**NATIONAL TECHNICAL UNIVERSITY OF ATHENS**

**SCHOOL OF RURAL, SURVEYING AND GEOINFORMATICS ENGINEERING**

**DEPARTMENT OF TOPOGRAPHY**

# *« Spatial Decision Support System for Offshore Wind Farm siting using Geographic Information Systems, Spatial Analysis and Optimization »*

---

**Ph.D. Thesis of:**

*Loukas P. Katikas*

**Supervisor:**

*Marinos Kavouras (Professor)*

**April 2022**

**NATIONAL AND TECHNICAL UNIVERSITY OF ATHENS**

**SCHOOL OF RURAL, SURVEYING AND GEOINFORMATICS ENGINEERING**

**DEPARTMENT OF TOPOGRAPHY**

# *«Spatial Decision Support System for Offshore Wind Farm Siting using GIS, Spatial Analysis and Optimization under Uncertainty»*

---

**Ph.D. Thesis of:**

***Loukas P. Katikas***

**Doctoral Supervisory Committee:**

***Marinos Kavouras (Professor)***

***Byron Nakos (Professor)***

***Phaedon Kyriakidis (Professor)***

**Margarita Kokla**
**(Ass. Professor)**

**Demetris Koutsoyiannis**
**(Professor)**

**Maria Papadopoulou**
**(Professor)**

**Nikolaos Mamasis**
**(Ass. Professor)**

---

**NATIONAL AND TECHNICAL UNIVERSITY OF ATHENS**

**SCHOOL OF RURAL, SURVEYING AND GEOINFORMATICS ENGINEERING**

**DEPARTMENT OF TOPOGRAPHY**

Loukas Panagiotis Katikas, 2022

Doctor of Philosophy, School of Rural, Surveying and Geoinformatics Engineering,

Department of Topography

## Acknowledgements

For most of the time, seeking the PhD degree is like finding ways and solutions out of a room in total darkness, all by yourself, with the most expected and unexpected ways. Without guidance, encouragement, help, support, positive thoughts and smiles from many others, this dissertation would not have finally entered the light by putting all pieces together. For these reasons, I would like to acknowledge the numerous people who have helped me get to this point. Knowingly or unknowingly, they all had a part to play in getting me through what most people recognise as a significant life hurdle, a PhD.

First and foremost, I would like to thank my supervisor Dr. Marinos Kavouras for his support throughout my PhD studies. He has guided me and trusted me over the years through a series of unexpected forks in the road (or preferably geospatially-speaking, path), leading to a rewarding research experience which I could not have predicted in advance. He has provided the ideal balance of tolerating a freedom to pursue research ideas, and also putting me back on track when I needed it towards finishing this PhD. He has always generously provided nudges and encouragement to take up opportunities for personal, academic and professional development and to show off my research to a broader extent.

I am also indebted to the other members of the supervisory board, Professors Vyronas Nakos and Phadon Kyriakidis for their constant help, support, encouragement and advice on my dissertation and journal papers. Their guidance has served me well and I owe them my great appreciation. Special thanks to my committee, Professors Demetris Koutsoyiannis, Margarita Kokla, Nikos Mamasis and Maria Papadopoulou for their support, guidance, helpful suggestions and patience throughout my research. I would also like to acknowledge and thank my school department along with the Civil Engineering Hydrology department for allowing me to conduct my research and providing any assistance requested all these years. Special thanks go to the members of staff development and human resources department for their continued support. Leda, Eleni, Nick, Andelina, Myra, Romanos and Anny, thank you for everything! Also, Dr. Panagiotis Dimitriadis is more than just a colleague and friend and I am really thankful for his support, his guidance and of course, his contribution to the wind-related publications.

Finally, and most importantly, I am heartily thankful to my friend, colleague and professor Themistoklis Kontos, my strong pillar, my source of scientific and programming inspiration, wisdom, knowledge and understanding. He has been the source of my strength throughout this journey and on his wings only have I soared. Six years of continuous coding on almost a daily basis via a laptop screen, numerous discussions, bugs, errors, applications, publications, conferences, difficulties but he has been always there. Without his support and overall, his presence, this PhD Thesis would not have been completed.

This PhD Thesis is also dedicated to my family and many friends. A special feeling of gratitude to my loving parents and my brother, Panagiotis, Eleni and Chris whose words of encouragement and push for tenacity ring in my ears and have never left my side and are very special. I also dedicate this dissertation to my many friends who have supported me and put up with me throughout this journey. I will always appreciate all they have done, especially for listening to my concerns, my thoughts and my unsolved programming problems for hours on a weekly basis. Namely, Peter, Kalliroi, Vaggelis, George, Jenny, Kostas, Marouan, Margarita, Stella, Nadia, Chris, Mike, Stella, John, THANK YOU GUYS, YOU ROCK AND YOU ARE THE REASON I HAD ALL THE GREAT TIMES WHEN I DIDN'T CODE!

*'The proper use of science is not to conquer nature but to live in it'*

- *Barry Commoner*

*'Θυμήσου: Προηγούνται οι επόμενοι!'*

## List of Publications

**Peer-Reviewed Journals**

**Katikas L., Kontos T., and M. Kavouras (2021):** An angle-weighted distance least cost path algorithm and trajectory smoothing techniques for offshore wind farm cost modelling*, Journal of Spatial Science (Under review).*

**Katikas L., Dimitriadis P., Koutsoyiannis D., Kontos T., Kyriakidis P. (2021):** A stochastic simulation scheme for the long-term persistence, heavy-tailed and double periodic behavior of observational and reanalysis wind time-series, *Applied Energy*;295*,* https://doi.org/10.1016/j.apenergy.2021.116873

**Hadjipetrou S., Liodakis S., Sykioti A., Fayad P., Katikas L., Park N.W., Kalogirou S., Akylas E., Kyriakidis P., (2021):** Offshore Wind Resource Assessment around Cyprus using Sentinel-1 Level 2 Ocean products, *Renewable Energy*;182:1228-1239*,* https://doi.org/10.1016/j.renene.2021.10.100

**Kontos T, Katikas L. (2018):** Delimiting Future Urban Sprawl Boundaries Using a GIS-based Model for Ecological Sensitivity Index Assessment and Optimization Techniques. The Case of Mytilene (Lesvos Island, Greece), *European Journal of Sustainable Development Research*;3(1), https://doi.org/10.20897/ejosdr/3975

**Conference Proceedings**

**Katikas L., Kontos T., and Kavouras M. (2019):** "A Least Cost Path Algorithm Implementation for the Transmission Cost Evaluation and Grid Connection of Future Offshore Wind Farms", Poster presented at: MESPOM Conference in Environmental Science, Policy & Management, Lesvos island, Greece, June 1-3 of June, 2019.

**Katikas L., Kontos T., Kavouras M., Kotroni V., Lagouvardos K. (2018):** Allocating continuous areas for future Offshore Wind Farm sitting using G.I.S, Spatial Analysis and Optimization techniques. The case of the North and Central Aegean Sea, Greece, Geomapplica International Conference, Syros-Mykonos islands, Greece, 25-29 of June 2018

**Kontos, T., Katikas, L., (2018):** Delimiting future Urban Growth Boundaries through the Ecological Sensitivity Index Assessment using a comprehensive G.I.S. based model and Optimization techniques. The case of Mitilini (Lesvos island, Greece), 11$^{th}$ International Conference of the Hellenic Geographical Society, Lavrion Technological and Cultural Park (LTCP), Lavrion, Greece

**Katikas L. and Kontos T. (2018):** "Suitability Assessment for Offshore Wind Farm Siting Using Exclusion Criteria and Spatial Economic Models. The Case of North and Central Aegean Sea", Conference in Environmental Science, Policy & Management, Lesvos island, Greece, June 1-3 2018

*«Spatial Decision Support System for Offshore Wind Farm siting using Geographic Information Systems, Spatial Analysis and Optimization»*

# Abstract


Planning an offshore wind project is considered as a highly complex and multivariable task since it involves a large number of parameters, controversial objectives and constraints to be considered. During the pre-feasibility and pre-planning stages for offshore wind farm site-prospecting, the current manual and sequential design approaches are not always sufficient to guarantee optimal solutions because inherent interactions and trade-offs are most of the times disregarded. Most of the already existing wind energy design tools are specifically built either for onshore environments or for specific offshore activities; hence most of them ignore many relevant key design aspects extended in both space and time. In addition, with the rapid evolution of the Geographic Information Systems (GIS) during the last two decades, numerous research studies, spatial modelling and spatial optimization approaches in the field of the Renewable Energy Sources (RES) gained attention. Highlighting the promising results occurred, considering the planning and designing procedures of such projects, in the near future, geospatial technology with its numerous services and fields can effectively be utilized for timely analysis and future planning assessments.

Considering the aforementioned challenges, this Ph.D. thesis proposes the development of a set of tools, as a Spatial Decision Support System (SDSS) entitled **SpOWNED-Opt** (**Sp**atial **Opt**imization for **O**ffshore **W**i**N**d **E**nergy **D**evelopment), in order to model, map, evaluate and identify continuous space for future OWF siting, towards the mathematical programming approach, based on GIS data structures and algorithms. Thus, the proposed tool can be defined as a more integrated GIS-based framework for the pre-feasibility assessment as also for parts of the Front and Engineering Stage of the Design (FEED) for offshore wind farm site-prospecting procedures in the North and Central Aegean Sea in Greece. In particular, the **SpOWNED-Opt** approach proposes a multi-level methodological framework for integrating different spatial modelling tools separated at four stages of development. The first stage consists of all preparative steps considering data acquisition pre-processing along with the screening analysis module, based on the Maritime Spatial Planning (MSP) guidelines and the national legislative regulations. Vector and raster data

are used expressing existing potential conflicts among human activities combined with socio-economic and environmental factors affecting the selection procedures. The second stage is linked to the cost assessment modules for the capital, operation and maintenance and decommissioning expenses (CAPEX, O&M and DECEX) approximation. An extensive review of all sub-cost components is carried out in order to formulate analytical expressions embedded in the SDSS. Moreover, graph-based optimization techniques are applied, based on Least Cost Path (LCP) algorithms upon raster surfaces in order to extract distance-based costs (transmission lines, installation, decommissioning and O&M costs).

The third stage focuses on the energy yield estimation and wind power output variability based on the UERRA Regional Reanalysis data. Different probabilistic models (Weibull, Burr Type II and XII, Gen. Gamma), reanalysis data errors quantification, wind speed intermittent characteristics and the second-order dependence structure are examined, analyzed and modelled in order to stochastically generate wind power output time series that are served as inputs to the last stage of the SDSS. The final module refers to a multi-objective integer non-linear programming (INLP) algorithm; as a unified framework that allows exploring in a rigorous and systematic mode numerous alternatives for offshore wind farm site-prospecting. The economic viability and the performance of the proposed wind farms are assessed along with the optimality of the different scenarios, from which the best ones are finally identified and mapped.

The novelty of this research lies both on the integrated nature of the SDSS and on the models used in the spatial modelling field. A critical advantage of the SDSS is that it addresses existing gaps on OWFs siting and overall, in RES location-allocation issues, by: i) introducing a holistic, step-by-step, spatial modelling framework, ii) providing a long-term planning approach, iii) implemented in a user-friendly graphical user interface (GUI), giving the opportunity to national and local authorities and stakeholders to delineate systematic assessment strategies in order to succeed an effective and sustainable renewable energy sources penetration.

**Keywords:** Geographic Information Systems (GIS), Spatial Modelling, Maritime Spatial Planning (MSP), Offshore Wind Farms (OWF), Least Cost Path (LPC), Numerical Weather Prediction (NWP), Probabilistic modelling, Stochastic simulation, Integer Programming (IP)

*«Δημιουργία Συστήματος Υποστήριξης Λήψης Χωρικών Αποφάσεων για τη Χωροθέτηση Θαλάσσιων Αιολικών Πάρκων με τη χρήση Συστημάτων Γεωγραφικών Πληροφοριών, Χωρικής Ανάλυσης και Βελτιστοποίησης»*

# Περίληψη


Οι διαδικασίες του σχεδιασμού, της αξιολόγησης και της χωροθέτησης ενεργειακών έργων, και πιο συγκεκριμένα Θαλάσσιων Αιολικών Πάρκων (ΘΑΠ), χαρακτηρίζονται από αρκετά μεγάλη πολυπλοκότητα και αβεβαιότητα. Η συνεκτίμηση διαφορετικών μεταβλητών και παραμέτρων, τα αμφιλεγόμενα συμφέροντα και στόχοι αλλά και οι περιορισμοί που ανακύπτουν, απαιτούν την υλοποίηση αναλυτικών μοντέλων διαχείρισης και μηχανισμών υποστήριξης λήψης βέλτιστων αποφάσεων. Τα ήδη υπάρχοντα εργαλεία διαχείρισης επικεντρώνονται είτε σε επίπεδο χωροθέτησης χερσαίων ενεργειακών έργων είτε σε μοντέλα μικρής κλίμακας και με στοχευμένη λειτουργικότητα για συγκεκριμένες διεργασίες. Αυτό έχει σαν αποτέλεσμα την απουσία μίας ολοκληρωμένης διαχείρισης του προβλήματος στο χώρο και το χρόνο κατά τα αρχικά στάδια του σχεδιασμού ενός ΘΑΠ. Παράλληλα, η εξέλιξη των Συστημάτων Γεωγραφικών Πληροφοριών (ΣΓΠ) και των Γεωεπιστημών γενικότερα τις τελευταίες δύο δεκαετίες αποτέλεσε ένα σημαντικό παράγοντα για την ανάπτυξη εφαρμογών, εργαλείων και μοντέλων χωρικής ανάλυσης στοχευμένα για τη διαχείριση και επίλυση προβλημάτων χωροθέτησης και αξιολόγησης ενεργειακών έργων. Αποτέλεσμα όλων αυτών των διεργασιών ήταν και είναι η ολοένα αποτελεσματικότερη μοντελοποίηση και αξιολόγηση των φυσικών και μη διεργασιών που λαμβάνουν χώρα στον πλανήτη μας.

Η παρούσα διδακτορική διατριβή επικεντρώνεται στην υλοποίηση ενός Συστήματος Υποστήριξης και Λήψης Χωρικών Αποφάσεων (ΣΥΛΧΑ), το **SpOWNED-Opt** (**Sp**atial **Opt**imization for **O**ffshore **W**i**N**d **E**nergy **D**evelopment), για την χωροθέτηση ΘΑΠ, λαμβάνοντας υπόψιν ένα σύνολο χωρικών παραμέτρων και μεταβλητών. Προτεινόμενη περιοχή μελέτης αποτελεί το κεντρικό και Βόρειο Αιγαίο, δεδομένου τόσο του υψηλού αιολικού δυναμικού όσο και της γεωμορφολογικής του πολυπλοκότητας. Ο διαχωρισμός των υπο-μοντέλων του προτεινόμενου ΣΥΛΧΑ είναι πολύ-επίπεδος και εντοπίζεται σε τέσσερα διαφορετικά στάδια. Στο πρώτο στάδιο γίνεται η διαχείριση και η προ-επεξεργασία των δεδομένων ενώ παράλληλα αποτυπώνονται οι περιορισμοί αποκλεισμού με βάση τις αρχές του Θαλάσσιου Χωροταξικού Σχεδιασμού (ΘΧΣ) και του εθνικού νομοθετικού πλαισίου. Κατά το δεύτερο στάδιο γίνεται η συστηματική αξιολόγηση

των οικονομικών δεδομένων για το ύψος της συνολικής επένδυσης αλλά, τα ετήσια κόστη λειτουργίας και συντήρησης αλλά και την απεγκατάσταση ενός ΘΑΠ, με τη σύνθεση αναλυτικών μοντέλων για κάθε μεταβλητή κόστους. Παράλληλα, με τη χρήση αλγόριθμων βέλτιστης χάραξης διαδρομών, βελτιστοποιούνται οι εκτιμήσεις για τα κόστη που συνδέονται με τον υπολογισμό αποστάσεων (ηλεκτρική διασύνδεση και κόστη εγκατάστασης, απεγκατάστασης και συντήρησης).

Κατά το τρίτο στάδιο του ΣΥΛΧΑ γίνεται η αξιολόγηση και προσομοίωση των ανεμολογικών χαρακτηριστικών και της παραγόμενης ενέργειας, αξιοποιώντας δεδομένα μοντέλων αριθμητικής πρόγνωσης υψηλής ανάλυσης. Από την αξιολόγηση της πιθανοτικής συμπεριφοράς των χρονοσειρών ανέμου, της κυκλοστασιμότητας αλλά και της μακροχρόνιας αυτοσυσχέτισης των χρονοσειρών, γίνεται η στοχαστική σύνθεση χρονοσειρών ενέργειας συνεκτιμώντας την μεταβλητότητα της στο χώρο. Τέλος, το τέταρτο και τελευταίο στάδιο του ΣΥΛΧΑ αποτελείται από το χωρικό μοντέλο εύρεσης βέλτιστων περιοχών, βασιζόμενο στις δομές του ακέραιου μη-γραμμικού δυναμικού προγραμματισμού. Σκοπός είναι η αξιοποίηση των προηγούμενων αποτελεσμάτων προκειμένου να επιλεγούν μία ή περισσότερες βέλτιστες περιοχές για τη χωροθέτηση ΘΑΠ. Μέσα λοιπόν από ένα σύνολο εναλλακτικών σεναρίων, μπορούν να επιλεγούν οι βέλτιστες στρατηγικές για την χάραξη πολιτικής σε τοπικό και εθνικό επίπεδο με στόχο την βιώσιμη διείσδυση των ΑΠΕ στον ενεργειακό εθνικό σχεδιασμό.

Η καινοτομία αλλά και ο τελικός στόχος της παρούσας διδακτορικής διατριβής είναι η απόδοση: i) ενός ολιστικού εργαλείου ανάλυσης του χώρου που θα είναι εύκολα προσαρμόσιμο ως προς τα κριτήρια που εξετάζει, ii) η εξασφάλιση της επαναληπτικής διαδικασίας και ανάλυσης πολλαπλών εναλλακτικών σεναρίων για την λειτουργία των ΘΑΠ και iii) η συμπερίληψη όλων όσων προαναφέρθηκαν σε ένα εύχρηστο αλλά αποτελεσματικό γραφικό περιβάλλον που θα μπορεί να αξιοποιηθεί από τους αρμόδιους ενδιαφερόμενους φορείς αλλά και από την ερευνητική και ακαδημαϊκή κοινότητα.

**Λέξεις κλειδιά:** Συστήματα Γεωγραφικών Πληροφοριών (ΣΓΠ), Χωρική Ανάλυση, Θαλάσσιος Χωροταξικός Σχεδιασμός (ΘΧΣ), Θαλάσσια Αιολικά Πάρκα (ΘΑΠ), Μοντέλα Χωρικής Βελτιστοποίησης, Εύρεση Βέλτιστης Διαδρομής, Στατιστική και Πιθανοτική ανάλυση, Στοχαστική προσομοίωση, Ακέραιος Προγραμματισμός

# Table of Contents

# List of Figures

# List of Tables

**Nomeclature**

*Abbreviations*

| | | | |
|---|---|---|---|
| SDSS | Spatial Decision Support System | LCP | Least Cost Path |
| GIS | Geographic Information Systems | SI | Sinuosity Index |
| RES | Renewable Energy Sources | MW | Mega Watt |
| LCC | Life Cycle Cost | PCF | Production Complexity Factor |
| LCoE | Levelized Cost of Energy | kV | kilo Volt |
| NPV | Net Present Value | AC | Alternative Current |
| CAPEX | Capital Expenditures | DC | Direct Current |
| O&M | Operation and Maintenance | HVAC | High-Voltage Alternative Current |
| DECEX | Decommissioning Expenditures | HVDC | High-Voltage Direct Current |
| MPAs | Marine Protected Areas | WF | Weather Factor |
| WT(s) | Wind Turbine(s) | VC | Vessel Capacity |
| ED | Euclidean Distance | HLCV | Heavy-Lift Crane Vessel |
| DH | Height Difference | AHTS | Anchor Handling Tug Supply |
| S | Slope | RDV | Rock Dumping Vessel |
| Lcd | least cost distance | JU | Jack-Up |
| BFS | Breadth First Search | CLV | Cable Laying Vessel |
| IQCP | Integer Quadratically Constrained Problem | | |
| ILP | Integer Linear Programming | | |
| INLP | Integer Non-Linear Programming | | |
| OWF(s) | Offshore Wind Farm(s) | GPD | Generalized Pareto Distribution |
| OWE | Offshore Wind Energy | SMA | Symmetric Moving Average |
| NWP | Numerical Weather Prediction | GHK | Generalized Hurst-Kolmogorov |
| UERRA | Uncertainties in Ensembles of Regional Re-Analyses | MEF | Mean Excess Function |
| | | PDF | Probability Density Function |
| MERRA | Modern Era Retrospective-Analysis for Research and Applications | CDF | Cumulative Density Function |
| | | AIC | Akaike Information Criterion |
| | | BIC | Bayesian Information Criterion |
| ERA | ECMWF Re-Analyses | GoF | Goodness of Fit |
| RAY | Rayleigh distribution | KS | Kolmogorov-Smirnov |
| W2 | Weibull distribution | RMSE | Root Mean Square Error |
| B3 | Burr (Type III) distribution | MAPE | Mean Absolut Percentage Error |
| B12 | Burr (Type XII) distribution | lnL | Log-Likelihood |
| PBF | Pareto-Burr-Feller distribution | STDE | Standard Deviation Error |
| GG | Generalized Gamma distribution | | |
| MLE | Maximum Likelihood Estimation | *Greek Letters* | |
| LSE | Least-Squares Estimation | | |
| MOM | Method of Moments | $\chi^2$ | Chi-Square |
| WT | Wind Turbine(s) | $\gamma$ | Climacogram function |
| MW/GW | Mega-Watt/Giga-Watt | $\lambda$ | Standardized variance |
| MWh | Mega-Watt Hours | $\mu_c$ | Mean value of *c* |
| CF | Capacity Factor | $\sigma_c$ | Standard deviation of *c* |
| POT | Peak Over Threshold | Γ(x) | Gamma function |
| | | Γ(x,y) | Lower incomplete gamma function |

# 1. Introduction

## 1.1 Offshore Wind Energy (OWE)

During the last three decades, renewable energy sources (RES) interest has been solidly revived due to the concerns of the climate change and global warming, carbon emissions reduction and energy supply (Díaz & Soares, 2020). International treaties as the Kyoto Protocol (UU.NN., 1998), the Paris Agreement (2015) (UU.NN., 2015), and the European 2030 climate and energy framework tried to handle the adverse climate effects and environmental degradation. Since the Intergovernmental Panel on Climate Change's (IPCC) Fifth Assessment Report (AR5)[1], and in front of the upcoming finalization of AR6 by the end of 2021 (IPCC, 2020), a consensus has been finalized by most of the countries worldwide that the global average temperatures should not exceed 2 °C above pre-industrial levels (IPCC, 2014). Most mitigation scenarios denote that the significant penetration of RES is critical to reach this target and succeed the optimal decarbonization scenarios and projections (Bosch et al. 2019).

Among different RES technologies, offshore wind energy (OWE) has experienced considerable growth since the beginning of the 21$^{th}$ century, becoming an economically competitive RES technology because of its unlimited and less variable resources, the increased efficiency and relatively low impact on marine activities and the environment (Akbari et al. 2019; Díaz & Soares, 2020). In particular, Offshore Wind Farms (OWFs) can reach higher capacities, in comparison with the onshore, on account of the i) higher, more constant, and often "smoother" wind speeds and ii) the taller and larger turbines allowing an increased energy production. The increased size and capacity of current wind turbines (WTs) led to the capital costs decrease, since fewer WTs, support structures and electrical infrastructures (in terms of the cabling lengths) are needed to reach the same OWF capacity (Bosch et al. 2019). Furthermore, the relative impact of OWFs installations on the marine ecosystems and biodiversity is not neglectable, although, with the appropriate planning and siting procedures and measures, can be minimized or even lead to a positive environmental footprint for a specific marine area (Spiropoulou et al. 2014; Soares-Ramos et al. 2020).

[1] The Synthesis Report (SYR) of the IPCC Fifth Assessment Report (AR5) provides an overview of the state of scientific knowledge concerning climate change, emphasizing new results since the publication of the AR4 in 2007.

From a historical point of view, the world's first OWF was installed in 1991 (Denmark). Despite of the tremendous development of OWE in the North and Baltic Sea, with more than half of the global installed capacity belonging to Denmark, UK, Belgium, Germany and Netherlands, no full-scale operational OWFs have been planned yet for the Mediterranean region (Akbari et al. 2019). Currently, more than 112 offshore wind projects are operating globally and there are 767 additional projects in different phases of development (Díaz & Soares, 2020). More than 30 GW of capacity have been already installed and the 90% of these projects are located mainly in European waters (North and Baltic Sea). The UK has an increased share of offshore wind capacity with 44% (10 GW of capacity), followed by Germany (34%), Denmark (7%), Belgium (6.4%) and Netherlands (6%) (Spyridonidou et al. 2020). In addition, France, Portugal, Norway, China, South Korea, Japan and the US have smaller but steadily increasing offshore capacities (Bosch et al. 2019) as long as countries like Greece, Finland, India, Brazil, Canada and Australia among others, begin to get involved in OWE deployment strategies. Projections for 2030 are estimating an increase of 150 GW (70 GW in Europe) in the total installed capacity, implying a tremendous scaling up of future offshore wind installations (Ioannou et al. 2020; Díaz & Soares, 2020).

Focusing on some technical aspects, the development of OWE is associated to the optimal exploitation of the available marine areas. Despite of the additional 250 GW of onshore wind farms planned to be installed up to 2030, finding new onshore sites is obstructive for many European countries, including Greece, due to socio-economic and environmental concerns (Jay, 2010; Ioannou et al. 2020). Consequently, this has advocated to the expansion of offshore wind industry, denoting at the same time that practices and principles of more integrated and holistic spatial planning and management approaches can be critical to the proper consideration of future OWFs. Furthermore, many Integrated Assessment Models (IAMs)[2] can only build viable global energy systems, towards more sustainable planning policies (Wang et al. 2017).

To allocate the most suitable coastal and offshore areas on which to site an OWF is crucial to the economic feasibility of a project, potential conflicts with other marine activities as also to the reduction of the environmental impact (Moller, 2008; Jay, 2010). Researchers, planners,

[2] IAMs are considered as models of using multidisciplinary research knowledge and usually contain numerous sub-models from many different areas (engineering, physics, chemistry, ecology, economics, politics), focused on the integrated assessment of environmental science, technology and policy issues.

policymakers and investors are interested in space management frameworks and cost-related assessments for OWF site-prospecting, in order to accelerate and succeed better planning forecasts for both incomes and outcomes of an offshore wind project (site-specific capital and operational expenditures, offshore wind and power potential etc.). As a result, robust approaches for applying econometric assessments across heterogeneous and complex spatial domains at different time scales, gives stakeholders better insights of the resulted sensitivities and uncertainties (Mytilinou & Kolios, 2019; Bosch et al. 2019).

The exploitation of the increased offshore potential in countries like Greece is vital, since substantial wind resources are observed in numerous locations like Cyclades, the North Aegean Sea, the Southern and Eastern Crete, and the southeast of Dodecanese (Karpathian archipelago). Recent energy demand estimates indicate that for small and sparsely populated countries like Greece, multi-megawatt OWFs (e.g. 500 MW) can cover an approximately 10% of the energy demand. However, considering the complex bathymetry and the intense marine and coastal activities, the proper locations of potential OWFs requires the installation of WTs at increased distances from the shoreline and whether is possible, in shallow depth areas (Spiridopoulou et al. 2014).

## 1.2 Geographic Information Systems (GIS)

GIS role starts at the very beginning of the OWF planning during the site prospecting analysis as also in some aspects of the Front-End Engineering Design[3] (FEED) stage. In parallel with the first OWFs deployment during the early 1990s, the development of GIS was vital for many geo-spatial problems as long as users were able to process large amounts of geographical data, which led to the construction of robust models and spatially explicit decision support tools. In general, the evolution of spatial modelling is based on four major disciplines of geographic content consisting of: i) quantitative geography, ii) regional science, iii) spatial statistics and finally, iv) computational geometry. Focusing on the last two, spatial statistics and computational geometry

[3] FEED phase includes specific reports and design tests related to the wind turbines selection, support structures design, electrical infrastructure and grid connection, O&M strategies, ports and harbours locations and logistics for an OWF.

use computers to build algorithms for analyzing or optimizing geometrical attributes, relations and phenomena. Among the different methods developed and evolved were the multi-criteria decision making (MCDM), route and network planning, spatial and temporal modelling and dynamic programming, as parts of the known as spatial analysis and optimization problems (Murayama & Thapa 2011).

These key aspects of GIS-based spatial modelling are that allow to collect, interpret, monitor, analyze and visualize data in order to understand spatial relationships, patterns and trends. In a broad sense, spatial modelling may be characterized as a collection of tools for analyzing, revealing, assessing and shedding light on complex spatial processes and structures of spatial phenomena occurring on the Earth's surface (Murayama & Thapa 2011; Goodchild & Longley, 2019). Furthermore, these systems are designed to support spatial decision-making, as a mechanism for dealing with regional, national, continental or even global planning. However, spatio-temporal modelling is still in a state of development seeking to always meet users' needs (Murayama and Thapa 2011). Hence, one key feature for the real-world applications of GIS, has been the system's ability to capture the process by which decisions are made (Goodchild 2013).

Despite the tremendous capabilities and the evolution of GIS science, there are rather few purely technical solutions to substantial real-world problems. As a result, some of the key drawbacks occur in spatial modelling incorporate: i) data availability, complexity and size, ii) relevant data quality control issues leading to increased uncertainty, iii) the capability to process in a short computational time, iv) spatial resolution, scale of analysis and data aggregation issues and finally, v) spatial problems complexity and interactions that most of the times preserve some unique spatial or temporal characteristics really difficult to be addressed and modelled (Goodchild & Longley, 2019). Involving optimum networks, pathfinding algorithms, dynamic programming approaches and location-allocation decision-making, is the highlight of spatial modelling techniques, providing decision makers the opportunity to map solutions and interactively modify preferences and the inherent trade-offs between various objectives (Tong & Murray, 2012).

## 1.3 Motivation

Keeping in mind the key trends and challenges of both OWE deployment and GIS modelling, and that the OWE sector is still succeeding a noteworthy share of the future RES, it is important that the unique characteristics and trade-offs of offshore wind installations are captured during the planning process. Many previous modelling efforts are seeking to incorporate spatio-temporal details as also to capture a logical connection between the environmental, economic, societal and geographical factors of the energy supply. Nevertheless, there is a gap concerning integrated Spatial Decision Support System (SDSS) tools for location-allocation problems such as OWF site-prospecting. Overall, technical reports and previous research studies highlighted several key opportunities that may help reduce OWE cost, (Rodriguez et al., 2015; Mytilinou & Kolios, 2019; Bosch et al. 2019) focusing on the:

1. Introduction of WTs with increased rated power (larger than 8, 10 or even 15MW) and reliability;
2. Deeper commercial floating support structures consideration (beyond 200 meters depth);
3. Integration of simple but efficient spatial planning tools in the offshore wind industry and enhanced assessment procedures at the pre-development and consenting phase;
4. Spatial heterogeneity assessment, as long as recent OWFs preoccupy larger offshore areas, which most of the times have increased depth variability and heterogeneous seabed and met ocean conditions;
5. Nowadays, there are more technological options available related to the type of WTs, cables, transformers and support structures that are available subject to multiple viable configurations and planning scenarios;
6. Increased collaboration, knowledge and data sharing among industry, investors, researchers and national authorities is vital.

Keeping in mind the aforementioned challenges, holistic and novel spatial models must be considered, and geographic science is providing an enormous potential of algorithms and tools. Some perennial drawbacks of energy-related geospatial modelling consist of:

1. Improving geographic methods for the spatio-temporal assessment of energy fluctuations, variability and demand;
2. There are several commercial wind farm design tools which are specifically built either for onshore environments or site-specific tasks;
3. Existing spatial optimization algorithms do not fully support multi-objective approaches targeted to marine space management and OWF optimal site prospecting;
4. Geospatially condensed models and analysis results can be a major advancement for multiple scale modelling (regional, national, continental).
5. The integration of a variety of heterogeneous spatial and non-spatial data, denotes a key challenge on unifying less uncertain results with more integrated sensitivity analyses.

Under the scope of these issues and challenges, the possibility to acquire, process, model and visualize different types of information, makes GIS a valuable and powerful field for RES planning in a macro and even micro scale level of development. On top of that, GIS systems accompany the entire lifecycle of an OWF and the integration of already operational data with the geographic content provides a holistic view of the planning processes and the inherent trade-offs, by enabling location-aware and practical decisions.

## 1.4 Research questions, aims and objectives

The research questions of the proposed thesis are formulated in the context of how GIS technologies can effectively be combined with renewable energy studies, as a powerful set of tools for more integrated and less uncertain planning procedures and assessment strategies. In order to address this statement, the following questions must be answered:

- *In recent literature research, if there are any existing integrated spatial modelling schemes to support OWE deployment beyond simple multi-criteria assessments?*
- *How to create a holistic and user-friendly Spatial Decision Support System (SDSS), based-on interconnected GIS tools and algorithms for less uncertain site-prospecting campaigns?*
- *How GIS structures and models can be a powerful tool to monitor, handle and assess complex spatial relationships towards OWF siting, as a multi-objective problem, using spatial modelling techniques that can be easily customized for any specific region worldwide?*
- *What kind of spatial optimization models must be established in order to gain vital cost- and energy-related information leading to less uncertain results, even in the pre-development and consenting stages?*
- *Which are the technical and economic characteristics of future OWFs and in an environmental and socio-economic scale of development, if RES investments such as offshore wind energy projects can be sustainable and profitable for Greece?*

To answer these questions, this work aims to provide an integrated methodological framework for OWFs site-prospecting, by providing it in a way that is accessible to end users. It builds from a bottom-up approach, characterizing space availability, economic trade-offs, wind energy generation potential from high resolution wind data, towards the optimal site-selection upon technical, societal, environmental and economic constraints. Given the problem definition, the motivation and the research questions, there are four systematic objectives, numbered below, that this thesis aims to address including:

1. The investigation of how to create a holistic Spatial Decision Support System (SDSS) framework to integrate, automate, optimize and iterate the planning of optimal OWFs areas. Demonstrate the utility of the model through a set of investigations of the influences on the inherent cost trade-offs of current and future OWFs.
2. Furthermore, the implementation of spatially explicit cost models, which comprise the OWF sub-cost components, based on up-to-date cost data and Least-Cost-Path (LCP)

algorithms. LCP algorithms are mostly applied in order to obtain more realistic transmission, installation and O&M corridors under real case scenarios, for cost evaluation based on both simplified and analytical cost estimations.

3. The application of an integrated offshore wind resource assessment framework considering the key statistical and probabilistic characteristics of wind. The first task is to quantify and map the most important wind speed characteristics using reanalysis data that spread out over many different wind regimes. The ultimate goal is to establish and test a stochastic simulation scheme for the North and Central Aegean Sea in order to analyze the power potential and the inherent variability of the energy yield.
4. Finally, the integration of the above-mentioned results in a robust and computationally efficient multi-objective optimization framework, specially tailored to the optimal site prospecting processes of future OWFs upon multiple objectives, including contiguity and compactness control of the resulted optimal areas.

## 1.5 Outline

This thesis was built heavily on open access and peer-reviewed journal papers in the fields of Geographic, Environmental and Energy fields, listed in the preamble of this thesis. The following paragraphs summarize the contents of each chapter:

**Chapter 1** briefly introduces the key aspects and challenges in the field of RES planning and modelling linked to the GIS context among with the motivation, research questions, objectives and the outline of the proposed research.

**Chapter 2** provides the state of the art in the offshore wind industry. It firstly presents the incentives for the development of OWFs, describing alongside the current status of OWE in Greece. The remainder of the background section then reviews the steps required for OWFs site prospecting, cost evaluation and energy estimation.

**Chapter 3** is briefly reviewing relevant GIS-based frameworks, spatial optimization models and spatial decision support tools used for OWE deployment. Moreover, the current state and future

challenges in the offshore wind resource assessment and stochastic simulation field are further analyzed and discussed.

**Chapter 4** describes the proposed study area characteristics, the data availability and scale of determination used for this work. At first, the key geophysical, economic and environmental characteristics of the North and Central Aegean Sea are illustrated. In addition, the data sources availability and their application in the subsequent modelling work are analyzed.

**Chapter 5** is extensively surveying the methods used for each model including the screening and economic assessment, the offshore wind assessment and stochastic simulation models, the site-prospecting optimization procedures and finally, the SDSS implementation using a standalone graphical user interface.

**Chapter 6** presents and discusses on the results of the proposed framework in terms of the exclusion scenarios applied, the life-cycle cost modelling results, the estimated long-term energy production and all siting scenarios as extracted from the site-prospecting optimization scheme in the SDSS. Finally, based on the results;

**Chapter 7** reviews the key findings of the modelling concepts, and the main benefits and drawbacks of the current work by discussing in parallel for future improvements and directions to be considered.

## References


1. **Akbari N., Jones D., Treloar R., (2019):** A cross-European efficiency assessment of offshore wind farms: A DEA approach, *Renewable Energy*:151;1186-1195
2. **Bosch J., Staffell I., Hawkes A. D., (2019):** Global levelised cost of electricity from offshore wind, *Energy*:189
3. **Díaz H., and Soares G., (2020):** Review of current status, technology and future trends of offshore wind farms, *Ocean Engineering*:209;107381
4. **Goodchild M. F., (2013):** Prospects for a Space–Time GIS, *Annals of the Association of American Geographers*
5. **Goodchild, M. F., & Longley, P. A., (2019):** Geographic Information Science. In: Fischer M., Nijkamp P. (eds) Handbook of Regional Science. Springer, Berlin, Heidelberg
6. **Ioannou A., Angus A., Brennan F., (2020):** Stochastic financial appraisal of offshore wind farms, *Renewable Energy*:145;1176-1191

7. **IPCC, (2014):** Climate Change 2014: Synthesis Report. Contribution of Working Groups I, II and III to the Fifth Assessment Report of the Intergovernmental Panel on Climate Change *[Core Writing Team, R.K. Pachauri and L.A. Meyer (eds.)]. IPCC, Geneva, Switzerland, 151 pp.*
8. **IPCC, (2020):** AR6 Synthesis Report: AR6 Climate Change 2021: Impacts, Adaptation and Vulnerability
9. **Jay S. (2010):** Planners to the rescue: Spatial planning facilitating the development of offshore wind energy, *Marine Pollution Bulletin*:60;493-499
10. **Moller B. (2011):** Continuous spatial modelling to analyze planning and economic consequences of offshore wind energy, *Journal in Energy Policy*:9;511-517
11. **Mytilinou V. and Kolios A. J. (2017):** A multi-objective optimization approach applied to offshore wind farm location selection, *Ocean Engineering and Marine Energy*:3;265-284
12. **Murayama Y., Thapa R. (2011):** Spatial Analysis and Modelling in Geographical Transformation Process: GIS-based Applications, The GeoJournal Library (eds.), 100, Springer Netherlands
13. **Soares-Ramos E. P. P., Oliveira-Assis L., Sarrias-Mena R., Fernandez-Ramirez L. M., (2020):** Current status and future trends of offshore wind power in Europe, *Energy*:202
14. **Spiridopoulou I., Karamanis D., and Kehayias G., (2014):** Offshore wind farms development in relation to environmental protected areas, *Sustainable Cities and Society*:14;305-312
15. **Spyridonidou S.**, Vagiona D.G., and Loukogeorgaki E., (2020): Strategic Planning of Offshore Wind Farms in Greece, *Sustainability*:12(3);905
16. **Tong D., and Murray A.T., (2012):** Spatial Optimization in Geography, *Annals of the Association of American Geographers*:102(6);1290;1309
17. **UU.NN., (1998).** Kyoto protocol to the united nations framework Kyoto protocol to the united nations framework. Rev. Eur. Community Int. Environ. Law 7, 214–217.
18. **UU.NN., (2015).** Approval of the Paris agreement. Conv. Framew. Clim. Change 70371, 1–40. Volker, P.J.H., Hah
19. **Wang, Z., Wu, J., Liu, C., & Gu, G., (2017):** Integrated Assessment Models of Climate Change Economics. Singapore: Springer Singapore
20. **Rodrigues S., Restrepo C., Kontos E., Teixeira Pinto R., Bauer P., (2015):** Trends of offshore wind projects, *Renewable and Sustainable Energy Reviews*:49; 1114 – 1135

# 2. State of the art in Offshore Wind

## 2.1 Offshore Wind Energy - General aspects

By the end of 2020, European Union (EU) set the target to reduce by 20% the $CO_2$ emissions, to generate 20% of its energy consumption using RES and to improve 20% of its energy efficiency, compared to the 1990 levels. These goals are extended to double the reduction of $CO_2$ emissions, with an increase up to 27% for renewables and 27% in energy efficiency by 2030 (Rodriguez et al. 2015; Díaz & Soares, 2020). Table 2.1.1 indicates that many European and Asian countries among with the US have already succeeded to decrease $CO_2$ and $SO_2$ emissions, focusing on renewable energy and offshore wind installations. Towards the aforementioned targets, the OWE sector plays a pivotal role in the short and long-term (2020, 2030 and 2050 respectively) international energy strategies. As a result, the global cumulative capacity produced by offshore wind farms is expected to increase from 19 GW registered in 2019 to 50 GW in 2022. Currently, more than 112 OWFs are operational, 53 under construction and more than 700 projects at different stages of development and planning (Figure 2.1.1).

**Table 2.1.1:** Homes powered annually by RES and $CO_2$/$SO_2$ emissions reduction (By the end of 2018 - 4C Offshore, 2019) (Source: Díaz & Soares, 2020)

| **Country** | *Homes powered annually* | *CO2 reduced annually (ton)* | *SO2 reduced annually (ton)* |
|---|---|---|---|
| **Belgium** | 617032 | 1247021 | 29002 |
| **Finland** | 59777 | 120809 | 2809 |
| **Denmark** | 916553 | 1852324 | 43079 |
| **Germany** | 3783716 | 7646885 | 177836 |
| **Ireland** | 17848 | 36071 | 839 |
| **Netherlands** | 791689 | 1600000 | 37209 |
| **Sweden** | 135383 | 273159 | 6364 |
| **UK** | 5204120 | 10517526 | 244594 |
| **China** | 1706862 | 3449492 | 80219 |
| **Japan** | 29266 | 59144 | 1376 |
| **South Korea** | 24789 | 50099 | 1165 |

| | | | |
|---|---|---|---|
| **Taiwan** | 5666 | 11451 | 266 |
| **Vietnam** | 70259 | 141993 | 3303 |
| **USA** | 21248 | 42942 | 999 |

Analyzing Figure 2.1.1 and Figure 2.1.2 there is a tendency for an increase in OWE investments and many key characteristics indicate the potential and the dynamics of OWFs during the last 20 years. When considering the capacity of wind generators, 6 – 8 MW are commonly used, compared to less than 3 MW until 2004. Alongside with the increased WTs capacities, the gross OWFs' capacity seems to increase, mainly due to the increased energy demand and the bigger OWE projects. Current trends denote, bigger WTs in terms of the hub height and rotor diameter in order to increase the available energy extracted and decrease the total support structures, WTs and inter-array cables and capital expenditures in general. Concerning the number of WTs, the vast percentage of OWFs is composed of less than 70 WTs with the future trends for mega-projects denoting an increase in the total WTs installed (more than 150). Besides, most of the operational wind farms have less than 400 MW total installed capacity. Regarding the average water depth and the distance from the shoreline, all the operating wind farms are located at a maximum depth of 50 m, while the 90% of installations are located in distances less than 60km from the shore (with maximum distances exceeding 120 km) (Díaz & Soares, 2020).

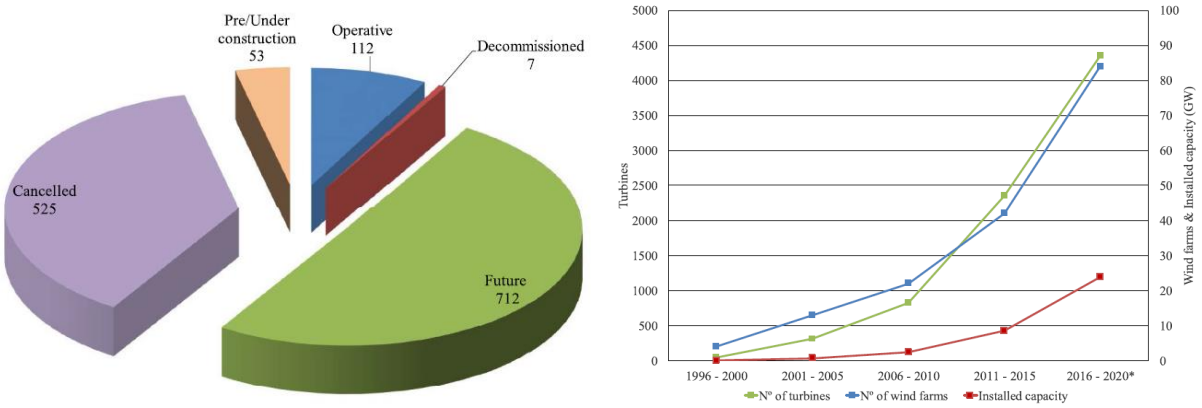


**Figure 2.1.1:** (Left) A general overview of offshore wind projects state (by the end of 2018 - 4C Offshore, 2019), (Right) Evolution of offshore wind farms with respect to the commissioning period (Source: Díaz & Soares, 2020)

Most future OWFs are likely to remain at a maximum depth of 50-100 meters (for fixed-bottom structures), but numerous projects expected and planned for higher water depths, up to 1000 meters, using floating support structures. This mostly concerns countries that have increased bathymetric profile relatively close to the shore, such as Greece, Portugal, Norway and Italy. Currently, only research prototypes of floating wind turbines exist, located in the North Sea, featuring five WTs with total capacity of 30 MW, in the Atlantic Ocean off the Portuguese coast, in the Baltic Sea and finally in Japan (4 MW) (Bento & Fontes, 2019; Maienza et al. 2020).

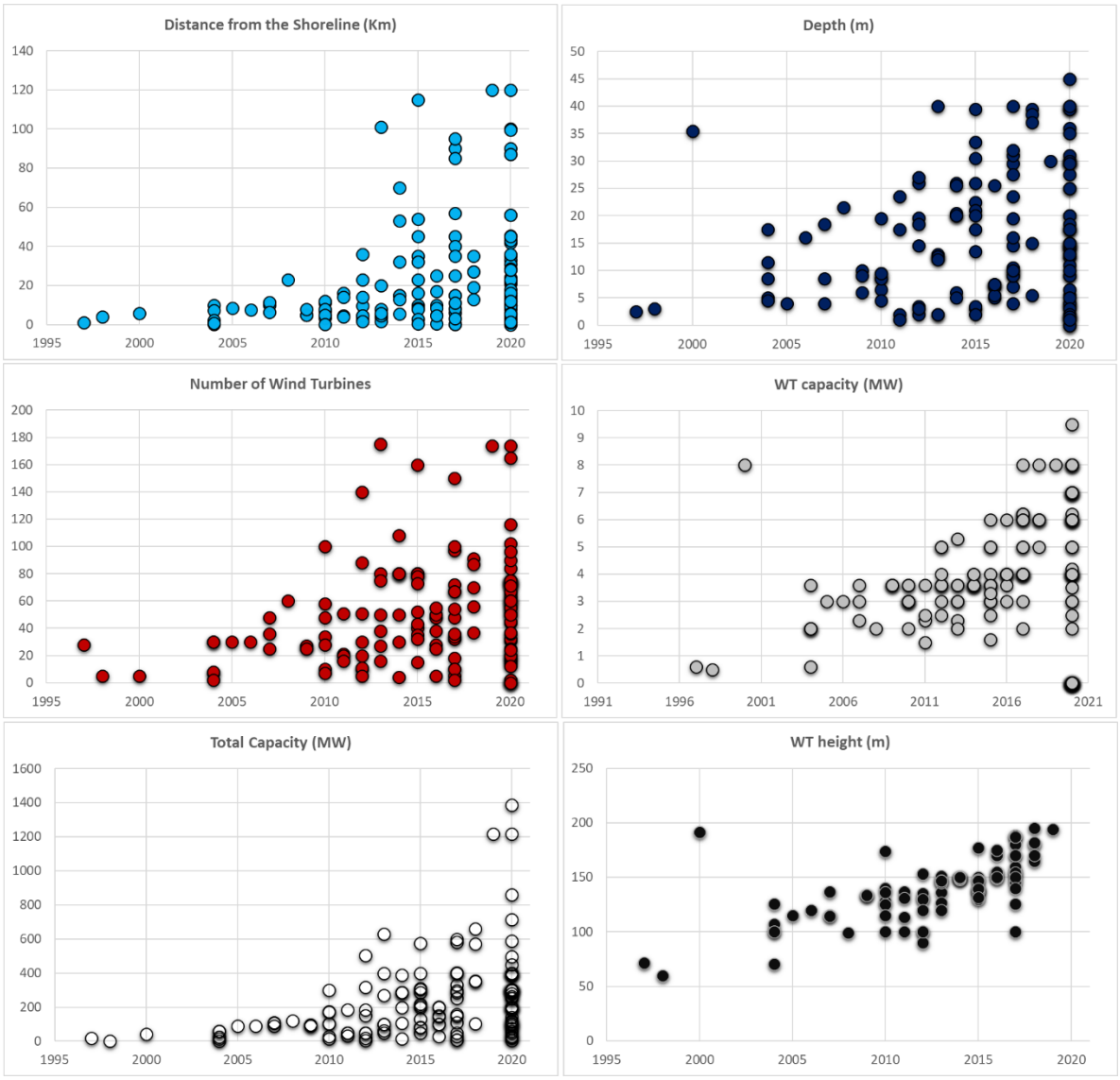


**Figure 2.1.2:** Distance from the shore, Depth, Number of WTs, WT capacity, Total OWF capacity and WT hub height (from the sea bottom) evolution from 1995 - 2020

(Sources: 4C Offshore, 2019; Díaz & Soares, 2020)

Despite of the accelerated development of OWFs installations by 2000 and onwards, when larger turbines and OWFs became available and experience was gained, Figure.2.1.1 clearly highlights that, there are still 525 projects cancelled by the end of 2018. Issues related to wind speed and power variability, harsh marine weather conditions, increased depths and distances from ports, harbors and the onshore grid connection points, lead to complex engineering, logistics and operational procedures consisting of the main challenges faced by the offshore wind industry (Akbari et al. 2019). On top of that, other non-technical reasons explaining this amount of cancelled offshore wind projects (mainly in EU) constitute of the lack of strategic spatial and environmental planning, the complex administrative procedures and further beyond due to the uncertainty of the entire support mechanisms (Spiropoulou et al. 2014; González and Arántegui, 2016). As a result, it seems unlikely that many countries worldwide will reach the total expected capacity for offshore wind by 2021 (larger than 43 GW) and despite of some exceptions (United Kingdom, Netherlands, Sweden and Denmark), most of the countries have deployed less RES investments than they planned.

## 2.2 Offshore Wind Farm Planning

As already discussed, OWFs are built further and further offshore, using bigger turbines and new foundation technologies are tested. Hence, it is crucial to have plans that can deal with these challenges and ensure cost-effective decision-making steps during the planning, construction and operation and maintenance stages. During the first years of OWE deployment, industry and policymakers thought developing an OWF was a straightforward alternative out from the drawbacks of targeting increased onshore wind capacities (Gerdes et al. 2010). However, the results from the offshore experience were not always as encouraging as expected and the increased manufacturing, installation and operational costs led to a lot of criticism. Nevertheless, research on OWF planning has improved our knowledge and understanding of the key factors affecting offshore wind investments. Furthermore, the interdisciplinary nature of planning procedures demanded a comprehensive evaluation of the OWF siting criteria (Ho et al. 2018).

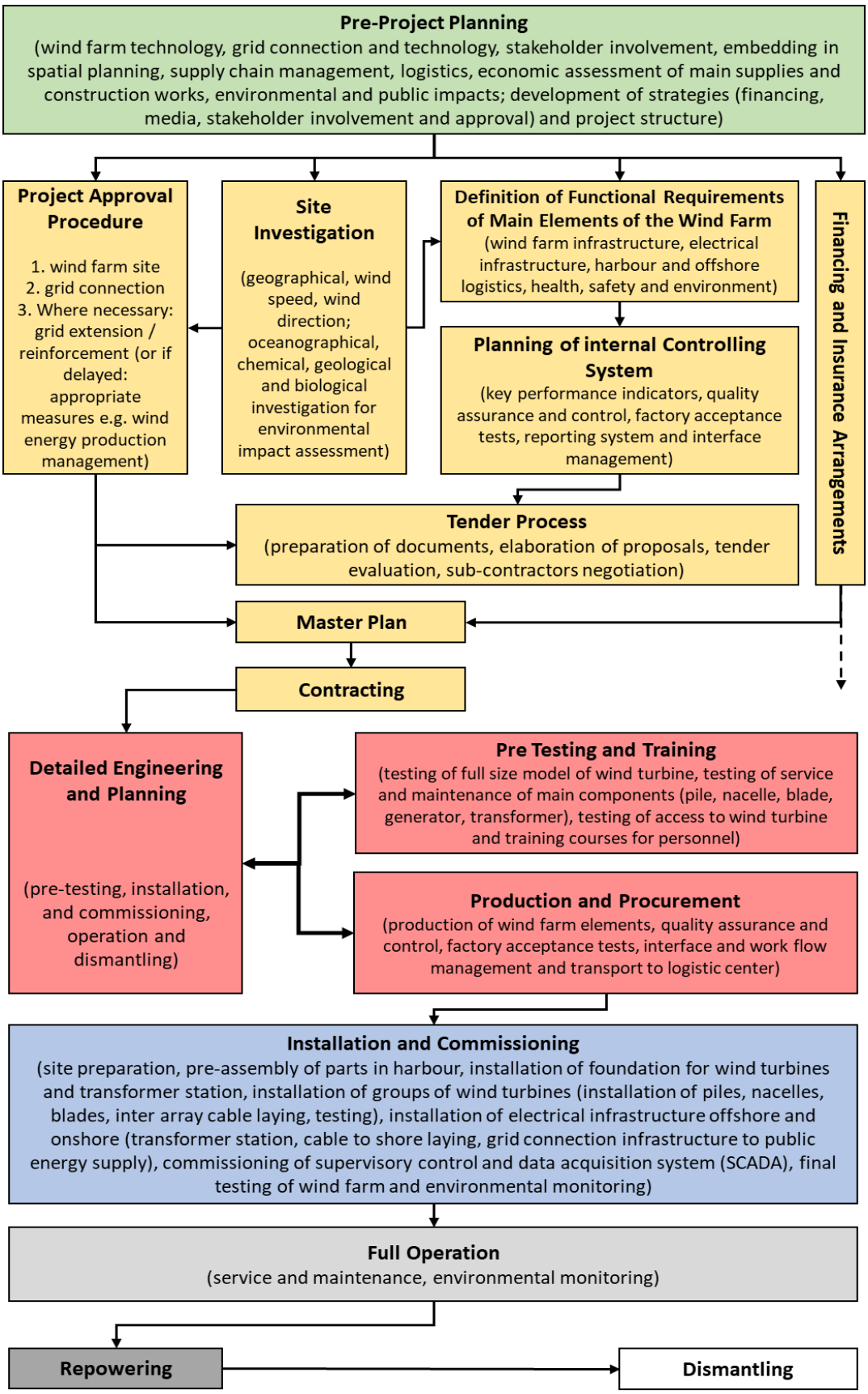
Pre-Project Planning
(wind farm technology, grid connection and technology, stakeholder involvement, embedding in spatial planning, supply chain management, logistics, economic assessment of main supplies and construction works, environmental and public impacts; development of strategies (financing, media, stakeholder involvement and approval) and project structure)
Project Approval Procedure
1. wind farm site
2. grid connection
3. Where necessary: grid extension / reinforcement (or if delayed: appropriate measures e.g. wind energy production management)
Site Investigation
(geographical, wind speed, wind direction; oceanographical, chemical, geological and biological investigation for environmental impact assessment)
Definition of Functional Requirements of Main Elements of the Wind Farm
(wind farm infrastructure, electrical infrastructure, harbour and offshore logistics, health, safety and environment)
Planning of internal Controlling System
(key performance indicators, quality assurance and control, factory acceptance tests, reporting system and interface management)
Financing and Insurance Arrangements
Tender Process
(preparation of documents, elaboration of proposals, tender evaluation, sub-contractors negotiation)
Master Plan
Contracting
Detailed Engineering and Planning
(pre-testing, installation, and commissioning, operation and dismantling)
Pre Testing and Training
(testing of full size model of wind turbine, testing of service and maintenance of main components (pile, nacelle, blade, generator, transformer), testing of access to wind turbine and training courses for personnel)
Production and Procurement
(production of wind farm elements, quality assurance and control, factory acceptance tests, interface and work flow management and transport to logistic center)
Installation and Commissioning
(site preparation, pre-assembly of parts in harbour, installation of foundation for wind turbines and transformer station, installation of groups of wind turbines (installation of piles, nacelles, blades, inter array cable laying, testing), installation of electrical infrastructure offshore and onshore (transformer station, cable to shore laying, grid connection infrastructure to public energy supply), commissioning of supervisory control and data acquisition system (SCADA), final testing of wind farm and environmental monitoring)
Full Operation
(service and maintenance, environmental monitoring)
Repowering
Dismantling

**Figure 2.2.1:** Planning stages of an OWF, Source: Gerdes et al. (2010)

In sight of some technical aspects, investigating for an optimal site is a complicated process related on various technical, environmental and socio-economic criteria, as well as to the relevant national legislation and marine spatial planning regulations. Offshore wind capacity is the most important factor and directly dependent to a wind project's financial efficiency. Furthermore, technical and geophysical factors must be examined as the water depth, the sea substrate conditions, possible tectonic faults, wave and currents characteristics etc. Finally, societal and environmental constraints are always play the most important role in the decision-making procedures. Distance from nearby coastal cities and recreational activities, conflicts among sea uses, environmentally vulnerable or protected sites, are some of the obstacles may arise during the planning and licensing procedures. Therefore, to identify potential conflicts, obstacles and constraints for potential suitable areas, numerous planning activities must be considered. Gerdes et al. (2010) have divided the project phases into seven categories required consisting of the (Figure 2.2.1):

- Pre-project planning,
- Detailed project planning,
- Procurement and production,
- Engineering, testing, installation and commissioning,
- Full operation,
- Repowering or Decommissioning,
- Dismantling

Translating these categories into Life Cycle Cost (LCC) analysis drivers, the main stages for OWF siting are separated into five categories (Figure.2.2.1) (Myhr et al., 2014; Shaffie et al., 2016; Ioannou et al., 2018;Bosch et al. 2019):

1. Pre-development and consenting (P&C),

2. Production and acquisition (P&A),
3. Installation and commissioning (I&C),
4. Operation and maintenance (O&M) and
5. Decommissioning and disposal (D&D)

Analyzing the aforementioned steps and the outline illustrated in Figure 2.2.1, the following actions must be applied:

**Pre-project planning** and **Development and Consenting** phase consists of the feasibility studies reports indicating how technically and economically feasible a project is. The first stage requires an initial investigation of potential sites' characteristics that allows the developers, planners and stakeholders to weight the associated risks, before a large investment is further proceed on other development activities. Particularly, numerous sets of reports are produced clarifying the most suitable areas for OWF installation, based on the marine spatial planning assessment, the OWF configuration (technology to be used), geotechnical and environmental surveys, logistics and supply chain strategies as also the overall impact and benefits of the offshore wind project to the public. A typical initial study and the associated reports will include some or all of the following studies (Jongbloed et al. 2014; Rodriguez et al., 2015; Cavazzi and Dutton 2016):

- Wind resource assessment based on in situ records among with high-resolution modelled and satellite data;
- Met-ocean conditions assessment and monitoring (i.e. waves and sea currents);
- Seabed analysis and water depth characteristics (foundation options);
- Proximity evaluation to the nearest high voltage grid and the nearest port with sufficient capacity;
- Additional support services and infrastructures evaluation (i.e. onshore substations, ports, harbors, logistics etc.);
- Minimum suitable available space by monitoring the current or future marine activities;

- Environmental impact assessments;
- Potential challenges for community acceptance;
- Technical feasibility and technology options;
- WTs layout, turbine selection, and energy production estimates;
- Cost and revenue projections

**Detailed project planning** consists of the project approval procedures. The final OWF marine area is further assessed to a more in-depth analysis (wind measurements and simulations, transmission infrastructures delineation and connection to the grid, optimal allocation of ports and harbors facilities, predictions for the operation and maintenance cost etc.), in order to formulate a finalized bid for a price per produced kWh. These steps consist of a prerequisite for the upcoming tendering process and contracting. Moreover, **engineering, testing, procurement and production** is also incorporated in this stage and involves a more detailed and site-specific engineering planning, called as FEED (Front-End Engineering Design). During FEED stage, testing of full-size models of WTs and foundations prototypes as well as training campaigns are also provided for the personnel linked to the operation and maintenance procedures. Finally, the hiring of contractors follows and production and acquisition of the OWF components starts (WTs, foundations, transition pieces, cables etc.) in order to be transported to the port facilities and the installation site accordingly.

Installation and commissioning phase refers to the installation of the entire OWF's infrastructures both offshore and onshore. The installation process begins with the site preparation activities, pre-assembly of parts followed by installation of the foundations and the offshore and onshore stations (if an onshore station exists). In later stages, the tower, the nacelle and the rotor blades are placed. Finally, the electrical infrastructure consist of the last stage where, the offshore and onshore substations are installed and the inter-array (cables connecting the WTs with the offshore substation or the transformer) and export transmission cables are connected to national grid. After installation, the commissioning tests are performed by monitoring in parallel for possible negative environmental impacts from the construction phase.

The operational phase is this stage where the operational standards and OWF's efficiency must be guaranteed among with the optimal maintenance strategies as well as the environmental monitoring procedures until the OWF is finally, decommissioned and disposed. This is the final stage of an OWF's life cycle as an opposite procedure of the installation stage, where the WTs, the foundations and the cables are detached. OWF components, depending on the selected waste management strategy, are either removed or recycled, the offshore site is cleared and finally, some post-decommissioning monitoring activities are performed to ensure that the environmental impact on the site is the least possible.

Reviewing the pre-feasibility and pre-planning stages, the optimal site(s) selection is the first crucial task. Knowing from the very beginning of a project, the optimal strategies to be followed is a very important step to reduce further uncertainties or delays. The economic situation preserves increased variability, especially when the grid connection costs and the distances to the shore increase. González and Arántegui (2016) highlight that the development of OWFs struggles with technical uncertainties that pose risks to the corresponding investments. These risks tend to increase the investment cost, subject to financing and contingency issues, and are critical for the delay, postponement or even the cancellation of an OWE project. As a result, it is becoming obvious that stable and positive conditions for OWE development can be gained from activities such as the integrated spatial planning for OWF site prospecting including all possible economic trade-offs and alternatives for successful, optimal and sustainable solutions.

## 2.3 Offshore Wind Energy Sector in Greece

Analyzing the Greek experience and since many onshore areas are covered with WT installations, OWFs have started to be considered. Since specific locations in the Greek territory like Cyclades, the Southern Crete, and the southeast marine areas of the Dodecanese have many advantages to those on land, OWE deployment seemed as a rather sustainable option to increase RES penetration. However, the increased depth variability, distance from the shoreline, environmental concerns, the public acceptance and the economic crisis during the period 2009-2017 are some of the main obstacles for further OWE deployment in Greece (Spiropoulou et al.

2014; Caralis et al. 2016; Christoforaki and Tsoutsos 2017). Particularly for Greece, the severe economic crisis was characterized by the lack of liquidity that blocked, delayed or cancelled numerous investments. One of the most successful support schemes, the Feed-in Tariff (FiT)[4], had a negative impact to the investments due to the economic circumstances and the increased FiT variability created huge concerns to the investors.


**Figure 2.3.1:** Proposed marine areas for OWE deployment based on CRES study (Sources: CRES, 2010)

Analyzing the legislative and regulatory frameworks in Greece, Law 3851/2010 specified procedures to accelerate the development of RES. Thus, for the first time in Greece, a tendering procedure was foreseen for the planning, construction and operation of OWFs (Article 6 - L3851/2010). According to this legislative framework, the state had to identify no conflicting sea uses or possible environmental consequences, assess the environmental impacts from the

[4] Feed-in Tariff (FiT) is defined as a policy mechanism designed to accelerate investment in RET, by offering long-term contracts to RE producers, typically based on the cost of generation of each technology (Pyrgou et al. 2016).

construction and operation of future OWFs by proposing environmentally acceptable marine areas. Upcoming steps consisted of issuing the approvals of environmental terms followed by an open public tender for the exploitation rights of the proposed sites (Ministry of Environment Energy & Climate Change 2010). The key target of this procedure was to attract investors for offshore wind development, by preparing the entire licensing procedure for them and facilitating them to start the construction of the OWFs immediately after the tendering procedure. As provided by Law 3851/2010, an initial governmental study (in cooperation with the Center of Renewable Energy Sources - CRES) has been conducted, indicating twelve areas for OWE deployment (Figure 2.3.1). Although, the tendering approach was cancelled almost one year later with the Law 4030/2011 (Caralis et al. 2016).

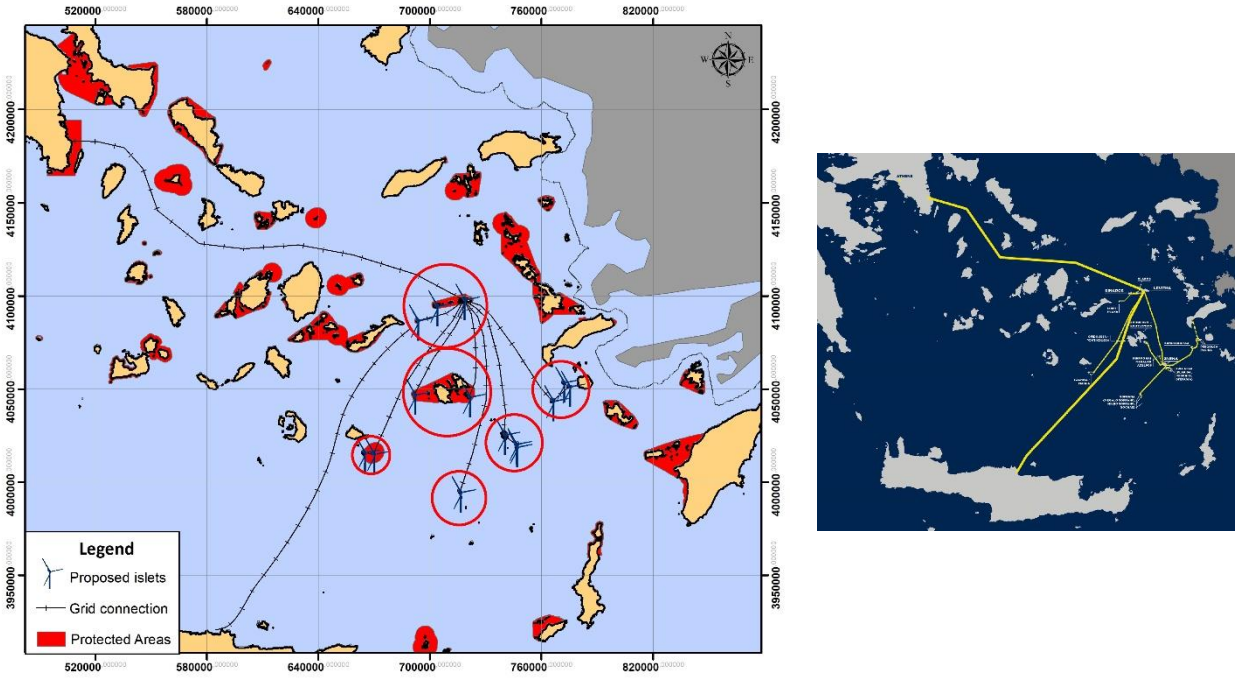


**Figure 2.3.2:** Aigaio project - Proposed OWFs for OWE deployment in 23 islets of the Aegean Sea, Sources (right image): Eunice Energy Group, (2019)

This preliminary assessment, provided by CRES, was only based on a few siting criteria (mainly technical, societal and environmental), which however were not specified, and it was unclear whether they include the criteria set by the Special Spatial Framework, of Law 2464/2008 requires (MEEC, 2008). For instance, some of the criteria included incorporated the wind speed characteristics, the exclusion of sites where the installation of an OWF is incompatible with other

marine activities and marine protected areas, without clarifying if all of the regulation measures or suggestions were considered. However, this study was not intended to be the final assessment for indicating the optimal OWFs areas subject to all relative socio-economic, technical and environmental factors (Ntoka, 2013).

Another example indicating the lack of holistic planning procedures during the design stage and the pre-feasibility assessments is the rejection of three proposed "offshore" wind energy projects (Aigaio project) in the broader area of Cyclades and Dodecanese islands (Central and South Aegean Sea). The proposed wind investment was planned to design three "offshore" wind farms in the selected study area. The total installed capacity was 582 MW consisting of 138 wind turbines in 23 remote islands and islets, approximately 245 kilometers of offshore transmission cables among with 75 kilometers of road network and 14 ports as support infrastructures (Figure 2.3.2). The final goal was to interconnect the Dodecanese islands with the onshore national grid, with Crete, and in later stages with the North Aegean islands and Cyprus. Finally, the proposed investment was rejected during the design phase mainly for environmental reasons. According to the Ministry of Environment and Energy and the Hellenic Ornithological Society (HOS), the environmental impact on the proposed areas would be of paramount importance. Almost all the proposed islands and islets are Marine Protected Areas (MPAs - NATURA) or consist of Special Protection Areas (SPAs) for marine and bird habitats (Figure 2.3.2) (Papakonstantinou et al., 2019).

Despite the above-mentioned preliminary steps, in Greece today, there is no prospect of offshore wind installations, despite of the occasional investors' interest during the last decade, mostly for offshore floating concepts. Along with the economic crisis and the uncertain support mechanisms, Ntoka (2013) highlights that Greece is lacking a central GIS that would provide information about additional parameters related to the available wind resources, the seabed characteristics, marine activities mapping and any other vital information that is necessary to be considered for offshore wind development. As a result, the planning procedures and pre-feasibility studies are becoming of an extreme cost without simplifying or accelerating the licensing procedures. Furthermore, Caralis et al. (2016) classified the uncertainties associated

with OWE deployment in the Mediterranean countries as a mixture of techno-economic and social aspects. These can be reported in two categories consisting of the:

- **Internal uncertainties** related to the projects' specifications and site-specific characteristics, affecting the cost of potential OWFs including: i) water depth and seabed conditions, ii) intense seismic activity in many offshore areas, iii) the lack of accurate wind potential evaluation strategies, iv) the limited offshore Grid in Mediterranean and finally, vi) due to environmental concerns.
- **External uncertainties** as part of the socio-economic environment of each country focusing on the: i) support schemes and the Feed-in tariffs (FiT), ii) the financing issues and finally, iii) social acceptance. Consequently, Greece faced all of the aforementioned issues mainly due to the economic crisis as also because it is considered as one of the main touristic destinations globally, thus, multiple pressures occurred on consenting authorities regarding the social and environmental impact.

Considering these uncertainty factors, several research studies have focused on the OWE deployment for the Greek marine territory. At a national level of development, Vasilakis et al., (2017) examined potential areas for hybrid offshore wind and wave energy systems and Spyridonidou et al. (2020) focused on potential marine areas for OWE deployment. Morever, Christoforaki and Tsoutsos (2017) focused on potential OWFs in Crete and Vagiona and Karanikolas (2017) for sustainable site prospecting procedures in the South Aegean Sea. The main conclusions of these studies are:

- Most of the eligible marine areas are located in the marine areas West and East of Crete, as well as in the North-central and Central Aegean.
- Suitability assessment results indicated that the most promising areas are significantly affected by the existence of increased water depths (> 500 m) or spatial constraints resulting from conflicting marine activities and the existence of protected zones.

- More detailed spatial and non-spatial data, integrated assessments, analytical cost estimation models and, most importantly, more accurate offshore wind resource measurements and assessments are critical.

## 2.4 Maritime Spatial Planning (MSP)

During the previous sections, the need for integrated, sustainable and successful spatial planning was highlighted considering OWE deployment. Analyzing the steps required for an integrated planning scheme, the first and most important step is to allocate marine areas for future OWF siting. Maritime spatial planning (MSP) can be defined as a spatio-temporal decision-making process for marine space management. Three key characteristics of MSP and the spatial planning in general are crucial as long as: i) it is future-oriented, ii) it is a public-sector activity, and iii) it is concerned with managing and protecting both of the human activities and the natural environment (Jay, 2010).

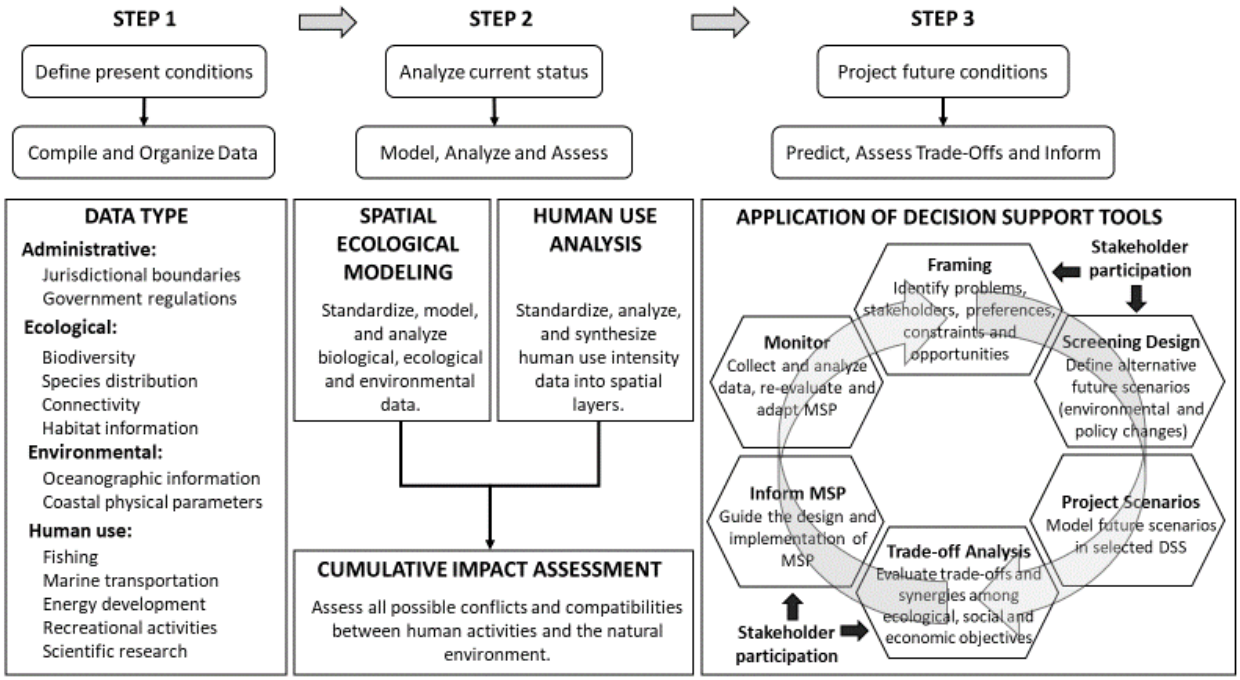


**Figure 2.4.1:** Marine Spatial Planning phases and sub-processes

(Source: Stamoulis et al., 2015)

Nowadays, most planning procedures that are based on a project or permit-specific approach, have been enhanced by more comprehensive, integrated and effective planning schemes. Contrary, with only a few exceptions (mainly in Europe and Asia), no clearly articulated spatial planning frameworks for the future use of marine areas existed since the end of the 20$^{th}$ century. This does not mean that marine activities globally are unregulated or do not allocate marine space, On the contrary, coastal and offshore areas have been regulated within individual economic sectors including shipping lanes, disposal areas, military security zones, fishing and aquaculture sites and marine protected areas (MPAs) (Table 2.4.1). Because of the intense and controversial human activities, not all uses are compatible with each other (see Figure 2.4.4) or have adverse effects, described as user–user conflicts, thus numerous studies have been conducted related to the oil and gas development and fisheries (Pascoe & Innes 2018), OWFs and aquaculture areas (Buck et al. 2017) or combined offshore energy converters (Cradden et al. 2016).

All of the aforementioned activities are grouped into three categories incorporating: i) maritime transports and military activities; ii) mining and natural resources exploitation, e.g. hydrocarbons, renewable energy, fishing etc. and, iii) uses interrelated for marine research, education and recreation (Douvere, 2008). Moreover, considering that the sea consists of three "dimensions", another categorization occurs separating marine areas in three layers including: i) the seabed, ii) the water column, and iii) the surface. To these three dimensions, the temporal perspective must be accounted, indicating: i) periodic marine activities with seasonal occurrences e.g. fishing, sailing, and recreational activities; and ii) activities performed in long-term scales e.g. for mining or military purposes (Tsilimigkas & Rempis 2017). Considering of these spatio-temporal variations, MSP should be able to provide an integrated planning framework for optimizing the use of marine areas, allocating space in a tractable way and enabling a mix of uses that are compatible with each other and the environment (Figure 2.4.1). As a result, MSP must be stated as a process that determines the spatial and temporal distribution of human activities in a manner of minimizing their environmental impact and ensuring sustainability to the greatest possible extent (Ehler et al., 2009).

From a technical point of view, an integrated MSP scheme consists of: i) multiple objectives, ii) conflicts and synergies of human activities, iii) the risk of cumulative effects to the environment, iv) spatial zoning and planning, and v) multiple scenarios examination (Figure 2.4.1). For this reason, practical tools must be established which ultimately assess these processes. As a result, GIS, Spatial Decision Support Systems (SDSS), multicriteria analysis and multi-objective optimization algorithms may be characterized as robust tools to facilitate 'what if' questions/scenarios from which planning options can be arise (Stelzenmuller et al. 2013).

**Table 2.4.1:** Potential synergies and conflicts among marine human activities and compatibility with other sea uses (green: compatible red: incompatible, blue: probably compatible) (Sources: Gee et al., 2006; Ehler & Doulvere, 2009)

| Compatibility with other sea uses | Offshore wind farms |
|---|---|
| Offshore wind farms | |
| MPAs | |
| Fisheries | |
| The sea and public good | |
| Cables | |
| Tourism | |
| Shipping routes | |
| Harbours and Ports | |
| Agriculuture run-off | |
| Sand and ravel extraction | |
| Oil and Gas exploration | |
| Dumping and dredging material | |
| Mariculture | |
| Coastal services centers | |
| Nature conservation | |
| Coastal protection | |
| Military use | |

| Offshore wind farms compatibility with other sea uses | | | |
|---|---|---|---|
| Commercial Fishing: Nets | | Dredged material disposal | |
| Commercial Fishing: Pots/traps | | Offshore airports | |
| Commercial Fishing: Spears/harpoons | | Offshore industrial production facilities | |
| Commercial Fishing: Trawls/dredges | | Offshore liquified natural gas terminals | |
| Commercial Fishing: Seine nets | | Offshore oil & gas exploration | |

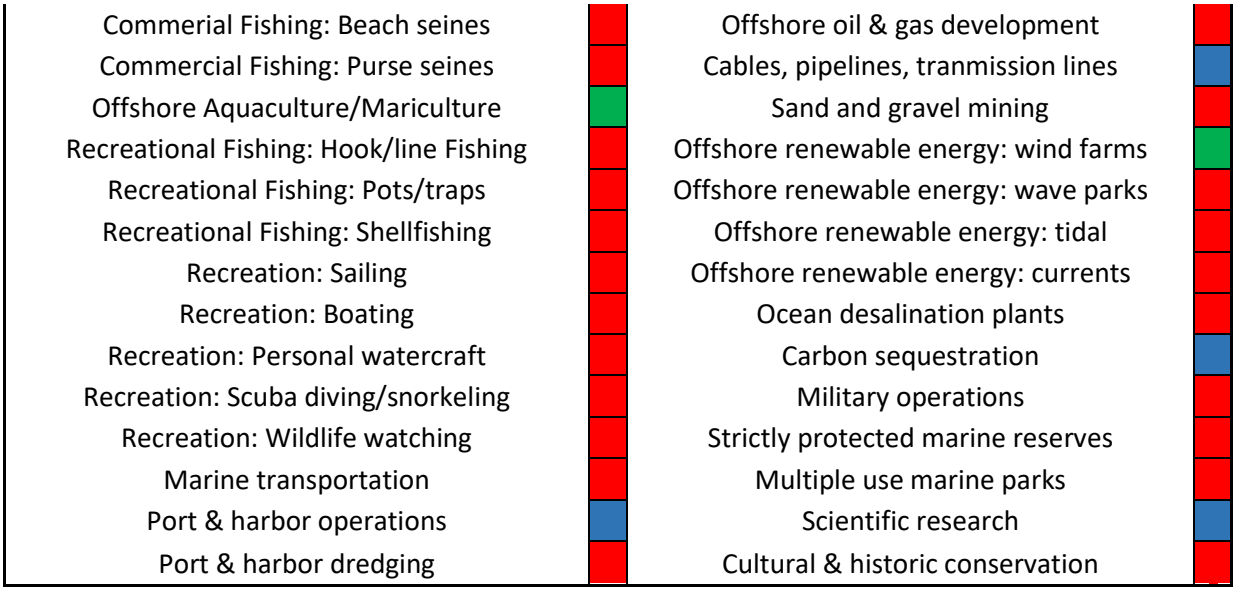


To address these issues, multiple spatial information is required on the current and future impact of human threats occur in marine environments. Many attempts have been made to address cumulative impacts by establishing the CHI index (Cumulative Human Impact) (Halpern et al., 2009; Korpinen et al., 2012; Batista et al., 2014; Henriques et al., 2014; Judd et al., 2015). Figure.2.4.2 demonstrates some efforts to monitor, map and assess current and future state and impact of the marine areas in the Atlantic Ocean among with the Baltic, North and the Mediterranean Sea accordingly. In addition, Belgium, Germany and the Netherlands have advanced the furthest in MSP, having already produced marine plans (Jay, 2010). Based on these integrated frameworks, many other countries worldwide evolved in MSP framework, including North America (White et al., 2012) and China (Li, 2006) as also many European countries. In the particular case of the European Union members, the EU Marine Strategy Framework Directive (MSFD 2008) indicated that strategies must be developed by July 2014 in order to achieve an optimal environmental status by the end of 2020.

For this reason, during the last decade integrated sectoral assessments and EU or nationally funded projects have been conducted. Indicative examples include MESMA for the monitoring and evaluation of marine areas (www.mesma.org), the “Towards COast to Coast NETworks of Marine Protected Areas (CoCoNet) (www.coconet-fp7.eu/), the MASPNOSE (www.surfgroepen.nl/sites/CMP/maspnose) and WindSPEED project (Jongbloed et al. 2014) for

MSP in the North Sea, BALANCE (www.balance-eu.org) and BaltSeaPlan (www.baltseaplan.eu) as a marine management tool for the Baltic Sea, PlanCoast (www.plancoast.eu) for Integrated Coastal Zone Management, KnowSeas (www.knowseas.com) for the European Seas sustainable management (Meyer et al. 2013) and finally, Marisca (http://www.marisca.eu) and Thal-Xor (www.mspcygr.info/thal-xor/) characterized as the first attempts for MSP implementations for Greece and the Aegean Sea.

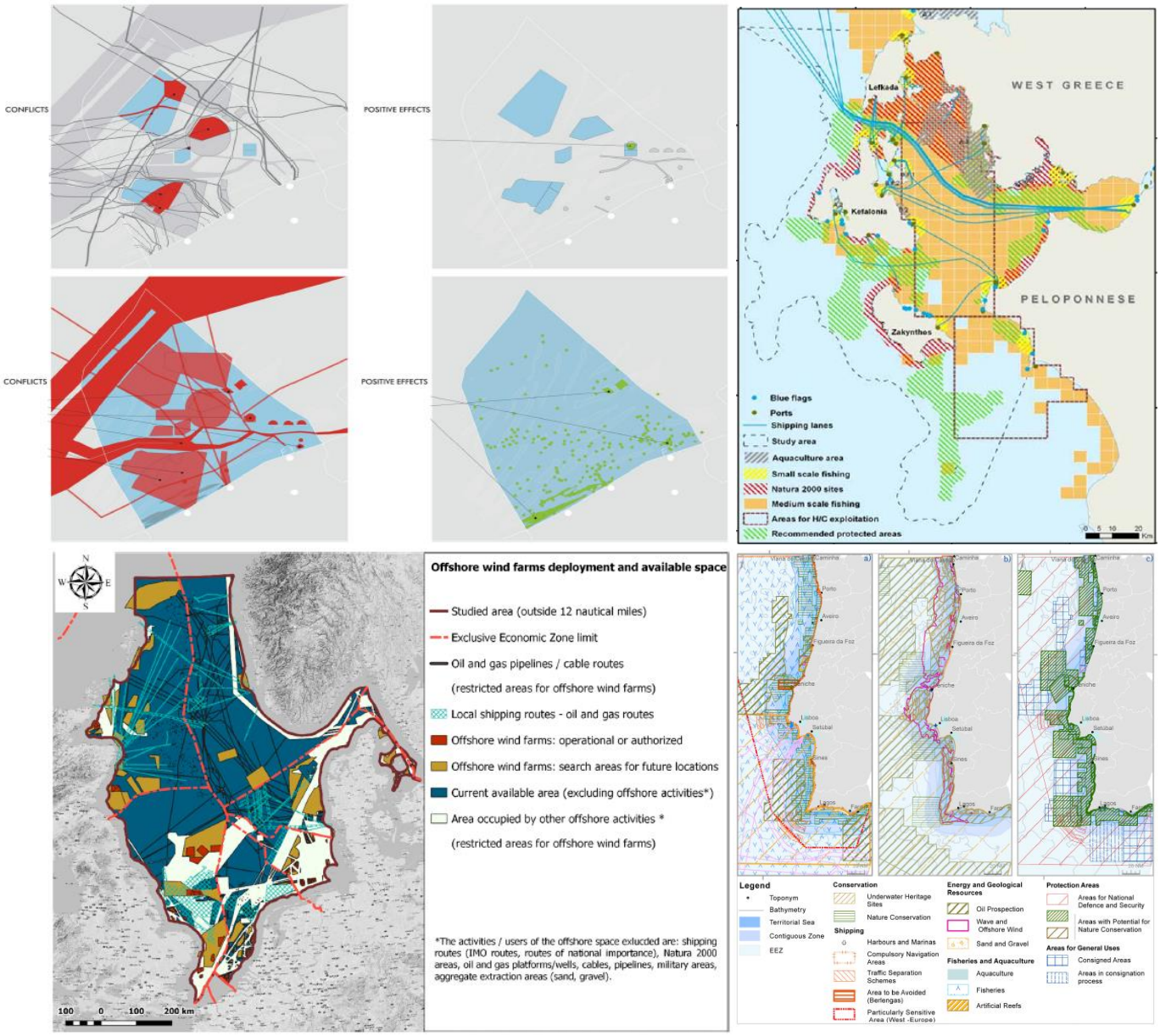

**Figure 2.4.2:** Marine Spatial Planning zoning and mapping procedures for: a) Belgium (Source: Doulvere, 2008) b) Greece (Source: Krassanakis et al., 2015), c) Baltic Sea (Source: Gusatu et al., 2020) and d) Portugal (Source: Fernandez et al., 2017)

As a concluding remark, despite of the fact that most national marine areas are still unexplored, the spatial limitations for OWE deployment due to lack of free marine space or incompatibility issues, highlight the need of integrated MSP plans. The temporal perspectives of technological development, as well as the spatial dimension of MSP, combined in the economics of OWE and other marine activities, mean that methods are required for the sustainable management of possible offshore areas (Moller, 2011). Already existing approaches from the north European countries as also the outcomes from many research projects may play a key role in terms of both the appropriate steps to be followed and for data availability purposes.

### 2.4.1 MSP in Greece

Focusing on the Greek experience on the MSP processes, despite the fact that discussions began in the mid 2000's, no specific plans have taken place yet. A few years later, MSP was incorporated in the 2011 spatial planning legislation through the National strategy for protection and management of the marine environment. Thus, Law 4030/2011 (OGG, 2011) delineated the new emerging principles focusing on: i) the need for integrated management of coastal zones and offshore areas, ii) the need for coordination and harmonization of previous policies and, iii) the development of synergies in order to avoid conflicting issues among marine activities (Tsilimigkas and Rempis 2017).

In addition, in 2014 with the adoption of the EU Directive 2014/89 for the MSP, a series of obligations and measures proposed (Papageorgiou, 2016). Based on this directive, Law 4269/2014 (OGG, 2014) provided the key directions for spatial management procedures. As a result, the General Framework of Spatial Planning and Sustainable Development (GFSPSD) defined the national level planning, but most importantly, the Special Frameworks on Spatial Planning and Sustainable Development SFSPSD set the guidelines for RES penetration (OGG, 2008). With the latter action, the principles for site prospecting of RES installations were set,

focusing on the offshore areas, inhabited islands and uninhabited islets management. As a result, areas of sufficient wind resources which are not part of regulatory prohibitions (i.e. shipping lines, military areas, protected areas etc.) were characterized available for further investigation. Specifically, as minimum requirements, the exclusion areas incorporate: i) the installation of OWFs less than 1500 meters from the coast, ii) the installation of offshore wind projects in enclosed bays with opening width less than 1500 meters, iii) the depth of the foundation or anchoring of the WTs must be determined by the capabilities of current technology, iv) a sufficient interconnection and transportation of electricity to the onshore system must be ensured with finally, v) the maximum distance of onshore cables to the substation do not exceeds 20 kilometers (Tsilimigkas and Rempis 2017).

Reviewing the steps followed during the last decade, it is increasingly being argued that detailed guidelines and legislative adjustments to promote offshore wind projects are lacking. However, the EU MSP Directive, might be critical to overcome deficiencies and drawbacks of the past, towards the adoption of new priorities and integrated planning approaches, leading to the optimal integration of wind energy projects into the marine environment at a national level.

## 2.5 Offshore Wind Farms Cost Evaluation

During the previous sections, the current and future trends of OWE, the benefits and the drawbacks of OWFs and the planning procedures for site prospecting were highlighted. However, despite of the beneficial characteristics of offshore wind technologies, the capital and installation cost as also the operation and maintenance procedures are characterized far more capital intensive than onshore wind power and most conventional RES technologies (Levitt et al. 2011). Analyzing the cost drivers of offshore wind projects, the following categories occur, consisting of: (Section 2.3) i) the pre-development and consenting (P&C) phase, ii) the production and acquisition (P&A), iii) the installation and commissioning (I&C) and finally, iv) operation and maintenance (O&M), and v) decommissioning and disposal (D&D or DECEX) stages (Figure.2.5.1). The P&C, P&A, I&C and D&D are always referred as the capital expenditures (CAPEX) and the

O&M phase incorporates all operational expenditures (OPEX) including all annual maintenance costs (Figure.2.5.1).

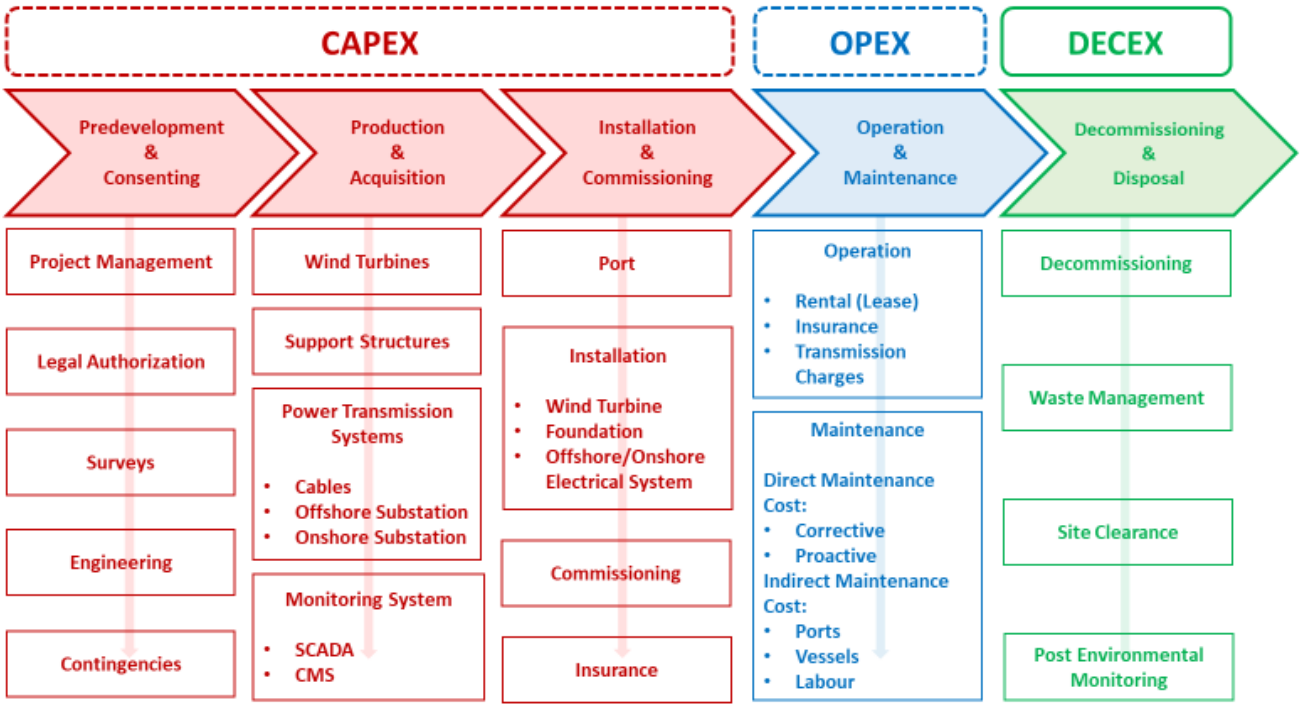


**Figure 2.5.1:** Cost breakdown structure (CB) for offshore wind farms (Sources: Myhr et al., 2014; Shaffie et al., 2016; Ioannou et al., 2018; Bosch et al., 2019)

Both CAPEX and O&M costs are varying in accordance with each OWF's site characteristics. As a result, the bathymetry and the met-ocean conditions indicate the type of foundations to be selected, the wind speed characteristics define the WT's rated power, the total installed capacity, the capacity factor, reliability, loads and availability of an OWF. Furthermore, the distance from the onshore network and the nearest ports has a direct impact to the electrical infrastructure and the accessibility of the transportation means respectively (Shaffie et al., 2016; Ioannou et al., 2018).

Cost breakdown structure illustrated in Figure 2.5.1 indicates all of the sub-processes applied during the life cycle of an offshore wind project. Therefore, all these procedures must be evaluated and quantified in terms of the Life-Cycle Cost (LCC) analysis. However, either the cost and the profitability assessment of a wind project is valueless if it fails to incorporate accurate economic data. Unfortunately, the number of sources for accurate economic data from

companies or already operational OWFs are very sparse leading to cumulative uncertainties in the profitability assessment. Among with the data availability issues, other factors influencing the cost evaluation procedures consist of the variable competitiveness in the supply chain, the volatility in the commodities prices and the prices given at different time scales with variable currencies and inflation rates (Gonzalez-Rodriguez, 2017).

Considering of these uncertainties, during the last two decades, OWE cost assessments have been carried out by several industries, governments and academic researchers wordwide. Most of these studies have focused on:

- Technology comparative studies (Kaldelis and Kapsali 2013; Myhr et al. 2014; Rodriguez et al. 2015; Soares-Ramos et al. 2020).
- Financial assessment methodologies and cost reduction scenarios (Levitt et al. 2011; Prässler and Schaechtele 2012; Weaver 2012; Schwanitz and Wierling 2016; Voormolen et al. 2016; Shaffie et al., 2016; Ioannou et al., 2018).
- Country-specific studies based on geospatial analytical cost expressions (Moller 2011; Hong and Moller 2011; Kim et al. 2013; Cavazzi and Dutton 2016; Nagababu et al. 2017) which are typically constrained to a specific site or type of site.
- Global-scale cost assessments by international organizations including the International Energy Agency (IEA), International Renewable Energy Agency (IRENA) and the European Wind Energy Association (EWEA).

The usefulness of these assessments and models mainly lies on: i) the need of accurate cost records during the last 30 years and ii) the integration of methodological frameworks in order to identify, analyze, evaluate and reduce the overall cost of key operations in the offshore wind industry. Consequently, the aforementioned outcomes may be used to enhance and assist the knowledge of both managers and stakeholders in making appropriate investment decisions (Shaffie et al., 2016). According to Levitt et al., (2011), the insights and benefits extracted from these studies are meaningful for addressing important decision-making questions concerning the measures, the policies and the components that are likely to have the greatest effect in reducing future costs.

The results of these assessments, considering the capital and O&M expenditures are summarized in Table 2.5.1 where the mean cost per MW of installed capacity and the mean O&M expenses in euro per MWh (megawatt hour) of the produced energy among different OWFs are demonstrated for the period 2001 – 2017.

**Table 2.5.1:** Cost breakdown (Capital and O&M expenditures) for offshore wind farms

| Capital expenditures cost | Year | CAPEX (million € 2020/MW) | Operation and Maintenance cost | Year | O&M (€ 2020/MWh) |
|---|---|---|---|---|---|
| Gonzalez-Rodriguez, (2017) | 2001 | 1.26 | Gonzalez-Rodriguez. (2017) | 2005 | 10.5 |
| | 2003 | 1.22 | | 2007 | 22.05 |
| | 2003 | 1.71 - 1.82 | | 2009 | 12.6 - 18.9 |
| | 2004 | 1.4 - 1.43 | | | |
| | 2005 | 1.51-2.33 | Levit et al.. (2011) | 2009 | 13.02 - 38.28 |
| Vormoolen et al., (2016) | 2000-2005 | 2.23 | | 2010 | 8.42 – 50.53 |
| | 2007 | 1.98 - 2.12 | Gonzalez-Rodriguez. (2017) | 2010 | 11.55 - 32.55 |
| | 2008 | 3.36 | Vormoolen et al.. (2016) | | |
| Ernst and Young (2009) | 2009 | 2.66-4.52 | Kolios & Brennan. (2018) | 2014 | 18.8 - 26.86 |
| | 2010 | 3.36-3.83 | | 2014 | 25.52 - 75.23 |
| Prassler and Schaechtele (2012) | 2010 | 3.44-4.02 | Noonan et al.. (2018) | 2017 | 28.91 |
| Vormoolen et al., (2016) | 2005-2010 | 2.98 | | | |
| | 2012 | 4.34 | | | |
| | 2013 | 3.26-5.06 | | | |
| | 2014 | 4.21-4.94 | | | |
| | 2015 | 3.74-4.74 | | | |
| Vormoolen et al., (2016) | 2010-2015 | 4.36 | | | |
| Noonan et al., (2018) | 2016 | 3.98 | | | |
| | 2017 | 3.63 | | | |

All cost values are expressed in 2020 euros($€_{2020}$) and the data have been obtained from cost review assessments, international organizations as also from companies reports. It is noticed that the reference prices have been normalized into the same reference monetary value (euros2020) for comparison purposes. The reviewed values have been converted from US dollars

or British pounds into euros, based on the currency exchange[5] values and increased according to the accumulated inflation[6].

CAPEX cost values indicate an obvious increase, mainly during the last decade. This tendency is explained due to the increase in the size of the OWF projects linked with the higher distances from harbor facilities, depths and WTs size and capacity. Furthermore, capital expenses seem to be stable or even decrease from 2013 and now on due to the increase of WTs' capacity leading to a smaller number of wind generators, support structures and inter-array cables inside an OWF. In contrast, operational expenditures seem to remain stable between 15–30 Euros/MWh (with an increase between 2008 - 2010). Although, long-term O&M costs are relatively uncertain compared to the CAPEX, mainly due to the lack of published data, the unpredictable repair activities and most importantly the uncertain failures increase as the OWF's equipment ages (Levit et al., 2011; Myhr et al., 2014; Shaffie et al., 2016).

The following sections analyze and discuss the most important components of CAPEX and O&M compiled from multiple sources. The extracted data are presented based on the cost component breakdown illustrated in Figure 2.5.2, including: i) design and project management cost, ii) WTs, iii) foundations and electrical infrastructure expanses, iv) installation cost and finally, v) operation and maintenance and decommissioning costs. In the last section some key cost and cash flow indicators are analyzed and discussed.

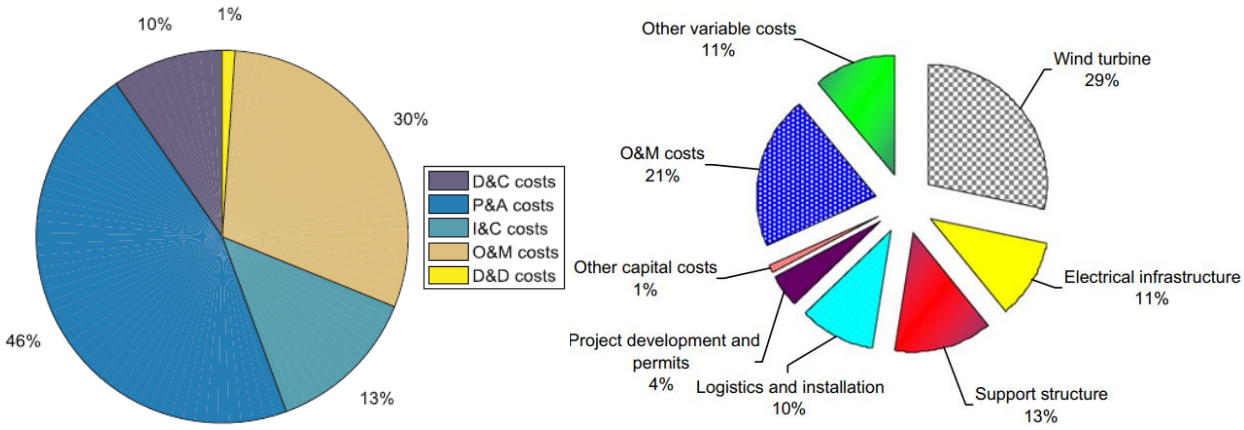


**Figure 2.5.2:** Cost breakdown structure (CB) for offshore wind farms (Sources: Kaldelis & Kapsali, 2013; Ioannou et al., 2018)

[5] https://www.statista.com/ have been used for the exchange rates calculations

[6] https://www.inflationtool.com/ have been used for the accumulated inflation extraction and approximation

### 2.5.1 Design and Project Management

Design and project management consists of a variety of tasks including the met-ocean surveys and monitoring campaigns, public relations and marketing, environmental-impact assessments, front-end engineering design (FEED), and the construction management. Detailed cost values extracted from Dicorato et al., (2011), Myhr et al., (2014), Shaffie et al., (2016), Gonzalez-Rodriguez, (2017), Ioannou et al., (2018) and Noonan et al., (2018) and Table 2.5.1.1 demonstrates the compiled values evolution for this stage of development during the period 2005 - 2018.

**Table 2.5.1.1:** Cost of Design and Development stage for the period 2005 – 2018 in million euros(m€) per MW

| Design & Project | Year | million €/MW (2020) |
|---|---|---|
| Gonzalez-Rodriguez, (2017) | 2005 | 0.093 |
| | 2006 | 0.054 |
| | 2007 | 0.092 |
| | 2009 | 0.114 |
| | 2010 | 0.097 - 0.384 |
| Dicorato et al., (2011) | 2011 | 0.053 |
| Myhr et al., (2014) | 2014 | 0.221 |
| Shaffie et al., (2016) | 2016 | 0.311 |
| Noonan et al., (2018) | 2016 | 0.519 |
| Noonan et al., (2018) | 2017 | 0.518 |
| Ioannou et al., (2018) | 2018 | 0.422 |

In Table 2.5.1.1 a relative increase is noticed, during the last decade, reaching values of 0.5 million euros/MW from approximately 0.1 during the period 2005-2011. These cost values are explained due to the complexity of the modern offshore wind projects, the increased depths (up to 60 meters), the remote distances from the closest onshore transmission networks and mostly due to the increased marine areas acquired for OWE deployment and as a result, costlier rental fees, engineering, environmental and seabed assessments are needed.

### 2.5.2 Wind turbines and substructures characteristics and cost

The manufacturing of a fully equipped WT is one of the costliest components for an OWF. Cost is usually proportional to the turbine's capacity and size (Ioannou et al., 2018). These WTs characteristics lead to higher capital costs due to the increased demand for raw materials (steel, copper etc.) and Table 2.5.1.2 demonstrates the evolution of the WT cost per MW of installed capacity from 2003-2017. Current statistics indicate an increase during the last decade of more than one million eurosper MW caused by the WTs characteristics (increased rotor diameter and hub height). In Figure 2.5.2.1 WTs' size of the current operational OWFs is demonstrated. Clear evidence that the current trend in offshore wind industry is the increase of the WTs size as long as most of the operational or planned OWFs are considered with turbine of a hub height above 100 meters with a rotor diameter of approximately 100 – 170 meters. According to Gonzalez-Rodriguez, (2017), the overall WT cost consists of i) the acquisition cost (85% of the total cost), ii) shipping and assembling (5%); and finally, iii) the electrical installation (10%).

**Table 2.5.1.2:** Cost of offshore wind turbines (WTs) for the period 2003 – 2017 in million €/MW

| WT prices | Year | million €/MW (2020) |
|---|---|---|
| Gonzalez-Rodriguez (2017) | 2003 | 0.471 - 0.651 |
| | 2004 | 1.226 |
| | 2005 | 0.341 - 0.624 |
| | 2006 | 0.357 |
| | 2007 | 0.356 - 0.496 |
| | 2009 | 0.403 - 0.970 |
| Vormoolen et al., (2016) | 2009 | 0.943 |
| | 2010 | 0.873 |
| | 2011 | 2.531 |
| | 2012 | 1.581 - 2.109 |
| | 2014 | 1.898 - 2.636 |
| Noonan et al., (2018) | 2016 | 1.743 |
| | 2017 | 1.541 |

According to Table 2.5.1.2 wind turbines' cost values until 2010 ranged between 0.35 - 0.9 million eurosper MW of installed capacity. By 2011 the cost of a single WT increased up to 2.5 million Euros/MW, mainly due to the size and the capacity increase as long as during the period 2015 - 2018 a decrease occurred, leading to a cost value of 1.5 million Euros/MW. It is also noticed

that these costs include only the production and acquisition cost and not the installation expanses. Indicatively, most recent studies highlight that the total cost of a 3.5, 8 and 10 MW wind generator has not a linear increase and is approximately 3, 12 and 15 million eurosrespectively, mainly due to the increase of the substructure size (tower and as a result the hub height) (Gonzalez-Rodriguez, 2017).

| Turbine diameter (m) | 30 - 65 | 65 - 100 | 100 - 135 | 135 - 170 |
|---|---|---|---|---|
| Wind farms | 4 | 30 | 63 | 15 |
| Turbines | 45 | 1094 | 3142 | 714 |

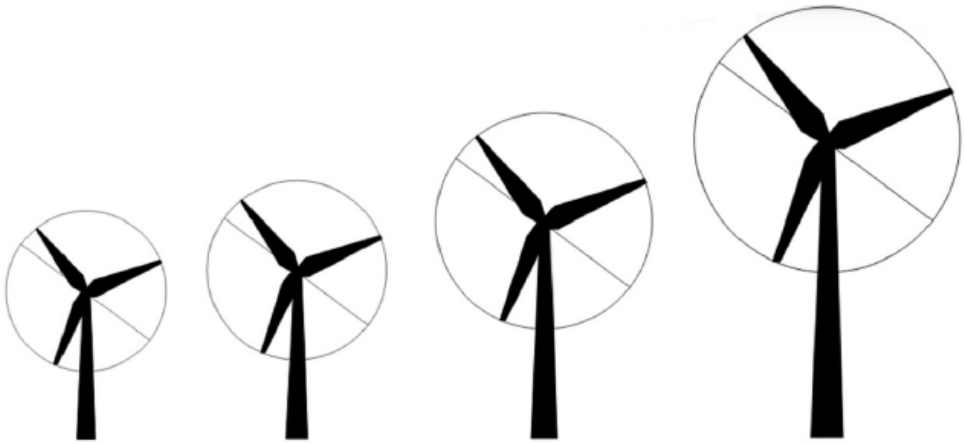

| Turbine height (m) | 60 - 95 | 95 - 130 | 130 - 165 | 165 - 200 |
|---|---|---|---|---|
| Wind farms | 5 | 33 | 56 | 18 |
| Turbines | 96 | 1154 | 2878 | 867 |

**Figure 2.5.2.1:** Wind Turbines size and rotor diameter of current operational OWFs (Source: Myhr et al., 2014; Shaffie et al., 2016; Ioannou et al., 2018; Bosch et al., 2019)

### 2.5.3 Different foundation technologies cost

The foundation cost is proportional to the sea depth and the selected foundation type is used (i.e. gravity, monopile, jacket or floating support structures). In turn, the type of foundation depends on the seabed characteristics, and to a minor extent, on the WT size and the met-ocean conditions (Dicorato et al., 2011; Gonzalez-Rodriguez, 2017).

Monopile support structure is the most commonly used foundation technology (75% of the operational OWFs), however, there is a tendency towards the jacket or even floating structures, as long as the water depth increases beyond 45-50 meters. In addition, the gravity foundations were mainly used during the first years of OWE deployment using its own weight to stabilize the support structure and is more suitable for shallow waters up to 20m. The tripod (or tripile) foundations consist of three piles inserted to the sea bottom connected to the tower through a large steel central shaft with a maximum depth capacity of 40 - 50 m. Jacket structures are composed of three or four legs for depths reaching up to 80 m., although, the optimal depth (considering the increased cost) is no more than 45 m (Díaz & Soarez, 2020; Soarez-Ramos et al., 2020). All of the proposed foundation technologies are illustrated in Figure 2.5.3.1. Considering the floating foundation technologies multiple conceptual prototypes have been developed. The Tension-Leg (TL) and Tension-Leg-Buoy (TLB) platforms, the WindFloat system and the Spar-Buoy buoyancy system are some of the proposed floating concepts already exist (Myhr et al., 2014). All these conceptual models are demonstrated in Figure 2.5.3.1 considering different stabilization, mooring and anchoring technologies.

**Table 2.5.3.1:** Cost of different foundation types for the period 2003 – 2018 in million eurosm€/MW

| Foundation cost | Foundation type | Year | million €/MW (2020) |
|---|---|---|---|
| Gonzalez-Rodriguez (2017) | Gravity based | 2003 | 0.47 |
| | Floating | 2004 | 1.23 |
| | Gravity based | 2005 | 0.34 - 0.62 |
| | Gravity based | 2006 | 0.36 |
| | Gravity based | 2007 | 0.36 |
| | Monopile | 2007 | 0.4 – 0.5 |
| | Mean value (Fixed sup.str.) | 2009 | 0.40 - 0.94 |
| Kausche et al., (2018) | Spar-type (Floating) | 2009 | 22.1 |
| | Monopile | 2010 | 0.87 |
| Kausche et al., (2018) | Semi-submersible (Floating) | 2013 | 5.95 |
| | Spar-type (Floating) | 2013 | 16.15 |
| Myhr et al., (2014) | Spar-type - TLB B (Floating) | 2014 | 0.99 |
| | Spar-type - TLB X3 (Floating) | 2014 | 1.27 |
| | Spar-type (Floating) | 2014 | 3.98 |
| | Semi-submersible (Floating) | 2014 | 7.98 |
| | Spar-type - SWAY (Floating) | 2014 | 2.92 |
| | Spar-type - TLWT (Floating) | 2014 | 1.02 |

| | | | |
|---|---|---|---|
| Kausche et al., (2018) | Semi-submersible (Floating) | 2016 | 11.9 |
| Noonan et al., (2018) | Mean value (Fixed sup.str.) | 2016 | 0.90 |
| | Mean value (Fixed sup.str.) | 2017 | 0.79 |
| Kausche et al., (2018) | Semi-submersible (Floating) | 2017 | 22.1 - 24.65 |
| | Spar-type (Floating) | 2018 | 2.55 |
| | Monopile | 2018 | 0.74 |

Analyzing the cost of a support structure, two major components must be accounted, one for material and manufacturing cost and another for the transport and installation procedures. Previous studies showed that the former cost does not vary much from one foundation type to another, for the fixed foundation technologies, but an increase by 2 % for each meter increase in water depth is observed and an increase of 80 % for each unit increase considering the load factor (Shaffie et al., 2016).

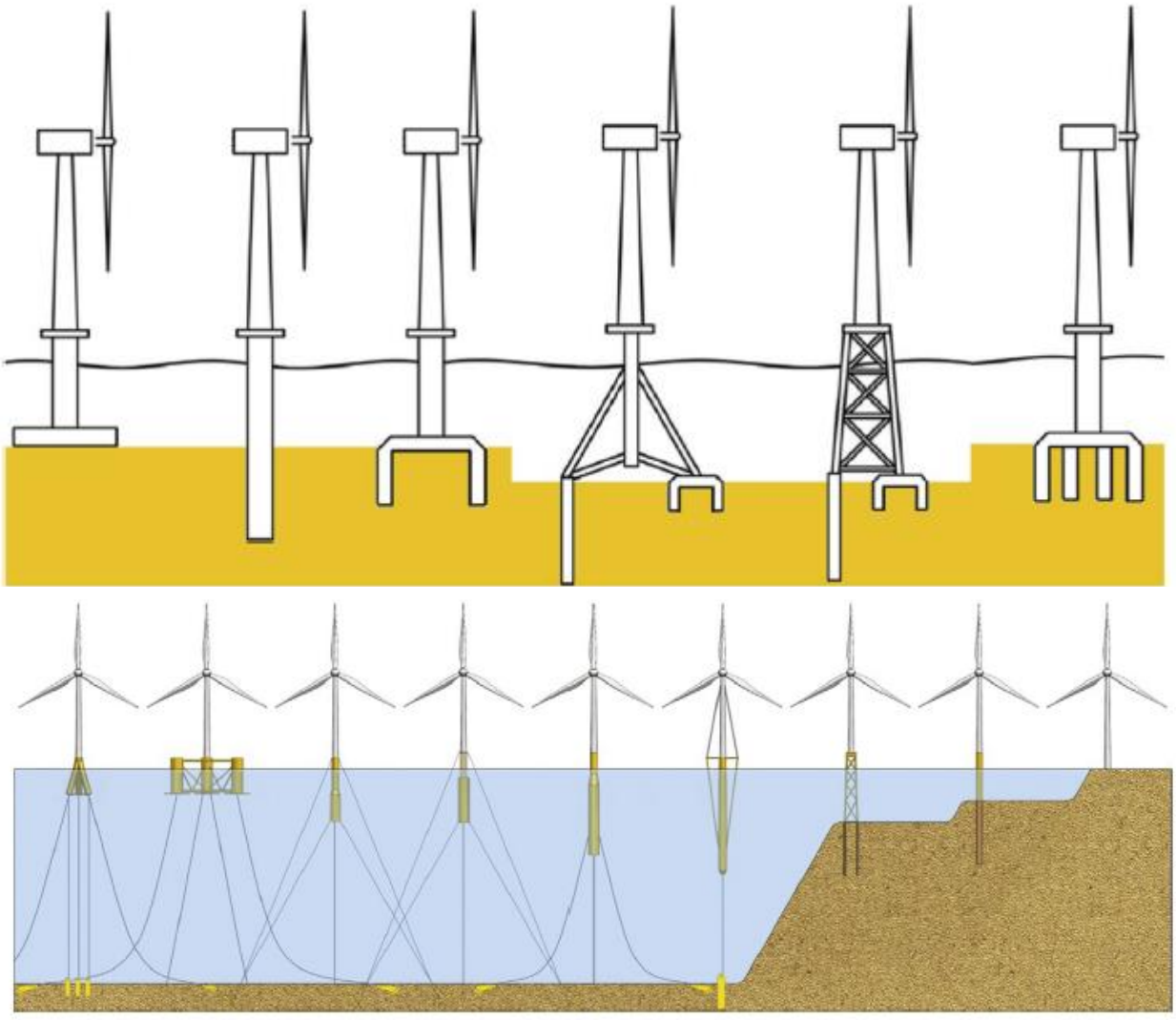

**Figure 2.5.3.1:** Foundation types: **Fixed-bottom support structures** (Top) from left to right; Gravity base, Monopile, Suction bucket, Tripod, Jacket, HRPC, **Floating structures** (Bottom) from left to right; TLWT, WindFloat, TLB B, TLB X3, Hywind II, SWAY, Jacket, Monopile and the onshore reference (Sources: Myhr et al., 2014; Díaz et al., 2020)

On the contrary, cost differences among floating foundations may considerably vary and is relevant to the floater, mooring and anchoring type selection. Table 2.5.3.1 summarizes foundation cost per foundation type expressed in million eurosper MW of installed capacity for the period 2003 – 2018. Fixed-bottom support structures present a small increase from 0.5 to 0.8 million eurosduring the last 15 years and small differentiations among the different foundation technologies are highlighted. For gravity-based foundation technologies the cost is 0.3 million Euros/MW and for monopiles and jacket technologies is 0.4 – 0.8 million Euros/MW approximately. A non-linear cost increase is observed for depths > 30 meters considering both monopile and jacket support structures. On the other hand, floating technologies seem to preserve controversial cost approximations related to each type of technology. Cost values ranging between 1 – 24 million Euros/MW with some of the spar-type floating technologies reaching cost values below 3 million Euros/MW. Noteworthy is that for the floating concepts, technological improvements and materials cost reductions have led to more competitive cost values, compared to the fixed-bottom foundations.

## 2.5.4 Electrical infrastructure standards and cost

The transmission system of an OWF consists of: i) the export cable connecting the offshore substation to the shore through offshore and onshore cables, ii) the collection system (inter-array cables) of the generated power and iii) the integration of the power through offshore and onshore substations among with the costs for transformers, converters (if needed), switch gears, compensation devices and other services. (Dicorato et al., 2011; Gonzalez-Rodriguez, 2017; Ioannou et al. 2018).

The entire power transmission system includes the collection of the power generated by the WTs, transferred to the substation and through the offshore export cables, the electricity is transmitted to the offshore substation, the onshore substation and the onshore transmission network accordingly (Figure.2.5.4.1). In terms of the power transmission technologies, two main alternatives exist, High Voltage Alternative Current (HVAC) and High Voltage Direct Current (HVDC) lines. The preference for HVAC transmission against HVDC for OWFs located up to 50 kilometers away from the shore is usual, mostly in order to avoid additional infrastructures. For this reason, in HVDC systems, power converters are additionally used to adapt and control the DC voltage both offshore and onshore (through the substations) as it is demonstrated in Figure.2.5.4.1. Moreover, medium voltage alternative current (MVAC) technologies are used for shorter distances from the shore and lower power ratings (e.g. 100 MW and near to shore up to 10-20 km). Based on the distance limitations, HVDC technology is considered as a technically viable and economical solution. However, costs in HVDC lines are typically higher than in HVAC or MVAC (Soares-Ramos et al., 2020).

**Table 2.5.4.1**: HVAC and HVDC technical characteristics for OWF concepts (Source: FOWIND, 2017)

| Transmission solution | HVAC | LCC based HVDC | VSC based HVDC |
|---|---|---|---|
| **Maximum available capacity** | 200 MW at 150 kV<br>350 MW at 245 kV | up to 1200 MW | 500 MW |
| **Voltage level** | Up to 245 kV | Up to ±500 kV | Up to ±150 kV |
| **Does transmission capacity depend on distance?** | Yes | No | No |
| **Total system losses** | Depends on distance | 2-3% | 4-6% |

In the offshore wind industry, 70% of the transmission systems in OWFs above 150 MW corresponds to HVAC lines. However, an increased share of HVDC transmission technologies occurred during the last decade (Soares-Ramos et al., 2020). Considering these technical aspects and offshore wind projects' trends and projections until 2030, distances from the shore, WTs rated power and the total installed capacity increase, the HVDC technology may gain an increase share of the technologies used in the offshore transmission networks. Table 2.5.4.1 and Figure.2.5.4.1 demonstrate some technical characteristics and layouts used for these technologies.

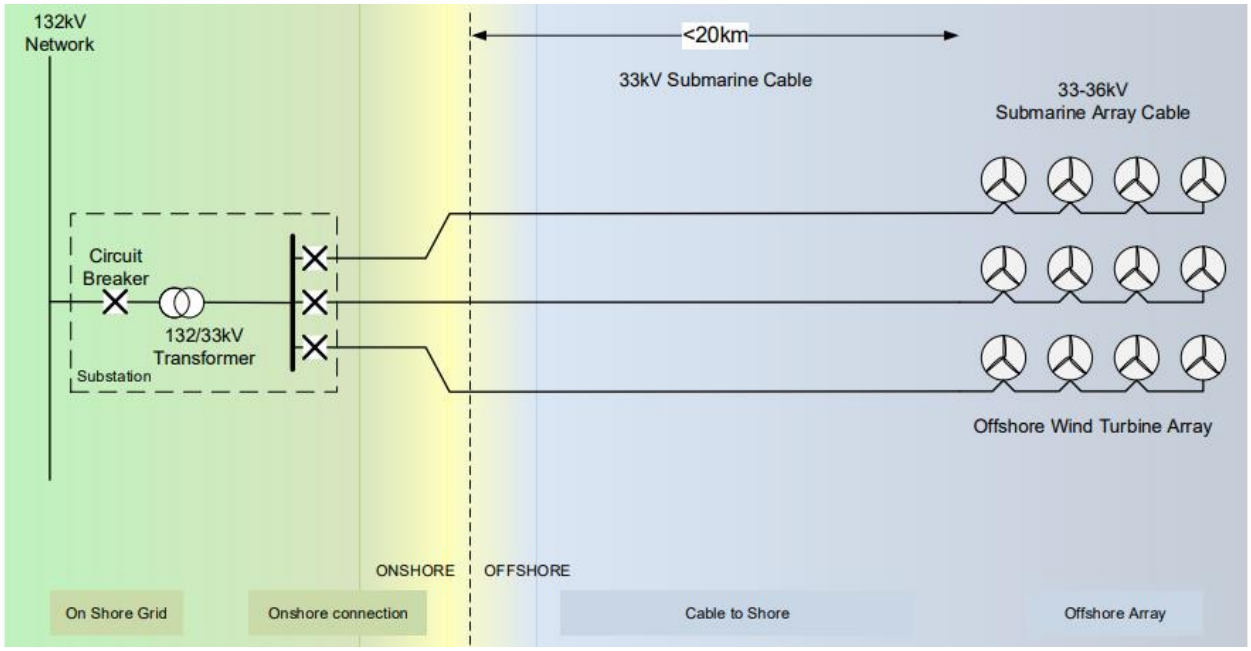
132kV
Network
<20km
33kV Submarine Cable
33-36kV
Submarine Array Cable
Circuit
Breaker
132/33kV
Transformer
Substation
Offshore Wind Turbine Array
ONSHORE
OFFSHORE
On Shore Grid
Onshore connection
Cable to Shore
Offshore Array

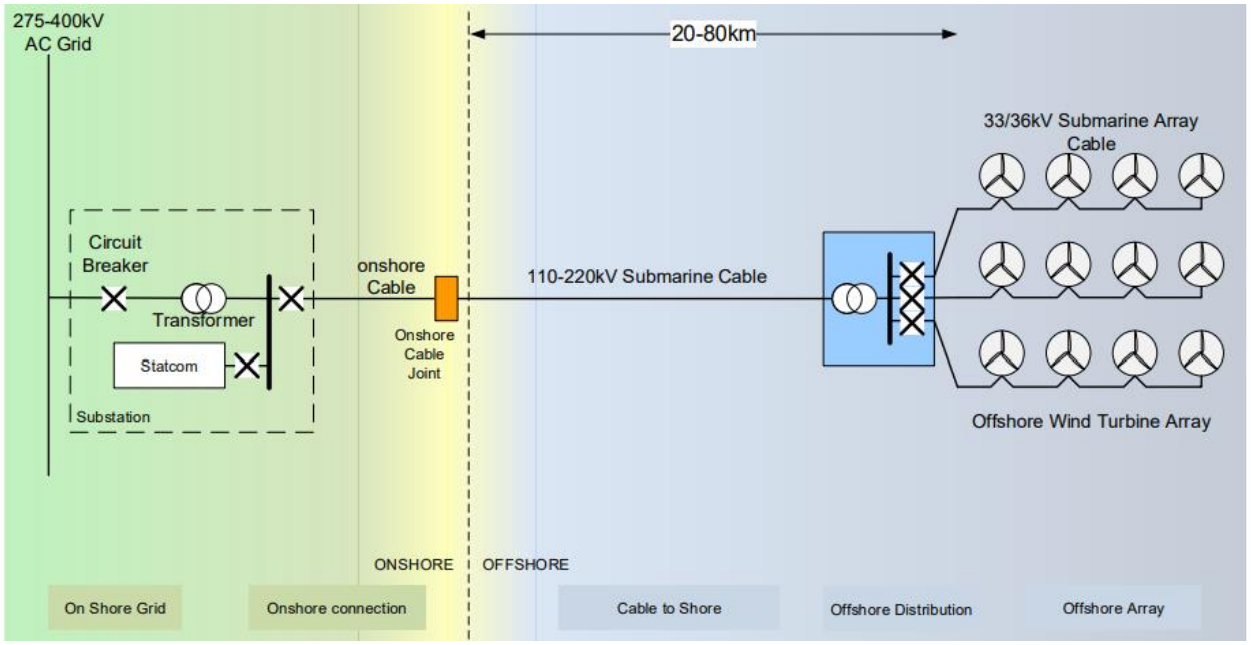
275-400kV
AC Grid
20-80km
33/36kV Submarine Array
Cable
Circuit
Breaker
Transformer
Statcom
Substation
onshore
Cable
Onshore
Cable
Joint
110-220kV Submarine Cable
Offshore Wind Turbine Array
ONSHORE
OFFSHORE
On Shore Grid
Onshore connection
Cable to Shore
Offshore Distribution
Offshore Array

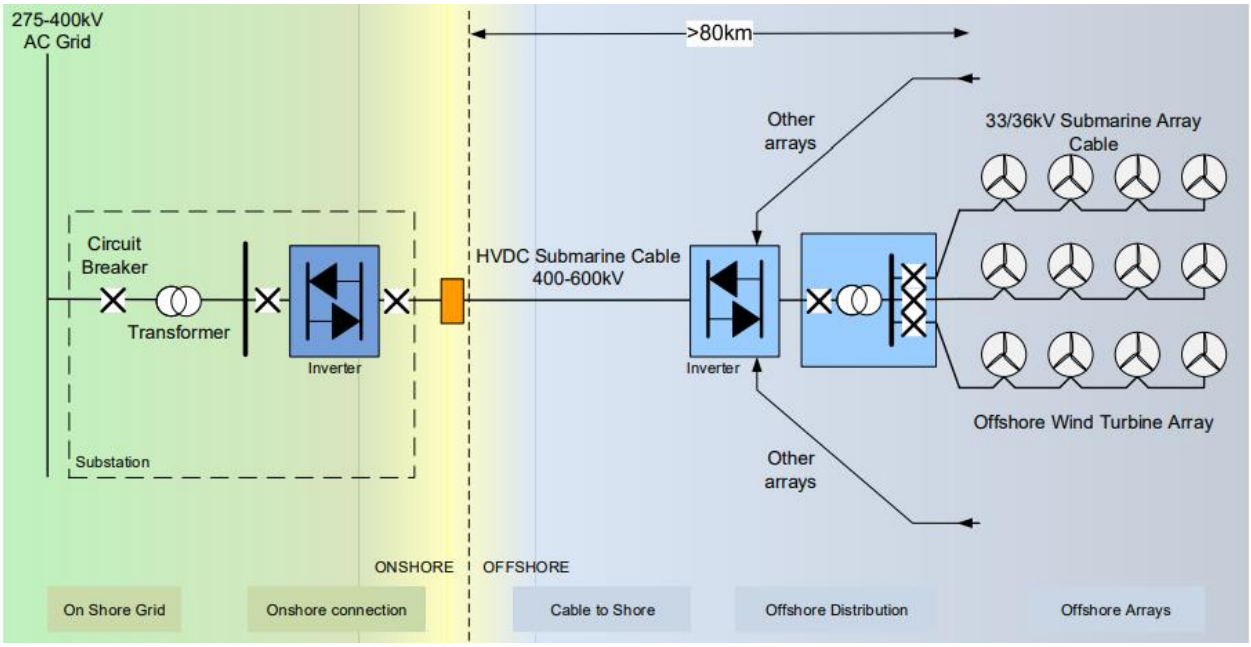


**Figure 2.5.4.1** : Illustrative MVAC, HVAC and HVDC connections (Source: FOWIND, 2017)

The total transmission system cost stands for both investment and operating expenses. Investment costs change with cable's rating power and technical characteristics among with the distance from the onshore network connection point. Table 2.5.4.2 summarizes the cost of offshore and onshore export cables based-on their technical characteristics (Ampacity, diameter and voltage) expressed in eurosper meter.

**Table 2.5.4.2:** HVAC and HVDC cables connection cost and technical characteristics

| Xiang et al., (2016) | **HVAC Offshore transport cables** | | |
|---|---|---|---|
| **Voltage (kV)** | **Section ($mm^2$)** | **Steady state current $I_{SSN}$ (A)** | **Euros/meter (2020)** |
| 132 | 600-1000 | 800-1000 | 850-1110 |
| 220 | 500-1000 | 700-1000 | 100-1300 |
| 400 | 800-2000 | 850-1100 | 1800-2800 |
| Xiang et al., (2016) | **HVDC Offshore transport cables** | | |
| **Voltage (kV)** | **Section ($mm^2$)** | **Steady state current $I_{SSN}$ (A)** | **Euros/meter (2020)** |
| +/– 150 | 1000-2000 | 1600-2400 | 850-1150 |
| +/– 300 | 1000-2000 | 1650-2400 | 1100-1500 |
| Gonzalez-Rodriguez (2017) | **HVAC Offshore transport cables** | | |
| **Voltage (kV)** | **Section ($mm^2$)** | **Capacity (MV A)** | **Euros/meter (2020)** |
| 132 | 500-1000 | 140-190 | 550-850 |

| | | | |
|---|---|---|---|
| 220 | 500-1000 | 250-320 | 890-1300 |
| Gonzalez-Rodriguez (2017) | **Onshore transport cables** | | |
| **Voltage (kV)** | **Section (mm²)** | **Capacity (MV A)** | **Euros/meter (2020)** |
| 220 | 500-1000 | 250-350 | 250-400 |

**Inter-Array Cables:** The inter-array cables connect each WT to the offshore substation(s). Currently, there are several topological options of an OWF regarding their inter-arraying design (ring, star topologies etc.) and many optimization tools consider inter-array topologies cost minimization among with power production maximization. Larger distances between WTs will lower the wake losses by increasing the inter-array cables cost. The amount of cabling required depends on the layout of the farm, the distance between the WTs, and the number of turbines (Kaizer & Snyder, 2012). The collection system applied can be divided into two cabling technologies including AC collection or DC collection. Although AC topologies are most commonly used, it is not always the most adequate option for an OWF. DC collection cables, or even the mix of two or more topologies, are a relatively new technology, and depends on the wind turbine generator type and capacity (Soarez-Ramos et al., 2020). Indicative examples are demonstrated in Figure 2.5.4.2.

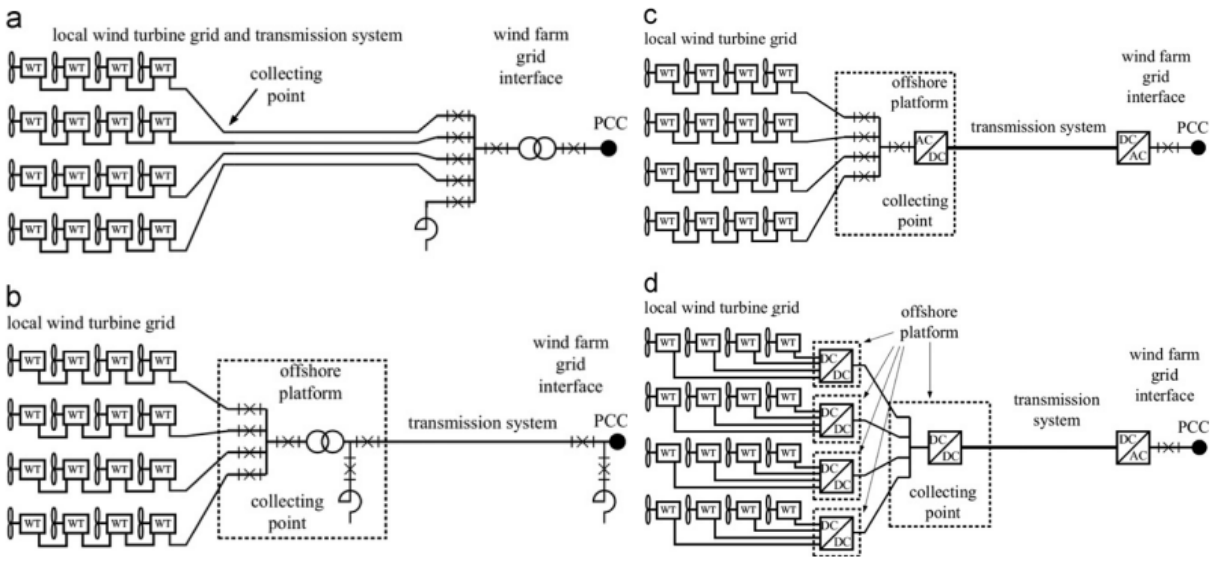


**Figure 2.5.4.2**: General layouts for OWFs between 60 and 300 MW. (a) Small AC wind farm, (b) large AC wind farm, (c) AC/DC wind farm and (d) large DC wind farm with two transformation steps. (Source: Madariaga et al., 2013)

Considering a small AC wind farm (Figure 2.5.4.2a), the MVAC collector system is applied both for connecting all WTs and directly transmitting the generated power to the onshore substation. For a large AC wind park (Figure. 2.5.4.2b), WTs are clustered within the MVAC collector system connected to an HVAC transmission system using an offshore substation. Moreover, an AC/DC wind project (Figure.2.5.4.2c) uses an HVDC link connecting the OWF with the onshore grid. Finally, the large DC layout is similar to that of a large AC wind farm (Figure.2.5.4.2d) and the key difference is the voltage transformation steps are needed among the WTs and the transmission system (Madariaga et al., 2013). The inter-array cables are typically medium-voltage (MV) with a rated power between 33 and 36 *kV*, but nowadays, some developers are considering the use of 66 *kV* cabling options. Similarly to the export cables, unit cost vary according to the cable section (*mm*) and nominal voltage (*kV*) (Ioannou et al. 2018). In Table 2.5.4.3 the resulting cost of inter-array cables is demonstrated in eurosper meter according to the cables' technical characteristics with values ranging between 150 – 600 euros/meter in accordance with the increase of the cable's diameter.

**Table 2.5.4.3:** Inter-array cables cost and technical characteristics

| Gonzalez-Rodriguez (2017)<br>**Inter-array cables (Type in mm)** | **Euros2020**<br>**Euros/meter** |
|---|---|
| 95 - 800 | 135 - 650 |
| Jin et al., (2019) | |
| 150 - 1600 | 164 - 610 |

**Substations.** When the OWF's transmission voltage is greater than 33 kV (36 or 66 *kV*), offshore transformer(s) must be constructed to raise the voltage to the desired level. In order to house the transformers, offshore substations with the appropriate power rating (MVA) for the project's capacity, will have to be built consisting of rather large, complex and very costly constructions (Kaizer & Snyder, 2012). An indicative example of the components that a substation accommodates is referred Ackerman (2005) for the Horns Rev OWF, located in the North Sea. An HVAC substation placed about 14m above mean sea level, established on a jacket foundation structure, is used including the following installations:

- 36 kV switch gear;
- 36/150 kV transformer;
- 150 kV switch gear;
- an emergency diesel generator;
- staff and service facilities;
- a helipad;
- a crawler crane;
- an MOB (man overboard) boat.

Furthermore, additional elements are needed at HVDC substations including insulated-gate bipolar transistor converters with a cooling system, smoothing coils and DC filters (Robak & Raczkowski, 2018).

**Table 2.5.4.4:** Offshore and onshore substation cost for the period 2003 - 2017

| Offshore Substation | Year | million euros/MW (2020) |
|---|---|---|
| Gonzalez-Rodriguez, (2017) | 2003 | 0.08 |
| | 2003 | 0.09 |
| | 2004 | 0.06 |
| | 2005 | 0.14 |
| | 2007 | 0.15 |
| | 2009 | 0.24 (HVDC) |
| | 2010 | 0.10 |
| | 2010 | 0.15 (HVDC) |
| Vormoolen et al., (2016) | 2016 | 0.22 |
| Noonan et al., (2018) | 2016 | 0.18 |
| | 2017 | 0.19 |
| **Onshore Substation** | **Year** | **million euros/MW (2020)** |
| Gonzalez-Rodriguez, (2017) | 2003 | 0.19 |
| | 2004 | 0.08 |
| | 2007 | 0.05 |
| Noonan et al., (2018) | 2016 | 0.08 |
| | 2017 | 0.10 |

Considering these technical installations needed and the support structure's size and complexity, the cost for an offshore substation is not negligible. Myhr et al., (2014) approximate this cost for a 500 MW OWF up to 150 million eurosfor an HVDV offshore substation as well as

Dicorato et al., (2011) indicates a 20 million euroscost for a HVAC substation of 150 MVA. An increase to the total substation's cost is highlighted by Gonzalez-Rodriguez (2017) exceeding 50-500% for HVDC platforms compared to the HVAC. Overall, the total substations cost has been approximated by a number of authors based on parametric expressions linking the total substation's cost to the total installed capacity (and accordingly the size of the substation) of an OWF (Gonzalez-Rodriguez, 2017; Ioannou et al. 2018). The associated results are presented in Table 2.5.4.4 with costs exceeding 0.2 million Euros/MW (i.e., approximately 100 million eurosfor a 500 MW offshore wind farm).

### 2.5.5 Installation costs

Installation procedures incorporate all activities involving the vessels' loading activities among with the transportation and installation of the OWF components. At first, the installation of the foundations is taking place among with the transition piece and the scour protection configurations. Next step consists of the erection of the tower and the rotor-nacelle assembly (RNA) of the WT. Accordingly, the installation of the offshore substation (if needed), the inter-array cables and finally the export cables are placed in position (Ioannou et al. 2018).

In general, installation costs are expressed as functions of the installation vessel type and day rates, the installation procedures duration and the personnel costs required for carrying out all of the operations (Myhr et al. 2014). Table 2.5.5.1 illustrates the average days of installation per foundation type and WT concept. Among fixed foundation technologies, installation time differences are relatively low, with the jacket foundations preserving the maximum amount of installation time with approximately 7 days. In contrast, floating concepts seem to preserve decreased installation times, mainly due to the installation strategy followed, where both the floater and the WT are assembled onshore and transferred to the OWF site.

**Table 2.5.5.1**: Days of installation per foundation type and wind turbine

| Foundation type | Days/foundation | Days/Turbine | Sources |
|---|---|---|---|
| Gravity | 4.645 | 3.654 | Arántegui et al., (2020) |
| Jacket | 7.567 | 8.143 | |
| Monopile | 3.574 | 3.821 | |
| Floating | 5 -7 | 1.1 | Bjerkseter & Ágotnes (2013) |
| Floating | 1.33 | 0.3 | James et al., (2015) |

**Table 2.5.5.2**: Wind turbines and Foundation concepts installation costs for the period 2003 – 2018 in million euros/MW of installed capacity

| WT installation cost | Year | million euros/MW (2020) | | |
|---|---|---|---|---|
| Gonzalez-Rodriguez, (2017) | 2003 | 0.99 | | |
| | 2003 | 1.11 | | |
| | 2007 | 0.56 – 1.51 | | |
| | 2009 | 0.94 – 2.02 | | |
| Myhr et al., (2014) (Floating) | 2014 | 0.61 | | |
| | 2015 | 1.27 - 1.59 | | |
| Kausche et al., (2018) (Floating) | 2018 | 0.52 | | |
| **Foundation installation cost** | **million euros/MW (2020)** | | | |
| **Fixed structures** | Gravity-based | Steel monopile | Steel jacket | Tripod |
| Myhr et al., (2014) | - | 1.02 | 1.46 | - |
| Gonzalez-Rodriguez, (2017) | | | | |
| 0 - 20 m | 0.38 | 0.61 | 0.51 | 0.76 |
| 20 - 30 m | 0.54 | 0.76 | 0.64 | 1.02 |
| 30 - 40 m | 0.91 | 1.02 | 0.96 | 1.15 |
| **Floating structures** | TLP | Spar-Buoy | Semi-Submers. | SWAY |
| Bjerksetter & Agotnes, (2013) | 0.041 | 0.035 | 0.047 | 0.019 |

Table 2.5.5.2 demonstrates both WT and foundation installation cost. Results highlight a relative stable installation cost for the WTs during the period 2003-2018 with values ranging between 0.6 - 2 million Euros/MW, although, in most concepts the installation cost is between 1.4 - 1.6 million Euros/MW. For the foundation installation cost, most differences occur relatively to the sea depth increase (e.g. from 20 to 40 meters) rather between the fixed foundation concepts. Correspondingly, the floating foundations are characterized by decreased installation

costs (approx. 0.04 million euros/MW), mainly due to the days and the vessel type needed for the installation process.

**Table 2.5.5.3**: Export and inter-array cables installation time and cost characteristics

| **Operational OWFs** | **Length (km)** | | **Total time (days)** | | **Inst. Rate (km/day)** | |
|---|---|---|---|---|---|---|
| No. of cables | Export | Inter-array | Export | Inter-array | Export | Inter-array |
| 2 | 12 | 15 | 49 | 105 | 0.5 | 0.14 |
| 3 | 4 | 17 | 60 | 60 | 0.2 | 0.28 |
| 1 | 26 | 22 | 130 | 150 | 0.2 | 0.15 |
| 1 | 7 | 22 | 5 | 90 | 1.4 | 0.24 |
| 2 | 13 | 32 | 60 | 180 | 0.4 | 0.18 |
| 2 | 36 | 51 | 70 | 161 | 1 | 0.32 |
| 3 | 11 | 18 | 60 | 90 | 0.6 | 0.2 |
| 3 | 10 | 21 | 30 | 60 | 1 | 0.35 |
| 1 | 28 | 45 | 30 | 150 | 0.9 | 0.3 |
| 3 | 15 | 27 | 40 | 90 | 1.1 | 0.3 |

| Kaizer & Snyder, (2012) ↑ | Gonzalez-Rodriguez, (2017) ↓ |
|---|---|
| **Offshore transport cables - Installation cost** | **Euros 2020** |
| **Year** | **euros/meter** |
| 2003 | 65.39 |
| 2004 | 90.70 |
| 2007 | 349.07 |
| 2009 | 673.89 |
| 2009 | 743.49 |
| 2010 | 165.57 |
| **Onshore transport cables - Installation cost** | **Euros 2020** |
| **Year** | **Euros/meter** |
| 2003 | 566.32 |
| 2007 | 223.58 |
| 2009 | 403.9-724.5 |
| **Inter-array cables installation cost** | **Euros 2020** |
| **Year** | **Euros/meter** |
| 2003 | 65.39 |
| 2007 | 83.31 - 349.07 |
| 2009 | 62.22 |
| 2010 | 142.37 - 153.97 |

Average installation rates for both export and the inter-array cables can be extracted by taking into account already operational OWFs. Based on the extended research studies applied by Kaizer & Snyder, (2012) and Gonzalez-Rodriguez, (2017), the total cables length (in kilometers) and the total installation time (in days) among with the cables' installation cost per meter are reported in Table 2.5.5.3. Average installation rates are estimated approximately at 0.6 and 1.6 km/day for the export and 0.2 to 0.3 km/day for the inner-array cables, respectively. The installation cost of export and inter-array cables preserve increased variations with values ranging between 65 - 743 euros and 62-349 euros per meter.

### 2.5.6 Operation and Maintenance (O&M) cost and Operational Expenditures

Operation and Maintenance (O&M) cost sums up to about 20% - 30% of the total costs of an OWF project as a sum of both the fixed and variable costs. The former incorporates all administrative costs, insurances, grid access fees and service contracts for scheduled maintenance, while the latter stand for the scheduled and unscheduled maintenance repairs (Maienza et al., 2020). Notable is that there is a difference between O&M and OPEX (Operational expenditures) as long as OPEX is included in O&M costs and must not be confused. Previous technical and research studies estimated that OPEX is about 50% of the total O&M costs for an OWF (IRENA, 2012; Vormoolen et al., 2016). The O&M costs are usually given on per MWh basis and they increase as the equipment is aging. However, in the case that O&M costs are expressed on per MW basis, it can be translated to currency per MWh by multiplying by 8760 h/year and the load factor (typically 0.35) (Gonzalez-Rodriguez, 2017).

According to Shaffie et al., (2016), the OPEX of an OWF includes the rental/lease payments, the insurance costs and the transmission charges. Focusing on the maintenance expenses, the maintenance activities aim to maximize the total availability (in % expressing the amount of time that the OWF has no downtimes) of the OWF while minimizing the costs associated with all type of failures. Thus, for the maintenance costs, two major categories exist, direct and indirect costs including the failed components transportation cost, maintenance technicians' salaries and overall, all spare parts required (Myhr et al., 2014; Shaffie et al., 2016).

In Table 2.5.6.1 all the reviewed values are demonstrated for the period 2005-2012. Cost values indicate a relative stable evolution for O&M (around 20 euros per MWh) with an exception during 2010 where an increase is observed. Notable is that further cost information related to O&M from 2012 and beyond was difficult to acquire as long as annual operating expenditures (OPEX) are not published for specific projects.

**Table 2.5.6.1:** Cost of the Operations and Maintenance cost for the period 2005 – 2012 in million euros(m€) per MWh

| Sources | Year | O&M (€ 2020/MWh) |
|---|---|---|
| Gonzalez-Rodriguez, (2017) | 2005 | 10.5 |
| | 2007 | 22.05 |
| | 2009 | 12.6-18.9 |
| Levit et al., (2011) | 2009 | 13 - 38.28 |
| | 2010 | 35.22 |
| | 2010 | 15.42 – 50.53 |
| Gonzalez-Rodriguez, (2017) | 2010 | 18.9 - 32.55 |
| Vormoolen et al., (2016) | 2012 | 19.78 |

## 2.5.7 Decommissioning and Dismantling costs

Decommissioning and disposal costs, commonly referred as DECEX, extends to the last stage of the OWF operational lifespan, and sums up around 1–3% of the total investment costs. It includes all the expenditures for removing all the OWF components and cleaning the area or possible repowering of the wind project (Bjerksetter & Agotnes, 2013; Maienza et al., 2020). OWF owners are obligated to remove almost all structures (subsea cables are partially removed) and clean the broader offshore area upon the termination of the lease for both environmental and economic considerations. Decommissioning activities are related to the removal of the WTs (i.e. nacelle, tower and transition piece) and the support structures as well as the balance of the plant components (substation(s), inter-array and export cables and scour protection). (Ioannou et al. 2018). Often, after the dismantling of offshore installations some materials, such as the steel of both WTs and foundations or the aluminum of the electrical cables are sold and considered as scrap revenues (Table 2.5.7.1).

**Table 2.5.7.1:** Cost of the decommissioning and dismantling procedures for the period 2012 – 2018 in million euros(m€) per MWh

| Decommissioning Cost | Year | million Euros/MW (2020) |
|---|---|---|
| Kaiser & Snaider, (2011) | 2010 | 0.11 - 0.16 |
| Prassler and Schaechtele (2012) | 2012 | 0.23 |
| Shaffie et al., (2016) | 2016 | 0.31 |
| Topham & McMillan, (2017) | 2016 | 0.17 - 0.29 |
| Gonzalez-Rodriguez et al., (2017) | 2017 | 0.12 |
| Kausche et al., (2018) (Floating) | 2018 | 0.037 |
| **Scrap revenues** | **Year** | **million Euros/MW (2020)** |
| Bjerksetter & Agotnes, (2013) (Monopile) | 2013 | 0.25 |
| Bjerksetter & Agotnes, (2013) (Jacket) | 2013 | 0.13 |
| Bjerksetter & Agotnes, (2013) (TLB - Floating) | 2013 | 0.15 |
| Bjerksetter & Agotnes, (2013) (Hywind - Floating) | 2013 | 0.33 |
| Bjerksetter & Agotnes, (2013) (WindFloat - Floating) | 2013 | 0.45 |
| Bjerksetter & Agotnes, (2013) (SWAY - Floating) | 2013 | 0.2 |

Table 2.5.7.1 demonstrates the evolution of DECEX values during the last decade for fixed and floating offshore wind projects, considering that decommissioning and dismantling cost as also scrap revenues differ per foundation technology. Notable is that most off these values are rough estimates as long as the vast majority of the total offshore wind projects are still operational. Discussing the cost values of Table 2.5.7.1, decommissioning estimations seem to be similar for all foundation technologies (approx. 0.15 – 0.3 million euros) although, increased differences are noticed in scrap revenues where jacket foundations preserve the lowest value in million euros per MW compared to monopile and floating structures.

## 2.5.8 Cost assessment indicators

During Sections 2.5.1 – 2.5.7, all sub-cost components of a potential OWE project were analyzed and discussed for different stages of development. A detailed cost breakdown of an OWF project is important for calculating the life cycle costs, the Levelized Cost of Energy (LCoE),

the Breakeven Price (BP) and the Net Present Value (NPV). A comprehensive consideration of all costs included is essential to predict the profitability of an offshore wind project as well as to compare alternative investment options, scenarios or technical aspects during the decision-making process. Generally, the LCoE describes the costs that are required to generate 1 unit of electricity (kW/hour). The LCoE (Equation 2.8.1) considers the initial capital expenditures (CAPEX) as well as all annual O&M costs and the annual energy production (AEP) sustained over the total project lifetime (Vormoolen et al., 2016; Kausche et al., 2018). An indicative example of the LCoE breakdown is demonstrated in Figure 2.5.8.1 for different support structures technologies, fixed and floating, indicating the differences per phase of development and the according support structure mechanism.

$$\text{LCoE} = \frac{CAPEX + \sum_{t=1}^{L} \frac{O\&M}{(1+i)^t}}{\sum_{t=1}^{L} \frac{AEP}{(1+i)^t}} \quad (2.5.8.1)$$

where *i* is the discount factor, *L* is the project's lifetime, *t* is the year of operation, *AEP* is the Annual Energy Production, which is related to the capacity factor (including wake and transport losses among with OWF's availability). CAPEX includes all capital expenditures and finally O&M stands for the operation and maintenance costs. Instead of *i* as the discount factor, the Weighted Average Cost of Capital (WACC) is used in some cases. WACC (Equation 2.5.8.2) is related to the financing costs of a project, expressed as a rate of return, comprising of the weighted average of the required returns on the dept and equity and is set to a base case of 8-10%, with high and low cases at 6% and 12%, respectively. WACC is expressed as (Myhr et al., 2014; Vormoolen et al. 2016):

$$\text{WACC (\%)} = share\ of\ equity * cost\ of\ equity(\%) + share\ of\ dept * cost\ of\ dept(\%) \quad (2.5.8.2)$$

Analyzing Equations 2.5.8.1 - 2.5.8.2, noteworthy is that WACC has a significant impact on the resulted LCoE. According to Ebenhock et al. (2015) and the sensitivity analysis that they

conducted for a proposed OWF, a reduction of the WACC by one percent point (i.e. from 9% to 8%), leads to a decrease of the LCoE by about 6 %. In Figure.2.5.8.2 is illustrated the cost of capital (left) across different countries with the highest values observed in South American countries and Greece from Europe. On the contrary, WACC exceeds around 5–7% in Japan, Germany and the UK and for the developed countries, 8.5% in China, 12.5% in India, 13% in Russia and 14.8% in Brazil.

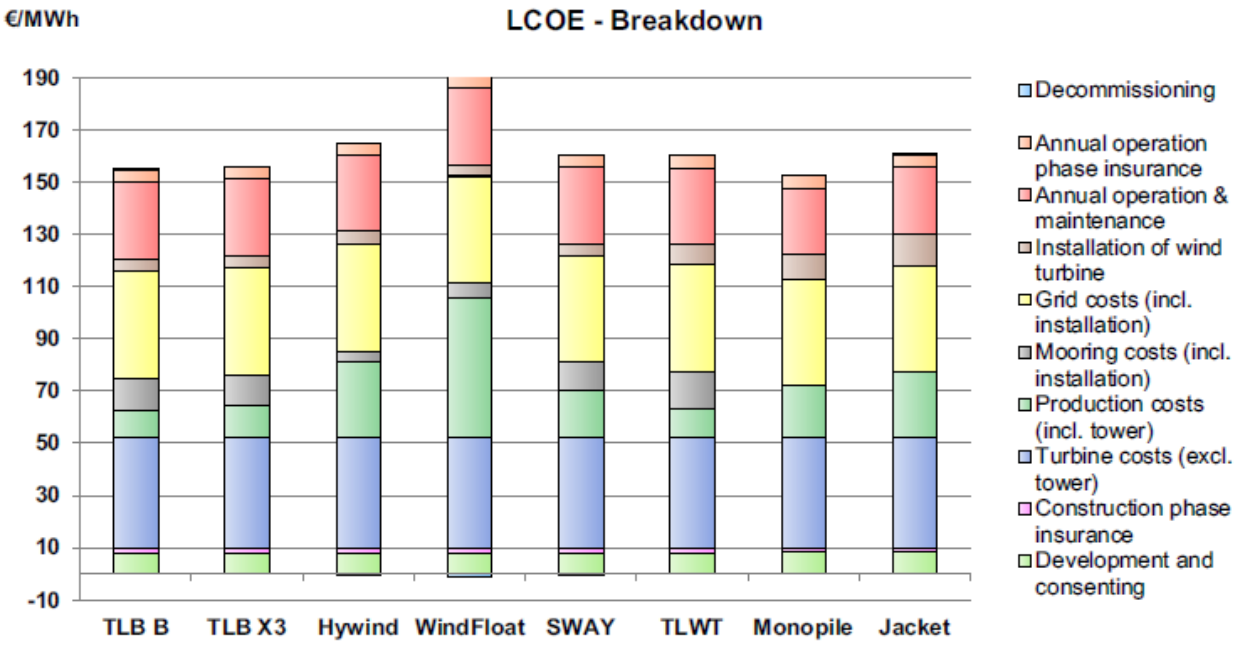


**Figure 2.5.8.1:** LCoE cost breakdown for the base case of the reference case, Sources: Myhr et al. (2014)

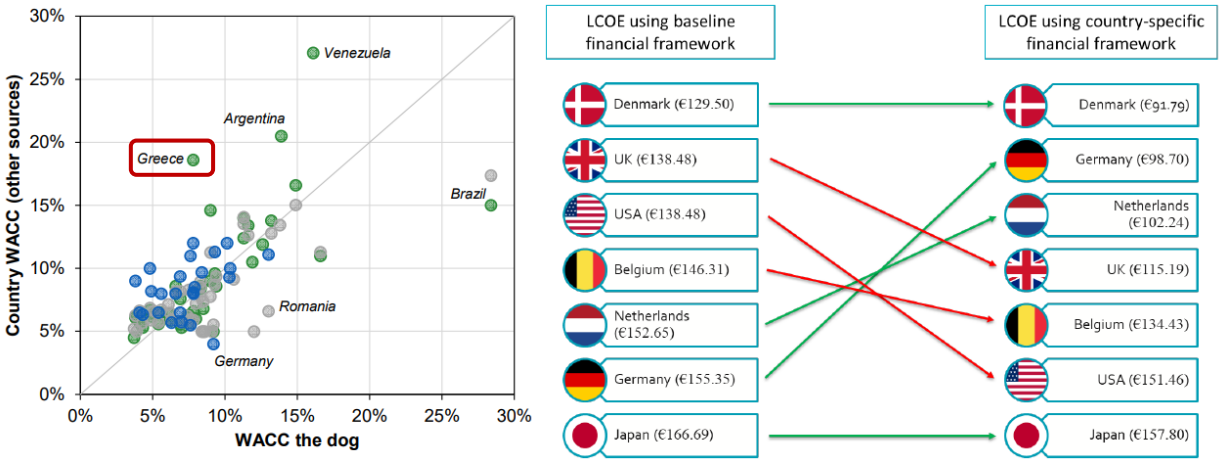


**Figure 2.5.8.2:** Comparison between the cost of capital across different countries (left), Impact of country-specific financial framework on LCOE (right), Sources: Bosch et al. 2019; Noonan et al. 2018

Indicative of the aforementioned LCoE values is that in 2017, the Final Investment Decisions (FID) stated that the UK offshore wind projects will reach a LCoE below 112€/MWh before 2020. In addition, a price of 70.88€/MWh was reported for offshore wind projects commencing in 2021/22, and 65.59€/MWh for 2022/23, compared to the 163€/MWh exceeded in 2010 (Bosch et al. 2019). These statistics indicate the tremendous efforts applied in order to reduce OWE costs, towards to more sustainable and efficient technological improvements. Another economic metric, valuable for an OWE project feasibility assessment, related to the LCoE among other parameters, is the Net present value (NPV) (Equations 2.5.8.3- Eq.2.5.8.4) expressed as the sum of the present values calculated for many periods (e.g. annual interval). As a result, different cash flows coming from expenses and revenues at different timescales must be evaluated and compared.

NPV parameters are based on the given discount rate and the internal profitability rate of a project (IRR). Formally, the IRR is derived by calculating the discount rate that sets the NPV to zero (Prässler & Schaechtele, 2012; Shaffie et al., 2016):

$$\mathrm{NPV}(d,N) = \sum_{t=0}^{N} C_t/(1+d)^t \qquad (2.5.8.3)$$

$$C_t = AEP_n\, P_n\, B_n \qquad (2.5.8.4)$$

where *Ct*, *d* and *N* represent, respectively, the cash flow at time *t*, annual interest rate and the number of years in which the investment takes place. Accordingly, $AEP_n$ is the estimated energy production of year *t*, $B_n$ represents tax benefits, capacity payments, etc., and $P_n$ (which is the resulting LCoE or Breakeven Price-BP) is the hypothetical energy price during that period.

Overall, the objective in these economic metrics and cost assessment studies is to select and place the components that optimize a specific economic indicator. Table 2.5.8.1 summarizes all LCoE values, technical characteristics and benchmark costs of indicative OWFs across different countries. By reviewing all relative cost indicators discussed in Section 2.5, differences among LCoE values are highlighted according to the technical characteristics and the “strategies” the

offshore wind projects were developed (WT size and number, bathymetry, distances from onshore network junctions and ports along with some key economic indicators).

**Table 2.5.8.1:** Indicative OWF site characteristics and relative cost indicators per country, **Source:** Noonan et al., (2018)

| OWF components | Unit | Netherlands | UK | Belgium | Denmark | USA | Germany | Japan |
|---|---|---|---|---|---|---|---|---|
| **LCoE** | **€/MWh** | **152.7** | **138.5** | **146.3** | **129.5** | **148.1** | **155.4** | **166.7** |
| Number of WTs | count | 150 | 69 | 42 | 50 | 76 | 60 | 14 |
| WT rated power | MW | 4 | 6 | 7 | 8 | 6 | 6 | 5.2 |
| Hub height | m | 89 | 100 | 106 | 105 | 100 | 100 | 127 |
| Rotor diameter | m | 130 | 154 | 154 | 164 | 154 | 154 | 136 |
| OWF capacity | MW | 600 | 414 | 294 | 400 | 456 | 360 | 72.8 |
| Foundation type | type | Monopile | Monopile | Monopile | Monopile | Monopile | Jacket | Monopile |
| Inter-array cables | type | 33 kV/185mm | 33 kV/185mm | 33 kV/185mm | 33 kV/185mm | 33 kV/185mm | 33 kV/185mm | 33 kV/185mm |
| Offshore substations | count | 2 | 1 | 1 | 1 | 1 | 1 | 0 |
| Offshore export cables | type | 220 kV/1000mm | 220 kV/1000mm | 220 kV/1000mm | 220 kV/1000mm | 220 kV/1000mm | 220 kV/1000mm | 33 kV/400mm |
| Onshore export cables | type | 220 kV/1000mm | 220 kV/1000mm | 220 kV/1000mm | 220 kV/1000mm | 220 kV/1000mm | 220 kV/1000mm | 33 kV/500mm |
| Water depth | m | 33 | 27 | 29 | 16 | 30 | 35 | 11.9 |
| Distance to port | km | 78 | 25 | 33 | 60 | 30 | 80 | 70 |
| Distance to O&M port | km | 78 | 25 | 33 | 50 | 30 | 60 | 3 |
| Distance to cable landfall | km | 120 | 50 | 40 | 33 | 30 | 60 | 3 |
| Onshore cable distance | km | 10 | 18 | 10 | 50 | 10 | 60 | 0 |
| Mean wind speed | m/s | 9.36 | 9.15 | 8.95 | 9.57 | 8.99 | 9.47 | 8.67 |
| Wave conditions | type | medium | medium | harsh | medium | mild | medium | medium |
| Seabed conditions | type | normal | normal | normal | normal | normal | normal | normal |

| | | | | | | | | |
|---|---|---|---|---|---|---|---|---|
| Depth equitity ratio | % | 70 | 70 | 75 | 70 | 55 | 75 | 70 |
| Cost of equity | % | 13 | 12.5 | 13 | 12.8 | 12.1 | 12 | 15 |
| Cost of dept | % | 4 | 4 | 5 | 4.8 | 6.8 | 4 | 3 |
| WACC (pretax nominal) | % | 6.7 | 6.55 | 7 | 7.15 | 9.16 | 6 | 5.98 |
| Annual inflation | % | 1.8 | 1.8 | 1.8 | 1.8 | 1.8 | 1.8 | 1.8 |
| WACC (pretax real) | % | 4.81 | 4.67 | 5.1 | 5.26 | 7.23 | 4.13 | 2.65 |
| **TOTAL CAPEX** | m€/MW | 4.023 | 3.349 | 3.458 | 3.395 | 3.518 | 3.979 | 3.666 |
| **TOTAL ANNUAL O&M** | m€/MW | 0.069 | 0.064 | 0.066 | 0.06 | 0.061 | 0.067 | 0.11 |

As a concluding remark, the need for integrated and accurate cost assessments is crucial but relatively uncertain due to the number and the heterogeneity of the factors affecting the cost estimates. Numerous cost comparative analyses have been conducted and the outcomes discussed analytically during these sections, however, more accurate data and up-to-date modelling approaches must be considered for further validation, or refinement of already existing knowledge (Levit et al., 2011)

## 2.6 Offshore Wind Resource Assessment

Site prospecting and successful OWF planning incorporate the accurate assessment strategies of the wind resources by quantifying in parallel the inherent wind power variability. Therefore, efficient wind energy projects rely on accurate wind resource estimates, which most of the times are costly and complex to obtain offshore due to the temporal and spatial sparseness of in-situ data. On this basis, alternate data sources, based on either satellite and modelled data (or fusion of them), are used (Petersen & Troen 2012; Badger et al. 2014; Doubrawa et al. 2015), in order to produce wind resource maps and project climate estimations.

On top of that, knowing that wind is a highly variable phenomenon, from gusts lasting a few seconds to seasonal and inter-annual variations spanning decades, the need for integrated wind resource strategies is a matter of crucial importance (Bett et al. 2017). The identification of significant sources of variation on a diurnal, seasonal and inter-annual basis in order to evaluate revenues risk, becomes even more challenging (Mytilinou & Kolios, 2019). For this reason, minimizing uncertainty in offshore wind power resource estimates improves results during the site prospecting phase of planning, and this can be accomplished by utilizing more accurate offshore wind speed data and probabilistic models (Hu et al. 2016). A comprehensive wind resource assessment framework usually entails the following tasks (Zhang et al. 2015):

1. **Site prospecting and measurement campaign;** Identification of one or multiple suitable sites using cartographic tools e.g. produced wind atlases. Next step consists of the characterization of the selected on-site(s) wind resources by recording the winds for 1–4 years as close as possible to hub height, with meteorological masts and supplemented data sometimes from remote sensing instruments, buoys and offshore platforms.
2. **Long-term extrapolation and microscale vertical extrapolation;** Extension of the measurements from first step up to 10 - 30 years long operation lifetime using historical observations from nearby surface coastal weather stations, reanalysis datasets from numerical weather prediction (NWP) models and correction techniques with statistical regression methods (e.g., Measure-Correlate-Predict) (Liléo et al. 2013).
3. **Wind farm layout design and gross energy production estimation;** Establishment of turbine locations applying optimization techniques (Grady et al. 2005) relative to wind resource estimation and wake effects phenomena using standard wake models (Frandsen et al. 2006; Larsen et al. 2007) or computational fluid dynamic models. The scope is to calculate the wind power potential over a year and over the lifetime for a site incorporating the associated energy losses and availability issues.
4. **Uncertainty quantification;** Careful evaluation of the resulted uncertainty associated with previous steps. These uncertainties in wind energy may be categorized into long-term and short-term. Long-term uncertainties are mainly introduced by variation of wind conditions

on intra and inter–annual variations, and other environmental, operational, and financial factors. On the contrary, short-term uncertainties mainly lie on the diurnal and inter-diurnal wind's variations, the turbulence intensity and the wake deficits from the WTs.

Quantification of uncertainties due to wind's horizontal and vertical variability remains one of the most challenging fields in offshore wind renewable energy sector. Therefore, multiple modelling techniques combining different sources of wind data are capable to handle, validate and reduce this uncertainty among observations, modelled reanalysis outputs and statistical analysis techniques. In particular, the final wind resource assessment uncertainty is quantified as a sum of uncertainties derived from: i) wind speed measurements, ii) probabilistic assessment of wind speeds and directions, iii) hub height extrapolation and finally iv) long-term resource assessment. Therefore, quality control and correction techniques, adjustment of errors and statistical tests must be applied (Lackner et al. 2008).

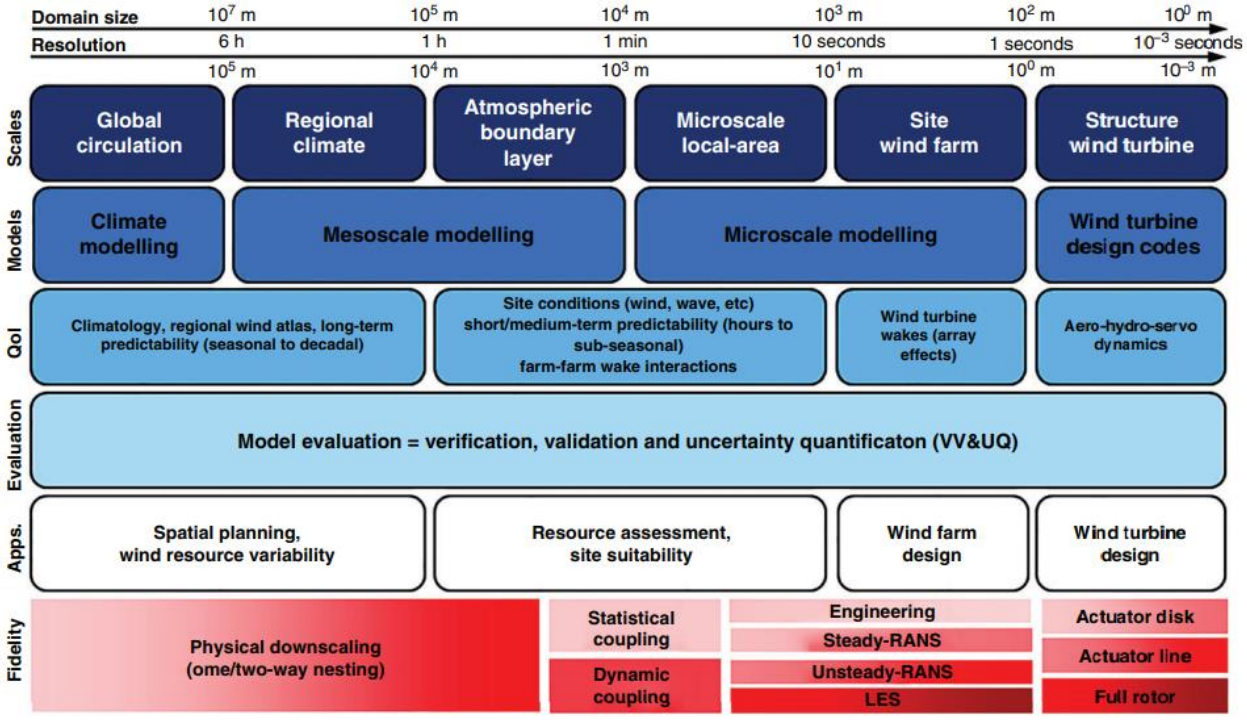


**Figure 2.6.1:** Wind assessment modelling framework indicating typical scales, relevant outputs for different applications, and high-level fidelity methods (Rodrigo et al. 2016)

These steps are briefly illustrated on Figure 2.6.1 for multiple steps applied and different temporal and spatial scales. Global circulation and regional climate models are mostly considered for long-term planning strategies incorporating climatological data, regional wind atlases and long-term simulation data (Petersen & Troen 2012; Badger et al. 2014; Doubrawa et al. 2015). In addition, meso and micro-scale models consist of the most valuable information for site-specific assessment strategies in order to reliably quantify short and medium-term wind variability as long as WTs wake interactions. Finally, for WTs aerodynamic, hydrodynamic and servo-elastic simulations more robust models and temporally complete wind time series data must be considered. Overall, when exploring wind energy resources for long-term assessment and planning purposes, the mean wind speeds (daily, monthly or annual) are not enough to characterize and understand the climate patterns at a specific area. However, many assessment indicators exist in order to analyze wind's probabilistic behavior, wind extremes, intermittency patterns and long-term periodicity and variations, which can be seen as key sources for representatively characterizing wind climatology and the associated uncertainties.

### 2.6.1 Offshore wind data availability

Considering the data availability and accuracy, wind data time series can be derived from any direct or indirect measurement or observation campaign and techniques (e.g. meteorological towers, lidar, sodar, satellite observations or numerical models). The wind industry's practice is to deploy a finite number of wind measurement campaigns in order to assess wind speed characteristics and the wind power density of an area during the pre-planning, the construction and the operation phase of an OWF.

As already stated, the collection of homogeneous offshore wind data is a challenging problem. A brief description of all available data and modelling techniques is presented in Figure 2.7.1 and Table 2.7.1. Becoming aware of the need for accurate data sources, the best-case scenario is to acquire in-situ measurements from masts, buoys or ships. Although, the sparsity and the lack of spatial and temporal coverage as well as the increasing cost for offshore meteorological observations has led to alternative sources for wind regimes characterization and assessment.

**Table 2.6.1:** Strengths, weaknesses and accuracy of different wind data types

| | Strengths | Weaknesses | Accuracy |
|---|---|---|---|
| **SAR** | High spatial resolution (<100m), Moderate swath coverage, Long term data (>15 years), Can estimate spatial variation of wind | Poor temporal resolution, Influence of non-wind signatures upon observations, Satellite continuity questions, Require scaling to turbine hub height | Std. dev. ±1-2 m/s |
| **SCAT** | Wide swath coverage, Long term data (>15 years), High temporal resolution, Can estimate spatial variation of wind | Low spatial resolution, Require scaling to turbine hub height | Std. dev. ±1-2 m/s |
| **NWP** | High temporal resolution, Can estimate spatial variation of wind | Moderate to low resolution, Accuracy questionable near to coast | Std. dev. ± 2 m/s |
| Wind Atlas (**WaSP**) | Simple to apply, Mature technology, Can estimate spatial variation of wind | Sensitivity to input observations | < 10% |
| **MCP** | Simple to apply Mature technology | Requires observations at offshore site, No spatial coverage | Lower than in |
| **In Situ** | Simple to apply, Gold standard of accuracy, Can directly measure the vertical wind profile | No spatial coverage, Installation and capital cost | ± 10% |

Becoming aware of the need for qualitative data sources, in situ measurements from masts, buoys or ships should be acquired. However, the sparsity of spatial and temporal coverage as long as the increasing cost has led to alternative sources for wind regimes characterization and analysis. For these reasons, Numerical Weather Prediction (NWP) models appear to be a valuable alternative source for wind data and are considered as a challenging multivariate, spatially continuous, and consistent source of records at various atmospheric time-scales (Sempreviva et al. 2008). NWP models and reanalysis data are often used to calculate and assess the offshore wind resources at a specific site with the key advantage of simulating high-quality wind data for any region globally at low computational cost or totally free of any charge. In addition, mesoscale models can use results from global and regional models or reanalysis datasets as input, by applying methods for obtaining energy estimations (Sempreviva et al. 2008; Hassager et al. 2014; Salvação & Soares 2016).

Two of the most wide-ranging reanalysis data sets used for wind resource assessment are the *ECMWF Re-Analysis Interim* product (ERA-Interim) (Kiss & Jánosi 2008) and the NASA's *Modern Era Retrospective-analysis for Research and Applications* (MERRA [Wang et al. 2019] and MERRA-2 [Grumber et al. 2019]). By 2018, the Copernicus Climate Change Service released the European project of Uncertainties in Ensembles of Regional Re-Analyses (UERRA) (Ridal et al. 2017; Aschroft et al. 2018) offering ensembles of European regional reanalysis at high spatial and temporal resolution (6 hours at 5.5 and 11 km) for more than five decades (1960 - today), with an additional estimate of the associated uncertainties in the output datasets. In addition to that, ERA5 reanalysis data were also released in 2019 by the Copernicus Services, consisting of the fifth generation of ECMWF global reanalysis, succeeding ERA-Interim and covering the entire globe from 1979 with a temporal resolution of 1 hour and a spatial coverage of approximately 30 km (Pelosi et al. 2020).

Previous research studies have used the aforementioned reanalysis products, mostly for large-scale assessments, such as wind resource (Del Jesus et al. 2014; Giannaros et al. 2017) and wind power assessments (Lizuma et al. 2013; Emmanouil et al. 2016), climatological analysis and long-term trends in wind speed (Kircher-Bossi et al. 2015; Carpar et al. 2020), for daily to annual scale variability assessment (Brower et al. 2013) or uncertainty quantification (Rose & Apt 2016; Torralba et al. 2017). Results from these studies indicate that until 2017, ERA-Interim was the dataset that provides the most accurate NWP wind simulation product with the lowest biases, errors and highest correlation scores compared to in situ records. Contrary, MERRA and MERRA-2, while they are covering an excessively large temporal resolution, they exhibit two disadvantages, a significant deviation from the observed means and a rather low spatial resolution at 50 km scale. Finally, considering UERRA and ERA5 reanalysis data, there is no extensive research in the validation of the models' realizations. However, in Ref. (Pelosi et al. 2020), comparisons between the UERRA (MESCAN-SURFEX) and ERA5 land datasets indicate small differences, compared to the observed wind speed data (see Pelosi et al. 2020, pg. 11, Fig.4). Similarly, in Hallgren et al. (2020), the authors compare several reanalysis products, including MERRA2, UERRA (HARMONIE) and ERA5. The authors concluded that both of UERRA and ERA5 outperform MERRA2, compared to 4 observational datasets from offshore masts in the Baltic Sea.

Particularly, authors notice that similar bias values occurred up to 150 meters above sea level. Finally, Dörenkämper et al. (2020) quantifies the added value of the mesoscale and microscale generated climatology produced by the Weather Research Forecast (WRF) and the Wind Atlas Analysis and Application Program (WAsP) accordingly, in accordance to the performance of the driving ERA5 reanalysis. Results showed a dramatic reduction of mean wind speed biases for the microscale models compared to the 291-mast data from multiple European sites. Alongside, the largest underestimations occurred in the broader Mediterranean region (Italy, Greece and Turkey), and specifically in Greece, with the mean wind speed bias ranging between 2.5 - 4 $ms^{-1}$.

## References


1. **4C Offshore, (2019):** https://www.4coffshore.com/. (Accessed 14 June 2020).
2. **Ackermann, T., (2005):** Transmission Systems for Offshore Wind Farms, *Wind Power in Power Systems*;479–503
3. **Akbari N., Jones D., and Treloar R., (2019):** A cross-European efficiency assessment of offshore wind farms: A DEA approach, *Renewable Energy*, 151;1186-1195
4. **Ashcroft L., Coll J.R., Gilabert A., Domonkos P., Brunet M., Aguilar E., et al., (2018):** A rescued dataset of sub-daily meteorological observations for Europe and the southern Mediterranean region, Earth Syst. Sci. Data;10:1613-1635
5. **Badger M., Badger J., Nielsen M., Hasager C., B., and Pena A. (2010):** Wind Class Sampling of Satellite SAR Imaginary for Offshore Wind Resource Mapping, *Journal of Applied Meteorology and Climatology*:49;2474-2492
6. **Batista M. I., Henriques S., Miguel P. P., and Cabal H. N., (2014):** Assessment of cumulative human pressures on a coastal area: Integrating information for MPA planning and management, *Ocean & Coastal Management*, 102;248-257
7. **Barbanti, A., Campostrini, P., Musco, F., Sarretta, A., and Gissi, E. (eds.) (2015)**: Developing a Maritime Spatial Plan for the Adriatic-Ionian Region. CNR-ISMAR, Venice, IT.
8. **Bento N., and Fontes M., (2019):** Emergence of floating offshore wind energy: Technology and industry, *Renewable and Sustainable Reviews*, 99;66-82
9. **Bett P.E, Thornton H.E., and Clark R.T., (2017):** Using Twentieth Century Reanalysis to assess climate variability for the European wind industry, *Theor. Appl. Climatol*;127:61-80
10. **Bjerkseter C., and Ågotnes A., (2013):** Levelised cost of energy for offshore floating wind turbine concepts. Department of Mathematical Sciences and Technology, University of Life Sciences;206.
11. **Bosch J., Staffell I., and Hawkes A. D., (2019):** Global levelised cost of electricity from offshore wind, *Energy*, 189

12. **Brower M.C., Barton M.S., Lled_o L., and Dubois J., (2013):** A Study of wind speed variability using global reanalysis data, AWSTruepower
13. **Buck B.H. et al. (2017):** The German Case Study: Pioneer Projects of Aquaculture-Wind Farm Multi-Uses. In: Buck B., Langan R. (eds) Aquaculture Perspective of Multi-Use Sites in the Open Ocean. Springer, Cham
14. **Caralis G., Chaviaropoulos P., Albacete V. R., Diakoulaki D., Kotroni V., Lagouvardos K., Gao Z., Zervos A., and Rados K., (2016):** Lessons learnt from the evaluation of the feed-in tariff scheme for offshore wind farms in Greece using a Monte Carlo approach, *J. Wind Eng. Ind. Aerodyn*., 157;63-75
15. **Carvalho D., Rocha A., Gómez-Gesteira M., and Santos C.S., (2014):** Offshore wind energy resource simulation forced by different reanalyses: Comparison with observed data in the Iberian Penisula, *Applied Energy*:134:57-64
16. **Carpar T., Ayat B., Aydoğan B., (2020):** Spatio-Seasonal Variations in Long-Term Trends of Offshore Wind Speeds Over the Black Sea; an Inter-Comparison of Two Reanalysis Data, Pure and Applied Geophysics:177;3013-3037
17. **Cavazzi, S., and Dutton, A. G.(2016)**: An Offshore Wind Energy Geographic Information System (OWE-GIS) for assessment of the UK's offshore wind energy potential, Part 1, *Renew. Energy*, 87, pg. 212–228
18. **Centre for Renewable Energy Sources and Saving (CRES), (2010):** Pre-study of offshore wind farms development in Greece. Procedure and criteria for the pre-Study and First Phase Results (in Greek).
19. **Christoforaki M., and Tsoutsos T., (2017):** Sustainable siting of an offshore wind park a case in Chania, Crete, *Renewable Energy*:109;624-633
20. **Cradden L., Kalogeri C., Martinez-Barrios I., Galanis G., Ingram D., and Kallos G., (2016):** Multi-criteria site selection for offshore renewable energy platforms, *Renewable Energy*:87(1);791-806
21. **Del Jesus F., Menendéz M., Guanche R., Losada I.J., (2014):** A wind chart to characterize potential offshore wind energy sites, Computers & Geosciences;71:62-72
22. **Díaz H., and Soares G., (2020):** Review of current status, technology and future trends of offshore wind farms, *Ocean Engineering*, 209;107381
23. **Dörenkämper M., Olsen B.T., Witha B., Hahmann H., Davis N.N., Barcons J., et al., (2020):** The Making of the New European Wind Atlas, Part 2: Production and Evaluation, Geoscientific Model Development:13;5079-5102
24. **Doubrawa P., Barthelemie R., J., Pryor S., C., Hasager C., B., Badger M., and Karagali I. (2015):** Satellite wind atlas as a tool for offshore wind resource assessment: The Great Lakes Wind Atlas, *Journal in Remote Sensing of Environment*:168; 349-3593
25. **Doulvere F., (2008):** The importance of marine spatial planning in advancing ecosystem-based sea use management, *Marine Policy*, 32(5);762-771
26. **Dicorato M., Forte G., Pisani M., and Ttrovato M., (2011):** Guideliness for assessment of investment cost for offshore wind generation, Renewable Energy, vol. 36, pp. 2043-2051
27. **Ehler C., and Douvere F. (2009)**: Marine Spatial Planning: a step-by-step approach toward ecosystem-based management. In: Intergovernmental Oceanographic Commission and Man and the Biosphere Programme. IOC Manual and Guides No. 53, ICAM Dossier No. 6. Paris: UNESCO. 2009 (English).
28. **Emmanouil G., Galanis G., Kalogeri C., Zodiatis G., Kallos G., (2016):** 10-year high resolution study of wind, sea waves and wave energy assessment in the Greek offshore areas, Renewable Energy;90:399-419

29. **Ernst & Young, (2009):** Cost of and financial support for offshore wind (Report), Prepared for the Department of Energy and Climate Change
30. **Eunice Energy Group, (2019):** Aigaio Project (Report) [Last accessed: 30/09/2020]
31. **Fernandez M. L., Esteves T. C., Oliveira E. R., and Alves F. L., (2017):** How does the cumulative impacts approach support Maritime Spatial Planning?, *Ecological Indicators*, 73;189-202
32. **FOWIND, (2017):** Grid integration study for offshore wind farm development in Gujarat and Tamil Nadu, Grid Integration Report, FOWIND Consortium
33. **Frandsen S., Barthelmie R., Pryor S., Rathmann O., Larsen S., and Hojstrup J. (2006):** Analytical Modelling of Wind Speeds Deficit in Large Offshore Wind Farms, *Journal in Wind Energy*, 9, pp. 39-53
34. **Gee, K., Kannen, A., Licht-Eggert, K., Glaeser, B., and Sterr, H. (2006):** Integrated Coastal Zone Management (ICZM): Strategies for coastal and marine spatial planning: The role of spatial planning and ICZM in the sustainable development of coasts and seas. Federal Ministry of Transport, Building and Urban Affairs (BMVBS) and Federal Office for Building and Spatial Planning (BBR). Final Report, Berlin, October 2006
35. **Gerdes G., Tiedemann A., and Zeelenberg S., (2010):** Case Study: European Offshore Wind Farms – A Survey for the Analysis of the Experiences and Lessons Learnt by Developers of Offshore Wind Farms, Final Report, Deutsche WindGuard GmbH, Deutsche Energie-Agentur GmbH, University of Groningen
36. **Giannaros T. M., Melas D., and Ziomas I., (2017):** Performance evaluation of the Weather Research and Forecasting (WRF) model for assessing wind resource in Greece, *Renewable Energy*:102;190-198
37. **Gonzalesz-Rodriguez A. G. (2017):** Review of offshore wind farm cost components, *Energy for Sustainable Development*, 37;10-19
38. **González J. S., and Arántegui R. L., (2016):** A review of regulatory framework for wind energy in European Union countries: Current state and expected developments, *Renewable and Sustainable Energy Reviews*, 56;588-602.
39. **Grady, S., Hussaini M.Y., and Abdullah M.M., (2005):** Placement of wind turbines using genetic algorithms, *Renew. Energy*:30;259–270.
40. **Gruber K.**, **Klöckl C., Regner P., Baumgartner J., and Schmidt J., (2019):** Assessing the Global Wind Atlas and local measurements for bias correction of wind power generation simulated from MERRA-2 in Brazil, *Energy*:189
41. **Gusatu L. F., Yamu C., Zuidema C., and Faaij A., (2020):** A Spatial Analysis of the Potentials for Offshore Wind Farm Locations in the North Sea Region: Challenges and Opportunities, *International Journal of GEO-Information:*9(2)
42. **Hallgren C., Arnqvist J., Ivanelli S., Körnich H., Vakkari V., Sahlée E., (2020):** Looking for an Offshore Low-Level Jet Champion among Recent Reanalyses: A Tight Race over the Baltic Sea, Energies:13(14);3670
43. **Hasager C.B., Mouche A., Badger M., Bingöl F., Karagali I., Stoffelen A., Peña A., and Longépé N., (2015):** Offshore wind climatology based-on synergetic use of Envisat ASAR, ASCAT and QuikSCAT, *Remote Sensing of Environment*;247-263
44. **Ho L. W., Lie T. T. Leong P. T. M., and Clear T., (2018):** Developing offshore wind farm siting criteria by using an international Delphi method, *Energy Policy*, 113;53-67
45. **Hong L., and Moller B. (2011):** Offshore wind energy potential in China: under technical, spatial and economic constraints, *Energy*:36;4482 - 4491

46. **Hu Q., Wang Y., Xie Z., Zhu P., and Yu D., (2016):** On estimating uncertainty of wind energy with mixture of distributions, *Energy*:112:935-962
47. **Ioannou A., Angus A., and Brennan F., (2018a):** A lifecycle techno-economic model of offshore wind energy for different entry and exit instances, *Applied Energy*:221;406-404
48. **IRENA, (2012):** Renewable Power Generation Costs in 2012: An Overview (Report), International Renewable Energy Agency
49. **James, R., and Ros M.C., (2015):** Floating Offshore Wind: Market and Technology Review, Carbon Trust, Prepared for the Scottish Government
50. **Jay S. (2010):** Planners to the rescue: Spatial planning facilitating the development of offshore wind energy, *Marine Pollution Bulletin*:60;493-499
51. **Jin R., Hou P., Yang G., Qi Y., Chen C., and Chen Z., (2019):** Cable routing optimization for offshore wind power plants via wind scenarios considering power loss cost model, *Applied Energy*:254;113719
52. **Jongbloed R.H., van der Wal J.T., and Lindeboom H.J., (2014):** Identifying space for offshore wind energy in the North Sea. Consequences of scenario calculations for interactions with other marine uses, *Energy Policy:*68;320-333
53. **Kaiser M.J., and Snyder B.F. (2012):** Offshore wind energy cost modelling: Installation and decommissioning, Green Energy and Technology, vol.85, Springer
54. **Kaldellis J.K., and Kapsali M., (2013):** Shifting towards offshore wind energy – Recent activity and future development, *Energy Policy*:53;136 – 148
55. **Kausche M., Adam F., Dahlhaus F., and Groobmann J., (2018):** Floating offshore wind – Economic and ecological challenges of a TLP solution, *Renewable Energy*:126;270-280
56. **Kim T., Park Jeong-I.I., and Maeng J. (2016):** Offshore wind farm site selection study around Jeju Island, South Korea, *Journal in Renewable Energy*:94;619-628
57. **Kirchner-Bossi N., Garćia-Herrera R., Prieto L., Trigo R.M., (2015):** A long-term perspective of wind power output variability, International Journal of Climatology;35:2635-2646
58. **Kiss P., and Jánosi I.M., (2008):** Comprehensive empirical analysis of ERA-40 surface wind speed distribution over Europe, *Energy Conversion and Management*:49:2142-2151
59. **Kolios A., and Brennan F., (2018):** Review of existing cost and O&M models, and development of a high-fidelity cost/revenue model for impact assessment, Deliverable Report (WP8 - D8.1), Reducing the cost of offshore wind energy and boosting the renewables industry (ROMEO research project)
60. **Krassanakis V., Kokkali, A., and Vassilopoulou, V. (2015):** Identification of spatial interactions among human uses in a marine Region of Central Western Greece, *11th Panhellenic Symposium on Oceanography and Fisheries*, Mytilene, Greece.
61. **Lackner M. A., Rogers A. L., and Manwell J. F. (2008):** Uncertainty Analysis in MCP-Based Wind Resource Assessment and Energy Production Estimation, *Journal in Solar Energy Engineering*: 130;10
62. **Levitt A.C. , Kempton W., Smith A.P. , Musial W., and Firestone J., (2011):** Pricing offshore wind power, *Energy Policy*:39(10);6408-6421.
63. **Li H., (2006):** The impacts and implications of the legal framework for sea use planning and management in China, *Ocean & Coastal Management*:49;717-726
64. **Liléo S., Berge E., Undheim O., Klinkert R., and Bredesen R.E. (2013):** Long-term correction of wind measurements. State-of-the-art, Guidelines and future work, Elforsk report, 13:18, pp.1–94

65. **Lizuma L., Avotniece Z., Rupainis S., and Teilans A., (2013):** Assessment of the Present and Future Offshore Wind Power Potential: A Case Study in a Target Territory of the Baltic Sea Near the Latvian Coast, Hindawi Publishing Corporation, *The Scientific World Journal*:10
66. **Madariaga A., Martín J.L., Zamora I., Martínez de Alegría I., and Ceballos S., (2013):** Technological trends in electric topologies for offshore wind power plants, *Renewable and Sustainable Energy Reviews*:24;32-44
67. **Maienza C., Avossa A. M., Ricciardelli F., Coiro D., Troise G., and Georgakis C. T., (2020):** A life cycle cost model for floating offshore wind farms, *Applied Energy*:266;114716
68. **Ministry of Environment, Energy and Climate Change (MEECC), (2008):** Specific framework for spatial planning and sustainable development for renewable energy sources;JMD 49828/2008, OGHE B' 2464/3-12-08
69. **Ministry of Environment Energy & Climate Change, (2010):** National Renewable Energy Action Plan In the Scope of Directive 2009/28/EC, Greece
70. **Moller B., (2011):** Continuous spatial modelling to analyze planning and economic consequenses of offshore wind energy, *Journal in Energy Policy*:39;511-517
71. **Myhr A., Bjerkseter C., Ågotnes A., and Nygaard T.A., (2014):** Levelised cost of energy for offshore floating wind turbines in a life cycle perspective, *Renewable Energy*:66;714-728.
72. **Nagababu G., Kachhwaha S.S., and Savsani V., (2017):** Estimation of technical and economic potential of offshore wind along the coast of India, *Energy*:138;9-91
73. **Noonan M., Stehly T., Mora D., Kitzing L., Smart G., Berkhout V., and Kikuchi Y., (2018):** IEA Wind TCP Task 26 – Offshore Wind International Comparative Analysis, International Energy Agency Wind Technology Collaboration Programme
74. **Ntoka C., (2013):** Offshore wind park sitting and micro-sitting in Petalioi Gulf, Greece, Master Thesis , M.Sc. (Eng.) "Sustainable Energy Planning and Management", Aalborg University, Denmark
75. **OGG (Official Government Gazette), (2008):** Special Framework for Spatial Planning and Sustainable Development for Renewable Energy Sources and Strategic Environmental Impact Assessment. Official Government Gazette 2464 B/ 03.12.2008. "Eidiko plaisio Chorotaxikoú Schediasmou kai Aeifóroy Anaptyxis gia tis Ananeosimes piges Energias kai tis stratigikis meletis periballontikon epiptoseon aytoy». Efimeris tis Kyverniseos 2464 B/03.12.2008.
76. **OGG (Official Government Gazette), (2011):** A New Way of Issuing Building Permits, Building Control and Other Provisions. Official Government Gazette 249-A/ 25.11.2011. [Neos tropos ekdosis adeion domisis, elenchou kataskevon kai loipes diatakseis, in Greek], Efimeris tis Kyverniseos 249-A/25.11.2011. Law 4030/2011.
77. **OGG (Official Government Gazette), (2014):** Regional planning and urban planning reformation - Sustainable development. Greek Official Gazette 142-A/ 28.06.2014. [Chorotaxiki kai poleodomiki metarithmisi e Viosimi anaptyksi, in Greek], Efimeris tis Kyverniseos 142-A/28.06.2014. Law 4269/2014.
78. **Papageorgiou M., (2016):** *Marine spatial planning and the Greek experience, Marine Policy*:74;18-24
79. **Papakonstantinou K., Kardakari N., Portolou D., Ntemiri K., Papadopoulos V., and Tsipelas N., (2019):** Environmental Impact Assessment Rejection for an Offshore Wind Project proposal in 14 protected islets located in the Aegean Sea, Hellenic Ornithological Society (Report)

80. **Pascoe S., and Pembroke-Innes J. (2018):** Economic Impacts of the Development of an Offshore Oil and Gas Industry on Fishing Industries: A Review of Experiences and Assessment Methods, Reviews in Fisheries Science & Aquaculture, *Reviews in Fishery Science & Aquaculture*:26(3)
81. **Pelosi A., Terribile F., D'Urso G., Chirico G.B., (2020):** Comparison of ERA-5 Land and UERRA MESCAN-SURFEX Reanalysis Data with Spatially Interpolated Weather Observations for the Regional Assessment of Reference Evapotranspiration, Water:12(6);1669
82. **Petersen L., E., Troen L., Jorgensen E. H., and Mann J. (2014):** The new European wind atlas, Published in *Energy Bulletin*:17;34-39
83. **Prässler T., and Schaechtele J., (2012):** Comparison of the financial attractiveness among prospective offshore wind parks in selected European countries, *Energy Policy*:45;86-101
84. **Pyrgou A., Kylili A., and Fokaides P.A., (2016):** The future of the Feed-in Tariff (FiT) scheme in Europe: The case of photovoltaics, *Energy Policy*:95;94-102
85. **Ridal M., Olsson E., Unden, P., Zimmermann K., Ohlsson A., (2017):** Uncertainties in Ensembles of Regional Re-Analyses - Deliverable D2.7 HARMONIE reanalysis report of results and dataset
86. **Rodrigo J. S., Arroyo R. A. C., Moriarty P., Churchfield M., Kosovic B., et al. (2016):** Mesoscale to microscale wind farm flow modelling and evaluation, WIREs Energy Environ.
87. **Rodrigues S., Restrepo C., Kontos E., Teixeira Pinto R., and Bauer P., (2015):** Trends of offshore wind projects, *Renewable and Sustainable Energy Reviews*:49; 1114 – 1135
88. **Robak S., and Raczowski R.M., (2018):** Substations for offshore wind farms: a review from the perspective of the needs of the Polish wind energy sector, *Bulletin of the Polish Academy of Sciences-Technical Sciences*:66(4)
89. **Rose S., and Apt J., (2016):** Quantifying sources of uncertainty in reanalysis derived wind speed, *Renewable Energy*:94:157-165
90. **Salvacão N., and Soares G., (2016):** Resource Assessment Methods in the Offshore Wind Energy Sector, In: Castro-Santos L., Diaz-Casas V. (eds) Floating Offshore Wind Farms, Green Energy and Technology. Springer, Cham:122-141
91. **Schwanitz V.J., and Wierling A., (2016):** Offshore wind investments – Realism about cost developments is necessary, *Energy*:106;170-181
92. **Sempreviva, A.M., Barthelmie, R.J., and Pryor, S.C., (2008):** Review of Methodologies for Offshore Wind Resource Assessment in European Seas, *Surv. Geophys*;29:471–497
93. **Shaffiee M., Brennan F., and Espinoza I.A., (2016):** A parametric whole life cost model for offshore wind farms, *Int. J. Life Cycle Assess*.:21;961-975
94. **Soares-Ramos E.P.P., Oliveira-Assis L., Sarrias-Mena R., and Fernandez-Ramirez L.M., (2020):** Current status and future trends of offshore wind power in Europe, *Energy*:202
95. **Spiropoulou I., Karamanis D., and Kehayias G., (2014):** Offshore wind farms development in relation to environmental protected areas, *Sustainable Cities and Society*:14;305-312
96. **Spyridonidou S., Vagiona D.G., and Loukogeorgaki E., (2020):** Strategic Planning of Offshore Wind Farms in Greece, *Sustainability*:12(3);905
97. **Stamoulis K.A., and Delevaux J.M.S., (2015):** Data requirements and tools to operationalize marine spatial planning in the United States, *Ocean & Coastal Management*:116;214-223

98. **Stelzenmuller V., Lee. J., South. A., and Rogers. S., (2010):** Quantifying cumulative impacts of human pressures on the marine environment: a geospatial modelling framework. *Marine Ecology-Progress Series:*398;19-32.
99. **Topham E., and McMillan D., (2017):** Sustainable decommissioning of an offshore wind farm, *Renewable Energy*:102;470-480
100. **Torralba V., Doblas-Reyes F.J., and Gonzalez-Reviriego N.G., (2017):** Uncertainty in recent near-surface wind speed trends: a global reanalysis intercomparison, *Environ. Res. Lett*:12
101. **Tsilimigkas G., and Rempis N., (2017):** Marine spatial planning and spatial planning: Synergy issues and incompatibilities. Evidence from Crete island, Greece, *Ocean & Coastal Management*:139;33-41
102. **Vagiona, D. G., and Karanikolas, N. M. (2012):** A multicriteria approach to evaluate offshore wind farms sitting in Greece, *Glob NEST J*:14; 235–243
103. **Voormolen J. A., Junginger H. M., and van Sark W.G.J.H.M., (2016):** Unravelling historical cost developments of offshore wind energy in Europe, *Energy Policy*:88;435-444
104. **Wang Y. H., Walter R. K., White C., Farr H., and Ruttenberg B., (2019):** Assessment of surface wind datasets for estimating offshore wind energy along the Central California Coast, *Renewable Energy*:133:343-353
105. **Weaver T., (2012):** Financial appraisal of operational offshore wind energy projects, Renewable and Sustainable *Energy Reviews*:16(7): 5110-5120.
106. **Winter C., Halpern B.J., and Kappel C.V., (2012):** Ecosystem service tradeoff analysis reveals the value of marine spatial planning for multiple ocean uses, *PNAS*:109(12);4696-4701
107. **Xiang X., Merlin M.M.C., and Green T. C., (2016):** Cost analysis and comparison of HVAC, LFAC and HVDC for offshore wind power connection, *12th IET International Conference on AC and DC Power Transmission (ACDC 2016)*, Beijing, 2016, pp. 1-6
108. **Zhang J., Draxl C., Hopson T., Monache L., D., Vanyve E., and Hodge B.M. (2015):** Comparison of numerical weather prediction based deterministic and probabilistic wind resource assessment methods, *International Journal in Applied Energy*:156;528-541

# 3. Literature review

## 3.1 GIS in Offshore Wind Farm Site Prospecting and Planning

During the last two decades, the use of GIS for the renewable energy technologies, and specifically for OWFs, has become relatively common. Considering some OWF planning technical aspects linked with the GIS utilities, researchers, planners and developers employed GIS at numerous stages, from screening processes to identify suitable areas, down to the micro-siting level of designing WTs arrays and detailed cable layouts. GIS allow managing, monitoring, mapping, measuring, modelling and interpreting data in order to understand relationships, patterns, and trends for current adjustments or further forecasting. Thus, GIS applications consist of an irreplaceable tool for the entire OWF pre-planning or even installation procedures and operation and maintenance processes.

The first attempts to assess the physical, technical and economic characteristics of a marine area through GIS as a key management tool mainly started in the North and Baltic Sea. Denmark, for instance, has carried out an integrated mapping framework to determine optimal areas (Moller, 2011). Similarly, in the UK, the Crown Estate[7] carried out a GIS-based effort for Round 1 and 3 projects to identify potential areas, considering technical and environmental characteristics and constraint factors etc. (Jay, 2010). Moreover, for the North and Baltic Sea, the WINDSPEED program was established (Schillings et al. 2012), a Decision Support System (DSS) to clarify potential OWE costs among other environmental and socio-economic parameters. Upon this framework, additional research efforts for analytical OWE cost evaluation were applied such as the SCREAM (Spatially Continuous Resource Economic Analysis Model) by using raster-based GIS structures and considered numerous geographical factors, technology and cost data as well as planning information (Moller, 2011; Hong & Moller 2011; Moller et al. 2012). A similar effort developed by Cavazzi and Dutton (2016) in order to identify the economically accessible offshore wind energy resources for the United Kingdom through the UK OWE-GIS. Outside Europe, similar studies have been conducted and significant results have been produced for China (Hong & Moller 2011; 2012), Japan (Abudureyimu et al., 2012), South Korea (Kim et al. 2013), India (Nagababu et

[7] The Crown Estate is constituted as a statutory corporation under the Crown Estate Act 1961. The Crown Estate's public function is to: invest in and manage certain property assets belonging to the monarch; and remit its revenue surplus each year to the Exchequer.

al. 2017), Egypt (Mahdy & Bahaz, 2018) and the US (Musial & Ram, 2010; Dvorak et al., 2009; Mekonnen & Gorsevski, 2015).

For the Mediterranean region, multiple studies have been conducted for Portugal (Castro-Santos et al., 2013), Italy (Beccali et al., 2015) and Greece (Vagiona and Karanikolas 2012; Ntoka 2013; Vagiona & Kamilakis 2017, Vagiona & Kamilakis 2019), which constitute the first efforts to allocate space for OWF development near-shore or offshore without using analytical cost expressions. Key parameters of these GIS-based models incorporate the major capital and financial components, foundation cost dependent on water depth and transmission and O&M cost in accordance with the distance from nearest ports or grid connection points. On top of these efforts, numerous studies have been conducted on the estimation of the wind resource potential among other parameters for the Mediterranean Sea and the Greek marine areas accordingly (Kotroni et al., 2014; Soukissian & Papadopoulos 2015; Soukissian et al., 2016; Giannaros et al., 2017).

Reviewing the spatial analysis methods used in these studies, Multi-Criteria Analysis (MCA) or spatial distribution mapping approaches are mostly applied. Although these efforts can play a key role in planning and decision-making procedures, they can be described as spatial multi-criteria evaluation frameworks. Thus, they are sensitive and highly dependent on the decision-makers' preferences and conflicting objectives. OWF planning procedures deal with techno-economic, environmental and social criteria by incorporating numerous spatial and non-spatial data. Consequently, a relevant number of alternate optimal scenarios may occur, that most of the times are disregarded in MCA tools. As an alternative, Malczewski & Jankowski, (2020) highlighted the efficiency of GIS-based multi-objective optimization tools to deal with spatial heterogeneity, contradictive objectives and preference information. Thus, combining spatial and preference data, defining contexts and spatio-temporal scales, quantifying uncertainties and effectively visualizing multi-objective spatial problems and solutions is of paramount importance in the emerging GIS science and decision-making.

Focusing on the spatially explicit cost assessment models, simplified cost expressions are mostly established for reproducing the spatial distribution of an OWF's sub-cost components. For example, Möller, (2011), Kim et al. (2013), Cavazzi and Dutton, (2016), Cradden et al., (2016),

Nagababu et al., (2017) and Mahdy and Bahaz, (2018) assumed fixed WTs costs irrespectively of the sea depth, the foundation type or the met-ocean characteristics. For the foundation cost, mostly fixed-foundation technologies are considered, and cost calculation expressions are mostly related to the sea depth without considering structures complexity and analytical installation cost estimations, rather than a per cent approximation proportional to the total foundation cost. However, Cavazzi and Dutton, (2016) introduced the first analytical expressions to approximate the spatial distribution of the installation cost for both the WTs and the foundations accordingly. In terms of the transmission cost estimation, distance approximation and accurate paths delineation consist of the most crucial cost factors affecting both manufacturing and installation expenses. Results for the transmission cost estimation indicate that mostly Euclidean distances (i.e. the straight line connecting two points) are used, leading to noticeable transmission cost underestimations. On top of that, the total transmission cost (i.e. export, inter-array cables, substations etc.) equations are mainly based on the distance from the onshore grid, accounting for the cost of the export cable. Relative inter-array cables and integration system cost are transferred as a fixed value proportional to the overall transmission cost. Similarly, for the O&M cost, distance from the nearest ports is determined in terms of the Euclidean distance, resulting to reduced maintenance expenses approximation.

On the contrary, when the site assessment procedures account for the estimated energy yield (in terms of the AEP), the mean wind speed or the wind power density is used. Particularly, Möller, (2011), Kim et al., (2013), Cavazzi and Dutton, (2016), Nagababu et al., (2017) and Vasileiou et al., (2017) acquired mean wind speed data from national wind atlases or reanalysis data in order to extract the Wind Power Density (WPD). Moreover, Yamagutchi and Ishihara, (2017), by applying a superimposition GIS-based interpolation scheme, extracted the energy yield and the capacity factors using offshore in-situ and reanalysis data. However, the wind speed and wind power variability among with multiple scenarios generation for future wind power estimates is lacking when spatially-explicit multi-criteria assessments are performed.

Considering more sophisticated and integrated frameworks, a few research efforts and sector-specific spatial models have been implemented during the last two decades. The first holistic attempt applied with Opti - OWECS program for the Baltic and North Sea. Simplified cost

models were combined with GIS in order to extract optimal areas for OWF siting, before a more in-depth assessment and further optimization processes, focusing on the structural and economic optimization of the selected OWF components (Cockerill et al., 2001). Furthermore, integrated studies have been conducted for the Netherlands, based on a GIS-based multi-objective optimization model, considering economic objectives and environmental constraints (Punt et al., 2009). Finally, a Web Based Participatory GIS (PGIS) system was established for the United States, as a multi-objective evaluation process, in order to extract the most promising areas for OWF siting, according to the users' preferences (Mekonnen & Gorsevski, 2015).

Focusing on the key characteristics of the aforementioned GIS-based studies, the following outcomes are highlighted: i) they are mostly rely on MCA frameworks based on simplified cost and energy-related indicators in terms of the suitability assessment and the siting alternatives, ii) spatially-explicit integrated and robust cost models are lacking in terms of the distance-based cost approximation i.e. transmission, installation and O&M cost and iii) wind power potential is extracted in accordance with the mean wind speed data or using the Weibull (or Rayleigh) distribution. Hence, some perennial challenges are still unexplored for incorporating and understanding both the spatial and temporal nature of OWE systems, not only considering cost and energy-related parameters, but also the geographic ones.

Spatio-temporal modelling has recently started to emerge and evolve, thus, developments in key fields such as high-performance computing applications and big data analysis allowed either to improve the models and validate them as also to create geospatial tools with minimized uncertainties and spatial simplifications. These challenges have already noticed by Resch et al. (2014) and reaffirmed by Camaro and Stoeglehner, (2018) and will be extensively discussed in Sections 3.2-3.3. The aforementioned challenges were seen as a breakthrough in GIS science, which could contribute to redefine the complex trade-offs of environmental and socio-economic issues in a tractable way, using alternate multi-objective analysis and optimization models. However, limitations still exist in terms of the data types used, software and hardware able to manage the relative spatial and non-spatial information and more integrated approaches to reproduce real word problems in a more systematic and accurate manner.

## 3.2 GIS and cost modelling using Least-Cost Path algorithms

Considering the distance-based cost indicators, already highlighted in the previous section, numerous models have been developed using GIS data structures. Finding optimal paths is a useful application in GIS and this topic gained attention in many other research fields such as environmental conservation, cartography, artificial intelligence and robotics, civil engineering and computer science. Nowadays, many commercial and open-source GIS platforms use Least-Cost Path (LCP) algorithms, however, simplified models are used with limited capabilities (Antikainen, 2013; Etherington, 2016). Algorithms' selection, multi-objectivity, obstacles avoidance, straightness and curvature control are some of the issues avoided in most of the traditional GIS platforms, mostly for computational efficiency reasons as long as graph-based network models are time-consuming.

From a theoretical point of view, in order to calculate optimal paths across a surface (referred as a resistance or cost surface), the discrete raster cells are converted into a lattice graph. The centroids of the cells (excluding NoData) become the graph's nodes, and the associated edges are formed connecting the orthogonal or diagonal neighbor nodes. There are three main network problem types, linked to the weights (resistances) to each node or edge that can be assigned. The first is the simplest, where costs are related to the node location, but are the same for all directions (Douglas, 1994), called isotropic. In spite the fact that many pathfinding problems can be solved using isotropic surfaces, the approach is limited to problems where the cost of movement is the same for all directions (Stefanakis & Kavouras, 1995). The second network problem type refers to the costs that are related to the direction, however, this anisotropic condition considers one prevailing direction over the entire surface. Lastly, network problems that can be solved by algorithms like Dijkstra may be of a third type, where costs of movement are entirely anisotropic. Thus, costs are varying over the surface and are direction dependent, but without any specific prevailing direction (Collischonn & Pillar, 2000).

Potential uses include travel planning, service management, location-allocation studies, road construction and irrigation systems, pipeline routing, among others. Multiple objectives were considered by several authors when selecting optimal paths, including environmental,

physical, regulatory, technical and economic parameters. For example, Stefanakis and Kavouras (1995) charted the shortest sea courses connecting offshore areas and ports under various models of travel costs whereas Zhou et al. (2011) developed a pathfinding algorithm for robots' navigation. Roadway planning models have been implemented based on spatial distances and anisotropic surfaces (Collischon & Pilar, 2000) or extreme slopes identification and directional constraints (Yu et al. 2003). Additionally, many efforts are focused on power transmission line routing based-on dynamic programming algorithms (Monteiro et al. 2005) or graph-based LCP algorithms (Ahmadi et al. 2008; Bagli et al. 2011). Moreover, graph-based models have been conducted for pipeline routing in the presence of obstacles, applying in parallel smoothing techniques (Kang & Lee 2017; Durmaz et al. 2019) or using genetic algorithms (Baioco et al. 2018). Finally, alternate implementation can be found for drainage basin analysis (Douglas, 1994), ecological conservation (Etherington, 2016) or animals' movement (Benhamou, 2004; Almeida, 2010).

A fundamental step from the emerging Movement Theory, and as a consequence in LPC algorithms, is the description of movement paths in terms of their straightness. The most widely known characteristic used to characterize and analyze movement paths is tortuosity (or sinuosity), and a variety of alternate indices have been proposed in many different research fields such as hydrology (rivers sinuosity) and cartography (fractal dimension of geographic objects) (Almeyda et al. 2010). These indices consist of the: i) Straightness Index (SI) expressed as the quotient of the Euclidean distance (between starting and end point) to the total path length; ii) Sinuosity Index (SI), derived from the mean step length, the mean cosine and sine of the turning angles and the coefficient of variation of the step length; iii) Mean Squared Displacement (MSD) expressed by the cartesian coordinates' trajectory change from the path; iv) Intensity Use (IU) calculated as the quotient of the total path length to the total area of movement and finally; v) the Fractal Dimension (FD) measured by propensity of a set of two points (as a curve) to cover the plane and is expressed by the slope extracted from the log-log plot of the ruler and the path length with a slope equal to 1 – F (Benhamou, 2004; Almeida, 2010). Previous studies have been extensively examined turns or angles prohibition and penalization as a constrained problem in both graph networks (Boroujerdi and Uhlmann 1998; Gutiérrez and Medaglia 2008) and grid-

based heuristic search implementations (Yakovlev et al. 2015). In addition, Winter (2002) defined and investigated an analytical model that handles cost of turns in different route planning scenarios, as also, Choi et al. (2009) considered the minimization of existence of curves upon an already established road network for optimal haulage routes of dump trucks. Nevertheless, these approaches either examine straightness as a single objective or as part of a multi-objective problem but in a limited spatial extend, mainly due to computational complexity reasons. Considering the geographical context, these studies can be linked with the angle or direction constraints in LCP algorithms for a 'fair' route or path, however, without extensively assessing the straightness of the resulted paths or even embedding the straightness as an objective to the optimization process.

Considering another spatial limitation in LCP models, most of the pathfinding algorithms generate paths consisting of straight lines and sharp turns that in most routing applications (e.g. cables or pipelines and shipping lanes routing) do not correspond to the reality. Indeed, the initial paths generated by LCP algorithms like Dijkstra usually do not satisfy the requirement of a "smooth" path considering that all the applications mostly work based on discrete surfaces. To address this problem and considering mostly continuous space many smoothing techniques have been tested focusing on polynomial interpolation, cubic and B-splines, Bezier and NURBS curves, implemented on robots' navigation (Zhou et al. 2011) and autonomous vehicle routing (Choi et al. 2008; Berglud et al. 2010) for computing obstacle-avoiding minimum curvature paths. On the other hand, it is emphasized that B-Splines and Bezier curves can lead to 'fairer' and faster smoothed lines or trajectories, although the control vertices must be found along the entire curve, which can be quite complex when considering discrete surfaces (Kang & Lee 2017; Ravankar et al. 2018). Nevertheless, it is very tough to ensure that the so-called 'smoothed' curve does not touch any possible obstacles as long as the optimized line path retains the same movement cost upon the discrete cost surface. Therefore, pipeline routing in the presence of obstacles and Laplacian smoothing technique is applied by Kang and Lee (2017) because of its simplicity and algorithms' time effectives to solve the problem.

As a concluding remark, some of the most important algorithms and paths' spatial characteristics were reviewed and analyzed in this section. Some key findings from already

existing LCP models mainly lie on the lack of integrated multi-objective approaches, in terms of the spatial attributes discussed above, upon real case scenarios. Novel and robust frameworks have been already established and tested for both their computational efficiency and the spatial attributes, embedded as objectives in graph-network problems. However, the aforementioned models are either used in limited spatial extents or by partially handling some of these attributes (i.e. straightness, curvature, multi-objectivity etc.).

## 3.3 Offshore Wind Farm siting and spatial optimization models

Having reviewed all of the critical aspects for OWE deployment in terms of the GIS-based cost and energy assessment and modelling, one last step remains focusing on the incorporation of the spatio-temporal information in a holistic optimization framework for OWF site-prospecting. According to Doulvere, (2008), "*Offshore wind economic sector, to remain economically viable, have to develop and function sustainably as well*". To achieve that, the wide range of variables, parameters and constraints, already highlighted in the previous sections, must be embedded in a rigorous and systematic spatial optimization scheme.

Considering spatial modelling and planning, multiple approaches for defining and assessing alternative options encompassing multi-criteria analysis (MCA) and overlay superimposition were reviewed in Section 3.1. Although these efforts produced significant results in location-allocation planning and management, multi-objective spatial optimization models may play a pivotal role on defining efficient and sustainable planning alternatives. Spatial optimization models have been extensively used as a prescriptive tool in numerous fields including land-use management, site-prospecting of public facilities, nature conservation or finding minimum paths (see Section 3.2). In addition, alternate optimization techniques are embedded in spatial optimization problems such as the Pareto optimality (Aerts et al 2005;Santé-Riveira et al 2007; Stewart & Janssen 2014; Sahebgharani, 2016) and goal programming approaches (Ligmann-Zielinska 2008; Billionnet, 2012; Liu & Kao 2012; Beyer et al 2016).

Accordingly, in the case of RES, and particularly for OWF site prospecting and WTs configuration, relevant research efforts can be found, although, the formulation of the spatial

problems is described by different methodological tools and for different planning and engineering purposes. In particular, most of these techniques are mostly applied on wind turbine level siting approaches and their layout configuration through wind distribution and power assessments, wind deficits analysis (wake effects[8])and interconnection cables (inter-array cables) cost minimization, or both of them (Valverde et al., 2014; Hou et al., 2019). Key parameters of these optimization algorithms are to maximize wind power production and minimize transmission cost into a given area, combining the optimum number of WTs and the array density (Katic et al., 1986; Mossetti et al., 1994). Due to the complexities of the wind flow within an OWF, all micro-siting models use heuristic approaches to optimize WTs placement (Elkinton et al. 2008; Valverde et al. 2014; González et al. 2014) or mixed heuristics and goal programming techniques (Perez et al. 2013). Similarly, González et al. (2010) used evolutionary algorithms, where the configuration of the WTs layout was optimized based on a cost model. Finally, Wan et al. (2012), optimized the layout of a wind farm considering continuous space and using particle swarm optimization (PSO) techniques.

Furthermore, some really challenging holistic projects such as the OWECOP (Elkinton et al., 2004) and OWFLO (Kooijman et al., 2011) developed over the last two decades based on GIS and multi-objective optimization models for site prospecting and assessment purposes as also for WTs micro-siting configuration using efficient cost and structural design optimization models accordingly. On top of these efforts, Jones and Wall (2015), using goal programming and decision-making methods tried to allocate potential areas for OWF siting. Their model examined both of the energy production and the associated costs embedded in a multi-objective optimization framework subject to environmental, social, technical, and economic aspects. However, their framework focused on specific selected sites (9 proposed areas) for OWE deployment in the UK. Finally, Mytinou and Kolios (2017), demonstrated the effectiveness of a robust optimization process and extracted satisfactory outcomes for the most suitable and cost-efficient OWFs locations in the UK. A comparison has been made among three state-of-the-art algorithms

[8] WTs extract energy from the wind and downstream there is a wake from the WT, where wind speed is reduced. As the flow proceeds downstream, there is a spreading of the wake and the wake recovers towards free stream conditions.

(NSGAII, NSGAIII and SPEA2) but similarly with the research of Jones and Wall (2015), their approach was tested among already selected areas for future OWFs site prospecting.

Although the these models are based on robust and efficient optimization algorithms, they are mostly based on either micro sitting purposes or for trade-offs quantification between the energy generation and the associated cost. In order to proceed on a "*tabula rasa*" site prospecting approach upon discrete surfaces (rasters), it is important to analyze some terms and spatial issues such as the "*compactness"* and *"contiguity".*

Compactness is characterized as an indicator that belongs to the spatial optimization analysis which in turn applies diverse analytic and computational techniques involving geographical objects (cells, lines, points, areas-cells) (Liegmann-Zielinska et al., 2008; Cao et al., 2012). In general, compactness describes the shape and the level of fragmentation among spatial units. Consequently, in order to obtain a compact area, contiguity among spatial units must be guaranteed i.e. neighbored geographical objects must be connected to each other (Santé-Rivera et al., 2008). These spatial indicators are mostly applied in land-use allocation models and natural reserves or ecological features assessment and modelling. In terms of the methods used to control compactness and contiguity, spatial optimization approaches are separated in two types as i) solution-based and ii) explicit constraint-based (Ligmann-Zielinska et al. 2008). Several techniques have been already implemented to calculate and control compactness, but the most common and effective methods are: i) the Integer Non-Linear Programming (INLP neighbor method) where compactness is modelled as a convex-quadratic function (Gabriel et al. 2006), ii) Integer Linear Programming (ILP neighbor method and minimization of shape index) (Kao & Lin 1996; Cao et al. 2012; Liu & Kao, 2013) where compactness is handled as a single objective, iii) ILP using buffer zones cells where the compactness is embedded as a constraint factor of the minimal buffer zone (Williams & ReVelle, 1996), iv) ILP using aggregated blocks where compactness is solved through the objective function (Aerts et al. 2003) and finally v) Spatial autocorrelation (Moran's method) where compactness is quantified as a spatial autocorrelation measure between -1 and 1 (Cao & Bo, 2010).

Similarly, contiguity can be explicitly structured as a spatial optimization problem or implicitly accounted for in a solution algorithm. The former approaches are based on graph theory

imposing network nodes connectivity (Williams, 2002; Datta et al. 2012; Billionnet, 2013). Williams (2002) examined contiguity using a dual-graph representation in order to prevent the formation of loops searching for continuous cells, however the algorithm's computational efficiency was relative to the size of the problem (i.e. the number of the initial cells). This problem was addressed by employing solely graph-based concepts combined with mixed integer programming (MIP) algorithms. In these approaches alternate implementations formulated contiguity constraints based on network flows (Shirabe 2005) or as a network partitioning problem (Datta et al. 2012) rather than utilizing paths and spanning trees. Duque et al., (2011) and Önal et al., (2006) forced contiguity by applying different models (Tree, Order and Flow based) using different sub-tour elimination functions (embedded as constraints) in the sub-graph when selecting nodes and arcs, however, compactness was not incorporated as an explicit criterion. The hybrid graph-based and MIP formulations were proved to be effective by employing cycle-breaking constraints, however, they have led to large and computationally difficult models (Önal et al., 2016).

For this reason, according to previous studies (Ligmann-Zielinska et al. 2008; Oehrlein & Haunet, 2017), ensuring connectedness of spatial units within an optimization model, tends to require a large number of constraints and variables explicitly devoted to the contiguity control, as a result, mostly graph-based models are established. All of the aforementioned research efforts are limited in applications with small spatial extents (i.e. a few decades or hundreds of pixels) or dedicated to serve specific tasks for particular land-use management problems. On the contrary, implicit or solution-based models examine contiguity as a not mathematically formulated part of the model rather than a necessary property. That being the case that Önal and Wang, (2008) suggested a cutting plane constraint (referred as Dantzig cuts) in order to eliminate sub-tours by ensuring optimal solutions' contiguity as an iterative check of sequential linear constraints. Similarly, Carvahal et al., (2015) and Oehrlein and Haunert, (2017) ensured contiguity using a cutting-planes scheme (i.e. a separation algorithm). In this manner, they reduced parts of the solution's space feasible region for a spatial aggregation modelling scheme, however, without examining compactness criteria. A key disadvantage of exact models, as NP-hard problems,

mainly lies on the computational effort needed to examine all feasible solutions, however, they consist of a solid alternative when they are combined with sophisticated optimization software.

As a concluding remark, heuristic and dynamic programming algorithms are extensively used throughout the literature in the wind industry. However, all the efforts reviewed in this section are focusing on either onshore wind projects or trade-offs assessment for pre-defined offshore areas as also, on micro-siting configurations of these systems. The lack of holistic spatial optimization approaches in order to control and evaluate numerous spatial properties and relationships among with spatially-explicit cost and energy indicators is highlighted. Solving multi-objective problems is inherently more difficult compared to single-objective approaches. Consequently, research on how to simultaneously model multiple-objectives, by optimizing in parallel contiguity and compactness for site-prospecting purposes, remains a challenging task.

## 3.4 Offshore wind resource assessment and stochastic modelling

According to Camargo & Stoeglehler, (2018), the promotion of sustainable and efficient support-schemes for RES penetration cannot be supported with solely GIS-based spatial models and assessment frameworks as already stated in Sections 3.2-3. Therefore, the full or even the partial integration of the temporal component in GIS-based models is a necessary further step. One of the key challenges occurs in both spatio-temporal GIS modelling, as also in offshore wind industry, is how to handle, model and evaluate spatio-temporal data. Consequently, the need of data models defining a minimal set of data types embedded in simple but efficient spatial analysis techniques, able to represent different kinds of spatio-temporal information is vital. Focusing on the wind-related applications, reanalysis data consist of a continuous and spatially complete information for wind energy modelling approaches. With either the technological and computational improvements during the upcoming decades, reanalysis data will play a pivotal role in wind resources modelling, exceeding reduced uncertainties and inaccuracies. However, for an efficient assessment and modelling scheme, both probabilistic and statistical properties of wind are considered as critical for site-prospecting purposes and uncertainty quantification. In this section, the above-mentioned characteristics are reviewed and discussed along with the

challenges occur in the field of the wind resource probabilistic and statistical assessment subject to an efficient and robust stochastic modelling scheme.

A key component for analytical and accurate wind resource assessment is to select the appropriate marginal and dependence structure for wind speed simulation and wind energy potential quantification. The most widely used probabilistic models for the characterization of mainly short-term wind speed time series is the two-parameter Weibull distribution (W2) or even the special case of the one-parameter Rayleigh (RAY) distribution (related to the W2 for shape parameter equal to 2) (Carta et al. 2009; Morgan et al. 2010; Hu et al. 2016; Jung & Schindler 2019). In their research, Carta et al. (2009), compared the W2 probability density function to 12 other distribution models and found that W2 has several advantages in terms of its flexibility and accuracy. However, the W2 distribution cannot achieve high accuracy results for all the wind regimes, such as those with high percentages of very low wind speeds or wind regimes with bimodal probabilistic characteristics. Therefore, additional suitable PDFs may be selected for different spatial domains in order to minimize errors in the wind speed and wind power estimation as long as for long-term data assessment, multi-parameter distributions seem to have a better fitting performance. For example, Morgan et al. (2011), Jung and Schindler (2019) and many others have noticed that under different wind regimes, multi-parameter distributions may fit wind time-series better. Consequently, other distributions used to characterize onshore and offshore wind speeds including the 3-parameter Generalized Gamma (GG), 3-parameter Beta, Kappa, Wakeby, Burr III and Burr–Generilized Extreme value distributions, providing an enhanced fitting accuracy in both observational (Lo Brano et al. (2011); Chioco and De Falco (2016); Jung et al. 2017) and reanalysis (Kiss & Janosi, 2008; Mert & Karakus 2015; Jung & Schindler, 2017) time series data.

Focusing on the Mediterranean region, specifically, for the Greek marine areas numerous studies have been conducted using W2 and RAY distribution (Kotroni et al. 2014; Soukissian et al. 2007; 2008; 2015; Giannaros et al. 2017) or other multi-parameter distributions like Wakeby and Kappa (Soukissian, 2013). In most of the these studies, the results indicate that the W2 distribution and comparisons with the RAY, lognormal, Gamma and inverse Gaussian distributions are sufficient for short-term data. However, all of the aforementioned studies using the W2 or

REY distribution are based either on a limited number of samples from confined geographic regions and short-term data or often explain that the better fits of the mixture models consist of a unique exception to the rule. As a result, for a reliable assessment and long-term evaluation of the wind frequency distribution, additional probabilistic assessment models and frameworks must be considered (Bett et al. 2017).

Moreover, statistical information about the wind speed PDF is also important for the assessment of wind energy potential and as a result for site-selection of potential OWFs (Morgan et al. 2010; Salvacao & Soares, 2016). Morgan et al. (2010) stated that the wind speed PDF is of paramount importance in estimating energy production for a specific wind turbine design and site prospecting campaign. According to recent research (Masseran et al. 2012; Hrafnkelsson et al. 2016), the largest uncertainty in the estimation of the energy output lies also on the optimal choice of wind speed parent distribution. In numerous studies, the assessment of the wind power density has been derived mainly from the W2 distribution. However, and similarly for the wind speed assessment, multi-parameter distributions tend to minimize the errors on the estimated wind power production, mainly due to the additional flexibility for an enhanced fitting performance in extreme wind speeds (Carta et al. 2009; Morgan et al. 2010; Soukissian 2013; Hu et al. 2016; Jung & Schindler 2019).

An extensive review, focusing on wind energy estimation methods, was provided by Carta et al., (2009), where the authors describe and analyze various approaches. Considering the calculation of the annual energy production (AEP), distributions similar to the W2 often result to less accurate results and tend to underestimate the AEP. In addition, Bensoussan et al. (2012) analyzed the process of calculating the AEP with a focus on the estimation uncertainty and concluded that the applied methods tend to overestimate AEP by roughly 9% in a single year simulation, and roughly 4% in the entire operational lifespan of an OWF. Similar to the uncertainties produced in wind power estimations, the extreme values analysis is of paramount importance and the selection of a less accurate model may lead to significant errors, especially in the estimation of the upper and lower wind energy power output quantiles (Chiodo & De Franco, 2016). Generally, probabilistic distribution models, depending on their tail behavior, can be categorized in heavy-tailed and light-tailed distributions (Neratzaki & Papalexiou, 2019). In order

to accurately assess the tail behavior, several methods exist focusing on graphical methods (log-log, generalized Hill ratio and mean excess plot) and Peak Over Threshold (POT) using the generalized Pareto distribution. These methods have been less applied in wind resource assessments and may provide additional vital information in decision making and model selection procedures (Neratzaki & Papalexiou, 2019).

In addition to the probabilistic properties, climate variations at multiple time scales should also be taken into consideration for an integrated RES exploitation. Offshore winds are typically characterized by diurnal, monthly, seasonal and inter-annual variation (IAV). As a result, knowing that the wind power is proportional to the third power of the wind speed, small fluctuations in wind speed may lead to significant differences in the extracted power output in both short and long-term periods (Kirchner-Bossi et al., 2014; Wang et al., 2019). According to Wang et al., (2019), during the previous years, research efforts have sparsely examined daily, seasonal or even long-term cycles at increased spatial extents and heterogeneous spatial datasets (i.e., reanalysis data). Moreover, the authors claim that temporally-averaged wind speeds (daily or monthly mean) utilization can lead to increased errors in energy production estimates, mostly due to the variance differences from short-term to long-term time scales. In this context, Suomalainen et al., (2012) denoted the necessity for new practices to be developed for wind's periodicities characterization for both assessment and stochastic generation purposes. On the contrary, at coarse time scales (annual or inter-annual), many studies have verified the presence of a long-range dependence. Studies analyzing wind power long-term variability patterns have been conducted for the broader areas of the US (Pryor et al., 2012), the Baltic Sea (Lizuma et al., 2012), the Eastern Europe (Kirchnner-Bossi et al., 2015), Greece (Soukissian et al. 2017) and the Black Sea (Carpar et al., 2019). Results of these studies highlight a 2-4% difference in the energy content for the middle of the 21$^{st}$ century, 4-30% difference for the Eastern Mediterranean Sea for the period 1995-2009, approximately 5% differences for the Western Mediterranean and East Atlantic area during the period 1871-2009 and finally, for the Black Sea occurred differences exceed in some cases a 30% for the 1979-2016 period. Overall, according to Pryor et al., (2012) the inter-annual variability differences contribute "*anywhere between 10 % and 25 %*" of the overall uncertainty in a wind project energy yield for a 10- year period.

In order to reproduce the aforementioned variations, the long-term persistence (LTP) is typically used. LTP consists of a measure which can be determined: i) directly from the data, however, missing data occurrences lead to underestimation of the actual persistence, ii) by the wind speed duration curves and finally iii) using the autocorrelation function (ACF) or iv) conditional probabilities (Scholz et al., 2014). An alternate method was proposed by Koutsoyiannis (2000), expressed through the Hurst coefficient (*H*) and the slope of the so-called climacogram function (i.e., the rolling variance of a process at continuous time scales). A key prerequisite for analyzing the Hurst-Kolmogorov dynamics is the acquisition of time series exceeding long time period records, in order to be able to detect multiple time scales variance (i.e. 5, 10 or even 100 years). Particularly, the long-term dependence structure of the wind process (referred as a Generalized Hurst-Kolmogorov-GHK process), can be described through the climacogram function, i.e., the variance of the mean process vs. time scale, denoted as $\gamma$ ($m^2/s^2$) (Equation 3.3.1). The justification for the use of climacogram compared to the autocorrelation function or power spectrum can be seen in Koutsoyiannis et al., (2018) proving that the climacogram has a lower statistical uncertainty from other stochastic tools. Consequently, the long-term persistent behavior of wind is expressed by the standardized GHK model:

$$\gamma = \lambda/(1 + k/q)^{2-2H} \tag{3.4.1}$$

where $\lambda = (1 + 1/q)^{2-2H}$ is the standardized variance of the discretized stationary process, $q$ is the shape parameter distinguishing the short-term from the long-term behavior, and $H$ is the Hurst parameter. The literature for wind-related Hurst-Kolmogov processes assessment is limited, thus, previous research efforts have been conducted by Bakker and van den Hark, (2012) for estimating the persistence and the associated trends in geostrophic wind speeds for wind energy yields in Norther Europe among with Dimitriadis and Koutsoyiannis, (2015) and Deligiannis et al., (2016) using the climacogram function as the second order dependence structure of a wind process for stochastic simulation purposes.

### 3.4.1 Offshore wind stochastic simulation

Nowadays, in the absence of long-term offshore wind in-situ records is critical to obtain robust wind speed and power output synthetic simulations by preserving the wind speed characteristics. To generate such wind speed synthetic time series, it is necessary to select and consider the optimal marginal dependence of wind speed as well as the diurnal, seasonal or even inter-annual wind speed intermittency while explicitly preserving the long-term persistence. Considering the long-term planning window for a potential OWF, several statistical methods exist in the literature that attempt to simulate by preserving the above statistical properties of wind speed (Carapelluci & Giordano, 2013). The more widely applied ones are the AR(MA) (Autoregressive Moving Average) (Aksoy et al., 2004; Castellanos & Ramesar 2006), parametric (Zárate-Miñano et al. 2013; Scholtz et al. 2014; Papaefthymiou & Klöckl, 2008) and non-parametric Markov (Suomalainen et al., 2012;Loukatou et al. 2018), Wavelet models combined with Artificial Intelligence (AI) algorithms (Pei et al., 2019) and hybrid optimization methods (Naimo, 2014).

The AR(MA) and Markov chain approaches are considered the oldest ones among stochastic wind generation schemes with satisfying results and modelling capabilities, considering the marginal and the dependence structure preservation (Koutsoyiannis, 2020). However, their strengths may also often act as drawbacks since they may be characterized by higher complexity with a quite extensive number of parameters, as for example, one for each periodicity resulting in 12x24 parameters for the estimation of the double periodical mean. Moreover, these approaches may not always guarantee the explicit preservation of the marginal structure with the autocorrelation function in cases of strong long-term persistence (Suomalainen et al., 2012; Naimo, 2014; Pei et al., 2019). On the contrary, wavelet, AI-based and hybrid methods have gained attention as non-parametric generation schemes with a satisfactory predictive capability and accuracy, yet, without avoiding the increased computational performance or the decreased predictive temporal windows, mainly for short-term forecasting applications (Carapelluci & Giordano, 2013).

Considering the aforementioned characteristic, an alternate modelling scheme was proposed by Koutsoyiannis (2000) in order to simulate long-term hydro-meteorological processes, based on two important features and innovations. First, the climacogram stochastic

tool (i.e., variance of average process vs. scale) used for the analysis of the dependence structure with focus on the variability of the wind process in a vast range of temporal scales, while also robustly dealing with the discretization and the bias effect in the wind speed model building. The second one was the applied Symmetric-Moving-Average (SMA) stochastic simulation algorithm, which is used for the simulation of hydrological processes while preserving, explicitly with the marginal moments and important stochastic properties such as intermittency and long-term persistence (Koutsoyiannis, 2000; Koutsoyiannis, 2016; Koutsoyiannis, 2020). Extensions of this scheme to the stochastic simulation of wind processes were introduced by Dimitriadis and Koutsoyiannis, (2015) and Deligiannis et al., (2016) and produced significant results. Nevertheless, according to the author's knowledge, further validation of the proposed model is crucial in terms of the wind data used (i.e. in situ, reanalysis etc.), alternate periodic characteristics including seasonal intermittency or alternate configurations to capture the double-cyclostationarity of the wind processes in both space and time.

Parsimonious, effective and rigorous stochastic simulation tools are essential as long as wind power uncertainty quantification is a highly complex and critical task in RES planning procedures. Some key features for further investigation are highlighted including: i) The climacogram stochastic tool (i.e., variance of average process vs. scale) may be used for the analysis of the dependence structure (Generalized Hurst-Kolmogorov process) with focus on the variability of the wind process in a vast range of temporal scales, while also robustly dealing with the discretization and the bias effect in the wind speed model building; ii) The applied Symmetric-Moving-Average (SMA) stochastic simulation algorithm, which may be established for the simulation of the wind process while preserving, explicitly with the marginal moments and important stochastic properties such as intermittency and long-term persistence and finally; iii) The representation of the wind double periodicity (diurnal and seasonal) using an implicit scheme, by reducing the number of parameters needed and applying empirical periodic equations.

## 3.5 Spatial Decision Support Systems in Offshore Wind Energy deployment

In Sections 3.1 - 3.4 many critical aspects of how GIS science can strengthen OWF planning and site-prospecting procedures were reviewed and the key challenges were noticed. However, a crucial question arises on how the aforementioned modelling efforts can be comprised to integrated and holistic decision support tools*?* The continuous development of geospatially based tools combined with multi-objective decision making, as well as their growing implementation in spatial management, location-allocation issues and policy making, led to the creation of Decision Support Systems (DSS) and Spatial Decision Support Systems (SDSS) (Malczewski, 2006). The scope of these models is to compute the characteristics of problem solutions, facilitate the evaluation of solution alternatives and assess their trade-offs (Keenan & Jankowski, 2019). DSS and SDSS are multidisciplinary tools which handle a wide range of sources including spatial data, non-spatial information as also shared knowledge and methods from multiple research fields. According to Wanderer and Herle, (2015), the structure of these systems preserves increased differentiations, from communication-oriented systems to data orientated, knowledge base or model and analysis-based systems, however, during this section the review is focusing on model and analysis-oriented systems based-on on mathematical and simulation methods.

Generally, DSS are computerized systems designed to help managers and stakeholders to choose one of several alternatives. They allow automating partially or completely critical stages of the decision-making processes requiring large amounts of data, in a relatively short amount of time. Some key features of these systems include: i) the ability to quantify the analyzed elements, ii) the huge quantity of possible alternatives and results as long as the model, in each case, will be different and iii) the assessment and quantification of levels of uncertainty by the determination of which elements are based on so-called robust data and methods. The latter feature of a DSS system is of crucial importance because it allows the user to specify the range of possible changes and the delineation of alternate scenarios (Kazak et al., 2017). A special case of DSS incudes SDSS, which similarly can store and process spatial data based on GIS structures, in order to handle spatially-dependent problems. SDSS usually involve multiple criteria decisions making (MCDM) approaches with geographic location in order to logically evaluate and compare

multiple criteria that are often conflicting to make the best possible decision and alternatives (Wanderer & Herle, 2015).

Focusing on RES and wind energy sector, DSS and SDSS arise in many scales of development of a project, from the pre-feasibility studies to the micro-siting level and they are designed to support the site prospecting and planning, installation procedures and operation of many energy-related projects. Considering the initial feasibility studies and pre-planning phases, DSS and SDSS have played key role as long as a series of requirements from various fields showed up. A number of GIS-based DSS and SDSS have been also proposed for site suitability prospecting and assessment. Ramírez-Rosado et al., (2008) and Noorollahi et al., (2016) developed a multi-criteria GIS-based DSS to identify potential onshore wind farms in Spain and Iran accordingly. Lejeune et al., (2010) and Goverski et al., (2013) developed similar GIS multi-criteria frameworks among with a standalone interface using QGIS and ArcGis software linked with Visual Basic for Application (VBA), as easy-to-use SDSS tools for non-experienced GIS users. Additionally, more complicated DSS tools were developed by Chang (2014) and Labati et al., (2018) for planning and coordination of onshore regional hybrid renewable energy systems as also for electric power prediction of onshore wind farms.

Considering OWFs planning, starting with the initial spatial planning and screening procedures, (MSP decision process), several DSS and SDSS are able to manage a wide variety of spatial data, producing outputs easily understood by the users (Ehler & Douvere, 2009; Stelzenmüller et al., 2013). Existing tools range from simple mapping tools to more robust modelling approaches (Stamoulis & Delevaux, 2015). Some indicative examples include the Continental Shelf Information System (CONTIS) for detailed planning of OWFs, produced by the German Federal Maritime and Hydrographic Agency (Schillings, 2012) and the GIS analysis tool developed in the UK and the Crown Estate as a Marine Resource System (MaRS) (Pahlke, 2007). In addition, an overview of systems used in the OWE sector was assembled by the EU-project POWER (Pushing Offshore Wind Energy Regions) (Pahlke, 2007; see Table 2.9.1) where already existing DSS tools, developed by universities, research foundations and private companies, were reviewed. The project concludes that ‘‘*DSS are rarely used in the offshore wind energy field*’. Furthermore, is highlighted that the systems dealing with the wider context of OWE are either

very rare or cover only a limited spatial extent. Based on these conclusions, a DSS was developed within the WINDSPEED project to analyze cross-border potentials for OWE in the North Sea analyzing various spatial constraint factors and cost indicators for OWE deployment (Wanderer, 2009; Schillings et al. 2012).

Another crucial factor for RES development and OWF siting is also focusing on the cost assessment procedures as already stated in Section 2.5. Analyzing the economic ingredients of an OWF, such as the capital and O&M expenditures, computational decision tools are of vital importance in order to analyze the inherent trade-offs. Recent efforts, as potential DSS schemes and tools, developed by Myhr et al., (2014), Koukal and Brietner (2014), Shaffie et al., (2016) and Ioannou et al., (2018) for the planning and coordination of RES in Brazil and the UK. Despite of the analytical cost evaluation efforts, there is a lack of the two-dimensional rendering (spatial distribution) of the associated costs as long as these efforts are focusing on site-specific analysis and evaluation. Additionally, as O&M expenses account for almost the 30% of the life cycle cost of an OWF, a number of researchers over the recent years have created DSS and SDSS for different purposes, such as to forecast the operations of an OWF or to delineate and estimate the associated maintenance strategies and costs (Li et al. 2016).

**Table 3.5.1:** Spatial Decision Support Systems (SDSS) in the Offshore Wind Energy sector

| Name | Company | Area | Type | Suitability |
|---|---|---|---|---|
| OWECOP | ECN, The Netherlands | Project development | Integrated | High |
| O&M DSS | ECN, The Netherlands | Operation & Maintenance Costs | Integrated | High |
| OWFLO | Uni. of Massachusetts, USA | Project development | Integrated | High |
| EeFarm | TU Delft, Netherlands | Grid Integration, Costs | Specific | Low |
| Maintenance Manager | ECN, The Netherlands | Operation & Maintenance Costs | Specific | High |
| GIS – cable route | ICBM, Germany | Project development | Specific | High, development discontinued |
| BMT MWCOST | BMT Cordah Ltd (UK) | Operation & Maintenance Costs | Specific | High |
| MaRS | The Crown Estate (UK) | Maritime Spatial Planning | Specific | High |

| | | | | |
|---|---|---|---|---|
| ---------- | Punt et al. (2009) (Netherlands) | Environmental Impact Assessment | Specific | High |

Some of the aforementioned SDSS are presented in Table 3.4.1 including:

- **OWFLO** is a project established by the Massachusetts Technology Collaborative (MTC), GE Energy, and the US Department of Energy. The researchers' objective was to develop a software tool that can be used by project developers and investors to model and understand the cost and energy trade-offs, focusing on the WTs micro-siting processes. As a result, the tool was specialized for WTs' layout analysis by applying cost and energy-based spatial optimization algorithms (Elkinton et al. 2005).
- **OWECOP** couples a GIS database with an Excel spreadsheet program. Spatial data are stored in a geodatabase including information about wind speed, wave height, bathymetry, and distance to shore. The Excel spreadsheets include different engineering and cost models for the WTs, for the support structure, electrical infrastructure, installation and O&M. For each location the site-specific parameters are translated to costs and the energy yield for a user-specified OWF (Kooijman et al. 2011).
- The **Maintenance Manager** and the **O&M DSS** have been developed by the Energy Research Centre of Netherland (ECN) to support operation and maintenance strategies as also grid connection modelling and assessment. Both of the models are structured such that planner, technicians and manufacturers provide to the system the turbine design data, information on spare parts and maintenance strategies in order to approximate operation and maintenance costs, strategies and alternative maintenance scenarios (Myhr et al., 2014; Ioannou et al., 2018a;2018b).
- **EeFarm** program helps to identify the most cost-effective electrical infrastructure (integration system, inter-array and export cables) solutions for OWFs planning. Overall, the dynamic program is focusing on the OWF control design, by the technicians and experts, and calculates the dynamic effects on the high voltage grid. On top of that, EeFarm calculates the steady state voltages and currents in an OWF by handling in parallel a number of different designs with AC and DC connections (Pahlke, 2007).

- **BMT MWCOST** is characterized as a statistical simulation software for the installation and O&M procedures and strategies of an OWF. It supports both the developers and operators to determine the predicted unavailability, loss of revenues, O&M planning, and the associated costs. Wind, wave and tidal characteristics are also taken into account to deal with the disruptions occur by weather conditions among with the effects of predicted and unpredicted equipment failures (Stratford, 2007).
- Finally, another SDSS is the **GIS-based assessment of alternative cable routes for interconnection** of OWFs platform from the University of Oldenburg focusing on the environmental impact of cable routes. Moreover, the same university developed **ANEMOS** as an interactive role game for OWE projects pre-planning. Game considers that three people are taking part in the game along with one approval authority and the project developers. The "players-planners" have to design a project, considering restricted areas and the associated costs and benefits, by sending in parallel a brief description of their proposal to the approval authority.

Reviewing already existing DSS and SDSS tools focusing on RES and OWFs site prospecting, several potential directions can be noticed as also many future prospects for further development can be highlighted. Keenan, (2003), almost 20 years ago, indicated that improvements in standard GIS software might be able to increase the amount of people who could easily use it directly for spatial decision-making and this statement is still up to date as long as open-source GIS platforms and applications are evolving. Moreover, according to Pahlke, (2007) and Wanderer, (2009), superior customization features, new tools and algorithms or custom spatial modelling frameworks in GIS software might allow easier modification of GIS for specific decisions. This requires the establishment of SDSS where users can understand and manage the key variables of interest while other most complicated processes may be performed without the need for extensive user interaction and *a-priori* sophisticated knowledge. Nevertheless, a successful implementation of SDSS tools for participatory decision-making, requires structured theoretical knowledge, easily understood by the stakeholders and planners, considering issues of an inter-disciplinary nature in a tractable way.

## 3.6 Conclusions and key findings from the Literature Review

Overall, findings from the literature review yield a need for the development of more integrated and sophisticated approaches and spatial models related to RES deployment and OWFs site prospecting at a local, regional or national level. Furthermore, the establishment of integrated SDSS tools is of paramount importance considering the evolution of the computational and algorithmic capabilities, data volumes and quality along with the spatial and temporal accuracy. In short, some of the key findings and challenges for the offshore wind industry, the research community and the geosciences overall, consist of:

1. Pre-planning and development for OWE deployment is a very complex and costly multi-objective process. As a result, more integrated spatial approaches and models must be established in order to reduce uncertainty and increase investors and stakeholders' interest, especially for areas where technical challenges occur.
2. The associated tools and feedback acquired from land-use management strategies constitutes of a great opportunity for more efficient marine space management tools under multiple spatial and non-spatial objectives;
3. Considering the spatial modelling of the cost-related indicators, multiple drawbacks and sources of uncertainty occurred. The lack of analytical cost information, biased or rough cost estimates along with the site-specific physical and economic characteristics are some of the key elements to be extensively appraised;
4. More integrated offshore wind resource assessments, new datasets validation and novel methodologies, considering the long-term probabilistic behavior of the offshore wind resources is critical. Furthermore, stochastic simulation tools for the uncertainty and the long-term power variability quantification must be further examined in spatial modelling approaches;
5. GIS-based frameworks for multi-objective OWF site-prospecting must be further optimized and adapted for a better understanding of real-word processes. More

integrated and analytical algorithms (e.g. distance -based or site-selection tools) must be incorporated in spatial modelling approaches and finally;

6. Holistic and easily customized SDSS are lacking at both research and commercial level. In order to increase the engagement and knowledge of researchers, national authorities, investors and the public, simple, robust and efficient decision-making schemes must be considered.

## References


1. **Abudureyimu, J. Hayashi, K., and Nagasaka K., (2012):** Analyzing the economy of off-shore wind energy using GIS technique, *APCBEE Procedia*:1;182 - 186.
2. **Aerts J.C.J.H, Herwijnen M.V., Janssen R., Stewart T.J., (2005):** Evaluating Spatial Design Techniques for Solving Land-use Allocation Problems, *Journal of Environmental Planning and Management*:48(1);121 - 142
3. **Ahmadi S., Ebadi H., and Valadan Zeoj M.J., (2008):** A new Method for Path Finding of Power Transmission Lines in Geospatial Information System Using Raster Networks and Minimum of Mean Algorithm, *Journal of World Applied Sciences Journal*:3(2);269-277
4. **Aksoy H., Toprak Z. F., Aytek A., Ünal N. E., (2004):** Stochastic generation of hourly mean wind speed data, *Renewable Energy:*29;2111-2131
5. **Almeida P.J.A.L., Vieira M.V., Kajin M., Forero-Medina G., and Cerqueira R., (2010):** Indices of movement behavior: conceptual background, effects of scale and location errors, *Zoologia*: 27(5):674-680
6. **Antikainen H., (2013):** Using the Hierarchical Pathfinding A* Algorithm in GIS to Find Paths through Rasters with Nonuniform Traversal Cost, *ISPRS Int. J. Geo-Inf*., 2;996-1014
7. **Bagli S., Geneletti D., and Orsi F., (2011):** Routeing of power lines through least-cost path analysis and multicriteria evaluation to minimize environmental impacts, *Environmental Impact Assessment Review*, 31(3);234-239
8. **Baioco J.S., Alves de Lima M.H., Albrecht C.H., Pires de Lima B.S.L., Jacob B.P., and Rocha, D.M., (2018):** Optimal Design of Submarine Pipelines by a Genetic Algorithm with Embedded On-Bottom Stability Criteria, *MathematicalProblems in Engineering*:1-21
9. **Beccali M., Galletto J., and Noto L. (2015):** Assessment of the technical and economic potential of offshore wind energy via a GIS application, *4th Int. Conference on Ren. Energy Research and Applications*, Palermo, Italy
10. **Benhamou S., (2004):** How to reliably estimate the tortuosity of an animal's path: straightness, sinuosity, or fractal dimension?,*Journal of Theoretical Biology*:229;209-220

11. **Bensoussan, A., Bertrand, P.R., Brouste A., (2012):** Forecasting the Energy Produced by a Windmill on a Yearly Basis. Stoch. *Environ. Res. Risk Assess*:26:1109–1122.
12. **Berglund T., Brodnik L., Jonsson H., Staffanson M., and Söderkvist I., (2010):** Planning Smooth and Obstacle-Avoiding B-Spline Paths for Autonomous Mining Vehicles, *IEEE Transactions on Automation Science and Engineering*:7(1)
13. **Bett P.E, Thornton H.E., Clark R.T., (2017):** Using Twentieth Century Reanalysis to assess climate variability for the European wind industry, *Theor. Appl. Climatol*.:127:61-80
14. **Beyer H.L., Dujardin Y., Watts M.E., Possingham H.P., (2016):** Solving conservation planning problems with integer linear programming, *Journal in Ecological Modelling*:328;14 - 22
15. **Billionnet A., (2016):** Designing connected and compact natural reserves, *Environ*. Model. *Asseess*:21;211-219
16. **Boroujerdi A., and Uhlmann J., (1998):** An efficient algorithm for computing least cost paths with turn constraints, *Information Processing Letters*:67;317-321
17. **Brower M.C., Barton M.S., Lled_o L., Dubois J., (2013):** A Study of wind speed variability using global reanalysis data, AWSTruepower
18. **Camargo L.R., and Stoeglehner G., (2018):** Spatiotemporal modelling for integrated spatial and energy planning, Energy, *Sustainability and Society*,8-32
19. **Campisi-Pinto S., Gianchandani K., Ashkenazy Y., (2020):** Statistical tests for the distribution of surface wind and current speeds across the globe, *Renewable Energy*:149:861-876
20. **Cao K., Bo H., (2010):** Comparison of Spatial Compactness Evaluation methods for Simple Genetic Algorithm based Land Use Planning Optimization problem, The International Archives of the Photogrammetry, *Journal in Remote Sensing and Spatial Information Sciences*:38, Part II
21. **Cao K., Huang B., Wang S. Lin H., (2012):** Sustainable land use optimization using Boundary-based Fast Genetic Algorithm, Journal in Computers, *Environment and Urban Systems*:36;257 – 269.
22. **Carapelluci R., Giordano L., (2013):** A methodology for the synthetic generation of hourly wind speed time series based on some known aggregate input data, *Applied Energy*:101;541-550
23. **Carpar T., Ayat B., Aydoğan B., (2019):** Spatio-Seasonal Variations in Long-Term Trends of Offshore Wind Speeds Over the Black Sea; an Inter-Comparison of Two Reanalysis Data, Pure and *Applied Geophysics*:177;3013-3037
24. **Carta J.A., Ramírez P., and Velázquez S., (2009):** A review of wind speed probability distributions used in wind energy analysis: Case studies in the Canary Islands, *Renewable and Sustainable Energy Review*s:13:933-955
25. **Castellanos F., Ramesar V.I., (2006):** Characterization and Estimation of Wind Energy Resources Using Autoregressive Modelling and Probability Density Functions, Wind Engineering:30(1)
26. **Castro-Santos L., García G.P., Costa P.A. and Estanqueiro A.I., (2013):** Methodology to design an economic and strategic offshore wind energy Roadmap in Portugal, *EnergyProcedia* [article in press], 10 p.
27. **Cavazzi, S. and Dutton, A. G.(2016)**: An Offshore Wind Energy Geographic Information System (OWE-GIS) for assessment of the UK's offshore wind energy potential, Part 1, *Renew. Energy*: 87:212–228
28. **Chiodo E., and De Falco P., (2016):** Inverse Burr distribution for extreme wind speed prediction: Genesis, identification and estimation, *Electric Power Systems Research*:141:549-561

29. **Choi Y., Park H., Sunwoo C., and Clarke K. C., (2009):** Multi-criteria evaluation and least-cost path analysis for optimal haulage routing of dump trucks in large scale open-pit mines. *International Journal of Geographical Information Science:*23(12);1541–1567
30. **Cockerill T. T et al. (2001):** Combined technical an economic evaluation of Northern European offshore wind resource, *Journal of Wind Engineering and Industrial Aerodynamics*:89; 689–711
31. **Collischonn W., and Pilar J.V., (2000):** A direction dependent least-cost-path algorithm for roads and canals, *International Journal of Geographical Information Science*,:14(4;397-406
32. **Cradden L., Kalogeri C., Martinez-Barrios I., Galanis G., Ingram D., and Kallos G., (2016):** Multi-criteria site selection for offshore renewable energy platforms, *Renewable Energy*:87(1);791-806
33. **Datta D., Malczewski J., Figueira J.R., (2012):** Spatial Aggregation and Compactness of Census Areas with a Multiobjective Genetic Algorithm: A Case Study in Canada, *Environment* and *Planning B: Urban Analytics and City Science*:39(2)
34. **Deligiannis I., Dimitriadis P., Daskalou O., Dimakos Y., and Koutsoyiannis D., (2016):** Global investigation of double periodicity of hourly wind speed for stochastic simulation; application in Greece, *Energy Procedia*, 97;278-285
35. **Dimitriadis P., and Koutsoyiannis D., (2015):** Climacogram versus autocovariance and power spectrum in stochastic modelling for Markovian and Hurst–Kolmogorov processes, *Stochastic Environmental Research & Risk Assessment:*29(6);1649–1669
36. **Dimitriadis P., and Koutsoyiannis D., (2015):** Application of stochastic methods to double cyclostationary processes for hourly wind speed simulation, *Energy Procedia*:76;406-411
37. **Dimitriadis P., and Koutsoyiannis D., (2018):** Stochastic synthesis approximating any process dependence and distribution, Stochastic Environmental Research and Risk Assessment:32: 1493-1515
38. **Douglas D.H., (1994):** Least-cost Path in GIS Using an Accumulated Cost Surface and Slopelines, *Cartographica*:31(3);37 - 51
39. **Doulvere F., (2008):** The importance of marine spatial planning in advancing ecosystem-based sea use management, *Marine Policy*:32(5);762-771
40. **Durmaz A.I., Unal E.O., and Aydin C.C., (2019):** Automatic Pipeline Route Design with Multi-Criteria Evaluation Based on Least-Cost Path Analysis and Line-Based Cartographic Simplification: A Case Study of the Mus Project in Turkey, *InternationalJournal of Geo-Information*:8(4);1-18
41. **Duque J.C., Church, R.L., and Middleton R.S., (2011):** The p-regions problem, *Geographical Analysis*:43;104-126
42. **Dvorak M.J., Archer C.L., and Jacobson M.Z., (2010):** California offshore wind energy potential, *Renewable Energy*:35(6);1244-1254
43. **Elkinton C.N, Manwell J.F, McGowan J.G, (2008):** Algorithms for Offshore Wind Farm Layout Optimization, *Wind Engineering*: 32; 67-83
44. **Etherington T.R., (2016):** Least-Cost Modelling and Landscape Ecology: Concepts, Applications, and Opportunities, *Journal of Current Landscape Ecology Reports*:1;0-53
45. **Gabriel S.A, Faria J.A, Moglen G.E., (2006):** A multi-objective approach to smart growth in land development, *Journal in Socio-Economic Planning Sciences:*40;212 - 248
46. **Giannaros T.M., Melas D., and Ziomas I., (2017):** Performance evaluation of the Weather Research and Forecasting (WRF) model for assessing wind resources in Greece, *Renewable Energy*:102(A);190-198

47. **Gutiérrez E., and Medaglia A.L., (2008):** Labeling algorithm for the shortest path problem with turn prohibitions with application to large-scale road networks, *Ann Oper Res*:157;169-182
48. **González J.S., Gonzalez Rodriguez A.G., Mora J.C., Santos J.R., and Payan M.B., (2010)**: Optimization of wind farm turbines layout using an evolutive algorithm, Renewable Energy:35;1671–1681
49. **Grady, S., Hussaini M.Y., and Abdullah M.M., (2005):** Placement of wind turbines using genetic algorithms, *Renew. Energy*:30;259–270.
50. **Gorsevski P. V., Cathcart S. C., Mirzaei G., Jamali M. M., Ye X., and Gomezdelcampo E., (2013):** A group-based spatial decision support system for wind farm site selection in Northwest Ohio, *Energy Policy*:55;374-385
51. **Hong L., Moller B. (2011):** Offshore wind energy potential in China: under technical, spatial and economic constraints, *Energy*:36;4482 - 4491.
52. **Hong L., Moller B. (2012):** Feasibility study of China's offshore wind target by 2020, *Energy*:48 ;268 – 277
53. **Hrafnkelsson B., Oddsson G.V., Unnthorsson R., (2016):** A Method for Estimating Annual Energy Production Using Monte Carlo Wind Speed Simulation, *Energies*:9:286
54. **Jay S. (2010):** Planners to the rescue: Spatial planning facilitating the development of offshore wind energy, *Marine Pollution Bulletin*:60;493-499
55. **Jones D. F., and Wall G. (2016):** An extended goal programming model for site selection in the offshore wind farm sector, *Annals of Operations Research*:245 (1-2);121-135
56. **Jones D.F., and Wall G., (2016):** An extended goal programming model for site selection in the offshore wind farm sector, *Annals of Operations Research*:245(1-2):121-135
57. **Jung C., Schindler D., Laible J., and Buchholz A., (2017):** Introducing a system of wind speed distributions for modelling properties of wind speed regimes around the world, *Energy Conversion and Management*:144:181-192
58. **Jung C, Schindler D., (2017):** Global comparison of the goodness-of-fit of wind speed distributions, *Energy Convers. Manag.*:133:216–34
59. **Kang J.Y., and Lee B.S. (2017):** Optimization of pipeline route in the presence of obstacles based on a least cost path algorithm and laplacian smoothing, *InternationalJournal of Naval Architecture and Ocean Engineering*:9;492-498
60. **Kao J. J. and Lin H.Y., (1996):** Multifactor Spatial Analysis for Landfill Siting, *Journal of Environmental Engineering*: 122; 902-908
61. **Kim T., Park Jeong-Il, and Maeng J. (2016):** Offshore wind farm site selection study around Jeju Island, South Korea, *Journal in Renewable Energy*:94;619-628
62. **Kooijman H. J. T.,Noord M. D., Volkers C. H., and Herman S. H.(2011):** Cost and potential of offshore wind energy on the Dutch part of the north sea, EWEC. Copenhagen, DK, pg. 218-21
63. **Kotroni V. ,Lagouvardos K., and Lykoudis S. ,(2014):** High - Resolution model - based wind atlas for Greece, Institute for Environmental Research, *Renewable and Sustainable Energy Reviews*:30;479–489
64. **Koukal A., and Breitner M. H., (2014):** Offshore Wind Energy in Emerging Countries: A Decision Support System for the Assessment of Projects, *47th Hawaii International Conference on System Science*, Waikoloa, HI, 865-874
65. **Koutsoyiannis D., (2000)** A generalized mathematical framework for stochastic simulation and forecast of hydrologic time series, *Water Resources Research*:36(6);1519–1533

66. **Koutsoyiannis D., (2016):** Generic and parsimonious stochastic modelling for hydrology and beyond, *Hydrological Sciences Journal*:61 (2);225–244
67. **Koutsoyiannis D., Dimitriadis P., Lombardo F., and Stevens S., (2018):** From Fractals to Stochastics: Seeking Theoritical Consistency in Analysis of Geophysical Data, In: Tsonis A. (eds) *Advances in Nonlinear Geosciences*. Springer
68. **Koutsoyiannis D., (2020):** Simple stochastic simulation of time irreversible and reversible processes, *Hydrological Sciences Journal:*65 (4);536–551.
69. **Li X., Ouelhadj D., Song X., Jones D., Wall G., Howell K. E., Igwe P., Martin S., Song D., and Pertin E., (2016):** A decision support system for strategic maintenance planning in offshore wind farms, *Renewable Energy*:99;784-799
70. **Ligmann-Zielinska A., Church R.L., and Jankwski P., (2008)**: Spatial optimization as a generative technique for sustainable multiobjective land-use allocation, *International Journal of Geographical Information Science*:22(6);601-622
71. **Liu K.H, Kao J.J., (2013):** Parallelized branch-and-bound algorithm for raster-based landfill siting, *Journal in Civil Engineering and Environmental Systems*:30(1);15 - 25
72. **Lizuma L., Avotniece Z., Rupainis S., Teilans A., (2013):** Assessment of the Present and Future Offshore Wind Power Potential: A Case Study in a Target Territory of the Baltic Sea Near the Latvian Coast, Hindawi Publishing Corporation, *The Scientific World Journal*:10
73. **Lo Brano V., Orioli A., Ciulla G., and Culotta S., (2011):** Quality of wind speed fitting distributions for the urban area of Palermo, Italy, *Renewable Energy*:36:1026-1039
74. **Loukatou A., Howell S., Johnson P., Duck P., (2018):** Stochastic wind speed modelling for estimation of expected wind power output, Applied Energy:228;1328-1340
75. **Malczewski J., (2006)**: GIS-Based Multicriteria Decision Analysis: A Survey of the Literature. *International Journal of Geographical Information Science*:20(7);703-726.
76. **Malczewski J., and Jankowski P., (2020):** Emerging trends and research frontiers in spatial multicriteria analysis, *International Journal of Geographic Information Science*:34(7);1257-1282
77. **Masseran N., Razali A.M., Ibrahim K., (2012):** An analysis of wind power density derived from several wind speed density functions: The regional assessment of wind power in Malaysia, *Renewable and Sustainable Energy Reviews*:16(8):6476-6487
78. **Mahdy M., and Bahaz A.S., (2018):** Multi criteria decision analysis for offshore wind energy potential in Egypt, *Renewable Energy*:118;278-289
79. **Mekonnen A.D., and Gorsevski P.V., (2015):** A web-based participatory GIS (PGIS) for offshore wind farm suitability within Lake Erie, Ohio. *Review inRenewable Sustainable Energy Rev.*:*41*;162–177.
80. **Möller B., (2011):** Continuous spatial modelling to analyze planning and economic consequenses of offshore wind energy, *Journal in Energy Policy*:39;511-517
81. **Möller, B., Hong, L., Lonsing, R., and Hvelplund, F., (2012)**: Evaluation of offshore wind resources by scale of development, *Energy*:48;314–322
82. **Monteiro C., Ramirez-Rosado I.J., Miranda V., Zorzano-Santamaria P.J., Garcia-Garido E., and Fernadez-Jimenez L.A., (2005):** GIS Spatial Analysis Applied to Electric Line Routing Optimization, *IEEE Transactions on Power Delivery*:20(2);934-942

83. **Mosetti, G., Poloni, C., and Diviacco, B. (1994):** Optimization of wind turbine positioning in large windfarms by means of a genetic algorithm, *Journal of Wind Engineering and Industrial Aerodynamics*:51(1);105-16.
84. **Morgan E.C., Lackner M., Vogel R.M., and Baise L.G., (2011):** Probability distributions for offshore wind speeds, *Energy Conversion and Management*:52:15-26
85. **Musial W., and Ram B., (2010):** Large-scale Offshore Wind Power in the United States, s.l., NREL.
86. **Myhr A., Bjerkseter C., Ågotnes A. and Nygaard T. A., (2014):** Levelised cost of energy for offshore floating wind turbines in a life cycle perspective, *Renewable Energy*:66;714-728.
87. **Murayama Y., and Thapa R., (2011):** Spatial Analysis and Modelling in Geographical Transformation Process: GIS-based Applications, The GeoJournal Library (eds.), 100, Springer Netherlands
88. **Naimo A., (2014):** A novel approach to generate synthetic wind data, *Procedia - Social and Behavioral Science*s:108;187-196
89. **Nagababu G., Kachhwaha S.S., and Savsani V., (2017):** Estimation of technical and economic potential of offshore wind along the coast of India, *Energy*:138;79-91
90. **Nerantzaki S., and Papalexiou S.M., (2019):** Tails of Extremes: Advancing a Graphical Method and Harnessing Big Data to Assess Precipitation Extremes, *Advances in Water Resources*
91. **Ntoka C. (2013):** Offshore wind park sitting and micro-sitting in Petalioi Gulf, Greece, Master Thesis , M.Sc. (Eng.) "Sustainable Energy Planning and Management", Aalborg University, Denmark
92. **Oehrlein J., and Haunert J.H., (2017):** A cutting-plane method for contiguity-constrained spatial aggregation, *Journal of Spatial Information Science*:15;89-120
93. **Önal H., and Briers R.A., (2006):** Optimal Selection of a Connected Reserve Network, *Operations Research*:54(2);379-388
94. **Önal H., and Wang Y., (2008):** A graph theory approach for designing conservation reserve networks with minimal fragmentation, *Networks: An International Journal*:51(2);142-152
95. **Önal H., Wang Y., Dissanayake S.T.M., and Westervelt J.D., (2016):** Optimal design of compact and functionally contiguous conservation management areas, European Journal of Operational *Research*:251;957-968
96. **Ouarda T.B.M.J., Charron C., Chebana F., (2016):** Review of criteria for the selection of probability distributions for wind speed data and introduction of the moment and L-moment ratio diagram methods, with a case study, *Energy Conversion and Management*:124:247-265
97. **Ouarda T.B.M.J., Charron C., (2018):** On the mixture of wind speed distribution in a Nordic region, *Energy Conversion and Management*:174:33-44
98. **Pahlke T., (2007):** Final Report, Software & Decision Support Systems for Offshore Wind Energy Expoitation in the North Sea (Version Final 1.1), Overspeed GmbH & Co. KG
99. **Papaefthymiou G., Klöckl B., (2008):** MCMC for Wind Power Simulation, IEEE Transactions on Energy Conversion:23(1)
100. **Pei S., Qin H., Zhendong Z., Yao L., Wang Y., Wang C., Liu Y., Jiang Z., Zhou J., Yi T., (2019):** Wind speed prediction method based on Empirical Wavelet Transform and New Cell Update Long Short-Term Memory network, Energy Conversion and Management:196;779-792
101. **Punt M.J., Groeneveld R.A., and van Ierland E.C., (2009)**: Spatial planning of offshore wind farms: A windfall to marine environmental protection? *Ecol. Econ.* :69; 93–103

102. **Ravankar A., Ravankar A.A., Kobayasi Y., Hoshino Y., and Peng C.C., (2018):** Path Smoothing Techniques in Robot Navigation: State-of-the-Art, Current and Future Challenges, *Sensors*:18(9);3170
103. **Resch B., Sagl G., Törnos T., Bachmaier A., Eggers J.B., Herkel S., Narmsara S., and Gündra H., (2014):** GIS-Based Planning and Modelling for Renewable Energy: Challenges and Future Research Avenues, *ISPRS International Journal of Geo-Information*:3;662-692
104. **Salvacão N., and Soares G., (2016):** Resource Assessment Methods in the Offshore Wind Energy Sector, In: Castro-Santos L., Diaz-Casas V. (eds) Floating Offshore Wind Farms, Green Energy and Technology. Springer, Cham:122-141
105. **Santé-Riveira I., Boullón-Magán M., Crecente-Maseda, Miranda-Barrós D., (2008):** Algorithm based on simulated annealing for land-use allocation, *Journal in Computers and Geosciences*:34;259 - 268
106. **Schillings. C., Wanderer. T., Cameron. L., vanderWal. J., Jacquemin. J., Veum. K., (2012):** A decision support system for assessing offshore wind energy potential in the North Sea. *Energy Policy*:49;541-551.
107. **Scholz T.S., Lopes V.V., Estanqueiro A., (2014):** A cyclic time-dependent Markov process to model daily patterns in wind turbine power production, Enegy,:67;557-568
108. **Shaffiee M., Brennan F., and Espinoza I. A., (2016):** A parametric whole life cost model for offshore wind farms, *Int. J. Life Cycle Assess.*:21;961-975
109. **Shirable T., (2004):** A model of contiguity for spatial unit allocation, *Geographical Analysis*:37(1);2-16
110. **Shirabe T., (2015):** A method for finding a least-cost wide path in raster space, *International Journal of Geographical Information Science*
111. **Soukissian T, Hatzinaki M, Korres G, Papadopoulos A, Kallos G, and Anadranistakis E., (2007):** Wind and wave atlas of the Hellenic seas. Hell. Cent Mar Res Publ.
112. **Soukissian T, Prospathopoulos A, Hatzinaki M, Kabouridou M. (2008):** Assessment of the wind and wave climate of the Hellenic seas using 10-Year hindcast results, *Open Ocean Eng J.*,:1, 1–12.
113. **Soukissian T., (2013):** Use of multi-parameter distributions for offshore wind speed modelling: The Johnson $S_B$ distribution, *Applied Energy*:111:982-1000
114. **Soukissian T. H., Papadopoulos A., (2015):** Effects of different wind data sources in offshore wind power assessment, *Renewable Energy*:77;101 – 114
115. **Soukissian T., Papadopoulos A., Skrimizeas P., Karathanasi, Axaopoulos P., et al. (2016a):** Assessment of offshore wind potential in the Aegean and Ionian Seas based on high-resolution hindcast models results, *AIMS Energy*:5(2);268-289
116. **Soukissian T, Prospathopoulos A, Hatzinaki M, Kabouridou M., (2016b):** Assessment of the wind and wave climate of the Hellenic seas using 10-Year hindcast results, *Open Ocean Eng. J.*:1:1–12.
117. **Suomalainen K., Silva C.A., Ferrão P., Connors S., (2012):** Synthetic wind speed scenarios including diurnal effects: Implifications for wind power dimensioning, Energy:37;41-50
118. **Standmark P., Ulén J., Kahl F., and Grady L., (2014):** Shortest Paths with Curvature and Torsion, *ed:IEEE International Conference on Computer Vision,* 1-8 Dec. 2013, **Available from:** http://openaccess.thecvf.com/content_iccv_2013/papers/Strandmark_Shortest_Paths_with_2013_ICCV_paper.pdf [Accessed 12 April 2020]
119. **Stefanakis E., and Kavouras, M. (1995):** On the Determination of the Optimum Path in Space, *International Conference on Spatial Information Theory*, COSIT, 241-257

120. **Suomalainen K., Silva C. A., Ferrão P., Connors S.** Synthetic wind speed scenarios including diurnal effects: Implifications for wind power dimensioning, *Energy*, 2012:37;41-50
121. **Zhang J., Draxl C., Hopson T., Monache L., D., Vanyve E. and Hodge B., M. (2015):** Comparison of numerical weather prediction based deterministic and probabilistic wind resource assessment methods, *International Journal in Applied Energy*:156;528-541
122. **Vagiona, D. G., and Karanikolas, N. M. (2012):** A multicriteria approach to evaluate offshore wind farms sitting in Greece. Glob NEST J:14; 235–243
123. **Vagiona D.G., and Kamilakis M., (2018):** Sustainable Site Selection for Offshore Wind Farms in the South Aegean-Greece, *Sustainability*:10(3);749
124. **Vanegas P., Cattrysse D, Orshven J. V., (2010):** Compactness in Spatial Decision Support: A Literature Review, D. Taniar et al. (Eds.): ICCSA 2010, Part I, LNCS 6016, Springer – Verlag Berlin Heidelberg, pp. 414 – 419
125. **Wan C., Wang J., Yang G., Gu H., and Zhang X. (2012):** Wind farm micro-siting by Gaussian particle swarm optimization with local search strategy, *Renewable Energy*, vol. 48, pp. 276–286
126. **Wang Y. H., Walter R. K., White C., Farr H., and Ruttenberg B., (2019):** Assessment of surface wind datasets for estimating offshore wind energy along the Central California Coast, Renewable Energy:133:343-353
127. **Wenwen L., Goodchild M.F., and Church R., (2017):** An efficient measure of compactness for two-dimensional shapes and its application in regionalization problems, *International* Journal *of Geographical Information Science*:27(6);1227-1250
128. **Williams J.C., ReVelle C.S., (1996):** A 0-1 programming approach to delineating protected reserves, *Journal in Environment and Planning B: Planning and Design*:23;607 - 624
129. **Winter S., (2002):** Modelling Costs of Turns in Route Planning, *Geoinformatica*:6(4);345-361
130. **Yakolev K., Baskin E., and Hramoin I. (2015):** Grid-based angle-constrained path planning, In: Hölldobler S., Peñaloza R., Rudolph S. (eds) KI 2015: Advances in Artificial Intelligence. KI 2015. Lecture Notes in Computer Science, 9324. Springer, Cham
131. **Yamaguchi A., and Ishihara T., (2014):** Assessment of offshore wind energy potential using mesoscale model and geographic information system, *Renewable Energy*:69;506-515
132. **Yu C., Lee J., and Mundro-Stasiuk, M.J., (2003):** Extensions to least-cost path algorithms for roadway planning, *International Journal of Geographical Information Science*:17;361-376
133. **Zárate-Miñano R., Anghel M., Milano F., (2013):** Continuous wind speed models based on stochastic differential equations, Applied Energy:104;42-49
134. **Zhou, F., Song, B., and Tian, G., (2011):** Bezier Curve Based Smooth Path Planning for Mobile Robot, *Journal of Information & Computational Science*:8(12);2441 - 2450

# 4. Study area and data acquisition

## 4.1 Study area presentation

The area of interest extends to the national marine territorial borders of Greece located in the southeastern Europe at the south part of the Balkan Peninsula. Greece is surrounded by the Aegean Sea in the east, the Ionian Sea in the west and by the Mediterranean Sea (Cretan and Karpathian Archipelago) in the south, having common marine boundaries with Albania and Italy (West), Libya, Egypt and Cyprus (South) and Turkey (East). The Aegean Sea comprises of multiple groups of islands and islets, including Cyclades in the southeast, Sporades along the eastern coast (western part of the Aegean Sea), Dodecanese on the eastern part of the Cretan Sea, and the northeastern Aegean Islands. Consequently, is characterized by an extended coastline comprising several landforms, including sandy coastal parts, rocky shores, cliffs, coastal lagoons and deltaic systems (Vasileiou et al., 2017; Topouzelis et al., 2018).

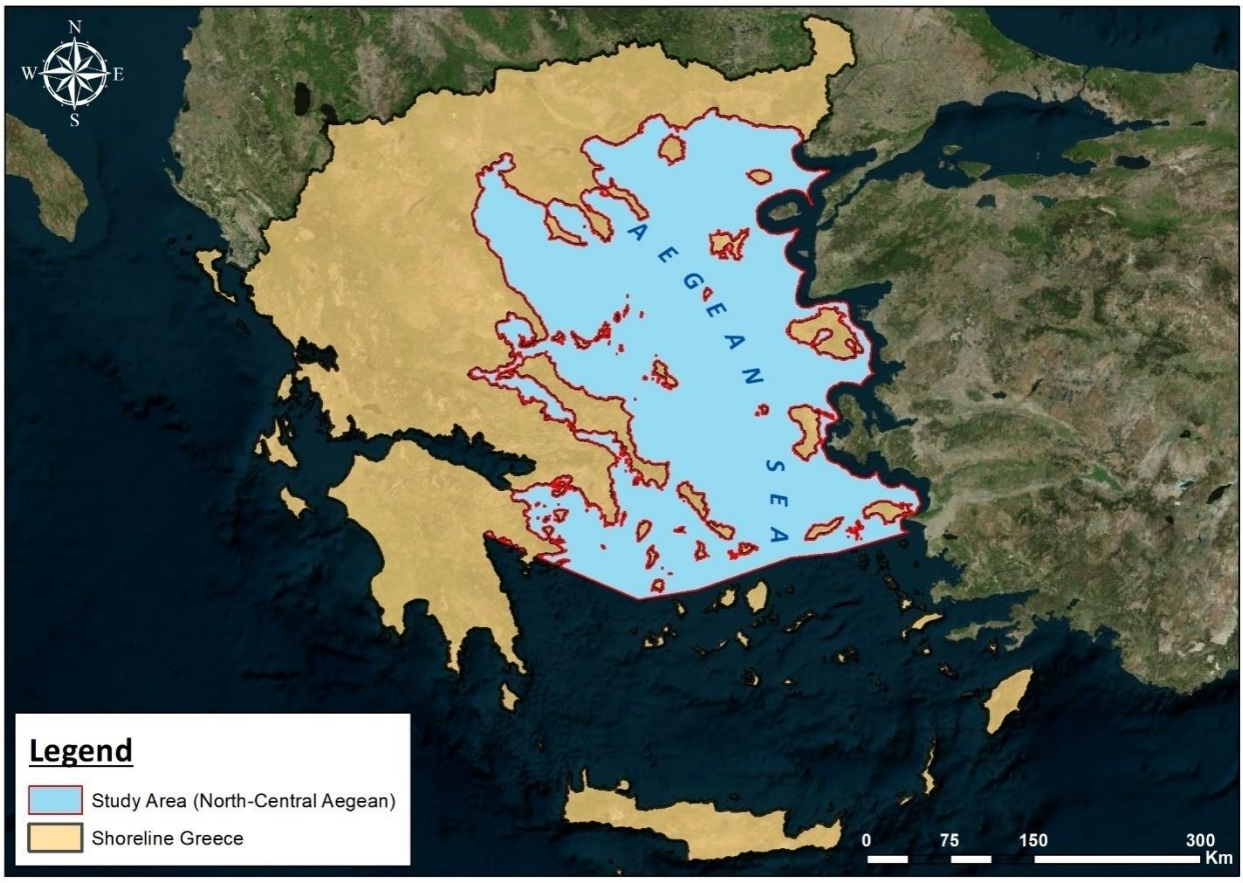


**Figure 4.1.1:** Study Area of North and Central Aegean Sea (light blue area)

Focusing on the Aegean's marine physical characteristics, situated at an area where the Asian, European, and African plates converge, the seafloor is characterized by a complex and heterogeneous geomorphology (Topouzelis et al. 2018). These distinctions are also reflected in the seawater circulation patterns and the sea temperature (Sini et al. 2017). Considering of these geophysical characteristics, notable is that both of the Northern and the Southern part of the study area are characterized by increased seismicity as long as numerous active tectonic faults exist (Sini et al. 2017; Vasileiou et al. 2017; Topouzelis et al. 2018). In Figure.4.1.1 the study area is presented (light blue color) which encompasses the international and Greek territorial waters with coordinates 39°N 25°E, where the North and Central Aegean Sea covers an area of approximately 155367 $km^2$. Also, Greece extends to an area of approximately 130000 $km^2$, while its permanent population corresponds to almost 11 million people. The extended coastal and marine areas in Greece enable the intense marine activities including tourism, shipping, fishing and aquaculture, military activities etc. During the following sections a more in-depth analysis of the physical and techno-economic characteristics of the broader study area will be discussed.

### 4.1.1 Physical characteristics

**Shoreline:** Greece is characterized by its extended coastline including numerous islands and small islets (Figure 4.1.1), most of them located in the Aegean Sea. The entire coastal zone of the country is of crucial importance, considering that most of the biggest cities, smaller towns and villages are located in short distances for the shore. Furthermore, 80% of the industrial activities, 90% of recreation and tourism areas, 35% of the cultivated land and many more important infrastructure facilities (e.g., airports, roads, electricity network, ports etc.) (Figure 4.1.1.1) are concentrated to the coastal parts (Lioutas & Tsimopoulou, 2010). As a consequence, the installation of OWFs close to the shore may lead to potential conflicts and social impact, considering the local communities. Visual impact, NIMBY[9] (Not in My Back Yard) situations as long

[9] **Not in My Backyard Phenomenon (NIMBY),** also called **Nimby**, a colloquialism signifying one's opposition to the locating of something considered undesirable in one's neighborhood.

as noise and aesthetics consequences may affect the legislative acceptance procedures and authorization for OWE deployment, but also affect many human activities occurring in the corresponding coastal areas.

**Bathymetry:** The most discouraging physical factor characterizing the Aegean Sea is the heterogeneous and intense bathymetric profile. Depths less than 250 meters, that technologically can be explored for OWE deployment, cover a short amount (< 50%) of the total marine areas (Figure 4.1.1.1c). In the case of fixed bottom structures (gravity based, monopile and jacket structures), a quite limited range of water depths (up to 60 - 100 m) may be considered adequate for their installation. On the other hand, floating structures can be utilized in significantly larger water depths (up to 250 or even 500 meters); however, there are still specific design challenges and technical limitations regarding the efficient design of the floaters, mooring lines and anchors that limit their installation depth.

The Northern Aegean, as already highlighted, contains extended shelf areas. To the South of this peninsula, a deep trench occurs, divided into three subbasins, the Sporades, Athos, and Lemnos Basin. Shallow areas are followed by deep basins, as with the deepest point being 1500m consisting of the West Anatolian fault. Accordingly, the Central and South part of the Aegean Sea consist of a "smoother" bathymetric profile, with the Cyclades islands plateau (Figure 4.1.1) being the main dividing physical feature with a maximum depth of 400m. Moreover, the Central Aegean is characterized by both extended deep areas, such as the Skyros and Chios basins and shallow areas to the northwester part of Lesvos with depths exceeding 250m. Cyclades broader area and southeaster Aegean are characterized by the shallowest depths, contrary, near to Dodecanese islands, the bathymetric profile exceeds of increased depth variations (Sini et al. 2017; Vasileiou et al. 2017; Topouzelis et al. 2018).

**Soil conditions and Tectonic faults:** Substrate sediments are characterized from large areas covered from sandy mud and fine mud substrates as long as hard bottom substrates and Posidonia oceanica meadows (Figure 4.1.1.1d). Resulting information from previous studies and European monitoring programs imply a total area of 2750 $km^2$ (1.3% of entire study area) for soft substrates, 1590 $km^2$ (0.7%) for seagrass beds, 164 $km^2$ (0.08%) for rocky substrates (Sini et al., 2017) and a total area cover of Posidonia oceanica beds of 449.39 $km^2$. As already stated, the

intensive seismic activity is remarkable in the Aegean Sea and the tectonic faults, illustrated in Figure 4.1.1.1e, are mapped and used as exclusion areas for OWF siting and site prospecting or as a factor under consideration for potential cost increase.

**Marine Protected Areas (MPAs):** The network of all protected areas is included and identified under the Birds and Habitat Directive (Special Protection Areas and Special Areas of Conservation, respectively[10]) (Figure 4.1.1.1g-h) among with all the Cultural heritage, as they have been institutionalized by the Ministry of Culture and Sports. Numerous species observed in the Greek seas, are under severe pressures due to the intense human activities, mostly in coastal areas. Such species include the Spur-winged plover (Hoplopterus spinosus), three species of sea turtles including Caretta-caretta, and the Mediterranean monk seal (Monachus monachus) (Lioutas & Tsimopoulou, 2010). Within the north and central Aegean Sea there are currently 5 National Parks and 186 Natura 2000 sites encompassing marine coastal waters (Figure 4.1.1.1g-h). The total surface area of designated waters for protection is 4455.8 $km^2$ (1.9%). This corresponds to 1.1 and 2.3% of the study area as National Parks and Natura 2000 sites respectively. Beyond these MPAs, in 2016, a new scheme was proposed for consultation by the Hellenic Ministry for the Environment, denoting the extension of the marine conservation areas network (61 new marine sites). Consequently, the total amount of MPAs will considerably increase, reaching more than 10% coverage of the Greek Territorial Waters (Papageorgiou, 2016).

**Wildlife preservation (Ecological Density – E.D index):** An alternate ecological index was proposed by Sini et al., (2017), in order to quantify the occurences of ecological features in the Aegean Sea. The Ecological Density (ED) index is a rather simplified but efficient measure to map and monitor the environmental state of an area. This metric has been developed within Marisca project to supplement and assess the nature conservation areas described in the previous paragraph (MPAs). The study area was divided into different cell sizes (2.5x2.5km up to 12 km from the shoreline and 12.5x12.5 $km^2$ far from the shore). Moreover, small spatial units of high feature diversity (>10 features) were scattered around different parts of the Aegean Sea (e.g Sporades).

[10] Natura 2000 sites have been designated specifically to protect core areas for a sub-set of species or habitat types listed in the Habitats and Birds Directives.

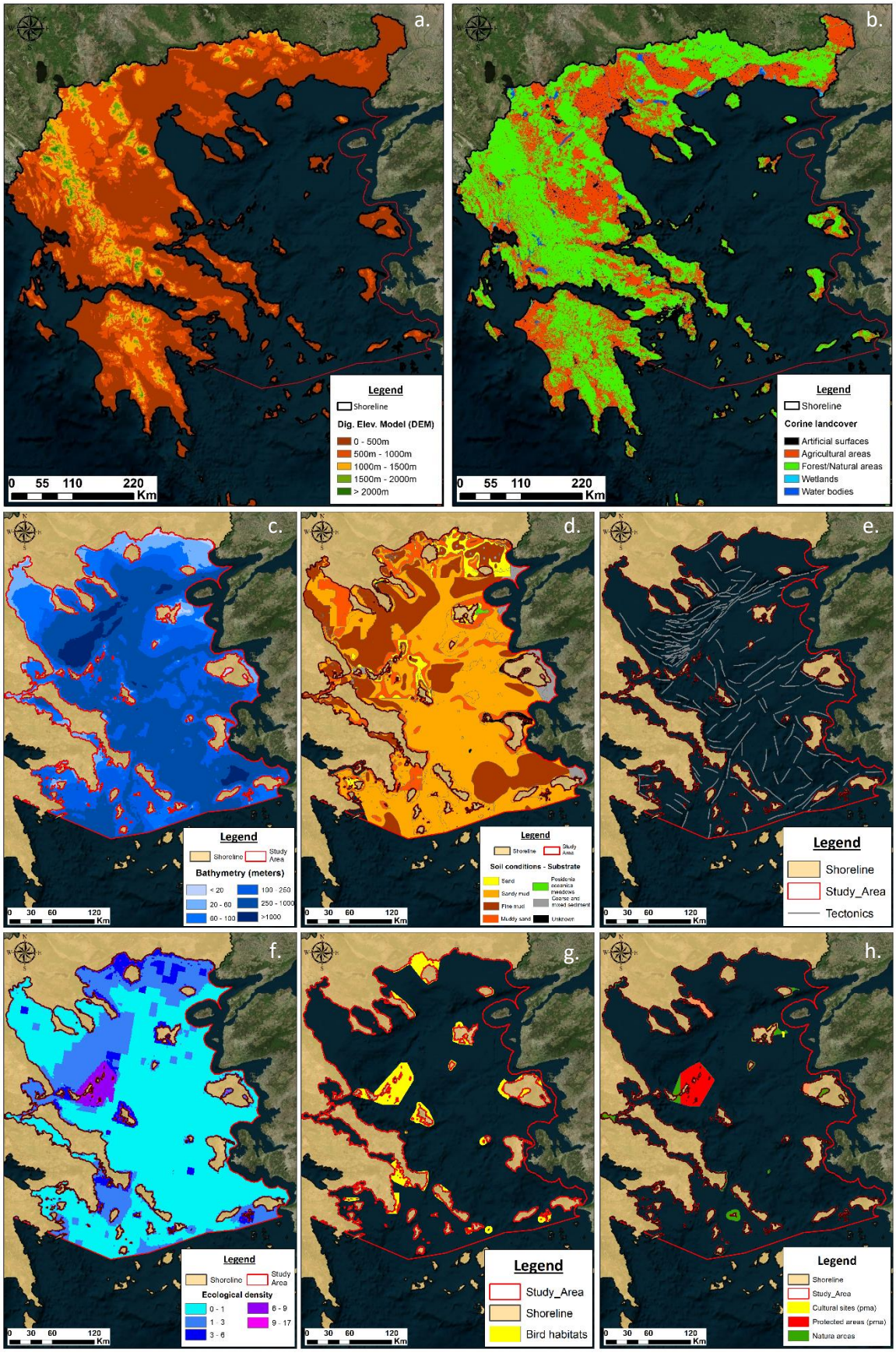
a.
Legend
Shoreline
Dig. Elev. Model (DEM)
0 - 500m
500m - 1000m
1000m - 1500m
1500m - 2000m
> 2000m
0 55 110 220 Km
b.
Legend
Shoreline
Corine landcover
Artificial surfaces
Agricultural areas
Forest/Natural areas
Wetlands
Water bodies
0 55 110 220 Km
c.
Legend
Shoreline
Study Area
Bathymetry (meters)
< 20
20 - 60
60 - 100
100 - 250
250 - 1000
>1000
0 30 60 120 Km
d.
Legend
Shoreline
Study Area
Soil conditions - Substrate
Sand
Sandy mud
Fine mud
Muddy sand
Posidonia oceanica meadows
Coarse and mixed sediment
Unknown
0 30 60 120 Km
e.
Legend
Shoreline
Study_Area
Tectonics
0 30 60 120 Km
f.
Legend
Shoreline
Study Area
Ecological density
0 - 1
1 - 3
3 - 6
6 - 9
9 - 17
0 30 60 120 Km
g.
Legend
Study_Area
Shoreline
Bird habitats
0 30 60 120 Km
h.
Legend
Shoreline
Study_Area
Cultural sites (pma)
Protected areas (pma)
Natura areas
0 30 60 120 Km

**Figure 4.1.1.1:** a) Digital Elevation Model (DEM), b) Corine landcover, c) Bathymetry, d) Soil conditions, e) Tectonic faults, f) Ecological Density, g) Bird habitats and h) Protected areas

The resulted grid comprises of 193 cells (2.5x2.5 $km^2$) and these spatial units correspond to 41% falling within Natura 2000 sites, 30% in locations where National Parks and Natura 2000 sites coincide, while 29% is located in areas exceeding no protection status. Overall, when the total number of ecological features per grid cell is considered, it becomes evident that cells with a high number of ecological features (>5 features) are most commonly found in coastal waters (Figure.4.1.1f). In addition, results indicated that the Northern Sporades, the Cyclades and the Dodecanese island complexes, as well as along some of the Thracian coasts preserve areas of increased importance, considering their ecological footprint.

### 4.1.2 Human activities

**Shipping routes:** The intense marine transportation activities (Figure 4.1.2.1a-b) is of paramount importance in Greece, because of the extended coastline and the existence of numerous inhabited islands. Both territorial and social cohesion depend on the existence of frequent and reliable shipping infrastructures, connecting 94 islands and serving more than 36 million passengers annually. Focusing on the cargo shipping density and marine operations, a total amount of 20 ports with more than one million tons of cargo are transported annually. Moreover, the high intensity shipping routes connecting the Black Sea with the rest of the Mediterranean Sea (via the Dardanelles Strait) play a key role for the international maritime transports. Focusing on some statistics of the general shipping activities, noteworthy is that i) Greek interests control more than 4000 vessels of various categories with 671 ships registered under the Greek flag in 2019 according to the Hellenic Chamber of Shipping (https://nee.gr/) and ii) worldwide, Greek interests control around 9.1% of the world's total number of vessels, 18% of the world fleet dead weight and 15.5% in terms of the gross tons. The aforementioned statistics are noticed in order to highlight both the tremendous efforts of the Greek shipping industry and the existence of a great number of infrastructures overall (Lioutas & Tsimopoulou, 2010).

**Cables and pipelines:** A fair number of electric and telecommunication cables exist or are planned in the North and Central Aegean Sea (Figure 4.1.2.1c). Most of them connect the numerous blocks of islands among each other or (Cyclades, Crete, Dodecanese and North Aegean islands) with the onshore infrastructures in both south and north Greece. The existence of already installed or planned undersea cables plays a key role in future OWF planning, considering the transmission lines or inter-array cables' paths delineation as also in site prospecting procedures and safety measures during planning and installation.

**Military zones:** Covering a wide range of activities, firing range zones, as military areas, are defined by the Greek government in the interest of training and security purposes (Figure 4.1.2.1f). The distribution of firing range and security areas is mostly observed to the coastal parts of the mainland as also to the nearshore marine areas in Cyclades and North Aegean islands consisting of totally exclusion criteria considering safety and national security reasons.

**Aquaculture and Fisheries:** Fishing activities and aquaculture (Figure 4.1.2.1d) cover a large amount of the study area mainly nearshore, depending on specific fishing techniques and aquaculture activities locations. This sector is considered vital for the national economy, because, despite of its small contribution to the GDP[11], it contributes to the social and economic inter-connection of the coastal zones and inhabitable islands. About 40000 people are occupied in fishing and aquaculture activities, with a fishing fleet of about 19000 vessels. The annual production in all categories (sea fisheries, aquaculture, lagoons etc.) acounts for a total of 231000 tons and notable is that the aquaculture production is estimated to 258k € (10% of the EU aquaculture production) (Lioutas & Tsimopoulou, 2010). Data used in this study, focus on i) heavy fishing using beam trawl or purse seine methods and ii) aquaculture sites extended across the north and central Aegean Sea, that could potentially come into conflict with OWFs and electric infrastructures. For this reason, these marine areas are partially or totally excluded during the constraints scenarios formulation.

[11] GDP is an indicator for a nation´s economic situation reflecting the total value of all goods and services produced less the value of goods and services used for intermediate consumption in their production.

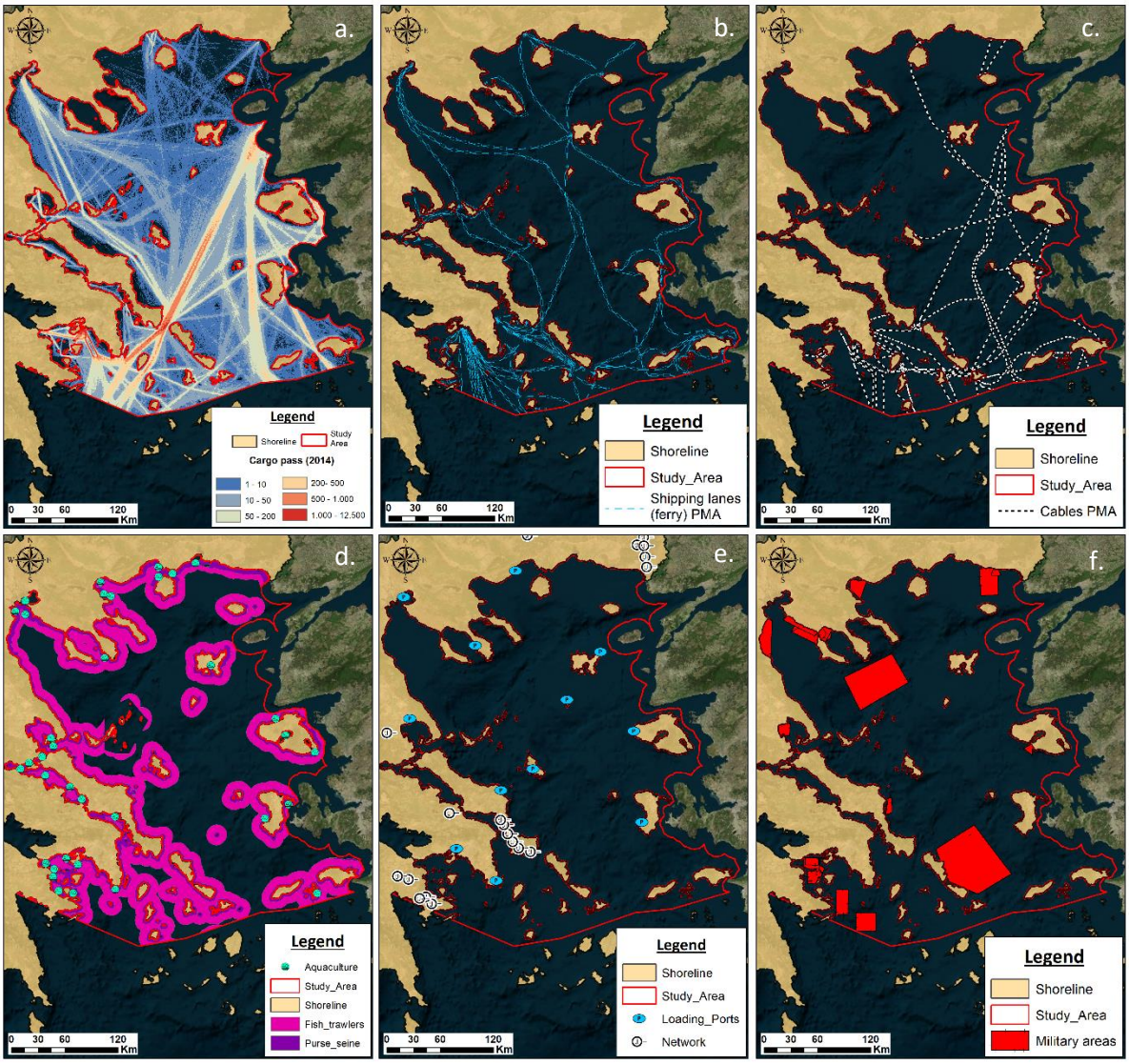


**Figure 4.1.2.1:** a) Cargo shipping density (2014), b) Commercial shipping routes, c) Cables-pipelines, d) Aquaculture-fishing zones, e) Ports and Network grid, f) Military areas

**Infrastructures :** Tourism constitutes one of the key economic activities in Greece by contributing annually a 18% of the GDP (more than 30 billion euros), resulting to 700000 jobs covering a 20% of all employees in Greece. Tourism and recreational activities are mostly located in the Greek coastal areas (90% of these activities are located near the coast) (Lioutas & Tsimopoulou, 2010). Considering the Greek legislation for the OWE (Section 2.4.1), no direct impact occurs, related to this type activities with an exception of the distances from coastal cities. However, the intense infrastructures in many coastal sites i.e. Chalkidiki, Pilio, Cyclades, North Aegean islands, Sporades etc. may cause tremendous conflicts and concerns to the local

communities. Consequently, multiple exclusion scenarios are considered focusing on the distances from the shoreline and coastal cities as well as the proximity to blue flag beaches and areas with intense recreational activities (Figure 4.1.2.1e).

### 4.1.3 Offshore wind characteristics

**Wind speed and power density characteristics:** According to Kotroni et al. (2014), Soukissian et al. (2007;2008;2014) and Emmanouil et al. (2016), the study area is characterized by increased wind velocities, mainly in the Northern-East, Central and Southern East Aegean. Based on these studies, the total wind energy potential for OWE exploitation in Greece, based on average wind speed data, approaches 1000 TWh (EEA, 2009) as approximately the 70% of the marine areas are characterized by a wind power class of 3 or better (typically up to 5-6 wind power classes are considered), while a 34% of these areas is classified in a wind power class of 4 or better.

Analyzing the offshore wind speed characteristics, results from previous studies indicate maximum intensities over the areas crossing the eastern part of the Aegean Sea (from north to south), with mean values exceeding 8 m/sec, 50 m above the mean sea level (Figure 4.1.3.2a-d). Considering the seasonal characteristics, wind speed is more intense during the winter period, with several low-pressure systems coming from the northern Europe. Increased wind speed values are also observed during the summer months, specifically in August, because of the etesian winds (meltemia) prevailing over Aegean Sea. During spring the mean wind speed preserves much less variability than in winter, with winds of the order of 5 m/s and during autumn the passage of low-pressure systems associated with southerly winds leads to slightly increased wind speeds across the study area, compared to spring values. Focusing on the variability patterns (Figure 4.1.3.3), the northwestern and western coastal part of the Aegean Sea is characterized by increased annual variability (high standard deviation values) as long as the inter-annual variability preserves relative increased values mostly in the broader coastal area of Alexandroupoli (Kotroni et al. 2014; Emmanouil et al. 2016; Soukissian et al. 2017).

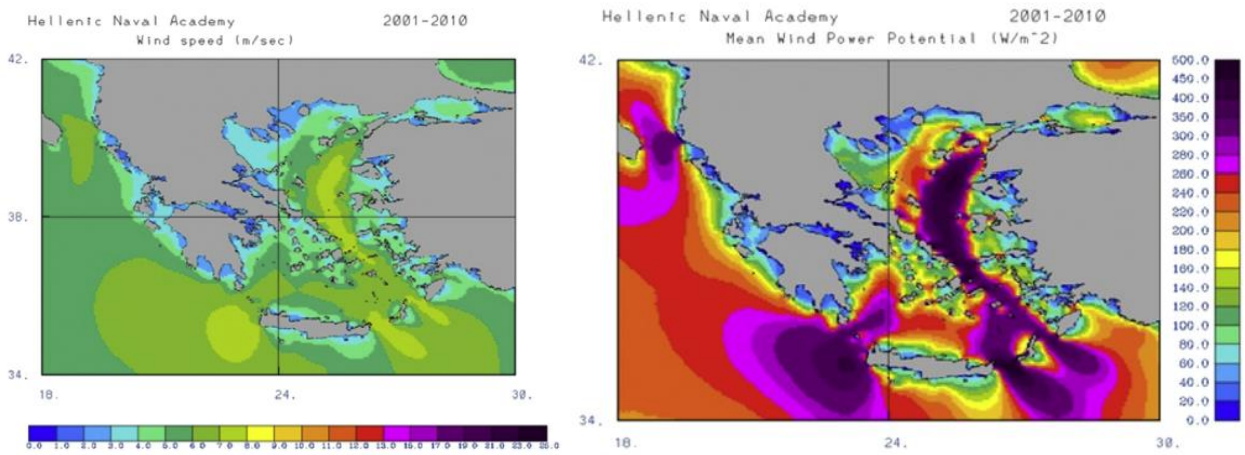


**Figure 4.1.3.1:** 10-years mean wind speed (2000 - 2010) (Left), Mean wind power density (W/m$^2$) (Right) **Source:** Emmanouil et al. (2016)

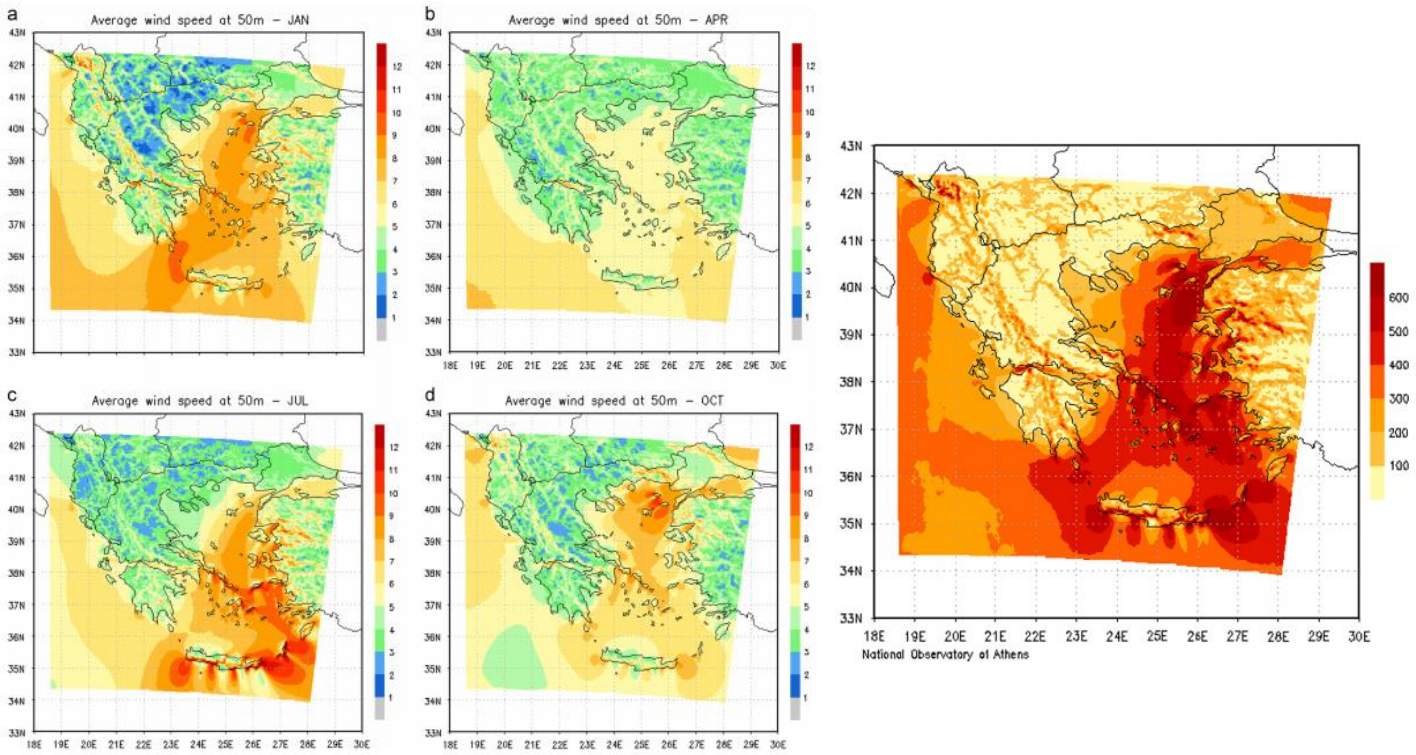


**Figure 4.1.3.2:** Monthly mean wind speed (Typical year) (a-d), Mean wind power density (W/m$^2$) (Right) **Source:** Kotroni et al. (2014)

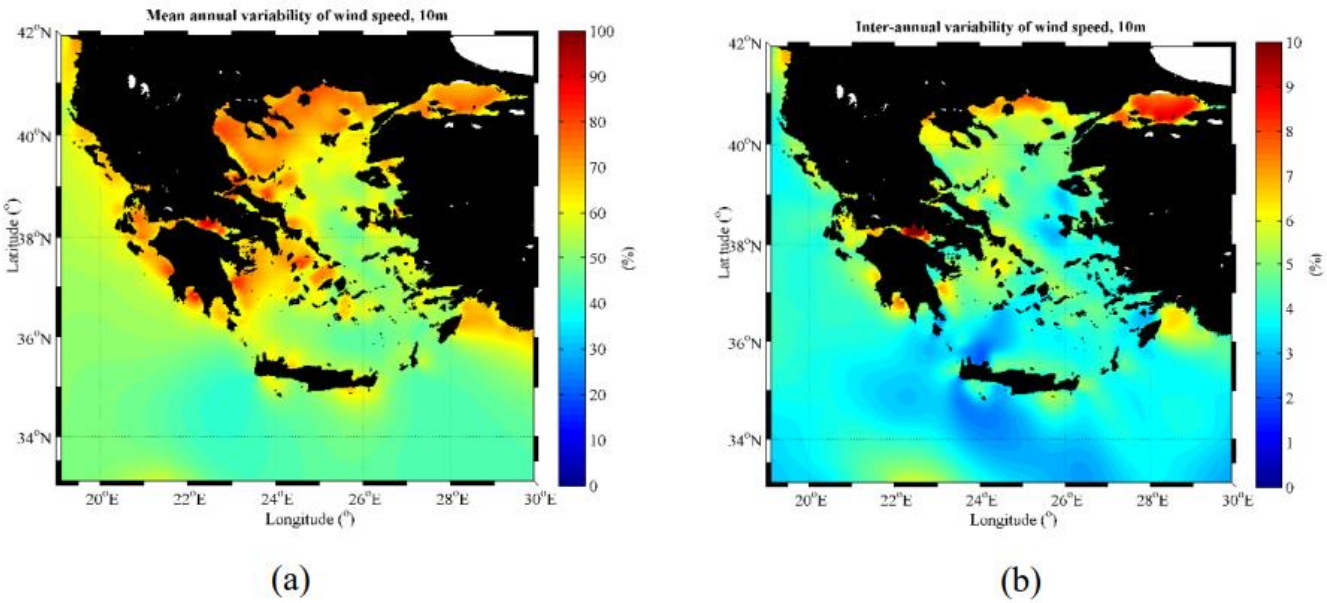


**Figure 4.1.3.3:** Spatial distribution of (a) mean annual variability, (b) inter-annual variability of offshore wind speed at 10 m asl for the period 1995–2009. **Source:** Soukissian et al. (2017)

Considering the wind power potential (Figures 4.1.3.1 – 3), in most areas across the Aegean Sea, the wind potential ranges between 200 – 600 W $m^{-2}$, reaching locally more than 700 W $m^{-2}$ (Kotroni et al. 2014; Emmanouil et al. 2016). Furthermore, based on a 15-year hindcast of wind data spanning from 1995 to 2009, Soukissian et al. (2017) estimated the overall highest values of the mean annual wind power density (~885 W/ $m^{-2}$) is depicted in the central Aegean Sea. Focusing on the behavior of wind power density at the seasonal scale results indicated that the highest values are observed during summer with values reaching 1172 W/ $m^{-2}$ over the southeastern Aegean Sea, winter follows with values exceeding 1090 W/ $m^{-2}$ over the North Aegean Sea, autumn with peak values near 806 W/ $m^{-2}$ over the central Aegean Sea, and finally, spring with the highest values approximating 773 W/ $m^{-2}$ over the central east and eastern Aegean Sea. Contrary, the lowest wind power availability is exhibited at the locations of the Thrace Sea, Thermaikos Gulf and the wider coastal and offshore areas in Pagasitikos Gulf and Western Sporades islands with the measured wind power potential reaching values below 150 W/ $m^{-2}$.

## 4.2 Data acquisition

In developing the core modules and algorithms of the SDSS, the first, and most crucial step, includes identifying, collecting and collating existing relevant data including both spatial and non-spatial information as also qualitative and quantitative particulars. In the current section, all available data used are presented among with their technical characteristics, the available sources and their purpose considering the framework development. All relevant data have been collected during the period of 2015 – 2020 and represent the status quo of the study area for this time period. Moreover, some of the datasets were used in more than one sub-process in the SDSS, highlighted by different color in the Table 4.2.1.1.

Fundamental information describing the spatial distribution of existing human activities, geo-physical and technical characteristics for the North and central Aegean Sea, as also, for the coastal continental part of eastern Greece was collected. Furthermore, detailed non-spatial cost data for OWF deployment related to the functions for calculating a location specific cost indicator were also gathered and analyzed. Table 4.2.1.1 lists the relevant spatial datasets collected and compiled in one harmonized spatial geodatabase consisting of:

1. **Geo-physical data:** Bathymetry, digital elevation model (DEM), marine soil conditions (substrate), landcover, tectonic faults, shoreline and wind speed time series derived from UERRA reanalysis dataset at 10m above sea level (see sub-section 3.2.2).
2. **Human activities:** coastal cities, recreational activities, subsea cables, aquaculture sites, ports, shipping lanes, fishing areas, military use exclusion zones and onshore grid transmission network junctions,
3. **Environmental data:** Marine wildlife density information, NATURA protected areas and nature conservation sites.

### 4.2.1 Geophysical and human activities spatial data

Coastal cities, blue flag beaches, available ports and NATURA 2000 areas obtained from the National portal for spatial datasets (http://www.geodata.gov.gr). Also, elecrical infrastructure

network connection points for RES connection digitized from maps of the Independent Power Transmission Operator (IPTO – http://www.admie.gr). Datasets for shipping density, shipping lanes, subsea cables, fishery and aquaculture are based on information derived from Thal-Xor program (http://www.mspcygr.info/thal-xor) for MSP monitoring in Aegean sea. Tectonic faults derived from EMODnet project database (https://www.emodnet.eu) of the European Marine Observation and Data Network along the European seas. Bird habitats spatial information derived from the Maritime Spatial Planning for the protection and Conservation of the biodiversity in the Aegean Sea – Marisca project (http://www.marisca.eu). Finally, Military zones data provided from the Hellenic Navy Hydrographic Service (HNHS).

**Table 4.2.1.1:** Data acquisition sources, type of spatial data and usage per spatial model

| Data | Source | Type | Usage | |
|---|---|---|---|---|
| **Shoreline** | http://geodata.gov.gr/ | Vector - Shapefile (Polygon data) | All sub-models | |
| **Shipping density (cargo/passs)** | http://www.mspcygr.info/thal-xor/ | Raster - Cell size ≈ 500 m | Exclusion analysis | |
| **Ecological density** | http://www.marisca.eu/index.php/en/ | Vector - Shapefile (Polygon data) | Site prospecting | |
| **NATURA** | http://geodata.gov.gr/ | Vector - Shapefile (Polygon data) | Exclusion analysis | |
| **Bird habitats** | http://www.marisca.eu/index.php/en/ | Vector - Shapefile (Polygon data) | Exclusion analysis | |
| **Fishing - Aquaculture** | http://www.mspcygr.info/thal-xor/ | Vector - Shapefile (Polygon data) | Exclusion analysis | |
| **Military areas** | https://www.hnhs.gr/en/ | Vector - Shapefile (Polygon data) | Exclusion analysis | |
| **Tectonic faults** | http://www.mspcygr.info/thal-xor/ | Vector - Shapefile (Polyline data) | Exclusion analysis | |
| **Cables** | http://www.mspcygr.info/thal-xor/ | Vector - Shapefile (Polyline data) | Exclusion analysis | |
| **Offshore wind** | https://cds.climate.copernicus.eu/cdsapp#!/dataset/reanalysis-uerra-europe-single-levels?tab=overview | Raster - Cell size ≈ 5500 m | Cost assessment | |
| **Digital Elevation Model (DEM)** | https://asterweb.jpl.nasa.gov/gdem.asp https://land.copernicus.eu/imagery-in-situ/eu-dem/ | Raster - Cell size ≈ 30 m | Exclusion analysis | Cost assessment |

| | | | | |
|---|---|---|---|---|
| **Bathymetry** | https://www.hnhs.gr/en/ | Raster - Cell size ≈ 500 m | Exclusion analysis | Cost assessment |
| **Onshore Transmission Junctions** | https://www.deddie.gr/en/ | Vector - Shapefile (Point data) | Cost assessment | |
| **Ports** | http://www.mspcygr.info/ | Vector - Shapefile (Point data) | Cost assessment | |
| **Landcover** | https://land.copernicus.eu/pan-european/corine-land-cover/clc2018 | Vector - Shapefile (Polygon data) | Cost assessment | |
| **Seabed Substrate** | https://www.emodnet.eu/geonetwork/emodnet/eng/catalog.search?node=emodnet#/home | Vector - Shapefile (Polygon data) | Cost assessment | |

All of the relevant vector and raster data are described above are store in a file geodatabase established in ArcGIS 10.5 software (ArcCatalog module). In spite of the fact that the entire structure of the proposed SDSS and sub-modules is based on open-source material and customized algorithms, current geodatabase is working only for storage and data validity and quality check purposes. As a result, an open-source geodatabase establishment is out of scope of the proposed research, although, in later stages an integrated scheme for data storage and quality control check will be integrated to the proposed framework.

Focusing on the data sources presented in Table 4.2.1.1, vector data are stored in the geodatabase as thematic shapefiles (feature classes) comprising a collection of geographic features. These features share the same geometry type (i.e., point, line, or polygon), the same attributes (number of features, identity number, name etc.), the same coordinate system (EPSG 2100 – Greek grid), and the usage of the acquired data, e.g. human activities, nature conservation data, geophysical characteristics etc. On the other hand, raster data are stored as unique raster datasets or catalogs. Each raster image is stored in *.tiff* format as its own thematic layer and if a categorization is needed (expressing common physical characteristics), multiple rasters are grouped into a raster catalog, as a collection of raster data (i.e., the DEM files extracted from ASTERDEM), mosaicked finally into a single raster dataset.

### 4.2.2 Offshore wind data

Two different types of long-term wind speed data (in-situ and reanalysis) were collected and analyzed in order to validate their accuracy as also to assess and quantify the wind energy potential. The in-situ measurements used during this study were acquired from 11 meteorological stations at coastal sites (in mainland and islands) and from 5 buoys (Figure 4.2.2.1) with time series covering a range from 1938 to 2018.


**Figure 4.2.2.1**: Study area representation and distribution of the coastal and offshore wind measurements (meteorological stations and buoys)

The data for Greek meteorological stations were obtained from the Hellenic National Meteorological Service (http://www.hnms.gr) and they were maintained from the National Oceanic and Atmospheric Administration (NOAA) (http://www.ndbc.noaa.gov/). All sites are equipped with propeller anemometers and data are reported every 1 to 6 hours, with sporadic periods of lower frequency (daily values) providing measurements at relatively low heights, with

anemometer heights (above sea level) ranging from 2 m to 120 m. Additionally, the buoys data were obtained from the POSEIDON marine monitoring and forecasting system, established in 2000 under the Hellenic Centre for Marine Research (HCMR) (http://www.poseidon.hcmr.gr) (Soukissian & Chronis, 2000). The buoys' offshore wind measurements are performed at 3 m height above sea level with recording interval of 600 seconds, and the measurements are delivered every 3 hours. Focusing on the data validity, the coastal stations have long-term records but represent coastal conditions, On the contrary, buoys capture offshore wind conditions but have limited or erroneous records because of technical and operation and maintenance reasons.

All of the descriptive and statistical characteristics for all of the stations and buoys are presented in Table 4.2.2.1. For both coastal and offshore measurements, a timestep of 6 hours interval was selected and the time series have been adjusted to 10 m height from the surface by using the log law expressed as:

$$u_z = \frac{u_{ref}}{\kappa} \ln\left(\frac{z-d}{z_0}\right) \qquad (4.2.2.1)$$

, where $u_z$ describes the wind speed at the required height $z$, $u_{ref}$ is referenced wind velocity ($ms^{-1}$), $\kappa$ is the Von *Kármán* constant (~0.41), $d$ is the zero-plane displacement and $z_0$ is the surface roughness (in meters). The roughness length $z_0$ for offshore areas is usually considered to be 0.002 m. and for suburb areas and woodlands is 0.2 (Mendis et al., 2007; Soukissian & Papadopoulos, 2015) while the zero-plane displacement $d$ is set as zero for both cases.

**Table 4.2.2.1:** Names, geographical coordinates, measurement time periods and descriptive information for met. stations and buoys data.

| NOAA | | | | | | | | | |
|---|---|---|---|---|---|---|---|---|---|
| **Mainland Stations** | **Location** | **Years** | **Height (m)** | **Lat** | **Lon** | **N (Obs.)** | **Min** | **Max** | **Zero Values (%)** |
| 166270 | **Alexandroupoli** | 1933 - 2018 | 7.3 | 40.85 | 25.95 | 138826 | 0.44 | 24.65 | 28 |
| 167160 | **Elliniko** | 1949 - 2018 | 21 | 37.88 | 23.74 | 104461 | 0.44 | 38.22 | 24 |
| 166220 | **Thessaloniki** | 1960 - 2018 | 6.7 | 40.52 | 22.97 | 185694 | 0.44 | 26.60 | 26 |

| | | | | | | | | | |
|---|---|---|---|---|---|---|---|---|---|
| 166653 | **Thessaly** | 1991 - 2018 | 16.5 | 39.17 | 23.5 | 28610 | 0.44 | 15.98 | 18 |
| **Islands Stations** | **Location** | **Years** | **Height (m)** | **Lat** | **Lon** | **N (Obs.)** | **Min** | **Max** | **Zero Values (%)** |
| 167060 | **Chios** | 1991 - 2018 | 4.6 | 38.34 | 26.14 | 93391 | 0.44 | 19.07 | 19 |
| 166670 | **Lesvos** | 1960 - 2018 | 18.3 | 39.05 | 26.59 | 127589 | 0.44 | 28.81 | 19 |
| 166500 | **Lemnos** | 1977 - 2018 | 4.3 | 39.91 | 25.23 | 101554 | 0.03 | 28.40 | 18 |
| 166840 | **Mykonos** | 1991 - 2018 | 123.4 | 37.43 | 25.34 | 96250 | 0.44 | 18.33 | 19 |
| 167320 | **Naxos** | 1979 - 2018 | 9.8 | 37.1 | 25.367 | 50328 | 0.44 | 38.13 | 8 |
| 167230 | **Samos** | 1978 - 2018 | 5.8 | 37.69 | 26.91 | 31767 | 0.44 | 42.65 | 5 |
| 166840 | **Skyros** | 1949 - 2018 | 13.4 | 38.96 | 24.49 | 15843 | 0.44 | 20.29 | 30 |
| **Buoys** | **Years** | **Dist. from the Shore (Km)** | **N (Samples)** | **Lat (Approx.)** | **Lon (Approx.)** | **Min (Non-Zeros)** | **Max** | **NaN-Zero Values (%)** | |
| **Athos** | 2000 - 2018 | 26.6 | 22123 | 39.96 | 24.72 | 0.00001 | 33.75 | 20-8 | |
| **Lesvos** | 2000 - 2011 | 21.5 | 14592 | 39.15 | 25.8 | 0.00001 | 33.75 | 16-7 | |
| **Mykonos** | 2001 - 2011 | 3 | 13371 | 37.51 | 25.45 | 0.001 | 67.51 | 16-5 | |
| **Petrokaravo** | 2008 - 2018 | 8.8 | 10428 | 37.6 | 23.56 | 0.01 | 18.59 | 35-1 | |
| **Skyros** | 2007 - 2010 | 10 | 4463 | 39.11 | 24.46 | 0.01 | 20.04 | 23-4 | |

The reanalysis wind speed data acquired for this study are based on the UERRA datasets. An important characteristic of UERRA is the recovery of sub-daily surface meteorological observations to provide inputs as also to assess the quality of future regional reanalysis products (Aschroft et al., 2018). The grid spatial resolution varies between 5.5 km and 11 km in a sub-daily timescale of 6-hours interval. The values are instantaneous meaning that it is valid for the last time step of the integration at the issued time step. The regional reanalysis differs in the NWP model and the data assimilation method used and as a result, COSMO (Consortium for Small-scale Modelling) was employed in the regional reanalysis and the Hirlam Aladin Regional Mesoscale model (HARMONIE-ALADIN) as a starting point to further increase the spatial resolution (Bazile et al., 2017).

Considering the models' capability to reproduce the wind regimes across Europe, the first validation of MESCAN-SURFEX reanalysis results presented by Kaiser-Weiss et al. (2019). In their assessment, they reported that high correlation coefficients indicated the precise capturing of time variability of the wind speed by regional reanalysis for the hourly, daily and monthly scale. However, the resulted data sources come with uncertainties highlighting that "*for threshold-based climate indices, are highly sensitive to bias issues*". Furthermore, they notice that the evaluation results differ with region, month of year, as well as with the temporal and spatial scale. For many wind regimes, and especially where topography varies, a local bias remains and therefore during this study the selected study area constitutes a great opportunity to quantitatively assess these issues. The statistical characteristics of the observational data are demonstrated in Table 4.2.2.1 and for the UERRA reanalysis data in Figure 4.2.2.2.

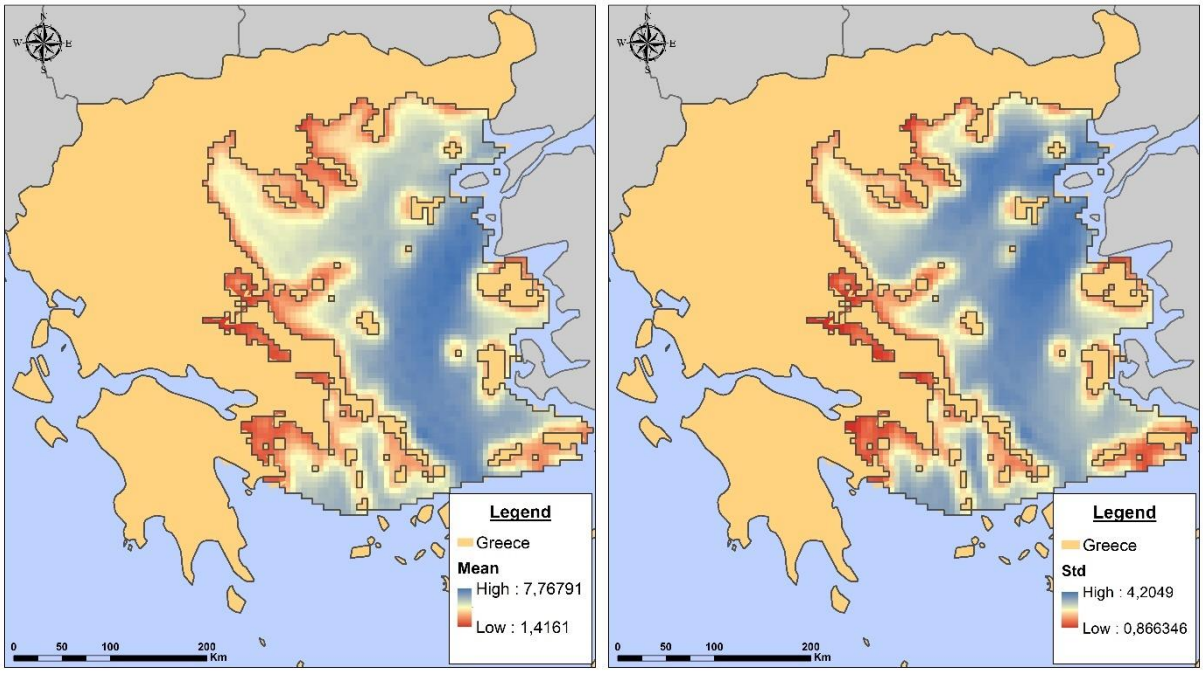

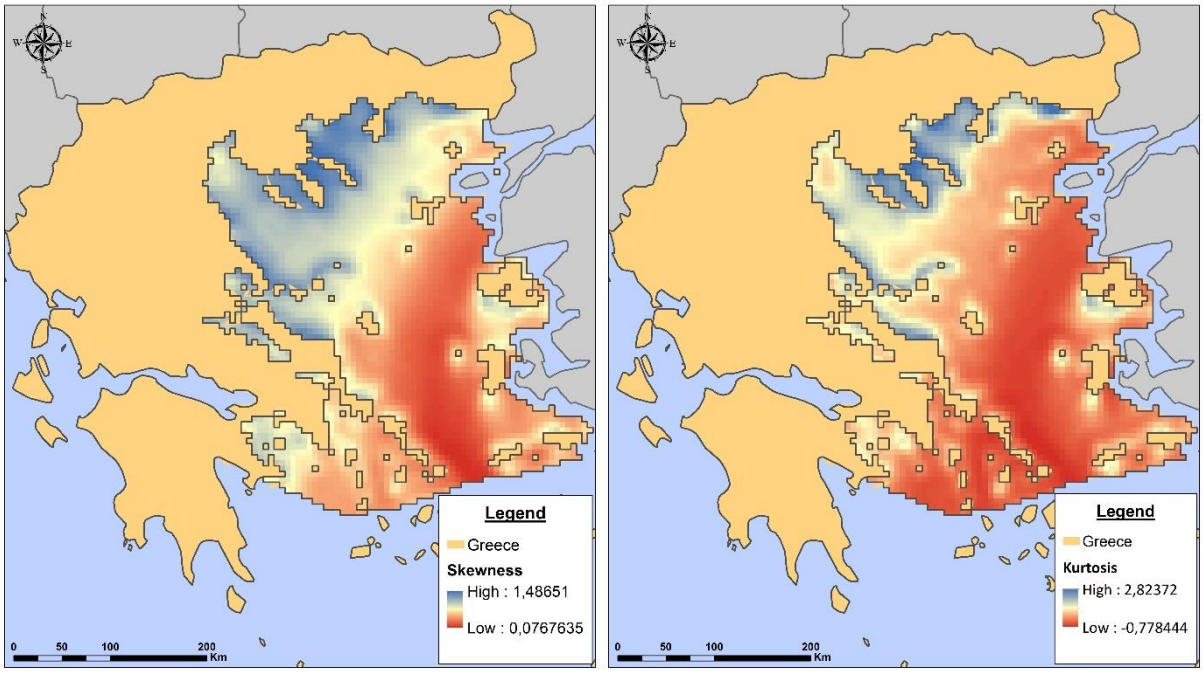


**Figure 4.2.2.2**: UERRA reanalysis statistical characteristics (Mean, Standard Deviation, Skewness and Kurtosis)

For comparison purposes, for both stages of statistical analysis (1. distribution fitting and 2. comparison of co-located samples), the collocation procedure in space (stage 1 and 2) and time (stage 2) was carried out. Particularly, the four nearest wind speed time series of the model were downscaled to the exact location of each station and buoy by applying the weighting mean scheme (Equation 4.2.2.2):

$$u = \frac{\sum_{i=1}^{4} \frac{u_i}{r_i^2}}{\sum_{i=1}^{4} \frac{1}{r_i^2}}, \quad i = 1,2,3,4 \qquad (4.2.2.2)$$

, where $u_1$, $u_2$, $u_3$ and $u_4$ describe the wind speeds at the four closest grid points surrounding a buoy or a coastal station, $r_1$, $r_2$, $r_3$ and $r_4$ stand for the corresponding distances from that exact location, and $u$ is the wind speed. Regarding the temporal collocation, the common time frame of a 6-hour timestep (00:00, 06:00, 12:00 and 18:00 UTC) was selected for both observational and reanalysis time series. Finally, in order to reduce further uncertainties, a quality control was performed on data from coastal sites and buoys. Since the anemometer response occurs at a minimum cut-in value, a portion of the erroneous values below the minimum recorded value was

removed (0–Station/Buoy minimum value above zero). As a result, to prevent this excessive number of calm recordings from skewing the selected distributions fit, a portion of these values was removed, while still allowing a fair number of low but legitimate wind speed values to remain for further processing.

### 4.2.3 OWF configuration and fixed-cost data

In order to analyze and assess the various cost and energy-related components, it will be useful to refer the OWF cost configuration steps, illustrated in Figure 2.1.2.1 (Sections 2.1.2.5), related to the sub-cost components of a project (Development and Consenting, Production and Acquisition, Installation and Commissioning, O&M and Decommissioning) as also to the annual energy calculation and power output.

The necessary information was collected from multiple sources based on the available literature review, mainly using specialized databases, governmental and manufacturers reports and research and review articles. It should be clear that there are numerous significant non-spatial variables that would greatly affect the total cost and energy production of a proposed OWF and to a lesser extent, the spatial costs as well. These parameters are:

- the model (WT type) and technical characteristics (power curve) of the proposed offshore wind turbines selected for the proposed OWF (Figure 4.2.2.1);
- the relationship between the number of turbines and energy output of an OWF considering the optimal number of WTs as also the optimal distances among wind generators to reduce wake losses and inter-array cables costs (wind turbines spacing – array density Figure 4.2.2.1);
- The estimated fixed costs for the first stage of planning a potential OWF (Development and Consenting) which includes: i) Legal Authorization, and ii) Contingencies (Table 2.5.1.1, Section 2.5.1);
- Associated materials (e.g., cost of steel), personnel and vessels' day rates considering the Production and acquisition as long as the installation and decommissioning phase;

- Fixed cost parameters considering the production and acquisition as also the installation phase, including: i) inter-array cables, ii) offshore and onshore substations (topside) and iii) Monitoring systems (e.g. SCADA) (Table 2.5.3.1 - Table 2.5.3.4, Section 2.5.3);
- During the Operation and Maintenance stage non-spatial costs are considered: i) the rental fees, insurance and transmission charges and ii) fixed costs such as the port fees, vessels costs during the maintenance procedures and labor expenses must also be considered (Table 2.5.5.1, Section 2.5.5);
- Parameters related to the total estimated losses including e.g., wake effects (power productions losses), transmission to the shore and inter-array cables' losses, downtime and availability factor, discount rate, loss of earning etc.
- Finally, during the decommissioning stage, additional costs must be considered denoting the entire decommissioning procedures, wastes management, site clearance and post monitoring procedures (Table 2.5.6.1, Section 2.5.6).

| | |
|---|---|
| **Rotor diameter (D)** | 128m |
| **Hub height** | 110m |
| **Rated Power** | 5.0 MW |
| **Control** | Individual blade pitching |
| **Cut-in wind speed** | 2 m/s |
| **Rated wind speed** | 14 m/s |
| **Cut-out wind speed** | 27 m/s |
| **Wind turbine spacing** | 7 D |

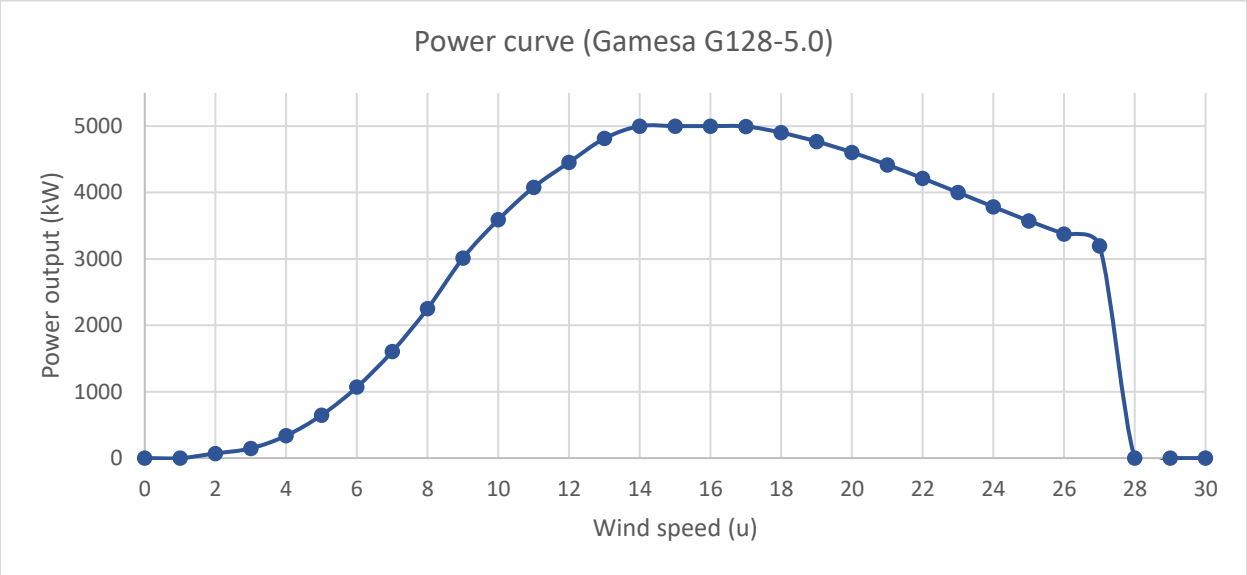

| | |
|---|---|
| **Rotor diameter (D)** | 164m |
| **Hub height** | 125m |
| **Rated Power** | 8.0 MW |
| **Control** | Individual blade pitching |
| **Cut-in wind speed** | 4 m/s |
| **Rated wind speed** | 13 m/s |
| **Cut-out wind speed** | 25 m/s |
| **Wind turbine spacing** | 7 D |

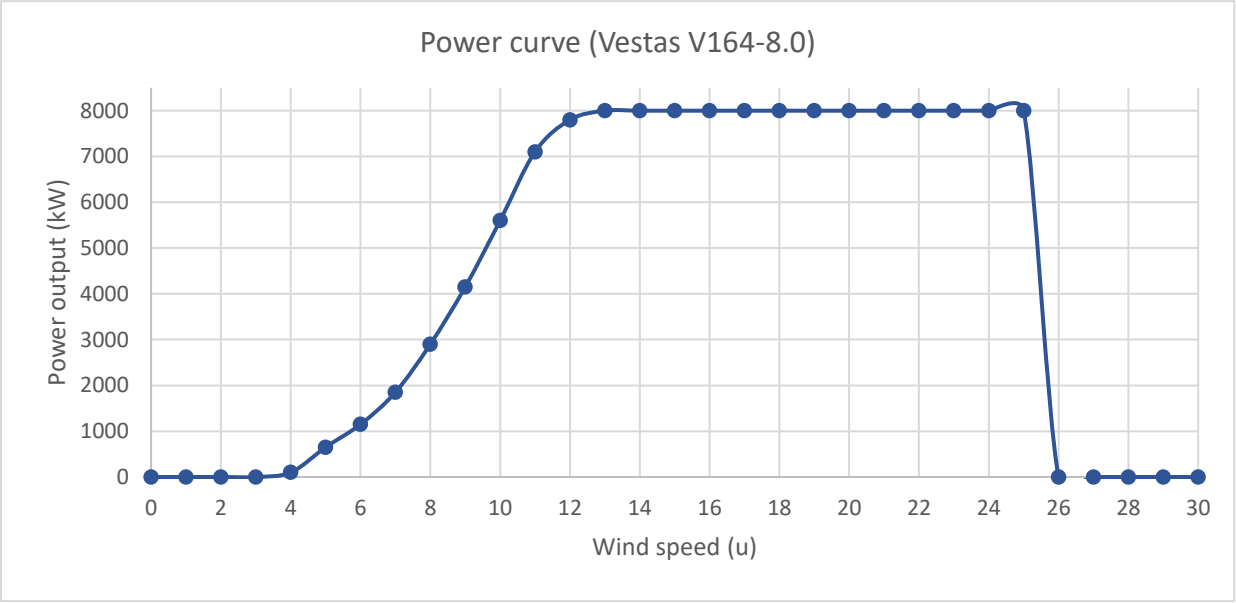


| | |
|---|---|
| **Rotor diameter (D)** | 190m |
| **Hub height** | 140m |
| **Rated Power** | 10.0 MW |
| **Control** | Individual blade pitching |
| **Cut-in wind speed** | 4 m/s |
| **Rated wind speed** | 11.5 m/s |
| **Cut-out wind speed** | 30 m/s |
| **Wind turbine spacing** | 7 D |

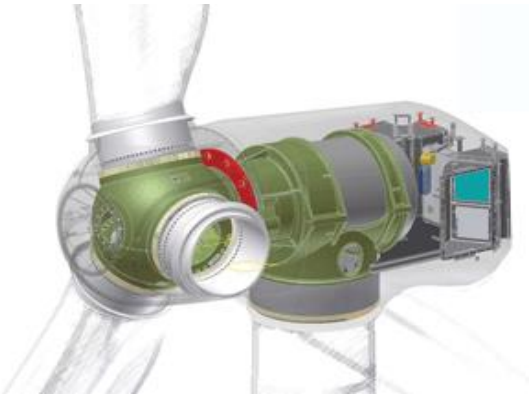

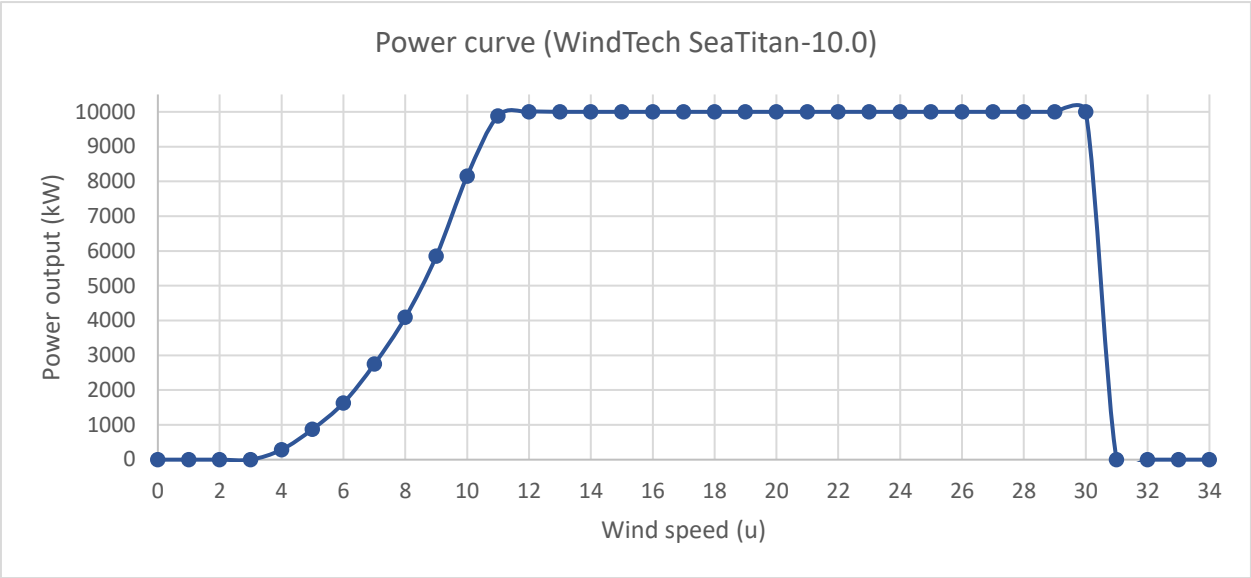


**Figure 4.2.3.1:** Specifications and Power curves of the selected Offshore Wind Turbines, Sources: a) Gamesa G-128 (Nagababu et al., 2017, photo: http://transfer-lbc.com/), b) Vestas V-164 (https://en.wind-turbine-models.com/, photo: https://mhivestasoffshore.com/), c) WindTech SeaTitan (AMSC, 2012)

Although the economic effects of the non-spatial variables may be rather simple to be estimated, the idea of trying to calculate the energy production and spatial fixed costs for hypothetically varying-sized OWFs, is a very complex task. The levelized costs approach, as already highlighted in the literature review (Section 2.5), provides a rather straightforward method for quantifying OWFs' costs across to the expected lifetime of the project. However, it has several limitations which are discussed below.

One of the most important cost parameters is the choice of discount rate expressed in per cent quantity. A low discount rate value could decrease dramatically the total LCoE and the opposite. According to previous studies, values ranging between 7 - 10% are representing a plausible mid-point in the range of discount rates. According to Heptonstall et al., (2012) and Myhr et al. (2014) there is a notable point that variations of ±2% in the discount rate contribute with an ±10 - 13% of the LCoE. Furthermore, another crucial parameter is the load factor which has a direct impact on the resulted LCoE by affecting a number of units of electricity a plant's costs are allocated over. Load factor assumptions affect numerous fields of an OWF's sub-costs

linked to the WT selection and downtime events due to components failures and the O&M cost as long as the fixed and variable maintenance costs are increase or decrease.

## 4.3 Data quality and scale determination

### 4.3.1 Data quality

The aim of the data quality assessment is to evaluate the origin of the data, identify the main sources of uncertainty, the spatio-temporal accuracy and the data integrity, reliability and completeness. Data evaluation is a critical step for both the modelling and assessment processes as long as the data quality may influence the reliability of the analyses and the interpretation of the expected results. However, data evaluation process is not always an objective task, because various aspects that affect data quality are arbitrary (e.g., geographic position, accuracy, spatial resolution or spatial/temporal extent), hence, suffer from intrinsic biases or uncertainties. In addition, metadata are not usually expressed in a quantitative manner or their documentation is poor and therefore, difficulties occur on extracting meaningful results linked to the overall data quality, especially when a large number of datasets is combined. The scope of this section is not to provide an in-depth analysis and assessment of the data quality, although, a characterization of the main key quality characteristics for each dataset is highlighted and discussed.

In particular, five different quality assessment metrics are referred consisting of the (Deviller et al., 2006; Li et al., 2012; Docan, 2012; Issaris et al., 2012; Sini et al., 2017):

1. **Lineage** which identifies the information necessary for reconstructing the history of a dataset and to deduce its potential usage (data sources, origin, reference domain, coordinate systems, data acquisition, compilation and derivation, data conversion, processing dates and transformations);
2. **Completeness** or data integrity is a measurable error of omissions observed between the data and the specifications expressing the presence and absence of features, their attributes and relationships;

3. **Temporal relevance** denotes the minimum duration of an event that is discernible and is affected by the interaction between the duration of the recording interval and the rate of change in the event;
4. **Spatial accuracy and resolution** refer to the fineness of detail that can be observed and the ability to resolve patterns over space characterized by absolute or external accuracy, relative or internal accuracy or gridded data position accuracy and finally;
5. **Logical consistency** denoting the spatial or temporal inconsistencies of a dataset. Considering spatial data, logical consistency determines whether the data are topologically correct.

Each of the aforementioned characteristics is divided into five quality categories with a score between 1 (high quality) and 5 (low quality) (see more in Sini et al., 2017-Table 3) and the results are demonstrated in Table 4.3.1. Data quality gradings are based on already existing analytical documentation and validation procedures provided for each data source or by topological rules testing for inconsistencies, gaps or inaccuracies. Moreover, when there is a lack of valid information or metadata entries, data quality scores are presumed to be rather low. An increased importance is given to the data related to the offshore wind speed time series and cost evaluation (bathymetry) (red color in Table 4.3.1) consisting for the key input parameters for the cost and site-prospecting models.

In particular, an extended assessment concerning the spatial and temporal accuracy is carried out for the offshore wind (UERRA reanalysis) datasets (see Section 6.3.3), although, UERRA reanalysis data seem to have a fair agreement with in-situ records but issues concerning spatial accuracy and resolution are highlighted (UERRA documentation/Metadata records). For errors in interval/ratio fields, such as DEM, bathymetry, landcover and marine soil substrate, error quantification is often performed by comparing a given data set against in situ (observed) data.

**Table 4.3.1**: Data quality control grading in terms of their lineage, completeness, spatio-temporal accuracy and logical consistency.

| Data | Lineage | Completeness | Temporal consistency | Spatial accuracy | Logical consistency |
|---|---|---|---|---|---|

| | | | | | |
|---|---|---|---|---|---|
| **Offshore wind** | 1 | 2 | 1 | 5 | 4 |
| **Bathymetry** | 4 | 4 | 2 | 3 | 2 |
| **Digital Elevation Model (DEM)** | 1 | 2 | 1 | 2 | 2 |
| **Landcover** | 1 | 1 | 1 | 3 | 3 |
| **Seabed Substrate** | 2 | 3 | 2 | 4 | 3 |
| **Ecological density** | 2 | 3 | 2 | 2 | 3 |
| **Bird habitats** | 2 | 3 | 2 | 2 | 3 |
| **NATURA areas** | 1 | 2 | 2 | 2 | 2 |
| **Ports** | 4 | 4 | 2 | 2 | 2 |
| **Tectonic faults** | 2 | 3 | 2 | 4 | 3 |
| **Fishing areas - Aquaculture** | 4 | 4 | 2 | 2 | 2 |
| **Cables** | 4 | 4 | 2 | 3 | 4 |
| **Shipping density (cargo/passs)** | 1 | 2 | 2 | 2 | 3 |

In view of the spatial data acquired, EU-DEM is a hybrid product based on SRTM and ASTER GDEM data fused by a weighted averaging approach. Data comparison measures such as RMSEs summarize elevation errors in EU-DEM as a single value of +/- 7 meters (EUDEM-Metadata). Considering CORINE landcover data, the accuracy of the landcover classification is the degree to which the map landcover agrees with the observed land cover classification. All CORINE features are delineated and classified on satellite images with better than 100 meters positional accuracy and 0.25 $km^2$ minimum mapping unit (CLC 2018-Metadata). On the contrary, seabed substrate and tectonic faults data derived from EMODNet project seem to preserve a lot of issues considering vertical, horizontal and temporal resolution and coverage (Pinardi et al. 2017). Finally, there is a clear lack of analytical documentation and metadata entities regarding the bathymetry data derived from the HNHS (https://www.hnhs.gr/).

### 4.3.2 Scale determination

The term scale is generally characterized by two dimensions comprising: a) the temporal scale, and b) the spatial scale. The spatial scale is comprised by namely: i) the size (e.g., municipality, province, continent), ii) the level (e.g., local, regional, national), and iii) the relation (as a complex mix that includes space, place and environment) (Goodchild, 2001a). In the context of geo-sciences, Goodchild (2001b) categorized four meanings for the term scale: i) implication of level of spatial detail, ii) representative fraction, iii) spatial extent and iv) process scale. Considering spatial modelling, scale determination plays a key role on quantifying and reducing data and results uncertainty. Therefore, it is crucially important to select the appropriate scale due to the data heterogeneity, accuracy and reliability. On the other hand, temporal scale identification gives a clear picture of the modelling scheme, targets and expected outputs. Temporal scale determination is linked to the data quality and volume, by expressing the capability of a spatial model to provoke from short to long-term analysis. Based on this statement, in order to obtain reliable results, the scale of analysis should match the temporal scale at which the processes under investigation are assumed to operate.

Focusing on OWF planning, many different scale measures can be identified linked with both the spatial and the temporal modelling context. For instance, data at the level of individual WTs have a high accuracy. However, a disadvantage at this scale is that the data tend to be commercial and costly and modelling procedures quite demanding and complex. On the other hand, when the spatial resolution decreases (increase of the cell size), vital information may be discarded or avoided. Thus, considering modelling purposes, the user must always clarify the level of detail in accordance to the data availability and the scope of the analysis. As a result, when coupling RES planning and GIS, there are at least three reasons why one has to work under pre-defined spatial and temporal scales in order to aggregate or disaggregate the data (Goodchild, 2001a):

1. Common scale (e.g., wind turbine level or wind farm level) for all data is required for the analysis or validation of the results when working with discrete surfaces (e.g., rasters);
2. Faster computing time is desired (depends on spatial and temporal resolution);

3. Inherent data uncertainty in both spatial and temporal extents;
4. Consideration of data privacy aspects are required (increasing spatial and temporal resolution may lead to data availability issues).

Hence, it is essential to apply methods that can store and process data at different scales and most importantly to homogenize spatial data under pre-defined spatial or temporal scales. Considering temporal scale determination, offshore wind data along with WT characteristics and cost-related information play a key role. The lack of a dense network of in-situ records along with the low temporal coverage (6 hours) of UERRA reanalysis data seems to be sufficient for a less uncertain long-term assessment framework (e.g., 1 year, 25 years, 50 years or more), although, for short-term wind resource assessment and wind power forecasting is not essential. Furthermore, the lack of analytical WTs technical specifications is crucial, considering energy production, load factors and failures rate for prediction and forecasting purposes in short-term periods (lasting from minutes to several months).

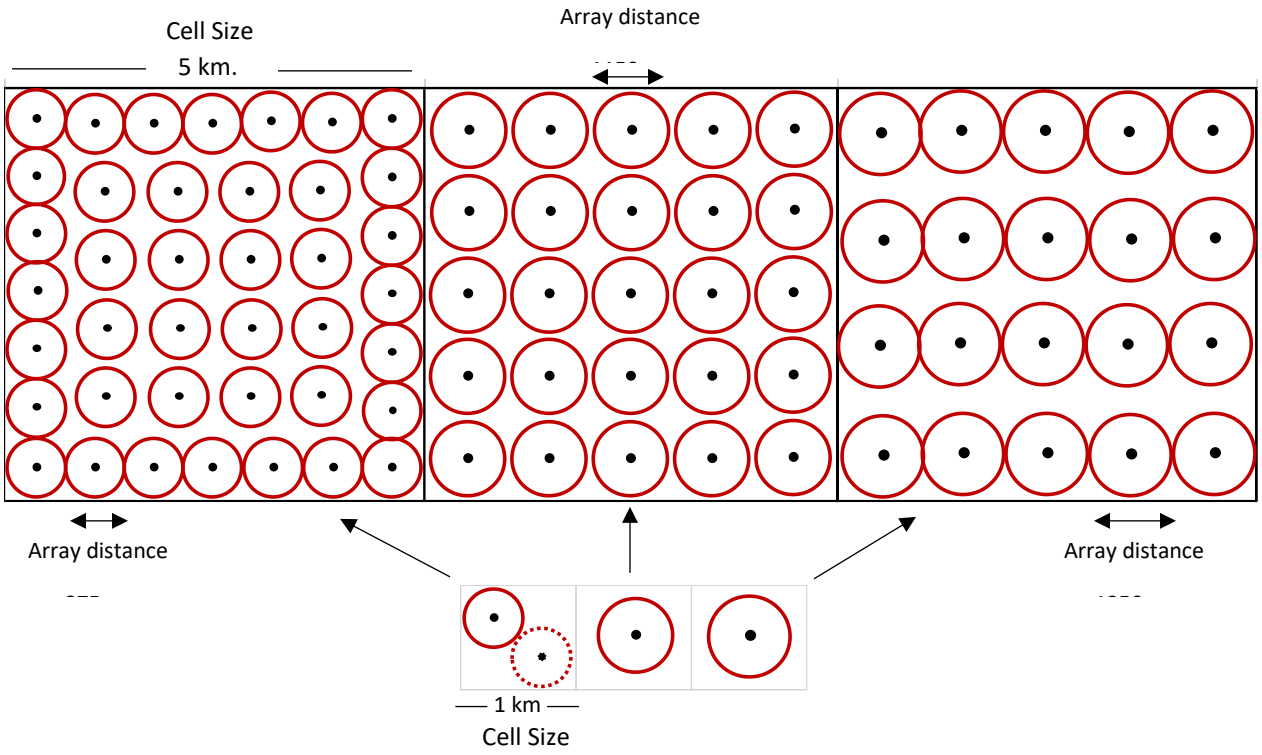


**Figure 4.3.2.1**: Scale determination differences for 1- and 5.5-kilometers cell size considering the total number of WTs consisting of the OWF

For the spatial scale determination, the purpose and the level of planning of each proposed model linked with the data accuracy indicates the identical spatial resolution in order to acquire less uncertain but valuable outputs. All raster datasets acquired have a spatial resolution ranging from approximately 25 - 5500 meters. In addition, considering the level of planning e.g., regional or national or the level of spatial generalizations to be applied, the proposed models are working at either WT or OWF level. However, a loss of vital spatial information has to be considered when modelling for instance, the foundation or the export cables cost where a cell size of 1000 or 5000 meters is not sufficient and leads to increased uncertainties. As an illustrative example, two different scenarios may be considered with a spatial resolution of 1 and 5-kilometers cell size (Figure 4.3.2.1).

In order to provide practical estimates of the wind energy production and the sub-costs of an OWF, technical parameters of the wind turbines and the OWF configurations such as the rotor diameter $D_{wt}$ (m), the WTs spacing in both axes (horizontal-$WD_{sps}$ and vertical-$WD_{spd}$ axis) must be pre-defined, in order to set the optimal number of WTs in each pixel. Therefore, when the OWF capacity is 500 MW, a total amount of 80, 50 and 40 WTs with installed capacity of 5, 8 and 10 MW is considered. Thus, using Equations 4.3.2.1 - 2, for a pixel size of 1000 m., and a wind turbine spacing of 8 and 6 times the rotor diameter (*D*), the total number of WTs per pixel is calculated as 1.95 (5 MW), 1.26 (8 MW) and 1.01 (10 MW) for a total number of pixels equal to 50 for reaching the 500 MW of installed capacity. Multiple regression model of Equation 4.3.2.1 is based on Borrmann et al., (2018) where descriptive data for more than 40 OWFs are demonstrated, considering the total area consumption and the WTs rated power, diameter and layout configuration. Thus, the total area required per WT and the number of pixels needed to reach a pre-defined capacity are estimated through:

$$WT_{area} = 0.0688\, WD_{spd} + 0.0485\, WD_{sps} + 0.0078\, D_{wt} - 1.2644 \qquad (4.3.2.1)$$

$$N_{pwts} \approx Cell_{size}{}^{2} / WT_{area} \qquad (4.3.2.2)$$

$$N_{pixels} = \sum_{i}^{I} N_{pwts} P_{wt}\,, \qquad for\ I = OWF_{cp} \qquad (4.3.2.3)$$

for $N_{pwts}$ as the total number of WTs per pixel, $P_{wt}$ stands for the rated power of each individual wind turbine and $N_{pixels}$ is the total pixels required to reach the installed capacity $OWF_{cp}$ set by the user.

Consequently, Figure 4.3.2.1 illustrates the final OWF output for different spatial resolutions (1 and 5 km.). Analyzing Figure 4.3.2.1, it is clear that for different cell sizes, the total amount of WTs per pixel differs. Therefore, in order to reduce uncertainties and the loss of vital information, a resampling of all raster surfaces to the minimal cell size is meaningful, for example, when the bathymetric data have increased accuracy (i.e., 500 m. or 1000 m.). Conversely, if the user increases the cell size to 10 km., some rough cost estimates may derive due to the resampling techniques applied and a significant loss of information occurs, subject that will be further analyzed, quantified and discussed in Sections 5 and 6.

## References


1. **AMSC, (2012):** SeaTitan 10 MW Wind Turbine, Maximum power per tower for offshore environment, AMSC Windtec Solutions
2. **Ashcroft L., Coll J.R., Gilabert A., Domonkos P., Brunet M., et al. (2018):** A rescued dataset of sub-daily meteorological observations for Europe and the southern Mediterranean region, 1877-2012, *Earth Syst. Sci. Data:*10:1613-1635
3. **Bazile. E., Abida. R., Verelle. A., Le Moigne P., and Szczypta C., (2017):** MESCAN-SURFEX surface analysis, deliverable D2.8 of the UERRA project
4. **Devillers, R., Jeansoulin, R., and Goodchild, M. F. (2006):** Fundamentals of spatial data quality. ISTE London.
5. **Docan D. C., (2013):** Spatial data quality assessment in GIS, *Recent Advances in Geodesy and Geomatics Engineering*, GENG2013 Conference Proceedings, WSEAS Press: Antalya, Turkey
6. **Emmanouil G., Galanis G., Kalogeri C., Zodiatis G., and Kallos G., (2016):** 10-year high resolution study of wind, sea waves and wave energy assessment in the Greek offshore areas, *Renewable Energy*:90;399-419
7. **Goodchild, M.F. (2001a):** Metrics of scale in remote sensing and GIS, *International Journal of Applied Earth Observation and Geoinformation*, 3(2);114–120.
8. **Goodchild, M.F. (2001b):** Models of scale and scales of modelling. In N. J. Tate & P. M. Atkinson (Eds.), *Modelling scale in geographical information* (pp. science:3–10). Chichester: John Willey & Sons
9. **Heptonstall P., Gross R., Greenacre P., and Cockerill T., (2012):** The cost of offshore wind: Understanding the past and projecting the future, *Energy Policy*:41;815-821

10. **Issaris, Y., Katsanevakis, S., Pantazi, M., et al. (2012):** Ecological mapping and data quality assessment for the needs of ecosystem-based marine spatial management: case study Greek Ionian Sea and the adjusted gulfs, *Mediterranean Marine Science*, 13(2)
11. **Kotroni V. ,Lagouvardos K., and Lykoudis S., (2014):** High - Resolution model - based wind atlas for Greece, Institute for Environmental Research, *Renewable and Sustainable Energy Reviews*:30;479–489
12. **Li D., Zhang J., and Wu H., (2012):** Spatial data quality and beyond, *International Journal of Geographical Information Science*:26(12);2277-2290
13. **Lioutas L., and Tsimopoulou V., (2010):** A Systematic Approach of Greek Coastal Zone Management, Delft University of Technology, MSc Thesis
14. **Mendis P., Ngo T., Haritos N., Hira A, Samali B., and Cheung J., (2008):** Wind loading on tall buildings, *EJSE Spec Issue Load Struct.:*3:41–54.
15. **Myhr A., Bjerkseter C., Ågotnes A., and Nygaard T. A., (2014):** Levelised cost of energy for offshore floating wind turbines in a life cycle perspective. *Renewable Energy*:66;714-728.
16. **Nagababu G., Kachhwaha S.S., and Savsani V., (2017):** Estimation of technical and economic potential of offshore wind along the coast of India, *Energy*:138;79-91
17. **Papageorgiou M., (2016):** Marine spatial planning and the Greek experience, *Marine Policy*:74;18-24
18. **Pinardi N., Simoncelli S., Clementi E., Manzella G., Moussat E., Quimbert E., et al. (2017):** EMODnet MedSea CheckPoint Second Data Adequacy Report (Version 1). European Marine Observation and Data Network.
19. **Sini M., Katsanevakis S., Koukourouvli N., Gerovasileiou V., Dailianis T., Buhl-Mortensen L., et al., (2017):** Assembling Ecological Pieces to Reconstruct the Conservation Puzzle of the Aegean Sea, *Front. Mar. Sci.*:17
20. **Soukissian T. H., and Chronis GTh., (2000):** POSEIDON: marine environmental, monitoring, forecasting and information system for the Greek Seas, *Mediter Mar. Sci.*:1(1):71-78
21. **Soukissian T, Hatzinaki M, Korres G, Papadopoulos A, Kallos G, and Anadranistakis E., (2007):** Wind and wave atlas of the Hellenic seas. *Hell. Cent Mar Res Publ.*
22. **Soukissian T., Prospathopoulos A., Hatzinaki M., and Kabouridou M. (2008):** Assessment of the wind and wave climate of the Hellenic seas using 10-Year hindcast results, *Open Ocean EngJ.*:1;1–12.
23. **Soukissian T. H., and Papadopoulos A., (2015):** Effects of different wind data sources in offshore wind power assessment, *Renewable Energy*:77:101 – 114
24. **Soukissian T. H., Karathanasi F., and Axaopoulos P. (2016):** Satellite Based Offshore Wind Resource Assessment in the Mediterranian Sea, *IEEE Journal of Oceanic Engineering*
25. **Soukissian T., Papadopoulos A., Skrimizeas P., Karathanasi, Axaopoulos P., et al. (2016):** Assessment of offshore wind potential in the Aegean and Ionian Seas based on high-resolution hindcast models results, *AIMS Energy*:5(2);268-289
26. **Topouzelis K., Makri D., Stoupas N., Papakonstantinou A., and Katsanevakis S., (2018):** Seagrass mapping in Greek territorial waters using Landsat-8 satellite images, *Int. J. Appl. Earth Obs. Geoinformation*:67;98-113

# 5. Site Selection Tools

## 5.1 Methodology and SDSS Outline

Two different geo-computational schemes are needed when trying to implement a SDSS: i) a spatial database management system (geodatabase) along with a GIS platform in order to handle and visualize all relevant spatial information (inputs and outputs) and ii) the spatial decision support tool (SDSS) with a graphical user interface (GUI) incorporating all of the spatial analysis routines. The ESRI's GIS products (ArcGIS software) are selected to establish the spatial database and to visually inspect all the inputs and outputs. As already highlighted, the implementation of an open-source geodatabase management system is out of scope of the proposed framework, at least for the initial stages of development. Focusing on the technical aspects, the core methodological framework is developed using an object-oriented programming language (Python) and a broad four-stage (pre-processing procedures are not included) methodology was applied (Figure 5.1.1) consisting of:

1. The **first part** of the SDSS consists of the statistical analysis of the offshore wind time series marginal structure using the most well-documented probabilistic models for wind-speed analysis (Weibull) and three-parameter Weibull-related distributions (Burr Type III and XII, Generalized Gamma), as well as the tails behavior and extremes response based on preliminary assessment indicators. Furthermore, in-situ records are compared with reanalysis data for assessing model's performance to reproduce coastal and offshore wind regimes and variability. The potential offshore wind power output and the corresponding errors for the entire study area, based on the UERRA reanalysis data, are determined and quantified. Finally, a generalized mathematical framework for stochastic generation of synthetic wind speed and power time series is applied based on some key statistical characteristics (wind's intermittency, long-term persistence and distribution functions). Based on the statistical and probabilistic offshore wind assessment results, multiple scenarios are developed focusing on the stochastic generation of offshore wind regimes in different time scales, periods and under multiple probabilistic models in order

to approximate relevant uncertainties of the LCoE and NPV linked with the long-term variability of the estimated power output.

2. The **second step** includes identifying, collecting and collating relevant spatial data based on the geomorphological, physical and national legislative regulations and MSP international guidelines in order to "filter" non-suitable areas for further OWF site prospecting. Fundamental information required for the SDSS are data records describing all coastal and marine human activities, nature conservation areas, technical restrictions and minimum distances from the shoreline. Finally, for the North and Central Aegean Sea, all exclusion areas are mapped using different restriction scenarios. In addition, the spatial distribution of existing sea use functions and their compatibility is assessed in terms of the associated conflicts among human activities and human-environment interactions.
3. The **third stage** comprises all cost models and functions related to the capital and decommissioning expenditures (CAPEX and DECEX) as well as the operation and maintenance (O&M) costs estimates. Spatially-explicit cost functions are established and presented for the OWF components in order to accurately estimate production and acquisition, installation, O&M and decommissioning cashflows. In addition, for distance-based cost functions, i.e., installation, O&M, transmission routes delineation and decommissioning activities, Least Cost Path (LCP) algorithms are established in order to delineate optimum corridors for the transmission cables paths and the vessels' routes respectively. The scope of the LCP models is to reduce uncertainties in the aforementioned cost calculations.
4. The **last stage** of the SDSS, entails the results from the first stage (energy yield and wind power variability), the second step (screening analysis), and the third stage (cost modelling). Furthermore, relative physical (bathymetry and wind power variability) objectives are used, in order to optimize (minimize or maximize according to the objectives and the user's preferences) the parameters extracted from the previous steps in a simplified version of the spatial optimization set-up. For the first configuration of the SDSS, a techno-economic assessment is applied based on the Levelized Cost of Energy

(LCoE) and the Net Present Value (NPV) indicators for quantifying the inherent trade-offs of the unit cost of electricity produced along with the current value of future cash flows. To accomplish this, a multi-objective spatial optimization framework is set for allocating continuous and compact optimal areas for OWF siting. Thus, an efficient integer programming model is used to identify multiple clusters of OWFs by maximizing revenues, compactness and guaranteeing contiguity while minimizing CAPEX, O&M and DECEX, by satisfying in parallel relevant technical and physical restrictions for all the selected cells of the final optimal areas.

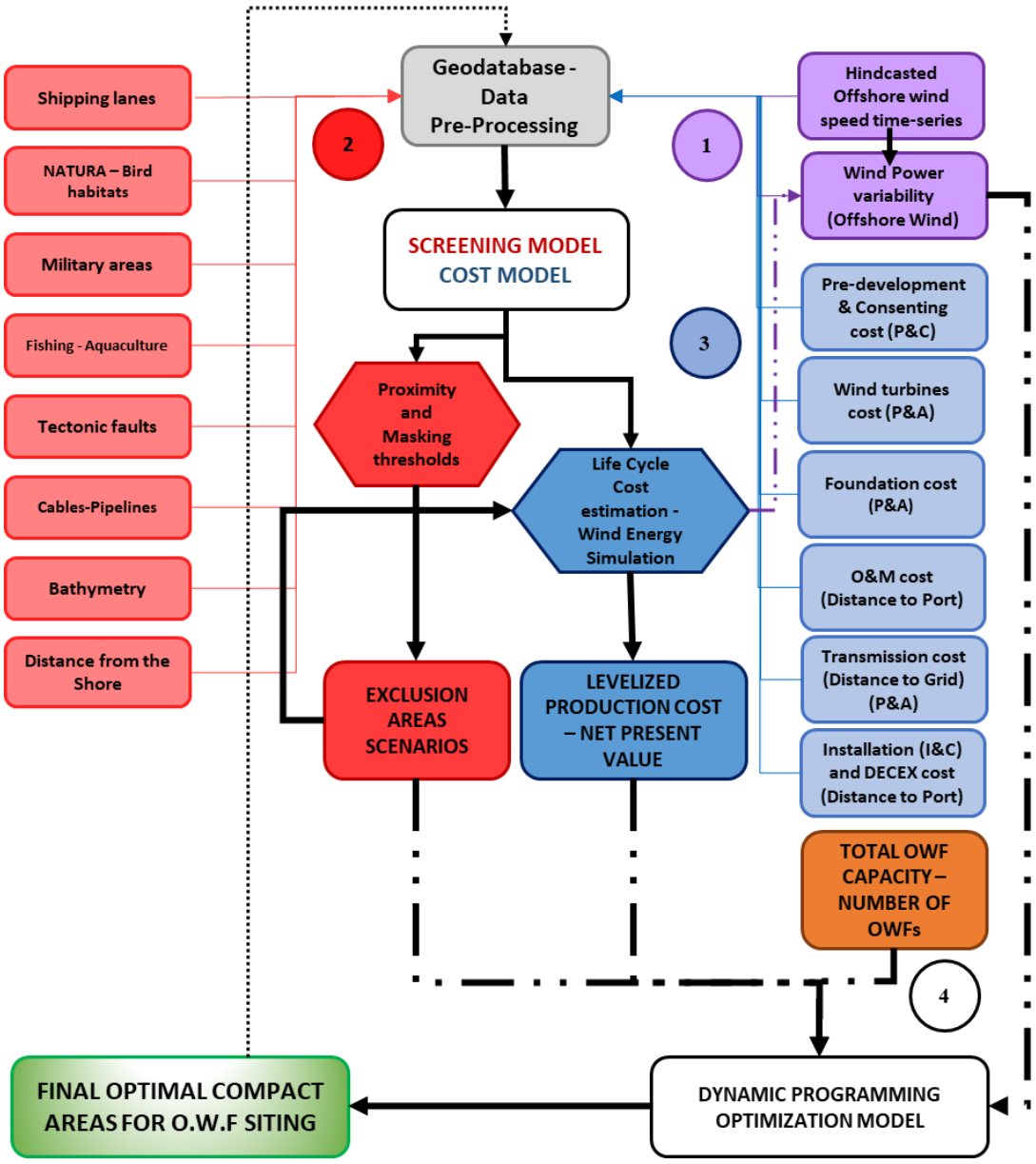


**Figure 5.1.1**: Methodology and sub-models outline

In order to establish the spatial modelling scheme illustrated in Figure 5.1.1, multiple Python libraries are used focusing on numerical computational tools and arrays operations (Numpy), scientific, statistical and technical computing (Scipy, Statsmodels), time series analysis (Pandas, Statsmodels), manipulation of complex networks (NetworkX), spatial data handling (GDAL, Rasterio, Fiona, PyShp, Shapely, netCDF) along with the Gurobi optimization suite (Gurobi Optimization, 2018) for mixed-integer programming. Gurobi Optimization was founded in 2009 (from the CPLEX optimization team) and revolutionized computer applications and the mixed-integer programming world (Gurobi Optimization, 2018). Finally, for the SDSS implementation Python's PyQT5 is selected in order to connect all sub-models with the GUI as also Qt Designer for the graphical environment customization due to its flexibility and easy integration with all of the sub-modules. The scope of the interface is to aid users' interaction with the computer system and to assist in the analysis of the outcomes.

## 5.2 Integrated Offshore Wind Resource Assessment and Modelling

The first step of the SDSS is based on three important features and innovations in either the wind resource assessment or stochastic wind simulation fields which are summarized as follows:

1. The climacogram stochastic tool (i.e., variance of average process vs. scale) is used for the analysis of the dependence structure (Generalized Hurst-Kolmogorov process) with focus on the variability of the wind process in a vast range of temporal scales, while also robustly dealing with the discretization and the bias effect in the wind speed model building (Dimitriadis & Koutsoyiannis, 2015).
2. The applied Symmetric-Moving-Average (SMA) stochastic simulation algorithm, which is used for the simulation of the wind process while preserving, explicitly with the marginal moments and important stochastic properties such as intermittency and long-term persistence (Koutsoyiannis, 2000; 2016; 2020; Dimitriadis & Koutsoyiannis, 2018).
3. The third feature, is that the double periodicity (diurnal and seasonal) of wind speed is also simulated using an implicit scheme by reducing the number of parameters, as discussed in previous studies (Aksoy et al., 2004; Suomalainen et al., 2012; Carapelluci & Giordano, 2013;

Scholtz et al., 2014), needed either based on averaged seasonal and diurnal data or by applying empirical periodic equations.

Along with the stochastic simulation scheme, the current research covers an extensive range of key issues in the wind resource assessment field, including:

4. The statistical similarities and associated errors between in situ records (buoys and meteorological stations) and the UERRA (MESCAN-SURFEX) reanalysis data as an alternative source for offshore wind speed time series as suggested by Carvalho et al., (2014);
5. The evaluation of multi-parameter (Weibull-related) marginal distributions that have been applied less in previous studies compared to the Weibull distribution, such as the Generalized Gamma, Burr III and Burr XII (Pareto-Burr-Feller) distributions; and finally,
6. A preliminary assessment of the wind extremes is performed in terms of the Mean Excess Function (MEF), the Generalized Pareto distribution fitting and the L-moments ratio diagram.

Starting from the wind resource assessment study, during this research one of the most common wind speed distributions is considered, the Weibull (W2) distribution. In addition, closely-related Weibull distributions are tested, such as the Burr-III, Burr-XII and Generalized Gamma (GG) that are also generalizations of numerous other distributions widely known in wind resource assessment such as gamma, lognormal, Pareto etc.

### 5.2.1 Weibull

The Weibull (W2) distribution constitutes the most widely accepted distribution for wind speed assessment and modelling (Monahan 2006; Carta et al. 2009; Jung and Schindler 2017). It is a generalization of the Rayleigh distribution (with shape parameter 2) and has been shown to fit both onshore and offshore wind samples better than Rayleigh due to its more flexible form (with the additional shape parameter). The Weibull PDF and CDF are expressed as:

$$f(x;k,c) = \frac{k*x^{-1}}{c^k} exp[-(\frac{x}{c})^k] \quad (5.2.1.1)$$

$$F(x;k,c) = 1\text{-}exp\left[-(\frac{x}{c})^{k}\right] \quad (5.2.1.2)$$

with $x \geq 0$, $k$ as shape parameter, $c$ as scale parameter and its first central moments (mean and variance) expressed as:

$$Mean = c\Gamma(1+\frac{1}{k}) \quad (5.2.1.3)$$

$$Variance = c^2[\Gamma\left(1+\frac{2}{k}\right) - \Gamma^2(1+\frac{1}{k})] \quad (5.2.1.4)$$

### 5.2.2 Burr (Type III)

Burr III (B3) distribution is obtained from a mixture of Weibull distributions. In regard to the wind speed or other meteorological variables, B3 provided a better congruity concerning the accuracy of fitting the empirical data (Chiodo & De Falco, 2016), although limited studies have been conducted for wind-related assessments. B3 and W2 are very similar in correspondence withthe central values of wind speed (Lo Brano et al., 2011), while a substantial difference is noticed in correspondence to the upper tail of the distribution. The B3 PDF and CDF are:

$$f(x;b,c,a) = \frac{bc}{a}(\frac{x}{a})^{-b-1}[1+(\frac{x}{a})^{-b}]^{-c-1} \quad (5.2.2.1)$$

$$F(x;b,c,a) = [1+(\frac{x}{a})^{-b}]^{-c} \quad (5.2.2.2)$$

with $x \geq 0$, $c$ and $a$ as shape parameters, $b$ as scale parameter and its first central moments:

$$\mu_r = b^r c\ Beta(\frac{ca+r}{c}, \frac{c-r}{c}) \quad (5.2.2.3)$$

$$Mean = \mu_1 \quad (5.2.2.4)$$

$$Variance = -\mu_1^2 + \mu_2 \quad (5.2.2.5)$$

$$Skewness = \frac{2\mu_1^3 - 3\mu_1\mu_2 + \mu_3}{(-\mu_1^2+\mu_2)^{3/2}} \quad (5.2.2.6)$$

for $c \geq r$ and $c$, $a$ *and* $b > 0$ (Shao, 2000).

### 5.2.3 Burr (Type XII - PBF)

Burr XII (B12) or Pareto-Burr-Feller (PBF) according to Koutsoyannis et al. (2018) appears to deviate from Weibull, Gamma, and Lognormal distributions (Pant & Headrick, 2013), characterized as a distribution with a much heavier tail. The B12 distribution has two different asymptotic properties, i.e., the Weibull distribution for low wind speeds and the Pareto distribution for large ones. Notable is that B12 has been used in a variety of independent fields (e.g. rainfall) emerging a strong physical and empirical justification (Koutsoyiannis et al. 2018). with the PDF and CDF of the proposed distribution expressed as:

$$f(x;b,c,a) = \frac{bc}{a}\left(\frac{x}{a}\right)^{b-1}\left[1+\left(\frac{x}{a}\right)^{b}\right]^{-c-1} \quad (5.2.3.1)$$

$$F(x;b,c,a) = 1-\left[1+\left(\frac{x}{a}\right)^{b}\right]^{-c} \quad (5.2.3.2)$$

with $x \geq 0$, $c$ and $a$ as shape parameters, $b$ as scale parameter. When c = 1, the B12 distribution becomes the Pareto II distribution, when a = 1, the Burr XII distribution becomes a special case of the Fisk distribution and for a → 0 becomes the Weibull distribution (Papalexiou & Koutsoyiannis, 2016). Its first central moments:

$$\mu_r = b^r c\, Beta\left(\frac{ca-r}{c}, \frac{c+r}{c}\right) \quad (5.2.3.3)$$

$$Mean = \mu_1 \quad (5.2.3.4)$$

$$Variance = -\mu_1^2 + \mu_2 \quad (5.2.3.5)$$

$$Skewness = \frac{2\mu_1^3 - 3\mu_1\mu_2 + \mu_3}{(-\mu_1^2+\mu_2)^{3/2}} \quad (5.2.3.6)$$

for $c*a \geq r$ and $c$, $a$ and $b > 0$.

### 5.2.4 Generalized Gamma

The 3-parameter generalized Gamma (GG) distribution includes the Weibull (for similar shape parameters $c \approx a$), Gamma, Pearson (Type 3), Exponential and other distributions as special cases of these probabilistic models. GG has been proposed as a wind speed model by several authors (Kiss & Jánosi 2008; Carta et al., 2009; Papalexiou & Koutsoyiannis, 2016) highlighting a better fitting flexibility and robustness to observed wind speed regimes compared to many other distributions. Analyzing the parameterization of GG distribution,it is mentioned that other forms also exist but one of the most commonly used is expressed by Equation 5.2.4.1-2 (Campisi-Pinto et al., 2020). Its PDF and CDF as also the first central moments are expressed by Equation 5.2.4.3-6:

$$f(x;b,c,a) = \frac{(a/b)^d}{\Gamma(c/a)}\, x^{c-1} exp^{-(x/b)^a} \quad (5.2.4.1)$$

$$F(x;b,c,a) = \frac{\gamma(c/a,(x/b)^a)}{\Gamma(c/a)} \quad (5.2.4.2)$$

$$\mu_r = \frac{b^r \Gamma(\alpha+\frac{r}{c})}{\Gamma(\alpha)} \quad (5.2.4.3)$$

$$Mean = b\frac{\Gamma(\alpha+\frac{1}{c})}{\Gamma(\alpha)} \quad (5.2.4.4)$$

$$Variance = b^2 \frac{\Gamma\left(\alpha+\frac{2}{c}\right)\Gamma(\alpha)-\Gamma(\alpha+\frac{1}{c})^2}{\Gamma(\alpha+\frac{1}{c})^2} \quad (5.2.4.5)$$

$$Skewness = \frac{\Gamma\left(\alpha+\frac{3}{c}\right)\Gamma(\alpha)^2-3\Gamma\left(\alpha+\frac{2}{c}\right)\Gamma\left(\alpha+\frac{1}{c}\right)\Gamma(\alpha)+2\Gamma(\alpha+\frac{1}{c})^3}{(\Gamma\left(\alpha+\frac{2}{c}\right)\Gamma(\alpha)-\Gamma(\alpha+\frac{1}{c})^2)^{3/2}} \quad (5.2.4.6)$$

where Γ() is the gamma function and γ() is the digamma function.

### 5.2.5 Parameters' estimation and Goodness of Fit tests

Multiple methods exist which can be used to estimate model parameters with desirable properties. Since the record length of the time series is rather large, differences among the proposed parameter estimation methods described below and the estimated parameters' values will not be critical compared to the differences among the selected probabilistic models.

The first parameter estimation method applied is the maximum likelihood estimation method (MLE) (Juntus et al. 1978; Ramirez & Carta, 2006; Morgan et al. 2011; Carta et al. 2009; Hu et al. 2016; Jung & Schindler, 2017). The MLE approximates the estimated values of the parameters which maximize the value of the probability of the observed sample (by maximizing the log-likelihood function). The resulting estimators are consistent, unbiased, asymptotically centered presenting an asymptotic normality and have a minimum variance as the sample size increases. The second method applied in order to estimate the distribution parameters is the least squares estimation method (LSE) (Lun & Lam, 2000; Carta et al. 2009; Yu et al. 2019). Applying the LSE method, the unknown values of the parameters of a PDF can be estimated by searching for the numerical values which minimize the sum of the squared residuals between the experimental and the modelled values. Normally, the LSE is applied to the cumulative or the tail distribution function and is considered as a general optimization problem, under linear constraints.

Finally, the third approach consists of the method of moments (MOM) (Jung et al. 2017; Koutsoyiannis et al. 2018; Campisi-Pinto et al. 2020) which includes the equation of the raw statistical moments or L-moments (linear combinations of probability weighted moments) of the sample with the corresponding population moments (Quarda et al. 2016). Subsequently, a system of equalities is applied, equal to the number of the unknown estimators, which allows the determination of the optimal parameters of the distribution. The key drawback is that this method does not use all the statistical information from the sample as long as only low-order moments are used (Dimitriadis & Koutsoyiannis, 2018). The key drawback is that this method does not use all the statistical information from the sample while only low-order moments are used (Dimitriadis & Koutsoyiannis, 2016).

In order to evaluate the fitting performance of the proposed probabilistic models, different Goodness of Fit (GoF) metrics are selected. The main scope of the fitting process evaluation is to identify persistence patterns for each model upon the selected GoF tests. For this reason, seven GoF metrics are applied to evaluate the fits of PDFs or CDFs to the empirical ones. Four of the seven GoF metrics are related to the probability and quantile-quantile (QQ) plot and the

remaining three are linked to the log-likelihood function and "penalize" the extra parameter of the multi-parameter distributions.

The selected GoF metrics are (Mohammadi et al. 2016; Ouarda et al. 2016; Jung & Schindler 2019): **i)** the Kolmogorov-Smirnov statistic (**KS**) which is defined as the maximum absolute difference between the sample's empirical CDF and the selected CDF, **ii)** the Chi-Squared statistic (**$\chi^2$**) which measures how similar the observed data sample distribution (PDF or CDF) is to a theoretical distribution, **iii)** the coefficient of determination (**$R_p^2$**), which measures the fit between the predicted probabilities at the class intervals obtained with a theoretical PDF (or CDF), **iv)** the root means square error (**RMSE**) and mean absolute percentage error (**MAPE**) which measure the difference between the empirical and the predicted relative probabilities or cumulative frequencies of each histogram and finally **v)** the log-likelihood **(*lnL*),** the Akaike Information Criterion **(*AIC*)** and the Bayesian Information Criterion **(*BIC*),** which are all related to the log-likelihood function of a distribution. With a given PDF $f_{\hat{x}}(u)$ fitted on a data sample having distribution parameter estimates $\hat{x}$, a high *lnL* in combination with low *AIC* and *BIC* values denotes a high fitting accuracy. Considering the *AIC* and *BIC,* there is a penalty term that increases with the increasing number of the model's parameters (Mohammadi et al., 2016; Ouarda et al., 2016; Jung & Schindler, 2017)

### 5.2.6 Energy output calculation

When planning an OWF it is important to know the expected wind power output of a single wind turbine (WT) or a cluster of WTs. In probabilistic modelling this can be achieved by calculating the average real wind turbine power output $\bar{P}_{real}$, obtained from the wind time series, compared to the $\bar{P}_{dist}$, which is an estimate of $P_w$ based on the $f_U(u)$. The most important step is the selection of a power curve of a WT referred as $P_w(u)$. Then, the $\bar{P}_{real}$, $\bar{P}_{dist}$ and $P_w(u)$ are estimated as (Equation 5.2.6.1-3):

$$\bar{P}_{real} = \frac{1}{N}\sum_{i=1}^{N} P_w(u_i) \quad (5.2.6.1)$$

$$\bar{P}_{dist} = \int_0^{\infty} P_w(u) f_u(u) du \quad (5.2.6.2)$$

And the relative error is expressed as:

$$R_pE = \frac{\bar{P}_{dist} - \bar{P}_{real}}{\bar{P}_{real}} 100 \qquad (5.2.6.3)$$

Using the power curves of Gamesa G128-5.0 (5 MW), Vestas V164-8.0 (8 MW) and WindTech SeaTitan-10.0 (10 MW) wind turbines, the nominal output for a year in MWh (8760 hours/year) is calculated (Table 5.2.6.1). A mathematical relationship developed for each wind as a fraction of time for each nominal wind speed and using the empirical power curve (Equation 5.2.6.4-6) to calculate the exact power output for each site. For each spatial unit area of 5.5x5.5 km$^2$ (cell) is considered that 40, 25 and 20 wind turbines can be sited, with a WT's spacing distance of 7-8xD, where D is the rotor diameter. With this interval, the influence of the wakes is limited and, thus, wake effects power losses are minimized.

$$P_{w5} = \begin{cases} 0 & & Vi < 2 \\ -0.2154\,(Vi^3) + 60.52\,(Vi^2) - 223.3\,Vi + 277 & (R^2 = 0.99) & 2 \le Vi \le 10 \\ 13.06\,(Vi^3) - 553.1\,(Vi^2) + 7896\,Vi - 32860 & (R^2 = 0.99) & 10 < Vi \le 13 \\ 5000 & & 13 < Vi \le 16.5 \\ 1.199\,(Vi^3) - 83.86\,(Vi^2) + 1739Vi - 6223 & (R^2 = 0.99) & 16.5 < Vi \le 27 \\ 0 & & Vi > 27 \end{cases} \qquad (5.2.6.4)$$

$$P_{w8} = \begin{cases} 0 & & Vi < 4 \\ -7600 + 41{,}66 * Vi^3 - 650 * Vi^2 + 3858{,}3 * Vi & (R^2 = 1) & 4 \le Vi \le 7 \\ 18100 - 25 * Vi^3 + 775 * Vi^2 - 6500 * Vi & (R^2 = 1) & 7 < Vi \le 11 \\ 7063.103 + 0.42 * Vi^3 & (R^2 = 0.99) & 11 < Vi \le 13 \\ 8000 & & 13 < Vi \le 25 \\ 0 & & Vi > 25 \end{cases} \qquad (5.2.6.5)$$

$$P_{w10} = \begin{cases} 0 & & Vi < 4 \\ 31.207\,(Vi^3) - 375.935\,(Vi^2) + 2068.446\,Vi - 3969.73 & (R^2 = 0.99) & 4 \le Vi \le 6 \\ 32.09\,(Vi^3) - 561.306\,(Vi^2) + 4338.149\,Vi - 11123.6 & (R^2 = 0.99) & 6 < Vi \le 10 \\ 158.632\,(Vi^3) - 6230.05\,(Vi^2) + 80050.58\,Vi - 327980 & (R^2 = 0.99) & 10 < Vi \le 11.5 \\ 10000 & & 11.5 < Vi \le 30 \\ 0 & & Vi > 30 \end{cases} \qquad (5.2.6.6)$$

**Table.5.2.6.1**: Specifications of the selected offshore WTs

| WT characteristics | Gamesa G128-5.0 | Vestas V164-8.0 | WindTech SeaTitan-10.0 |
|---|---|---|---|
| **Rotor diameter (D)** | 128m | 164m | 190m |

| Hub height | 105m | 125m | 140m |
|---|---|---|---|
| **Rated Power** | 5.0 MW | 8.0 MW | 10.0 MW |
| **Control** | Pitch control | Pitch control | Pitch control |
| **Cut-in wind speed** | 2 m/s | 4 m/s | 4 m/s |
| **Rated wind speed** | 14 m/s | 13 m/s | 11.5 m/s |
| **Cut-out wind speed** | 27 m/s | 25 m/s | 30 m/s |
| **Wind turbine intervals** | 8 D | 8 D | 8 D |

Wind power estimation has been carried out at indicative hub heights for the selected WTs at 105, 125 and 140 meters respectively. Hence, the wind speeds (at 10 m) are extrapolated to the required height and the log-law (Equation 5.2.2.1, Section 5.2.2) is applied.

### 5.2.7 Stochastic generation of synthetic wind time series

In this section, the stochastic synthesis for offshore wind simulation is demonstrated based on reanalysis data. Considering the lack of offshore measurements and based on the results extracted from the integrated wind resource assessment during the previous sections, our goal is to demonstrate a stochastic generation scheme using UERRA reanalysis wind speed time series. Each step of the stochastic analysis already described in previous sections is applied in order to simulate the marginal structure, the seasonal characteristics and the second order structure with long-term persistence.

Particularly, to account for the double periodicity, heavy-tail distribution, and long-term persistence, evident in hydrometeorological processes (Dimitriadis, 2017), the stochastic algorithm proposed by Dimitriadis and Koutsoyiannis (2015) is applied in offshore wind speed. An outline of the appropriate steps to be followed during the stochastic generation scheme is presented in Figure 5.2.7.1 including:

1. Selection of the appropriate probabilistic model for the entire sample, with fitting configurations and estimation of parameters for each periodic cycle (e.g., diurnal and seasonal).
2. Persistence evaluation based on the climacogram function.

3. Symmetric Moving Average (SMA) scheme for explicitly approximating the marginal probability function of the process by preserving its first four central moments, which are found adequate, and the second-order dependence structure.
4. For the stochastic simulation of the offshore wind time-series, a generalized long-range dependence is applied (GHK model), that requires as inputs the first four central moments estimated from the fitted probability function distribution, the Hurst parameter ($H$) and the scale parameter ($q$) of the GHK model ($H$), and the length of the synthetic time series ($N$).

***Stochastic simulation algorithm set-up***

**Step 1:** Initialize the number of simulations ***N*** and the total time series length ***L***.

**Step 2a:** Define seasonal cycles scale (e.g., monthly, seasonal).

**Step 2b:** Define diurnal cycles scale (e.g., hourly, six-hours).

**Step 3:** Fit a low-parameter parent-distribution (with *m* parameters) to the entire sample (e.g., Weibull, Burr3, Burr12, Gen.Gamma).

**Step 4a:** Estimate for each periodic cycle the first ***m*** moments (e.g., 4x4x***m*** estimations for the 3-monthly / 6-hourly cycles), or more robustly, and particularly in case of a sample with short length, fit low-parameter empirical expressions of double periodicity and theoretically estimate the first ***m*** moments for each cycle.

**Step 4b:** Theoretically estimate the ***m*** parameters of the parent-distribution but now for each cycle (i.e., in total ***m*** parameters of the parent-distribution for each cycle).

**Step 4c:** Transform each cycle (through the inverse expression of the parent-distribution), so that it follows the parent-distribution with the fitted parameters to the entire sample (**Step 3**).

**Step 5:** Theoretically estimate (i.e., from the parent-distribution) the first four (or more) central moments of the process.

**Step 6a:** Fit a low-parameter model to the empirical second-order dependence structure of the sample (e.g., GHK model with Hurst parameter ***H*** and scale parameter ***q***) using the Climacogram stochastic metric.

**Step 6b:** Theoretically estimate the coefficients ($\boldsymbol{a_j}$) of the SMA scheme.

**Step 6c:** Theoretically estimate the first four (or more) central moments of the white noise ($\underline{\boldsymbol{v}}$) of the SMA scheme.

**Step 7a:** Run SMA model (i.e., $\boldsymbol{x_j} = \sum_{j=-n}^{n} \boldsymbol{a}_{|j|} \boldsymbol{v}_{i+j}$).

**Step 7b:** Transform back each value of the synthetic timeseries that belongs to a cycle to the parent-distribution but with the parameters of the specific cycle (as estimated in **Step 4b**).

**Figure 5.2.7.1.** SMA-GHK simulation scheme outline

Compared to the aforementioned simulation scheme, one may adopt the mean, standard deviation and skewness estimated directly from data in order to fit the double periodicity of wind but would result in a highly over-parameterized model involving 12 (months) × 24 (hours) = 288 parameters for each statistical measure. An alternative, suggested only when the double periodicity of the examined wind stations (or pixels) can be considered weak, is to divide each periodicity to longer time-periods. For example, one may divide the 12-months annual period to 4 seasons (i.e., with three-months duration each) and the 24-hours diurnal period to 4 six-hour period (i.e., with six-hour duration each). However, still this model will include 4 (seasons) × 4 (six-hours) = 16 parameters for the mean, standard deviation and skewness respectively. Also, in order to ensure that all these parameters can be robustly estimated from data, the observed timeseries must have a large length and a good quality of records. Alternatively to the proposed 6-step double periodicity model demonstrated above, a fair approach is to obtain the key statistical characteristics through analytical periodic expressions with an extremely lower number of parameters for the mean, the standard deviation and the skewness wind speed. The proposed model includes only 8 parameters (compared to the 288x3 or 16x3) ensuring more robust statistical estimations.

The proposed solution assumes that only the mean and standard deviation exhibit an evident double periodicity, whereas the higher-orders (e.g., skewness, kurtosis) may be assumed unaffected by the diurnal periodicity of wind and partially affected only by the seasonal variation. The proposed models are based on a global analysis including thousands of wind stations performed by Deligiannis et al. (2016), but here, we further advance these expressions for the standard deviation and the skewness coefficient. So, the double periodicity of the mean, of the standard deviation and of the skewness coefficient of the wind process can be simulated by the functions shown in (Equations 4.2.7.1-3), respectively:

$$\mu_c = \left(a_1 + a_2 \cos\left(2\pi \frac{t_m - \alpha_m}{12}\right)\right) \exp\left(\cos\left(2\pi \frac{t_h - \alpha_h}{24}\right)\right) + a_3 cos\left(2\pi \frac{t_m - \alpha_m}{12}\right) + a_4 \quad (5.2.7.1)$$

$$\sigma_c = \left(b_1 + b_2 \cos\left(2\pi \frac{t_m - b_m}{12}\right)\right) \exp\left(\cos\left(\pi \frac{t_h - b_h}{24}\right)\right) + \beta_3 cos\left(2\pi \frac{t_m - b_m}{12}\right) + b_4 \quad (5.2.7.2)$$

$$s_c = \left(c_1 \sin\left(4\pi \frac{t_m - c_m}{12}\right)\right) + c_2 \quad (5.2.7.3)$$

, where $\mu_c$, $\sigma_c$ and $s_c$ (m/s) is the mean and the standard deviation for each season and 6-hour interval as also $s_c$ is the seasonal skewness of the process. Respectively, $a_1$, $a_2$, $a_3$, $a_4$, $b_1$, $b_2$, $b_3$, $b_4$, $c_1$ and $c_2$ are models' parameters, $t_m$ and $t_h$ is the continuous time in seasons and hours and finally, $a_m$, $a_h$, $b_m$, $b_h$ and $c_m$ are coefficients depicting the season and hour of maximum wind speed mean and standard deviation varying from 1 to 4 season and 1 to 24 (0, 6, 12, 24) hours.

Indicative results from the fitted models are demonstrated in Figure 5.2.7.2. highlighting the offshore wind behavior and the high fitting performance. Notable is that the observed double periodicities considering the mean and standard deviation of offshore wind align with the results of Bagiorgas et al. (2012) and Shu et al. (2015) where similar monthly and daily cycles were reported. The daily and seasonal cycles of both the mean wind speed and its standard deviation may present differences above 1 m/s. However, in wind power assessment and modelling these differences should not be neglected in the estimation of the energy production as well as in the wind turbines loads, and thus, it is considered crucial to always check for evidence in double periodicity, especially for the mean and the standard deviation of wind speed. For illustration purposes the proposed stochastic generation scheme is based on the estimated diurnal and seasonal probabilistic characteristics of the Lesvos station and UERRA reanalysis data.

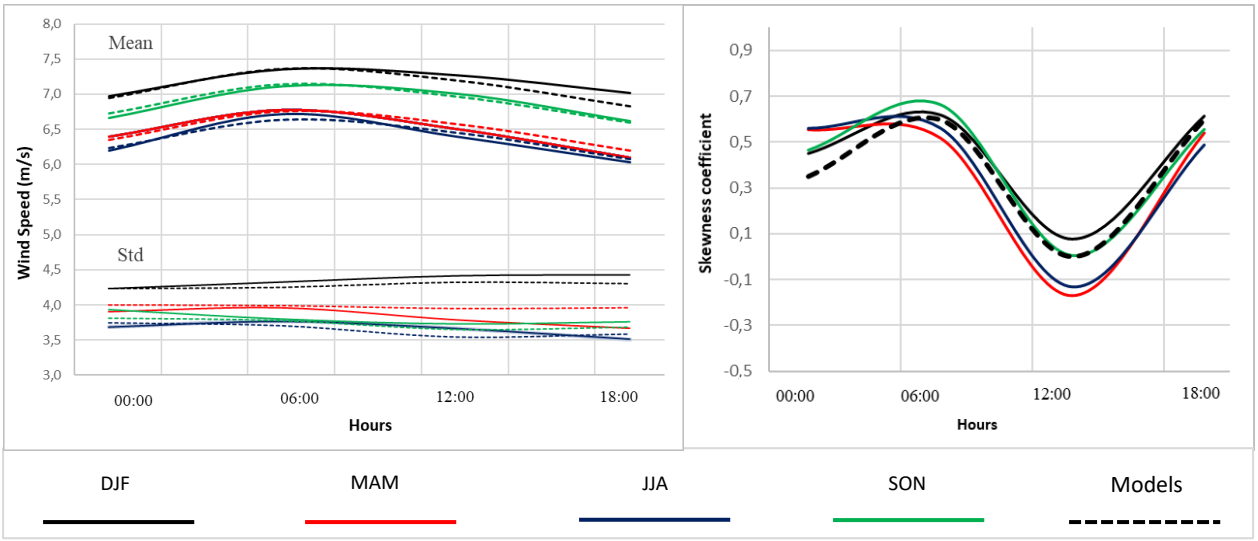


**Figure 5.2.7.2.** Seasonal-Hourly Mean, Standard Deviation and Skewness for the Lesvos buoy based on the observed (solid lines) and modeled (dashed lines) data, based on the Eq.5.2.7.1-3

For the proposed seasonal and hourly (6-hours interval) variations, the marginal characteristics of the reanalysis time series are calculated including the probabilistic models that had the best fitting performance during the assessment stage (Section 5.2.6). As a result, for each season and each time interval, each distribution is fitted to the data in order to extract the marginal characteristics. Besides the marginal properties, the dependence structure is also important for the stochastic synthesis. Particularly, the long-term dependence structure of the wind process (referred as a Generalized Hurst-Kolmogorov-GHK process), as extracted from the previous sections, is modelled through the climacogram, i.e., the variance of the mean process vs. time scale, denoted as $\gamma$ ($m^2/s^2$). The long-term persistent behaviour of wind is expressed by the standardized GHK model:

$$\gamma = \lambda/(1 + k/q)^{2-2H} \quad (5.2.7.4)$$

where $\lambda = (1 + 1/q)^{2-2H}$ is the standardized variance of the discretized stationary process, $q$ is the shape parameter distinguishing the short-term from the long-term behavior, and $H$ is the Hurst parameter. Also, the average marginal PDF for the standardized process is fitted and calculated based on the B12 (Equation 5.2.3.1-6) and GG (Equation 5.2.4.1-6) distributions that showed the best fitting performance for both in situ and reanalysis data. Note that by assuming stationarity and ergodicity, the standardization of the wind process is capable of homogenizing all-time series recorded at different locations (this process should not be confused with normalization procedures based on non-linear transformation). Thus, the simulated process is expressed as the sum of the products of coefficients (not parameters) defined by:

$$x_j = \sum_{j=-n}^{n} a_{|j|} v_{i+j} \quad (5.2.7.5)$$

, whereas $v_i$ is the white noise term and $a_j$ can be analytically or numerically calculated (Equations 5.2.7.5-6) up to lag $n$ (see Dimitriadis and Koutsoyiannis, 2018, equations 5-6). For the GHK process, an explicit expression for the coefficients $a_j$ is derived through the Fourier transform of the discrete power spectrum of the coefficients expressed as:

$$s_d^{\alpha}(\omega) = \sqrt{2 s_d(\omega)} \quad (5.2.7.6)$$

where $s_d^{\alpha}(\omega)$ and $s_d(\omega)$ are the power spectra of the SMA coefficients and the discrete time process, whereas $\omega = D/k$ is the dimensionless frequency, for $D$ expressing the time series resolution.

## 5.3 Data pre-processing

Data processing (pre-processing) represents activities which have a goal to transform the data acquired into the required form for further analysis. It is not a process in terms of analysis and synthesis of the data, but rather their pre-processing for later modelling stages, considering the heterogeneity of the input data and the prerequisites to set-up all optimization algorithms and simulation tools. During this stage, the user is asked to select the spatial resolution (cell size) and the boundaries of the study area.

To this end, the entire pre-processing stage can be divided into sub-steps including: i) data restructuring, ii) geometric transformations and change of a map projection or data conversion as also, iii) mosaicking (merging) of several layers as one layer and resampling procedures. Geometric transformation and change of a map projection involve the process of converting geographic coordinates to rectangular (projected) plane coordinates. In case of raster data, the part of the geometric transformation is also incorporating the process of resampling. During resampling, the position of the center of each cell of new representation in the coordinate system of original representation is calculated by transformation equations. Consequently, by using different methods it is possible to assign the attribute value. For example, the method of the nearest neighbor assignment for discrete data (e.g., Land-use/Landcover and seabed substrate) or method of the bilinear interpolation or Cubic convolution for continuous data (e.g., Digital Elevation Model, bathymetry and offshore wind speed rasters) are applied. Finally, data conversion is the process of transforming vector data to raster or the opposite procedure, based on the pre-defined spatial extent, the mask of the study area and the pre-defined spatial

resolution (cell size). During rasterization (conversion of vector to raster format) the vector layers are overlaid by a raster grid of fixed-size cells and the specified attribute is assigned to it.

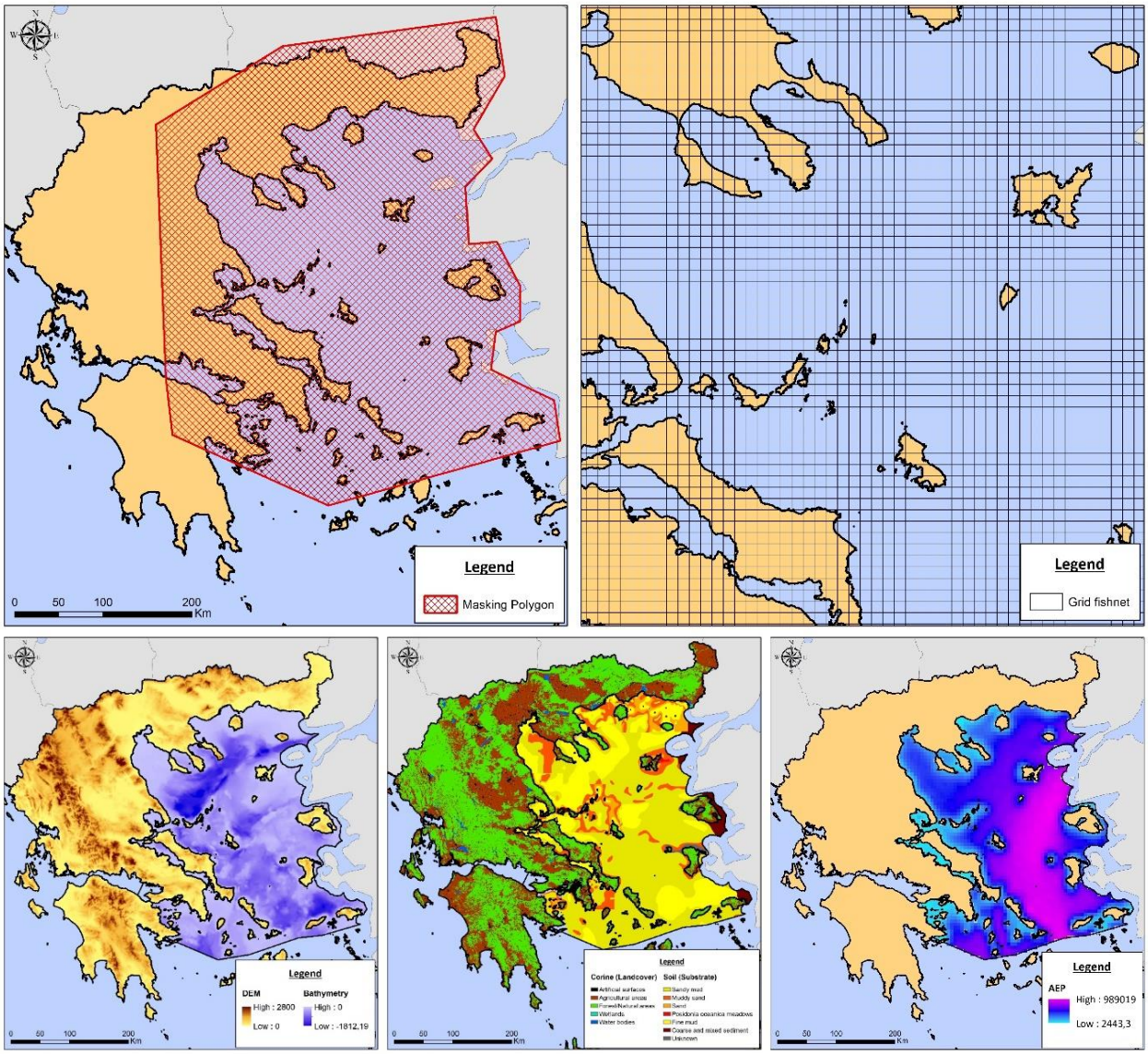


**Figure 5.3.1**: Mask of the Study Area intersecting all of the input data (top left), Fishnet grid of 5 km spatial resolution (top right), Input raster datasets (bottom left and right maps)

An increased emphasis is given to the aforementioned procedures considering the heterogeneity of the input data structures, the different types of data and the spatial resolution used for the sub-models' tuning procedures. The SDSS structure is giving the capability to the user to predefine and control all pre-processing tools, considering the input variables and the parameters and methods used. The spatial analysis upon raster surfaces is based on matrix

operations, where the matrix "overlays" a geographic area, and the information of each matrix entity corresponds to the numerical value associated with each respective location. As a result, all of the available datasets must be transformed (resampled) under a common spatial resolution (cell size) defined by the user (Figure 5.3.1). To achieve the resampling procedures, a vector grid (fishnet) is established including polygons having an extent equal to intersect all available vector and raster information needed. The size of each side of the polygon features (cells of the fishnet) is either set by the user or is defined by the maximum cell size of the initial data (e.g., the UERRA reanalysis data with approx. 5.5 km cell size). Notable is that the total size of the potential OWF(s) and the number of WTs per cell are proportional to the fishnet's cell size. For example, considering a 1 km cell size, a maximum amount of 1 or 2 wind generators per pixel (see Figure 5.3.2.1) is set, on the contrary, for a 5 km cell size, an entire OWF may be considered, consisting of 20 – 45 wind generators, depending on the WT's size and the rated power.

To this end, during the pre-processing stage all the cost- and energy- related raster data are processed in order to be able to further proceed to the next stages of the SDSS based on the user's preferences (Stage 2,3 and 4 – Figure 5.1.1). Having the key input data presented in Figure 5.3.1, consisting of the UERRA reanalysis data, DEM, bathymetry, CORINE landcover and seabed substrate, the final "resampled" outputs will be produced based on the fishnet resolution using a so-called zonal statistics approach[12]. According to zonal statistics approach, a new attribute is added to each polygon of the fishnet linked to the pixel's information from each raster dataset. The final attribute value per feature (polygon) and raster dataset can be extracted by calculating the minimum, maximum or mean values for continuous data and based on the most frequent value for discrete data.

Furthermore, in order to guarantee that all of the raster data overlap in accordance to the land or sea coverage (e.g., when a cell of offshore wind data exist, it is obligatory to obtain the relevant depth and seabed substrate characteristics otherwise the cell is set as NoData record), intersection calculation rules are applied. Some indicative examples are demonstrated in

[12] Using Zonal Statistics analysis, a statistic is calculated for each zone defined by a zone dataset, based on values from another dataset (a value raster). A single output value is computed for every zone in the input zone dataset.

Figure.5.3.2, where different cases of overlapping areas, no data cells (gaps) between the land-sea transition or overlapping cases with both land and sea raster surfaces can be observed.

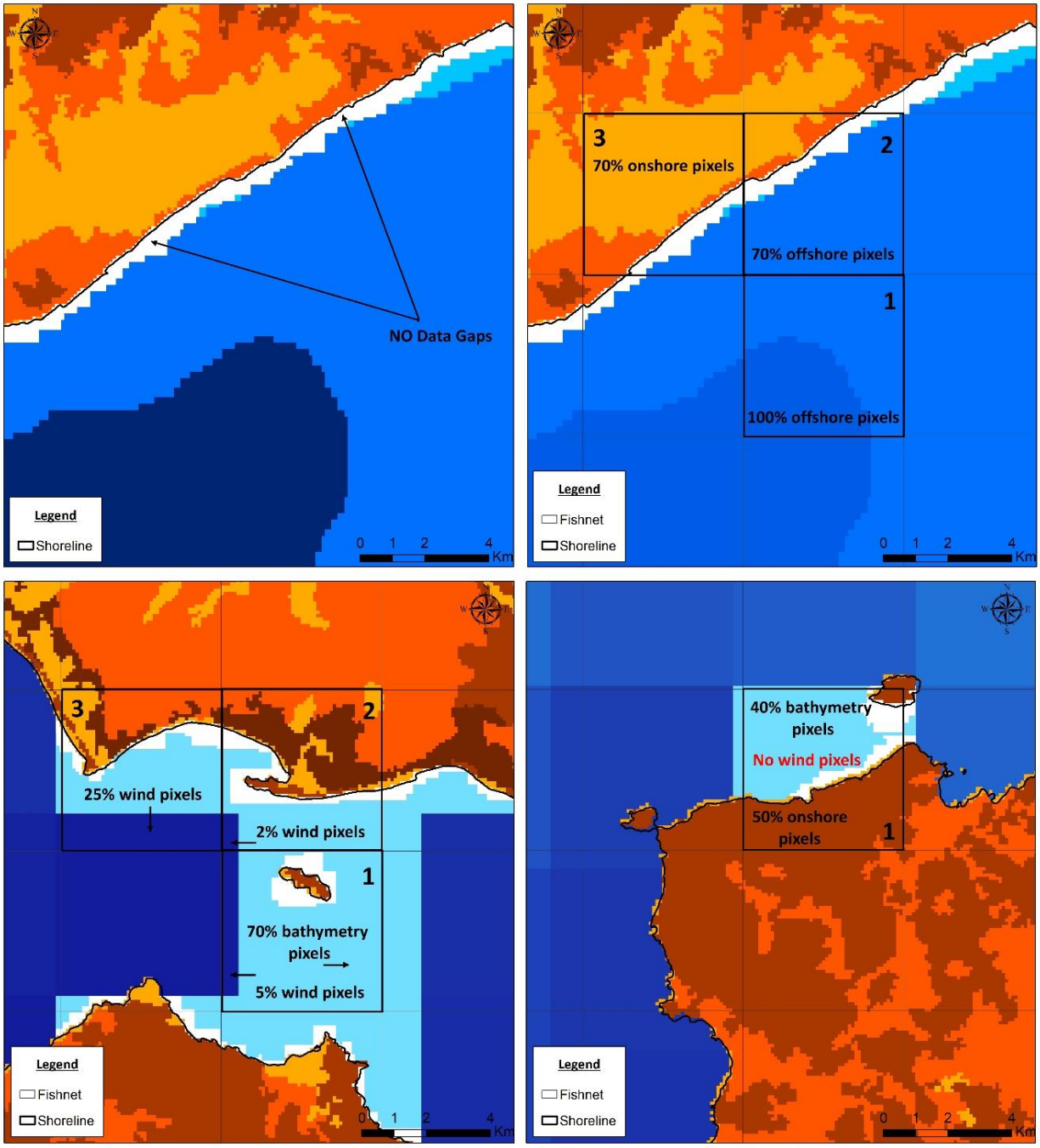


**Figure 5.3.2**: Zonal statistics examples with overlapping areas and NoData gaps between offshore wind, DEM, bathymetry and seabed substrate raster surfaces

To overcome these drawbacks, an overlapping percentage coverage rule is set in order to clarify whether a polygon attribute is translated to land or sea values, considering that a loss of information from the offshore wind data (UERRA reanalysis dataset) is vital. As a result, areas with offshore wind data coverage of e.g., 25% or less (Figure 5.3.2) are considered as land polygons, with the prerequisite that DEM, seabed substrate, bathymetry and CORINE pixels exist above each selected cell of the fishnet. Once the final rasters are extracted for both land and sea areas, merging procedures are applied for both DEM and bathymetry rasters and CORINE and offshore soil substrate respectively. All the resulting raster surfaces are stored for later stages of the SDSS and particularly, the Least-Cost-Path delineation algorithms and the spatial optimization scheme, where the graph network must be established, and all arrays of equal dimension for the final stage of the site-prospecting optimization algorithm.

## 5.4 Screening assessment based on the MSP and National legislation

For determining the unsuitable or unrestricted marine areas for OWF siting (**Stage II** of the proposed SDSS framework, Figure 5.1.1) a set of exclusion criteria is selected as well as economic, technical and social constraints based on the National legislation framework and the MSP regulations. As a consequence, utilization restrictions are imposed by the various human activities and the environmental requirements related to the conservation and the protection of marine areas (MPAs). Furthermore, societal, technical and economic factors are considered, focusing on public acceptance of potential OWFs or conflicts with other non-sea related economic activities (tourism, industry etc.) and the current technological status for OWE deployment (technical restrictions).

Therefore, different scenarios are adopted, considering the level of restrictions rules (Table 5.4.1), the number of the selected constraints and the possible conflicts among existing sea uses. For the proposed research, a dual approach was applied comprised of the: i) desk-based research for the collection, analysis and interpretation of the spatial and non-spatial data gathered and, ii) the mapping and visualization of the different scenarios. In more depth, these procedures are conducted as follows:

1. The desk-based research consists of a literature review for identifying the status-quo of spatial claims and interactions in the Central and North Aegean Sea, which implied: i) the synthesis of the main marine activities from multiple data sources, followed by, ii) the collection, classification and digitization of georeferenced data sets for the identified current activities using ArcGIS software.
2. Furthermore, trends and potential conflicts for current or future management scenarios of the national marine areas are identified. This information is the result of reviewing: i) national legal documents and reports as also, ii) the MSP guidelines applied in similar studies for different countries, considering OWE deployment.
3. At last, the finalized assumptions, in the form of three different scenarios and their spatial implications are embedded as a separate module to the SDSS (Table 5.4.1).

In the following paragraphs all restriction rules are analyzed, consisting of the following activities and physical constraints:

- **Shipping lanes (National):** The national shipping lanes of passenger vessels need a route of safe passage in travelling from place to place. Therefore, exclusion zones (buffers) are considered in order to avoid areas, for safety and economic reasons (displacements in shipping routes might cause the delineation of longer and costly paths regarding fuel consumption). During the most optimistic scenario, no restricted areas occur for national shipping routes.
- **Shipping density (IMO):** This criterion mainly involves areas with intense cargo and passenger vessels traffic, according to the International Maritime Organization (IMO). At the planning stage, areas with increased shipping densities render the siting of an OWF harder to achieve, mainly for safety reasons. For this reason, the fewer the shipping densities are per spatial unit (pixel), the higher the suitability is given to that area, in order to effectively eliminate possible conflicts. As a result, different cut-off values are selected for each scenario for eliminating non-suitable areas.

- **Cables and pipelines:** A fair number of electric and telecommunication cables exist in the Aegean Sea. Vectorized data include all of the known telecommunications or energy transfer cable infrastructures. For the most optimistic scenario no restrictions are considered considering this criterion where, according to the literature review, partial compatibility may exist among OWF installations and already existing cables. In contrast, for the first and second scenario, exclusion zones (buffer zones) are defined in order to provide protection and maintenance access.
- **Wildlife preservation, nature conservation zones and Marine Protected Areas (MPAs):** Considering the environmental impact, all protected areas that are identified under the Birds and Habitat Directive as Special Protection Areas and Special Areas of Conservation respectively are considered. In view of the bird habitats, the siting of OWFs is allowed only if a special ornithological study exists, however, for the current scenarios' development all protected areas are excluded. An exception occurs for the third scenario where the birds' habitats are not excluded.
- **Military zones:** Covering a wide range of activities – including firing ranges, munitions dumping, submarine maneuvers, aerial exercises and others, military zones are defined by governments in the interest to training and security characterized as total exclusion areas for OWE deployment. All of the aforementioned areas are excluded for the first and second scenario. An exception occurs for the third scenario, where military zones are not considered as exclusion areas.
- **Fisheries and aquaculture:** Fishing activities partially cover almost all the coastal areas in Greece, depending on targeted fish species and fishing techniques. The resulting conflicting areas can be characterized from seasonal or even annual variations depending on fish stocks and fishing activities types. Notable is that accurate fisheries and fishing density data do not exist for the selected territory and therefore, data on fishing areas are based on the Thal-Xor project where two different fishing zones are delineated denoting trawlers and pure-seine fishing activities. For the more conservative scenario all these activities are excluded.

- **Bathymetry:** In accordance to the bathymetric profile, only a specific number of areas are considered suitable for offshore support structures. For the bottom-fixed structures, depth up to 20-30 meters are selected for the monopile foundations and 70 meters depth is the upper limit for jacket foundations. In the case of floating structures, a quite limited range of water depths (e.g., up to 250-500 m) is considered economically viable for their installation. For the current research, only an upper depth limit is used in order to define marine areas unsuitable for OWE deployment equal to 200, 500 and 1000 meters, focusing on the current and future technologies that are still under development.
- **Distance from the Shoreline:** Distance from the shoreline consists of a critical factor, considering the suitability areas assessment process. The installation of OWFs close to the shore leads to negative environmental and societal impact as already discussed in Section 2. In this context, marine areas with distances smaller than 5 and 10 kilometers are considered unsuitable for OWF siting for the first two scenarios as for the third scenario no distance restrictions are applied. Notable is that the aforementioned upper limits considered also cover all of the National legislative restrictions included in 4269/2014 (OGG, 2014) Law related to the distances from the shoreline and coastal cities as also the restrictions of OWE deployment in closed bays.

All of the data for the selected criteria have been collected during 2015–2019 and represent the status quo for this time period (e.g., shipping density raster maps, cables infrastructure, military zones or protected and nature conservation areas).

**Table 5.4.1**: Exclusion analysis criteria and gradings – Calculation rules

| Criteria | Scenario 1 (Conservative) | Scenario 2 (Moderate) | Scenario 3 (Optimistic) |
|---|---|---|---|
| **Bathymetry** | >200 m (Exclusion) | >500 m (Exclusion) | >1000 m (Exclusion) |
| **Distance from the shoreline** | > 10 km | > 5 km | > 2 km |
| **Tectonic faults** | 1000 m (Buffer) | 500 m (Buffer) | 250 m (Buffer) |
| **Shipping lanes (IMO)** | >100 ships/year (Exclusion) | >200 ships/year (Exclusion) | >300 ships/year (Exclusion) |

| | | | |
|---|---|---|---|
| **Shipping lanes (National)** | 2000 m (Buffer) | 1000 m (Buffer) | 500 m (Buffer) |
| **Marine Protected Areas (MPAs)** | 500 m (Natura), 2 km (Bird Hab.), 3 km (Cult. sites) (Buffer) | 500 m (Natura), 1 km (Bird Hab.), 1 km (Cult. sites) (Buffer) | 500 m (Natura), 500 m (Bird Hab.), 500 m (Cult. sites) (Buffer) |
| **Military areas** | Exclusion | Exclusion | No restriction |
| **Fishing areas** | Exclusion | No restriction | No restriction |
| **Aquaculture** | 500 m (buffer) | No restriction | No restriction |
| **Cables** | 500 m (buffer) | 250 m (buffer) | No restriction |

Although the first stage is critical focusing on the screening assessment process for OWE deployment, the scope of the first stage has a great impact on later procedures of the SDSS. Considering the spatial optimization models, when comparing a Dynamic Programming (DP) approach upon a raster surface with different grid sizes (total number of pixels), it turned out that the optimization time increases rapidly (geometrically or even exponentially for graph-based implementations) with the grid size. With the current technological and computational power, smaller grids may be solved within seconds, however, larger grids may need a few hours or even days on an average computer.

Therefore, by minimizing the available space for OWF site prospecting, the raster space (the total pixels remaining) is reduced. This means that, if for example the initial selected area consists of e.g., 100000 pixels, after the screening assessment a reduced number of "suitable" cells will remain for further analysis. This impacts the execution (running) time of the spatial optimization algorithms during cost evaluation and site prospecting stages.

## 5.5 Offshore Wind Farm cost modelling

OWF planning and spatially-explicit cost approximation incorporates an increased volume of data and demanding spatial analysis techniques. Overall, in econometric science, capital cost estimates can be approximated using either an engineering (bottom-up) or a comparative (top-down) approach. In the former approach, the cost model incorporates all of the system's cost component estimates, which when summed, yield a total estimate of the capital cost (e.g., of an

OWF). The engineering approach is useful for estimating the costs of a particular project but requires site-specific information and is subject to optimism bias. On the contrary, in the latter approach (comparative approach), cost data from existing projects are used as a basis for analogy. As a result, if the physical infrastructure in two regions is similar, then the project characteristics may be similar even if other characteristics of planning, development and installation strategies are different. However, numerous drawbacks may occur due to the underlying environmental, contractual or scale economies differentiations among projects with the same technical or physical characteristics.

Consequently, for the cost modules embedded in the SDSS, three different types of models are established based on: i) a reference class of existing projects where previous cost information is used for comparative cost estimations (e.g., cost estimations on per MW basis), ii) already existing analytical cost expressions that are already applied and tested in relevant studies and finally, iii) a bottom-up modelling scheme based-on analytical cost estimates subject to site-specific technical and engineering criteria (Kaizer & Snyder, 2012). Focusing on the latter modelling framework, notable is that there are simplifying assumptions that may limit the accuracy of model outputs. However, the emphasis is on a comprehensive framework to integrate spatially-explicit cost calculation rules during the pre-development stages rather than an analytical micro-siting modelling approach. Thus, individual cost modules could later be upgraded by more sophisticated engineering and structural optimization modelling schemes.

**Cost estimation:** During the following sections the total sub-cost components of an OWF will be analyzed and discussed. All relative cost functions used in the SDSS express: i) development and consenting expenses ($Cost_{dc}$), ii) the production and acquisition cost ($Cost_{wt}, Cost_{tr}, Cost_{fd}$), iii) the installation cost ($Cost_{install}$), iv) operation and maintenance cost ($Cost_{om}$) and finally, v) decommissioning cost ($Cost_{dec}$), consisting of the total Capital Expenditures (CAPEX), Operation and Maintenance (O&M) and Decommissioning expenditures (DECEX). Production and acquisition costs are mostly related to the manufacturing complexity and the material consumption. An exception occurs for the transmission cables (inner and export cables), where the total cost is expressed as a combination of the cables' technical characteristics and length. Accordingly, installation, O&M and decommissioning cost are linked to the personnel, marine

operations and vessels needed but most importantly, to the measured distance each marine area is located from the nearest ports and onshore transmission junctions. Therefore, accurate shipping routes and cables' corridors must be considered in order to obtain more realistic and less uncertain costs. In both cases, the automation of the routing process integrates a detailed spatial modelling of the problem based-on accurate spatial information, cost data and experts' knowledge in order to reduce efforts in the revision of a future project.

The overall cost breakdown is expressed in Equations 5.5.1 - 4. Throughout the cost model, the most up-to-date cost expressions are employed and compared with spatially-explicit cost models established in previous research studies. Consequently, the user is able to select: i) more generic regression formulas for per MW cost evaluation, ii) simplified equations based on the key technical aspects of an OWF (number of WTs, depth, Euclidean distance from ports and the onshore grid etc.) or finally, iii) analytical cost models by decomposing each sub-cost component in its structural elements, e.g., design and consent, acquisition and manufacturing, installation cost, O&M and decommissioning and disposal cost. Overall, the total life-cycle cost of an OWF is modelled using the following formulas:

$$CAPEX = Cost_{wts} + Cost_{tr} + Cost_{fds} + Cost_{install} + Cost_{dc} + Cost_{decom} \quad (5.5.1)$$

$$Cost_{install} = Cost_{install\_wt\_fd} + Cost_{install\_cables} + Cost_{install\_sub} \quad (5.5.2)$$

$$Cost_{decom} = Cost_{remove} + Cost_{revenues} \quad (5.5.3)$$

$$Cost_{om} = Cost_{oper} + Cost_{main} \quad (5.5.4)$$

**Cost spatial adjustments:** The overall OWFs' life cycle costs are estimated based on different spatial scales (i.e., at a WT level or for the entire OWF). In particular, development and consenting, transmission system manufacturing cost, the total installation and decommissioning cost along with the O&M expenses are calculated at an OWF level. On the contrary, WTs and foundations manufacturing costs are estimated on per unit basis (per WT). Consequently, all cost components must be adjusted to a common spatial scale for both levels of spatial information. Thus, by defining the total installed capacity of the OWF ($OWF_{cap}$) and the spatial resolution, the total number of WTs per pixel is defined (see Section 4.3.2). The overall installation cost is estimated using Equations 5.5.2, 5.5.7, 5.5.9 and 5.5.11 by dividing the total costs with the OWF capacity

and then multiplied with the WT capacity ($WT_{cap}$) and the number of pixels needed to reach the desired capacity. For example, for a 200 MW OWF and a pixel size of 1000 meters, by assuming two 5 MW wind generators per pixel ($n_{wt\_px}$), a total sum of 20 pixels ($n_{pixels}$) is considered. Similarly, for the export and inter-array cables and the substation, the manufacturing and installation cost are divided with the total wind farm capacity and multiplied with the wind generators' capacity and the number of WTs per pixel. On the contrary, the total WTs and foundations cost is estimated on per WT basis and is simply multiplied with the optimal number of WTs per pixel and the total pixels required to reach the desirable capacity.

$$Cost_{dc} = (Cost_{dc}/OWF_{cap})WT_{cap}n_{wt\_px}n_{pixels} \quad (5.5.5)$$

$$Cost_{\_wt\_fd} = Cost_{wt\_fd}\, n_{wt\_px}n_{pixels} \quad (5.5.6)$$

$$Cost_{install} = ((Cost_{install\_wt\_fd} + Cost_{install\_cables} + Cost_{install\_sub})\, OWF_{cap})WT_{cap}n_{wt\_px}n_{pixels} \quad (5.5.7)$$

$$Cost_{cables} = (Cost_{cables}/OWF_{cap})WT_{cap}n_{wt\_px}n_{pixels} \quad (5.5.8)$$

$$Cost_{substation} = (Cost_{sub}/OWF_{cap})WT_{cap}n_{wt\_px}n_{pixels} \quad (5.5.9)$$

$$Cost_{om} = (Cost_{om}/OWF_{cap})WT_{cap}n_{wt\_px}n_{pixels} \quad (5.5.10)$$

$$Cost_{decom} = (Cost_{decom}/OWF_{cap})WT_{cap}n_{wt\_px}n_{pixels} \quad (5.5.11)$$

All of the aforementioned calculation rules have been set up in such a manner that it is versatile to allow the user to calibrate all relative inputs "at will". OWF costs were based on a number of known costs gathered, essential trends, assumptions and regression models from the extensive OWF literature research, presented in Section 2.5. In the proposed models the following characteristics of one or more OWFs are provided by the user including:

1. The total installed capacity of the OWF(s);
2. Specific wind generator model and the wind class limits per WT;
3. Hub height of the WT and the rotor diameter;
4. Water Depth limits in order to estimate the foundations cost characteristics;

5. Potential ports, harbors and onshore network junctions' locations for distance-based cost evaluation;
6. Installation vessels' types and daily rates, personnel count and installation strategies and configurations;
7. Export, inter-array and onshore cable characteristics;
8. Total number of Offshore and Onshore Substations and their equipment;
9. Cost of Steel – Procured cost in euros per ton of steel;
10. Manufacturing complexity factor related to the production and acquisition phase;
11. Cost-related parameters such as the inflation rate, factor development, electricity celling price and lifetime of the project;

### 5.5.1 Sources of error, bias and uncertainty

Apart from the wind and technical related uncertainties such as wind speed and wind power assessment, WT and inter-array availability, wake and electrical losses, downtime periods or degradation factors affecting an OWF's efficiency, additional cost uncertainties must be considered when estimating life cycle costs of an offshore wind project. Mostly, this type of uncertainties includes (Kaiser & Snyder, 2012):

1. **Sample size and heterogeneity:** The available cost data are limited and diverse in terms of the project size, geographic region, year of construction and monetary values, operating status, and the current technologies used during a specific period. As a result, small samples from relevant projects along with the heterogeneous technical characteristics and technologies used, lead to less robust analytical models.
2. **Data reliability:** Much of the cost data are not always acquired from relevant wind industries, technical reports or integrated modelling frameworks. As a result, referenced data sources or cost assessment models may or may not include all relative cost information, factors affecting the associated cost components and the overall cost of an OWF. On top of that, it is possible that the frequency and the quality of these sources is

biased, based on the novelty or the developers' preferences for an OWF, which is significantly affecting cost estimates.

3. **Exchange and inflation rate fluctuations:** Offshore wind projects have been deployed during the last 30 years in several countries worldwide. Between these projects, the capital costs or the O&M costs have been reported and assessed in different currencies e.g., euros, dollars, pounds etc., and different time intervals. These facts lead to increased uncertainties during the cost modelling as long as the exchange rates fluctuate over time and inflation rates are currency specific. Therefore, for comparison purposes all monetary values must be converted to a standardized format which is either neglected or can cause errors or bias to the resulted cost estimates.
4. **Spatial resolution and generalization issues:** Spatially dependent cost approximations such as the foundation, transmission, installation and O&M are exposed to the spatial data quality, resolution and measurement uncertainty. As a result, the quantification of the reference data uncertainty along with the pre-processing generalizations or simplifications to the input data may be critical to the resulted cost estimation.

### 5.5.2 Wind turbines cost

According to Gonzalez-Rodriguez (2017) the overall WT cost is divided in three sub-cost components: i) acquisition cost (accounted for approx. 85% of the overall cost), ii) shipping and assembling (approx. 5% of the overall cost) and iii) electrical installation (the remaining 10% of the overall cost). The cost of shipping and installation procedures depends on the distance to the potential OWF site; however, it constitutes the least significant factor. For the WTs' overall cost approximation multiple sources of data are used considering the analytical cost equations based on expressions denoting either the overall per MW cost or activity-based costs (e.g., acquisition, shipping and assembling and electrical installation). Table 5.5.2.1 and Equation 5.5.2.1 – 5.5.2.4 demonstrate previous cost functions based on data from industries, companies and developers related to OWE development. Consequently, according to Dicorato et al. (2011), WTs cost, for rated power of 2-5 MW, is expressed as:

$$Cost_{WT} = (2.95\ 10^3 \ln(P_{WT}) - 375.2)/1000 \quad (\text{m€}) \qquad (5.5.2.1)$$

where $P_{WT}$ is the rated power in MW for a single WT. Transport and installation costs have to be added to the cost expressed by Equation 5.5.2.1, corresponding to 10% of the WT manufacturing cost. According to Moller et al. (2012), overall WT cost is expressed through a simplified expression on per MW basis expressed as:

$$Cost_{WT2} = 1.1\ P_{WT}\ (\text{m€}) \qquad (5.5.2.2)$$

Similarly, Cavazzi and Dutton (2016), define WT cost as 1.6 m€/MW and based on their research, the WT's cost is increased by 50% in the case of floating turbines. Notable is that the aforementioned cost values (1.1 and 1.6 million Euros) correspond to the market values during the specific research period the aforementioned studies were carried out (2011 and 2016 respectively). One of the latest research studies, established by Gonzalez-Rodriguez (2017), highlights that the WTs' total cost can be expressed as:

$$Cost_{WT3} = 1.374\ P_{WT}^{\ 0.87}\ (\text{m€}) \qquad (5.5.2.3)$$

A significant drawback of Equations 5.5.2.1 - 5.5.2.3 is that they express WTs' cost estimates for the period 2007-2017, where a short number of commercial WTs beyond 8 MW have been installed worldwide and relevant cost estimates were lacking. Hence, reviewed cost data beyond 2017 (expressed in million $Euros_{2020}$) are illustrated in Table 5.5.2.1. Based on these data, Equation 5.5.2.4 models the cost of a potential WT as a polynomial function of the total power output, fitted in the cost per MW for each WT. The coefficient of determination ($R^2$) is 0.9144 (Figure 5.5.2.1) and based on this expression the user can approximate the overall cost of a WT with rated power beyond 8 MW.

$$Cost_{WT4} = 0.1176\ P_{WT}2\ +\ 0.5953\ P_{WT}\ +\ 1.133 \quad (\text{m€}) \qquad (5.5.2.4)$$

All of the equations are used in the SDSS as an alternate option to approximate and compare WT's overall cost for non-experienced users.

**Table 5.5.2.1**: Offshore wind turbines' overall cost approximation (manufacturing cost)

| Rated Power (MW) | Cost (million euros2020) |
|---|---|
| 2 | 2.257 - 3.792 |
| 3 | 2.174 - 5.666 |
| 3.6 | 3.203 - 4.913 |
| 4 | 4.616 - 6.12 |
| 5 | 5.376 - 6.466 |
| 6 | 9.506 - 9.987 |
| 7 | 11.404 |
| 8 | 12.774 - 13.25 |

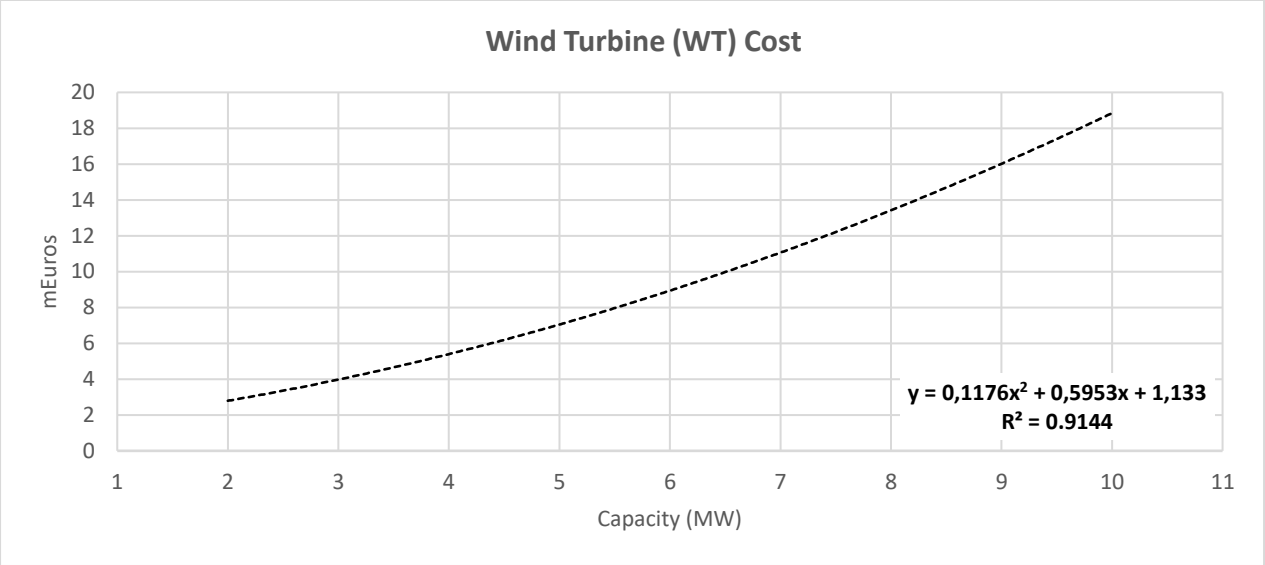


**Figure 5.5.2.1**: Offshore wind turbine cost estimation (Polynomial fitting)

Although the coefficient of determination of Equation 5.5.2.4 is admissible, the increase of a WT cost, regarding its power output and size, is not always linear for both the production and installation process and therefore more analytical functions must be considered. The hub height and as a consequence the tower mass, the rotor diameter and radius along with the nameplate capacity of each WT play a pivotal role to the total cost estimation. As a result, variable cost approximations are established for each wind turbine generator as long as the raw materials consumption differs non-linearly considering the RNA (Rotor-Nacelle-Assembly) and the tower (substructure) mass and the total weight.

Based on Fingersh et al. (2006) and Perkin et al., (2015), for a WT scaling cost model, the total top (RNA) and tower mass can be approximated using multiple linear and non-linear analytical expressions. Based on the proposed framework, WT's components are divided to the: i) tower, ii) rotor blades, iii) rotor hub and bearings, iv) gearbox, v) generator, vi) pitch and yaw system, vii) converters and transformers, viii) mechanical breaks, ix) main shaft and x) the entire electrical infrastructures (e.g., inner cables etc.). Consequently, the total cost is expressed as a function of the total component's mass with the WT's capacity, the rotor diameter and the hub height. Multiple adjustments are applied in some of the equations in order to adjust current technological improvements (e.g., the tower height, mass and cost, blades' fabrication materials, gearbox technologies etc.). Analyzing these costs, one of the costliest components of a WT are the blades (approx. 25% of the total WT cost). In Equations 5.5.2.6 - 7 each blade's and nacelle's mass and costs are calculated by:

$$Blade_{mass} = 0.4483\ {P_{wt}}^2 - 2.922\ P_{wt} + 24.905$$
$$Blade_{cost} = ((0.4019\ R^3 + 90000)BCE + 2.7445 R^{2.5025} GDPE)/0.72 \qquad (5.5.2.6)$$

$$Nacelle_{mass} = 244.56 \ln(P_{wt}) - 152.64$$
$$Nacelle_{cost} = 11.537\ P_{wt} + 3849.7 \qquad (5.5.2.7)$$

where *R* is the rotor radius, *BCE* is the blade material cost escalator and *GDPE* the labor cost escalator set as 1 (both escalator parameters may vary as the manufacturing complexity increases, e.g., > 1) and $P_{wt}$ is the rated power of the WT in kilowatts. Blade and nacelle mass equations are extracted using the data in Table 5.5.2.2 where different offshore WT models are reported for rated powers ranging from 3.6 up to 12 MW.

**Table 5.5.2.2**: Offshore wind turbine blades and nacelle characteristics, Sources: Desmond et al., (2016), en.wind-turbine-models.com, wind-energy-the-facts and Rampion, (2015)

| Model | **Rated power (MW)** | **Radius (m)** | **Blade (tons)** | **Nacelle (tons)** |
|---|---|---|---|---|
| Siemens 3.6-107 | 3.6 | 53.5 | 25 | 125 |
| E112 | 4.5 | 57 | 20 | - |
| M500 | 5 | 58 | 17 | 233 |
| NREL | 5 | 63 | 17.74 | 240 |

| | | | | |
|---|---|---|---|---|
| Repower 5M | 5.075 | 63.25 | 18 | 300 |
| Bard VM | 5.276 | 61 | 26 | 280 |
| Vestas V-164-8 | 8 | 82 | 33 | 375 |
| LW | 8 | 82 | 35 | 285 |
| Vestas V-164-10 | 10 | 82 | 35 | 390 |
| DTU | 10 | 89.15 | 41.71 | 446 |
| GE Haliade | 12 | 107 | 55 | - |

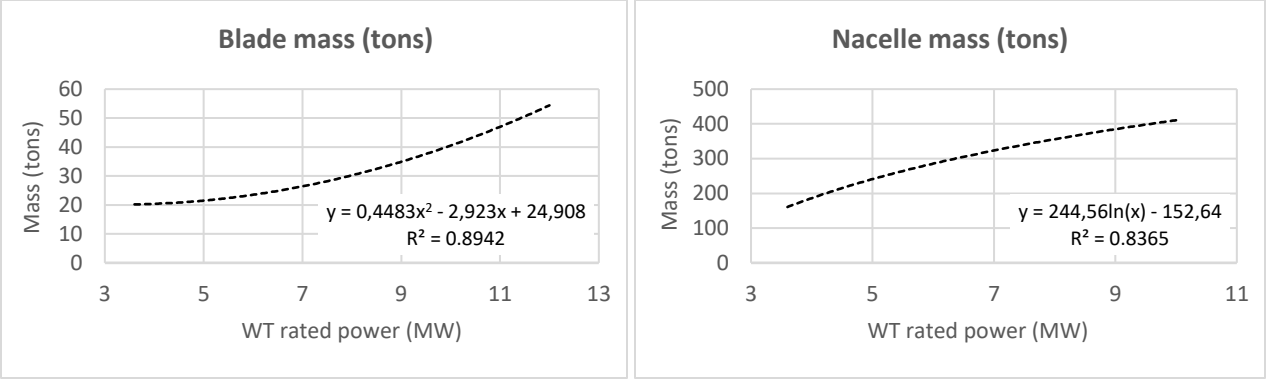


**Figure 5.5.2.2**: Wind turbine blades' and nacelle's cost modelling (Regression results)

Accordingly, the hub mass and cost are proportional to the total individual blade mass and are expressed as:

$$Hub_{mass} = 0.954\ Blade_{mass} + 5680.3$$
$$Hub_{cost} = 4.25\ Hub_{mass} \quad (5.5.2.8)$$

The pitch system cost is related to the sum of the pitch bearing and pitch system mass and is calculated as a function of the total blades' mass. Thus, pitch system total cost is formulated as:

$$Pitch\_Bearing_{mass} = 0.1295\ (3\ Blade_{mass}) + 491.31$$
$$Pitch\_System_{mass} = 1.328\ Pitch\_Bearing_{mass} + 555$$
$$Total\_Pitch\_System_{cost} = 2.28\ (0.2106\ D^{2.6578}) \quad (5.5.2.9)$$

In addition, the nose cone (spinner), the rotor blades' bearings, the low-speed shaft, the gearbox, the generator and the break are extracted using Equation 5.5.2.10 - Equation 5.5.2.15. Gearboxes

and generators are considered as the most complicated components of a WT, accounting of a total 15% of the entire WT's cost.

$$Nose\_cone_{mass} = 18.5D - 520.5$$
$$Nose\_cone_{cost} = 5.57\ Nose\_cone_{mass} \quad (5.5.2.10)$$

$$Low\_speed\_shaft_{cost} = 0.01\ D^{2.887} \quad (5.5.2.11)$$

$$Bearing_{mass} = ((800D)/600 - 0.033)0.0092\ D^{2.5}$$
$$Bearing_{cost} = 35.2\ Bearing_{mass} \quad (5.5.2.12)$$

$$Gearbox_{cost} = 16.45\ {P_{wt}}^{1.249} \quad (5.5.2.13)$$
$$Break_{cost} = 1.9894\ P_{wt} - 0.1141 \quad (5.5.2.14)$$
$$Generator_{cost} = 54.73\ P_{wt} \quad (5.5.2.15)$$

Yaw system among with the mainframe and the platform railing are also approximated in relation to the rotor diameter *D* (Equation 5.5.2.16 - Equation 5.5.2.18). Total yaw system cost is almost twice of the bearing and the mainframe cost and is related to the drive train type of each wind turbine generator.

$$Yaw\_system_{cost} = 2\ (0.0339\ D^{2.964}) \quad (5.5.2.16)$$
$$Mainframe_{cost} = 9.489\ \ D^{1.953} \quad (5.5.2.17)$$
$$Platform\_railing_{mass} = 0.125\ Mainframe_{mass}$$
$$Platform\_railing_{cost} = 8.7\ Platform\_railing_{mass} \quad (5.5.2.18)$$

Finally, Equation 5.5.2.19 expresses the hydraulic and cooling system as also the nacelle's total mass and cost proportional to the WT's capacity. Moreover, Equation 5.5.2.20 describes the total cost for the remaining electrical connections, including switchgear and any tower wiring, the power converter and the transformer as also the control and monitoring systems.

$$Hydro\_cooling_{cost} = 12\ P_{wt} \quad (5.5.2.19)$$

$$Electronics_{cost} = 180\ P_{wt} + 70000 \quad (5.5.2.20)$$

As already highlighted, adjustments have been applied to some of the cost expressions including the tower mass and the associated cost. Therefore, relevant cost data were examined which are illustrated in Table 5.5.2.3. Wind generator's capacity, hub height and the rotor diameter are some of the key factors that influence the total tower mass and cost approximation. According to Dicorato et al., (2011), Myhr et al. (2014), Shaffie et al. (2016) and Gonzalez-Rodriguez et al. (2017), the total tower expenses account for approximately 25% of the entire WT cost. Based on these data, the tower cost was adjusted to the relative WT's cost, considering the material and the manufacturing cost, proportional to the tower mass. As a result, Equation 5.5.2.21 presents the total tower mass and cost as a function of the wind generator capacity, the hub height and the rotor diameter.

**Table 5.5.2.3**: Offshore wind turbines and tower mass characteristics

| Source | Capacity ($P_{wt}$) (MW) | Hub height (H) (m) | Tower Mass (tons) |
|---|---|---|---|
| De Vries, (2011) | 2 | 78 | **190** |
| De Vries, (2011) | 2,3 | 80 | **250** |
| Energinet, (2015) | 3 | 65 | **150** |
| De Vries, (2011) | 3 | 80 | **280** |
| Energinet, (2015) | 3.6 | 60 | **180** |
| De Vries, (2011) | 3.6 | 90 | **210** |
| Energinet, (2015) | 4 | 68 | **210** |
| Desmond et al. (2016) | 5 | 90 | **348** |
| Energinet, (2015) | 8 | 84 | **340** |
| Desmond et al. (2016) | 8 | 110 | **558** |
| Energinet, (2015) | 10 | 125 | **620** |
| Desmond et al. (2016) | 10 | 119 | **605** |
| Gaertner et al. (2020) | 15 | 150 | **860** |
| **Regression** | | | |
| *P-value* | 0.007 | 0.001 | - |
| Multiple $R^2$ | | 0.985 | |

$$Tower_{mass} = (24.072\ (P_{wt}) + 4.848\ H - 221.339)\ 1000 \text{ (in Kg)}$$

$$Tower_{cost} = 3.2\ Tower_{mass} \text{ (in Euros)} \quad (5.5.2.21)$$

Using the sum of the Equation 5.5.2.6 - Equation 5.5.2.21, the total WT cost is extracted in Euros$_{2020}$ using Equation 5.5.2.22. An additional 13% is added to the total cost for "marinization" procedures (e.g., special preparation for all components to increase their survivability in the extremes of an offshore ocean environment). Finally, the total WT cost is adjusted to the current monetary values (using the exchange and inflation rates from the 2003 period).

$$WT_{cost} = 1.63\ (3\ Blade_{cost} + Nacelle_{cost} + Tower_{cost} + Electronics_{cost} + Hydro\_cooling_{cost} + Platform\_railing_{cost} + Mainframe_{cost} + Yaw\_system_{cost} + Generator_{cost} + Break_{cost} + Gearbox_{cost} + Bearing_{cost} + Low\_speed\_shaft_{cost} + Nose\_cone_{cost} + Total\_Pitch\_System_{cost} + Hub_{cost}) \quad (5.5.2.22)$$

### 5.5.3 Foundation cost

Foundation cost is given by three major components consisting of the manufacturing cost, the cost of transport and installation and the cost of the preparative activities at the site related to the scour protection (Dicorato et al., 2011; Gonzalez-Rodriguez, 2017). Many parametric expressions link the cost of the support structures with water depth, WT's capacity, as well as with the cost of material usage and fabrication (i.e., cost of steel etc.), however, a lot of uncertainties arise due to the site-specific characteristics (depth, soil, wave and current conditions). Dicorato et al. (2011) and Gonzalez-Rodriguez, (2017) highlight that for bottom-fixed structures, an increase per one meter (m) of additional water depth has an impact of 2% in the total foundation cost. Also, an increase of 80% to the total foundation cost is considered when specific WT characteristics occur, related to the hub height and the rotor diameter (expressed as the load factor *LF*). Specifically, according to Dicorato et al., (2011) foundation cost is based on three different empirical equations defined as:

$$Cost_{found1} = ((8.17 D_m + 389.3)/1000)\ 1{,}1527 \quad (5.5.3.1)$$

$$Cost_{found2} = ((320\ P_{WT}(1 + 0.02(D_m - 8))(1 + 0.8\ 10^6(LF - 10^5)))/1000)\ 1.1527 \quad (5.5.3.2)$$

$$LF = h\left(\frac{d}{2}\right)^2 \quad (5.5.3.3)$$

$$Cost_{found3} = ((5.382(D_m - 5) + 306.77) / 1000)\ 1.1527 \quad (5.5.3.4)$$

expressed in million euros (2020) per foundation, where $D_m$ is the depth, *LF* is the load factor for *h* and *d* (in meters) as the hub height and the rotor diameter respectively. When *LF* reaches 1.1x10$^6$ m$^3$, foundation cost resulted from Equation 5.5.3.2 increases by 80%. From these analytical expressions, Dicorato et al., (2011) indicate that Equation 5.5.3.2 has the better fitting accuracy compared to real cost observed. To the above-mentioned cost functions, an increase of additional 50% of manufacturing cost must be considered for transport and installation procedures. On the other hand, several authors applied different analytical expressions for separating foundation cost per depth range values, considering different polynomial equations per foundation technology. Thus, according to Moller (2011) the total foundation cost can be expressed as:

$$Cost_{found4a} = (((499{D_m}^2 + 6219D_m + 311810)1.4)/1000000)1.117 \quad (5.5.3.5)$$

$$Cost_{found4b} = (((440{D_m}^2 + 19695D_m + 90169)1.4)/1000000)1.117 \quad (5.5.3.6)$$

for 0 < $D_m$ < 25 and $D_m$ ≥ 25 respectively, where $D_m$ is the depth in meters and the total cost is expressed in (m€/MW). Although these expressions are sufficient for bottom-fixed structures, increased overestimations are noticed for depth values beyond 40 meters. Moreover, the transportation and installation costs are included as fixed constant values and therefore, no differentiation occurs considering site-specific characteristics and distance from nearest harbors and ports facilities. A more analytical calculation scheme was presented by Cavazzi and Dutton, (2016), including floating support structures cost approximation, incorporating the transportation and installation cost. According to their research the total foundation cost can be extracted from:

$$Cost_{monop} = ((0.0011{D_m}^2 + 0.0023D_m + 1.2253)\ 1.261)1.055 \quad (5.5.3.7)$$

$$Cost_{jacket} = ((0.0008{D_m}^2 + 0.0154D_m + 1.5847)\ 1.261)1.055 \quad (5.5.3.8)$$

$$Cost_{floating} = ((0.0017D_m + 3.732)\ 1.261)1.055 \quad (5.5.3.9)$$

expressed in m€/MW and the cost results are proportional to the water depth ($D_m$). Based on these equations, the total installation cost is added as a function of the time spent to reach the offshore site ($[days]_{to-site}$) (Equation 5.4.3.10), including the distance to the closest harbor ($D_{dist}$), the total days to install the support structures ($[days]_{install}$), the vessel speed ($[speed]_{jack-up}$) and cost ($[cost]_{jack-up}$) and finally the total working hours ($[hours]_{working-day}$) and the number of foundation installed per visit-trip of the jack-up vessel ($[n]_{per-visit}$):

$$[days]_{to-site} = ((2\{\frac{D_{dist}/1000}{[speed]_{jack-up}[hours]_{working-day}[n]_{per-visit}}\})\}\ [cost]_{jack-up} \quad (5.5.3.10)$$

$$Cost_{found5} = (aD_m{}^2 + bD_m + c) + ([days]_{install}+[days]_{to-site})\ \left([cost]_{jack-up}\right)1.261)0.055) \quad (5.5.3.11)$$

where the total foundation cost is expressed in m€/MW for the production, transportation and installation procedures (Equation 5.5.3.10-11) and parameters *a, b* and *c* are defined by Equation 5.5.3.7 - 5.5.3.9 for the monopile, jacket and floating support structures respectively. Finally, the latest foundation cost functions were established by Bosch et al. (2019) including:

$$Cost_{monop2} = (((201D_m{}^2 + 612.93D_m + 411.464)/1000)0.892)1.013 \quad (5.5.3.12)$$

$$Cost_{jacket2} = (((114.24D_m{}^2 \pm 2.270D_m + 531.738)/1000)0.892)1.013 \quad (5.5.3.13)$$

$$Cost_{floating2} = (((773.85D_m + 680.651)/1000)0.892)1.013 \quad (5.5.3.14)$$

expressed in m€/MW for monopile (0 - 25m), jacket (25 - 55m) and floating (55 - 1000m) support structures, including transportation and installation costs. Notable is that for all of the foundation cost expressions presented (Equation 5.5.3.1 - Equation 5.5.3.14), all monetary values are converted to Euro 2020 costs, based on the average exchange (from US dollars and British pounds) and inflation rates (Euro) of/from the according year the research was completed or based on the cost information given by the authors.

**Bottom-fixed support structures:** Similarly to the WTs analytical cost approximation, foundation cost estimates are highly uncertain due to the site-specific characteristics, the met-ocean

conditions or relevant technical or economic aspects. For instance, steel and fuel prices are volatile and are highly differentiated among countries (China, EU and the US) and other exogeneous factors (e.g., the COVID-19 pandemic crisis, oil crisis). According to Myhr et al., (2014), a base price of 775 euros per ton for bulk steel was assumed, increased in 1000 euros per ton including transport cost (transport to and from the manufacturing facilities). Moreover, a fuel cost of 640 euros per ton was used in their cost model, accounting for volatility in both steel and fuel costs, taking into consideration high and low scenarios of ±40%. Based on the EU fuel[13] and steel[14] price data, current steel prices preserve a decrease of 10% compared to the values used by Myhr et al. (2014) and the fuel values seem to remain steady. It is noticed that the fuel cost values are mostly incorporated in the day rates of the installation vessels as long as the steel values are used to estimate the manufacturing cost of the WT tower and the foundations.

**Table 5.5.3.1**: Monopile and jacket support structures characteristics

| Energinet, (2015) | | | | | |
|---|---|---|---|---|---|
| **Monopile foundations** | **Rated Power (MW)** | | | | |
| **Pile** | **3** | **3.6** | **4** | **8** | **10** |
| Diameter at seabed (m) | 5 | 5.5 | 6 | 6.5 | 7.75 |
| Pile length (m) | 35-55 | 35-60 | 40-65 | 50-70 | 50-80 |
| Penetration length(m) | 15-30 | 15-30 | 16-31 | 18-34 | 20-39 |
| Weight (tons) | 200-600 | 250-700 | 300-800 | 450-1000 | 550-1250 |
| **Transition piece** | | | | | |
| Length (m) | 15-20 | 15-20 | 15-24 | 20-30 | 20-31 |
| Outer diameter (m) | 4,5 | 4,5 | 5 | 6 | 6,5 |
| Weight (tons) | 150-250 | 150-250 | 160-260 | 200-370 | 250-420 |
| **Total Mass** | **350-850** | **400-950** | **460-1060** | **650-1370** | **800-1720** |
| **Jacket foundations** | | | | | |
| Mass jacket+Tran.piece (tons) | 250 | 350 | 400 | 1000 | 1100 |
| Mass of piles (tons) | 150 | 200 | 250 | 500 | 600 |
| Pile length (m) | 30-50 | 30-50 | 30-50 | 35-60 | 40-70 |
| **Total Mass** | **400** | **550** | **650** | **1500** | **1700** |

[13] https://www.eea.europa.eu/data-and-maps/indicators/fuel-prices-and-taxes/assessment-4

[14] https://worldsteelprices.com/european-steel-prices/

In Table.5.5.3.1 the structural characteristics for both monopile and jacket foundations are demonstrated. Data in Table.5.5.3.1 denote that the total mass of both structures differs according to the selected WT size as also jacket foundations are generally less massive than monopiles. For the monopile support structures, Table.5.5.3.2 captures all the relevant information related to the operational depth and the monopiles' structural characteristics consisting of the pile diameter, the total and penetration depth[15] and the total weight of the support structure from previous OWF projects. Based on these data, a strong relation occurs between the pile diameter (and therefore the size of the WT), the sea depth and the total length of the monopile structure. Accordingly, the following rules can be used: i) for monopiles with 6 m of diameter, the penetration pile length is about 7 times the diameter; ii) in case of monopiles with 7 m of diameter, the driving length is about 5 times the diameter; and iii) in case of monopiles with 8-9 m of diameter, the driving length is about 4-5 times the diameter (Negro et al., 2017). Using these assumptions, a multiple regression model is set to approximate the total monopile's mass based on the key structural characteristics (diameter, total length and sea depth). The results are presented in Table.5.5.3.2 based on 32 observations and the adjusted $R^2$ is 0.891, indicating a very satisfying agreement between the observed and the modelled data.

$$\text{Pile}_{\text{mass}} = 19.627 Depth_{sea} + 116.597 D_{pile} - 419.426 \quad (5.5.3.15)$$

$$\text{Pile}_{\text{cost}} = Cost_{steel\_ton} Pile_{mass} + PCD(Cost_{steel\_ton} Pile_{mass}) \quad (5.5.3.16)$$

for $D_{pile}$ as the mean diameter of the monopile structure, $Depth_{sea}$ is the sea depth in meters and *PCD* is the production escalator factor indicating the structure difficulty to be constructed for *PCD* values greater than zero (i.e., 1 is assumed for monopiles and 4 for jacket structures according to Myhr et al., 2014).

**Table 5.5.3.2**: Monopile foundation characteristics

| **Indicative OWFs,** Source: Negro et al., (2017) | | | | |
|---|---|---|---|---|
| **Depth (m)** | **Diameter (m)** | Total Length (m) | Penetration length (m) | **Weight (tons)** |

[15] The driving length of the pile beyond the sea bottom surface (Negro et al., 2017)

| | | | | |
|---|---|---|---|---|
| **5** | **4** | 38 | 33 | **247** |
| **5** | **5** | 52 | 44 | **400** |
| **7.5** | **4.2** | 42 | 32 | **200** |
| **7.5** | **4.3** | 35 | 22 | **310** |
| **7.5** | **5** | 50 | 35 | **423** |
| **9** | **4** | 25 | 14 | **250** |
| **9** | **4.7** | 40 | 28 | **235** |
| **10** | **4** | 42 | 28 | **230** |
| **11.5** | **4.5** | 45 | 32 | **300** |
| **12.5** | **5.2** | 48 | 31.7 | **480** |
| **12.5** | **7** | 85 | 60 | **650** |
| **15** | **7** | 20.4 | 35.4 | **488.1** |
| **15** | **9** | 25 | 40 | **841** |
| **17** | **5** | 54 | 35 | **630** |
| **17.5** | **4.75** | 60 | 39 | **530** |
| **19.5** | **5.2** | 61 | 40 | **530** |
| **20** | **5** | 72 | 48 | **550** |
| **20** | **6** | 70 | 42 | **700** |
| **20** | **7** | 22.4 | 42.4 | **577.1** |
| **20** | **9** | 27 | 47 | **1011.5** |
| **21** | **6** | 70 | 47 | **720** |
| **22.5** | **6** | 70 | 45 | **800** |
| **25** | **7** | 23.2 | 48.2 | **647.8** |
| **25** | **9** | 29 | 54 | **1186.4** |
| **26** | **5.9** | 66 | 37 | **700** |
| **26** | **6** | 65 | 34 | **730** |
| **26** | **6** | 60 | 28 | **700** |
| **27** | **6** | 68 | 38 | **805** |
| **30** | **7** | 27 | 57 | **764** |
| **30** | **9** | 30 | 60 | **1308** |
| **35** | **7** | 33 | 68 | **942.6** |
| **35** | **9** | 33 | 68 | **1477.7** |
| **40** | **7** | 38 | 78 | **1252.2** |
| **40** | **9** | 39 | 79 | **1719.8** |
| **Regression results** | | | | |
| **P-value** | **P-value** | Multiple $R^2$ | 0.947 | |
| 1,63E-07 | 1.79E-07 | $R^2$ | 0.891 | |

Although the mass of the monopile foundations is greater than the jacket support structures, the overall cost impact on LCoE values indicates that the monopiles are economically more favorable than the jackets for water depths up to 30-40 meters (Damiani et al., 2016; Arantegui et al. 2018). Hence, for water depths beyond 30 meters, jacket support structures are considered. Jacket support structures are different and more complex than the monopiles because of the number of elements to be considered. The main structure consists of the steel legs, the horizontal and diagonal braces as also from the foundation piles mounted into the seabed surface and the transition piece to the top of the structure. The dimensions of the jacket foundations are site-specific and specifically tailored to the seabed characteristics at a specific area or the WT's type and size (capacity) (Hensel et al., 2012; Myhr et al., 2014; Damiani et al., 2016). Foundation piles' length and mass are very dependent on the soil conditions when different substrate characteristics occur (sand, clay etc.). Moreover, the leg dimensions and the mass increase are both relative to the water depth, the WT capacity and the hub height. On the contrary, the mass of the foundation piles, decreases with the increase in the leg dimensions, however, differentiations in the soil stiffness (soft soils - higher pile mass) increase the total mass of the piles (Energinet, 2015; Sandal, 2017).

Based on the aforementioned characteristics, multiple data were gathered from industry or analytical modelling frameworks in order to quantify the jacket and foundation piles mass differences according to water depth and WT size. In Table 5.5.3.3 these data are demonstrated for the total jacket and piles mass characteristics.

**Table 5.5.3.3**: Jacket support structures mass characteristics (piles and top structure) for different depth values and WT capacities

| Sources | Wind Turbine capacity (MW) | Depth (m) | Pile mass (Clay) (tons) | Jacket mass (tons) |
|---|---|---|---|---|
| Wijngaarder, (2013) | 3.6 | 20 | 200 | 177 |
| Wijngaarder, (2013) | 3.6 | 40 | 200 | 216 |
| Wijngaarder, (2013) | 3.6 | 60 | 200 | 461 |
| Damiani et al., (2016) | 5 | 20 | 280 | 400 |
| Damiani et al., (2016) | 5 | 30 | 290 | 470 |
| Hensel et al., (2012) | 5 | 30 | 380 | 300 |
| Damiani et al., (2016) | 5 | 40 | 385 | 500 |

| | | | | |
|---|---|---|---|---|
| Hensel et al., (2012) | 5 | 45 | 390 | 380 |
| Damiani et al., (2016) | 5 | 50 | 400 | 550 |
| Damiani et al., (2016) | 5 | 60 | 415 | 620 |
| Damiani et al., (2016) | 5 | 65 | 425 | 680 |
| Damiani et al., (2016) | 6 | 10 | 310 | 500 |
| Wijngaarder, (2013) | 6 | 20 | 320 | 335 |
| Damiani et al., (2016) | 6 | 25 | 330 | 510 |
| Damiani et al., (2016) | 6 | 30 | 340 | 520 |
| Wijngaarder, (2013) | 6 | 40 | 350 | 468 |
| Wijngaarder, (2013) | 6 | 60 | 380 | 669 |
| Wijngaarder, (2013) | 8 | 20 | 500 | 606 |
| Wijngaarder, (2013) | 8 | 40 | 500 | 646 |
| Wijngaarder, (2013) | 8 | 60 | 500 | 713 |
| Energinet, (2015) | 10 | 20 | 600 | 900 |

Manufacturing cost is evaluated through a technology or complexity factor according to Hensel et al., (2012) and Myhr et al., (2014) respectively. For the latter approach this factor is equal to 4 (multiplied by the total support structure mass, 1 is for the piles final cost) and reflects the manufacturing complexity. The former approach indicates that the Technology Type factor (referred as TT) is approximately between 1-2 for both the jacket and the piles construction, depending on the soil conditions. For this study this factor is considered equal to 1.7 for both the jacket and the piles cost. Finally, an additional mass increase of 200 tons is considered for the transition piece and is added to the total jacket support structure mass expressed in Equation 5.5.3.20.

$$\text{Jacket}_{\text{mass}} = 91.847\ WT_{cap} + 4.972 D_s - 208.476 \quad (5.5.3.18)$$

$$\text{Piles}_{\text{mass}} = 1.972 D_s - 52.997 \quad (5.5.3.19)$$

$$\text{Total\_Jacket}_{\text{cost}} = (\text{Jacket}_{mass} Cost_{steel\_ton}) + (\text{Piles}_{mass} Cost_{steel\_ton}) + PCD\ (\text{Jacket}_{mass} Cost_{steel\_ton}) + PCD\ (\text{Piles}_{mass} Cost_{steel\_ton}) + (200\ Cost_{steel\_ton}) \quad (5.5.3.20)$$

Multiple regression results are presented in Table 5.5.3.4 where the relationship between the bathymetry and the WT's capacity for both the jacket structure and the piles is established. The adjusted $R^2$ value is 0.77 and 0.81 respectively and the small *p*-values for the regression

coefficients indicate that the predictor variables are statistically significant for either the piles and the jacket mass equations.

**Table 5.5.3.4**: Multiple regression results for the total jacket mass approximation

| **Regression Statistics (Support Str.)** | | **Regression parameters** | *Coefficients* | *P-value* |
|---|---|---|---|---|
| *Observations* | 21 | *Intercept* | -208.476 | 0.029283 |
| *Multiple R* | 0.89 | *WT capacity (MW)* | 91.847 | 3.04E-07 |
| *R Square* | 0.7959 | *Depth (m)* | 4.972 | 0.000317 |
| *Standard Error* | 82.181 | | | |
| **Regression Statistics (Piles)** | | **Regression parameters** | Coefficients | *P-value* |
| *Observations* | 21 | *Intercept* | -52.997 | 0,029312 |
| *Multiple R* | 0.91 | *WT capacity (MW)* | 60.095 | 2.81E-08 |
| *R Square* | 0.829 | *Depth (m)* | 1.9724 | 0.005327 |
| *Standard Error* | 45.682 | | | |

**Floating support structures:** Considering floating support structures, two different foundation technologies are selected consisting of the Spar-Buoy (SB) and the Semi-Submersible (SSB) models. Multiple cost data, were also acquired from previous cost models, technical reports as also from already existing offshore floating projects and are illustrated in Table 5.5.3.5 (Bjerkseter & Agotnes, 2013; Myhr et al., 2014; Kausche et al., 2018; Maienza et al., 2020). The total manufacturing cost for the proposed floating structures is divided in three sub-cost components incorporating: i) the sub-structure (floater), ii) the mooring lines and iii) the anchors. In Table 5.5.3.6 the technical and cost data for different floating concepts are listed. According to these data, a clear site-dependent relation occurs for each floating prototype concept based on the mooring and anchoring depth, the WT size and soil conditions among other parameters.

It is noticed that for estimating the mooring lines length of each floating concept is a complex engineering operation, however, some rough estimates may be considered in order to highlight the cost differences which are proportional to the water depth increase. In particular, all of the catenary mooring systems utilize a combination of steel wire and chain (Myhr et al., 2014) and the length differentiations are solely related to the depth, as presented in Table.5.5.3.7 where the cost per meter of mooring type is estimated (Bjerkseter & Agotnes, 2013). The

moorings' manufacturing cost is proportional to the mass per meter for each mooring system, its length, its diameter, the cost per kilogram of the mooring material and finally the total number of mooring lines. Similarly, for the anchoring manufacturing cost, the water depth and the mooring lines length are considered.

**Table 5.5.3.5**: Offshore wind floating structures characteristics (mass and costs)

| | **Depth range (meters)** | | | |
|---|---|---|---|---|
| Myhr et al., (2014) | 70 -200 meters | 70 -200 meters | 100 -500 meters | 40 -1000 meters |
| ***Structural characteristics for 200 meters depth*** | TLB B | TLP | Hywind II (Spar-Buoy) | WindFloat (Semi-Submersible) |
| Material consumption (tons) | 445 | 417 | 1700 | 2500 |
| Material cost (m€) | 0.497 | 0.465 | 1.899 | 2.793 |
| Manufacturing complexity | 110% | 130% | 120% | 200% |
| Manufacturing cost (m€) | 0.546 | 0.605 | 2.279 | 5.587 |
| Total production cost (m€) | 1.043 | 1.07 | 4.178 | 8.38 |
| ***Mooring and anchoring*** | | | | |
| Total line length (m) | 1767 | 2508 | 1950 | 2840 |
| Total line cost (m€) | 0.977 | 0.108 | 0.131 | 0.184 |
| Anchors mass (tons) | 40 | 53 | 17 | 17 |
| Anchors cost (m€) | 1.164 | 1.901 | 0.382 | 0.509 |
| **Total cost (m€)** | **3.184** | **3.079** | **4.691** | **9.073** |
| Kausche et al., (2018) | | | | |
| ***Depth (30 meters)*** | | TLP | | |
| **Total cost (m€)** | | **4.49** | | |
| Maienza et al., (2020) | | | | |
| ***Depth (130-140 meters)*** | | TLP | Spar-buoy | Semi-Submersible |
| Mass of platform (tons) | | 965 | 989 | 696 |
| Mass of anchoring (tons) | | 8.1 | 8.1 | 3.15 |
| Mass of mooring lines (tons) | | 4.64 | 93 | 132.6 |
| Length of mooring (m) | | 85 | 390 | 450 |
| **Total cost (m€)** | | **5.42** | **6.022** | **5.073** |

The cost of manufacturing the sub-structure (floater) is dependent on the mass and the size of each wind generator (Table.5.5.3.6). Moreover, the manufacturing cost is proportional to the

labor costs on the harbor where the offshore wind floating platforms are constructed. In this context, the cost of materials, direct labor and the activities cost are the main parts of the calculation process.

According to Bjerkseter & Agotnes, (2013) and Myhr et al., (2014) the reference cost values, considering a 5MW turbine generator, are 4.178 million euros for the spar-buoy and 8.38 million euros for the semi-submersible, including material and manufacturing cost. Highlighting that there is a lack of accurate cost data, different cost scaling factors are used. For example, Kikuchi and Ishihara (2019) indicated that there is an approximately 2.2 mass increase in the total support structure of the semi-submersible floater by increasing the WT's rated power from 5 to 10 MW of installed capacity, using the Equation 5.5.3.21. Moreover, based on Myhr et al., (2014), Wang et al., (2020) and data from industries involved in the Hywind project (Equinor, 2018), the structure mass ($Mass_{SB}$) of the spar-buoy floating concepts is extracted. Results indicate that for the spar-buoy floaters a 1750 tons floater is assumed for a 5 MW wind generator, as also 3500 and 5000 tons for the 8 and 10 MW wind turbine models. Both variables are multiplied by a production complexity factor (*PCF*) as illustrated in Equations 5.5.3.22 and 5.5.3.23.

$$\text{Mass}_{\text{SSB}} = 335P_{rated} + 1972 \quad (5.5.3.21)$$

$$Cost_{SSB} = PCF\ Mass_{SSB}\ Cost_{steel\_ton} \quad (5.5.3.22)$$

$$Cost_{SB} = PCF\ Mass_{SB}\ Cost_{steel\_ton} \quad (5.5.3.23)$$

**Table 5.5.3.6**: Examples of the total anchoring and mooring cost and length approximations, Source: (Myhr et al., 2014)

| **Floating Concept** | Hywind II (Spar-Buoy) | WindFloat (Semi-Submersible) |
|---|---|---|
| Anchors | 3 x DPA | 4 x DPA |
| **Anchor costs (€)** | **363853** | **485138** |
| Fibre rope length (m) | - | - |
| Chain total length (m) | 1800 | 2640 |
| Wire length (m) | 150 (250 €/m) | 200 (250 €/m) |
| Mooring line costs (€) | 126604 (x3) | 179799 (x4) |
| **Total mooring costs (€)** | **378000** | **718000** |

**Table 5.5.3.7**: Anchoring and Mooring length and cost data based on the depth profile and the WTs' array spacing, Source: Fontana, (2019)

| Depth - D (m) | Mooring line length (m) | Spacing - WD (m) | Cost per meter (€) | Cost per Mooring Line (€) | Anchor cost (DEA) (€) |
|---|---|---|---|---|---|
| 100 | 420 | 750 | 775.60 | 325752 | 95000 |
| 250 | 500 | 750 | 854.04 | 427020 | 89000 |
| 500 | 700 | 750 | 880.19 | 616133 | 55000 |
| 750 | 930 | 750 | 575.17 | 534908.1 | 22000 |
| 1000 | 1170 | 750 | 470.59 | 550590.3 | 11000 |
| 100 | 560 | 1000 | 1002.20 | 561232 | 113000 |
| 250 | 620 | 1000 | 932.48 | 578137.6 | 133000 |
| 500 | 800 | 1000 | 749.47 | 599576 | 68000 |
| 750 | 1020 | 1000 | 627.46 | 640009.2 | 31000 |
| 1000 | 1250 | 1000 | 278.87 | 348587.5 | 10000 |
| 100 | 700 | 1250 | 1420.50 | 994350 | 186000 |
| 250 | 750 | 1250 | 915.05 | 686287.5 | 152000 |
| 500 | 920 | 1250 | 601.32 | 553214.4 | 61000 |
| 750 | 1120 | 1250 | 453.16 | 507539.2 | 30000 |
| 1000 | 1330 | 1250 | 296.30 | 394079 | 17000 |
| 100 | 840 | 1500 | 1795.24 | 1508001.6 | 296000 |
| 250 | 890 | 1500 | 740.75 | 659267.5 | 115000 |
| 500 | 1030 | 1500 | 723.32 | 745019.6 | 88000 |
| 750 | 1220 | 1500 | 514.17 | 627287.4 | 42700 |
| 1000 | 1440 | 1500 | 148.15 | 213336 | 9600 |

Costs per mooring line and per anchor are listed in Table 5.5.3.7. Data were collected from Fontana (2019) and were also compared to previous research studies from Bjeckseter and Agotnes, (2013) and Myhr et al., (2014). Considering a single-line mooring configuration, it is assumed that all WTs are utilizing drag embedment anchors (DEAs), as they are the most cost-efficient anchor type, and are suitable for different soil types. Data in Table 5.5.3.8 indicate that for larger water depths and WTs spacings (array density), longer line lengths with smaller chain sizes are the more suitable. Thus, the magnitude-length of the suspended line increases as both water depth and the WTs spacing distance increases. As a result, smaller chain sizes are equally efficient for developing the restoring forces provided to the mooring system. On the contrary, for shallow waters (i.e., < 200-250 meters) and increased array densities (wind turbines spacing), the

length of the suspended line decreases and heavier and costlier chains are required. Similarly, for the anchors size and cost, increased depths, WTs spacing and mooring lines length and magnitude, lower cost values are observed. Consequently, moorings and anchors cost are both calculated via:

$$Mooring_{length} = 0.752D_{sea} + 0.453\,WD_{array} + 8.663 \quad (5.5.3.22)$$

$$Mooring_{cost\_meter} = -0.746\,Mooring_{length} + 1332.36 \quad (5.5.3.23)$$

$$Mooring_{cost} = N_{moorings}(Mooring_{cost\_meter}Mooring_{length}) \quad (5.5.3.24)$$

$$Anchors_{cost} = N_{anchors}(-680{,}77\,D_{sea} - 228.996\,WD_{array} + 672.224Mooring_{length} + 81112) \quad (5.5.3.25)$$

for $D_{sea}$ as the water depth, $WD_{array}$ the WTs spacing in meters as also $N_{moorings}$ and $N_{anchors}$ are the total number of mooring lines and anchors. Multiple regression results for each mooring line and anchor cost are presented in Table 5.5.3.8 and modelled by Equation 5.5.3.22 - 25. Adjusted $R^2$ values above 0.8 and *p*-values below the significance level of 0.05 highlight the satisfying agreement of the fitted models and the statistically significant association between the response variables and the mooring and anchor cost.

**Table 5.5.3.8**: Anchoring and Mooring length and cost regression results

| **Anchor cost** | ***Coefficients*** | ***P-value*** | ***Adjusted R Square*** |
|---|---|---|---|
| Intercept | 81112.396 | 0.01 | 0.848 |
| Depth (m) - *D* | -680.772 | 0.0001 | |
| Spacing (m) – *WD* | -228.995 | 0.015 | |
| Chain length (m) | 672.224 | 0.001 | |
| **Mooring length** | ***Coefficients*** | ***P-value*** | ***Adjusted R Square*** |
| Intercept | 8.663 | 0.017 | 0.983 |
| Depth (m) - *D* | 0.752 | 4.62759E-16 | |
| Spacing (m) - *WD* | 0.453 | 2.37068E-11 | |
| **Mooring cost** | ***Coefficients*** | ***P-value*** | ***Adjusted R Square*** |
| Intercept | 1332.356 | 4.73964E-11 | 0.804 |
| Chain length (m) | -0.746 | 2.86513E-07 | |

### 5.5.4 Electrical Infrastructure Cost evaluation

Balance of Plant (BoP) economic dispatch evaluation has been carried out from various sources based on descriptive mathematical formulations for the export and inter-array cables as also for the integration system cost estimation (see Dicorato et al. 2011; Hong & Moller 2011; Moller et al. 2012; Myhr et al., 2014; Cavazzi & Dutton, 2016; Shaffie et al., 2016; Nagababu, Kachhwaha & Savsani, 2017; Ioannou et al., 2018). In order to evaluate the total electrical infrastructure cost, the following sub-systems must be accounted, including: i) the OWF's collection system by means of the inter-array cables, ii) the integration of the power through offshore and onshore substations (if exist) and finally, iii) the transmission of the electricity from the offshore substation to the shore through the export cables and to the onshore substation through the onshore cables.

**Export cables cost:** According to Dicorato et al., (2011) the export cable(s) cost is expressed as a relation of the cables' technical characteristics, the distance from the onshore grid as well as by the technical characteristics of the integration system (substations, transformers). The cost of the cable section per meter is calculated from:

$$Cost_{export} = \left(\alpha + \beta e^{\left(\frac{\gamma I_n}{10^5}\right)}\right) 1.153 \qquad \text{(in €)} \qquad (5.5.4.1)$$

for $I_n$ expressing the cable's ampacity (*A*) (Table.5.5.4.2) and $\alpha$, $\beta$ and $\gamma$ are coefficients depending on nominal voltage level (Table.5.5.4.1). Consequently, the total transmission system cost ($C_{TS}$) is defined by Equation 5.5.4.2 in the presence of an offshore substation as:

$$C_{TS} = n_{HV}\left(Cost_{export} + Cost_{install}\right)d_{sea} + n_{HV}Cost_{onshore}(1 - a_{ol})\, d_{shore} + n_{olHV}c_{olHV}a_{ol}d_{shore} + n_{HV}C_{SG\_HV} \qquad (5.5.4.2)$$

where $C_{TS}$ is the total transmission cost in Euros, $Cost_{install}$ is 830 €/meter of cable installed, $n_{HV}$ is the number of export cables, $d_{sea}$ is the distance of the potential OWF from the coast, $d_{shore}$ is the total length of onshore connection to the onshore transmission system and $c_{olHV}$ is 311 €/meter or 403 in €/meter for 150 and 230 kV cables voltage respectively. Moreover, $Cost_{onshore}$

is 1844 €/m or 2248 €/m for 150 and 230 kV, $a_{ol}$ represents the amount of $d_{shore}$ covered by overhead lines in the range of 0-1 and $n_{olHV}$ is the number of overhead lines. Finally, $C_{SG\_HV}$ expresses the switch gears cost and is considered as 0.506 or 0737 and 1.072 or 1.464 million Euros, depending on the insultation system (AIS or GIS) and for 150 and 230 kV cables distributively (see Dicorato et al., 2011, pg.4-6).

Alternatively, $Cost_{export}$ and $Cost_{onshore}$ in Equation 5.5.4.2 can be replaced with more recent cables cost estimates which were derived from Table.5.5.4.2 and modelled using Equations 5.5.4.3 - 5.5.4.5. In particular, the cost of transmission cables is proportional to the cable's voltage (kV), the cable section diameter in $mm^2$and the ampacity (*A*) for different types of cable technologies (AC and DC) and for both offshore and onshore cables. Data gathered for the period 2014-2020 and adjusted to $Euros_{2020}$. For each cable technology and purpose of use, multiple regression models are established in order to estimate cable's cost per meter for different voltage and diameter levels. For the onshore transmission cables, similar cost estimates were considered for both AC and DC cables as long as small differences occur for different voltage and diameter values. Thus, for HVAC offshore cables cost per meter can be calculated from:

$$Cost_{exportAC} = 0.804\, D_{cable} + 3.286\, V_{cable} - 101.9 \quad (5.5.4.3)$$

$$Cost_{exportDC} = 0.329\, D_{cable} + 0.581\, V_{cable} + 509.95 \quad (5.5.4.4)$$

$$Cost_{onshore} = 0.223\, D_{cable} + 1.828\, V_{cable} - 225.759 \quad (5.5.4.5)$$

**Table 5.5.4.1:** Cost coefficients for export cables

| kV | α | β | γ |
|---|---|---|---|
| 132 | 249.72 | 26.48 | 379.5 |
| 239 | 403.02 | 13.94 | 462.1 |

**Table 5.5.4.2:** HVAC and HVDC cables connection cost and technical characteristics

| Xiang et al., (2016) | Offshore HVAC | | |
|---|---|---|---|
| **Voltage (kV)** | **Section ($mm^2$)** | Steady state current $I_{SSN}$ (A) | **Euros/meter (2020)** |
| 132 | 600 | 818 | 884 |
| 132 | 800 | 888 | 1026 |
| 132 | 1000 | 949 | 1110 |

| | | | |
|---|---|---|---|
| 220 | 500 | 732 | 1052 |
| 220 | 630 | 808 | 1097 |
| 220 | 800 | 879 | 1259 |
| 220 | 1000 | 942 | 1291 |
| 400 | 800 | 870 | 1808 |
| 400 | 1000 | 932 | 2002 |
| 400 | 1200 | 986 | 2195 |
| 400 | 1400 | 1015 | 2389 |
| 400 | 1600 | 1036 | 2583 |
| 400 | 2000 | 1078 | 2777 |
| Cole et al., (2014) | **Offshore HVDC** | | |
| +/– 320 | 300 | - | 633 |
| +/– 320 | 2500 | - | 1396 |
| +/– 500 | 1500 | - | 1181 |
| +/– 500 | 2500 | - | 1548 |
| Xiang et al., (2016) | **Offshore HVDC** | | |
| **Voltage (kV)** | **Section ($mm^2$)** | **Steady state current $I_{SSN}$ (A)** | **Euros/meter (2020)** |
| +/– 150 | 1000 | 1644 | 865 |
| +/– 150 | 1200 | 1791 | 942 |
| +/– 150 | 1400 | 1962 | 1013 |
| +/– 150 | 1600 | 2123 | 1084 |
| +/– 150 | 2000 | 2407 | 1162 |
| +/– 300 | 1000 | 1644 | 1104 |
| +/– 300 | 1200 | 1791 | 1214 |
| +/– 300 | 1400 | 1962 | 1311 |
| +/– 300 | 1600 | 2123 | 1407 |
| +/– 300 | 2000 | 2407 | 1517 |
| Gonzalez-Rodriguez (2017) | **Offshore HVAC** | | |
| **Voltage (kV)** | **Section ($mm^2$)** | **Capacity (MV A)** | **Euros/meter (2020)** |
| 132 | 500 | 138 | 546 |
| 132 | 630 | 151 | 624 |
| 132 | 800 | 177 | 728 |
| 132 | 1000 | 189 | 849 |
| 220 | 500 | 250 | 889 |
| 220 | 630 | 273 | 998 |
| 220 | 800 | 295 | 1119 |
| 220 | 1000 | 314 | 1280 |
| Jin et al., (2019) | | | |
| 220 | 1600 | 1200 | 610 |
| Cole et al., (2014) | **Onshore transport cables (HVAC)** | | |
| **Voltage (kV)** | **Section ($mm^2$)** | **Capacity (MV A)** | **Euros/meter (2020)** |

| | | | |
|---|---|---|---|
| 150 | 1200 | - | 317 |
| 150 | 2000 | - | 422 |
| 220 | 1200 | - | 554 |
| 220 | 1400 | - | 580 |
| 220 | 2000 | - | 659 |
| 400 | 800 | - | 712 |
| 400 | 2000 | - | 897 |
| Gonzalez-Rodriguez (2017) | **Onshore transport cables (HVAC)** | | |
| 220 | 500 | 273 | 246 |
| 220 | 630 | 297 | 281 |
| 220 | 800 | 314 | 316 |
| 220 | 1000 | 348 | 387 |
| Cole et al., (2014) | **Onshore transport cables (HVDC)** | | |
| +/– 320 | 500 | - | 576 |
| +/– 320 | 2400 | - | 791 |
| +/– 500 | 1500 | - | 905 |
| +/– 500 | 2500 | - | 1055 |

**Table 5.5.4.3:** HVAC and HVDC cables regression results for both offshore and onshore cables

| **Regression variables** | ***Coefficients*** | ***P-values*** | ***Adjusted $R^2$*** | ***St.Error*** |
|---|---|---|---|---|
| **Offshore HVAC cables** | | | | |
| Voltage (kV) | 3.286 | 2,18E-08 | 0.991 | 64.99 |
| Section (mm) | 0.804 | 6,43E-08 | | |
| Intercept | -101.9 | 0,0818 | | |
| **Offshore HVDC cables** | | | | |
| Voltage (kV) | 0.581 | 0,0752 | 0.724 | 124.1 |
| Section (mm) | 0.329 | 0,0003 | | |
| Intercept | 509.95 | 0,0013 | | |
| **Onshore cables** $(Cost_{onshore})$ | | | | |
| Voltage (kV) | 1.828 | 8,61E-05 | 0.897 | 65.6 |
| Section (mm) | 0.223 | 0,0003 | | |
| Intercept | -225.23 | 0,02 | | |

Multiple regression results in Table 5.5.4.3 indicate a satisfying fitting performance in terms of the adjusted *R* square and p-values for the onshore and offshore AC cables cost approximation. On the contrary, increased errors are noticed for the HVDC offshore cables where “weak”

statistical significance occurred for the voltage (kV) predictor. More generic cost functions for transmission cost estimates are given in Equation 5.5.4.6 - 5.5.4.9 which include the total production, acquisition and installation. For example, Hong and Moller (2012) express the total transmission cost as a linear function of distance to the shore and the onshore substation is defined by:

$$C_{TS2} = \ (0.38d_S + 0.4d_l + 76.6)\ 10^6 \quad (5.5.4.6)$$

where $C_{TS2}$ is the electrical cost in €, $d_S$ is the shortest subsea distance to coast and $d_l$ is the shortest land distance to the onshore substation (network junction) in kilometers ($km$). Finally, according to Cavazzi and Dutton (2016) the total transmission, collection and installation cost is expressed in terms of the days to reach a potential OWF site along with the onshore and offshore cable length and the capacity of the OWF.

$$[days]_{to-site} = \ 2\{\frac{Near_{dist}/1000}{[speed]_{jack-up}})\} \quad (5.5.4.7)$$

$$Cost_{install} = ([days]_{install} + [days]_{to-site})[cost]_{jack-up} + [cabling]_{length}([cabling]_{cost} + [cable\_install]_{cost}) \quad (5.5.4.8)$$

$$Cost_{transmission} = (Cable_{DIST}/1000)\ [n]_{cables}[cost]_{cable} + [n]_{offshore}[cost]_{offshore} \quad (5.5.4.9)$$

where $Cable_{DIST}$ is the distance with the onshore transmission junction, $[n]_{cables}$ is the number of HVAC or HVDC export cables, $[cost]_{cable}$ is the cost of cable expressed in million euros per kilometer, $[n]_{offshore}$ and $[cost]_{offshore}$ is the number and the cost of the offshore substations and $[capacity]_{wind}$ is the total capacity of the OWF. In order to reckon in the cost of inter-array cables, the total installation cost of the WTs is calculated including cabling connection expenses between the WTs and the offshore substation(s). Therefore, the following parameters and variables must be accounted where: i) $Near_{dist}$ is the distance from the port, $[speed]_{jack-up}$ and $[cost]_{jack-up}$ are the speed and the cost of the jack-up installation vessel, $[hours]_{working-day}$ is the total working hours per day, $[n]_{per-visit}$ is the number of the WTs installed per trip and finally,

$[cabling]_{length}$, $[cable\_install]_{cost}$ and $[cabling]_{cost}$ are the total length, the cables' manufacturing cost and the installation cost of the collection system.

**Inter-Array Cables:** Array cables consist of medium Voltage (MV) submarine cables, and similarly to the HV cables, unit cost varies according to the cable section and the nominal voltage. A voltage of 30-36 kV is the most frequently used in internal array systems of OWF. However, with the increase of the rated power of the turbines in OWF, the trend is to increase the voltage rating as well. Hence, a rated voltage of 66 kV has been proposed in several works, and, although it has not been implemented yet, it might be the future trend for the internal array (Soarez-Ramos et al., 2020).

**Table 5.5.4.4:** Inter-array cables cost and technical characteristics

| Gonzalez-Rodriguez (2017)<br>**Inter-array cables (Type in mm)** | **Euros2020**<br>**Euros/meter** |
|---|---|
| 95 | 135 - 405 |
| 150 | 202 - 438 |
| 400 | 338 - 541 |
| 630 | 507 - 564 |
| 800 | 533 - 649 |
| Jin et al., (2019) | |
| 150 | 164.2 |
| 240 | 213.1 |
| 500 | 346.3 |

In Table.5.5.4.4 the resulting cost of inter-array cables is presented in euros per meter according to the cables' technical characteristics (section diameter in *mm*) with values ranging between 150 – 600 euros/meter. Based on these data the inter-array cables cost ($C_{CS}$) is calculated with the following expression (Dicorato et al., 2011):

$$C_{CS} = Cost_{cable}\ Cables_{length} + (Cost_{linstall}\ Cables_{length}) \quad (5.5.4.10)$$

where $Cables_{length}$ is the total inter array cables length and $Cost_{cable}$ (€/meter) is the manufacturing cost per meter of cable in Euros. $Cost_{linstall}$ refers to the transportation and installation cost per cable meter accounting for 420.84 euros per meter of cable installed (Dicorato et al., 2011). The manufacturing cost per meter is calculated using Equation 5.5.4.11

and Table.5.5.4.2 for a nominal voltage of 30-36 kV. Finally, the total cables cost is extracted using Equation 5.5.4.12 where the total inner-cables cost is modelled as a function of the total WTs to be installed ($n_{wt}$) and their nameplate capacity ($P_{wt}$).

$$Cost_{cable} = 0.5858\ Cable_{voltage} + 87.708 \quad (5.5.4.11)$$

$$Cables_{length} = 696.11\ n_{wt} + 126.226\ n_{wt}P_{wt} - 16179 \quad (5.5.4.12)$$

**Table 5.5.4.5:** Inter-array cables length for indicative OWFs, Sources: Barring-Gould, (2014), Nexans, (2016), Rampion, (2018), Bormmann et al., (2018)

| | **Number of WTs** | **MW** | Rotor D (meters) | WT spacing (column)*D | WT spacing (row)*D | **Inter-array length (meters)** |
|---|---|---|---|---|---|---|
| Nysted | **73** | **165.6** | 82.4 | 7.8 | 5 | **48000** |
| Horns Rev I | **80** | **160** | 80 | 8.7 | 6.1 | **63000** |
| Alpha Ventus | **12** | **60** | 121 | 8.7 | 5.5 | **16000** |
| Thornton Bank | **54** | **352.2** | 126 | 6.7 | 5.3 | **51000** |
| Kentish Flats | **30** | **90** | 90 | 7.4 | 6.7 | **21000** |
| P, Amalia | **60** | **160** | 80 | 7.4 | 6.9 | **45000** |
| Horns Rev 2 | **92** | **209.3** | 93 | 9.3 | 5.4 | **70000** |
| Riffgat | **30** | **108** | 120 | 7.1 | 3.2 | **18000** |
| ENBW Baltic 1 | **21** | **48.3** | 93 | 12.1 | 4.8 | **20000** |
| Bard Offshore 1 | **80** | **400** | 122 | 9.7 | 6.3 | **107000** |
| Rodsand 2 | **90** | **207** | 93 | 9.4 | 5.8 | **73000** |
| Thanet | **100** | **300** | 90 | 8.8 | 5.5 | **75000** |
| Greater Gabbard | **140** | **504** | 107 | 10.3 | 8 | **173000** |
| Amrubank West | **80** | **288** | 120 | 8.8 | 3.8 | **86000** |
| ENBW Baltic 2 | **80** | **288** | 120 | 6.5 | 5 | **88000** |
| Borkum Riffgrund 1 | **75** | **312** | 120 | 7.7 | 5.5 | **97000** |
| Butendiek | **80** | **288** | 120 | 7.1 | 5 | **90000** |
| Dantysk | **80** | **288** | 120 | 11.1 | 6.5 | **108000** |
| Gode Wind | **97** | **582** | 154 | 6.8 | 4.9 | **140000** |
| Nordsee One | **54** | **332.1** | 126 | 7.6 | 5.5 | **70000** |
| Sandbank | **72** | **288** | 130 | 8.9 | 6.9 | **105000** |
| Arkona | **60** | **360** | 154 | 6.4 | 4.7 | **76000** |
| Borkum Riffgrund 2 | **56** | **448** | 164 | 6.8 | 4.1 | **105000** |
| Merkur | **66** | **366** | 150 | 6.9 | 4.8 | **84600** |
| Anholt | **111** | **399.6** | 120 | 9.9 | 6 | **160000** |
| London Array | **175** | **630** | 120 | 8.3 | 5.3 | **210000** |

| Regression results | Number of WTs | MW | Intercept |
|---|---|---|---|
| *Coefficients* | 696.11 | 165.6 | -16179.9 |
| *Standard Error* | 126.226 | 29.233 | 7172.865 |
| *P-value* | 1.31E-05 | 9.13E-06 | 0.033904 |
| Adjusted R Square | 0.904 | | |

Thus, the total length of array cables required is dependent to the OWF layout configuration and often varies with the number and the size of the WTs, the WTs spacing in order to reduce wake losses and the power transmitted within the OWF. Hence, the optimal layout configuration and accurate inter-array cables length and cost approximation is most of the times a challenging and complex spatial optimization task that is not under consideration in the proposed research thesis. However, the regression results presented in Table 5.5.4.5 and Equation 5.5.4.12 are solely used for evaluating and comparing the influence of other key parameters (i.e., inter-array cables length reduction scenarios respectively to the number of the WTs), rather than the exact OWF layout.

**Integration system cost:** The most cost-efficient electric power transmission method to reduce cable losses is by means of the offshore and onshore substations, which are considered appropriate for projects located at a distance of >20 km offshore. The total substations cost has been estimated by a number of authors who proposed parametric expressions by linking the total integration system cost to the total OWF capacity (and the size of the substations) (Shaffie et al., 2016; Gonzalez-Rodriguez, 2017; Ioannou et al. 2018). For instance, Shaffie et al., (2016) utilize a linear regression model in order to approximate offshore substation's total cost proportional to the OWF size (MW). Thus, the cost for an offshore substation can be estimated as follows:

$$C_{IS} = (583.3 + 107.9\, n_{wt}P_{wt})10^3 \text{ , for } n_{wt}P_{wt} \geq 100 \text{ MW} \qquad (5.5.4.14)$$

expressed in euros, where $P_{wt}$ is the WT's rated power and $n_{wt}$ the number of WTs in the OWF. Furthermore, several authors reviewed the cost for both offshore and onshore substations on per

MW basis and the results are presented in Table 5.5.4.6. Consequently, the cost for an offshore substation may be alternatively estimated from:

$$C_{IS2} = (0.19\, n_{wt} P_{wt})\, 10^6 \qquad (5.5.4.15)$$

expressed in euros and the constant 0.19 is the cost per MW as extracted from Table.5.5.4.3.

**Table 5.5.4.6:** Offshore and onshore substation cost for the period 2003 - 2017

| Offshore Substation | Year | million Euros/MW (2020) |
|---|---|---|
| Gonzalez-Rodriguez, (2017) | 2003 | 0.09 |
| | 2004 | 0.06 |
| | 2005 | 0.14 |
| | 2007 | 0.07 - 0.15 |
| | 2009 | 0.24 |
| | 2010 | 0.10 - 0.15 |
| Vormoolen et al., (2016) | 2016 | 0.22 |
| Noonan et al., (2018) | 2016 | 0.18 |
| | 2017 | 0.19 |
| **Onshore Substation** | **Year** | **million Euros/MW (2020)** |
| Gonzalez-Rodriguez, (2017) | 2003 | 0.19 |
| | 2004 | 0.08 |
| | 2007 | 0.05 |
| Noonan et al., (2018) | 2016 | 0.08 |
| | 2017 | 0.10 |

Highlighting that offshore substation are designed specifically for each OWF project, the aforementioned expressions consist of rough and highly uncertain estimates. For this reason, more robust analytical cost models for the substation cost are given by Dicorato et al. (2011), using parametric equations and linking the offshore substation cost to: i) the MV/HV transformer(s) cost ($Cost_{transformer}$), ii) the MV switchgear cost, ($C_{SG\_MV}$), iii) HV switchgear cost, ($C_{SG\_HV}$) , iv) HV busbar cost, ($Cost_{bb}$), v) Diesel generator cost, ($Cost_{diesel_{generator}}$), and finally vi) the top of the substation platform cost. The expressions of the individual cost components expressed in million euros are the following:

$$Cost_{transformer} = (-153.05 + 131.1\ A_{TR}^{0,4473})/1000 \quad (5.5.4.16)$$

for transformers up to 150 MVA. For transformers up to 50 - 800 MVA, the total cost is extracted by:

$$Cost_{transformer} = (42.688\ A_{TR}^{0,4473})/1000 \quad (5.5.4.17)$$

where $A_{TR}$ is the rated power of transformer (MVA). For the medium voltage switchgear, the cost is calculated as:

$$C_{SG\_MV} = (40.543 + 0.76\ V_n)/1000 \quad (5.5.4.18)$$

where $V_n$ is the nominal voltage (*V).*

$$Cost_{diesel\_generator} = (21{,}242 + 2.069 n_{WT} P_{WT})/1000 \quad (5.5.4.19)$$

$$Cost_{substation} = (2534 + 88.7 n_{WT} P_{WT})/1000 \quad (5.5.4.20)$$

for $n_{WT}$ as the number of WTs and $P_{WT}$ the rated power of each wind turbine in MW. Finally, considering the grid interface, additional costs must be accounted for compensation devices, shunt reactors and SCADA systems. Shunt capacitor cost is estimated about 20k euros per $MV_{Ar}$ and SCADA system cost is approximately 77k euros per WT. For the total integration system cost $C_{IS}$, Equations 5.5.4.10 - 14 are needed among with the following parameters expressing, i) $n_{cl}$ is the number of clusters, ii) $n_{TR}$ is the number of transformers, and iii) $n_{HV}$ is the number of HV circuits. Then, the total cost is expresses as:

$$C_{IS3} = n_{TR} Cost_{transformer} + (n_{cI} + n_{TR}) C_{SG\_MV} + n_{HV}\left(2C_{SG\_HV} + C_{BB}\right) + (Cost_{diesel\_generator} + Cost_{substation}) + C_{RPR} \quad (5.5.4.21)$$

where $C_{SG\_HV}$ and $C_{BB}$ are constant and calculated as 0.439 - 1.25 and 2.65 - 2.9 million euros(m€) for cables of 150 and 230 kV voltage respectively. Finally, cost contribution from reactive power

regulation devices ($C_{RPR}$) must be added to the total integration cost ($C_{IS}$) using the following expression:

$$C_{RPR} = n_R(0.66Cost_{transformer}) + 0.02n_C + 0.077n_{SVC} \quad (5.5.4.22)$$

where $n_R, n_C$ and $n_{SVC}$ are the numbers of needed reactors, capacitors and SVCs respectively. Finally, onshore substation cost is assumed to be half of the offshore substation cost according to the data illustrated in Table 5.5.4.3 for the reference cost values of the years 2016-2017 and previous research studies and technical reports (Myhr et al., 2014; Shaffie et al., 2016).

$$C_{on\_sub} = C_{of\_sub} / 2 \quad (5.5.4.21)$$

### 5.5.5 Offshore wind farm installation cost modelling

Installation and commissioning phases refer to all activities involving the loading, transportation and installation of the OWF components (WTs, foundations, transmission cables, substations etc.), all preparative actions in the selected OWF area (site clearance, scour protection) as well as those actions related to the port activities, commissioning of the OWF and insurance during construction (Shaffie et al., 2016). Particularly, when the OWF components are assembled or transferred to the port staging area, the construction activities start with the: i) scour protection for each foundation (for bottom-fixed installations), ii) the transportation and installation of the foundations and the transition piece are taking place next, followed by the tower erection, the rotor-nacelle assembly (RNA) deposition and the blades installation and finally iii) the offshore substation is placed along with iv) the inter-array cables, the offshore and onshore export cables and the onshore substation (if needed).

Some of the critical factors affecting the total installation cost incorporate: i) the installation strategy to be followed, ii) the vessel type selection, iii) the distance from the nearest port-harbor and finally, iv) the weather conditions affecting both offshore and onshore installation activities (referred as bad weather allowance or weather factor) (Kaizer & Snyder, 2012; Bjekseter &

Agotnes, 2013). Starting from the vessel types needed for the installation procedures, Table.5.5.5.1 illustrates the daily rental costs expressed in euros($€_{2020}$). According to the foundation concept and the installation strategy to be applied, different vessel types and quantities may be needed to complete the installation and commissioning of an OWF. In the finalized vessels' daily rates, fuel costs, port taxes and mobilization-demobilization costs must be included, however, these cost data are not always clarified, thus, the cost values illustrated in Table 5.5.5.1 consist of indicative examples gathered from previous studies and technical reports.

**Table 5.5.5.1:** Day-rates estimates in $Euros_{2020}$, for different vessel types and installation procedures

| | **Vessel cost** | | | |
|---|---|---|---|---|
| **Vessel Type** | **Day rate (Euros)** | **Day rate (Euros)** | **Day rate (Euros)** | **Day rate (Euros)** |
| **Source →** | Myhr et al., (2014) | Smith et al., (2016) | Ahn et al., (2016) | Ioannou et al., (2018) |
| Heavy lift Crane vessel (HLCV) | 593000 | - | - | 740000 (+565000 mob.-demob. cost) |
| WTIV - Jack-up vessel | 219000 | 90000-180000 | 140000 - 235000 | 112600 (+458000 mod.-demob. cost) |
| Crane barge | - | - | 75000 - 94000 | - |
| Cargo barge | - | - | 28000 - 47000 | - |
| Tug boat | 18000 | - | 940 - 4700 | - |
| Anchor handling, tug and supply (AHTS) | 101000 (+210000 mob. - demob. cost) | - | - | - |
| Cable Laying Vessel (CLV) | - | - | - | 187000 (Inter-array) - 211000 (Export) (+500000 mod.-democ. cost) |
| Rock Dumping Vessel (RDV) | - | - | - | 15600 (+12000 mob.-demob. cost) |
| Platform Supply Vessel (PSV) | 49000 (+90000 mob. - demob. cost) | 60000-90000 | - | - |
| Diving Support Vessel (DSV) | - | 23000-37000 | - | - |
| Workboat | - | 2300-3800 | - | - |

**Total travel time:** Installation procedures are calculated on a per trip basis and the total time per trip is the total sum of the travel, loading, installation time, and intra-field movement time if needed (from one foundation or WT site to the other) adjusted by the weather limitations (or weather factor - WF). The travel and the intra-field movement time expressed in Equation 5.5.2.1 and Equation 5.5.2.4, determined by the average speed of the vessel (*S*, km/hour) which are listed in Table 5.5.5.2 and the distance to the nearest port (*D*, kilometers) where all the operations will take place. Moreover, loading and installation time are fixed values listed in Table 5.5.5.3, customized by a time increase factor according to the operation to be performed and the size of the WTs. In the upcoming sections (Section 5.5.7) of this chapter, more detailed and accurate pathfinding algorithms are analyzed for distance, cost and paths extraction and delineation.

For the total travel time of transfer vessels, the mean vessel speed is used based on the installation strategy and the configurations to be followed during installation activities (Table 5.5.5.2). For example, an AHTS vessel speed is different considering different installation scenarios for floating concepts. Furthermore, the total per-trip installation time ($Install_{time}$, hours), total loading time ($Load_{time}$, hours) and total per-trip intra-field movement time ($Move_{time}$, hours) are functions related to the vessel's capacity (VC, units/trip) and installation (I, hours), loading (L, hours) and intra-field movement (M, hours) time expressed as (Kaizer & Snyder, 2012):

$$Travel_{time} = 2\frac{D}{S} \quad (5.5.5.1)$$

$$Install_{time} = (VC)\ I_{hours} \quad (5.5.5.2)$$

$$Load_{time} = (VC)\ L_{hours} \quad (5.5.5.3)$$

$$Move_{time} = (VC)\ M_{hours} \quad (5.5.5.4)$$

$$Total\_trip_{time} = Travel_{time} + Install_{time} + Load_{time} + Move_{time} \quad (5.5.5.5)$$

Loading, installation, and movement time are also adjusted using a weather-adjustment factor (WF - Table 5.5.5.2) to account for the proportion of time that transfer vessels or the quayside cranes can operate due to unfavorable or extreme weather conditions. Hence, a WF value of 100 (normalized to a scale between 0-1) indicates that there are no weather delays, while a WF = 55 means that almost half of the time the installation vessels or quayside cranes are unable to

perform any operation. In general, inshore and nearshore WFs are increased by approximately 15-20% compared to operations performed offshore (Myhr et al., 2014).

**Table 5.5.5.2**: Concept-depending vessels speeds and operational windows (Weather Factor)

| **Concept** | ***Spar-Buoy*** | ***Spar-Buoy*** | ***Semi-Submersible*** | ***Semi-Submersible*** |
|---|---|---|---|---|
| **Operation** | **Speed (km/h)** | **WF (%)** | **Speed (km/h)** | **WF (%)** |
| Own transport (AHTS) | 27.78 | 95 | 27.78 | 95 |
| Towing complete WTs (AHTS) | 5.56 | 55 | 9.26 | 60 |
| Towing floater-tower (AHTS) | 7.51 | 60 | 11.11 | 70 |
| Towing floater (AHTS) | 8.72 | 65 | 12.03 | 75 |
| PSV vessel (3 WTs/trip) | 33.3 | 80 | 33.3 | 80 |
| **Concept** | ***Monopiles*** | *WF (%)* | ***Jacket*** | *WF (%)* |
| Jack-Up vessel | 22 | 80 | 22 | 80-85 |
| **Concept** | ***Substation*** | WF (%) | *Spar-Buoy – Semi-Sub.* | *WF (%)* |
| Heavy-Lift vessel | 16.6 | 55 | 16.6 | 45-65 |
| **Concept** | ***Scour protection*** | WF (%) | | |
| Rock Dumping Vessel (RDV) | 25 | 95 | | |
| **Concept** | ***Cable installation*** | WF (%) | | |
| Cable Laying Vessel (CLV) | 25.9 | 80 | | |
| **Concept** | ***Decommissioning*** | WF (%) | | |
| Diving support vessel | 22 | 85 | | |
| **Concept** | ***Decommissioning*** | WF (%) | | |
| Workboat | 26 | 85 | | |

**Table 5.5.5.3**: Time consumption and vessels characteristics for each installation procedure

| **Bottom-fixed** | **Vessel Type** | **Vessel Capacity** | **Load time** | **Install time** | **Move time** |
|---|---|---|---|---|---|
| Wind Turbines | Jack-Up | 9,6,4 (10,8,5 MW) | 4 hours/lift | 29 hours | 4 hours |
| Foundations | Jack-Up | 6,4,3 (10,8,5 MW) | 3 hours/lift | 48 - 96 hours | 4 hours |
| Scour protection | RDV | 24000 (tons) | 12 hours/trip | 4 hours/WT | 0.9 hours |
| Substation | HLCV | - | 24 hours | 72 hours topside (0.115 hour/m for each pile) | 8 hours/pile |
| **Floating** | **Vessel Type** | **Vessel Capacity** | **Load time** | **Install time** | **Move time** |
| Wind Turbines | AHTS - Tug boats (2) | 1 | 7 hours | 16 hours | - |

| | | | | | |
|---|---|---|---|---|---|
| Foundations | AHTS - Tug boats (2) | 2 | 43 hours | (for towing incomplete WTs) | - |
| Mooring | AHTS - Tug boats (2) | 15 sets | 24 hours | 6 hours/line | - |
| Anchoring | AHTS - Tug boats (2) | | | 8 hours/anchor | 1 hours/anchor |
| Substation | AHTS - Tug boats (4) | - | 48 hours | 45 hours | - |
| **Cables** | **Vessel Type** | **Vessel Capacity** | **Load time** | **Install time** | **Move time** |
| Inter-array | CLV | 7500 tons | - | 1.5 km/day | - |
| Export | CLV | | - | 0.8 km/day | - |

**Vessels' capacity:** In order to estimate the total number of trips needed during the installation process, the vessels' capacity must be set (e.g., for the Jack-Up, the AHTS and the RDV vessels). For the WTs and foundations installation operations, three different scenarios are considered using 5, 8 and 10 MW wind generators. For each scenario, the total number of the total structure components, consisting of the pile or jacket sub-structure, the transition piece and the tower including the RNA (the top structure), must be accounted. Thus, a vessel capacity of 9, 6 and 4 is considered for the RNA and the towers and 6,4 and 3 foundations (including the transition piece) (Table 5.5.5.3). Subsequently, for the scour protection operations, the total rock-dumping vessel's capacity is needed (in tons) and the scour volume per WT. Finally, for the floating concepts, the AHTS vessel capacity is needed for either the anchors loaded per trip and the floaters to be towed offshore. number of the components adjusted to each individual WT that the installation vessel can carry is expressed as a function of the vessel's capacity ($VC_i$) calculated as follows:

$$JU\_Num_{trips} = \frac{n_{wts}}{VC_{wt}} + \frac{n_{fds}}{VC_{fd}} \quad (5.5.5.6)$$

$$RDV\_Num_{trips} = \frac{n_{wt}}{VC_{rdv}} \quad (5.5.5.7)$$

$$AHTS\_Num_{trips} = \frac{n_{wt}\, n_{anchors}}{VC_{anc}} + \frac{n_{floaters}}{VC_{fl}} \quad (5.5.5.8)$$

for $n_{wts}$ as the total number of WTs and towers, $n_{fds}$ the number of foundations to be installed, $VC_{wt}$ and $VC_{fd}$ the jack-up vessel's capacity for either the top and the support-structures, $n_{wt}$ is

the total number of WTs to be installed, $VC_{rdv}$ the RDV vessel capacity and finally, $n_{anchors}$ and $n_{floaters}$ consist of the total number of anchors and floaters to be carried and installed towards the AHTS vessel's capacity for both the anchors and the floaters expressed as $VC_{anc}$ and $VC_{fl}$ respectively.

Indicative examples for estimating the total installation cost for either bottom-fixed and floating concepts are demonstrated in Tables 5.5.5.3 - 5.5.5.5. For the installation procedures, a total number of 15 employees, working 12-h shifts, is required to perform the installation tasks, resulting in a total of 30 workers stationed on the vessels used in addition to the vessel crew (these values are established irrespective of the OWF size). Estimated installation cost for both monopiles and jackets as also for spar-buoy and semi-submersible floating concepts are shown in Tables 5.5.5.4 - 5.5.3.6, where the number of operations, duration in days and operational weather windows, expressed as the Weather Factor (WF), are also illustrated. In order to calculate each procedure's (row) cost, the following expression is used:

$$Cost_{procedure} = Unit_{cost}((Count)Duration) + \left( (Count)\ Duration \left(\frac{100-WF}{WF}\right)\right) Unit\_cost \quad (5.5.5.9)$$

where $Count$ is the total amount of the loading, transportation and installation actions or vessels used among with the personnel needed, $Duration$ is expressed in hours denoting the total amount of time needed for each procedure including Total_Install$_{time}$, *WF* is the weather factor in order to adjust each operation's time to the weather conditions and unavailability issues and finally, $Unit\_cost$ is expressing the vessels, personnel and mobile cranes cost in Euros(€), as presented in Table 5.5.5.1.

**i) Foundations' installation and scour protection:** At first, a Rock Dumping Vessel (RDV) is used in order to ensure the structural stability of each WT foundation either for monopiles or jacket structures. In order to estimate the scour installation cost per WT and overall, for the entire OWF, the Rock Dumping Vessel's (RDV) day rates are needed among with the vessel's capacity, the estimated scour volume per WT and the RDV's operational characteristics. Considering the scour volume for both monopile and jacket foundations, data extracted from Energinet, (2014) for

multiple WTs' capacities (i.e., 3, 3.6, 4, 6 and 8 MW). The total scour volume for both monopiles ($Scour_{mp}$) and jacket ($Scour_{jc}$) is calculated using the following expressions:

$$Scour_{mp} = 14.641\, P_{wt}^3 - 292.08\, P_{wt}^2 + 2176.5 P_{wt} - 202.38 \quad (5.5.5.10)$$

$$Scour_{jc} = 22.095\, P_{wt}^3 - 422.27\, P_{wt}^2 + 2907.5 P_{wt} - 3944.7 \quad (5.5.5.11)$$

where the results are estimated in tonnes/WT and $P_{wt}$ refers to the WT's capacity in MW.

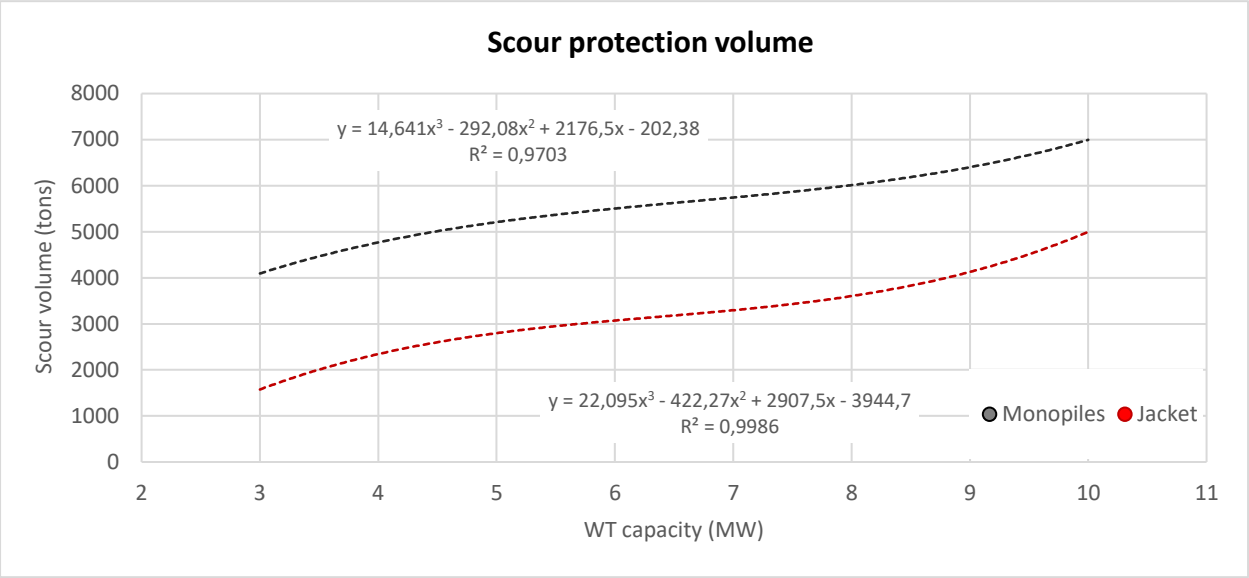


**Figure 5.5.5.1**: Polynomial fitting results for scour volume estimation

Scour volume results indicate increased estimates for the monopile foundations compared to the jacket structures and consequently, differentiations will occur in the total number of trips needed for the RDV. The total number of trips to be performed is therefore expressed by:

$$Num_{trips} = (n_{wt}\, Scour_i)/VC_{RDV} \quad (5.5.5.12)$$

where $n_{wt}$ expresses the total WTs to be installed, $Scour_i$ is the scour volume in tons as estimated by Equations 5.5.5.10 - 5.5.5.11 and $VC_{RDV}$ is the RDV's capacity obtained by Table 5.5.5.3. The travel time cost is adjusted using a WF of 95% and Equation 5.5.5.9 as also the dumping time (16 hours) per trip is adjusted using a WF of 80%. Finally, the load time remains constant for each trip

and the total estimated cost for the RDV to complete the scouring protection activities is calculated using the sum of Equations 5.5.5.13 - 14 defined as:

$$Cost_{scour\_tr} = (Num_{trips} * Travel_{time})Cost_{RDV} + \left(Num_{trips} * Travel_{time}\left(\frac{100-WF}{WF}\right)\right)Cost_{RDV} \quad (5.5.5.13)$$

$$Cost_{scour\_in} = (Num_{trips} * Dumping_{time})Cost_{RDV} + \left(Num_{trips} * Dumping_{time}\left(\frac{100-WF}{WF}\right)\right)Cost_{RDV} + (Num_{trips} * Loading_{time})Cost_{RDV} \quad (5.5.5.14)$$

**ii) WT and foundation installation:** For the bottom-fixed concepts (monopile and jacket structures) the installation process is straightforward. Subsequently, a high-capacity jack-up installation vessel picks up the components for one or more turbines (related to the vessel's deck area and tons capacity), delivers them to the offshore site and performs the installation activities. Moreover, the offshore substation is installed using a Heavy Lift Crane Vessel (HLCV) for both the topside and the jacket support structure (or optionally a Jack-Up vessel for the jacket foundation). Finally, the inter-array and the export cables are installed using a Cable Laying Vessel (CLV).

On the contrary, for the floating concepts, installation procedures differentiate in terms of the complete WT-foundation transportation and placement as also for the substation installation steps to be followed. Two different installation strategies for floating concepts are proposed. The first one is based on complete installation near-shore using crane barges and tugboats before towing the complete WT and floater to the offshore site using an Anchor Handling Tug Supply (AHTS) vessel where the mooring and anchoring procedures are followed. The second installation strategy is based on towing the substructure (with or without the WT's tower) using an AHTS vessel, the RNA and the hub using a Platform Supply Vessel (PSV), where the WT components are installed offshore using an HLCV. Similarly, the floating offshore substation is towed to the offshore site (both of the topside and the floater) using an AHTS vessel and tugboats. Cables for the floating concepts are similarly installed compared to the bottom-fixed concepts. Finally, for either fixed and floating concepts, a mobile crane is deployed in loading of the OWF components onto the supply vessels with a day rate between 6500-8500 euros.

**Table 5.5.5.4**: Monopile foundation and WT installation cost (indicative values)

| **Monopile Foundations** | Operation | Count | Duration (days) | Unit cost (€) | WF (%) | Total cost (€) |
|---|---|---|---|---|---|---|
| Jack-up | Quayside lifts | **2** | 0.13 | **170000** | **80** | 55250.0 |
| Jack-up | Transportation | **1** | 0.25 | **170000** | **80** | 53125.0 |
| Jack-up | Substructure installation | 1 | **3** | **170000** | **55** | 927272.7 |
| Jack-up | Personnel usage | **30** | 3.38 | **393.7** | **57** | 70037.2 |
| **Wind turbine** | | | | | | |
| Jack-up | Quayside lifts | **3** | 0.17 | **170000** | **80** | 108375.0 |
| Jack-up | Transportation | **0.15** | **0.11** | **170000** | **80** | 3541.7 |
| Jack-up | Turbine installation | 1 | **1.5** | **170000** | **55** | 463636.4 |
| Jack-up | Personnel usage | **30** | 1.78 | **393.7** | **59** | 35655.4 |
| **Total days and cost per WT** | | | **5.16** | | | **1716893.3** |

Foundation type will impact the time required for installation. Jackets take longer to install than monopiles because they are heavier, more complex, and more piles must be lifted and driven into place. If the installation vessel transports the foundations, the distance to port, vessel speed, and the number of foundations carried per trip determines the travel and loading time. Installation vessel travel time may be eliminated by transporting foundations on barges or towing them to site. The number of installations impacts both the total time and the time required per foundation (Kaizer & Snyder, 2012).

**Time adjustment:** Considering that three different WT models that are used, a normalized installation duration adjustment factor is applied in order to express the installation time increase relative to the complexity and the size of the offshore WTs and the support structures. According to Beiter et al., (2016), this relation is expressed as:

$$Time_{increase} = 0.071622\ P_{WT} + 0.779730 \qquad (5.5.5.15)$$

, where $P_{WT}$ is the WT's nameplate capacity in MW. As it is observed there is a linear relation ($R^2$ = 0.98) between the WT nameplate power and installation time and this finding is in accordance with the results from Arantegui et al. (2018), where a linear relation exists (nameplate capacity and installation time of both WTs and foundations) if the outliers due to extreme weather conditions are removed. In Table 5.5.5.3, time consumption (blue colored values), for each

installation operation, are adjusted using Equation 5.5.5.15 in order to quantify the overall installation time increase proportional to the WTs' and foundations' size and mass characteristics.

**Table 5.5.5.5**: Jacket foundation and WT installation cost (indicative values)

| **Jacket Foundations** | Operation | Count | Duration (days) | Unit cost (€) | WF (%) | Total cost (€) |
|---|---|---|---|---|---|---|
| Jack-up | Quayside lifts | **2** | 0.13 | **170000** | **80** | 55250.0 |
| Jack-up | Transportation | **1** | 0.25 | **170000** | **80** | 53125.0 |
| Jack-up | Substructure installation | 1 | 4 | **170000** | **55** | 1236363.6 |
| Jack-up | Personnel usage | **30** | 4.38 | **393.7** | **57** | 90758.2 |
| **Wind turbine** | | | | | | |
| Jack-up | Quayside lifts | **3** | 0.17 | **170000** | **85** | 102000.0 |
| Jack-up | Transportation | **1** | **0.11** | **170000** | **85** | 22222.2 |
| Jack-up | Turbine installation | 1 | **2** | **170000** | **55** | 618181.8 |
| Jack-up | Personnel usage | **30** | 2.28 | **393.7** | **59** | 45664.8 |
| **Total days and cost per WT** | | | **6.66** | | | **2223565.6** |

Depending on floating support structure technology, floating WTs may be installed using numerous already established or experimental methods (Bjerkseter & Agotnes, 2013). Several transportation methods have been suggested to reduce the installation cost of offshore wind floating concepts. Two main installation strategies consist of: i) Assembly inshore, towing of complete turbine and ii) Towing of substructure and assembly offshore. The latter procedure includes both pre-joined turbines and a strategy where floater and tower are pre-joined, and only the turbine is installed offshore. The following assumptions are made considering floating concepts installation (Myhr et al., 2014):

1. One AHTS can tow either one complete turbine or two floaters;
2. PSV transit speed is 33.3 km/hour with WF of 80% with a capacity of three turbines;
3. Loading of solid ballast and rigging for Spar-Buoy and Semi-Submersible is performed inshore by a crane barge with an WF of 65-80% and 24-hours duration overall;
4. Overall, inshore WF are increased by approximately 15-20% compared to the operations performed offshore, due to better weather conditions;

5. Time consumption to attach the mooring system is assumed to six hours per line with a WF 60%;
6. 8 hours of installation time to place each anchor system;
7. 30 min per 100 m of depth is added to the installation time for both mooring lines and anchors.

For all concepts, different WT's inshore assembly strategies may be selected (i.e., the number of total lifts inshore and offshore), however, the two-part turbine lift is by complete tower and assembled nacelle with rotor. This implies that it is convenient to assemble most of the major parts on ground level, minimizing lifts and the need for larger crane facilities. The total cost to mount the turbine on the Spar-Buoy and Semi-Submersible concepts is 0.836 million euros and 0.685 million euros for the 5MW wind generator respectively. An increase of 10 and 15% is assumed for the 8 and 10MW concepts leading to 0.919/0.753 and 0.961/0.787 million euros for both WTs installed in Spar-Buoy and Semi-Submersible floaters.

**Table 5.5.5.6**: Spar-Buoy and Semi-Submersible floater, mooring and WT installation cost based on different installation strategies (indicative values)

| **Spar-Buoy Lifting operations** | Operation | Count | Duration (days) | Unit cost (€) | WF (%) | Total cost (€) |
|---|---|---|---|---|---|---|
| Quayside crane | Quayside lifts | **4** | 0.08 | **6384** | **80** | 2553.6 |
| Crane barge | Rigging | 1 | 0.08 | **58525** | **80** | 5852.5 |
| Crane barge | Ballast | 1 | 1 | **58525** | **65** | 90038.5 |
| Crane barge | 3 near-shore lifts | 1 | 0.63 | **58525** | **77** | 47884.1 |
| **Loading, Assistance and Transportation** | | | | | | |
| Tug boats | Loading | 2 | 0.33 | **12000** | **80** | 9900.0 |
| Tug boats | Up-ending | 2 | 0.50 | **12000** | **65** | 18461.5 |
| Tug boats | Assistance | 2 | 0.63 | **12000** | **77** | 19636.4 |
| Tug boats | Transportation | 2 | **0.80** | **12000** | **59** | 32542.4 |
| Tug boats | Mooring | 2 | **0.75** | **12000** | **60** | 30000.0 |
| Tug boats | Anchors ($Install_{time}$) | 2 | **1.33** | **12000** | **60** | 53200.0 |
| Tug boats | Anchors ($Move_{time}$) | 2 | **0.16** | **12000** | **60** | 6400.0 |
| AHTS | Transportation | 1 | **0.18** | **96833** | **59** | 29177.6 |
| AHTS | Mooring | 1 | **0.75** | **96833** | **60** | 121041.3 |
| AHTS | Anchors ($Install_{time}$) | 1 | **1.33** | **96833** | **65** | 148973 |

| | | | | | | |
|---|---|---|---|---|---|---|
| AHTS | Anchors ($Move_{time}$) | 1 | 0.16 | 96833 | 80 | 14524 |
| Personnel | Personnel usage | 30 | 5.67 | 393.7 | 77 | 86937.8 |
| **Total days and cost per WT** | | | **5.67** | | | **717122.6** |

| **Semi-Submersible Lifting operations** | Operation | Count | Duration (days) | Unit cost (€) | WF (%) | Total cost (€) |
|---|---|---|---|---|---|---|
| Quayside crane | Quayside lifts | 5 | 0.08 | 6384 | 80 | 3192.0 |
| Crane vessel | Rigging | 1 | 0.17 | 565037 | 70 | 137223.3 |
| Crane vessel | Ballast | 1 | 1 | 565037 | 65 | 869287.7 |
| Crane vessel | 4 Offshore lifts | 1 | 0.67 | 565037 | 51 | 742303.5 |
| **Loading, Assistance and Transportation** | | | | | | |
| Tug boats | Transportation | 2 | 0.50 | 12000 | 76 | 15789.5 |
| Tug boats | Up-ending | 2 | 0.00 | 12000 | 65 | 0.0 |
| Tug boats | Mooring | 2 | 1.00 | 12000 | 60 | 40000.0 |
| Tug boats | Assistance | 2 | 0.67 | 12000 | 51 | 31529.4 |
| Tug boats | Anchors ($Install_{time}$) | 2 | 0.75 | 12000 | 65 | 27692.3 |
| Tug boats | Anchors ($Move_{time}$) | 2 | 1.33 | 12000 | 65 | 49107.7 |
| AHTS | Transportation | 1 | 0.44 | 96833 | 76 | 56627.5 |
| AHTS | Up-ending | 1 | 0.00 | 96833 | 65 | 0.0 |
| AHTS | Mooring | 1 | 1.00 | 96833 | 60 | 161388.3 |
| AHTS | Assistance | 1 | 0.67 | 96833 | 51 | 127212.0 |
| AHTS | Anchors ($Install_{time}$) | 1 | 0.75 | 96833 | 65 | 148973 |
| AHTS | Anchors ($Move_{time}$) | 1 | 1.33 | 96833 | 80 | 14524 |
| PSV | Loading | 1 | 0.25 | 48948 | 80 | 15143.3 |
| PSV | Transportation | 1 | 0.13 | 48948 | 75 | 8158.0 |
| PSV | Assistance | 1 | 0.50 | 48948 | 51 | 48228.2 |
| Personnel | Personnel usage | 30 | 6.99 | 393.7 | 51 | 161867.3 |
| **Total days and cost per WT** | | | **6.82** | | | **2658246.9** |

**iii) Export and inter-array cables installation:** For export and inter-array cables all relevant information were derived from Kaizer and Snyder, (2012), Myhr et al., (2014), and Ioannou et al., (2018) focusing on the Cable Laying Vessel (CLV) daily rates and installation rates for both types of cables. Table 5.5.5.7 illustrates some indicative installation cost values for both export and inter-array transmission cables. Notable is the increased variability of installation cost values, mainly for export cables (approx. 100-800 euros per meter), due to the site-specific

characteristics, vessels cost differences among different countries as long as because of different cables' technologies used for each project.

**Table 5.5.5.7**: Transmission cables installation cost (export and inter-array) per meter. Indicative values from various projects and sources for 2003-2014

| Kaizer & Snyder, (2012); Myhr et al., (2014); Gonzalez-Rodriguez, (2017) | | | |
|---|---|---|---|
| **Offshore transport cables - Installation cost** | **Euros2020** | **Inter-array cables - installation cost** | **Euros2020** |
| **Year** | **Euros/meter** | **Year** | **Euros/meter** |
| 2003 | 65.39 | 2003 | 65.39 |
| 2004 | 90.7 | 2007 | 83.31 |
| 2007 | 349.07 | 2007 | 91.75 |
| 2009 | 673.89 | 2007 | 349.07 |
| 2009 | 743.49 | 2009 | 62.22 |
| 2010 | 165.57 | 2010 | 153.97 |
| 2011 | 140-527 | 2010 | 142.37 |
| 2013 | 376-879 | 2013 | 202.23 |

For the proposed model, the total installation cabling cost is expressed as a function of the daily installation rates ($r$ in km/h) extracted from Table 5.5.5.7, the daily Cable Laying Vessel's cost ($Cost_{CLV}$ including ROV and mobilization-demobilization cost), the Weather Factor (WF) and finally the total cables' distance *D* (Ioannou et al., 2018).

$$CI_{export} = Cost_{CLV}\ (D_{export}\ r_{export}) + \left( D_{export}\ r_{export} \left(\frac{100-WF}{WF}\right)\right) Cost_{CLV} \quad (5.5.5.16)$$

$$CI_{inner} = Cost_{CLV}\ (D_{inner}\ r_{inner}) + \left( D_{inner}\ r_{inner} \left(\frac{100-WF}{WF}\right)\right)\ Cost_{CLV} \quad (5.5.5.17)$$

Reviewing the reported values of Table 5.5.5.8, a value of 1.2 and 0.5 kilometers/day is selected for the export and inter-array cables respectively. In addition, a day rate of 187000 and 211000 for the CLV is selected (inner and export values) by adding 500000 euros to the total cost for mobilization-demobilization procedures.

**Table 5.5.5.8**: Export and inner cables installation rates expressed in km/day

| Source | **Export** ($r_{export}$) (km/day) | **Inter-array** ($r_{inner}$) (km/day) |
|---|---|---|
| Kaizer & Snyder, (2012) | 0.2 – 1.4 | 0.14 – 0.63 |
| Ioannou et al,(2018) | 1.6 | 0.6 |

**iv) Substation installation cost:** Substation installation cost is evaluated for both bottom-fixed (jacket) and floating foundation concepts. The installation activities for the floating concept are similar to the floating WTs transportation and installation procedures. As a result, an onshore crane is used for both installation strategies (jacket and floating) in order to either lift the substation's jacket and topside to a barge or to tow the floater and the topside to the tugboats. Offshore procedures for both concepts start with the preparation and installation of the anchors (floating) or piles (jacket) at the offshore site using an AHTS or a HLCV vessel. The installation time for the bottom-fixed concept is comprised of the jacket foundation installation time and the installation of the substation's topside part. On the contrary, for the floating concept, the total installation time mainly lies on the transportation time and the mooring and anchoring activities time consumption. The total trip time from the port to the installation site and vice versa is estimated by Equation 5.5.5.1 - 4 and Table 5.5.5.4 and the total installation time of the substation is illustrated in Table 5.5.5.8 using Equation 5.5.5.9 where the total installation cost is expressed as the sum of sub-costs for each onshore and offshore operation adjusted by the WF and multiplied by each vessel's day rates including the personnel used for the operations.

In Table 5.5.5.9, different types of vessels used for the installation activities is described, $N_{piles}$ for the bottom-fixed concept is the total number of the jacket structure piles assumed as 4, $R_{piles}$ is the rate pilling of piles expressed in meters per hour and is assumed as 0.115 (Ioannou et al., 2018), $D_{piles}$ is the depth of the piles in meters with a pre-defined value of approximately 30-60 meters, transportation time (blue color) is site-specific and proportional to the distance from the nearest port and finally the installation time for the substation's topside is estimated to be approximately 24-48 hours as already referred in Section 2.5.5. Subsequently, onshore lifts and loading time for both concepts is estimated as double compared to the jacket and floating foundations lifting operations presented in Tables 5.5.5.3-5. Vessels' transportation speeds and operations WFs are extracted by Table 5.5.5.2 based on the minimum speed used for the complete WT towing concept (5 km/h) for either the bottom-fixed and floating concepts. Finally,

for the floating concept, the number of mooring lines and anchors to be considered, is set as 10 based on data provided by Quintana, (2016) considering the total mass of both floater and the topside of the substation (1000-2000 and 2000-5000 tons respectively).

**Table 5.5.5.9**: Jacket and floating substation concept installation cost breakdown

| **Jacket Substation** | Operation | Count | Duration (days) | Unit cost (€) | WF (%) | Total cost (€) |
|---|---|---|---|---|---|---|
| Quayside crane | Quayside lifts ($Load_{time}$) | **2** | 0.5 | **6384** | **65** | 9821.538462 |
| Barge | Transportation ($Travel_{time}$) | 2 | 2 | **35000** | **65** | 323076.9231 |
| Tug boats | Transportation ($Travel_{time}$) | 2 | **2** | **12000** | **65** | 110769.2308 |
| Tug boats | Loading | 2 | 0.5 | **12000** | **80** | 15000 |
| Tug boats | Assistance | 2 | 1 | **12000** | **77** | 31168.83117 |
| Heavy Lift Crane V. | Transportation ($Travel_{time}$) | 2 | **1** | **565037** | **77** | 1467628.571 |
| Heavy Lift Crane V. | Offshore lifts ($Install_{time}$) | 2 | 2 | **565037.7** | **55** | 4109365.091 |
| Heavy Lift Crane V. | Ples (Installtime) | 4 ($N_{piles}$) | $R_{piles}xD_{piles}$ 40x0.115 | **565037.7** | **55** | 3544327.391 |
| Heavy Lift Crane V. | Personnel usage | 15 | 0.67 | **393.7** | **51** | 7758.205882 |
| **Total days and cost** | | | **9.12** | | | **9618915.783** |
| **Floating Substation** | Operation | Count | Duration (days) | Unit cost (€) | WF (%) | Total cost (€) |
| Quayside crane | Quayside lifts ($Load_{time}$) | **2** | 0.5 | **6384** | **65** | 9821.538462 |
| Tug boats | Loading | 4 | 0.33 | **12000** | **65** | 24369.23077 |
| Tug boats | Assistance | 4 | 0.63 | **12000** | **77** | 39272.72727 |
| Tug boats | Transportation ($Travel_{time}$) | 4 | **1.8** | **12000** | **55** | 157090.9091 |
| Tug boats | Mooring ($Install_{time}$) | 10 | 0.25 | **12000** | **60** | 50000 |
| Tug boats | Anchors ($Install_{time}$) | 10 | 0.33 | **96833** | **65** | 491613.6923 |
| Tug boats | Anchors ($Move_{time}$) | 9 | 0.16 | **96833** | **80** | 174299.4 |
| AHTS | Transportation ($Travel_{time}$) | 1 | **1.8** | **96833** | **55** | 316908 |
| AHTS | Mooring ($Install_{time}$) | 10 | 0.25 | **96833** | **60** | 403470.8333 |
| AHTS | Anchors ($Install_{time}$) | 10 | 0.33 | **96833** | **65** | 491613.6923 |
| AHTS | Anchors ($Move_{time}$) | 9 | 0.16 | **96833** | **80** | 174299.4 |
| AHTS | Personnel usage | 15 | 0.67 | **393.7** | **51** | 7758.205882 |
| **Total days and cost** | | | **13.88** | | | **2330696.091** |

### 5.5.6 Operation and Maintenace Expenditures (O&M) cost

The operation and maintenance (O&M) cost of an OWF is divided into two parts, one for the operational expenses (OPEX) and the other one for the maintenance expenses consisting of the preventing, the corrective (including predicted and unpredicted failures) and the proactive maintenance procedures (Myhr et al., 2014; Shaffie et al., 2016).

OPEX costs are assumed as all the expanses related to the rental/lease payments to the local authorities and landowners, the offshore wind infrastructures insurance costs and the transmission charges that are paid to the authorities who are managing the national electrical grid. In addition, maintenance expenses consist of the costs related to the transport of failed components, technicians who carry out the repair/replacement actions and all consumables and spare parts required for an OWF maintenance. OPEX may be considered as constant expanses, contrary, maintenance costs are highly depending on the distance to harbor, the OWF's capacity, the number of the WTs, the total number of failures, the number and type of the maintenance vessels used as also in the weather conditions and the maintenance strategies followed. Literature review (Section 2.5.6) clearly indicates that the overall O&M cost per MW basis has been decreased during the last decade due to the optimized maintenance strategies. However, maintenance costs quantification is a complex task with highly variable and uncertain parameters. Despite of the analytical tools established in the offshore wind industry for more accurate costs approximation, more generic frameworks and analytical equations may approximate O&M expenses in a rather satisfactory manner.

Particularly, Equations 5.5.5.3.1 - 5.5.5.3.4 demonstrate O&M cost calculation formulas based on the distance from the nearest harbors, the OWF capacity and the number of the wind generators. According to Moller (2011) O&M cost expressed in m€ is:

$$C_{om} = \begin{cases} 0.00026\, d_p + 17 & if\ d_p < 50000 \\ 0.0001\, d_p + 25 & if\ d_p \geq 50000 \end{cases} \quad (5.5.6.1)$$

where $d_p$ is the distance from harbor in meters and the intercept term accounts for the operational expenses. Similarly, the cost function used on Nagababu et al. (2017) is expressed in m€ as:

$$C_{om2} = 1.4(0.29\left(\frac{d_p^2}{1000}\right) + 159\left(\frac{d_p}{1000}\right) + 50415)n_{wt}P_{wt}\ /10^6 \qquad (5.5.6.2)$$

where $n_{wt}$ is the number of the WTs and $P_{wt}$ is the nameplate capacity of each WT. According to Cavazzi and Dutton (2016):

$$C_{om3} = (fixed_{cost} + port_{fees} + (\frac{\left(\frac{d_p}{1000}\right)var_{cost}}{100}))n_{wt}P_{wt}\ 8760 \qquad (5.5.6.3)$$

in m€, where $var_{cost}$ is a constant value in euros (9 euros) per 100 km and $port_{fees}$ among with $fixed_{cost}$ are expressed in €/MWh calculated as 5 and 26 €/MWh respectively.

Finally, Ioannou et al. (2018) consider all operational expenditures as a function of the WT's nameplate capacity ($P_{wt}$), the total installed capacity of the OWF ($P_{wf}$) and the distance from the nearest port-harbor ($d_p$) expressed in euros (€) as:

$$Cost_{om4} = -6.349 * 10^8 P_{wt}^{0.187} + 2.595 * 10^{-19} \exp(0.83d_p) + 8.413 * 10^5 P_{wf} + 9.506 * 10^8 \qquad (5.5.6.4)$$

where the $Cost_{opex}$ is expressed in €. Noteworthy is that the regression expression in Equation 5.5.6.4, was estimated based on the extracted results for the O&M approximation using the Netherlands Operation and Maintenance (ECN O&M) tool for a 500 MW offshore wind farm. Coefficient of determination of the resulted regression was 0.986, indicating a satisfactory fitting performance to the resulted data, however, only for limited configurations considering the OWF size, distance from the nearest harbor and weather conditions.

### 5.5.7 Other costs

Having analyzed the key cost components and the associated models, related to the OWF's manufacturing and installation phase, two procedures are still remaining to be evaluated, consisting of the Development and Consenting and the Decommissioning and Disposal phase. The

former stage is actually the first phase of an OWF conceptualization and planning as long as the latter is the last stage to be accomplished after the operational period (approx. 25 years) of a wind project. Withing the next two sections, the total cost evaluation schemes will be demonstrated accounting for a rather small, but not negligible, cost of the total life cycle cost of an OWF.

#### 5.5.7.1 Development and Consenting cost

From the early stages of the conceptualization of an OWF, many procedures and studies must be accomplished in order to assess and ensure the economic feasibility of a project. These costs, according to Shaffie et al., (2016) comprise the: i) the project management, ii) legal authorization and licensing of the project, iii) the conducted surveys e.g. wind resource assessment campaigns and met-ocean conditions monitoring, iv) engineering activities, such as seabed assessment and connection to the onshore grid, structural design testing regarding the WTs and foundation types etc. and finally, v) the associated contingencies translated as the unpredictable annual expenses and allowance for replacement of the most expensive components. Most of the reports notice that the total cost during this stage accounts for a total 10-14% of the total CAPEX. Particularly, Hong & Moller (2011) express the development and consenting cost as:

$$Cost_{consent} = 0.1\ CAPEX \quad (5.5.7.1.1)$$

Accordingly, Dicorato et al., (2011), propose a per MW expression:

$$Cost_{consent2} = 0.13\ MW_{install} \quad (5.5.7.1.2)$$

Finally, Shaffie et al., (2016), for their Life Cycle Cost assessment express the sum of this stage's costs for a 500 MW offshore wind project as:

$$Cost_{consent3} = 0.14\ CAPEX \quad (5.5.7.1.3)$$

where Myhr et al., (2014) expressed the total development and consenting cost as a function of the number of WTs in the OWF calculated based on the following equations for both fixed and floating concepts:

$$Cost_{consent\_fixed} = 0.823\ N_{WT} + 32.2 \quad (5.5.7.1.4)$$

$$Cost_{consent\_floating} = 0.564\ N_{WT} + 43.4 \quad (5.5.7.1.5)$$

estimated in million euros ($€_{2020}$).

### 5.5.7.2 Decommissioning and Disposal cost (DECEX)

OWF decommissioning activities are expected to follow the same process as installation, but in a reverse order. This means that the equations and the data presented in Equations 5.5.5.1 - 4 and Tables 5.5.5.1, 5.5.5.4 will be used to estimate the total duration of the decommissioning process related to the vessels' costs, capacity and the number of technicians needed to accomplish the removal procedures. Consequently, a jack-up vessel is used for the decommissioning of the offshore WTs and bottom-fixed foundations, tugboats and an AHTS vessel for the floating concepts removal (and the floating substation) and a Heavy-Lift crane vessel for the jacket substation removal. In parallel, additional support vessels (Diving Support boats, Dynamic Positioning Vessels and workboats) and cutting equipment will be used for the cables' extraction (cables are most of the times partially removed), the monopiles and jackets inspection and removal and the substation preparative decommissioning operations (Smith et al., 2016; Ioannou et al., 2018).

One key assumption to be considered is that the OWFs components are not reused, but rather recycled and sold for scrap. As a result, it is expected that for steel-intensive components (e.g., WTs tower and foundations), the total decommissioning-disposal cost differences might be negative, considering the scrap revenues (Bjeckseter & Agotnes, 2013; Myhr et al., 2014).

Focusing on the decommissioning operations, two strategies are applied in order to transfer the components to the shore using the techniques of:

1. Cut, Lift, Carry (e.g., for WTs, monopile and jacket foundations as also for the substation)
2. Detach and Tow (floating WTs and substation)

**Table 5.5.7.2.1**: Removal time consumption per decommissioning operation

| Removal (per WT) | Operation | Duration (days) | Removal | Operation | Duration (days) |
|---|---|---|---|---|---|
| WT (Workboat) | Preparation 1 | 1.2 | Cables (ROV) | Cable protection | 0.4 |
| WT (Jack-Up) | Preparation 2 | 0.2 | Cables (ROV) | Preparation 1 | 0.1 |
| WT (Jack-Up) | $Uninstall_{time}$ | 2 | Cables (CLV) | Preparation 2 | 0.3 |
| Foundation (Dive b.) | Preparation 1 | 1 | Cables (CLV) | $Uninstall_{time}$ | 0.8/0.5 |
| Foundation (Jack-Up) | Preparation 2 | 0.5 | Substation (Workboat) | Preparation 1 | 3 |
| Foundation (Jack-Up) | $Uninstall_{time\ 1}$ | 1 | Substation (Dive boat) | Preparation 2 | 12 |
| Foundation (Jack-Up) | $Uninstall_{time\ 2}$ | 1.5 | Substation (Tug) | Load-Assist | 1 |
| Foundation (PSV) | Preparation 1 | 0.5 | Substation (HLCV) | Preparation 1 | 0.4 |
| Foundation (PSV) | Disc. ballast | 0.5 | Substation (HLCV) | $Uninstall_{time\ 1}$ | 2 |
| Foundation (PSV) | Dicom. Moorings | 1 | Substation (HLCV) | Preparation 2 | 1 |
| Foundation (AHTS) | Preparation 2 | 0.5 | Substation (HLCV) | $Uninstall_{time\ 2}$ | 2 |
| Foundation (AHTS) | Detach moorings | 0.5 | Substation (PSV) | Preparation 1 | 1 |
| Foundation (AHTS) | $Uninstall_{time\ 1}$ | 0.5 | Substation (PSV) | Disc. ballast | 0.5 |
| | | | Substation (PSV) | Dicom. Moor. | 0.5 |
| | | | Substation (AHTS) | Preparation 2 | 0.5 |
| | | | Substation (AHTS) | Detach Moor. | 1 |
| | | | Substation (AHTS) | $Uninstall_{time}$ | 2 |

**WTs and foundations decommissioning:** For the bottom-fixed concepts, the sequence of the marine operations consists of the preparation stage, using workboats and diving vessels, the cutting stage using specialized equipment, the removal stage by lifting the WTs and foundation components to the transfer vessels and finally the transportation stage to the disposal facilities. Subsequently for the floating concepts, the preparation stage includes the moorings detachment and removal, anchors decommissioning and finally the towing of the floater and the topside to the tugboats and the AHTS vessel in order to be transferred onshore. One key assumption for the floating concepts is that they are first detached (cutting the mooring lines) and then transferred to the shore using AHTS vessels and tugboats. Similarly to the installation time adjustment

considering that three different WT models are used, which leads to different structural masses per WT and foundation concept, a normalized installation duration adjustment factor is also applied using Equation 5.5.5.15 in order to express the installation time increase.

**Table 5.5.7.2.2**: WTs and foundations' decommissioning cost estimation per operation

| WTs removal | Operation | Count | Duration (days) | Unit cost (€) | WF (%) | Total cost (€) |
|---|---|---|---|---|---|---|
| Workboat | Preparation | 1.2 | 1.2 | 5000 | 80 | 1.2 |
| Workboat | Transportation | 0.3 | 0.3 | 5000 | 90 | 0.3 |
| Jack-Up | Transportation | 0.25 | 0.25 | 150000 | 85 | 0.25 |
| Jack-Up | Preparation | 0.2 | 0.2 | 150000 | 80 | 0.2 |
| Jack-Up | WT ($Uninstall_{time}$) | 1.6 | 1.6 | 150000 | 75 | 1.6 |
| Jack-Up | Preparation | 0.1 | 0.1 | 150000 | 80 | 0.1 |
| Jack-Up | Transit to next WT | 0.3 | 0.3 | 150000 | 85 | 0.3 |
| Cutter | Cut and prepare | 1.2 | 1.2 | 7500 | 85 | 1.2 |
| Personnel | Personnel usage | 2.45 | 2.45 | 350 | 51 | 2.45 |
| **Total days and cost** | | | 5.15 | | | **518284,3137** |

| Fixed concepts removal | Operation | Count | Duration (days) | Unit cost (€) | WF (%) | Total cost (€) |
|---|---|---|---|---|---|---|
| Diving boat | Cut and prepare | 1 | 0.5 | 30000 | 75 | 20000.00 |
| Diving boat | Transportation | 1 | 0.7 | 30000 | 85 | 24705.88 |
| Jack-Up | Transportation | 1 | 0.2 | 150000 | 85 | 35294.12 |
| Jack-Up | Preparation | 1 | 0.5 | 150000 | 80 | 93750.00 |
| Jack-Up | Foundation 1 | 1 | 1 | 150000 | 75 | 200000.00 |
| Jack-Up | Foundation 2 | 1 | 1.5 | 150000 | 80 | 281250.00 |
| Jack-Up | Transit to next fd. | 1 | 0.3 | 150000 | 85 | 52941.18 |
| Personnel | Personnel usage | 15 | 3.5 | 393.7 | 51 | 40527.94 |
| **Total days and cost** | | | 4.7 | | | **748469.1176** |

| Floating concepts removal | Operation | Count | Duration (days) | Unit cost (€) | WF (%) | Total cost (€) |
|---|---|---|---|---|---|---|
| PSV | Transportation | 1 | 0.3 | 48948 | 90 | 16316.00 |
| PSV | Prepare WT | 1 | 0.5 | 48948 | 80 | 30592.50 |
| PSV | Disconnetct ballast | 1 | 0.5 | 48948 | 70 | 34962.86 |
| PSV | Dicom. Moorings | 1 | 1 | 48948 | 75 | 65264.00 |
| Tug boats | Transportation | 2 | 1.2 | 12000 | 75 | 38400.00 |
| AHTS | Transportation | 1 | 1.2 | 96833 | 75 | 154932.80 |
| AHTS | Prepare | 1 | 0.5 | 96833 | 80 | 60520.63 |

| | | | | | | |
|---|---|---|---|---|---|---|
| AHTS | Tow and detach moorings | 1 | 0.5 | 96833 | 65 | 74486.92 |
| AHTS | Moorings and anchors | 1 | 0.2 | 96833 | 70 | 27666.57 |
| Personnel | Personnel usage | 15 | 2.4 | 393.7 | 51 | 27790.59 |
| **Total days and cost** | | | **4.9** | | | **503142.28** |

**Cables' removal:** Further to the removal of the WT components, the balance of the plant, including the cables and the offshore substation, must be removed. Export and inter-array cables can be cut in smaller sections (i.e., 2km) while they are removed, hence, a dynamic positioning CLV is used with a ROV for the removal and cutting operations. For the cables' decommissioning procedures, the user specifies the total amount of cables (%) that are removed, thus during this study, a 40% of the initial cables' length is assumed to be left in situ after the decommissioning of an OWF. An indicative example of the cables' decommissioning cost estimation is illustrated in Table 5.5.7.2.3 for a 500MW offshore wind project.

**Table 5.5.7.2.3**: Export and inter-array cables decommissioning cost estimation per operation

| Export/Inter-array | Operation | Count | Duration (days) | Unit cost (€) | WF (%) | Total cost (€) |
|---|---|---|---|---|---|---|
| Cable protection rem. | Remove protection | 1 | 8 | 15000 | 70 | 171428.57 |
| Cable protection rem. | Survey cable | 1 | 8 | 15000 | 70 | 171428.57 |
| CLV | Transportation | 1 | 12 | 170000 | 80 | 2550000.00 |
| CLV | Prepare | 1 | 4 | 170000 | 75 | 906666.67 |
| CLV | Cable removal | 1 | 40 | 170000 | 65 | 10461538.46 |
| CLV | Transit to next cable section | 1 | 0.1 | 170000 | 80 | 21250.00 |
| Cable deburial tool | Debury cable | 1 | 40 | 18000 | 65 | 1107692.31 |
| Personnel | Personnel usage | 15 | 84.1 | 393.7 | 51 | 973828.53 |
| **Total days and cost** | | | **84.1** | | | **16363833.11** |

**Offshore substation decommissioning:** At last, the offshore substation is removed. Two different decommissioning strategies are applied for either the bottom-fixed and the floating substation concepts respectively. For the former, the topside and the jacket foundation preparation are performed using a diving vessel and workboats, followed by the topside and the jacket removal (including the jacket piles) using an HLC vessel by loading the removed components onto a transit barge towed by 2 tugboats back to the disposal port in order to unload and return to the site.

For the floating substation, the decommissioning activities are similar to the floating WTs removal. A PSV is used for all preparative activities before the decommissioning stage followed by the transportation of both the floater and the substation by tugboats and the AHTS. Finally, the AHTS removes the anchors and the moorings and returns to the disposal port. In Table 5.5.7.2.4 all the operations are demonstrated among with the total decommissioning activities duration and cost. In Table 5.5.7.2.4, the distance from the port is set as 40 km and the vessels' transit speeds along with the weather factors (WF) deriving from Table 5.5.5.2.

**Table 5.5.7.2.4**: Substation's decommissioning operation and cost estimation per operation

| **Jacket Substation** | Operation | Count | Duration (days) | Unit cost (€) | WF (%) | Total cost (€) |
|---|---|---|---|---|---|---|
| Workboat | Preparation | 1 | **13.03** | **5000** | **80** | 81437.50 |
| Diving boat | Cut and prepare | 1 | **13.03** | **30000** | **85** | 459882.35 |
| Barge | Transportation | 1 | **3** | **35000** | **65** | 161538.46 |
| Tug boats | Transportation | 2 | 3 | **12000** | **65** | 110769.23 |
| Tug boats | Assistance | 2 | **3** | **12000** | **80** | 15000.00 |
| Tug boats | Loading | 2 | 0.63 | **12000** | **77** | 19636.36 |
| Heavy Lift Crane V. | Transportation | 1 | 3.5 | **565037** | **77** | 2568350.00 |
| Heavy Lift Crane V. | Prepare topside | 1 | 0.4 | **565037** | **55** | 410936.00 |
| Heavy Lift Crane V. | Detach, Lift, Load | 1 | 2 | **565037** | **51** | 2215831.37 |
| Heavy Lift Crane V. | Prepare jacket | 1 | 1 | **565037** | **55** | 1027340.00 |
| Heavy Lift Crane V. | Detach, Lift, Load | 1 | 2 | **565037** | **51** | 2215831.37 |
| Personnel | Personnel usage | 15 | 0.67 | **393.7** | **51** | 7758.21 |
| **Total days and cost** | | | **13.3** | | | **9294310.86** |

| **Floating Substation** | Operation | Count | Duration (days) | Unit cost (€) | WF (%) | Total cost (€) |
|---|---|---|---|---|---|---|
| PSV | Transportation | 1 | **0.5** | **48948** | **90** | 27193.33 |
| PSV | Prepare Substation | 1 | 1 | **48948** | **80** | 61185.00 |
| PSV | Disconnetct ballast | 1 | 0.5 | **48948** | **70** | 34962.86 |
| PSV | Dicom. Moorings | 1 | 0.5 | **48948** | **75** | 32632.00 |
| Tug boats | Transportation | 4 | **1** | **12000** | **65** | 73846.15 |
| Tug boats | Prepare | 4 | 0.5 | **12000** | **65** | 36923.08 |
| Tug boats | Tow and detach moorings | 4 | 1 | **12000** | **65** | 73846.15 |
| AHTS | Transportation | 1 | **1** | **96833** | **75** | 129110.67 |
| AHTS | Prepare | 1 | 0.5 | **96833** | **60** | 80694.17 |
| AHTS | Tow and detach moorings | 1 | 1 | **96833** | **65** | 148973.85 |

| | | | | | | |
|---|---|---|---|---|---|---|
| AHTS | Moorings and anchors | 1 | 2 | **96833** | **80** | 242082.50 |
| Personnel | Personnel usage | 15 | **7.5** | **393.7** | **51** | 86845.59 |
| **Total days and cost** | | | **9.5** | | | **1028295.343** |

**Site clearance:** According to Kaizer and Snyder, (2012), the last stage during the decommissioning phase is site clearance and verification expressed as the process of removing or addressing potentially adverse impacts from debris and seafloor disturbances overall due to OWF components and facilities. For the entire offshore area, the authors consider that the total site clearance cost is proportional to the total area expressed in km$^2$ using the following formula:

$$Area_{owf} = -51.5 + 0.41D_{wt} + 0.65n_{wt} \quad (5.5.7.2.1)$$

where $D_{wt}$ is the WT's rotor diameter and $n_{wt}$ is the total number of WTs in the OWF. By assuming a total cost of 26000 - 92000 €$_{2020}$/ km$^2$, the total site clearance cost can be estimated using a mean value of 59000 €/ km$^2$.

**Scrap revenues:** When all of the aforementioned OWF components are transported to the shore, most of them will be reused, recycles or will be sold for scrap (Myhr et al., 2014). For the latter scenario, all steel and copper-based components must be cut into smaller pieces in order to be transferred to the selected facilities. However, the cost for processing the materials and transporting them to the selected facilities are not considered in this thesis, since the costs are small relative to the total decommissioning cost.

In order to estimate the scrap revenues, Table 5.5.7.2.5 illustrates the components' initial mass for an indicative OWF comprised of 40 WTs, 40 km from the shore with 45 km of inter-array cables. Reviewing Sections 5.5.2 - 5.5.4, all of the OWF's components mass volumes (tower, nacelle, foundations and substation) are extracted and saved in raster files. On the contrary, the volume and hence mass of copper in cables is set as fixed and is typically ranging 5 to 10 tons/km for inter-array cables and 15 to 20 tons/km for the export cables. In addition to the initial mass estimation, a recovery factor (%) for the OWF components is set for the total recovered

components mass. When the total recovered mass is estimated, a steel and copper scrap price of 115 euros/ton and 3880 eoros/ton is set (iscrapapp.com).

**Table 5.5.7.2.5**: Recovery percentage and scrap revenues (indicative values)

| **Components** | Weight (tons) | Recovery factor (%) | No. Units | Rec. Weight | Revenues (€) |
|---|---|---|---|---|---|
| Nacelle (steel) | 150 | 75 | $n_{wt}$ | **4500** | 517500 |
| Towers (steel) | 350 | 95 | $n_{wt}$ | **13300** | 1529000 |
| Foundations fixed (steel) | 700 | 95 | $n_{wt}$ | **26600** | 3059000 |
| Foundations Floating (steel) | 2500 | 95 | $n_{wt}$ | **95000** | 10925000 |
| Transition Piece (steel) | 200 | 90 | $n_{wt}$ | **7200** | 828000 |
| Substation (steel) | 1200 | 80 | $n_{sub}$ | **960** | 110400 |
| Cable (export) (Copper) | 17 | 95 | ***Length (40)*** | **646** | 2183480 |
| Cable (array) (Copper) | 7 | 95 | ***Length (45)*** | **299.25** | 1011465 |
| **Total revenues (Fixed)** | | | | | **8227380** |
| **Total revenues (Floating)** | | | | | **16093380** |

In Table 5.5.7.2.5 some rough estimates are presented in order to highlight how the scrap values in some cases reduce drastically or even eliminate the decommissioning cost. Hence, the scrap revenues for either the tower and the foundations can potentially outweigh decommissioning cost, mostly for offshore floating structures that are steel-intensive.

### 5.5.8 Least Cost Path (LCP) algorithms for the Installation, Decommissioning and O&M cost

In this Section, the Least Cost Path (LCP) algorithms used for the transmission lines production and installation cost, the overall installation and decommissioning costs (wind turbines, foundations, scour protection, substation) and the operation and maintenance cost are illustrated and discussed. All functions used in the algorithms' set-up are distance-based in terms of the distance from the nearest onshore network junction, the nearest port/harbour and the distance from the shoreline.

Figure 5.5.8.1.1 illustrates the flowchart with all the appropriate steps were followed along with the data used in order to estimate the aforementioned costs. Thus, a graph-based representation of the study area is used to set-up the cost surfaces and extract all optimal paths for each pixel in the Central and North Aegean Sea, using the Dijkstra algorithm, followed by the different sub-procedures (smoothing techniques) applied to reduce the inherent uncertainties of the extracted paths and costs when working upon discrete surfaces (raster data structures).

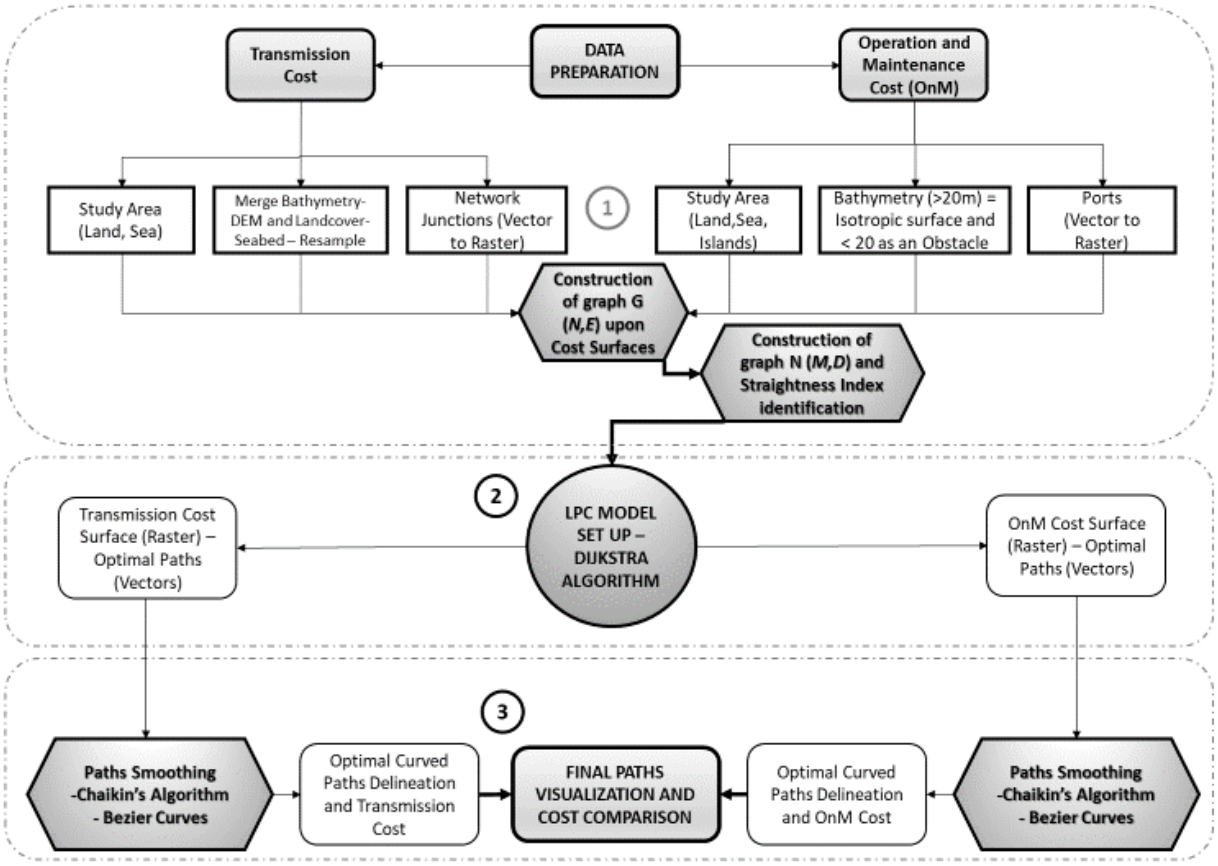


**Figure. 5.5.8.1.1**: Flowchart and methodology outline based on the: 1) Data preparation, 2) LCP set-up and 3) Smoothing techniques

### 5.5.8.1 Preparation of data layers and LCP algorithm set up

In order to integrate GIS data structures in a graph-based modelling environment, preparative operations of input rasters using common data processing methods in GIS (mosaicing several layers as one layer, converting vector format into raster format, resampling and

reclassification) are applied on the initial data (Figure 5.5.8.1.1). Using the cost surfaces, a raster-based representation of space can be transformed into a graph by treating the center point of each cell as a node and connecting each node to the other cells. During the graph creation several procedures are applied in order to set up properly the algorithms for both Transmission and O&M cost evaluation and paths delineation as presented in Table 5.5.7.1.1 and Figure 5.5.7.1.1 (***Process 2***). All of the objectives are normalized into a common numerical scale (from 0 to 5) considering that completely different spatial indices are combined (e.g., elevation, bathymetry, slopes, distances, straightness, landcover and substrate). Considering landcover and substrate types for the transmission paths' delineation, soft substrate areas (e.g., muddy sand or sandy mud) and non-forest areas were graded with the highest normalized score values (= 4) for a cable pass-through.

**Table 5.5.8.1.1:** Objectives, criteria, obstacles and weighting factors for the LCP algorithms

| | **Objective** | **Criteria** | **Obstacles** | **Weighting** |
|---|---|---|---|---|
| **Transmission Cost LCP** | Cost Minimization (Anisotropic Surface) | 3D Distance - Slope Differences - Straightness | Urban areas, Posidonia Oceanica-NoData cells | Slopes - Straightness - Landcover - Distance |
| **O&M Cost LCP** | Cost Minimization (Isotropic Surface) | 2D Distance - Straightness | Island - Mainland - NoData cells | Bathymetry - Straightness - Distance |

Additionally, during the graph creation the connectivity rules must be identified between neighboring cells. Since there is an infinite number of movement options in two-dimensional space, there are also multiple ways to approximate connectivity. The most commonly used connectivity pattern is to link a cell to its four orthogonal and four diagonal neighbors, amounting to eight movement angles (Queen's Pattern – Yu et al. 2003). Considering that the cells of the raster are assigned with cost values defining the cost of movement per distance unit through the cell, the cost of each step connecting the centers of two neighboring cells can be calculated based-on their distance (2D or 3D) adjusted by the terrain slope of the underlying cells.

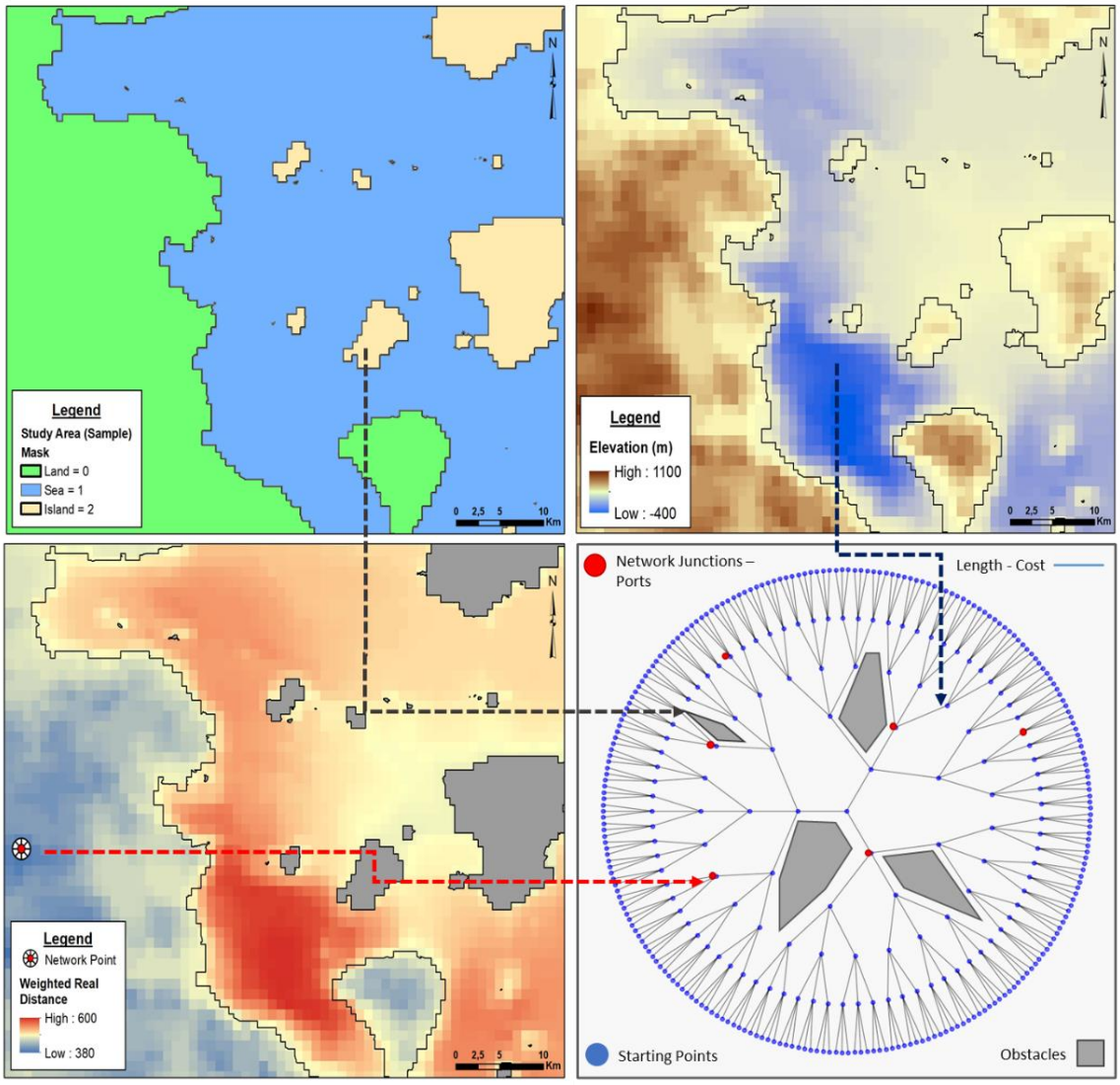


**Figure 5.5.8.1.2**: Graph *G(V,E)* construction upon raster surfaces

The center of non-null cells (ports or network junctions, mainland and offshore areas) is considered as the nodes (*V*), and weighted edges (*E*) are created between neighboring nodes (Figure.5.5.8.1.2), formulating the final primal graph *G (V, E)*. For each edge the attributes: a) distance, b) slope, c) land or soil type and d) mask value (land-sea-island), are stored. The 3D distance between the centroids of the neighbouring cells is calculated using the equations 1-3, while the slope is calculated using Equation 5.5.8.1.4.

$$R_{Dist}=\sqrt{ED^2 + DH^2}, \qquad (5.5.8.1.1)$$

$$ED = cell\_size \sqrt{(Xi - Xj)^2 + (Yi - Yj)^2} \quad (5.5.8.1.2)$$

$$DH = C_i - C_j, \quad (5.5.8.1.3)$$

$$S = \frac{DH}{ED} \quad (5.5.8.1.4)$$

where *ED* is the horizontal distance between two neighbor cells, *DH* is the vertical distance (height difference), *S* is the actual slope from cell *i* to neighbor cell *j* and $R_{Dist}$is the 3D distance measure. For the O&M cost the distance between two neighbor cells is the *ED* measure, while for the transmission cost is the $R_{Dist}$ measure.

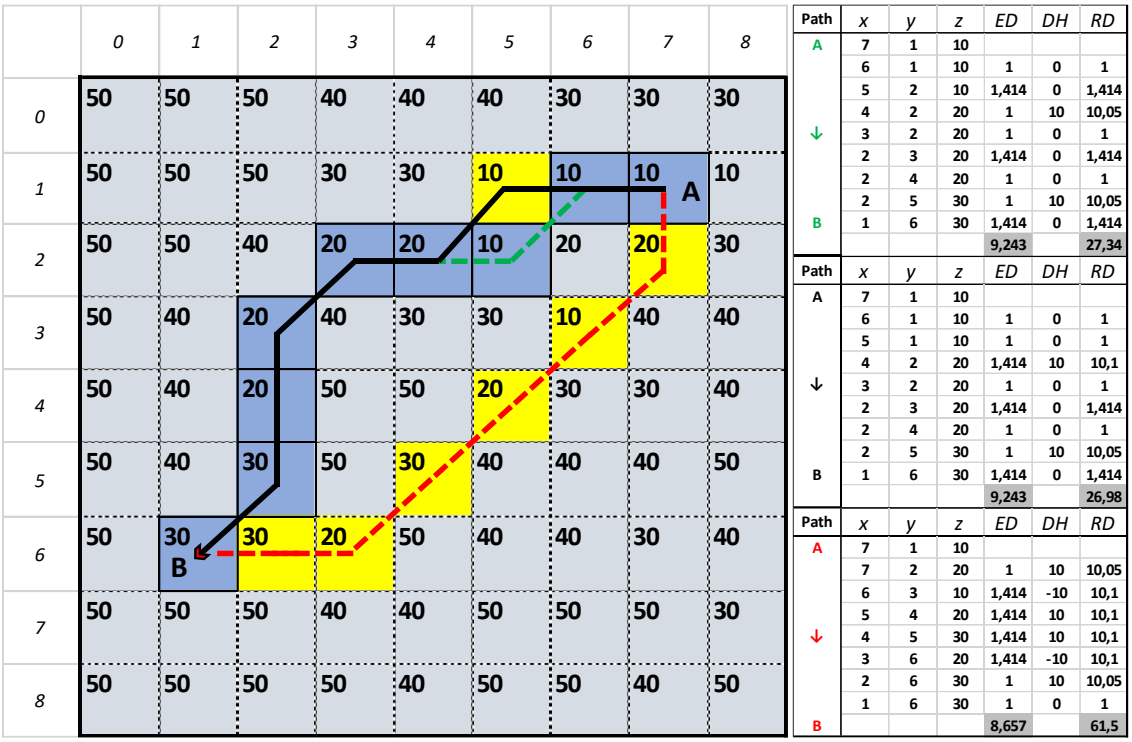


| | 0 | 1 | 2 | 3 | 4 | 5 | 6 | 7 | 8 |
|---|---|---|---|---|---|---|---|---|---|
| 0 | 50 | 50 | 50 | 40 | 40 | 40 | 30 | 30 | 30 |
| 1 | 50 | 50 | 50 | 30 | 30 | 10 | 10 | 10 | 10 |
| 2 | 50 | 50 | 40 | 20 | 20 | 10 | 20 | 20 | 30 |
| 3 | 50 | 40 | 20 | 40 | 30 | 30 | 10 | 40 | 40 |
| 4 | 50 | 40 | 20 | 50 | 50 | 20 | 30 | 30 | 40 |
| 5 | 50 | 40 | 30 | 50 | 30 | 40 | 40 | 40 | 50 |
| 6 | 50 | 30 | 30 | 20 | 50 | 40 | 40 | 30 | 40 |
| 7 | 50 | 50 | 50 | 40 | 40 | 50 | 50 | 50 | 30 |
| 8 | 50 | 50 | 50 | 50 | 40 | 50 | 50 | 40 | 50 |

| Path | x | y | z | ED | DH | RD |
|---|---|---|---|---|---|---|
| A | 7 | 1 | 10 | | | |
| | 6 | 1 | 10 | 1 | 0 | 1 |
| | 5 | 2 | 10 | 1,414 | 0 | 1,414 |
| | 4 | 2 | 20 | 1 | 10 | 10,05 |
| ↓ | 3 | 2 | 20 | 1 | 0 | 1 |
| | 2 | 3 | 20 | 1,414 | 0 | 1,414 |
| | 2 | 4 | 20 | 1 | 0 | 1 |
| | 2 | 5 | 30 | 1 | 10 | 10,05 |
| B | 1 | 6 | 30 | 1,414 | 0 | 1,414 |
| | | | | 9,243 | | 27,34 |

| Path | x | y | z | ED | DH | RD |
|---|---|---|---|---|---|---|
| A | 7 | 1 | 10 | | | |
| | 6 | 1 | 10 | 1 | 0 | 1 |
| | 5 | 1 | 10 | 1 | 0 | 1 |
| | 4 | 2 | 20 | 1,414 | 10 | 10,1 |
| ↓ | 3 | 2 | 20 | 1 | 0 | 1 |
| | 2 | 3 | 20 | 1,414 | 0 | 1,414 |
| | 2 | 4 | 20 | 1 | 0 | 1 |
| | 2 | 5 | 30 | 1 | 10 | 10,05 |
| B | 1 | 6 | 30 | 1,414 | 0 | 1,414 |
| | | | | 9,243 | | 26,98 |

| Path | x | y | z | ED | DH | RD |
|---|---|---|---|---|---|---|
| A | 7 | 1 | 10 | | | |
| | 7 | 2 | 20 | 1 | 10 | 10,05 |
| | 6 | 3 | 10 | 1,414 | -10 | 10,1 |
| | 5 | 4 | 20 | 1,414 | 10 | 10,1 |
| ↓ | 4 | 5 | 30 | 1,414 | 10 | 10,1 |
| | 3 | 6 | 20 | 1,414 | -10 | 10,1 |
| | 2 | 6 | 30 | 1 | 10 | 10,05 |
| | 1 | 6 | 30 | 1 | 0 | 1 |
| B | | | | 8,657 | | 61,5 |

**Figure.5.5.8.1.3**: LCP example considering 3D distance and slopes

A typical example of how the optimal paths are extracted, regarding the 3D real distance, is demonstrated in Figure 5.5.8.1.3. By evaluating the paths, from A to B, it is clear that the northern paths (black and green) are equal to 9 units (pixels) with the Euclidean distance equal to 9.243 and the southern path (red) is equal to 8 units with a distance equal to 8.667. Considering only the Euclidean distance, the optimal path is the red one, although, the optimum answer of the problem, regarding its crossing on pixels with a slighter slope, is the path with the continuous

black line with a value of 26.98 in the real 3D distance. The reason is that despite of the fact that the sum of the weights of both green and black paths are equal, the slopes crossing between pixels are different (the path with the black color has lower slope differences, hence a lower 3D distance value). The example below illustrates that a balance must be created between sum of pixels weight and path length parameters in order to choose the optimum path linked to its characteristics.

Another important aspect in LCP algorithms for routing problems is the straightness of the optimal paths. Determining a cable route or a shipping lane path in a grid-based graph presents a slightly different problem, as any sharp bends (turns of an increased angle) in such routes are not acceptable. A crucial requirement is to identify the minimum number and the angle of turns, in order to guarantee the straightness of the path. Obviously, this requirement calls for a not only 'safe' but also 'fair' LCP path. Indeed, the initial paths generated by the Dijkstra's Algorithm usually do not satisfy this requirement.

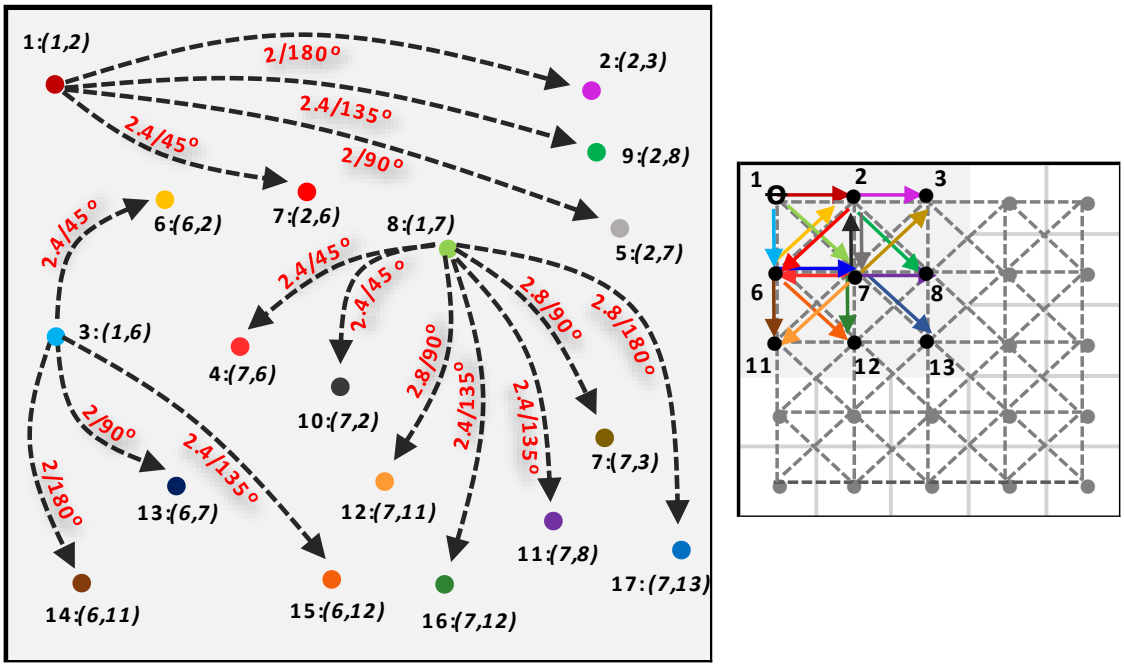


**Figure.5.5.8.1.4**: Construction of graph *N* – Straightness calculation based-on dual graph

To address this problem, a dual graph of the plane graph *G(V, E)* is used. Considering that a pair of points always lie on a straight line, at least three points are needed in order to determine

the curvature-straightness cost. To achieve this, a directed graph *N(M, L)* is constructed in which each node *M* of *N* corresponds to an edge of the graph *G* and the edges *L* are holding the angle information between two connected edges of graph *G* as a node combination in *N*. Therefore, any edge *L* connecting two nodes *M* corresponds to the interaction of three nodes *V* of the graph *G* with possible angle values ranging from 45° degrees to 180°. In this manner we can compute the straightness cost (e.g., score of 1 for straight paths and 4 for peaks) of any path through the original graph *G* and Figure.5.5.8.1.4. shows the same paths from graph *G* to *N* considering all available combinations in a 3x3 sub-graph and the according angles values. For each edge *L* of graph *N* the attributes of: a) the total distance, b) the minimum slope, c) land or soil type and d) the turn angle, are stored and scaled as illustrated in Table 5.5.8.1.2.

**Table.5.5.8.1.2:** Criteria scaling for the Least Cost Path algorithms of the Transmission and the Operation and Maintenance cost estimation

| Transmission Paths | Weighting Factors | | | | |
|---|---|---|---|---|---|
| **Landcover/Soil Substrate** | **Value** | **Angle** | **Value** | **3D Distance length** | **Value** |
| Urban | 10^3 | 45° | 2 | Minimum 3D distance | 1 |
| Posidonia Oceanica | 10^3 | 90° | 1.5 | Maximum 3D distance | 2 |
| Bare soil/Agricultural | 1 | 135° | 1.2 | | |
| Sundy mud, Fine mud, Muddy sand, Sand | 1 | 180° | 1 | | |
| Water surfaces (Onshore) | 1.2 | | | | |
| Coarse or Unkown Sediment | 2 | | | | |
| Forest areas | 2 | | | | |
| Operation and Maintenance Paths | Weighting Factors | | | | |
| **Angle** | **Value** | **2D Distance length** | **Value** | **Bathymetry** | **Value** |
| 45° | 2 | Minimum 2D distance | 1 | <= 20 meters | 10^3 |
| 90° | 1.5 | Maximum 2D distance | 2 | > 20 meters | 1 |
| 135° | 1.2 | | | | |

| | | |
|---|---|---|
| 180° | 1 | |

For estimating the final edge weight, Equation 5.5.8.1.5 is used where the product of the landcover/sea substrate, the angle and the distance length is assigned to each edge expressed by:

$$Edge_{weighted\_length} = Land\_Sea_{value} \, Angle_{value} \, Distance_{value} \quad (5.5.8.1.5)$$

, where the $Distance_{value}$ expresses the three-dimensional length for the Transmission cost surfaces and the two-dimensional length for the O&M rasters respectively, $Angle_{value}$ is the turns' normalized score and finally, $Land\_Sea_{value}$ is the normalized scores of the landcover and sea substrate type for the Transmission paths delineation. Finally, for the O&M paths, a homogenous surface is considered with a restriction value of below 20 meters of depth as indicated in Table 5.5.8.1.1.

With this weighted dual-graph, the accumulated-cost of a path between any two vertices on the graph *N* can be measured as the sum of the edge weights along that path. The LCP modelling uses graph theory shortest-path algorithms such as Dijkstra's Algorithm in order to find a least-cost distance between a start node (*i* as origin – any offshore pixel center) and an end node (*j* as destination – Ports or Network junctions) that is the minimum possible sum of edge weights (Equation 4.5.7.1.5) between vertices along the shortest-path:

$$lcd_{i,j} = min \sum_{i=1}^{j-1} e_{i,i} + 1 \quad (5.5.8.1.6)$$

Dijkstra's Algorithm works in an iterative vertex by vertex spreading manner and results in a Dijkstra tree that branches out one vertex at a time to find the shortest paths from the source vertex, or tree root, to the other vertices (Etherington, 2016). The accumulated sum of edge weights leading to "closest" destination node is converted into a raster surface, and the optimal path is converted into a vector polylines shapefile. After the optimal paths' delineation, cost functions are applied, leading to a raster cost surface for the transmission and O&M cost.

### 5.5.7.2 Paths smoothing and obstacles avoidance

One major drawback of raster-based LCP implementations, as highlighted in the literature review, is the lack of curved turns present in raster-based paths and therefore smoothing techniques can be applied in order to lead to more accurate results (Figure 5.5.8.1.1 - ***Process 3***). The distortion resulted includes two types of errors, an elongation and a deviation error (Antikainen 2013). The elongation error is due to the discrete surface presence unavoidably connecting each cell center to the center of one of the neighbored cells and as a consequence the distance increases. This leads to the deviation error which is translated as the discrepancy between the total distance measured upon discrete surfaces and the continuous space.

In Chaikin (1975), an algorithm is proposed for efficient curve generation involving a line as $P = P_o, P_1, P_2 \ldots\ldots P_k$. Considering of a line (or polygon) and using a process of repetitive "chopping off corners," a smooth limit curve derives with many vertices looking smooth when displayed in the plane. It can be proved that the resulting curve produced from this corner cutting approach will converge into a quadratic B-spline curve. The advantage of this approach is that the resulting curve will never "over-shoot" and leads to curved lines or polygons similar to the initial shapes (Reisenfeld 1975). According to Chaikin's algorithm, given the set of initial control points (Chaikin 1975) as:

$$P^0 = \{P_j^0\}_{j=0}^{n+1},\ P_j^0 \in R^d \text{ and let } P^k = \{P_j^k\}_{j=0}^{2^k n+1}$$

as the set of control points at level $k$ ($k \geq 0$, $k \in Z$), and $\{P_j^{k+1}\}_{j=0}^{2^{k+1} n+1}$ satisfying the following rules recursively:

$$\begin{cases} P_{2i}^{k+1} = a\, P_k^i + (1-a)\, P_{i+1}^k & ,0 \leq i \leq 2^k n \\ P_{2i+1}^{k+1} = \beta\ P_i^k + (1-\beta)\, P_{i+1}^k & ,0 \leq i \leq 2^k n \end{cases} \qquad (5.5.8.2.1)$$

where $\alpha$, $\beta$ are two arbitrary corner-cutting parameters between 0 and 1. When $\alpha = 3/4$, $\beta = 1/4$, the Chaikin's corner-cutting subdivision scheme is applied. The procedure of Equation 5.5.8.2.1. continues to subdivide in a binary manner until the set of points is sufficiently dense for the

display application intended (referred as refinement). The resulted curve is demonstrated in Figure.5.5.8.2.1 where Chaikin's corner cutting implementation can efficiently transform Dijkstra paths to curved smoothed lines mainly in the turning points of the line. In order to examine for more accurate optimal and smoothed results Bézier curves are further applied upon Chaikin's results. For every two points (Equation 5.5.8.2.2 - 5.5.8.2.3), we need to take the lower part and the upper part in the line between them using the ratio 1:3 and in a simpler form is expressed as:

$$\text{Lower Point} = (P_i)\alpha + (P_{i+1})\beta \quad (5.5.8.2.2)$$

$$\text{Upper Point} = (P_i)\beta + (P_{i+1})\alpha \quad (5.5.8.2.3)$$

It is also needed to add the edge points, so the line will not shrink. The resulted curve is demonstrated in (Figure 5.5.8.2.1e) Chaikin's corner cutting implementation as its name insists can efficiently transform Dijkstra paths to curved smoothed lines mainly in the turning points of the line. In order to examine for more accurate optimal and smoothed results Bézier curves are further applied upon Chaikin's results.

Compared to other type of curves, the Bézier curve is completely contained within the convex hull of its control points, which are used to define an optimal curve (Choi et al., 2008). In regard to the topological characteristics, a Bézier curve has fewer turning (intermediate) points, which control the shape of the curve by transforming the slope of the curve changing its sign. The more the intermediate points are, the closest the final curve is "fitted" to the initial line or path (Zhou et al., 2011). For this reason, the Chaikin's corner cutting procedure from the previous step is used in order to increase the number of the intermediate points in the angled parts of the Dijkstra path. Given a set of control points $P = P_o, P_1, P_2 \ldots\ldots P_n$, the corresponding Bézier curve (Figure 5.5.8.2.3f) is defined as:

$$P(\lambda) = \sum_{i=0}^{n} B_i^n(\lambda) Pi, \quad 0 \leq \lambda \leq 1 \quad (5.5.8.2.4)$$

where $B_i^n(\lambda)$ is a Bernstein polynomial and *Pi* is the $i^{th}$ vector of the control points. The Bernstein polynomials (Equation 5.5.8.2.5), which are the base functions in the Bézier curve expression, are defined as:

$$B_i^n(\lambda) = \binom{n}{i}\lambda^i(1-\lambda)^{n-i},\ i = 0,1,\ldots\ldots,n \qquad (5.5.8.2.5)$$

The tangent vectors at the start and last point are given by $P_1-P_0$ and $P_n-P_{n-1}$, respectively. The second derivative at start point must be determined by $P_0$, $P_1$ and $P_2$ and the last point must be determined by $P_{n-2}$, $P_{n-1}$ and $P_n$ (Zhou et al., 2011).

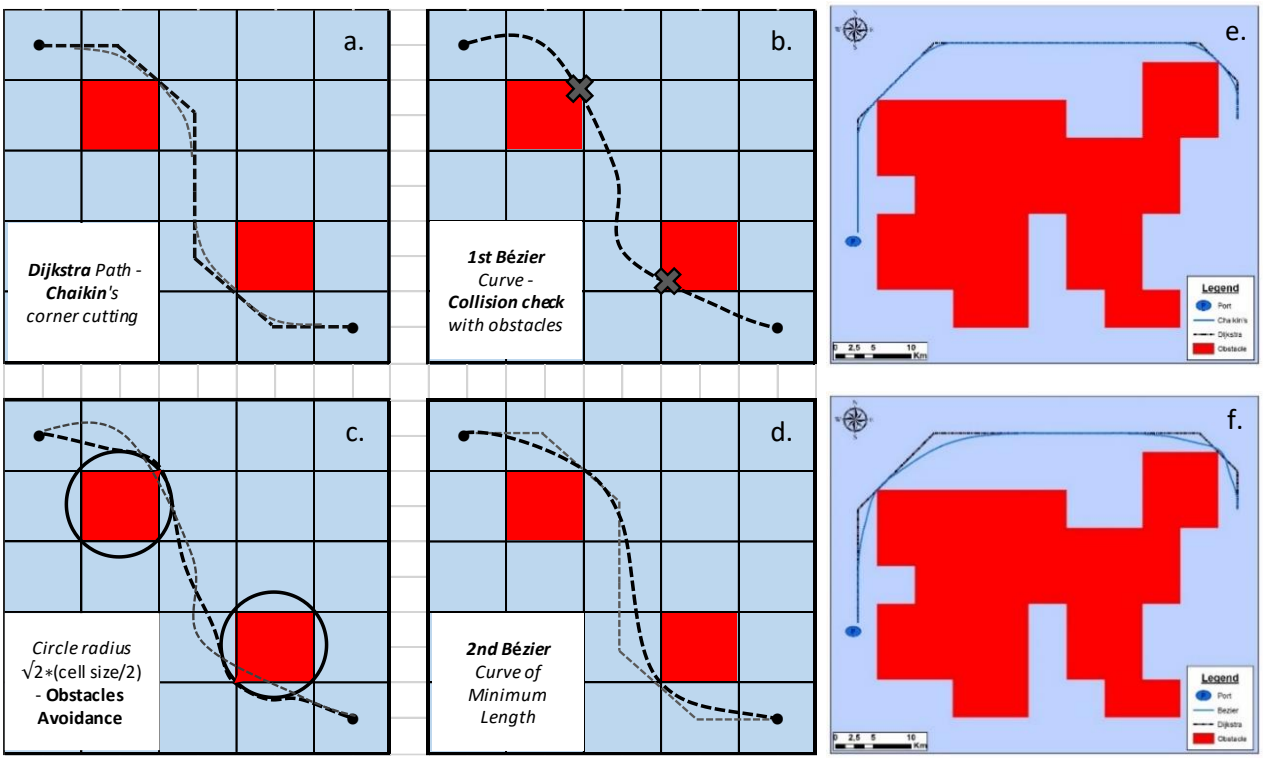


**Figure 5.5.8.2.1**: Bézier curve delineation (a-d), Dijkstra path - Chaikin's corner cutting (e) and Bézier curve (f) example

One of the most crucial steps in order to delineate the optimal Bézier curves smoothed paths was to handle and control obstacles avoidance. When referring to obstacles for O&M paths allocation or for Transmission lines delineation, all islands, urban areas, NoData cells and bathymetry values less than 20 meters are considered as obstacles according to each cost

calculation (see Table 5.5.8.1.2). The concept of controlling and refining Bézier curve points that intersect any of the above obstacles is focusing on the collision check first with a cell-pixel and second with the circle that surround and tangent this pixel (Figure 5.5.8.2.1c).In a more extensive description, upon finalized optimal Dijkstra paths (Figure 5.5.8.2.1a), the Chaikin's corner cutting algorithm is applied to obtain the first curved paths and also to increase the control points for the first Bézier curve delineation. The first collision check with the rectangular areas (pixels) considered as obstacles is applied and a circle with radius $\sqrt{2}$ x (cell size/2) as tangent to the pixel is drawn (Figure 5.5.8.2.1c). The second collision check with the circle and the first Bézier curve points is applied and the points that are included in the circle are switching their coordinates with the closest points of the circles' perimeter as it is presented in (Figure 5.5.8.2.1c) until the algorithm checks that no other control points collide with any obstacles. When all of the first Bézier curve control points are calibrated, the second and final Bézier curve is applied in order to delineate the final smoothed line avoiding all possible obstacles (Figure 5.5.8.2.1).

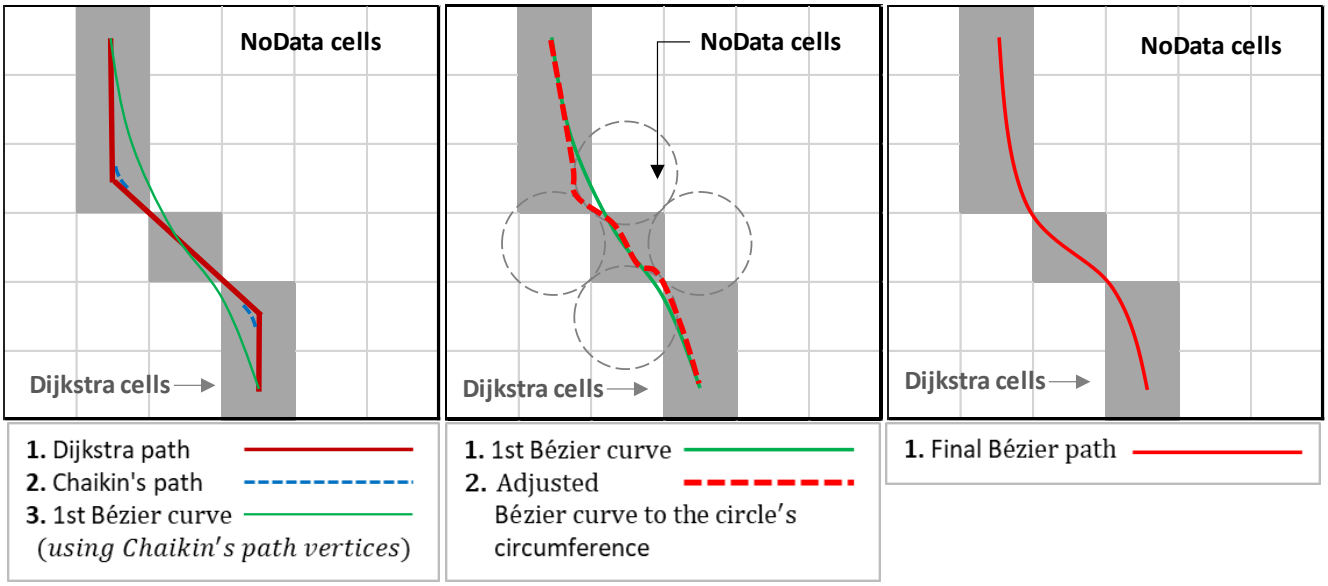


**Figure 5.5.8.2.2:** Transmission lines Bézier curve delineation based on the initial Dijkstra path, the Chaikin's path and the NoData circles' circumference

This procedure differs when considering the trajectories smoothing techniques upon non-homogenous raster surfaces (Transmission line paths) where the optimal Bézier curves are "forced" to lay withing the area of the optimal Dijkstra path to avoid potential differentiations in

the results optimal costs (the sum of the edge weight). An illustration of this procedure is presented in Figure 5.5.8.2.2.

## 5.6 Levelized Cost of Energy (LCoE) and Net Present Value (NPV) model

The Levelized Cost of Energy (LCoE) is the most common economic metric for comparing the cost of different generation types, measured in terms of cost per unit energy output (€/MWh). LCoE is the minimum cost of one unit of electricity (MWh) produced by an OWF averaged throughout the useful life span which is estimated based on Equation 5.6.1, where $C_I$ is the total investment cost per unit marine area (including cost of turbine, grid connection, turbine foundation and installation costs) in €/km$^2$, $C_{om}$ is the annual operation and maintenance cost per unit marine area in €/km$^2$/y, a is the annuity factor and *AEP* is the mean annual power production (MWh) generated from a specific turbine type in one year (Cockerill et al. 2001; Moller et al. 2012).

$$LCoE = \frac{C_I + \sum_{t=1}^{L} \frac{C_{om}}{(1+i)^t}}{\sum_{t=1}^{L} \frac{AEP}{(1+i)^t}} \quad (5.6.1)$$

where *L* is wind farm life span in years, *i* is the discount factor and *t* is the operational year. Twenty to twenty-five years of technical and economic lifetime (*t*) is assumed for a 2 - 7% annual discount rate (*i*). When working with LCoE, it is important to highlight the difficulty to obtain precise costs for individual existing WTs or planned OWFs due to commercial sensitivities, lack of information or technological development or deficit from year to year (i.e., variable O&M costs, energy production decline etc.) or even potential differences in the electricity celling price. For this purpose, the cash flows arising at different temporal scales are converted to a common reference point (year) by using the following net present value (NPV) formula (Levitt et al. 2011; Shaffie et al. 2016):

$$NPV = FiT\ E_{out}\left[\frac{(1+r)^n-1}{r(1+r)^n}\right] - C_I\left[1 + C_{o\&m}\frac{(1+r)^n-1}{r(1+r)^n}\right] \quad (5.6.3)$$

where *FiT* is the electricity celling price, $E_{out}$ is the annual energy generated by an offshore wind turbine, $C_I$ is the initial investment cost (CAPEX), $C_{o\&m}$ is the operation and maintenance cost of an offshore wind turbine, *r* is the interest rate and finally, *n* is the total lifetime of an offshore wind project. It is noticed that both Equations 5.6.3 and 5.6.4 are the key primary objectives embedded to the spatial optimization framework that will be further discussed in next Section.

## 5.7 Offshore Wind Farm site prospecting and multi-objective optimization

Formulating an optimization problem generally contains three basic steps: defining decision variable(s), formulating objective function(s) and defining problem constraint(s). The model is non-linear if the objective function and/or some of the constraints are non-linear. Moreover, Gabriel et al. (2006) highlight in their model the class of quadratic problems as part of non-linear problems, however, the relaxed version of these problems are simply convex, quadratic programs with linear constraints and thus represent a reasonable computational burden given the state of the art in optimization solvers. In order to solve multi-objective optimization problem two main processes can be applied in general, i) the weighting method and ii) the constrained method (Gabriel et al. 2006). The proposed algorithm is characterized as an Integer Quadratically Constrained optimization problem based on Branch and Bound algorithm upon linear constraints and multiple factors modelling of weighted summation to do the superposition calculation. The entire optimization scheme is implemented using *Gurobi* optimization package (Gurobi Optimization, 2018).

Since the problem is characterized as «*Integer*», a Boolean model is used where the decision variables are associated to each potential WT location in a Binary form where the values of 0 and 1 are expressed as the suitability or non-suitability of a cell as part of the solution. This is translated as a combination of the minimization of either the LCoE or the NPV values and Compactness for each selected cluster of cells. Whether, a cluster is part of an optimal solution

means that each cell *i,j* of each cluster formulates the minimum values of LCoE (or maximum NPV) in a way that the total perimeter of all selected cells is minimized (see Figure 5.7.1).

Start spatial optimization process (OWF_INLP_.py)
- Import gurobi, numpy, gdal, shapely
- **Define model parameters**
  - Number of total clusters (TOTAL_CLUSTERS)
  - Offshore Wind Farm Capacity required (TOTAL_MW)
  - Criteria weights ($W_k$)
  - Define whether is a Minimization or Maximization problem (*Min_Max*)
  - Normalization scheme
- **Create model object**
  - Add variables $X_{i,j}$ for any *i* in (0, Rows+1) and *j* in (0, Columns+1)
  - Add *k* "cost" surfaces values $C_{k,i,j}$ for any *i* in (1, Rows) and *j* in (1, Columns)
  - ***Add Contiguity Lazy constraint*** to check any optimal solution
    - Check contiguity using BFS algorithm for every (*i,j*) in current solution
    - If non-contiguous cells then:
      - sum($X_{i,j}$) <= TOTAL_CELLS-1, for every (*i,j*) in current solution
  - ***Add Optimization Constraints***
    - sum($X_{i,j}$) = TOTAL_PIXELS mega-watts for any *i* in (0, Rows+1) and *j* in (0, Columns+1)
    - sum($X_{0,j}$) = 0, for any *j* in (0, Columns+1)
    - sum($X_{Rows+1,j}$) = 0, for *j* in (0, Columns+1)
    - sum($X_{i,0}$) = 0, for any *i* in (0, Rows+1)
    - sum($X_{i,Columns+1}$) = 0, for any *i* in (0, Rows+1)
  - ***Set Objective***
    - If *Min_Max* = min then:
      - $X_{i,j}(W_1 * C_{0,i,j} + W_2 * C_{1,i,j} + W_3 * C_{2,i,j} + (W_4 *$ (4-sum(*x*[neighbors])))
    - Elif *Min_Max* = max then:
      - $X_{i,j}(W_1 * C_{0,i,j} + W_2 * C_{1,i,j} + W_3 * C_{2,i,j} + (W_4 *$(sum(*x*[neighbors])))
- **Create solution array**
- **Save solution array to raster(s)**

**Figure 5.7.1**: Spatial Optimization algorithm pseudo-code

### 5.7.1 Compactness minimization and Contiguity control

**Minimum compactness index (CP).** Compactness optimization is based on the normalized discrete compactness measure (NDC) (Wenwen et al., 2017) consisting of a simplified approach applied by Kao and Lin, (1996). In this study, compactness index is expressed as the total length

of cluster cells' edges that do not have common borders with any other cluster cell, leading the model to make more regular and rectangular patches. Considering a hypothetical area of 30 cells, Figure.5.7.1.1 illustrates the alternatives and the optimal final solution regarding compactness, for a continuous cluster with size of 5 cells.

Consequently, in Figure 5.7.1.1A-F the four optimal alternatives (minimized total sum), having a value of -211, must be further evaluated based on their compactness. As mentioned above, the most compact cluster is the one with the smallest perimeter which is calculated by the free edges of all cells. Therefore, the first three scenarios (blue color areas) have a cluster perimeter equal to 12, while the fourth is equal to 10 and is the optimal solution. Notable is that the continuity of the optimal solutions is guaranteed without applying the contiguity constraint, because the model seeks to minimize fragmentation and calculate the smallest perimeter (in terms of each cell's free edges). However, with small weights in compactness criteria (i.e. <= 0.1), contiguity is not always guaranteed and fragmented clusters may occur. In addition, due the spatial optimization objective's non-linearity, by increasing the compactness weight, the computational effort to obtain optimal solutions is increasing exponentially.

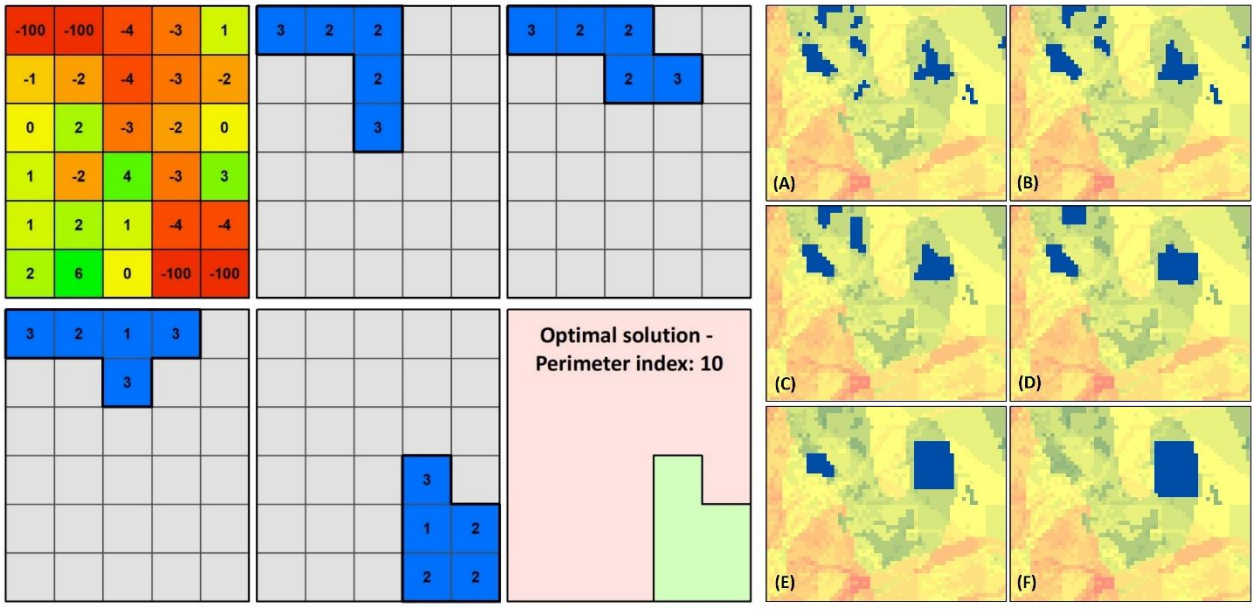


**Figure 5.7.1.1:** Compactness calculation according to the total cluster perimeter minimization (left), different levels of fragmentation and perimeter minimization (A-F, right)

**Contiguity control.** Contiguity control is based on the approach described by Lee, (1961) upon the Breadth-first search (BFS) algorithm for traversing or searching tree or graph data structures. Although the algorithm in the optimization problem is a dynamic programming implementation, the contiguity check is handled as a graph-based problem, considering each potential optimal solution as a graph consisting of edges and nodes. In the current approach, contiguity is not mathematically embedded in the optimization problem rather, it is stated as a necessary property of a valid solution. Consequently, Oehrlein and Haunert, (2017) indicate that the simplest approach following this strategy is to first compute an optimal solution and if the solution satisfies all constraints of the initial model, the solver stops, otherwise solves the problem again until a global optimal solution is carried out.

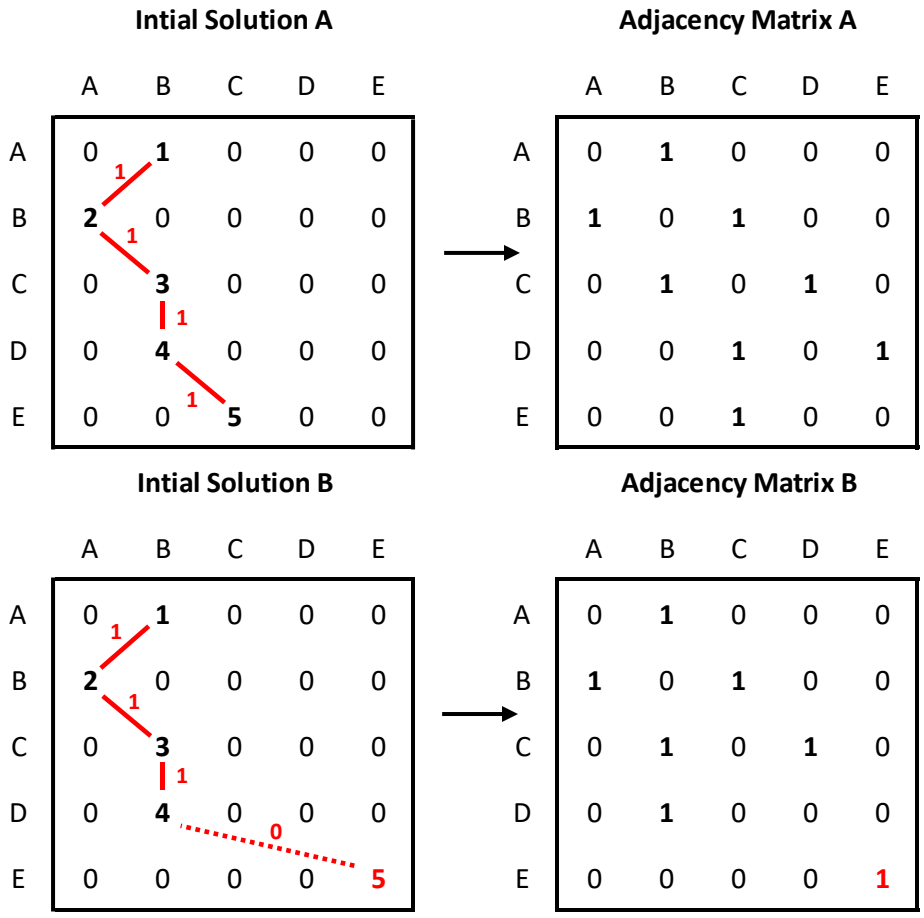


**Figure 5.7.1.2:** Contiguity check using BFS algorithm for each Gurobi optimizer solution

### 5.7.2 Size, data and complexity of the study area

In the proposed model, raster based formatted files are used (e.g., TIFF images) which are transformed into arrays as input for the optimization algorithm. Each raster cell represents either LCoE or NPV values in arrays format. The initial datasets used as inputs for the model are in raster format and the algorithm was tested for a variable spatial resolution with cell sizes of 1000, 2000 and 5000 meters.

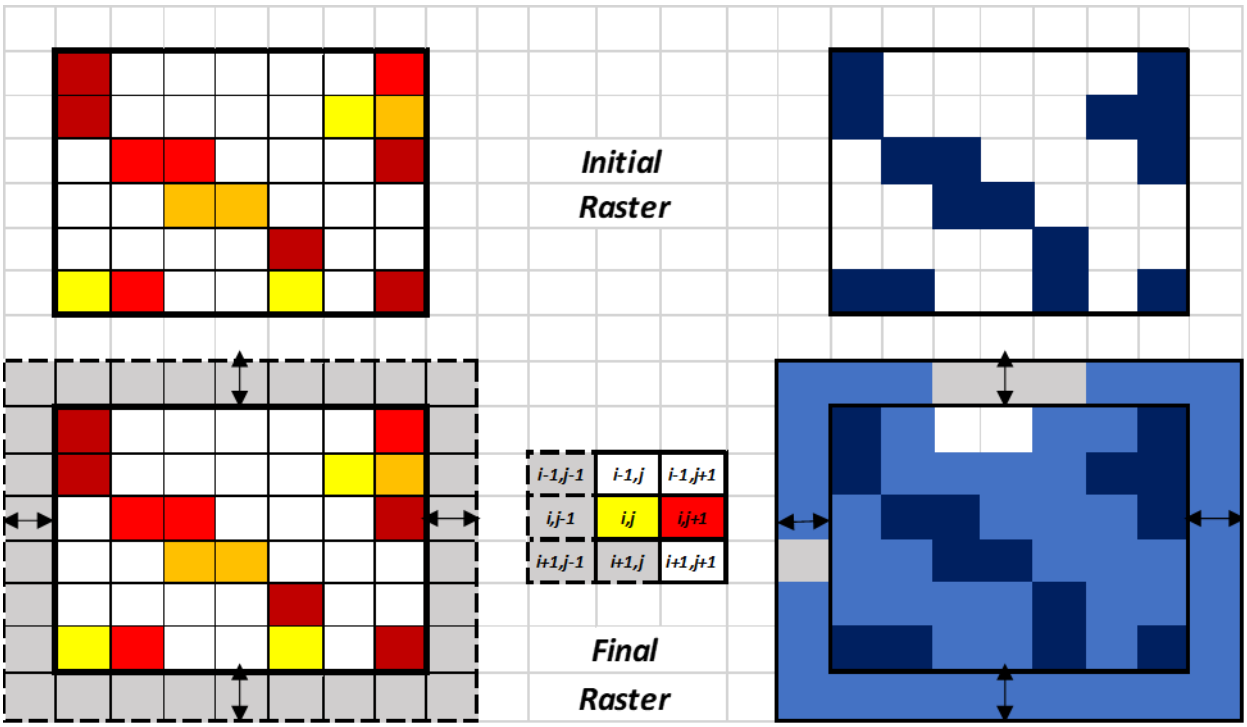


**Figure 5.7.2.1:** (Left) Initial raster array image with decision variable $C_{i,j}$ and (Right) Customized final raster array with decision variable $X_{i,j}$ (binary) that calculates all available neighbors participating in compactness and perimeter calculations

Compactness calculation for each cell state is affected by neighboring cell's state regarding ecological sensitivity index. For our model, we express as neighborhood of a cell the two-dimensional square lattice composed of a central cell and its eight adjacent cells (Von Neumman Neighborhood) (Fotakis & Sidiropoulos, 2012). Among the total number of cells, NoData values

of the raster file are not included but the model is capable to handle them in spite the fact that these values do not participate in the final optimal solution. These can include borders, backgrounds, the sea or other data considered to not have valid values.

Therefore, we have to customize the model to be able to search for an optimal solution above or near the boundary cells of the study area considering that the initial input raster is expressed as $C_{i,j}$ for *i* as the total number of rows and *j* as the total number of columns. In order to be able to account cross defined neighbors for the cells above the coastline we must add two additional rows and columns forming a final raster dataset $X_{i,j}$ for i = i + 2 and j = j + 2 as it is showed in Figure 5.7.2.1. Finally, the IQCP model contains 115345 discrete variables (binary) and 35234 constraints.

### 5.7.3 Decision variables, Objectives and Constraints

**Minimum LCoE index**. Levelized Production Cost index, and therefore, suitability of a cell i,j for WT sitting considering the minimization of the cost is expressed as the identification of minimum values for LCOE for a cell considering the values of its neighbor cells.

**Maximum Net Present Value index.** Model's second objective is based upon the maximization of NPV for future OWF site-prospecting. Thus, areas with negative NPV values are excluded from the optimization algorithm.

**Maximum compactness of OWF siting areas.** In this study, the maximum compactness is accomplished by minimizing the total cluster's perimeter. The continuity of the resulted cluster cells is guaranteed because the model seeks the minimum perimeter.

**Multiple factors optimization.** For a problem with consideration of multiple factors, the objective function of the model should be modified adding the weight factor of each objective and can be expressed as:

$$Minimize = \sum_{(i,j\in C)}(w_{\mathrm{LCoE}}(\mathrm{LCoE5}_{i,j}x_{i,j,1} + \mathrm{LCoE8}_{i,j}x_{i,j,2} + \mathrm{LCoE10}_{i,j}x_{i,j3})) + \sum_{(i,j\in C)}(w_{Perim}x_{i,j,0}V_{i,j}) \quad (5.7.3.1)$$

$$V_{ij} = M - \frac{M}{4}(x_{i,j-1,0} + x_{i,j+1,0} + x_{i-1,j,0} + x_{i+1,j,0}) \quad (5.7.3.2)$$

$$Maximize = \sum_{(i,j\in C)}(w_{NPV}(NPV5_{i,j}x_{i,j,1} + NPV8_{i,j}x_{i,j,2} + NPV10_{i,j}x_{i,j3})) + \sum_{(i,j\in C)}(w_{Perim}x_{i,j,0}V_{i,j}) \quad (5.7.3.3)$$

$$V_{ij} = \frac{M}{4}(x_{i,j-1,0} + x_{i,j+1,0} + x_{i-1,j,0} + x_{i+1,j,0}) \quad (5.7.3.4)$$

where *x* is the set of all raster cells$_{i,j}$ with total I rows and J columns, $w_{perim}$ is the weight for compactness, $w_{LCOE}$ and $w_{NPV}$ are the weights for the Levelized Production Cost and Net Present Value respectively. For each cell *i,j*, $LPC_{i,j}$ and $NPV_{i,j}$represent the values of the Levelized Production Cost and Net Present Values of the 5, 8 and 10 MW wind turbines respectively. Finally, $V_{ij}$ represents the total cell edges contribute to the cluster perimeter; $x_{i,j,wt}$ (for *wt* = 0,1,2,3) is a binary variable (0 or 1) that represents whether the cell *ij* belongs to final cluster or not and *M* is the maximum value of the normalization scale for both of the objectives. For *wt = 1* the 5 MW wind turbines are contributing to the optimal solution, for *wt = 2* or *3* the 8 and 10 MW wind turbines are part of the solution and finally *wt = 0* consists of all optimal combinations for the different WT types.

**Optimization constraints:** The seven constraints for the proposed model ensure: i) the total number of selected optimal cells, equal to the desired size of the OWF (in MW) (Equations 5.7.3.3-4), ii) none of the optimal cells exist at a pseudo-row or a pseudo-column of the raster (Equation 5.7.3.6-9), iii) in each cell only one type of WTs (5, 8 or 10 MW multiplied by the total number of WTs per cell) is allowed to be placed (Equation 5.7.3.5) and iv) the contiguity (referred as Lazy constraint callback via Gurobi optimizer) of the optimal solutions (Equation 5.7.3.10).

$$\sum_{(i,j\in P)}(MW5_{i,j}x_{i,j,1} + MW8_{i,j}x_{i,j,2} + MW10_{i,j}x_{i,j,3}) \leq l_b TOT_{MW} \quad (5.7.3.3)$$

$$\sum_{(i,j\in P)}(MW5_{i,j}x_{i,j,1} + MW8_{i,j}x_{i,j,2} + MW10_{i,j}x_{i,j,3}) \geq u_b TOT_{MW} \quad (5.7.3.4)$$

$$\sum_{(i,j\in P)}(x_{i,j,wt}) = 1 \text{ , for } wt \in (1,3) \quad (5.7.3.5)$$

$$\sum_{j=0}^{J+1} x_{0,J,0} = J + 2 \quad (5.7.3.6)$$

$$\sum_{j=0}^{J+1} x_{I+1,J,0} = J + 2 \quad (5.7.3.7)$$

$$\sum_{i=0}^{I+1} x_{i,0,0} = J + 2 \quad (5.7.3.8)$$

$$\sum_{i=1}^{I+1} x_{i,J+1,0} = J + 2 \quad (5.7.3.9)$$

where $x_{I,J,wt}$ is the set of all raster cells$_{i,j}$ including 2 pseudo-rows and 2 pseudo-columns at the start and the end of the raster extent with total I+2 rows and J+2 columns, $MW_{i,j}$ is the total sum of MW of installed capacity per cell considering the 5, 8 and 10 MW wind generators, $TOT_{MW}$ is the total installed capacity of each OWF and finally, $l_b$ and $u_b$ are the lower and upper bounds of the total installed capacity ($TOT_{MW}$). Focusing on the contiguity constraint, Equation 5.7.3.8 defines that the sum of the edges (between cells *i,j*) in each solution must be equal to the number of the total cells participating in the current solution minus 1, as defined by the BFS algorithm and is expressed as:

$$\sum_{(i,j \in S)} x_{i,j,wt} = N - 1 \quad (5.7.3.10)$$

where $S \dot{\subseteq} C$ is an alternative solution but with non-continuous raster cells. An outline of the spatial optimization scheme is illustrated in Table 5.7.3.1 in the form of a pseudocode denoting the appropriate steps to be followed for exporting all optimal clusters (OWFs) in the form of raster files, referred as the solution array.

## 5.8 SDSS interface set-up

The last chapter of this Section discusses the development of a Python-based Graphical User Interface (GUI) for the proposed SDSS. The SDSS (**SpOWNED-Opt**) incorporates the following procedures: data pre-processing, data analytics, spatial-explicit cost models, spatial optimization algorithms, wind speed probabilistic assessment and wind power simulation embedded in a graphical user interface (GUI). The aforementioned components have a wide range of interoperability characteristics as long as data objects can represent a spatial dataset (vector or raster), a number (parameter), a model as a stand-alone script or a shared function. In particular, Figure 5.8.1 illustrates the complete framework of **SpOWNED-Opt** with the modules and their integration methods using Python libraries.

The pre-processing module performs all spatial configurations needed (i.e., reprojections, masking and clipping, rasterization and resampling) and sends the spatially calibrated data to the exclusion analysis core module, followed by the cost evaluation and offshore wind assessment and wind power simulation modules. The final spatial optimization module calculates the optimum strategy and saves the optimal solution(s) in the form of maps. Then, the optimal solution(s), along with the previous modules' exports, are stored and saved in the predefined user's folders comprising of the raster and vector outputs, charts and tables for the cost and energy-based calculation rules, as well as the reports from the spatial optimization algorithms, including the LCP and the Integer Programming algorithms.

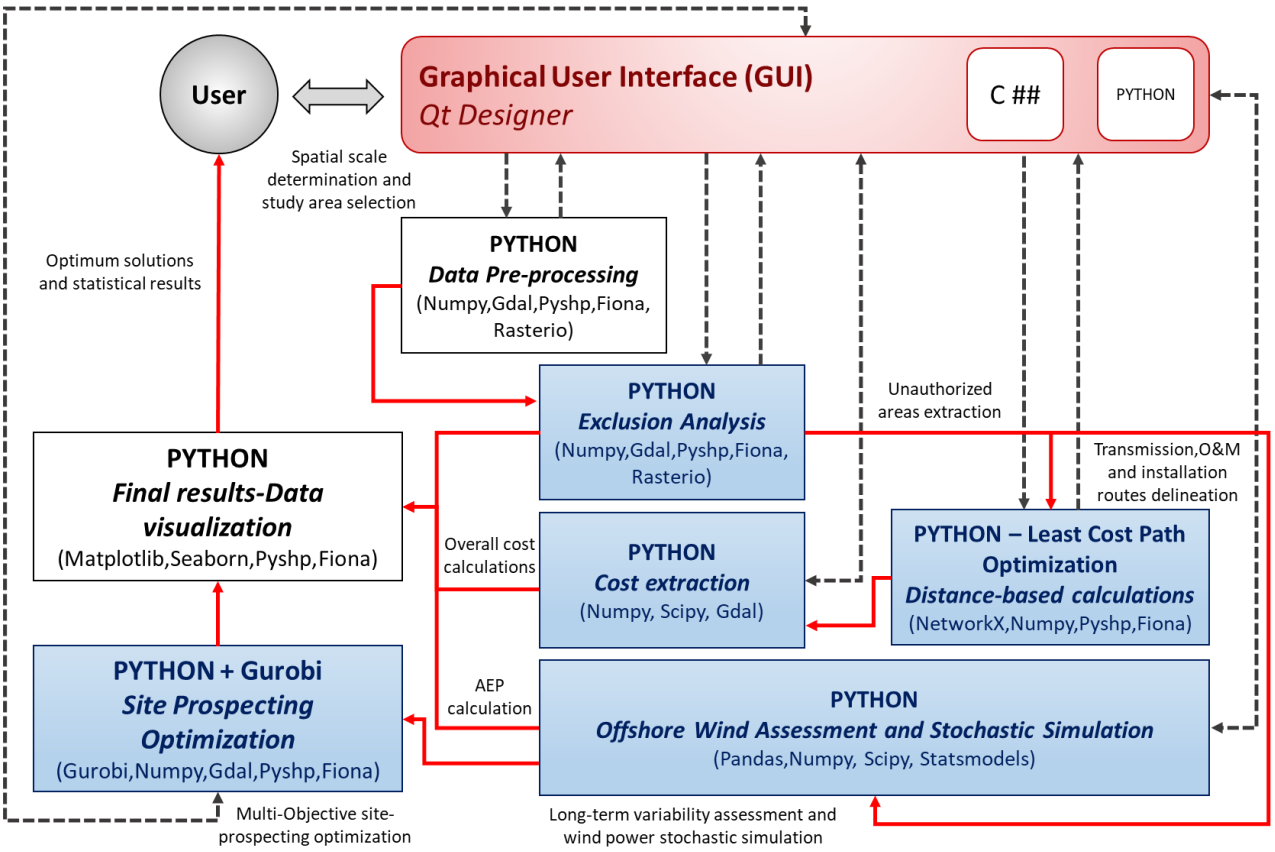


**Figure 5.8.1**: SDSS and the Graphical User Interface (GUI) outline and computing tools used for the implementation

Normally, setting-up GUI can be thought of as a combination between programming and graphic design configurations. Deeper knowledge of a user's needs is crucial for both usability and graphical appearance purposes. A GUI application generally consists of a main window and most

of the times one or more dialog boxes. The main window usually incorporates a menu bar, a status bar, and other widgets whereas a dialog box is made up of buttons and is created to communicate information to the user and prompt them for inputs and outputs. Thus, the programming part of a GUI is often a matter of finding the right components, to complete a task, and then applying the necessary programming steps to make them operational. Focusing on the technical aspects of the SDSS, Qt Designer (https://doc.qt.io) and PyQt5 (https://pypi.org/project/PyQt5/) are used in order to set-up the GUI environment.

Qt Designer is the Qt tool for designing and building GUIs with Qt Widgets. Both windows and dialogs boxes can be composed and customized in a what-you-see-is-what-you-get (WYSIWYG) manner and test them using different styles and layouts. Typically, there are two methods to build an application interface. The first method is a pure code implementation, and the second method is to draw UI (User Interface) using the Qt Designer Tool and each UI element is known as a Widget. Using the Qt Designer application's drag and drop interface, the developer is able to create and customize dialogs, windows, and widgets. This means that rather than spending a huge amount of time on layout and design, someone can get into coding the functionality of an application much faster. Consequently, a combination of pure code and Qt Designer can be used, using the visual tool to create the layout, and importing it into another script, adding another layer of functionality on top of the design. An illustration of the Qt Designer main window is shown in Figure 5.8.2 where the following elements are categorized as:

1. The **Form Editor** stands for the visual representation of the form;
2. The **Widget Box** containing all widgets that can be used in a form;
3. The **Object Inspector** which displays the form as a hierarchical tree;
4. The **Property Editor** which enumerates the properties of the selected widgets;
5. The **Action Editor/Signal & Slots Editor** in order to handle the connections multiple objects.

**QWindow:** When creating a GUI application, windows and dialogs are the most important elements to handle. The window generally consists of menus, a toolbar, and other kinds of widgets within it that can often act as the main interface in a GUI application.

**QDialog:** Using dialog boxes in an application can make it both easier to develop a GUI and for the user to better understand and navigate through an application. A dialog box will appear when the user needs to be prompted for additional information in order to continue, often to gather input such as an image or a file. That value could then be used to save a file, close a document, or cancel an action. Dialog boxes can also be used to display options or information while a user is working in the main window. Dialogs are the top-level window (often pop up), mostly used for short-term tasks and brief communications with the user. This may include checkboxes, radio buttons, text input, and other features.

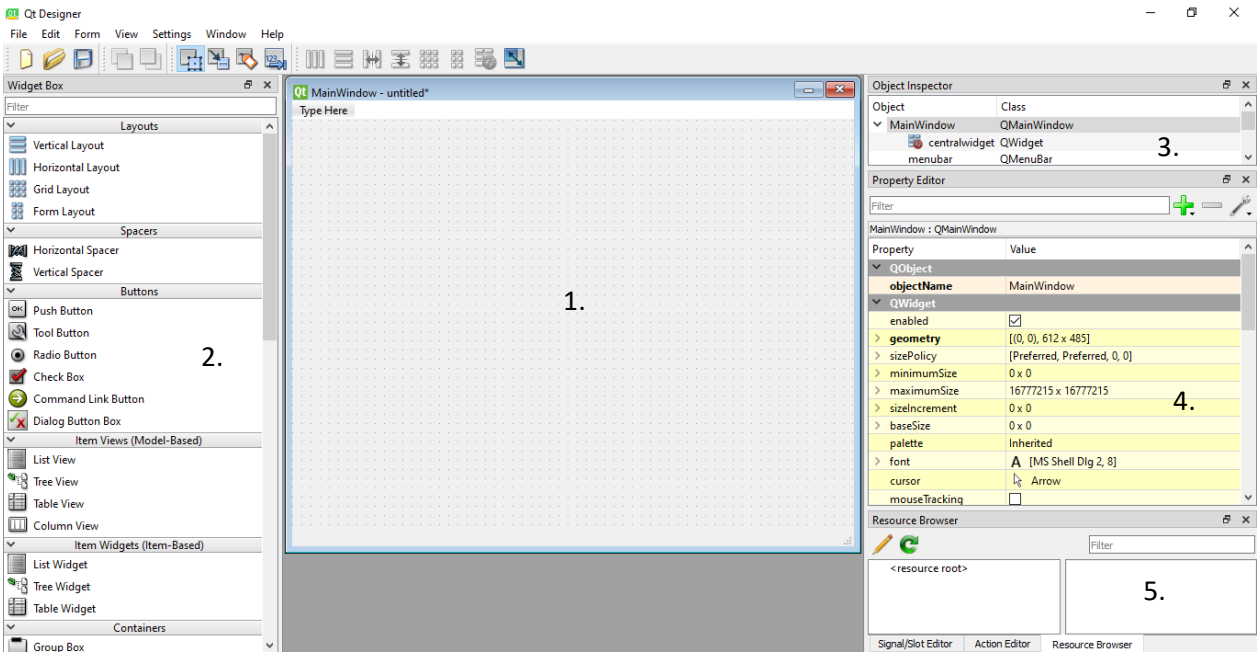


**Figure 5.8.2**: QT Designer user interface including: 1) the form editor, 2) the Widget object, 3) the object inspector, 4) the property editor and, 5) the actions, slots and signals editor

**QWidgets:** In computer programming, a widget is an element of a graphical user interface that displays an information arrangement changeable by the user. Widgets are interfaces used for tasks and communications with the user. GUI widgets span a large range of interaction solutions: selecting a file; triggering an action; choosing options; or even direct manipulation of graphical objects. The defining characteristic of a widget is to provide a single interaction point for the direct manipulation of a given kind of data. Widgets are basic visual building blocks, which, combined in an application, hold all the data processed by the application and the available interactions on this data. Basic widgets include, and are not limited to, buttons, labels, text

editors, scroll bars, progress bars, radio buttons, and check boxes. For example, a custom widget could include three checkbox widgets, two button widgets, and a text editor widget. The appropriate widgets and useful concepts that are covered in this chapter include:

- **QLabel** for labelling different widgets, adding titles, names or descriptive characteristics
- **QPushButton** is one of the most common widgets for giving computer simple commands
- **QRadioButton** as an option button that can be switched on (checked) or off (unchecked)
- **QCheckBox** which can act as a binary switch button.
- **QLineEdit** and **QPlainTextEdit** which give the user fields to input information (messages, store input and output paths etc.)
- **QMessageBox** is useful for displaying alert messages, procedures processing, log outputs etc.
- **QProgressBar** uses the concept of steps by specifying the minimum and maximum possible step values for displaying the percentage of steps that have been completed during a process.

**QSignals:** A feature of the Qt framework is its event loop implementation allowing the code to be triggered when certain events occur, for instance a key being pressed or an on-screen button being clicked. QSignals are translated in "signals and slots" where the signals are “triggered” when a particular event occurs, and these can be connected to one or more slots, which define the actions to be taken.

**QThread:** Qt class provides a platform-independent implementation of threads. A QThread represents a separate thread of control within the application; it shares data with all the other threads within the process but executes independently in the way that a separate program does on a multitasking operation system. Implementing a new thread just requires denning a class that inherits from QThread class and implementing its run() method. Then, when a new thread is to be created, the previously defined class has to be instantiated, and the start() method has to be called to begin the execution of the new thread. When the thread has been set up, it calls the previously defined run() method. Execution of the thread ends when it returns from this method.

Each QThread can have its own event loop, which can be started calling exec() from run() method. Having an event loop in a thread makes it possible to connect signals from other thread to slots in this thread, using a mechanism called queued connections, which allows communication between threads.

The integration of the above-mentioned functionalities is demonstrated in Figures 5.8.3 - 4 where the Qt Designer outputs along with the PyQt5 sample codes are discussed. For each one of the sub-modules in the GUI, the following logic is followed: i) the user imports the main spatial data regarding the offshore wind farm and the task to be completed, for instance, the bathymetry raster in order to calculate the foundations' manufacturing cost, the UERRA reanalysis wind data to estimate the wind power production etc. and secondly, ii) the user introduces additional inputs (as parameters) for each task such as the cost of steel for the manufacturing cost, the hub height, the rotor diameter and the wind turbine capacity for the energy assessment and simulation. In fact, the user is not expected to know deeply about specific variables, and the intention is to perform the calculations with the minimum number of the variables needed. For this reason, all models are provided to the user at different scalability levels, in terms of the difficulty and the complexity for estimating the life-cycle costs, the non-suitable areas and the produced energy. In brief some key characteristics and further insights of a GUI are expressed as follows:

1. The GUI presents a progression of tabs that follow the spatial modelling processes, input parameters set-up, input and output storage paths, simulation control and monitoring and results visualization;
2. The user either accepts the defaults for various parameters, or makes modifications to the relevant input data;
3. The user launches the spatial modelling functions via a button click and supervises the algorithms' execution via the dialog boxes;
4. Results can be monitored in real-time as they are produced by each code and store all of the results in the pre-defined folders.

An example of the wind power simulation dialog box is presented in Figure 5.8.3 where some of the aforementioned widgets are integrated by allowing the user to set the input and

output data, select wind turbine models, method to estimate the produced energy (simplified or analytical), the "*run*" button and the message box as also, the results display widget. Once each structural part of the GUI is created, including the Main Window and all Dialog Boxes as illustrated in Figure 5.8.3, the file is saved with the extension *.ui* for storing all GUI graphical elements.

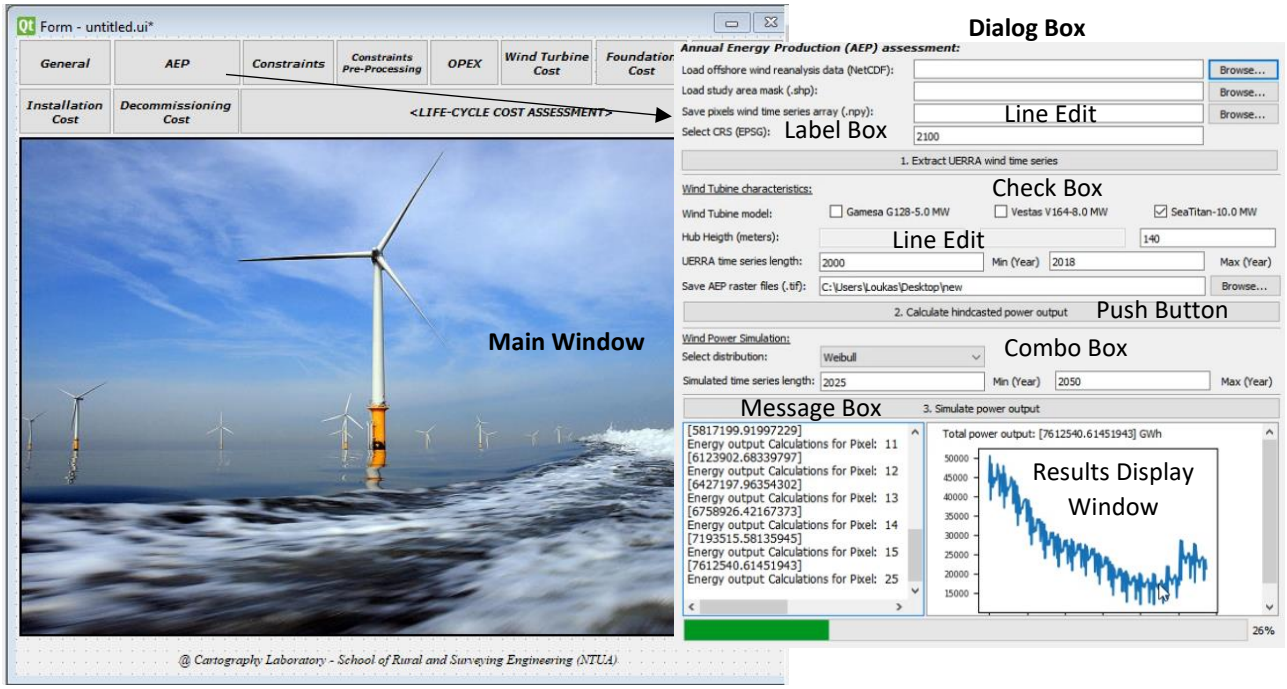


**Figure 5.8.3:** Qt Designer representation of the main GUI Window and an indicative Dialog Box

However, all of the GUI elements are not still activated. To succeed that, an additional Python binding is needed in order to connect/activate each Qt Designer window, the dialog box and connect each widget to a specific functionality. There are two primary Python bindings for the Qt Designer, PyQt and PySide. PyQt is developed by Riverbank Computing (PyQt5 Reference Guide) and allows Python to access almost all of the functionality of Qt Designer. Thus, PyQt5 provides the common ground between Python and a windowed GUI, as exported from the Qt Designer (*.ui* file). Hence, PyQt5 consists of a library of methods for connecting different windows, widgets, buttons, etc. and Figure 5.8.4 illustrates a set of classes and functions for loading a *.ui* file and connecting anything that is included to the Dialog Box with a particular functionality (if needed).

a.

```
class Ui(QMainWindow): #Set Main GUI Window class
     def __init__(self):
          super(Ui, self).__init__()
          uic.loadUi('C:\\MainGUI.ui', self) #Load .ui file
          self.setWindowTitle("SpOWNED-Opt") #Set title to the main window
          self.button = self.findChild(QToolButton, 'toolWT') #Find parent Window
          self.button.clicked.connect(self.OpenWindow)
          self.show()

     def OpenWindow(self):
          app = QApplication(sys.argv)
          ex = OnMWindow()
          ex.exec()
```

b.

```
class OnMWindow(QDialog):
    def __init__(self):
        super(OnMWindow, self).__init__()
        uic.loadUi('C:\\Turbines.ui', self)
        self.setWindowTitle("Wind Turbines Cost Calculation") #Set window title
        self.show()
        self.labelButtonTextMW = self.findChild(QLabel,'label1') #Identify label
        self.addbuttonMW = self.findChild(QRadioButton,'radio0') #Identify radio button
        self.loadButtonTextMW = self.findChild(QLineEdit,'line0') #Identify line text
        self.addbuttonMW.toggled.connect(self.enable) #Do something on button click
        self.group = QButtonGroup() #Create buttons group
        self.group.addButton(self.addbuttonMW)  #Add to buttons group
        self.group.addButton(self.addbuttonCostAnalytical)
        #Identify push button
        self.addbutton_In = self.findChild(QPushButton,'pushLoad')
        self.addbutton_In.clicked.connect(self.browse_data) #Call function on click
        self.addbutton_Out = self.findChild(QPushButton,'pushLoad2')
        self.addbutton_Out.clicked.connect(self.save_data) #Call function on click
        self.runmsg = self.findChild(QPlainTextEdit,'plainText') #Display messages
        self.runbutton_WT = self.findChild(QPushButton,'pushWTCost') #Run module
        self.runbutton_WT.clicked.connect(self.Send_WT_Cost) #Call main function
```

c.

```
def Send_WT_Cost(self):
         objWorker = Worker() #Set the Worker Class to send the function
         thrWorker = QThread(parent=self)
         Input_Rasters = str(self.load_Inras.text()) #Get input raster path as text
         Output_Rasters = str(self.load_Outras.text()) #Get output raster path as
text
         objWorker.moveToThread(thrWorker)
         #Pass arguments to the function
         thrWorker.started.connect(partial(objWorker.WT_cost,Input_Rasters,
Output_Rasters)
```

d.

```
class Worker(QObject):  #Initialize Worker Class object
    mySignal = pyqtSignal(str)  #Messages data types as strings
    def __init__(self, parent=None):
        super(Worker, self).__init__(parent)
        self._stopped = True
        self._mutex = QMutex()

    @pyqtSlot()
    def WT_cost(self,Input_Rasters,Output_Rasters): #Pass function's arguments
        #Pass messages to the display window
        self.mySignal.emit("Opening surface raster...")
        FUNCTION CALCULATIONS.....  #Run function to open and save raster dataset
        self.mySignal.emit("Cost raster is saved!")
```

**Figure 5.8.4:** PyQt5 code representation for: a) loading the Main Window (*.ui*), b) loading the Dialog Box, reading all widgets included and linking widgets to c) specific functions or d) classes (Workers) with specific functionality (i.e., estimate WT cost)

The functions of Figure 5.8.4 use directly the PyQt5 facilities to load a GUI as a *.ui* file and add title (Figure 5.8.4a), to access all available widgets included in the *.ui* file and link these widgets to a particular functionality, for example, to load or save files and folders when clicking a button, to call a specific function and model or to display messages (Figure 5.8.4b). Furthermore, Figure 5.8.4c presents how to pass arguments from the GUI (e.g., a text box with an input path) to certain functions or how to update (emit) messages as signals linked to specific text message boxes.

Finally, Figure 5.8.4d, similarly to Figure 5.8.4c, presents a class's interoperability to a particular function (Figure 5.8.4c), labeled as Worker threads, which are secondary threads of execution that one can use to offload long-running tasks from the main thread (the GUI execution primal thread) and prevent GUI freezing (PyQt5 Reference Guide). Based on the aforementioned functionalities, all dialog boxes are connected to the Main Window and all models described in the previous sub-sections are integrated via Python programming language and embedded to the GUI as a separate Dialog Box, as presented in Figure 5.8.3. The visual representations and the codes for all of the sub-modules of the GUI are provided in Appendix III Section of the dissertation.

## References


1. **Ahn D., Shin S.C., Kim S.Y., Kharoufi H., and Kim H.C., (2017):** Comparative evaluation of different offshore wind turbine installation vessels for Korean west-south wind farm, *International Journal of Naval Architecture and Ocean Engineering*:9(1);45-54
2. **Antikainen H., (2013):** Using the Hierarchical Pathfinding A* Algorithm in GIS to Find Paths through Rasters with Nonuniform Traversal Cost, *ISPRS Int. J. Geo-Inf*., 2;996-1014
3. **Bagiorgas H.S., Mihalakou G., and Rehman S., (2012):** Offshore wind speed and wind power characteristics for ten locations in Aegean and Ionian Seas, *J. Earth Syst Sci*:121:975-987
4. **Baring-Gould I., (2014):** Offshore Wind Plant Electrical Systems, BOEM Offshore Wind Renewable Workshop, National Renewable Energy Laboratory (NREL)

5. **Beiter F., Musial W., Smith A., Kilcher L., Damiani R., Maness M., et al., (2016):** A Spatial-Economic Cost Reduction Pathways Analysis for U.S Offshore Wind Energy Development from 2015-2030, National Renewable Energy Laboratory (NREL), Task No.WE15.CA02 (Technical Report)
6. **Bjerkseter C., and Ågotnes A., (2013):** Levelised cost of energy for offshore floating wind turbine concepts. Department of Mathematical Sciences and Technology, University of Life Sciences; p. 206.
7. **Borrmann R., Rehfeldt K., Wallasch A.K., and Lüers S., (2018):** Capacity Densities of European Offshore Wind Farms, Report produced by Deutsche WindGuard GmbH, Coherent Linear Infrastructures in Baltic Maritime Spatial Plans, Interreg Baltic Sea Region – Project Baltic LINes
8. **Bosch J., Staffell I., and Hawkes A.D., (2019):** Global levelised cost of electricity from offshore wind, *Energy*:189
9. **Burnecki, K., Misiorek, A., and Weron, R., (2005):** in Statistical Tools for Finance and Insurance (ch.13: Loss Distributions), ed. P. Čižek, W. Härdle, & R. Weron (Berlin: Springer),289
10. **Campisi-Pinto S., Gianchandani K., and Ashkenazy Y., (2020):** Statistical tests for the distribution of surface wind and current speeds across the globe, Renewable Energy:149:861-876
11. **Carta J.A., Ramírez P., and Velázquez S., (2009):** A review of wind speed probability distributions used in wind energy analysis: Case studies in the Canary Islands, *Renewable and Sustainable Energy Reviews*:13:933-955
12. **Cavazzi S., and Dutton A. G.(2016)**: An Offshore Wind Energy Geographic Information System (OWE-GIS) for assessment of the UK's offshore wind energy potential, Part 1, *Renew. Energ.*: 87;212–228
13. **Chaikin G., (1974):** An algorithm for high speed curve generation, *Computer Graphics and Image Processing*:3;346–349
14. **Chiodo E., and De Falco P., (2016):** Inverse Burr distribution for extreme wind speed prediction: Genesis, identification and estimation, *Electric Power Systems Research*:141:549-561
15. **Cole S., Marinot P., Rapoport S., Papaefthymiou G., and Gori V., (2014):** Study of the benefits of a meshed offshore grid in Northern Seas region (Final Report), Report prepared by Tractebel Engineering – Ecofys - PWC, European Commission
16. **Damiani R., Dykes K., and Scott G., (2016):** A Comparison Study of Offshore Wind Support Structures with Monopiles and Jackets for U.S. Waters, National Renewable Energy Laboratory (NREL), *The Science of Making Torque from Wind (TORQUE 2016)*, Munich, Germany, October 5-7
17. **de Vries, W. (2011):** Final report WP 4.2 - Support Structure Concepts for Deep Water Sites. Delft: Delft University of Technology.
18. **Deligiannis I., Dimitriadis P., Daskalou O., Dimakos Y., and Koutsoyiannis D., (2016):** Global investigation of double periodicity of hourly wind speed for stochastic simulation; application in Greece, *Energy Procedia*:97;278-285
19. **Desmond C., Murphy J., Blonk L., and Haans W., (2016):** Description of an 8 MW reference wind turbine, *Journal of Physics: Conference Series*:753
20. **Dicorato M., Forte G., Pisani M., and Ttrovato M., (2011):** Guideliness for assessment of investment cost for offshore wind generation, *Renewable Energy*:36;2043-2051
21. **Dimitriadis P., and Koutsoyiannis D., (2015):** Application of stochastic methods to double cyclostationary processes for hourly wind speed simulation, *Energy Procedia*:76;406-411

22. **Dimitriadis P. G., (2017):** Hurst-Kolmogorov dynamics in hydrometeorological processes and in the microscale of turbulence, Ph.D. thesis, Department of Water Resources and Environmental Engineering, National Technical University of Athens, Greece
23. **Dimitriadis P., and Koutsoyiannis D., (2018):** Stochastic synthesis approximating any process dependence and distribution, *Stochastic Environmental Research and Risk Assessment*:32: 1493-1515
24. **Smith G., Drunsic M., Reynolds P., and Whitmore A., (2016):** Assessment of Offshore Wind Farm Decommissioning Requirements, Report prepared from DNV-GL for Ontario Ministry of the Environmental and Climate Change
25. **Energinet, (2015):** Offshore Wind Farms at Vesternhav Nord, Vesterhav Syd, Saeby, Sejero Bugt, Smalandsfarvandet and Bornholm, Technical Project Description for Offshore Wind Farms (200MW), Report
26. **Etherington T.R., (2016):** Least-Cost Modelling and Landscape Ecology: Concepts, Applications, and Opportunities, *Journal of Current Landscape Ecology Reports*:1;0-53
27. **Gabriel S.A, Faria J.A, and Moglen G.E., (2006):** A multi-objective approach to smart growth in land development, *Journal in Socio-Economic Planning Sciences:*40;212 - 248
28. **Equinor, (2018):** Hywind Offshore Wind Floating Project, Equinor - Norwegian state-owned multinational company [last accessed: 16/09/2020]
29. **Fingerish L., Hand M., and Laxson A., (2006):** Wind Turbine Design Cost and Scaling Model. Technical Report NREL/TP-500-40566, National Renewable Energy Laboratory, CO, December 2006.
30. **Fontana C., (2019):** A Multiline Anchor Concept for Floating Offshore Wind Turbines, Ph.D. Thesis, Department of Civil Engineering, University of Massachusetts Amherst
31. **Gaertner E., Rinker J., Sethuraman L., Zahle F., Anderson B., et al., (2020):** Definition of the IEA 15-Megawatt Offshore Reference Wind, Golden, CO: National Renewable Energy Laboratory (NREL)
32. **Gonzalesz-Rodriguez A.G., (2017):** Review of offshore wind farm cost components, *Energy for Sustainable Development*:37;10-19
33. **Gurobi Optimization (2018):** *Gurobi Optimizer*, version 8.0., [last accessed 22 June 2020].
34. **Hu Q. Wang Y., Xie Z., Zhu P., and Yu D., (2016):** On estimating uncertainty of wind energy with mixture of distributions, *Energy:*112:935-962
35. **Ioannou A., Angus A., and Brennan F., (2018a):** A lifecycle techno-economic model of offshore wind energy for different entry and exit instances, *Applied Energy*:221;406-404
36. **Ioannou A., Angus A., and Brennan F., (2018b):** Parametric CAPEX, OPEX, and LCOE expressions for offshore wind farms based on global deployment parameters, *Energy Sources Part B: Economics, and Policy*:13(5);281-290
37. **Ioannou A., Angus A., and Brennan F., (2020):** Stochastic financial appraisal of offshore wind farms, *Renewable Energy*:145;1176-1191
38. **James R., and Ros M.C., (2015):** Floating Offshore Wind: Market and Technology Review, Carbon Trust, Prepared for the Scottish Government
39. **Jin R., Hou P., Yang G., Qi Y., Chen C., and Chen Z., (2019):** Cable routing optimization for offshore wind power plants via wind scenarios considering power loss cost model, Applied Energy, 254;113719

40. **Jung C., Schindler D., Laible J., and Buchholz A., (2017):** Introducing a system of wind speed distributions for modelling properties of wind speed regimes around the world, *Energy Conversion and Management:*144:181-192
41. **Jung C., and Schindler D., (2017):** Global comparison of the goodness-of-fit of wind speed distributions. *Energy Convers. Manag*.:133:216–34
42. **Justus C.G., Hargraves W.R., Mikhail A., and Graber D., (1978):** Methods for estimating wind speed frequency distributions. *Journal of Applied Meteorology*:17:350–353
43. **Kaiser M.J., and Snyder B.F. (2012):** Offshore wind energy cost modelling: Installation and decommissioning, Green Energy and Technology, vol.85, Springer
44. **Kao J. J. and Lin H.Y., (1996):** Multifactor Spatial Analysis for Landfill Siting, *Journal of Environmental Engineering*: 122; 902-908
45. **Kausche M., Adam F., Dahlhaus F., and Groobmann J., (2018):** Floating offshore wind – Economic and ecological challenges of a TLP solution, *Renewable Energy*:126:270-280
46. **Kiss P.**, **Jánosi I.M., (2008):** Comprehensive empirical analysis of ERA-40 surface wind speed distribution over Europe, *Energy Conversion and Management*:49:2142-2151
47. **Koutsoyiannis D., Dimitriadis P., Lombardo F., and Stevens S., (2018):** From Fractals to Stochastics: Seeking Theoritical Consistency in Analysis of Geophysical Data, In: Tsonis A. (eds) *Advances in Nonlinear Geosciences*. Springer
48. **Lacal-Arantégui, Yusta J.M., and Domínguez-Navarro J.A., (2018):** Offshore wind installation: Analysing the evidence behind improvements in installation time, *Renewable and Sustainable Energy Reviews*:92;133-145
49. **Lo Brano V., Orioli A., Ciulla G., and Culotta S., (2011):** Quality of wind speed fitting distributions for the urban area of Palermo, Italy, *Renewable Energy:*36:1026-1039
50. **Maienza C., Avossa A. M., Ricciardelli F., Coiro D., Troise G., and Georgakis C. T., (2020):** A life cycle cost model for floating offshore wind farms, *Applied Energy*:266;114716
51. **Mohammadi K., Alavi O., Mostafaeipour A., Goudarzi N., and Jalilvad M., (2016):** Assessing different parameters estimation methods of Weibull distribution to compute wind power density, *Energy Conversion and Management*:108:322-335
52. **Möller B., (2011):** Continuous spatial modelling to analyze planning and economic consequenses of offshore wind energy, *Journal in Energy Policy*:39;511-517
53. **Möller B., Hong L., Lonsing R., and Hvelplund F., (2012)**: Evaluation of offshore wind resources by scale of development, *Energy*:48;314–322
54. **Monahan A.H., (2006):** The Probability Distribution of Sea Surface Wind Speeds. Part II: Dataset Intercomparison and Seasonal Variability, *American Meteorological Society:*19
55. **Morgan E. C., Lackner M., Vogel R. M., and Baise L.G., (2011):** Probability distributions for offshore wind speeds, Energy Conversion and Management:52:15-26
56. **Myhr A., Bjerkseter C., Ågotnes A. and Nygaard T.A., (2014):** Levelised cost of energy for offshore floating wind turbines in a life cycle perspective, *Renewable Energy*:66;714-728.
57. **Nagababu G., Kachhwaha S.S., and Savsani V., (2017):** Estimation of technical and economic potential of offshore wind along the coast of India, *Energy*:138; 79-91

58. **Negro V., López-Gutiérrez J.S., Esteban M. D., Alberdi P., Imaz M., and Serraclara J.M., (2017):** Monopiles in offshore wind: Preliminary estimate of main dimensions, *Ocean Engineering*: 133;253-261
59. **Nexans, (2016):** Integrated Cable Solutions for Offshore Wind Development, Report, Nexans
60. **Noonan M., Stehly T., Mora D., Kitzing L., Smart G., Berkhout V., and Kikuchi Y., (2018):** IEA Wind TCP Task 26 – Offshore Wind International Comparative Analysis, International Energy Agency Wind Technology Collaboration Programme.
61. **Ouarda T.B.M.J., Charron C., Chebana F., (2016):** Review of criteria for the selection of probability distributions for wind speed data and introduction of the moment and L-moment ratio diagram methods, with a case study, *Energy Conversion and Management*:124:247-265
62. **Ouarda T.B.M.J., Charron C., (2018):** On the mixture of wind speed distribution in a Nordic region, *Energy Conversion and Management*:174:33-44
63. **OWEC Tower, (2017):** Foundations for Offshore Wind Turbines & Taiwan Offshore Wind Industry Solutions, 8th Communication Platform Conference of Taiwan Offshore Wind – Energy Industrial Cooperation
64. **Pant M.D., Headrick T.C., (2013):** A Method for Simulating Burr Type III and Type XII Distributions through L-Moments and L-Correlations, *Applied Mathematics*
65. **Papalexiou S.M., and Koutsoyiannis D., (2016):** A global survey on the seasonal variation of the marginal distribution of daily precipitation, *Advances in Water Resources*:64:131-145
66. **Perkin S., Garrett D., and Jensson P., (2015):** Optimal wind turbine selection methodology: A case-study for Búrfell, Iceland, Renewable Energy:75;165-172
67. **PyQT5 Reference Guide,** Version 5.15 (last accessed 27 July 2021)
68. **Quintana J.A., (2016):** Alternative Installation Methods for Offshore Wind Substations, Master Thesis Submitted for the Sustainable Engineering: Renewable Energy Systems and the Environment Master Program, Supervisor: Prof. Johnstone C., University of Strathclyde
69. **Ramirez P., and Carta J.A., (2006):** The use of wind probability distributions derived from the maximum entropy principle in the analysis of wind energy: a case study, *Energy Conversion and Management*:47:2564–77
70. **Rampion Offshore Wind, (2018):** The South's coast first offshore wind farm, Rampion Offshore Wind
71. **Riesenfled R.F., (1975):** On Chaikin's Algorithm*, Computer graphics and image processing*:4; 304-310
72. **Sandal K., (2017):** Design optimization of jacket structures for mass production, Models and applications, Ph.D. Thesis submitted in the Technical University of Denmark, DTU, Department of Energy, Supervisor: Professor Jesper Mathias Stolpe
73. **Shaffiee M., Brennan F., and Espinoza I. A., (2016):** A parametric whole life cost model for offshore wind farms, *Int. J. Life Cycle Assess.*:21;961-975
74. **Shao Q., (2000):** Estimation for hazardous concentrations based on NOEC toxicity data: an alternative approach, *Environmentrics:*11:583-595
75. **Shu Z.R., Li Q.S., and Chan P.W., (2015):** Investigation of offshore wind energy potential in Hong Kong based on Weibull distribution function, *Applied Energy:*156:362-373
76. **Soares-Ramos E. P. P., Oliveira-Assis L., Sarrias-Mena R., Fernandez-Ramirez L. M., (2020):** Current status and future trends of offshore wind power in Europe, *Energy*:202

77. **Vattenfall Wind Power Ltd, (2018):** Environmental Statement Volume 2, Chapter 1: Project Description (Offshore), Document Reference: 6.2.1, GoBe Consultants Ltd
78. **Wang S., Nejad A. R., Bachynski E. E., and Moan T., (2020):** Effects of bedplate flexibility on drivetrain dynamics: Case study of a 10 MW spar type floating wind turbine, *Renewable Energy*:161;808-824
79. **Wenwen L., Goodchild M.F., and Church R., (2017):** An efficient measure of compactness for two-dimensional shapes and its application in regionalization problems, *International Journal of Geographical Information Science*:27(6);1227-1250
80. **Wijngaarden M., (2013):** Concept design of steel bottom founded support structures for offshore wind turbines, BSc Thesis, Delft University of Technology, Faculty of Civil Engineering and Geosciences, Supervisor: Professor P. G. F. Sliggers
81. **Xiang X., Merlin M. M. C., and Green T. C., (2016):** Cost analysis and comparison of HVAC, LFAC and HVDC for offshore wind power connection, *12th IET International Conference on AC and DC Power Transmission (ACDC 2016)*, Beijing, 2016, pp. 1-6
82. **Zhou F., Song B., and Tian G., (2011):** Bezier Curve Based Smooth Path Planning for Mobile Robot, *Journal of Information & Computational Science*:8(12);2441 - 2450

# 6. Results and Discussion

## 6.1 Screening analysis and constraints assessment

Overall, screening analysis scenarios clearly indicate a low availability of suitable locations for OWE deployment in nearshore areas and in shallow waters, even when considering its multi-use with other human activities. However, areas beyond 10 km from the shore with water depths greater than 100 meters attract greater opportunities for future OWF planning. For the quantification of the current available space, three scenarios were developed where most of the major marine activities were fully or partially excluded. These scenarios are based on Table 5.4.1 of Section 5.4 consisting of different exclusion criteria linked to the water depth limits, distance from the shoreline, shipping routes and tectonic faults, marine protected areas and military zones regulations among other criteria. Considering the technical, physical and economic restrictions, Scenario A (conservative) is the most stringent, Scenario B (moderate) entails some synergies among sea uses and Scenario C (optimistic) has no restrictions among sea uses with an exception to the marine protected areas and the major IMO and national shipping lanes.

By analyzing the results of the different scenarios, the remaining available space is concentrated in areas with a water depth below 1000 m., with a total available space between 10392 $km^2$ and 67452 $km^2$, which can host 104 – 674 GWs of installed capacity, at a wind power density (WPD) of 86 - 1258 $W/m^2$ and 98 - 1341 $W/m^2$ for 100 and 150 meters above sea level respectively. However, available space and fair met-ocean conditions (mean wind speed and wind power density) for bottom-fixed structures with water depth below 70 meters impose some major technical restrictions for potential offshore wind projects. For distances greater than 10-20 km. and for water depths beyond 200 m., large-scale floating OWFs constitute a more beneficial option for OWE deployment in the broader Central and North Aegean Sea. However, these calculations do not take into account the conflicts with future offshore activities (planned offshore wind farms, platforms or cables and pipelines).

The results for each scenario are illustrated in Table 6.1.1 and Figures 6.1.1-3 where the total available space is estimated and mapped as also, the maximum installed capacity, the mean wind speed and the mean wind power density for either bottom-fixed or floating concepts.

**Table 6.1.1:** Screening analysis scenarios for potential OWE deployment based on different exclusion criteria and barriers among sea-uses

| Indicator | Conservative | Moderate | Optimistic |
|---|---|---|---|
| | Scenario A | Scenario B | Scenario C |
| *Total Area ($km^2$)* | 10392 | 34851 | 67452 |
| *Total Area (Fixed) ($km^2$)* | 1297 | 2500 | 5577 |
| *Total Area (Floating) ($km^2$)* | 9095 | 32342 | 61879 |
| *Installed capacity in GW (Total)* | 104 | 348.5 | 674 |
| *Installed capacity in GW (Fixed)* | 13 | 25 | 55.1 |
| *Installed capacity in GW (Floating)* | 91 | 323.5 | 618.7 |
| *Min Wind 10 m. (Total) ($m/s^{-1}$)* | 1.99 | 1.99 | 1.99 |
| *Max Wind 10 m. (Total) ($m/s^{-1}$)* | 7.61 | 7.94 | 8.19 |
| *Min Wind 10 m. (Fixed) ($m/s^{-1}$)* | 1.99 | 1.99 | 1.99 |
| *Max Wind 10 m. (Fixed) ($m/s^{-1}$)* | 7.5 | 7.58 | 7.61 |
| *Min Wind 10 m. (Float) ($m/s^{-1}$)* | 3.19 | 2.64 | 2.51 |
| *Max Wind 10 m. (Float) ($m/s^{-1}$)* | 7.6 | 7.94 | 8.19 |
| *Min WPD 100 m. (Total) ($W/m^2$)* | 86.3 | 86.3 | 79.2 |
| *Max WPD 100 m. (Total) ($W/m^2$)* | 1076.4 | 1128.3 | 1258.1 |
| *Min WPD 100 m. (Fixed) ($W/m^2$)* | 86.3 | 86.3 | 79.2 |
| *Max WPD 100 m. (Fixed) ($W/m^2$)* | 976.8 | 983.1 | 1131.8 |
| *Min WPD 100 m. (Float) ($W/m^2$)* | 151.3 | 136.2 | 135.4 |
| *Max WPD 100 m. (Float) ($W/m^2$)* | 1076.4 | 1128.3 | 1258.1 |
| *Min WPD 150 m. (Total) ($W/m^2$)* | 98.6 | 98.6 | 96.5 |
| *Max WPD 150 m. (Total) ($W/m^2$)* | 1191.2 | 1248.6 | 1341.6 |
| *Min WPD 150 m. (Fixed) ($W/m^2$)* | 98.6 | 98.6 | 96.5 |
| *Max WPD 150 m. (Fixed) ($W/m^2$)* | 1068 | 1075.9 | 1318.1 |
| *Min WPD 150 m. (Float) ($W/m^2$)* | 170.8 | 137.6 | 132.1 |
| *Max WPD 150 m. (Float) ($W/m^2$)* | 1191.2 | 1248.6 | 1341.6 |

**Scenario A (Conservative):** The first scenario is characterized by low-energy targets planning considering all potential restrictions from both the national legislation and the MSP guidelines. Based on the current scenario, a small part of the broader study area seems to be feasible for future OWE deployment (Figure.6.1.1a) by maintaining the renewable energy goals at a low level until 2030 and 2050. In a sectoral planning context, the economic, social and

environmental pressures (fisheries, military areas, MPAs, visibility concerns, IMO and national shipping lanes etc.) lead to a higher consideration of their spatial claims concerning future planning aspects and possible co-existence among different sea uses. Thus, the management of marine space is based on the exclusion of the current activities, whereas the multi-use of space is not considered. As a result, the total available space is approximately 10392 $Km^2$, (1297 $km^2$ and 9095 $km^2$ for depths below 70 m. and between 70 m. and 200 m. respectively). Mean wind speed at 10 m. above sea level exceeds 7.61 $m/s^{-1}$ and the WPD at 100 m. and 150 m. reaches 1076 $W/m^2$ and 1191 $W/m^2$ (Table 6.1.1).

The differences between areas for bottom-fixed and floating installations, concerning the mean wind speed and the WPD, are rather low, mainly due to the limited available space for WTs placement, hence a total deviation of 0.1 $m/s^{-1}$ occurred for the mean wind speed and 100 $W/m^2$ for the WPD at 100 m. and 150 m. height above sea level. The most promising areas are located to the Eastern part of Thasos island (North Aegean Sea), in areas around Agios Efstratios island (North-East Aegean Sea) and finally, to the Western part of Lesvos island. Moreover, the sea depth in the aforementioned areas ranges between 35 m. and 200 m. with mean wind speeds between 4.4 $m/s^{-1}$ and 7.6 $m/s^{-1}$.

**Scenario B (Moderate):** The second scenario, illustrated in Figure 6.1.1b, considers a less conservative planning approach, with some co-existence examples among sea uses to be allowed (i.e., with fisheries and aquaculture areas). Distance from the shoreline is reduced from 10 km. to 5 km., depth limit increases from 200 m. to 500 m. for floating structures and all buffering zones from human activities are diminished. Consequently, the total available area increases to 34851 $Km^2$ with 2500 $Km^2$ of available space for monopile and jacket support structures and 32342 $Km^2$ for the floating concepts. The total GWs of installed capacity increase to 348.5 (from 104 GW in Scenario A), the mean wind speeds exceed 7.94 $m/s^{-1}$ for the windiest areas and finally, the mean WPD at 100 m. and 150 m. increases up to 1128 $W/m^2$ and 1248 $W/m^2$ respectively (Table 6.1.1). In accordance to Scenario A, the most promising areas occurred, for water depths beyond 35 m., at the Central and Central North Aegean Sea (to the broader Eastern part of Sporades islands). However, many windiest areas are “unlocked”, mostly in the Northern part of Lesvos Island with

the mean wind speeds exceeding 7.9 $m/s^{-1}$, although the water depth in these areas ranges between 150 m. and 300 m.

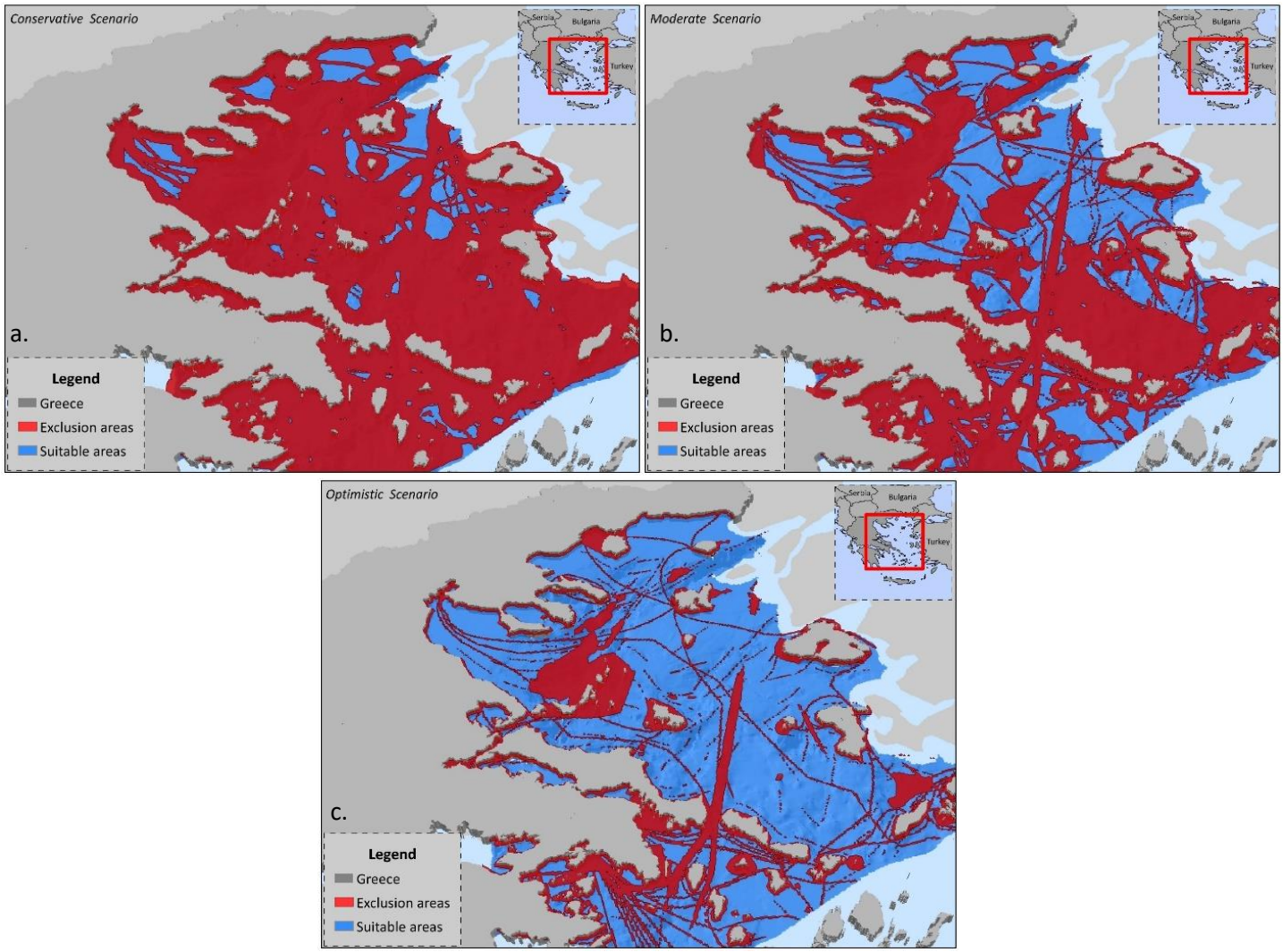


**Figure 6.1.1:** a) Scenario A, b) Scenario B and c) Scenario C of the screening assessment indicating the excluded areas (red color) and the suitable areas (blue color), d) Constraints pre-processing and e) Constraints' set-up Graphical User Interfaces

**Scenario C (Optimistic):** For the last, and most promising scenario, the results highlight an increased capacity and available space for the design and enforcement of integrated OWF planning. In a densely utilized space such as the Aegean Sea, this leads to the application of increased synergies among sea uses for the interaction between OWFs and fisheries, military areas or cables and pipelines infrastructures. In Figure 6.1.1c can be clearly observed that most

of the excluded areas incorporate all of the NATURA 2000 network, decreased distance from the shoreline (2 km.), increased shipping densities for the major IMO shipping routes (> 300 ships per cell unit, compared to the 100 and 200 of Scenarios A and B and no conflicts with the national shipping lanes. Moreover, the water depth limit increases to 1000 m. and a buffer of 250 m. is considered for the proximity to the tectonic faults. As a result, the remaining available space for OWF site-prospecting reaches 67452 $Km^2$ (5577 $km^2$ and 61879 $km^2$ for the bottom-fixed and the floating concepts) and the total GWs of installed capacity reach 674 GW, mostly in areas of water depths beyond 70 m. (55 GW for depths below 70 m.).

The maximum wind speed reaches 8.2 $m/s^{-1}$ for the windiest areas with maximum mean WPD values in the range between 1258 $W/m^2$ and 1318 $W/m^2$ at 100 m. and 150 m. above sea level (Table 6.1.1). Most of the excluded areas are located to the broader Sporades area (where the National Park of Alonisos is located), the Western part of the Anatolian fault with depths exceeding 900 m. and finally, to the Northern part of Cyclades and Dodecanese islands to the broader area of Eastern and Western parts of the Central Aegean Sea. Considering the windiest areas that are "unlocked" with the current scenario, only the available space for the floating technologies preserved increased differentiations in conjunction to the maximum mean wind speed. As a result, most of the offshore areas between Eastern Evoia and the Western part of Chios, Lesvos and Lemnos islands have potentially optimal meteorological conditions with wind speeds between 6.1 $m/s^{-1}$ and 8.2 $m/s^{-1}$, however, the intense bathymetric profile in these areas is noticed with depths exceeding 500 m.

Considering the cell size increase impact (i.e., from 1000 m. to 5000 m.), Figure 6.1.2 illustrates the "loss" of information resulted from the resampling techniques applied in terms of the total exclusion areas quantification. Consequently, for the conservative scenario (A), the total excluded, and suitable zones are estimated as 82898 $km^2$ and 10392 $km^2$, 82584 $Km^2$ and 10612 $km^2$ and finally, 83000 $km^2$ and 10175 $km^2$ for the 1000 m., 2000 m. and 5000 m. cell size respectively (Figure 6.1.2a - c). Thus, a decrease of 0.37% and an increase of 0.12% are observed by resampling from 1000 to 2000 and 5000 m. cell size respectively. Moreover, for the moderate scenario (B), these areas are estimated as 58448 $Km^2$ and 34842 $km^2$, leading to a decrease of 0.56% and 1.15% for the excluded and the suitable areas (Figure 6.1.2d - f). Finally, for the

optimistic scenario (C), these areas are estimated as 25894 km$^2$ and 67396 km$^2$, decreased by 1.81% and 0.65% by resampling from 1000 m. cell size to 2000 m. and 5000 m. respectively (Figure 6.1.2g-i).

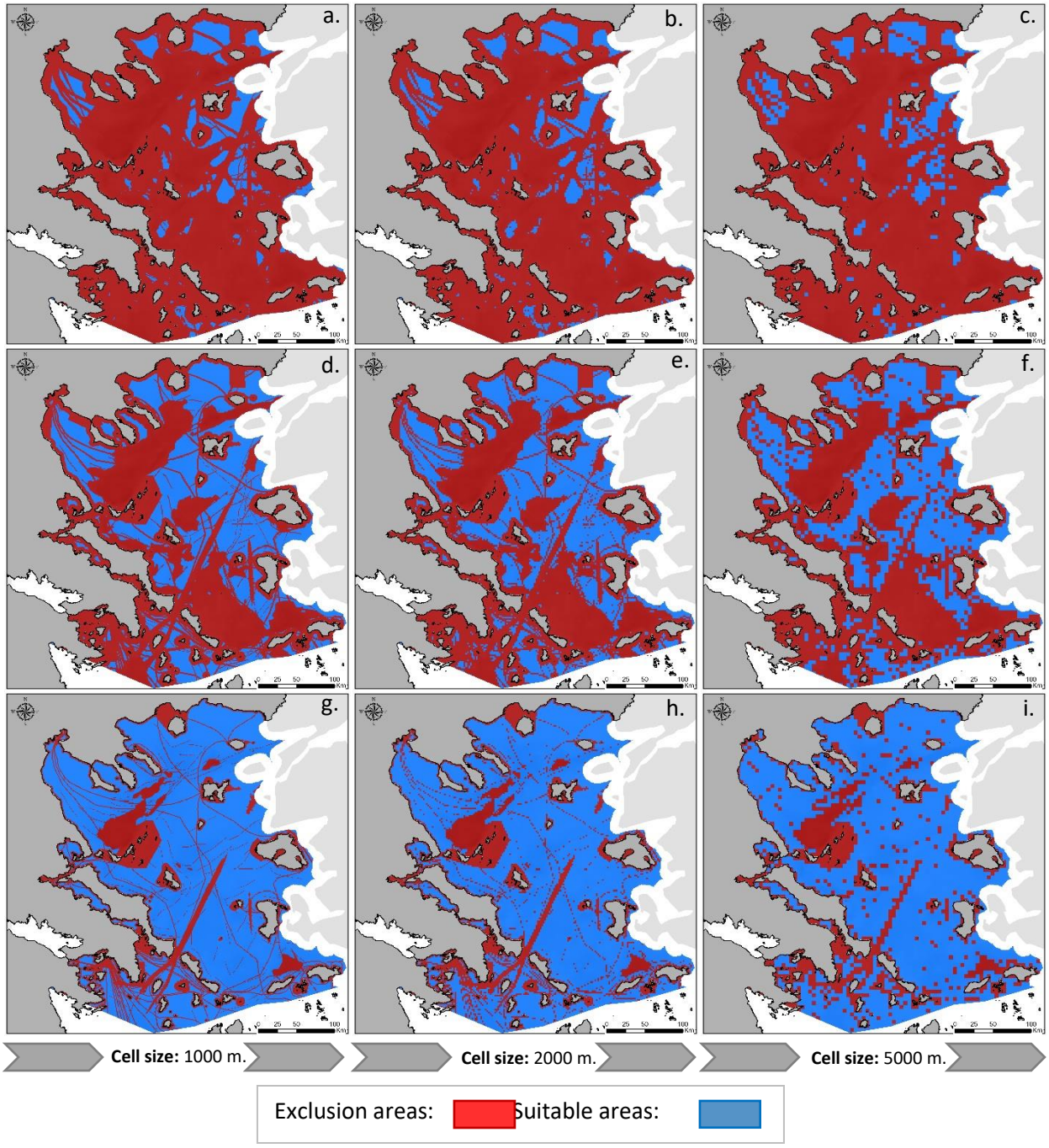


**Figure 6.1.2:** Cell size increase impact on the total exclusion areas quantification for Scenario A (a-c), Scenario B (d-e) and Scenario C (g-i)

## 6.2 Life – Cycle Cost modelling results

In this Section, an overview of the case study results is presented in line with the overall cost estimates for the different lifecycle assessment phases incorporating the: a) Development and Consenting (D&C), b) Production and Acquisition (P&A), c) Installation and Commissioning (I&C), d) Operation and Maintenance (O&M) and finally e), Decommissioning and Disposal (D&D). It is noticed that the aforementioned cost estimates are expressed on per wind turbine basis, however, the development and consenting, the balance of plant manufacturing and acquisition cost, the installation and commissioning cost and the decommissioning cost are firstly estimated at a wind farm level and then are reduced to a single wind turbine level, in terms of the WT's installed capacity.

### 6.2.1 Development and Consenting Cost (D&C)

For the development and consenting cost, results are presented in Figure 6.2.1, expressed in million euros per mega-watt (m€/MW). The final cost differentiations are expressed in terms of the distance from the nearest port and the depth increase, considering the cost variations for site-specific surveys, engineering activities and the associated contingencies (unpredictable annual expanses). Consequently, an increase of the total cost occurs for the remote marine areas with increased depth, mainly in the Central Aegean Sea.

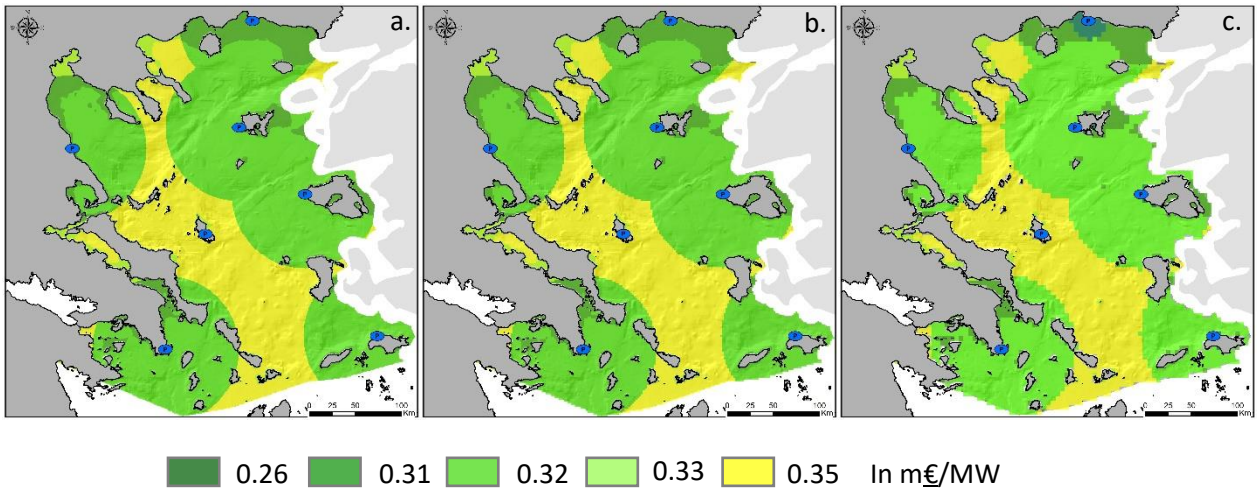

**Figure 6.2.1:** Development and Consenting cost (m€/MW) estimation for a cell size of: a) 1000 m., b) 2000 m. and, c) 5000 m.

The final cost values range between 0.26 million €/MW and 0.32 million €/MW for areas closer to the nearest port facilities such as the Eastern part of the Aegean Sea (Alexandroupoli, Lemnos, Lesvos, Chios, Samos), the broader Attica region and the North-Western part of the study area from the Northern part of Evoia to Thermaikos Gulf. On the contrary, the highest values occurred in Sporades and Cyclades islands, where the development and consenting cost was estimated in the range between 0.32 million €/MW to 0.35 m€/MW. These costs are "translated" to approximately 1.6, 2.56 and 3.2 million euros for the 5MW, 8MW and 10MW wind generators respectively. It is also noticed, that in these areas, although the proximity to the nearest ports was acceptable, increased water depths beyond 200 meters occurred, leading to slightly increased costs during this stage of development.

### 6.2.2 Wind turbines cost (P&A)

The results for the wind turbines production and acquisition cost are illustrated in Figure 6.2.2.1, considering three different wind turbine models of 5MW, 8MW and 10MW for the Gamesa G-128, Vestas V-164 and the SeaTitan respectively. Results for the selected wind turbine types were estimated as 7.9 million Euros, 13.2 million euros and 17.6 million euros, including tower and marinization procedures costs. Consequently, the cost is increased, mainly for the 8 and 10 MW wind turbines, because of the selected hub heights (125 and 140 meters) considered for this study. It is noticed that the aforementioned cost estimates are only useful for giving an indication of the relative costs differentiations, and not to estimate the absolute costs or provide site-specific accurate estimations based on the IEC standards, however, the results were compared to the results from the most recent reports and market prices.

On the contrary, by comparing these cost estimates with previous studies, increased overestimations occurred due to the inflation and exchange rates applied, the different economic and technological status based on the period that these studies were conducted as well as due to the lack of accurate data for the real wind turbines costs or analytical estimates of the sub-costs

as for instance, the tower cost or the electrical infrastructure cost. In Figure 6.2.2.2, all cost estimates are illustrated and compared using the models of Dicorato et al. (2011), Hong and Moller (2011), Cavazzi and Dutton (2016), Rodriguez et al. (2017), Fingers et al. (2006) (which was updated by Perkins et al. 2015) and finally, all primary cost data used in this study for the last 15 years.

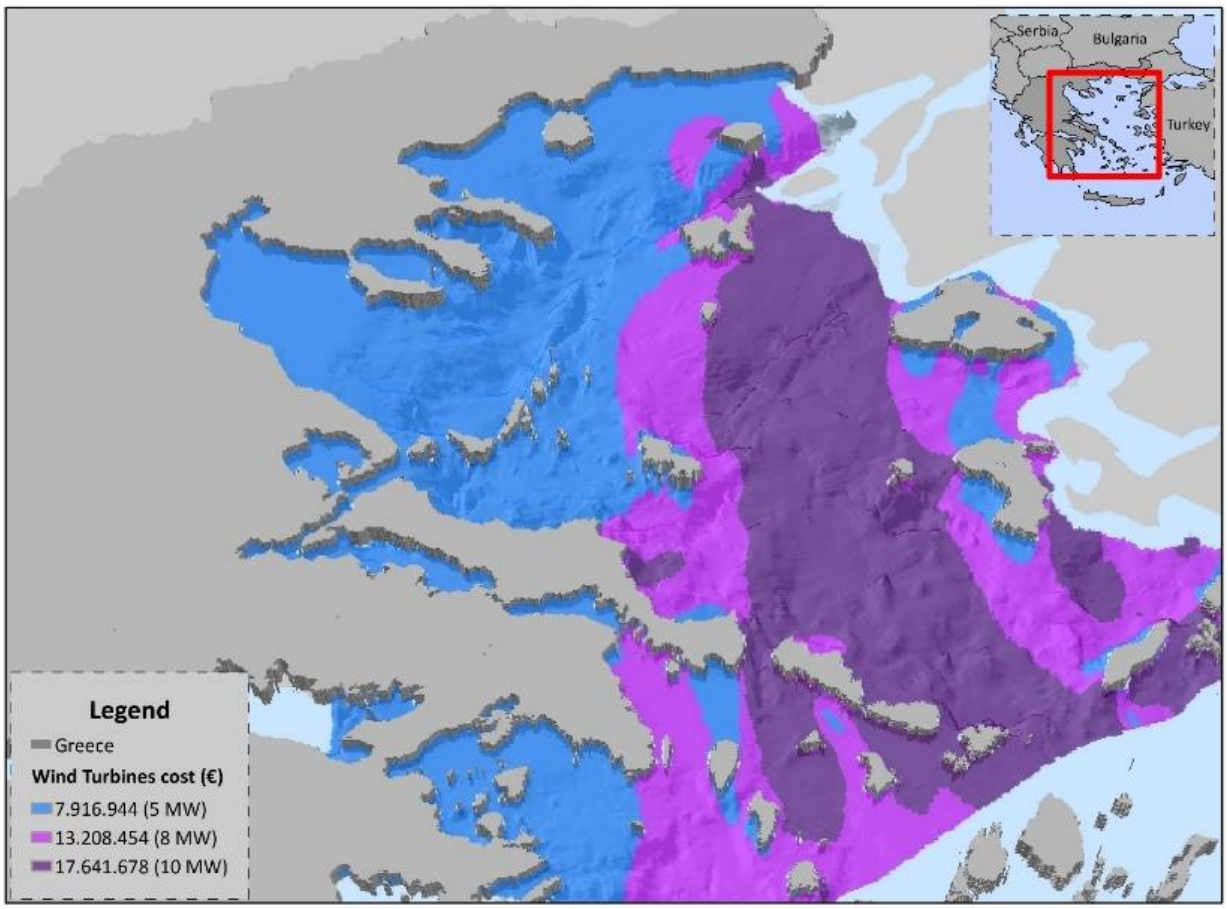


**Figure 6.2.2.1:** Wind turbines production and acquisition cost (€/WT type) estimation

Results indicate that the model used by Dicorato et al. (2011) extremely underestimates wind turbine cost where the authors state that the mathematical expression used in their study is efficient for wind turbine capacities between 2 MW and 5 MW. Furthermore, Hong and Moller (2011) also underestimate the total wind turbine cost, by assuming 1.1 million euros per MW, however, Cavazzi and Dutton (2016) considered 1.6 million euros per MW which seems to describe more precisely the WTs' cost estimates. On the contrary, the review conducted by Rodriguez et al. (2017) provides increased discrepancies for the wind turbine cost estimates,

compared to the current economic and technological status. Finally, the customized model of Fingers et al. (2006) as well as the regression model's results indicate small differences, with the total cost for the 5 MW wind turbine to be estimated between 7 and 7.91 million euros, for the 8 MW in the range between 13.21 – 13.42 million euros and 17.64 – 18.84 million euros for the 10 MW wind turbine respectively.

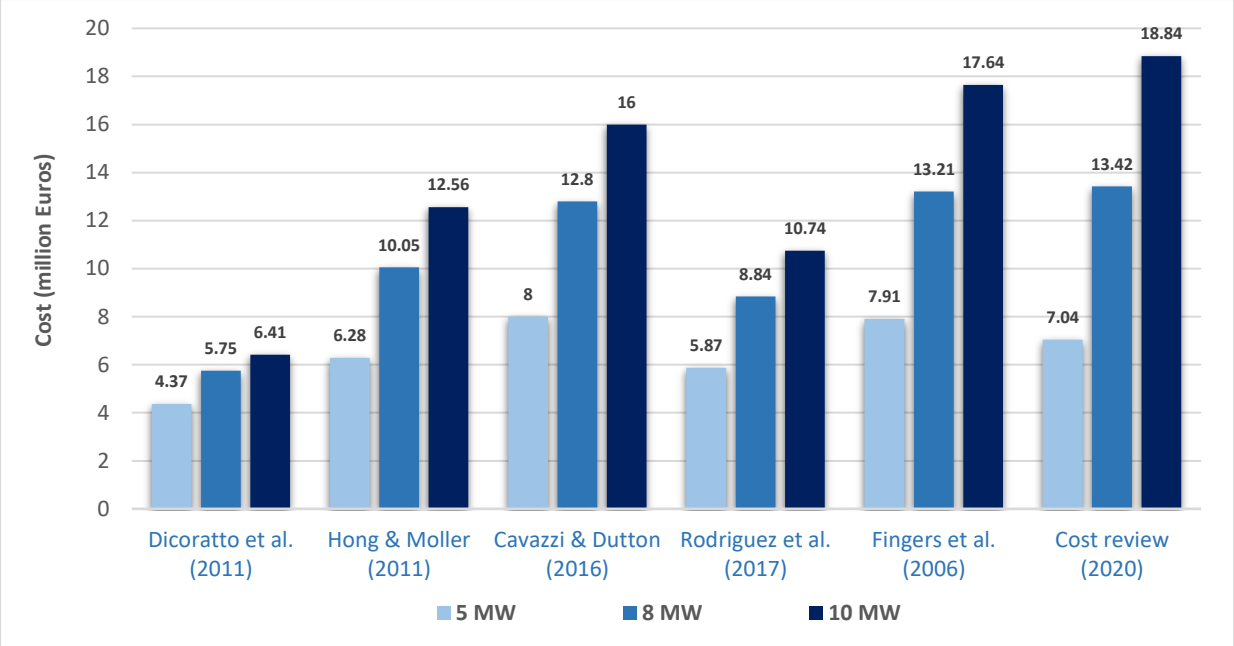


**Figure 6.2.2.2:** Wind turbine types cost comparisons with previous research studies and cost models

### 6.2.3 Foundation cost (P&A)

The foundation size is strongly dependent on the water depth and the size of the wind turbine to be attached (i.e., hub height and rotor diameter). As a result, the foundation cost, which in the case of steel solutions (i.e., monopile, jacket or floating support structures) depends on the price of this commodity, is estimated based on the steel consumption and the complexity of each support structure. Monopiles preserve lower manufacturing costs compared to the jacket and the floating foundations in spite of the fact that monopiles exceed greater masses in terms of the steel consumption. These facts explain the increased differences between monopile, jacket and floating concepts where the costs for the Spar-Buoy and the Wind Float concepts is 2 - 3 times greater than the jacket and 7 times from the monopile support structures.

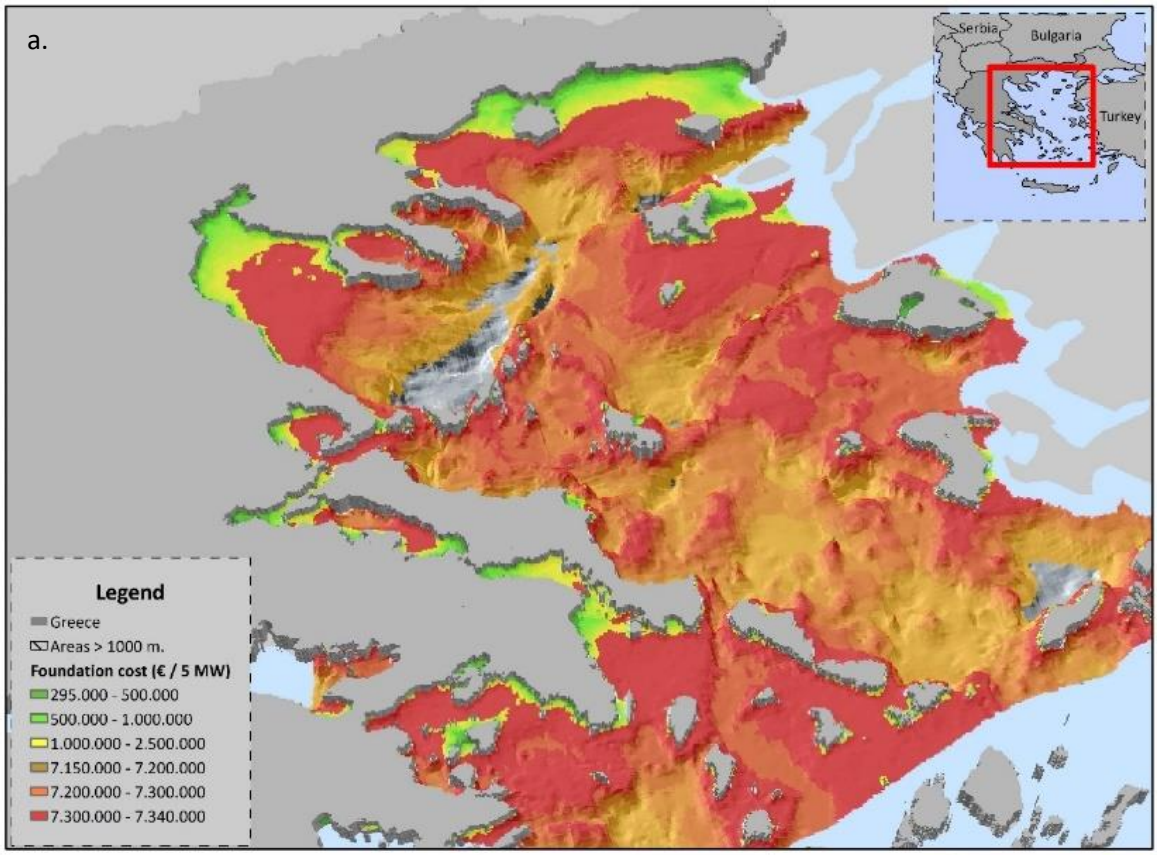
a.
Serbia
Bulgaria
Turkey
Legend
Greece
Areas > 1000 m.
Foundation cost (€ / 5 MW)
295.000 - 500.000
500.000 - 1.000.000
1.000.000 - 2.500.000
7.150.000 - 7.200.000
7.200.000 - 7.300.000
7.300.000 - 7.340.000

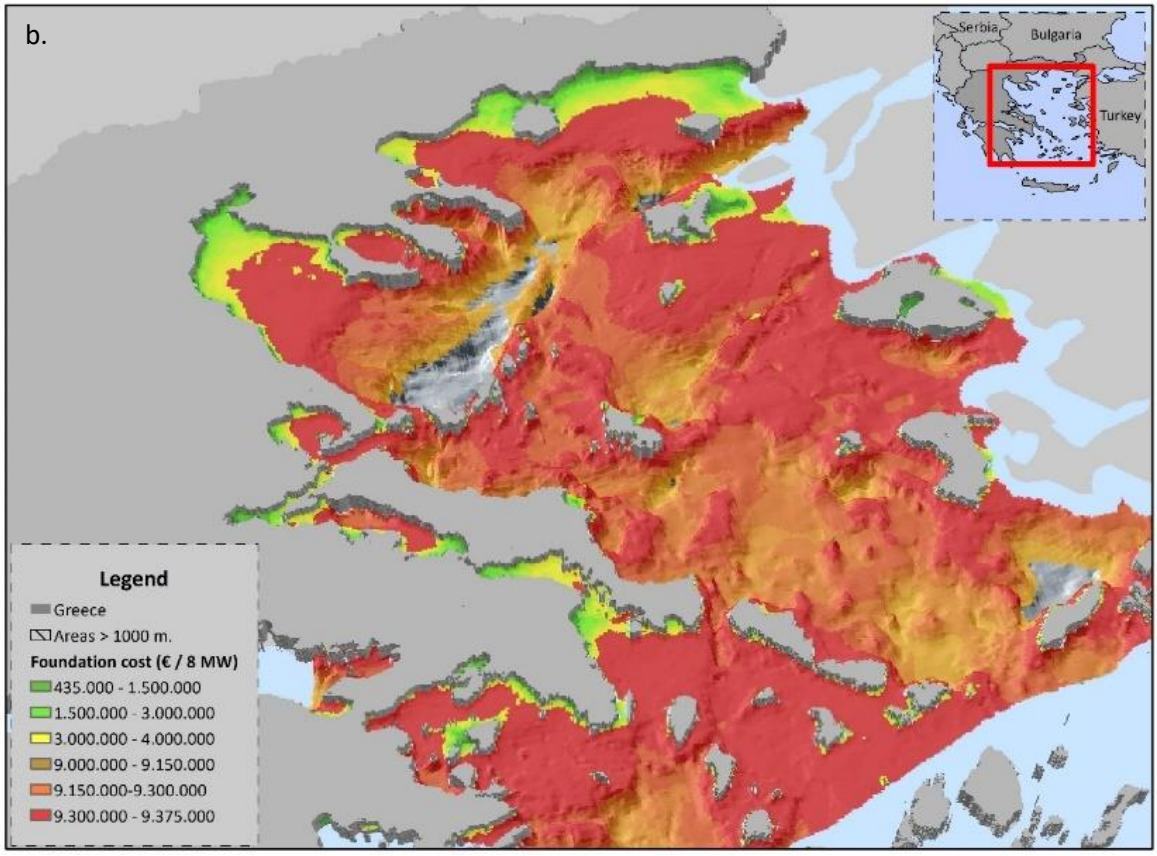
b.
Serbia
Bulgaria
Turkey
Legend
Greece
Areas > 1000 m.
Foundation cost (€ / 8 MW)
435.000 - 1.500.000
1.500.000 - 3.000.000
3.000.000 - 4.000.000
9.000.000 - 9.150.000
9.150.000-9.300.000
9.300.000 - 9.375.000

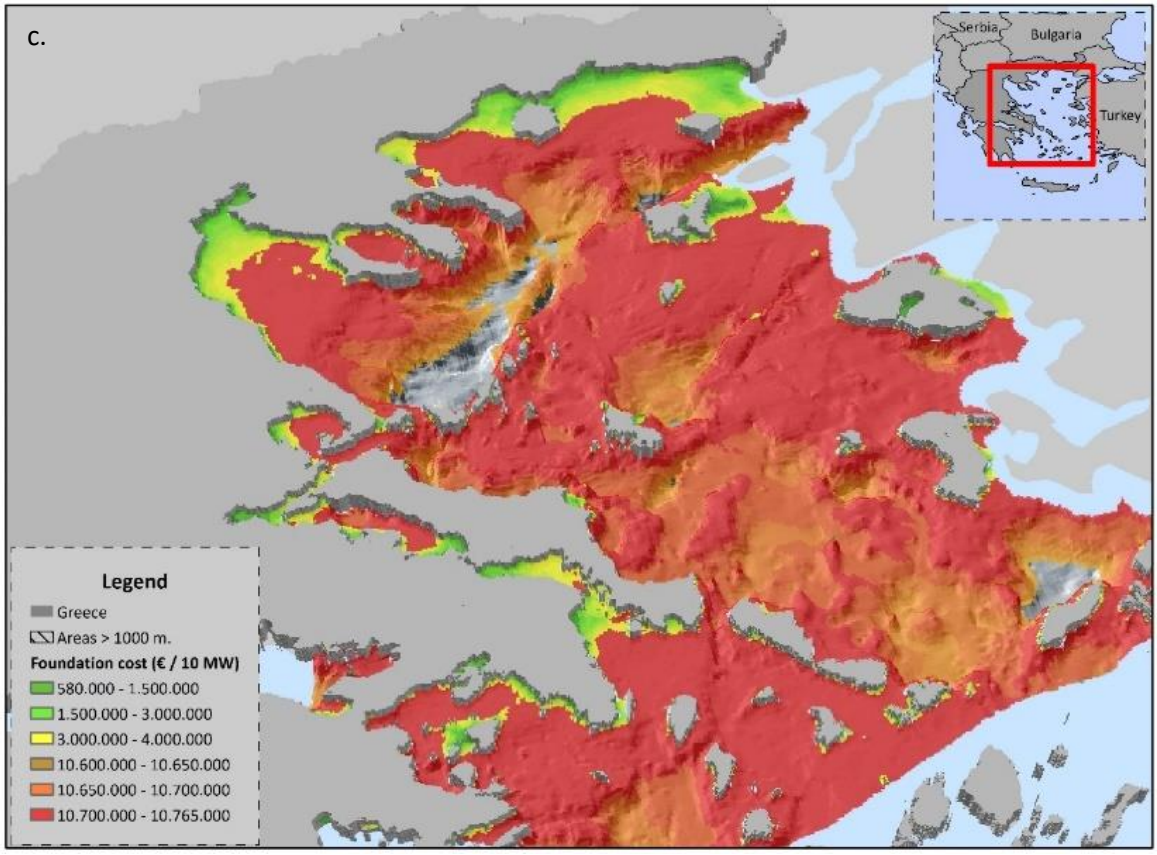


**Figure 6.2.3.1:** Foundation cost estimation for different wind turbine sizes including: a) 5 MW, b) 8 MW and c) 10 MW wind generators

In Figure 6.2.3.1 the estimated foundation costs are presented for the 5 MW, 8 MW and 10 MW wind generators respectively. Cost values for the bottom-fixed foundations, including monopile and jacket support structures, range between 0.295 and 4.5 million euros. In particular, for the monopile foundations the cost is estimated in the range between 0.294 and 0.901 million euros for a 5 MW wind turbine, 0.43 and 1.05 million euros for an 8 MW and between 0.58 and 1.21 million euros for a 10 MW wind generator. For the jacket foundations, these costs increase in 1.6 – 2.4 million euros, 2.7 – 3.5 million euros and finally, 3.44 – 4.24 million euros for the 5, 8 and 10 MW concepts respectively. The estimated cost of the floating support structures is estimated at approximately 7.2, 9.1 and 10.76 m€ for the 5, 8 and 10 MW concepts.

In Figure 6.2.3.1a - c, green and dark green colors indicate areas with shallow water depths (below 30 meters depth) where monopile technologies may be considered, yellow color specifies

areas with water depths up to 70 meters for the jacket technologies and finally, orange, brown and red colors underline areas that only floating concepts (semi-submersible or spar-buoy) may be selected.

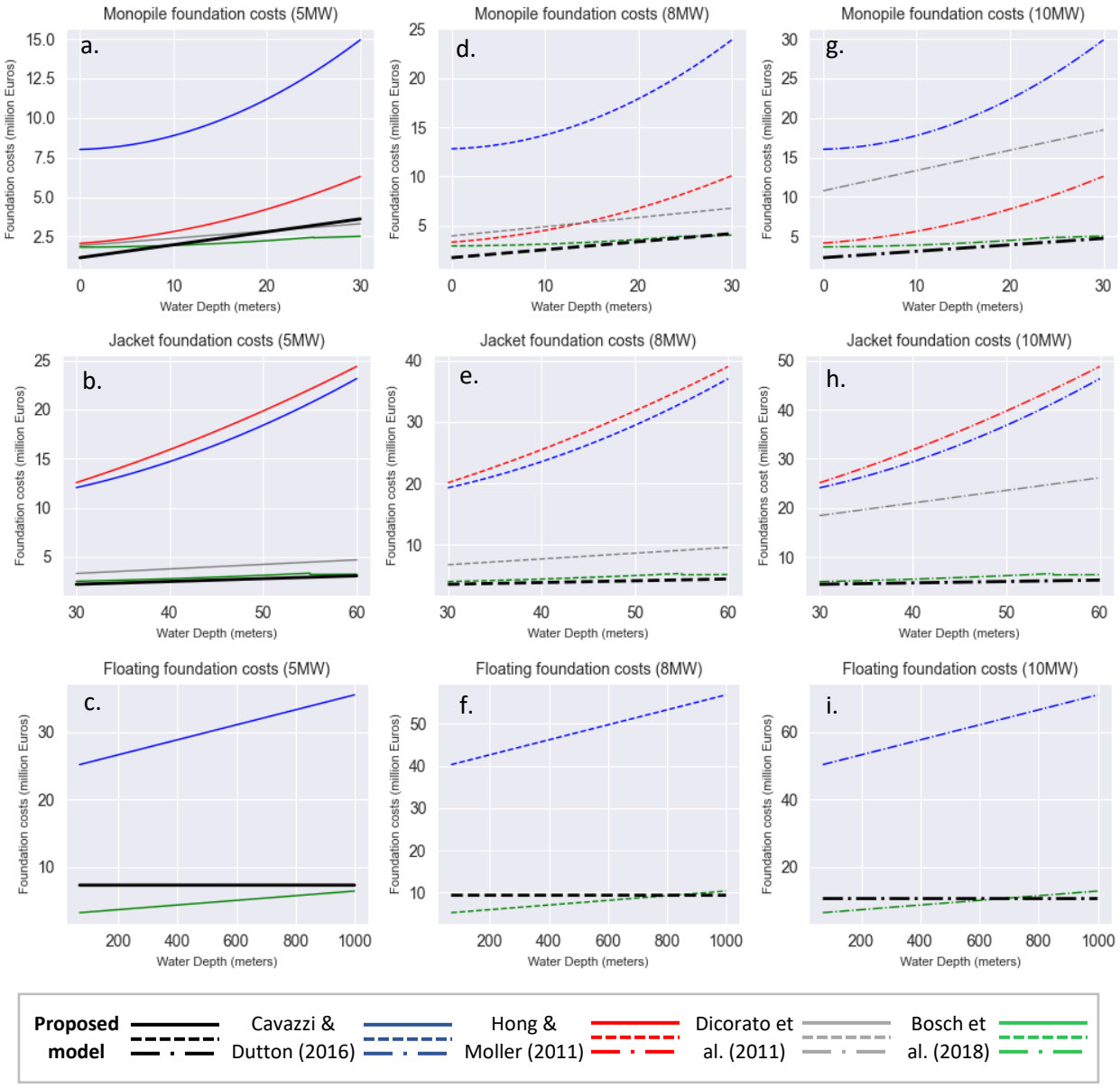


**Figure 6.2.3.2:** Foundation cost comparisons compared to previous studies for 5 MW (a-c), 8 MW (d-f) and, 10 MW (g-i) concepts (excluding installation cost)

Overall, the most promising areas, in terms of the minimum costs, are located nearshore (with the exception of the Eastern Lemnos offshore areas) in the Northern part of the Aegean Sea (Alexandroupoli, Thassos and Thermaikos Gulf), in the Northern and Southern Euboean Gulf and

finally, in the broader area of Attica region as well as in Lemnos and Lesvos islands. In contrast, the most promising areas considering the floating concepts are located at remote offshore areas of the Central Aegean Sea and the Northern part of the Anatolian Fault (brown areas in Figure 6.2.3.1). Although in these areas water depth exceeds 400 meters, the cost for the mooring lines and the anchors decreases. The reason is that while the water depth increases, anchoring and mooring costs slightly decrease because of the decreasing mooring lines diameter and the anchors size reduction.

In Figure 6.2.3.2, the foundation cost results are compared to the outcomes derived from previous studies. Results indicate increased variabilities in the foundation costs estimates for either the fixed-bottom or the floating concepts. According to Cavazzi and Dutton (2016), monopiles production and acquisition cost ranges between 8 and 30 million euros, considering a 5MW, 8MW and 10MW wind turbines respectively. Moreover, according to Dicorato et al., (2011), the total foundation cost for water depths up to 30 meters is estimated between 2.5 and 12 million euros, where the largest overestimations occurred for wind turbines of capacity greater than 8MW. On the contrary, results observed by Hong and Moller (2011), Bosch et al., (2018) and the proposed model indicate similar cost estimates for the monopile foundation concepts in the range between 2 and 11 million euros.

Focusing on the jacket foundations, increased overestimations occurred using the model applied by Cavazzi and Dutton (2016) and Hong and Moller (2011). Similarly to the monopile foundation costs, the other three models maintained similar cost estimates between 3 and 15 million euros (an exception occurred for the 10MW using the model of Dicorato et al. 2011). Finally, for the floating concepts, similar cost estimates (i.e., 3 - 12 million euros) extracted from the proposed model and Bosch et al. (2018) analytical equations, however, using the model established by Cavazzi and Dutton (2016), increased discrepancies occurred where an overestimation of 500% is noticed with the foundation cost values exceeding 60 million euros.

Analyzing foundation costs discrepancies due to the resampling configurations applied for the 2000 meters and 5000 meters cell size, Figure 6.2.3.3 illustrates the percentage differences of the cost estimates for the resampled bathymetry rasters. Consequently, for the foundation cost estimates, with the exception of a cell size increase from 1000 m. to 5000 m., most areas

preserve low percentage differences (± 5 %). Nevertheless, the highest discrepancies occurred in the "transition" areas from 30 m. to 40 m. water depth and from 70 m. to 100 m. depth, where different foundation types may be selected.

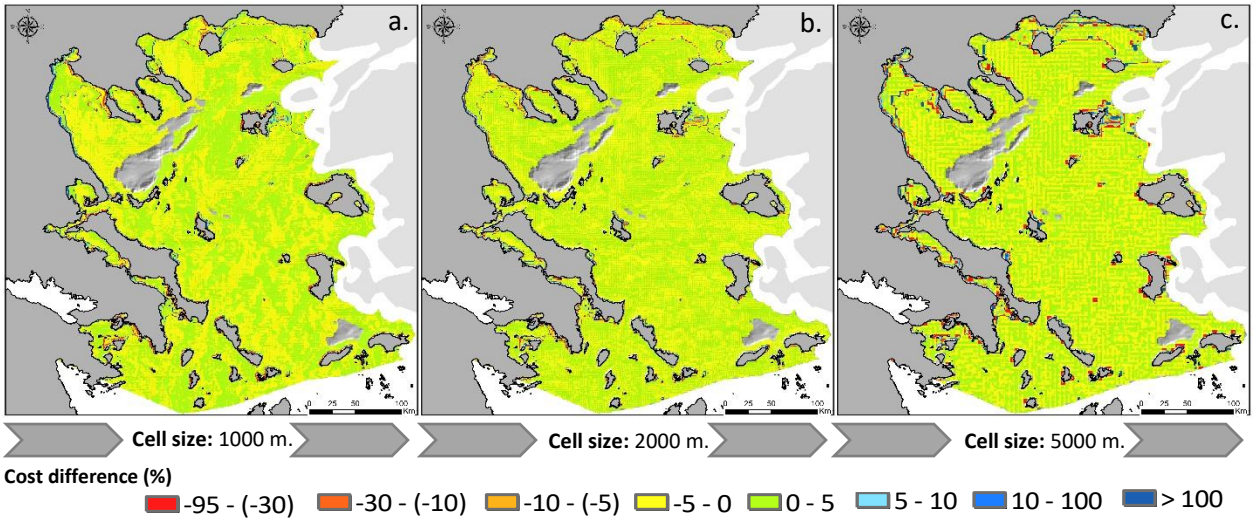


**Figure 6.2.3.3:** Foundation cost percent differences for different resampled rasters for: a) 1000 m., b) 2000 m. and c) 5000 m.

These results are not suspicious as long as when the bathymetry raster is resampled to 2000 m. and 5000 m., the mean depth of the initial pixels is preserved to the resulted pixels. Consequently, areas that monopile foundations have been selected for the 1000 m. raster surface are now differentiated due to the resampled pixels and lead to areas of increased water (or decreased based on the resampling method used) depth and thus, to the selection of either jacket or floating foundations.

### 6.2.4 Distance-based cost calculations (P&A – I&C)

For the distance-based modelling scheme, including installation, decommissioning, transmission and O&M costs, different cost models and algorithmic settings were tested in order to extract the final cost surfaces. The LCP Dijkstra algorithm and all of the smoothing techniques were implemented in Python scripting language and embedded in a GIS application and successfully tested in selecting optimal point-to-point transmission lines, installation and decommissioning routes and finally, O&M optimal corridors. All the results for the North and

Central Aegean Sea are presented in maps, as extracted from the algorithm (final cost assessment for each pixel and the optimal routes presented as vectorized paths). Also, the straightness control, based-on the Sinuosity Index, is analyzed and discussed along with the statistical results of the smoothing techniques applied.

The main raster images, in order to establish the graphs *G* and *N*, comprise of 88 (width) and 93 (height) on a total of 8184 pixels with a cell size of 5 km. Accordingly, the total number of nodes (non-null cells) and edges for the graph *G* is 3727 and 29970 and for graph *N* this number increases up to 29970 and 412447 respectively. Once the graph-based network is established, the Dijkstra's algorithm is applied to calculate the optimal paths counting to 161755 candidate paths (not optimal) for graph *N.* These numbers increase drastically when considering a decrease of the spatial resolution in 2 km and 1 km, where the total size of the study area increases to 220 and 440 (width) with 233 and 466 (height) respectively. Consequently, the size of graphs *G* and *N* expands to 23299 nodes with 187323 edges and 187323 nodes and 2566325 edges for the 2 km cell size and 93290 nodes with 749118 edges and 749118 nodes with $10^7$ edges for the 5 km cell size. These numbers are estimated for the O&M, the installation and commissioning and the decommissioning algorithm's set up, where only the offshore pixels are accounted for the total size of graphs *G* and *N.* For the transmission cost modelling (i.e., the export cables delineation) the graphs' total size increases by approximately 15%, considering the onshore pixels where the onshore network junctions are located.

As a result, the computational performance for the optimization procedures in such dense dual graphs is computationally demanding and time consuming. Hence, it is noticed that the algorithm was tested only for the scenarios of 2000 m. and 5000 m. cell size as well as for the 1000 m. cell size the computational time needed for the running tests approximated a time window of several months to a conventional computer. There are three aspects concerning the processing steps including the: pre-processing, the actual pathfinding phase and finally the smoothing stage. While the second phase is obviously the more critical one, it clearly depends on the size of both graphs (running time increase geometrically to the size of the graph). For the pathfinding stage, the algorithm needs less than 5 and 30 seconds for each path delineation and weighted cost extraction considering 2000 m. and 5000 m. cell size. Considering the total number

of paths and optimal paths to be searched, the total running time of the pathfinding stage was 4 and 19 days (2 and 5 km cell size) for the paths' delineation to the nearest port and this running time increased to 12 and 43 days approximately for the transmission paths respectively. The performance of the first stage is also important in real-world applications and for this case study the graph and dual graph set up lasts less than half an hour and 8 hours with the spatial resolution increase (0.2% of the total running time). For the last stage, smoothing techniques are implemented in less than 15 and 190 minutes for the total amount of the optimal paths (0.1% of the total running time). These results indicate a rather poor computational performance, although, the computational effort of pathfinding stage is more or less directly dependent on the number of nodes of graphs *G* and *N*.

#### 6.2.4.1 Transmission lines cost results (P&A)

Balance of plant (BoP) production and acquisition cost results (including inter-array, export cables cost and the substation's construction cost) are illustrated in Figures 6.2.4.1.2-3, based on both the simplified mathematical formula used by Hong and Moller (2011), and the analytical cost model established by Dicorato et al. (2011). All costs are expressed in €/MW (Figure 6.2.4.1.2) and €/Wind turbine capacity (for 5,8 and 10 MW) (Figure 6.2.4.1.2) in order to highlight cost differences of electrical devices per WT as also the cost differentiations among inter-array cables length, proportional to the wind turbine spacing.

At first, Figure 6.2.4.1.1 presents the export cables paths, as extracted from the LCP algorithm along with the finalized smoothed paths (Figure 6.2.4.1.1b,c), based on the Chaikin's algorithm and the Bézier curves configurations. Algorithm's capability to avoid obstacles (NoData, Urban and Posidonia Oceanica areas) is remarkable, as well as its efficiency to calculate and draw all least cost path corridors and extract the raster cost surfaces for potential OWFs connection corridors to the onshore network junctions. Analyzing the final cost estimates, the most promising areas, considering only the cables cost, seem to be nearshore as expected, as also to the North and Central Aegean Sea (in the Eastern part of Sporades islands, Alexandroupoli etc.). Total cost increases mainly in the Northeastern, Eastern and Southern Aegean areas where distances greater than 200 km occurred and the connection to the grid seems to be infeasible with the cable

costs values ranging from 1.5 to 1.9 million euros/MW or 3 - 4 million euros/MW (Figure 6.2.4.1.2) considering the different cost models.

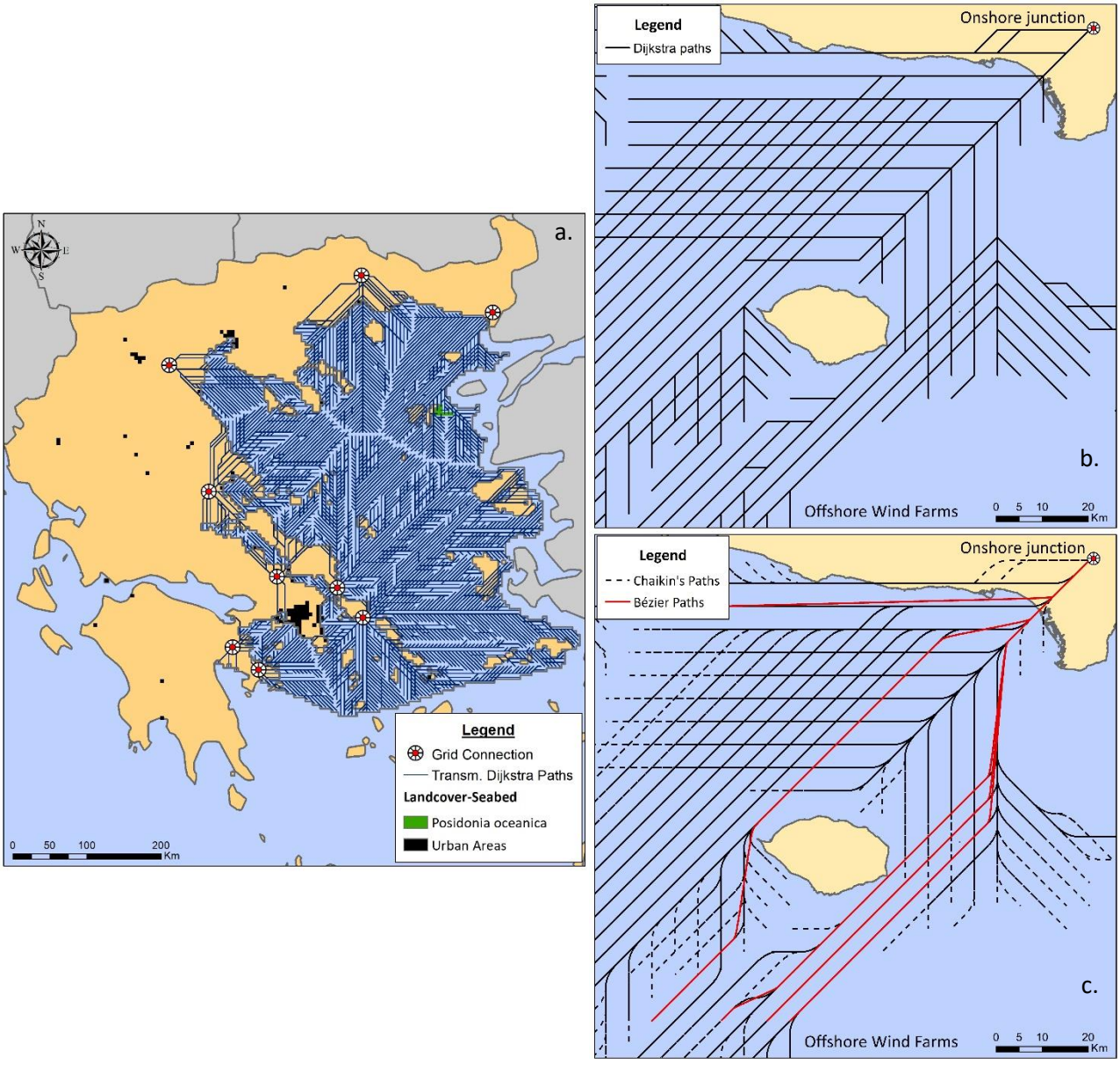


**Figure 6.2.4.1.1:** Dijkstra transmission lines delineation (a) (export cables) and smoothed vectorized paths (b,c)

BoP costs range between 0.4 million euros/MW (green areas) to 1.93 (red areas) m€/MW (Figure 6.2.4.1.2b) and 0.9 - 3.98 million euros/MW (Figure 6.2.4.1.2a) for the models used respectively. The aforementioned cost values are incorporating the transmission cost as

extracted from the smoothed Dijkstra paths, through the LCP model. It is noticed that a cost reduction of 1% (approx. 20000€/MW) occurred using Chaikin's corner cutting smoothing algorithm and for the Bézier curves, a total reduction of 5% (approx. 40000€/MW) is noticed. On the cost estimates per wind turbine type (Figure 6.2.4.1.4), increased differentiations occurred, where the final production and acquisition cost for the 5MW wind turbine was estimated in the range between 5-19 million euros/MW, 7.7-30 million euros/MW for the 8MW and 9 - 38 million euros/MW for the 10MW respectively.

The increased variability of the total BoP cost is explained by the different export cable types (AC, HVAC or HVDC) selected based on the distance of a potential OWF from the nearest onshore network junction (Figure 6.2.4.1.3d), the size of the OWF and the WTs' nameplate capacity (and as a result the WTs' spacing and the inter-array cables length). For instance, considering a 500MW wind park, Figure 6.2.4.1.3a-c illustrates the total BoP cost for the 5MW, 8MW and 10MW wind generators. For an OWF consisting of 100 WTs of 5MW, the total cost ranges between 480 and 1930 million euros. When considering 62 WTs of 8MW, these costs reach 477 – 1860 million euros and finally, for an OWF of 50 WTs with 10MW of nameplate capacity, the total BoP cost ranges between 450 – 1925 million euros. It is noticed that as long as the WTs capacity increases, the total number of WTs needed to reach the OWF's capacity decreases and as a result, the inner-array cables cost is smaller. Moreover, for distances greater than 200 km. from the onshore network junctions, for all of the OWF configurations, the total BoP is drastically increasing above 1700 million euros.

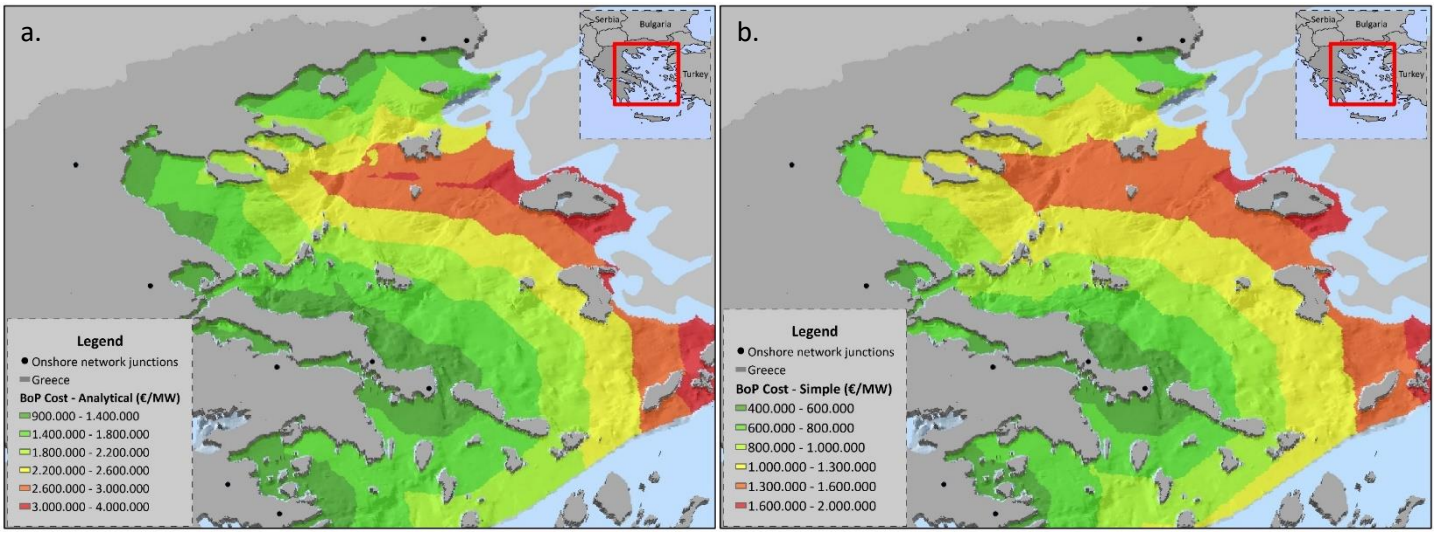

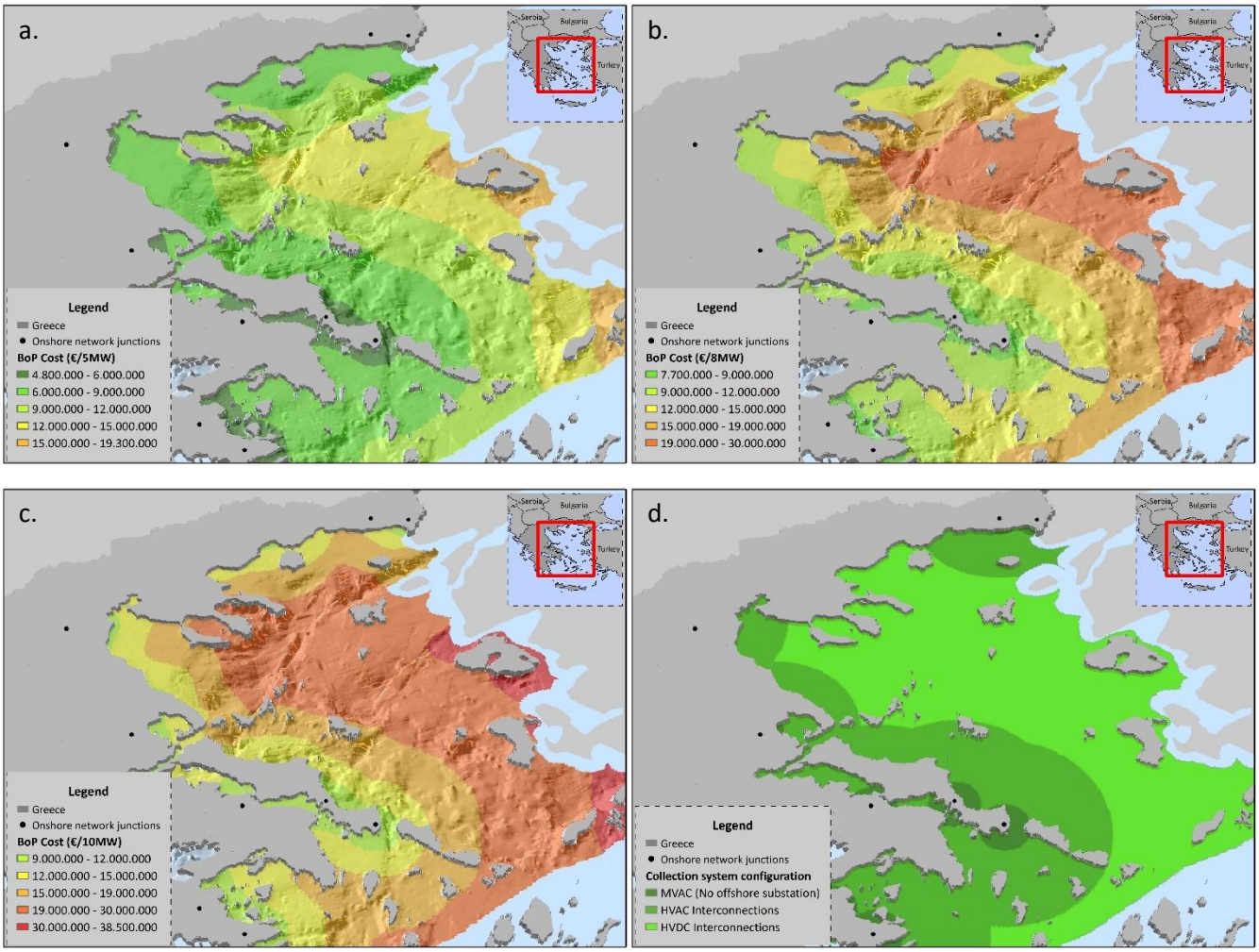


**Figure 6.2.4.1.3:** Estimated Balance of Plant production and acquisition cost based on the Dicorato et al. (2011) model on per wind turbine basis for the a) 5MW, b) 8MW and c) 10MW wind generators. d) Collection and interconnection system configuration schemes

Finally, Figure 6.2.4.1.4 illustrates the variability of the total BoP cost estimates in terms of the spatial resolution decrease (cell size increase) from 5000 meters to 2000 meters and 1000 meters respectively. For the analytical model, a difference between 1.2 - 2.25% occurred from the 1000 m. to the 2000 m. cell size, 3.5 - 5% from the 2000m. to the 5000 m. and finally, a total percentage difference between 5.9 - 6.15% occurred from the 1000 m. to the 5000 m. cell size. On the contrary, for the simplified cost model, these differentiations range between 0.5 - 0.6%

from the 1000 m. to the 5000 m., with the smaller percentage errors occurred from the 1000 m. to the 2000 m. and from the 2000 m. to the 5000 m.

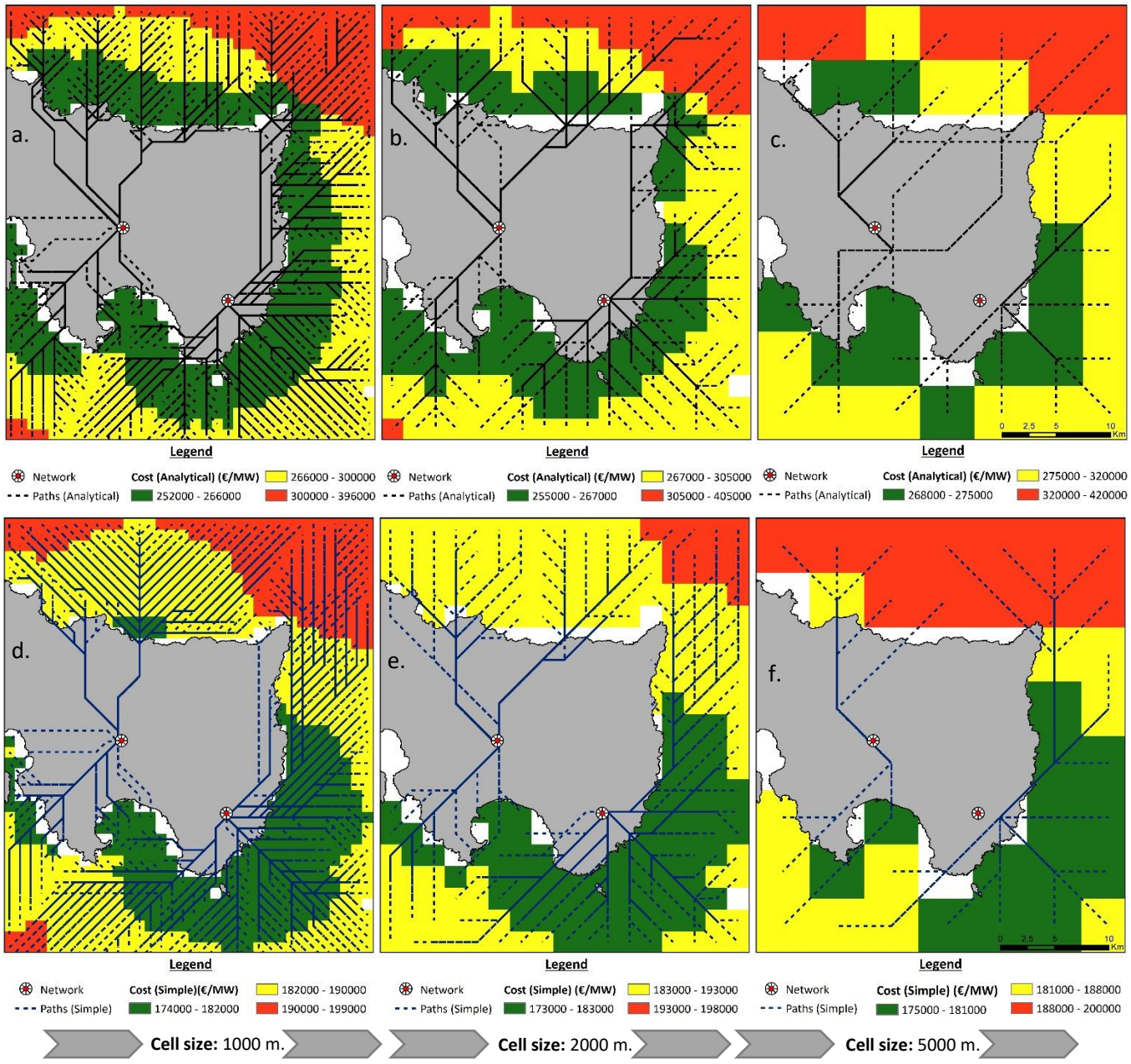


**Figure 6.2.4.1.4:** Dijkstra export cables delineation and cost differences for a cell size of a,d) 1000 m., b,e) 2000 m. and c,f) 5000 m. using the Dicorato et al. (2011) model (a-c) and the Hong & Moller (2011) model (d-f)

### 6.2.4.2 Operation and Maintenance cost results (O&M)

The annual O&M cost (Figures 6.2.4.2.1-2) ranges from 71500 - 100000 €/MW for areas within approximately 30 km. from the nearest port. For distances beyond 30 km., O&M cost exceeds up to 180000 €/MW mainly in the South and Central Aegean Sea and the North Euboean Gulf (Figure 6.2.4.2.1a). These costs increase by 20% up to 55% when the model established by Cavazzi and Dutton (2016) is selected (Figure 6.2.4.2.1b). A cost reduction obtained using the Chaikin's corner cutting smoothing algorithm of 1.5% (approx. 3000€/MW) and the final cost ranges between 71500 - 168000 €/MW. For the Bézier curves smoothed corridors, a total reduction of 6.5% (approx. 12000€/MW) occurred and the O&M cost ranges between 71500 - 158000 €/MW.

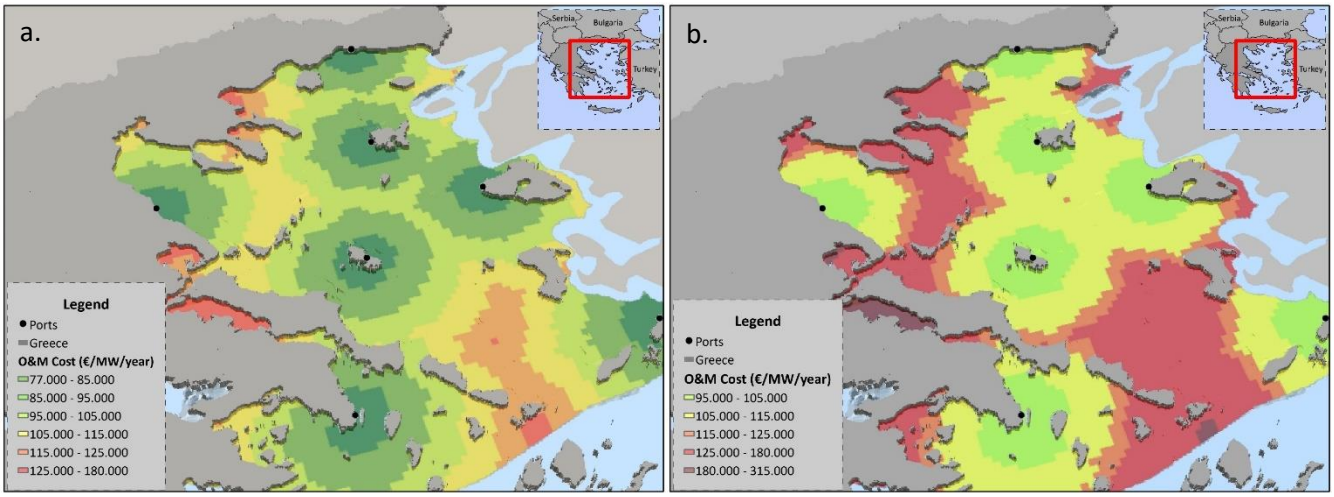


**Figure 6.2.4.2.1:** O&M cost estimates based on the models' proposed by a) Hong and Moller (2011) and b) Cavazzi & Dutton (2016)

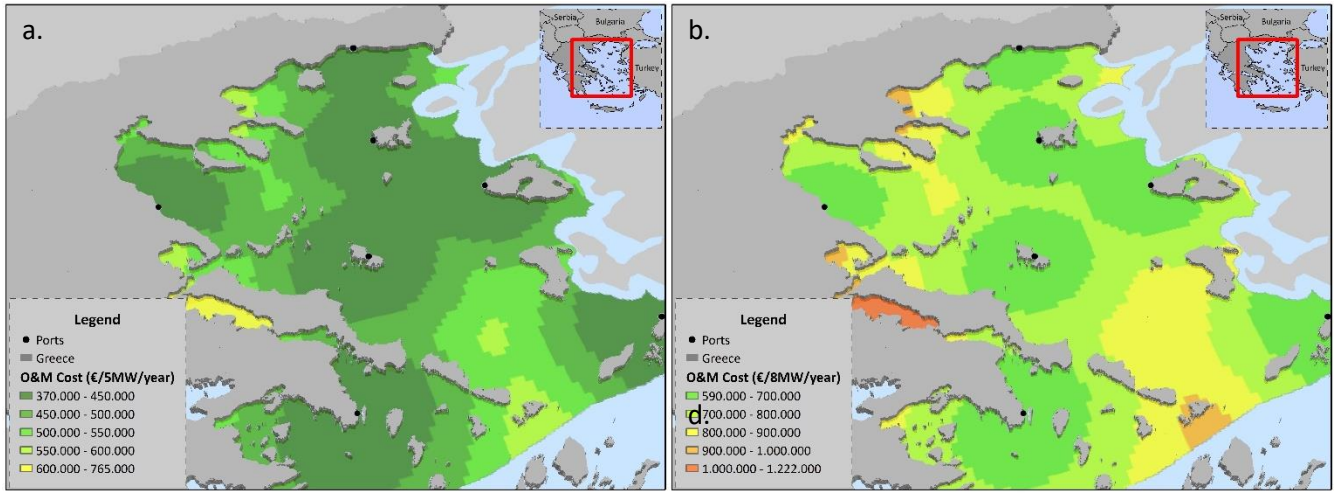

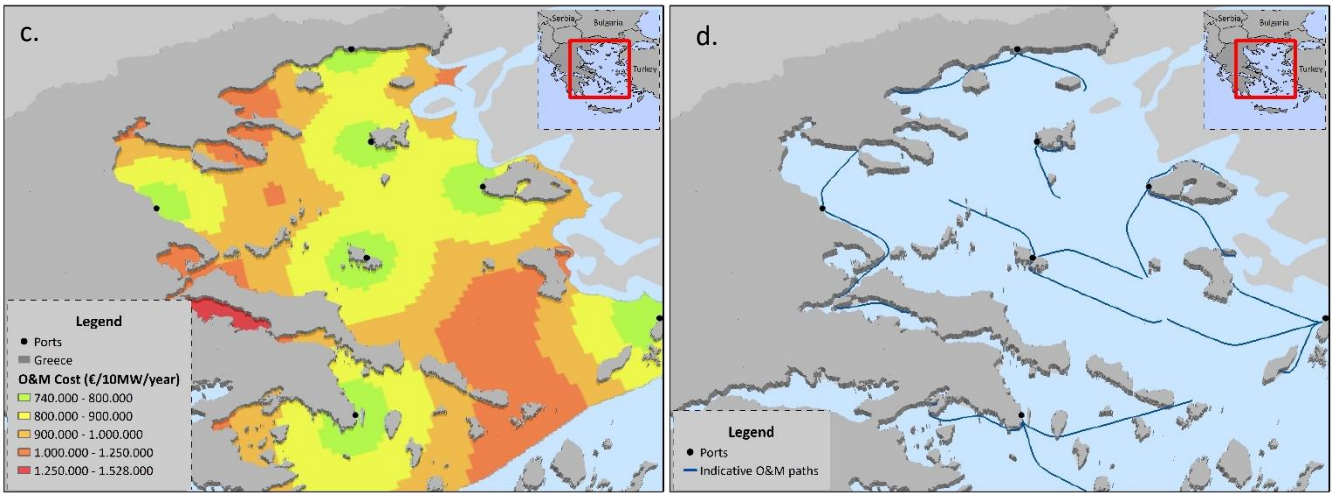


**Figure 6.2.4.2.2:** O&M cost estimates based on the model proposed by Hong and Moller (2011) for the a) 5MW, b) 8MW and c) 10MW wind turbines. d) Indicative curved paths from the shortest port

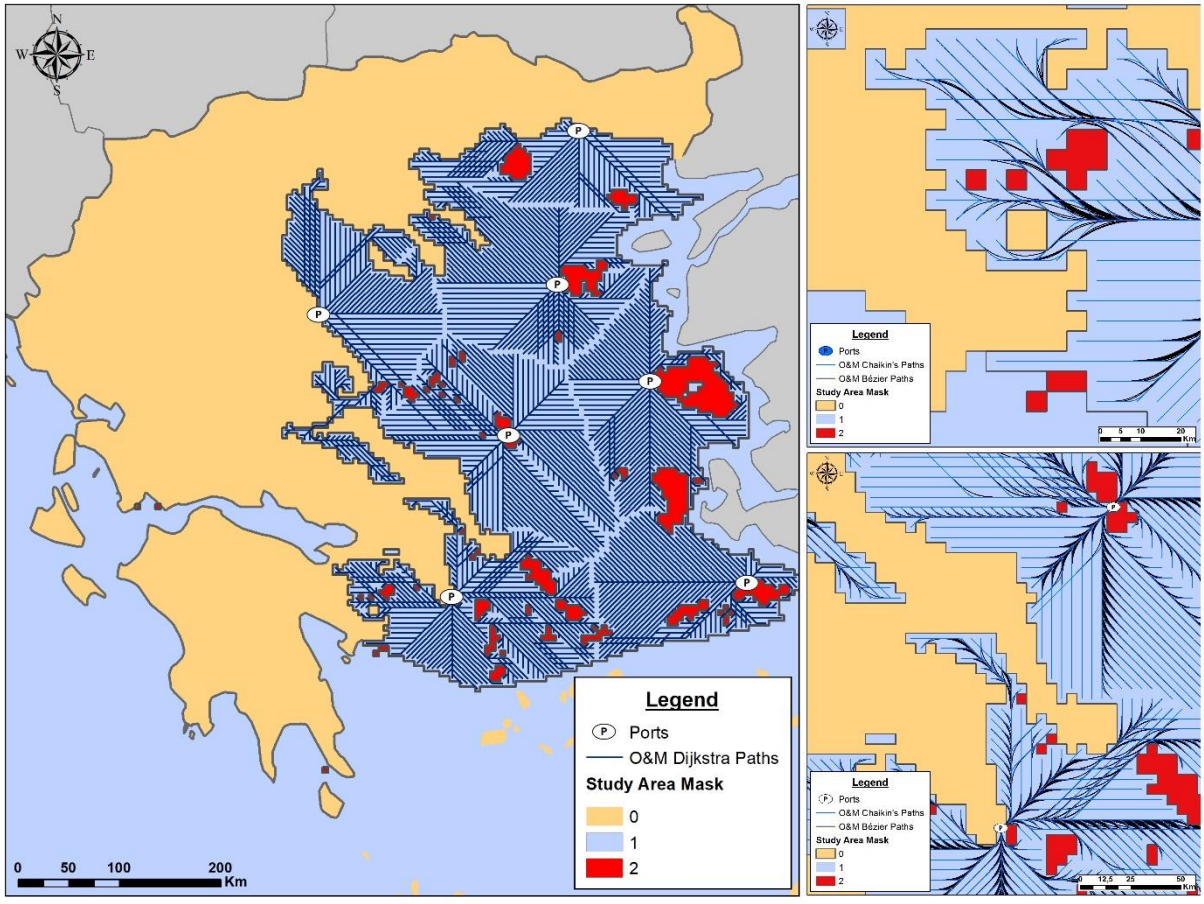


**Figure 6.2.4.2.3:** Dijkstra O&M vectorized paths (left) and curved paths using Chaikin's corner cutting algorithm and Bézier curves (right)

In terms of the total annual O&M for each different wind turbine (i.e., 5, 8 and 10MW), Figure 6.2.4.2.1a-c illustrates the total cost estimates based on the cost expression from Hong and Moller (2011). The final costs estimated between 370000€ and 760000€ for the 5MW concepts, from 590000€ to 1200000€ for the 8MW and finally, from 740000€ to 1500000€ for the 10MW concepts respectively. It is noticed that further cost assessment was applied based on the model of Cavazzi and Dutton (2016), considering the fixed and the variable costs values for each wind turbine model linked to the differences that might occur in the full load hours and the total failures of each wind turbine (i.e., increased number of failures for the 8 and 10MW concepts).

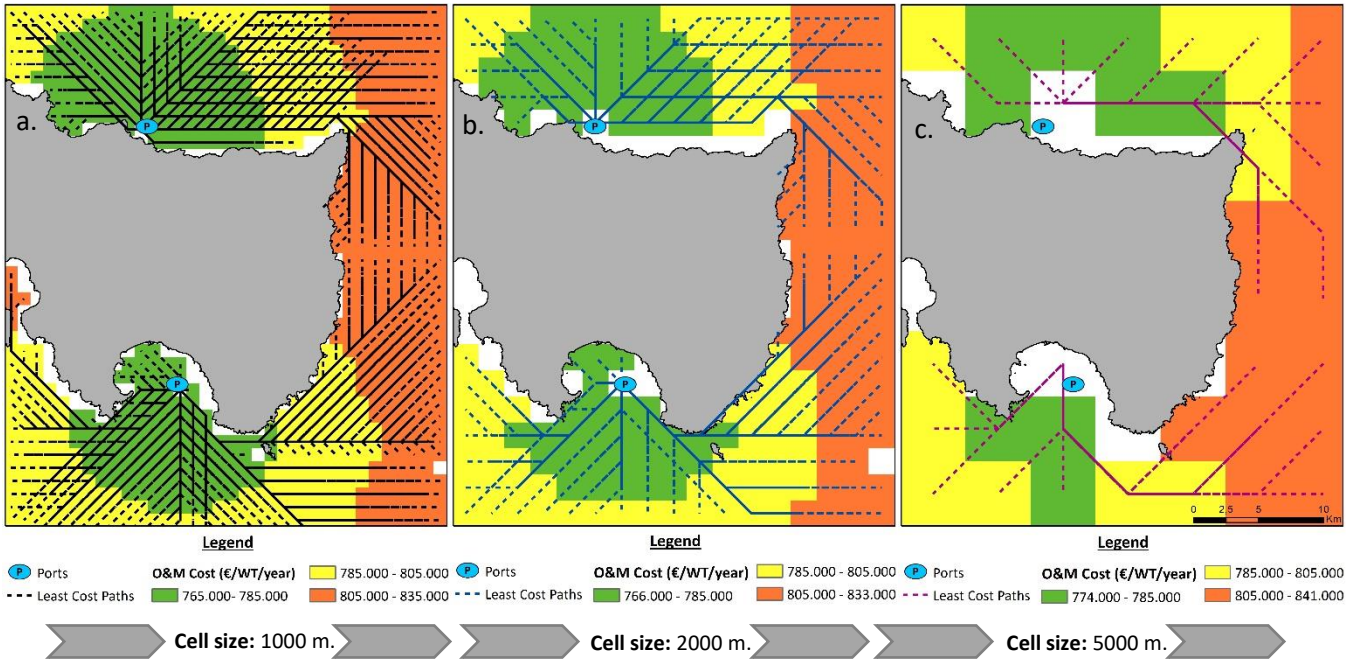


**Figure 6.2.4.2.4:** Dijkstra O&M routes delineation and cost differences for a cell size of a) 1000 m., b) 2000 m. and c) 5000 m. using the model applied by Hong & Moller (2011)

In addition to the aforementioned cost results, Figure 6.2.4.2.2d and Figure 6.2.4.2.3 illustrate the final vectorized paths as extracted by the Dijkstra algorithm and the smoothing techniques applied upon the initial Dijkstra paths. In terms of the paths optimality and the cost reduction associated to the smoothing techniques, results indicate increased cost differences between the initial Dijkstra and the smoothed paths (see Table 6.2.4.6.1). These results are expected because of the homogenized raster cost surface used, as long as the only criterion in

order to extract the optimal paths was the total length and thus, only the directional measures were used, without considering the 3D length, the landcover or the slope parameters (as applied in the transmission lines). In addition, the impact of the cell size increase from 1000 m. to 2000 m. and 5000 m. is presented in Figures 6.2.4.2.4. The cost differences approximate a 0.5 - 1.2% percentage error from 1000 m. to 5000 m. and these errors are further reduced to 0.2 - 0.8% when resampling the initial data from 1000 m. to 2000 m and from 2000 m. to 5000 m. respectively.

It is also highlighted that the proposed algorithm is not used to accurately delineate shipping routes for navigation purposes, however, some of the criteria used in this modelling scheme consist of a solid base for more accurate distance-based calculations by incorporating turns control, obstacles' avoidance and finally, length's minimization rather than simply estimating Euclidean distances or simplified pathfinding approaches. In this context, the most important aspect was to propose a multi-objective LCP optimization scheme that delivers more accurate results instead of using simplified GIS functions utilized in previous studies. Comparisons with these approaches indicated that the cost estimates are highly underestimated when using non-integrated LCP algorithms. For the transmission lines, the installation and decommissioning cost and finally, the O&M costs, a mean underestimation of approximately 60% and 80% respectively were noticed.

### 6.2.4.3 Installation and commissioning cost results (I&C)

Focusing on the installation and commissioning costs, Figure 6.2.4.3.1 presents the costs variations for the 5,8 and 10 MW wind generators expressed in euros(€). The total installation and commissioning cost incorporates all the OWF's installation procedures, as already highlighted in the previous Section (5). Consequently, the final cost values express the wind turbine, the foundation, the export and inner array cables and the offshore (or/and onshore) substation installation configurations and procedures for either the bottom-fixed or the floating concepts. It is noticed that all cost estimates are reduced at a wind turbine level, even for the cables installation and the offshore substation(s), where the total cost of the entire OWF is calculated

first (e.g., for a reference 500MW or 1000MW offshore wind farm) and then these costs are downgraded to a single wind turbine level.

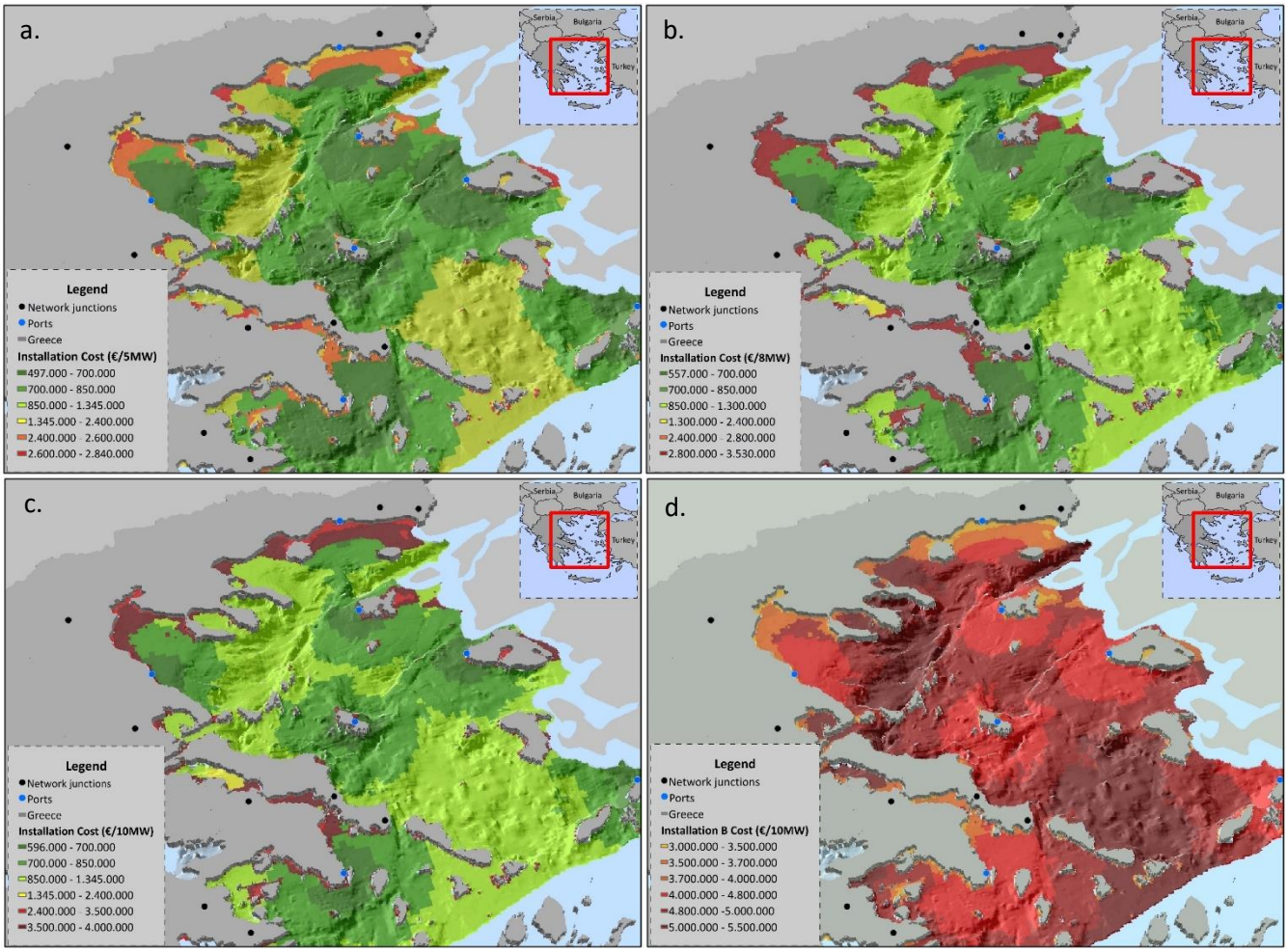


**Figure 6.2.4.3.1:** Installation and Commissioning cost (Towing of complete WTs for the floating concepts) for the a) 5MW, b) 8MW and c) 10MW wind turbines. d) Installation and Commissioning cost for the 10MW wind turbines (Towing only the floaters for the floating concepts)

In Figure 6.2.4.3.1a-c the total cost estimates for both the bottom-fixed and the floating concepts are demonstrated. It is highlighted that for the floating concepts these results are based on the installation scenario where the entire wind turbine (including the floater) is towed to the potential site as long as the same procedure is followed for the floating offshore substation. Consequently, for the 5MW concept (Figure 6.2.4.3.1a), the cost ranges from 0.5 to 2.8 million euros, for the 8MW wind turbines these costs increase up to 0.6 to 3.5 million euros (Figure

6.2.4.3.1b) and finally, for the 10MW, the installation cost is estimated in the range between 0.6 and 4 million euros (Figure 6.2.4.3.1c). On the contrary, considering the floating concepts, when the installation scenario (B) is considered, in terms of the vessels used and the installation strategies that are followed, the final installation cost is drastically increasing. Hence, for towing only the floater and transporting the topside of the wind turbine (tower and RNA), the installation cost increases to 3 - 5 m€, considering a reference wind generator of 10MW (Figure 6.2.4.3.1d). Similar differences occurred for the 5MW and 8MW concepts.

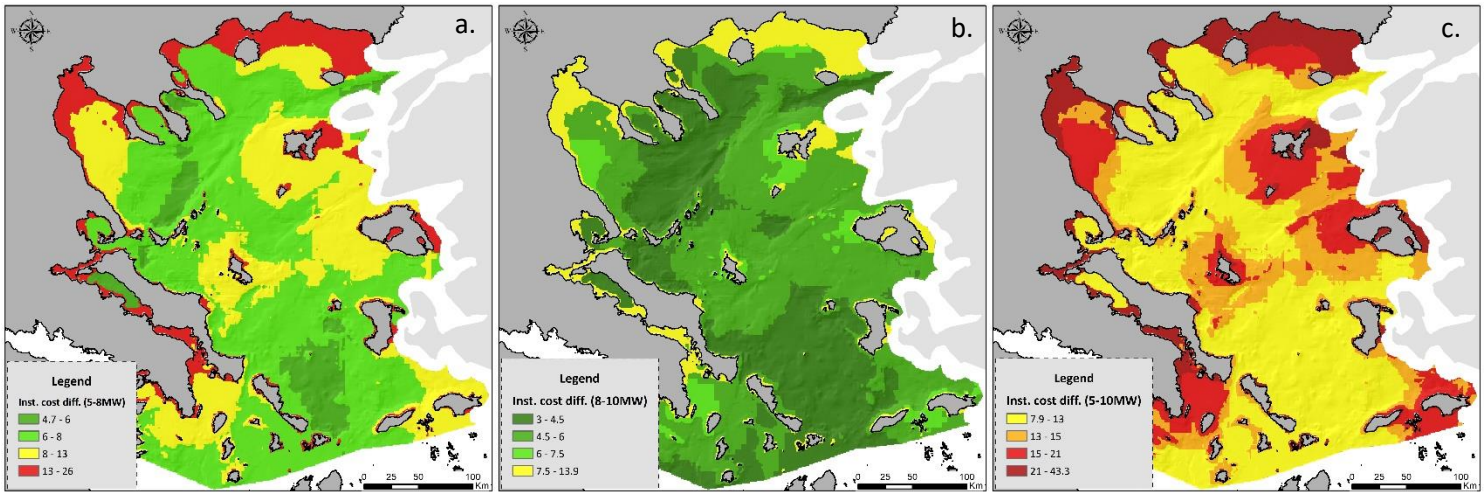


**Figure 6.2.4.3.2:** Installation and Commissioning cost (Towing of complete WTs for the floating concepts) for the a) 5MW, b) 8MW and c) 10MW wind turbines.

In terms of the cost variability among the selected wind turbines, Figure 6.2.4.3.2a-c demonstrates the cost differences (in percentage differences) between the 5MW and 8MW (Figure 6.2.4.3.2a), the 8MW and 10MW (Figure 6.2.4.3.2b) and finally, the 5MW and 10MW concepts (Figure 6.2.4.3.2c). These differences are highlighting the time increase of the installation process when the size of the wind turbine and the foundation increases, and as a result, the installation days and the total vessels' costs. Furthermore, increased cost differences occurred when considering either a bottom-fixed offshore substation or a floating substation, mainly due to the vessels needed to complete each installation procedure. Consequently, these differences are quantified in the range of 5 - 26% when increasing the wind turbine capacity from 5MW to 8MW, 3 - 14% from 8MW to 10MW and finally, a cost increase of 8 - 43% occurred when considering a 10MW wind turbine instead of 5MW.

Along with the cost variability due to the cell size increase, Figure 6.2.4.3.3 illustrates the cost uncertainty, for an indicative area, due to the spatial resolution decrease from 1000 m. to 2000 m. and 5000 m. cell size. Thus, when resampling the initial data from 1000 m. to 2000 m. cell size, installation cost is overestimated by 1.4% for nearshore areas and underestimated by 1.4% for offshore areas. However, these differences might exceed 100% in specific areas due to the loss of valuable information in terms of the water depth values (i.e., depth cut-off values to consider either bottom-fixed or floating concepts). These differences are highlighted in the dashed black circles of Figure 6.2.4.3.3b-c. These values, increase to a 7% difference for the offshore areas when resampling from 2000 m. to 5000 m. and for the nearshore areas these differences might exceed 110%.

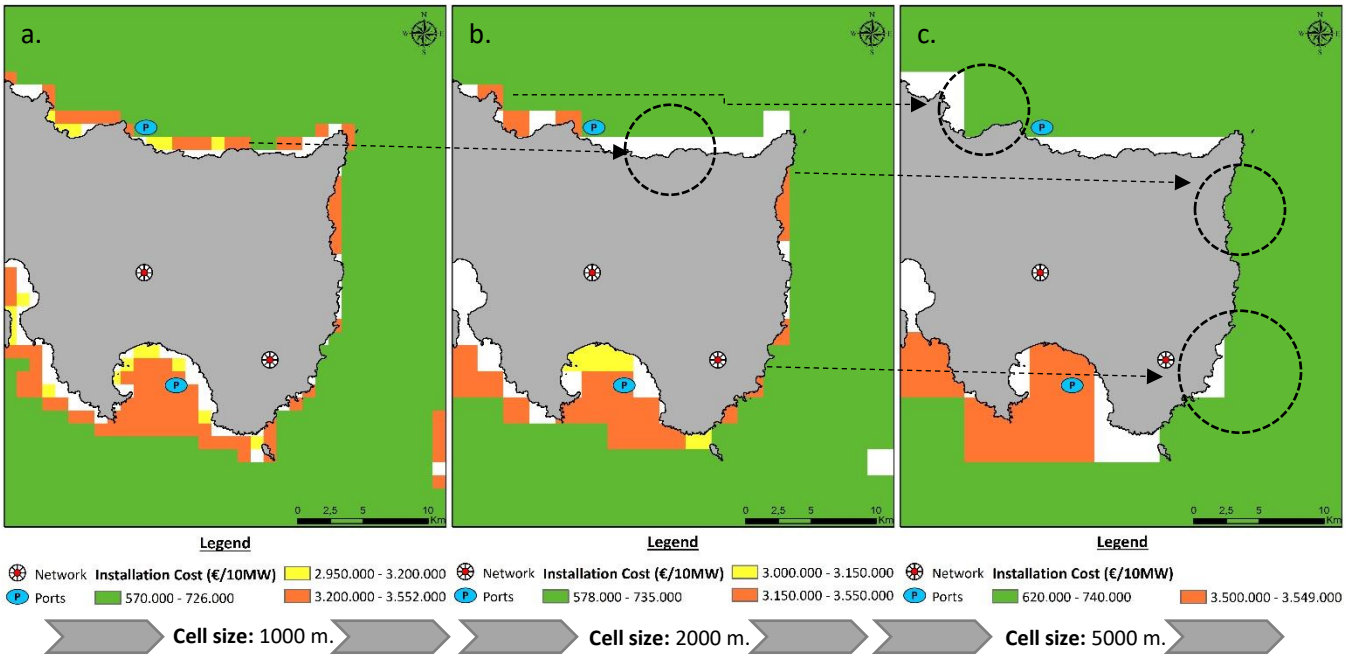


**Figure 6.2.4.3.3:** Dijkstra O&M vectorized paths and Annual O&M cost raster (upper and bottom left), Dijkstra and smoothed vectorized paths (right)

### 6.2.4.4 Decommissioning and Disposal cost results (D&D)

In the current section, all decommissioning and disposal (or dismantling) cost results are presented and discussed. The average cost of decommissioning an offshore wind farm is approximately reaching 35 - 60% of the installation cost according to previous research studies

(see Myhr et al. 2014, Shaffie et al. 2016 and Ioannou et al. 2018). Overall, the removal of a complete wind turbine is assumed to take more time for the bottom-fixed concepts compared to the floating concepts (1 - 2 days more the bottom-fixed foundations) and the decommissioning time is adjusted to the size and the capacity of each wind turbine, similarly to the installation time adjustments. Furthermore, the removal of the bottom-fixed offshore substations requires more time than the floating concepts (4-5 days less for the floating substations). The removal of the substation is assumed to take 80 - 90 % of the time taken to install the offshore substation. Similarly, the same time percentage is considered for the decommissioning of the support structures and the removal of the mooring and anchoring systems for both the substation and the wind turbines. Finally, the removal of the subsea cables is usually taking 10 - 20 % of the time taken to lay, because most of the times inter-array and export cables are partially removed. For this study, only the export cables are considered to be removed.

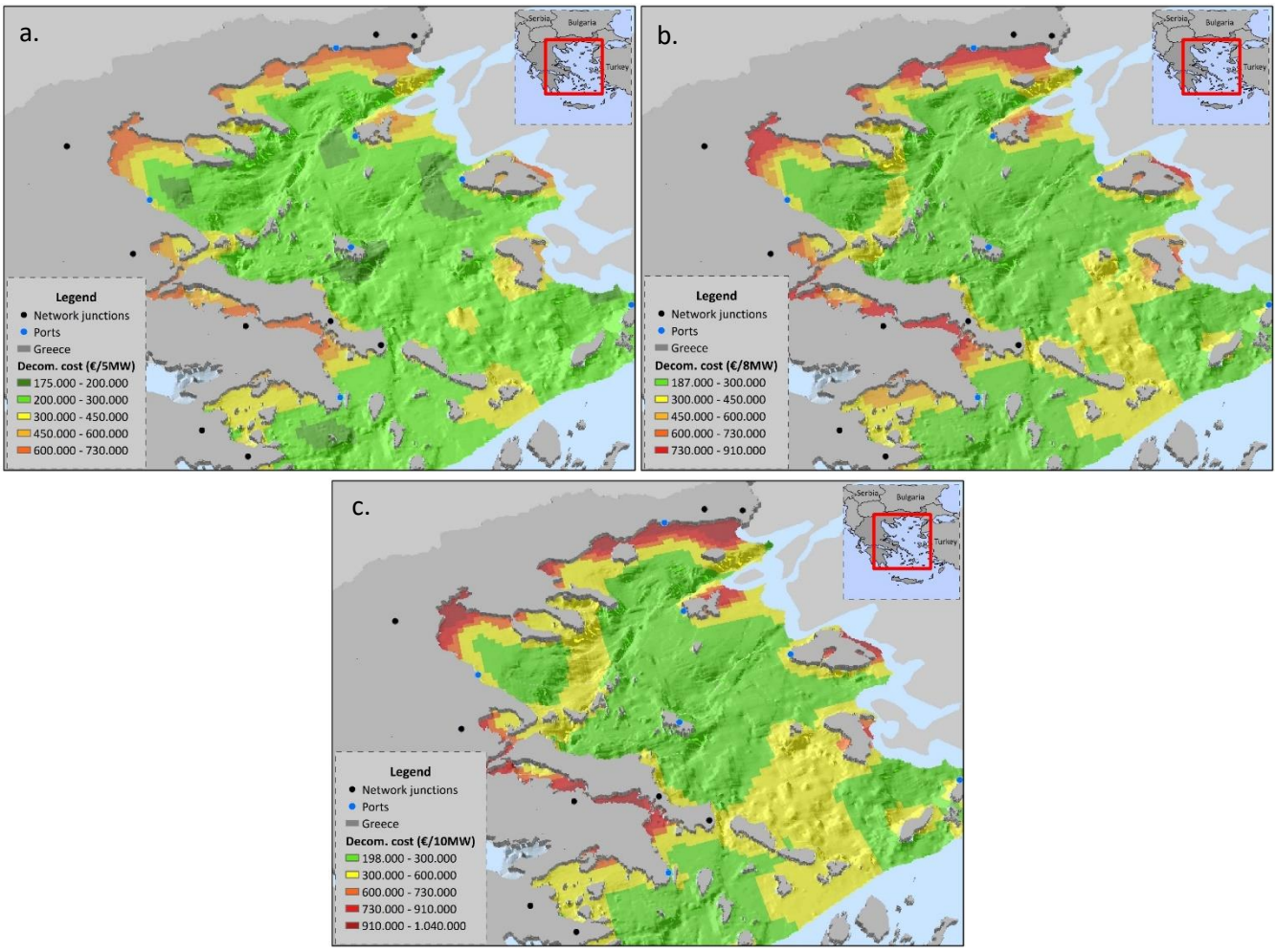

**Figure 6.2.4.4.1:** Total Decommissioning Cost per WT (including scrap revenues, see Figure 6.2.4.4.2) for a) 5MW, b) 8MW and c) 10MW

Results in Figure 6.2.4.4.1 indicate a total decommissioning cost between 0.18 - 0.73 m€ for the 5MW wind turbines (Figure 6.2.4.4.1a), 0.19 - 0.93 m€ for the 8MW (Figure 6.2.4.4.1b) and 0.2 - 1.04 m€ for the 10MW wind turbines (Figure 6.2.4.4.1c) respectively. Similarly to the installation process, the floating concepts lead to relatively inexpensive decommissioning costs compared to the bottom-fixed concepts. Thus, in the aforementioned cost results, the upper bounds highlight the decommissioning costs for either monopile and jacket concepts and the lower cost values describe the WindFloat and the Spar-Buoy concepts (0.15 - 0.6 million euros). In addition, Figure 6.2.4.4.2 presents the spatial distribution of the scrap revenues for each foundation concept (including the tower, the RNA and the export cables). The jacket structures rely on relatively low material consumption, giving low returns from scrap steel, compared to the monopiles. Additionally, either the WindFloat or the Spar-Buoy concepts, are expected to gain more from scrap steel, mainly because of the steel-intensive floaters where their mass exceeds 4000 tons.

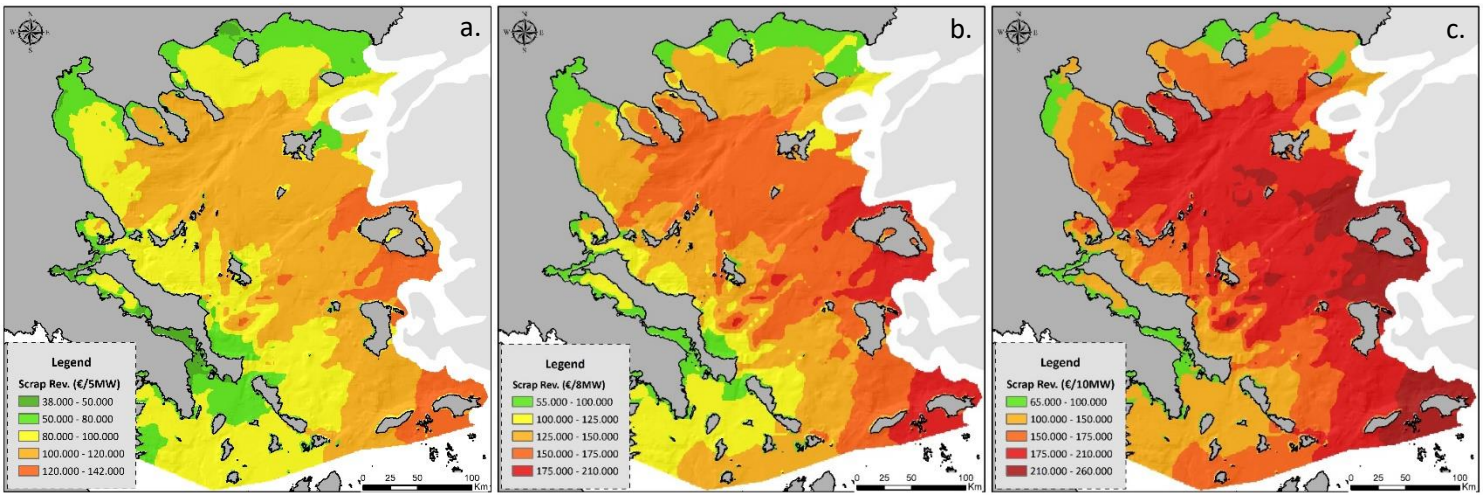


**Figure 6.2.4.4.2:** Scrap revenues (including WTs, foundations and export cables) for a) a 5MW, b) 8MW and c) 10MW wind turbines

The total wind turbines and foundations mass is extracted from the production and acquisition phase (P&A) where all of the cost equations are linked to the estimated mass for both the topside (wind turbine and tower) and the foundation type that is selected. Finally, it is noticed that since the scrap steel or copper prices are extremely volatile, it is difficult to estimate the scrap price 20 or 25 years in advance, thus, an average steel scrap price is estimated to be 90€ - 110€ per ton and a value of 1800€ per ton for the copper scrap revenues. The total scrap revenues for the 5MW wind turbines are estimated in the range between 38000 - 142000€ (Figure 6.2.4.7.2a), 55000 - 240000€ for the 8MW (Figure 6.2.4.7.1b) and 65000 - 260000€ for the 10MW wind turbines (Figure 6.2.4.7.2c).

Finally, the cost differences in terms of the cell size increase from 1000 m. to 2000 m. and 5000 m. are similar to the installation cost estimates (see Figure 6.2.4.3.3) as long as the same input data are used consisting of the distances from the closest onshore network junction (export cables decommissioning) and the distance from the nearest port/harbor (vessels' paths delineation) in order to estimate the total travel and removal time.

### 6.2.4.5 Paths' straightness control (Sinuosity Index)

As it was underlined in Section 3.2, many different indices are referred in the global literature for straightness quantification and assessment, mostly from research fields focusing on hydrology (rivers sinuosity) or animal paths movement (Benhamou 2004). Among these indices, Sinuosity Index (*SI*) is mostly applied, expressed in many different mathematical forms. According to Benhamou (2004) and Almeida *et. al.* (2010) *SI* is expressed as:

$$SI = 2[p(\frac{1-c^2-s^2}{(1-c^2)+s^2} + b^2)]^{-0.5} \qquad (6.2.4.5.1)$$

where *p* is the mean step path length, *c* is the mean cosine of turning angles, *s* is the mean sine of turning angles and *b* is the coefficient of variation of step length. Although, this index seems to be efficient for generating or assessing strongly sinuous paths, is not efficient for straight or straight-like paths. For this reason, a customized sinuosity index ($SI_n$) is established and is taken

under consideration focusing on the weighted segment's length, the real total length and the Euclidean distance connecting the start and the end of the path expressed as:

$$SI_n = |(\left(\frac{\sum_{i=0}^{j} p_i * \cos(a_{i,i+1})}{length_n{}^2}\right) * ED)^{-1}| \quad (6.2.4.5.2)$$

where $p_i$ is each segment's length, $\cos(a_i)$ is the cosine of the angle formulated between two neighbored segments (*i, i+1*), length$_n$ is the sum of all segments' lengths ($p_i$) and *ED* is the Euclidean distance. The scaling of the proposed customized *SI* indicates that paths occurring values of 1 are straight lines and as long as the path is meandering *SI* increases, considering that a circled meander path exceeds values to infinity (proportional to the circle radius and the total number of circle's perimetric points). Using the proposed sinuosity index as a straightness assessment metric, algorithm's capability to extract optimal results regarding the user's set up is remarkable and accurate in accordance to the objective's optimal values.

In Figure 6.2.4.5.1a-f the straightness assessment and controlling of the proposed algorithm are demonstrated, in both maps and histograms, expressed by the customized *SI* reduction according to the angles control (weighting). In particular, for a selected sampled area of nearly 300 different paths in the Saronic Gulf, results indicate a total mean *SI* reduction of 0.05 units for O&M paths and 0.1 for the transmission line routes respectively. In some cases, *SI* is reduced by one unit (e.g., from 3 to 2) mainly in the transmission paths delineation and this comes into sight due to the anisotropy of the cost surface upon multiple objectives (in comparison to the O&M paths where only the distance and the straightness are optimized). These differences may seem to be rather small although, difference of 0.05 - 0.1 indicates one or more angles' of 135$^o$ degrees elimination and higher decrease is mostly occurred for angles of 45$^o$ degrees reduction or elimination. Results for the entire study area in Figure.6.2.4.5.1e.-7f climax that *SI* values range between 1 - 1.4 and 1 – 1.2 for the O&M and transmission paths. Increased *SI* for the O&M paths is explained due to the obstacles' existence where the algorithm forces to avoid them leading to semi-circular segments.

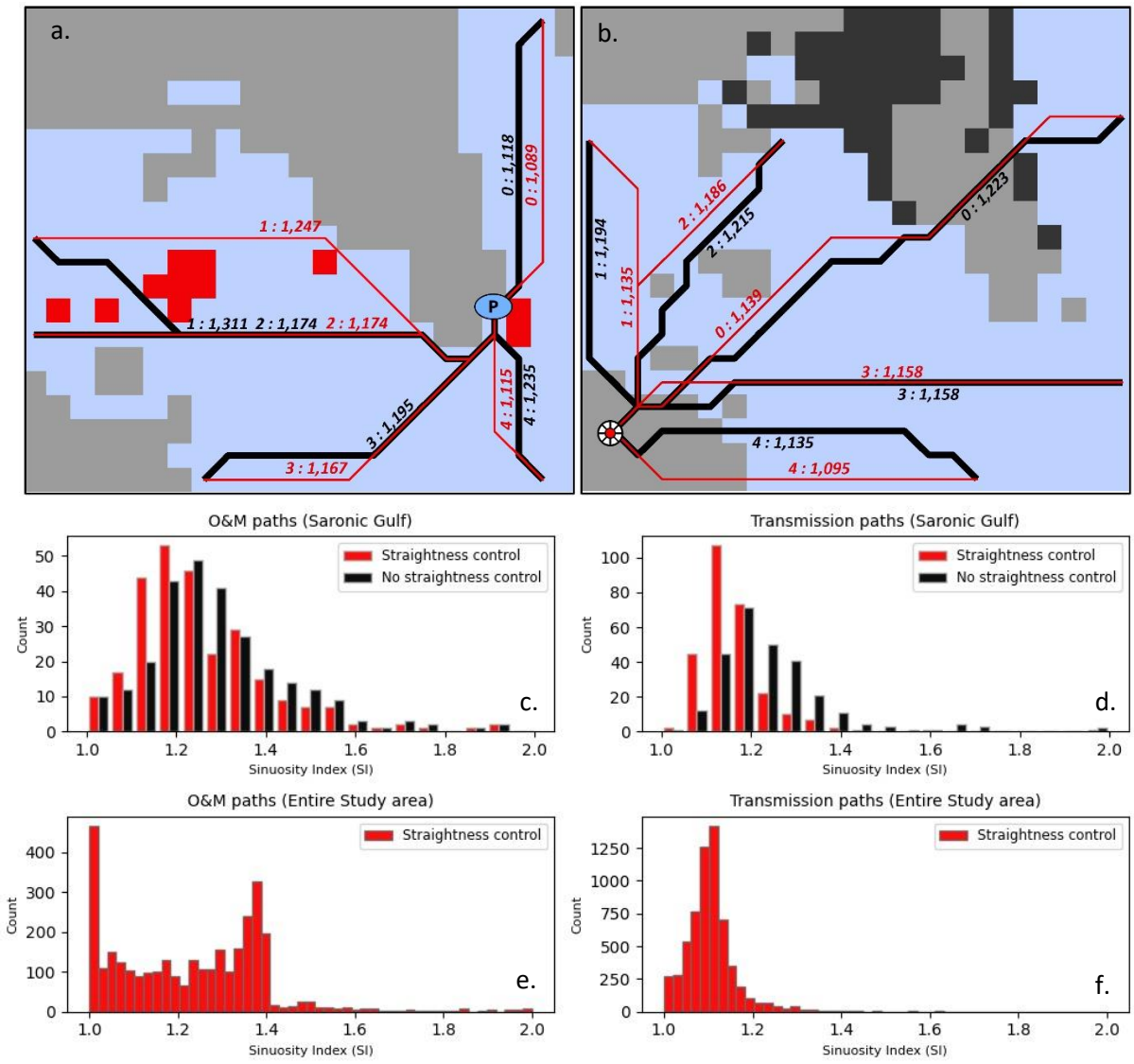


**Figure 6.2.4.5.1:** Sinuosity Index (*SI*) assessment results: a) - d): O&M and Transmission paths with equal and unequal straightness control (maps and histograms), e) - f): O&M and Transmission paths *SI* histogram for the entire study area

### 6.2.4.6 Path smoothing techniques

In this section path smoothing techniques and final cost evaluation are discussed and demonstrated in Table 6.2.4.6.1 as also in Figure 6.2.4.6.1. In general, considering smoothing results, Chaikin's algorithm and Bézier curves lead to additional length and cost minimization. Regarding O&M, the results are satisfactory with no constraints violation in regard to the paths'

agreement upon the homogenous cost surface. On the other hand, considering the transmission paths delineation in a 3D surface, and in order to guarantee that the smoothed paths will not cross pixels that were not part of the initial Dijkstra solution, different configurations were applied leading to decreased length and cost minimization.

**Table 6.2.4.6.1:** Transmission and O&M statistical results using Dijkstra and Smoothing techniques

| **Transmission Length** | ***Dijkstra Stats.*** | ***Chaikin's Stats.*** | ***Bézier Stats.*** | ***Dijkstra-Chaikin's Difference*** | ***Dijkstra-Bézier Difference*** | ***Chaikin's-Bézier Difference*** |
|---|---|---|---|---|---|---|
| **Mean** | 131653 | 130980 | 130076 | -0.583 | -1.279 | -1.779 |
| **Standard Error** | 800.01 | 797.57 | 764.98 | 0.005 | 0.007 | 0.01 |
| **Median** | 125222 | 124604 | 123665 | -0.510 | -1.107 | -1.765 |
| **Standard Deviation** | 62713 | 62521 | 61530 | 0.372 | 0.613 | 0.921 |
| **Minimum** | 7072 | 7072 | 7071 | -3.457 | -4.065 | -6.889 |
| **Maximum** | 308681 | 307284 | 303705 | 0.000 | 0.000 | -0.001 |
| **OnM Length** | ---------- | | | | | |
| **Mean** | 81722 | 81264 | 80358 | -0.622 | -1.672 | -1.058 |
| **Standard Error** | 497.59 | 495.04 | 485.73 | 0.007 | 0.013 | 0.009 |
| **Median** | 77426 | 77148 | 76378 | -0.490 | -1.467 | -0.987 |
| **Standard Deviation** | 39006 | 38806 | 38076 | 0.535 | 1.033 | 0.683 |
| **Minimum** | 5000 | 5000 | 5000 | -8.897 | -8.205 | -6.733 |
| **Maximum** | 290061 | 287001 | 267677 | 0.000 | 0.410 | 0.401 |

For the transmission cost evaluation, a mean difference between 0.5% – 1.2% occurred with the lower bound expressing the differences among Dijkstra and Chaikin's paths and the upper bound reveals the total cost differences among Dijkstra and Bézier paths. Additionally, for the O&M, the installation and decommissioning paths a total reduction between 0.65% – 1.67% occurred. The higher reduction levels are explained for the configurations applied for the smoothing techniques upon homogenous (i.e., O&M) and non-homogenous (transmission) raster surfaces as illustrated in Figure 6.2.4.6.1. The former smoothed paths (Figure 6.2.4.6.1b) are allowed to cross neighboring pixels, hence, the total route length is further reduced compared to

the restrictions applied for the transmission cables paths which were forced to lay withing the initial Dijkstra pixels (Figure 6.2.4.6.1a).

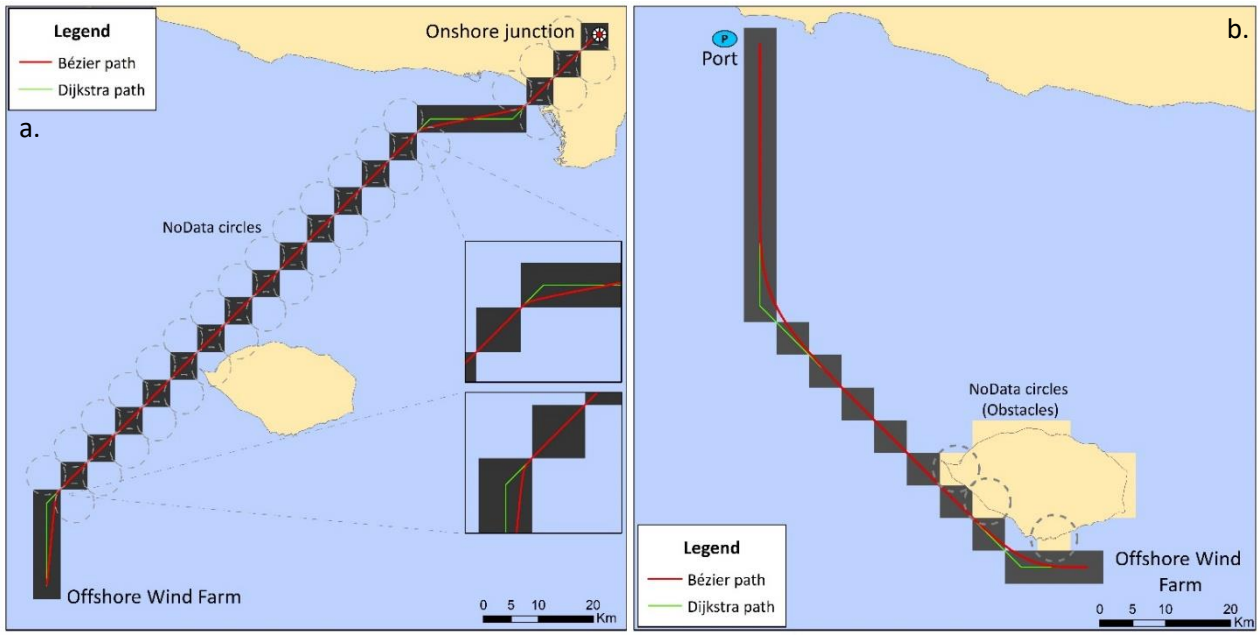


**Figure 6.2.4.6.1:** Bézier curve results for the a) Transmission lines (non-homogenous cost raster) and, b) O&M paths (Homogenous cost rasters)

## 6.3 Offshore Wind Resource Assessment and Simulation

In this section, for the observed regions of the North and Central Aegean Sea, the preliminary wind resource assessment and the stochastic simulation scheme results are illustrated. At first, the GoF test results, the graphical fitting representations, the optimal wind speed frequency distributions, the preliminary extreme values response analysis and the long-term persistence evaluation are determined and discussed. In accordance to the aforementioned procedures, the stochastic simulation of long-length offshore wind speed time series is demonstrated along with future scenarios for the annual energy production estimation and uncertainty quantification.

### 6.3.1 Distribution fitting and PDF models' comparison

In this section, for the observed regions of the North and central Aegean Sea, GoF test results, graphical fitting representations and optimal wind speed frequency distribution among all of the considered distribution models are determined and demonstrated. In Table 6.3.1.1 the optimal parameters for each distribution model are presented using MLE, LSE and MOM methods. For the W2 and B12 distributions the LST method provided better fitting results, for B3 the MLE and for GG the MLE and MOM methods. It is noteworthy that for B3, B12 and GG distributions, the Basin-Hopping non-linear optimization framework (Zhou et al. 2019) was applied in order to guarantee parameters' estimation optimality. Without the proper optimization set-up, several drawbacks in the estimation procedure linked to the constraints (or bounds) violations occurred (e.g., for B3 shape $c > 4$ and for B12 $cb > 4$). Moreover, for B12 and GG, in some cases, increased values observed in the shape and scale parameters, mainly in cases where the observational or the reanalysis time series tend to fit better with the W2 distribution. Therefore, the optimal set-up of the optimization algorithm must be guaranteed in either MLE, LSE or MOM method.

**Table.6.3.1.1:** Probability Density Function (PDF) parameters for the Stations/Buoys and the UERRA time series

| Stations/Buoys | W2 (k) | W2 (c) | B3 (c) | B3 (b) | B3 (a) | B12 (c) | B12 (b) | B12 (a) | GG (c) | GG (b) | GG (a) |
|---|---|---|---|---|---|---|---|---|---|---|---|
| **Athens** | 1.977 | 4.973 | 4.001 | 0.414 | 5.175 | 2.984 | 1.340 | 4.424 | 16.454 | 0.466 | 0.010 |
| **Dimokritos N.** | 1.874 | 5.450 | 4.804 | 0.311 | 6.458 | 2.394 | 2.595 | 7.126 | 3.750 | 0.921 | 1.135 |
| **Lemnos** | 1.884 | 6.301 | 6.628 | 1.674 | 5.066 | 2.177 | 4.119 | 11.055 | 3.459 | 0.949 | 1.496 |
| **Thessaloniki** | 1.648 | 4.512 | 4.386 | 2.823 | 4.401 | 2.644 | 1.513 | 4.135 | 13.988 | 0.448 | 0.010 |
| **Mytilene** | 1.750 | 5.419 | 4.033 | 2.006 | 3.732 | 2.506 | 1.596 | 5.265 | 14.535 | 0.441 | 0.010 |
| **Naxos** | 1.732 | 8.396 | 4.894 | 0.286 | 11.422 | 1.844 | 8.600 | 25.733 | 1.306 | 1.474 | 6.741 |
| **Chios** | 2.331 | 6.480 | 5.182 | 0.476 | 6.904 | 2.848 | 3.327 | 9.088 | 3.200 | 1.244 | 2.306 |
| **Mykonos** | 1.792 | 6.636 | 4.195 | 0.691 | 6.060 | 2.292 | 2.384 | 8.351 | 5.452 | 0.723 | 0.537 |
| **Alex. Pap.** | 2.097 | 5.154 | 5.428 | 0.340 | 6.225 | 2.208 | 12.123 | 15.514 | 1.302 | 1.795 | 4.316 |
| **Samos** | 2.205 | 7.801 | 6.989 | 0.244 | 10.294 | 2.295 | 13.938 | 24.041 | 1.032 | 2.163 | 7.659 |
| **Skyros** | 2.264 | 4.533 | 4.330 | 0.519 | 4.247 | 4.615 | 0.867 | 3.430 | 21.079 | 0.512 | 0.010 |
| **Athos (B)** | 1.324 | 5.738 | 4.855 | 0.196 | 9.697 | 1.399 | 10.967 | 30.319 | 0.446 | 2.266 | 9.727 |
| **Lesvos (B)** | 1.616 | 7.378 | 6.826 | 0.169 | 11.458 | 1.686 | 15.520 | 36.583 | 0.482 | 2.588 | 11.028 |
| **Mykonos (B)** | 1.704 | 8.418 | 10.677 | 0.111 | 13.285 | 1.791 | 17.277 | 40.509 | 0.620 | 2.259 | 11.130 |
| **Petrokaravo (B)** | 1.652 | 5.801 | 6.580 | 0.178 | 9.111 | 1.688 | 16.266 | 29.607 | 0.482 | 2.688 | 8.632 |
| **Skyros (B)** | 1.698 | 6.705 | 5.633 | 0.225 | 9.817 | 1.770 | 16.108 | 31.417 | 0.607 | 2.347 | 9.005 |

| UERRA | W2 (k) | W2 (c) | B3 (c) | B3 (b) | B3 (a) | B12 (c) | B12 (b) | B12 (a) | GG (c) | GG (b) | GG (a) |
|---|---|---|---|---|---|---|---|---|---|---|---|
| Athens | 1.653 | 2.989 | 4.983 | 0.264 | 4.203 | 1.706 | 18.990 | 16.410 | 1.008 | 1.645 | 2.971 |
| Dimokritos N. | 1.648 | 4.885 | 4.990 | 0.259 | 6.966 | 1.723 | 13.660 | 21.573 | 1.130 | 1.529 | 4.424 |
| Lemnos | 1.620 | 5.010 | 4.949 | 0.255 | 7.227 | 1.694 | 15.004 | 24.033 | 0.903 | 1.726 | 5.404 |
| Thessaloniki | 1.592 | 3.187 | 4.040 | 2.101 | 2.775 | 1.833 | 3.885 | 5.976 | 7.140 | 0.548 | 0.072 |
| Mytilene | 1.751 | 4.402 | 6.014 | 0.217 | 6.449 | 1.807 | 15.774 | 19.774 | 0.730 | 2.141 | 5.357 |
| Naxos | 1.874 | 5.677 | 7.039 | 0.191 | 8.394 | 1.947 | 19.413 | 25.524 | 0.667 | 2.437 | 7.122 |
| Chios | 1.860 | 4.088 | 6.502 | 0.213 | 5.842 | 1.918 | 17.867 | 18.009 | 0.675 | 2.393 | 5.108 |
| Mykonos | 1.756 | 4.821 | 4.680 | 0.315 | 6.079 | 1.822 | 14.354 | 20.236 | 1.239 | 1.544 | 4.072 |
| Alex. Pap. | 1.923 | 4.849 | 7.888 | 0.172 | 7.185 | 1.953 | 19.505 | 21.834 | 0.514 | 2.995 | 6.686 |
| Samos | 1.935 | 4.459 | 8.869 | 0.150 | 6.773 | 1.985 | 22.148 | 20.910 | 0.467 | 3.239 | 6.328 |
| Skyros | 1.498 | 3.629 | 4.003 | 1.728 | 3.485 | 1.699 | 4.484 | 7.914 | 3.751 | 0.719 | 0.486 |
| Athos (B) | 1.681 | 6.798 | 4.087 | 0.360 | 8.542 | 1.762 | 10.958 | 25.466 | 1.286 | 1.445 | 5.504 |
| Lesvos (B) | 2.229 | 8.143 | 10.185 | 0.151 | 11.568 | 2.270 | 20.716 | 30.556 | 0.413 | 4.067 | 11.338 |
| Mykonos (B) | 1.887 | 4.420 | 8.388 | 0.155 | 6.773 | 1.949 | 19.203 | 19.748 | 0.497 | 3.019 | 6.206 |
| Petrokaravo (B) | 1.608 | 3.927 | 4.365 | 0.302 | 5.378 | 1.668 | 13.875 | 18.416 | 1.397 | 1.315 | 2.893 |
| Skyros (B) | 1.788 | 6.321 | 4.762 | 0.313 | 8.231 | 1.878 | 11.276 | 22.174 | 1.178 | 1.619 | 5.582 |

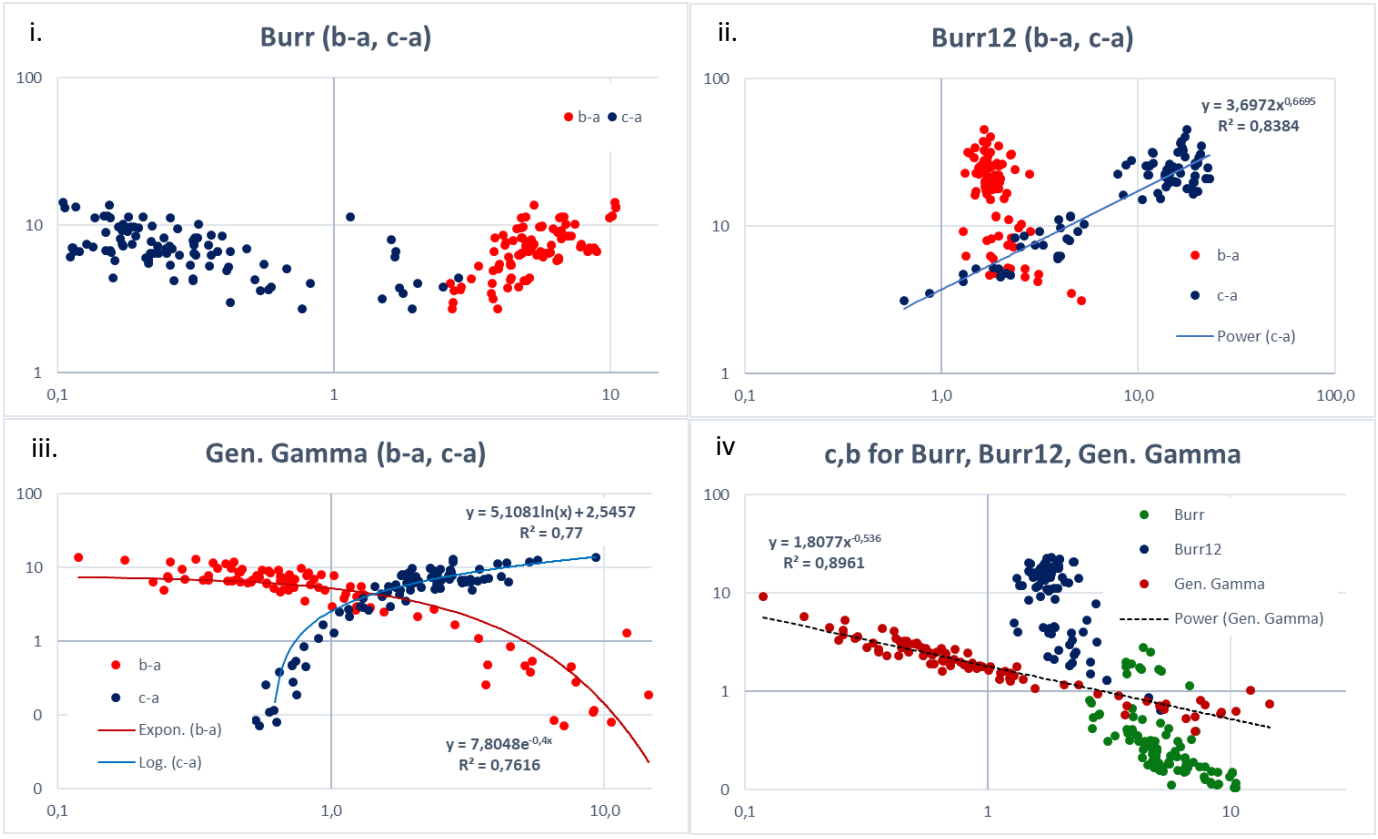


**Figure 6.3.1.1:** Estimated shape - scale (b,c - a) parameters plot for i) Burr3, ii) Burr12 and iii) Gen.Gamma, and iv) Estimated shape - shape (c - b) parameter plot for all distributions

Analyzing the results of Table.6.3.1.1, an increased variability of the scale value (*a*) is observed for all distributions, highlighting the differentiations of the mean wind speed across the study area. Furthermore, short variations are noticed for the shape value of W2 (*k*) between 1.5 – 2, for shape (*b*) of B3 distribution ranging from 0.2 to 1 and for shape (*b*) of B12 ranging between 1.4 - 4.5 (see also the applications with similar results for the shape parameter in Koutsoyiannis et al., (2018) [sect. 5.2] and Dimitriadis and Koutsoyiannis, (2018) [sect. 4.3]. By contrast, for B12, in some cases shape (*c*) and scale (*a*) parameters present slightly increased values highlighting the wide range of the parameter estimates that B12 can acquire. Considering the GG distribution, increased variability in the estimated parameters is mostly observed for the in-situ measurements since for the reanalysis data the shape (*c,b*) and scale (*a*) values are less variable. Here, it is noted that the fluctuation of the estimated parameters is also partially attributed to statistical bias due to the limited length for some of the timeseries and the long-term behavior of the wind process (Koutsoyiannis 2020).

**Table 6.3.1.2:** Ranked PDFs indicating the best fit for each goodness-of-fit statistic for the Stations/Buoys and UERRA reanalysis time series

| Station / Buoys | *K/S Test* | | | $R^2$ | | | $Chi^2$ | | | *RMSE* | | | *MAPE* | | | *Log Lik. Est. (L)* | | | *Ranks (per Station/Buoy)* | | | |
|---|---|---|---|---|---|---|---|---|---|---|---|---|---|---|---|---|---|---|---|---|---|---|
| | MLE | LST | MOM | MLE | LST | MOM | MLE | LST | MOM | MLE | LST | MOM | MLE | LST | MOM | MLE | LST | MOM | W2 | B3 | B12 | GG |
| **Athens** | B12 | B12 | B12 | B12 | W2 | GG | B12 | GG | GG | B12 | GG | GG | B12 | GG | B12 | GG | GG | GG | 1 | 0 | 8 | **9** |
| **Dimokritos North** | B3 | B3 | GG | B3 | B3 | B3 | B3 | B12 | B3 | B12 | B12 | B3 | B3 | B12 | B3 | B12 | B12 | B12 | 0 | **10** | 7 | 1 |
| **Lemnos** | B12 | B3 | GG | GG | W2 | GG | GG | B12 | W2 | GG | GG | GG | B12 | B12 | B12 | GG | GG | GG | 2 | 1 | 5 | **10** |
| **Thessaloniki** | B12 | W2 | GG | B3 | B12 | B12 | B12 | W2 | GG | B12 | W2 | GG | B12 | W2 | GG | B3 | B3 | GG | 4 | 3 | **6** | 5 |
| **Mytilene** | B3 | W2 | GG | GG | GG | GG | GG | W2 | GG | B3 | W2 | GG | GG | W2 | B12 | GG | GG | GG | 4 | 2 | 1 | **11** |
| **Naxos** | GG | B3 | W2 | W2 | GG | GG | B12 | GG | B12 | B12 | B12 | GG | GG | B12 | B12 | B12 | W2 | B12 | 3 | 1 | **8** | 6 |
| **Chios** | GG | B3 | GG | GG | W2 | GG | GG | W2 | B3 | GG | GG | GG | B12 | B12 | B3 | B12 | B12 | B12 | 2 | 3 | 5 | **8** |
| **Mykonos** | GG | B3 | B12 | GG | W2 | GG | B12 | W2 | B12 | GG | W2 | GG | B12 | GG | B12 | GG | GG | W2 | 4 | 1 | 5 | **8** |
| **Alex. Pap.** | GG | GG | GG | B12 | B3 | B12 | B12 | GG | B3 | B12 | GG | GG | B12 | W2 | B3 | B12 | B12 | W2 | 2 | 3 | **7** | 6 |
| **Samos** | W2 | GG | GG | W2 | GG | GG | W2 | B3 | W2 | W2 | GG | GG | GG | B3 | B12 | GG | GG | W2 | 6 | 2 | 1 | **9** |
| **Skyros** | B12 | GG | GG | B3 | B3 | B3 | B12 | GG | B12 | B12 | GG | B12 | B12 | GG | B12 | B3 | GG | B3 | 0 | 5 | **7** | **6** |
| **Athos (B)** | B3 | B12 | B3 | B12 | GG | GG | B12 | W2 | GG | B12 | GG | GG | B12 | W2 | GG | B12 | GG | GG | 2 | 2 | 6 | **8** |
| **Lesvos (B)** | B3 | GG | GG | B3 | GG | GG | B3 | GG | W2 | B3 | GG | GG | GG | W2 | GG | B3 | B3 | W2 | 3 | 6 | 0 | **9** |
| **Mykonos (B)** | B3 | B3 | B3 | B3 | B3 | GG | B3 | B3 | B3 | B3 | B3 | B3 | B3 | B3 | B3 | B3 | B3 | B3 | 0 | **17** | 0 | 1 |
| **Petrokaravo (B)** | GG | B3 | GG | GG | GG | GG | GG | GG | GG | GG | GG | GG | GG | B12 | GG | B3 | GG | GG | 0 | 2 | 1 | **15** |
| **Skyros (B)** | GG | GG | GG | GG | GG | GG | GG | GG | GG | GG | GG | GG | GG | B12 | GG | B12 | B12 | B12 | 0 | 0 | 4 | **14** |
| ***Ranks (per Test-Method)*** | | | | | | | | | | | | | | | | | | | **↑33** | **↑58** | **↑71** | **↑126** |
| **W2** | 1 | 2 | 1 | 2 | 4 | 0 | 1 | 5 | 3 | 1 | 3 | 0 | 0 | 5 | 0 | 0 | 1 | 4 | → | | **33** | |
| **B3** | 5 | **7** | 2 | 5 | 4 | 2 | 3 | 2 | 4 | 3 | 1 | 2 | 2 | 2 | 4 | 5 | 3 | 2 | → | | **58** | |
| **B12** | 4 | 2 | 2 | 3 | 1 | 2 | **7** | 2 | 3 | **7** | 2 | 1 | **8** | **6** | **7** | **6** | 4 | 4 | → | | **71** | |
| **GG** | **6** | 5 | **11** | **6** | **7** | **12** | 5 | **7** | **6** | 5 | **10** | **13** | 6 | 3 | 5 | 5 | **8** | **6** | → | | **126** | |

| UERRA | K/S Test | | | $R^2$ | | | $Chi^2$ | | | RMSE | | | MAPE | | | Log Lik. Est. (L) | | | Ranks (per Station/Buoy) | | | |
|---|---|---|---|---|---|---|---|---|---|---|---|---|---|---|---|---|---|---|---|---|---|---|
| | MLE | LST | MOM | MLE | LST | MOM | MLE | LST | MOM | MLE | LST | MOM | MLE | LST | MOM | MLE | LST | MOM | W2 | B3 | B12 | GG |
| **Athens** | W2 | GG | GG | B3 | GG | GG | W2 | B12 | GG | GG | GG | GG | GG | B12 | GG | GG | B12 | W2 | 2 | 1 | 3 | **12** |
| **Dimokritos North** | W2 | GG | W2 | W2 | B3 | GG | W2 | B3 | W2 | W2 | GG | GG | GG | B12 | W2 | GG | B12 | B12 | **7** | 2 | 3 | 6 |
| **Lemnos** | GG | B3 | GG | GG | B3 | GG | GG | B3 | GG | GG | GG | GG | GG | B12 | GG | GG | B12 | W2 | 1 | 3 | 2 | **12** |
| **Thessaloniki** | GG | W2 | GG | GG | GG | B12 | GG | W2 | GG | GG | W2 | B12 | GG | W2 | B12 | GG | W2 | B12 | 5 | 0 | 4 | **9** |
| **Mytilene** | GG | B3 | GG | GG | B3 | GG | GG | B3 | GG | GG | B3 | GG | GG | W2 | GG | GG | B3 | GG | 1 | 5 | 0 | **12** |
| **Naxos** | GG | B3 | GG | GG | B3 | GG | GG | B3 | GG | GG | B3 | GG | W2 | GG | W2 | GG | GG | GG | 2 | 4 | 0 | **12** |
| **Chios** | GG | B3 | GG | GG | B3 | GG | GG | B12 | GG | GG | B3 | GG | B3 | B12 | GG | GG | B12 | GG | 0 | 4 | 3 | **11** |
| **Mykonos** | GG | B3 | W2 | W2 | GG | B12 | B12 | B3 | B12 | B12 | B3 | GG | GG | B12 | W2 | GG | B12 | W2 | 4 | 3 | **6** | 5 |
| **Alex. Pap.** | GG | B3 | GG | GG | B3 | GG | GG | GG | GG | GG | GG | GG | GG | B12 | GG | GG | B12 | GG | 0 | 2 | 2 | **14** |
| **Samos** | GG | B3 | GG | GG | B3 | B3 | GG | GG | GG | GG | GG | GG | GG | B12 | GG | GG | GG | GG | 0 | 3 | 1 | **14** |
| **Skyros** | GG | B3 | GG | GG | B3 | GG | GG | W2 | GG | GG | W2 | GG | GG | W2 | GG | GG | GG | GG | 3 | 2 | 0 | **13** |
| **Athos (B)** | GG | B3 | W2 | GG | W2 | W2 | GG | W2 | W2 | GG | W2 | W2 | GG | B12 | W2 | GG | B12 | W2 | **9** | 1 | 2 | 5 |
| **Lesvos (B)** | B3 | B3 | GG | B3 | B3 | B3 | B3 | GG | GG | B3 | GG | B3 | GG | B12 | GG | B3 | B3 | B3 | 0 | **11** | 1 | 5 |
| **Mykonos (B)** | GG | B3 | GG | GG | B3 | B3 | GG | B3 | GG | GG | B3 | GG | GG | GG | GG | GG | GG | GG | 0 | 5 | 0 | **13** |
| **Petrokaravo (B)** | GG | B3 | GG | W2 | GG | GG | B12 | B3 | GG | W2 | B3 | GG | W2 | B3 | W2 | GG | B12 | W2 | 4 | 4 | 2 | **8** |
| **Skyros (B)** | GG | GG | GG | W2 | B12 | GG | GG | GG | W2 | W2 | GG | GG | GG | W2 | W2 | GG | GG | W2 | 6 | 0 | 1 | **11** |
| ***Ranks (per Test-Method)*** | | | | | | | | | | | | | | | | | | | **↑45** | **↑50** | **↑31** | **↑162** |
| **W2** | 2 | 1 | 3 | 4 | 1 | 1 | 2 | 3 | 3 | 3 | 3 | 1 | 2 | 3 | 6 | 0 | 1 | 6 | → | | **45** | |
| **B3** | 1 | **12** | 0 | 2 | **10** | 3 | 1 | **7** | 0 | 1 | 6 | 1 | 1 | 1 | 0 | 1 | 2 | 1 | → | | **50** | |
| **B12** | 0 | 0 | 0 | 0 | 1 | 2 | 2 | 2 | 1 | 1 | 0 | 1 | 0 | **10** | 1 | 0 | **8** | 2 | → | | **31** | |
| **GG** | **13** | 3 | **13** | **10** | 4 | **10** | **11** | 4 | **12** | **11** | **7** | **13** | **13** | 2 | **9** | **15** | 5 | **7** | → | | **162** | |

Considering the complexity of the probabilistic models, Figure.6.3.1.1 demonstrates the relations found between the shape (*c,b*) and scale (*a*) parameters for B3, B12 and GG distributions. For B12 and GG distributions shape-scale and shape-shape plots show mathematically power-based and polynomial and exponential relations in *b*-*a*, *c*-*a* and *c*-*b* plots (Figure.6.3.1.1- upper right plot and lower left and right plots). On the other hand, for the B3 distribution (Figure.6.3.1.1 – upper left and lower right) no clear dependency among shape and scale parameters occurs.

Analyzing the fitting performance of the probabilistic models, all the GoF results are demonstrated in Table.6.3.1.2. (see Appendix II for the quantitative GoF results) based-on the ranking performance for each distribution per station-buoy-reanalysis pixel and per method of parameter estimation. In particular, B12 and GG distributions achieved the best fit in 14 out of 16 cases, B3 provided the best fit in 2 cases and W2 in none of the observational data. The GG distribution outperforms the other probabilistic models in almost all of the GoF tests, mostly using LSE and MOM methods. Regarding the buoys' measurements, B3 and GG distributions provided the best fit in all the locations and W2 distribution's rankings were the lowest for all of the locations. Overall, W2 had the maximum optimal fitting scores in 1 station, although, the rankings of the remaining three distributions (B3, B12 and GG) were similar.

For the reanalysis data, the GG distribution presents the best fitting scores for 11 out of 16 modelled time series datasets. B3 and B12 distributions had better fits in 1 station and W2 in 2 stations. All of the distributions, with the exception of GG, produced worse results than the observational data in the GoF metrics. Especially for B3 and B12 distributions, using LST method, the rankings performance improved, although, GG distribution outperforms W2, B3 and B12 in almost all cases. In addition, a notable advantage of GG distribution is that the corresponding $R^2$ values and KS test statistics exhibit consistently high scores for all of the examined locations. *AIC* and *BIC* on the other hand, penalize models that have an increased number of parameters and therefore form a "fairer" metric for distributions' comparison. Results indicated small differences for in-situ and reanalysis data in terms of the *AIC* values (-20 for W2 and approximately -19 for B3, B12 and GG) and *BIC* values (-2 for W2 and approximately 8 for B3, B12 and GG). Among the 3-parameter probabilistic models, slightly better scores occurred for the B3 and B12 distributions considering *BIC* scores and for the *AIC* scores GG performed better than the other two distributions. These results, suggest that the B3, B12 and GG distributions can provide an alternative and efficient solution for wind speed fitting purposes considering the one additional parameter. On the other hand, it is important to note that in almost all the GoF tests, small differences were observed compared to the W2 distribution, highlighting the fitting accuracy for all the probabilistic models. Some fitting plots are presented for both observational and reanalysis data in Figure.6.3.1.2.

The majority of the criteria discussed and demonstrated above do not take into account the parsimony of the models (e.g., the number of the parameters). AIC and BIC on the other hand, penalize models that have a larger number of parameters and therefore form a more "global" metric for distributions' comparison. Results indicate small differences for in-situ and reanalysis data in terms of the AIC values (-20 for W2 and approximately -19 for B3, B12 and GG) and BIC values (-2 for W2 and approximately 8 for B3, B12 and GG). Furthermore, among the 3-parameter probabilistic models slightly better scores occurred for the B3 and B12 distributions considering BIC scores and for the AIC scores GG performed better than the other two distributions.

a.

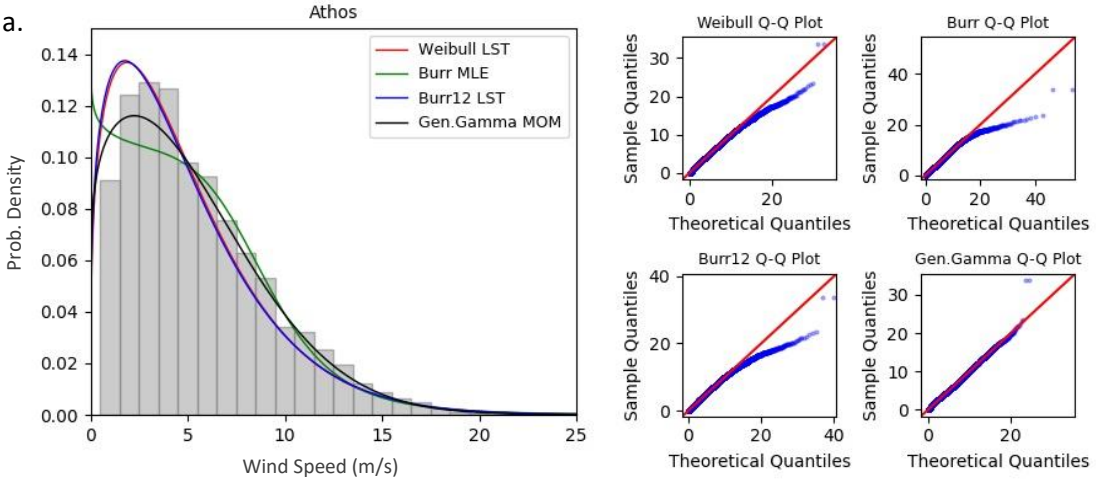
Athos
Weibull LST
Burr MLE
Burr12 LST
Gen.Gamma MOM
Prob. Density
Wind Speed (m/s)
Weibull Q-Q Plot
Burr Q-Q Plot
Burr12 Q-Q Plot
Gen.Gamma Q-Q Plot
Sample Quantiles
Theoretical Quantiles

b.

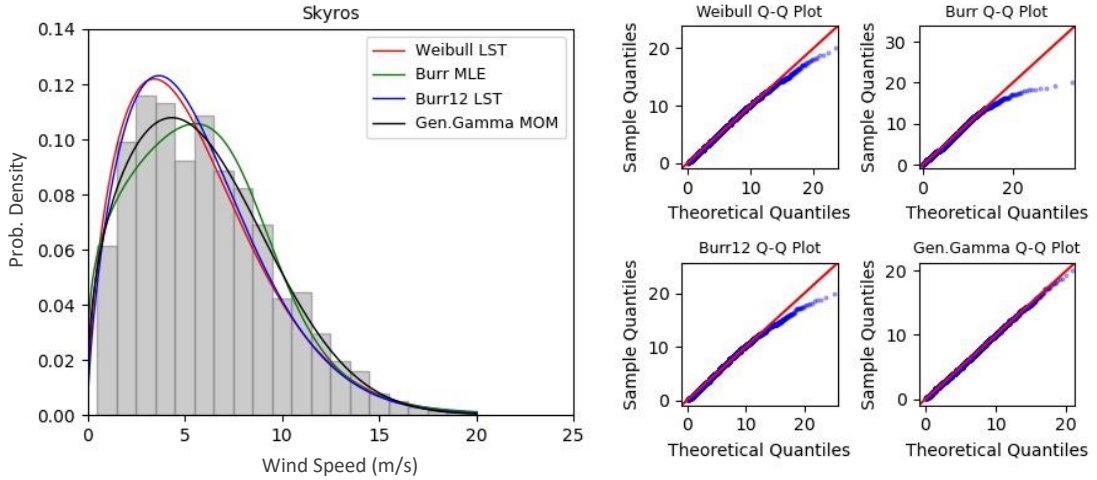
Skyros
Weibull LST
Burr MLE
Burr12 LST
Gen.Gamma MOM
Prob. Density
Wind Speed (m/s)
Weibull Q-Q Plot
Burr Q-Q Plot
Burr12 Q-Q Plot
Gen.Gamma Q-Q Plot
Sample Quantiles
Theoretical Quantiles

c.

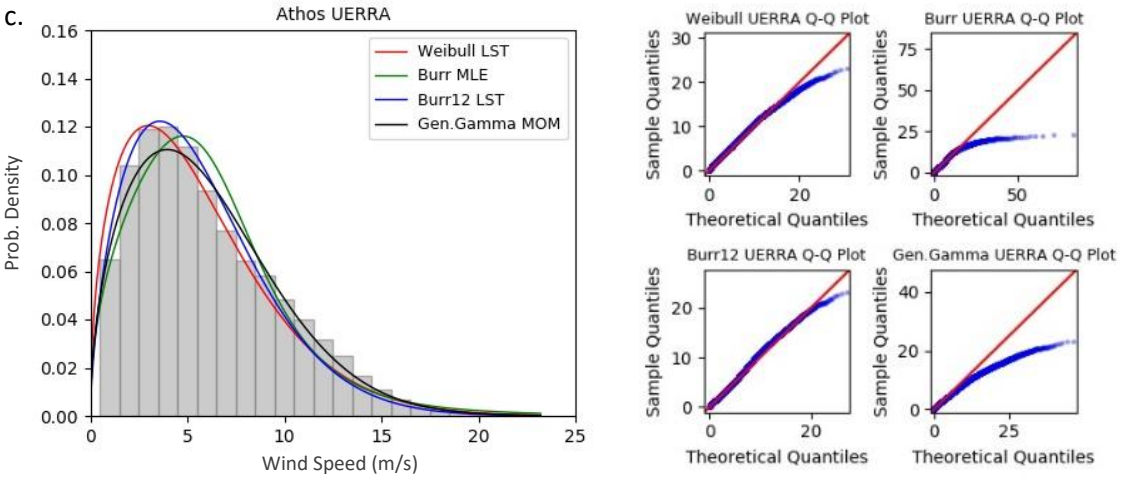
Athos UERRA
Weibull LST
Burr MLE
Burr12 LST
Gen.Gamma MOM
Prob. Density
Wind Speed (m/s)
Weibull UERRA Q-Q Plot
Burr UERRA Q-Q Plot
Burr12 UERRA Q-Q Plot
Gen.Gamma UERRA Q-Q Plot
Sample Quantiles
Theoretical Quantiles

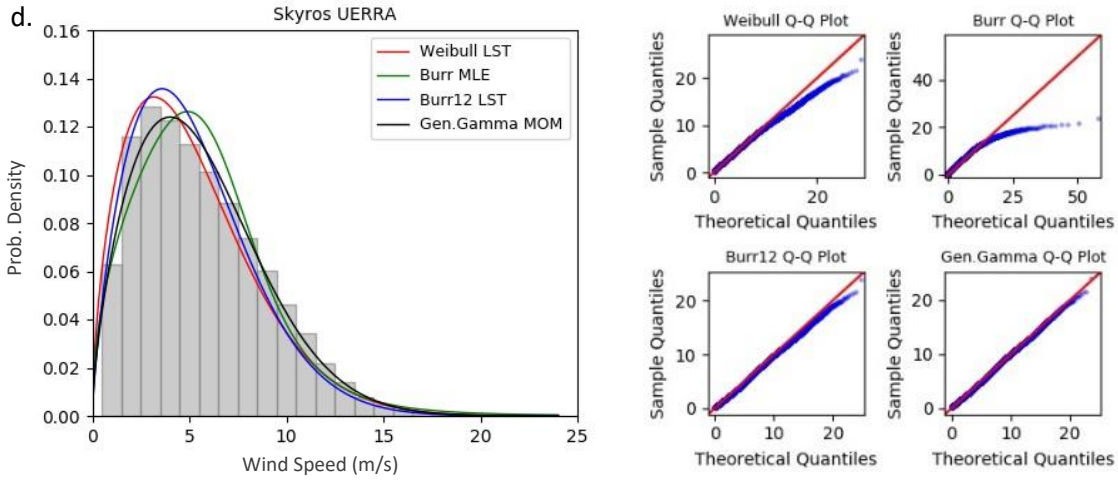


**Figure.6.3.1.2:** Wind speed histograms and quantile-quantile plots for the fitted Weibull, Burr3, Burr12 and Gen.Gamma distribution for a) Athos buoy, b) Skyros station, c) Athos and d) Skyros UERRA pixels

As a conclusion, B3, B12 and GG distributions provided high frequency rankings considering the best fit for all of the locations and consequently, they are considered as the most well-grounded candidates for the probabilistic modelling of coastal and offshore wind speed regimes for the Central and North Aegean Sea. The principal drawback, as already mentioned, is that they present greater complexity in the estimation of the parameters (constrained lower bounds for the shape parameters), whichever estimation method was used. W2 distribution often provided fairly satisfactory fits and could be adopted as a rather fair solution, if simplicity (parsimonious model) in the distribution form is considered. GG and B12 distributions perform better, however, small differences observed in almost all of the GoF metrics between the examined probabilistic models. Considering the latter statement, it may be argued that the use of a two-parameter distribution should be preferred over three-parameter distributions in cases of small statistical differences. However, the three-parameter distributions can capture more accurately the tails of the distribution, and thus, the wind energy, which depends entirely on the third-order moment.

### 6.3.2 Extreme values performance

In order to further evaluate the probabilistic models' fitting performance, a preliminary extreme values assessment is performed in terms of the Mean Excess Function (MEF), the Generalized Pareto distribution (Wang 2016) fitting and the L-moments ratio diagram (as a graphical method) for the extreme values in each station, buoy and reanalysis pixel. Graphical methods are considered as a useful tool for preliminary exploratory analysis and tail characterization. The MEF is a graphical method for tail behavior characterization comprising distributions like those of Pareto, Lognormal, Weibull, Gamma, and Exponential (Burnecki et al. 2005). More advanced and complex distributions, like the Generalized Gamma, the Burr type III and XII have an asymptotic behavior matching one of the aforementioned tails (Nerantzaki & Papalexiou 2019). Figure.6.3.2.1 illustrates the shapes of the MEF plots for the observational and reanalysis data in Chios, Dimokritos stations and Lesvos buoy respectively. Moreover, the shape parameter values of the Generalized Pareto distribution (GPD) (MLE method was applied to estimate parameters) and the expected variability of the GPD shape parameter for different wind speed threshold values is utilized to identify sequence changes (Appendix I). When the shape $c$ of the GPD is close to 0, it simplifies to an exponential distribution, for $c > 0$ to an ordinary uniform distribution and finally when $c < 0$, a Pareto type II distribution occurs.

Results climax highly negative shape parameters at low threshold evolving to near zero (or even positive) *shape* at large thresholds highlighting the sub-exponential tails (Exponential and Pareto shaped tails) of the wind datasets. Examining the MEF plots, GG, B3 and B12 distributions seem to reproduce better the upper quantiles of the wind speed datasets (zero or positive slope above threshold in the MEF plots). In contrast, W2 fails to reproduce the aforementioned extremes behavior in most of the total cases, although, W2 distribution performed better results for the reanalysis data "extreme" values where no increased peaks occurred. Furthermore, the results with the shape parameter stability plots (Appendix I) for the entire range of wind speeds highlight that above a threshold of 15-20 m/s an increased negative value for the shape parameter $c$ occurs, indicating Pareto shaped tails for most of the buoy observational data. Finally, the threshold values, considering MEF plots and the shapes of the GPD, for the observational data were selected as 12 m/s and for the reanalysis data as 8 m/s.

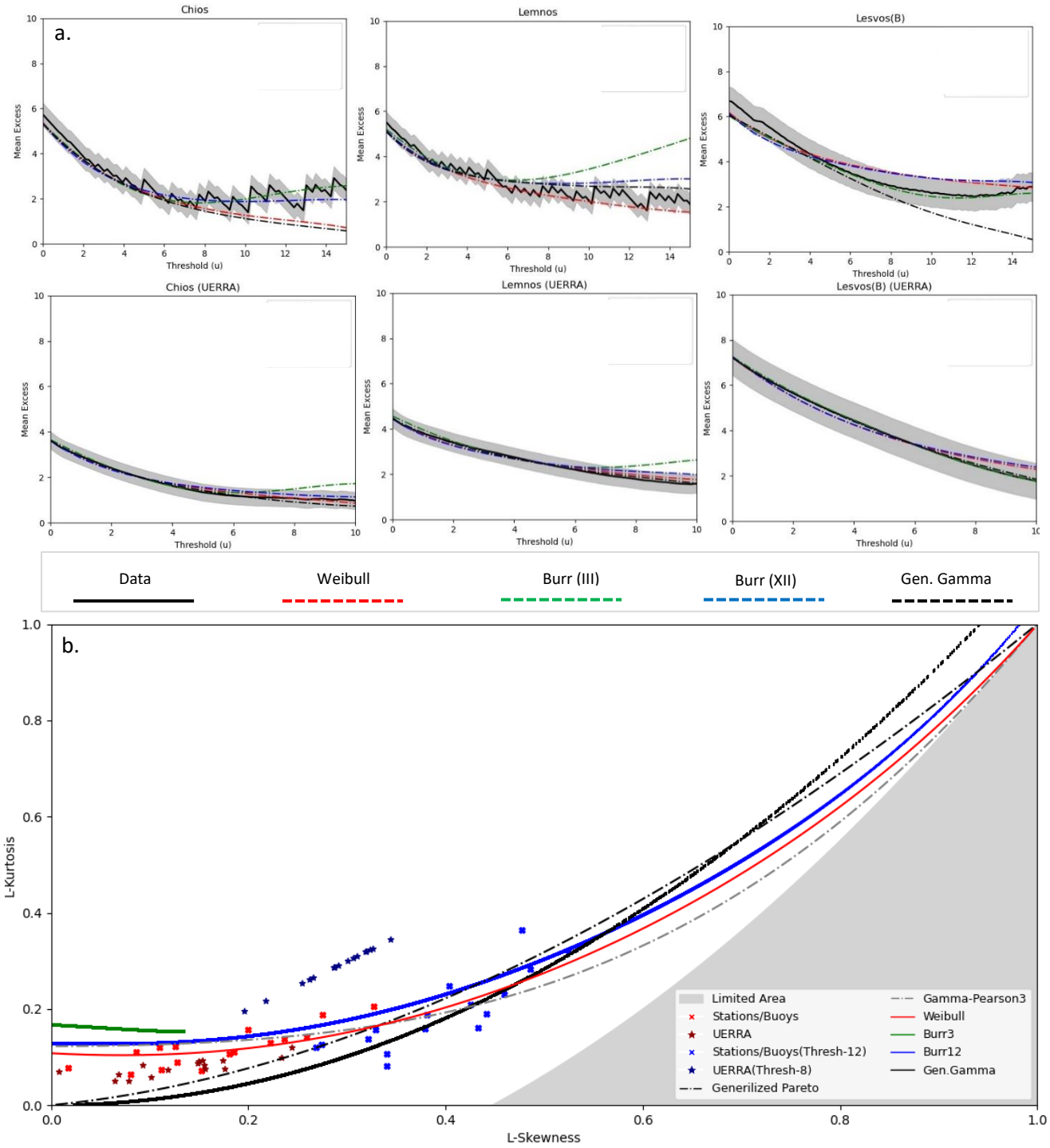


**Figure.6.3.2.1:** a) Mean excess plots for indicative in-situ and reanalysis data, b) L-moment ratios plot including all station/buoys and UERRA pixels.

Along with the threshold values identification using MEF and modified GPD shape values plots, the L-moment ratios (L-skewness and L-kurtosis) are respectively defined by $\tau_3=\lambda_3/\lambda_2$ and

$\tau_4$=$\lambda_4/\lambda_2$ and graphically compared to the empirical L-moment ratios plot of the selected distributions. The L-moment ratio plot allows analyzing the flexibility of the different distributions as well as the capability and flexibility of a probabilistic model to take many different values of skewness and kurtosis, linked to the shape of the distribution. The results are presented in Figure.6.3.2.1 where the extreme values (above the selected thresholds – blue marks) time series are coinciding with the empirical L-moments ratio curves of the Burr, Generalized Gamma, Gamma and Generalized Pareto distribution for the observational data. Conversely, for the reanalysis data time series, the $\tau_3$ and $\tau_4$ values are identified above the upper limit of both B12 and GG distributions.

### 6.3.3 Reanalysis statistical comparison with in-situ records

Concerning the spatially and temporally co-located samples of in-situ and reanalysis data, the results are "contentious". In general, the skewness and kurtosis values between the wind climate observations and numerical predictions present small differences at monthly and seasonal scales (Figure.6.3.3.1b,d). On the contrary, increased discrepancies occurred for the center of gravities (mean wind speed) and the variance in terms of the monthly, seasonal and annual statistical characteristics (mean-standard deviation plots in Figure.6.3.3.1a,c and Table 6.3.3.1). Considering the long-term persistence agreement, a climacogram assessment was carried out for detecting the long-term behaviour of a process, expressed as the variance (or standard deviation) of an averaged process *x(t)* (assuming stationary) versus averaging time scale *m* (symbolized by *γ(m)*, see Dimitriadis and Koutsoyiannis - sec.1.2 [2018]). Apart from the graphical representation and the assessment of the climacograms, the long-term persistence can be expressed using the Hurst coefficient *H*, which equals the half of the slope of the climacogram in a logarithmic plot, plus 1. Accordingly, the climacograms (Figure 6.3.3.1) and the Hurst coefficient (*H*) (Table 6.3.3.1) between the co-located samples are in good agreement with a positive bias occurring between the observational and modelled data due to smoothing techniques that are often applied in reanalysis datasets (zero values and extremely high peaks are lacking).

**Table.6.3.3.1:** Hurst coefficient (H) results for the co-located time series and standardized time series

| *Hurst coef. (H)* | Stations | UERRA | *Hurst coef. (H)* | Stations-Buoys | UERRA |
|---|---|---|---|---|---|
| **Athens** | 0.929 | 0.889 | **Alex. Pap.** | 0.882 | 0.846 |
| **Dimokritos North** | 0.887 | 0.879 | **Samos** | 0.932 | 0.841 |
| **Lemnos** | 0.889 | 0.865 | **Skyros** | 0.881 | 0.862 |
| **Thessaloniki** | 0.901 | 0.851 | **Athos (B)** | 0.862 | 0.823 |
| **Mytilene** | 0.911 | 0.831 | **Lesvos (B)** | 0.832 | 0.801 |
| **Naxos** | 0.827 | 0.811 | **Mykonos (B)** | 0.836 | 0.829 |
| **Chios** | 0.911 | 0.875 | **Petrokaravo (B)** | 0.899 | 0.887 |
| **Mykonos** | 0.896 | 0.839 | **Skyros (B)** | 0.811 | 0.791 |

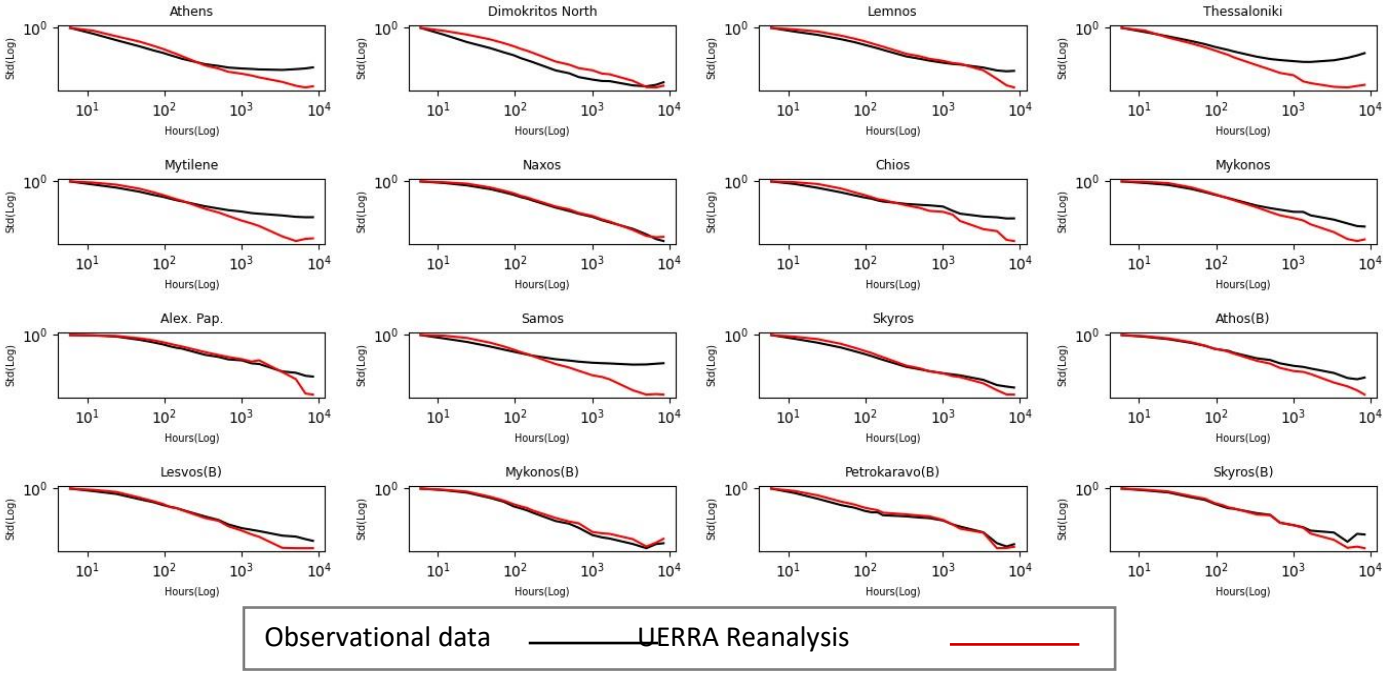


**Figure 6.3.3.1:** Climacograms of the co-located observational and reanalysis data samples

The second part of the analysis illustrates the comparison of both reanalysis and observational data related to the: (a) bias error, (b) root mean squared error (RMSE), (c) standard deviation error (STDE) and (d) coefficient of determination ($R^2$) estimation. All of these metrics, illustrated in Table 6.3.3.2, can successfully quantify the differences and similarities among the co-located samples, although STDE is considered to be of high importance for the model performance evaluation as it indicates a constant error in models' results. An increased STDE

value indicates that the model's error is random and, hence, the simulation has a low physical foundation, even if showing lower bias and RMSE values (Giannaros et al. 2017).

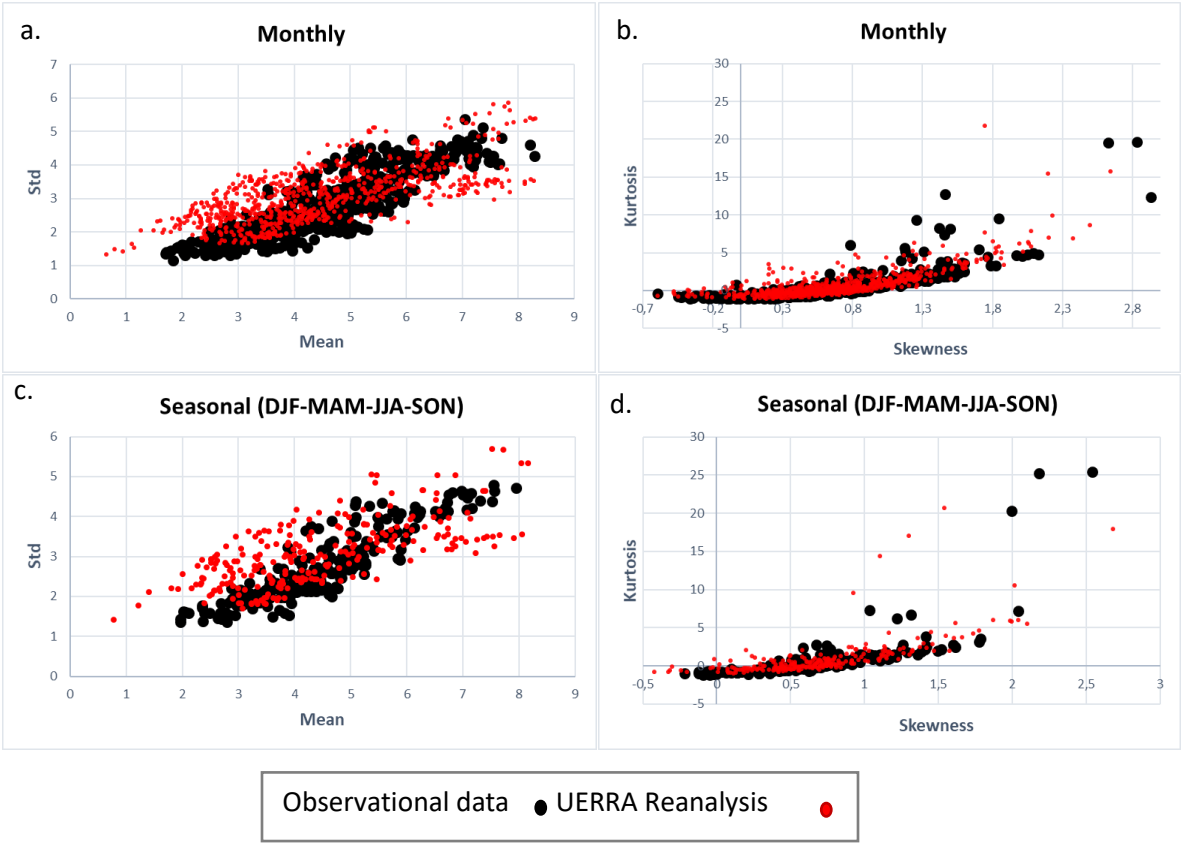


**Figure 6.3.3.2:** a) Monthly and b) Seasonal mean-standard deviation plots, c) Monthly and d) Seasonal skewness-kurtosis plots

**Table.6.3.3.3:** Statistical results and comparison of the 6-hour interval observed wind speeds and UERRA reanalysis data (co-located samples)

| Stations (NOAA) | Years (Co-located) | N (Samples) | Mean | Std | Skew | E.Kurt | $R^2$ | Bias | RMSE | STDE |
|---|---|---|---|---|---|---|---|---|---|---|
| **Alexandroupoli** | 1980 - 2018 | 103982 | 3.384 | 3.111 | 0.758 | 0.761 | 0.71 | -0.96 | 2.429 | 2.227 |
| **UERRA Alexandroupoli** | | | 4.352 | 2.73 | 0.778 | 0.35 | | | | |
| **Elliniko** | 1980 - 2018 | 67331 | 2.632 | 2.335 | 0.825 | 1.481 | 0.66 | **-0.046** | **1.764** | **1.763** |
| **UERRA Elliniko** | | | 2.679 | 1.667 | 0.818 | 0.653 | | | | |
| **Thessaloniki** | 1980 - 2018 | 146299 | 3.129 | 3.094 | 1.698 | 5.154 | 0.62 | **0.29** | 2.423 | 2.405 |
| **UERRA Thessaloniki** | | | 2.838 | 1.886 | 1.122 | 1.124 | | | | |
| **Alex. Pap.** | 1991 - 2018 | 15843 | 2.552 | 2.206 | 0.781 | 1.185 | 0.69 | -0.766 | **1.927** | **1.768** |
| **UERRA Alex. Pap.** | | | 3.319 | 2.22 | 1.172 | 1.494 | | | | |
| **Chios** | 1991 - 2018 | 28610 | 4.15 | 3.207 | 0.464 | -0.208 | **0.79** | **-0.166** | 2.058 | 2.051 |
| **UERRA Chios** | | | 4.281 | 2.29 | 0.375 | -0.324 | | | | |

| | | | | | | | | | | |
|---|---|---|---|---|---|---|---|---|---|---|
| **Mytilene** | 1980 - 2018 | 106743 | 3.483 | 2.831 | 1.179 | 2.110 | 0.71 | -0.553 | 2.133 | 2.06 |
| **UERRA Mytilene** | | | 3.937 | 2.312 | 0.597 | -0.045 | | | | |
| **Lemnos** | 1980 - 2018 | 123935 | 5.184 | 4.165 | 0.738 | 0.594 | **0.84** | 0.69 | 2.488 | 2.389 |
| **UERRA Lemnos** | | | 4.488 | 2.822 | 0.763 | 0.294 | | | | |
| **Mykonos** | 1991 - 2018 | 31767 | 3.983 | 2.494 | 0.253 | -0.357 | 0.76 | -0.458 | **1.713** | **1.651** |
| **UERRA Mykonos** | | | 4.442 | 2.119 | 0.283 | -0.618 | | | | |
| **Naxos** | 1980 - 2018 | 48926 | 6.780 | 4.818 | 0.646 | 0.113 | 0.78 | 1.731 | 3.614 | 3.173 |
| **UERRA Naxos** | | | 5.049 | 2.804 | 0.475 | -0.407 | | | | |
| **Samos** | 1980 - 2018 | 91169 | 4.985 | 3.548 | 0.342 | 0.475 | 0.66 | -1.35 | 3.012 | 2.693 |
| **UERRA Samos** | | | 3.639 | 1.985 | 0.532 | 0.132 | | | | |
| **Skyros** | 1980 - 2018 | 71903 | 4.034 | 3.319 | 0.924 | 2.031 | **0.81** | **-0.228** | **1.996** | **1.983** |
| **UERRA Skyros** | | | 4.262 | 2.532 | 0.815 | 0.555 | | | | |
| **Buoys** | **Years (Co-located)** | **N (Samples)** | **Mean** | **Std** | **Skew** | **Kurt.** | **$R^2$** | **Bias** | **RMSE** | **STDE** |
| **Athos** | 2000 - 2018 | 22123 | 4.892 | 3.898 | 0.918 | 0.731 | 0.75 | -0.871 | 2.901 | 2.727 |
| **UERRA Athos** | | | 5.771 | 3.741 | 0.846 | 0.321 | | | | |
| **Lesvos** | 2000 - 2011 | 14592 | 6.611 | 3.931 | 0.768 | 2.045 | 0.61 | 1.161 | 3.172 | 3.167 |
| **UERRA Lesvos** | | | 5.449 | 2.911 | 0.564 | 0.163 | | | | |
| **Mykonos** | 2001 - 2011 | 13371 | 7.215 | 4.492 | 1.276 | 13.56 | 0.75 | 0.632 | 3.061 | 2.998 |
| **UERRA Mykonos** | | | 6.682 | 3.358 | 0.1673 | -0.538 | | | | |
| **Petrokaravo** | 2008 - 2018 | 10428 | 5.12 | 3.188 | 0.539 | -0.157 | **0.78** | 1.067 | 2.27 | 2.004 |
| **UERRA Petrokaravo** | | | 4.053 | 2.497 | 0.749 | 0.251 | | | | |
| **Skyros** | 2007 - 2010 | 4463 | 5.709 | 3.712 | 0.564 | -0.115 | **0.82** | **-0.103** | 2.06 | **1.957** |
| **UERRA Skyros** | | | 5.813 | 3.346 | 0.626 | -0.073 | | | | |

Concerning the buoys' co-located samples, none of the statistical tests can be considered as acceptable as long as only in one buoy (Skyros) the results presented a good agreement. Conversely, the examined co-located wind speed time series preserved better results in almost all of the coastal sites where a good agreement occurred for Athens, Alexandros Papadiamantis (Skiathos), Chios and Skyros coastal stations. These unclear results, concerning the model's performance, could be potentially due to the complex "topography" of the wider Aegean Sea, consisting of numerous islands, which could have influenced the initial simulation of the wind field. Taking into account the addressed issue (presence of islands), an assumption can be made that the spatial resolution (i.e., 5.5 km) and the associated smoothing, resampling or neglecting of orography patterns, lead to the insufficient capture of local effects on wind flow. Thus, an increased spatial resolution, a more accurate representation of the topography and the inclusion of additional observational data could lead to more accurate realizations.

### 6.3.4 Wind Power output Assessment

The wind speed is extremely important for the estimated energy that a commercial WT can convert to electricity. The reason is that the energy content of the wind varies with the third power of the average or the instantaneous wind speed. When the fitting performance of a probabilistic models is expressed in terms of the real or theoretical power output, then the results tend to be more controversial. Consequently, the proposed distributions resulted in rather low relevant errors, smaller than 10%, for the examined locations considering in-situ observations (12 out of 16 stations and buoys) and smaller than 5% for the UERRA reanalysis data (14 out of 16 stations and buoys) (Figure 6.3.4.1a,b). For the different parameters' estimation techniques (MLE, LSE and MOM), B3 distribution while applying MOM method resulted in increased errors in both observational and reanalysis data and the negative error increases using LST for the reanalysis data (Figure 6.3.4.1c). For the in-situ data B3, B12 and GG provided the minimum error scores using LST, with B12 and GG achieving the lowest standard deviation values. For the reanalysis data, W2, B12 and GG lead to similar results, highlighting that W2 performed better than the observational data scenario. Summarizing, B12 and GG distribution seem to perform the best for both observational and UERRA data and in contrast to the GoF tests in the previous sections, the W2 distribution, "succeeded" in this case in highlighting its applicability in wind power assessment in spite of the fact that it has one less parameter.

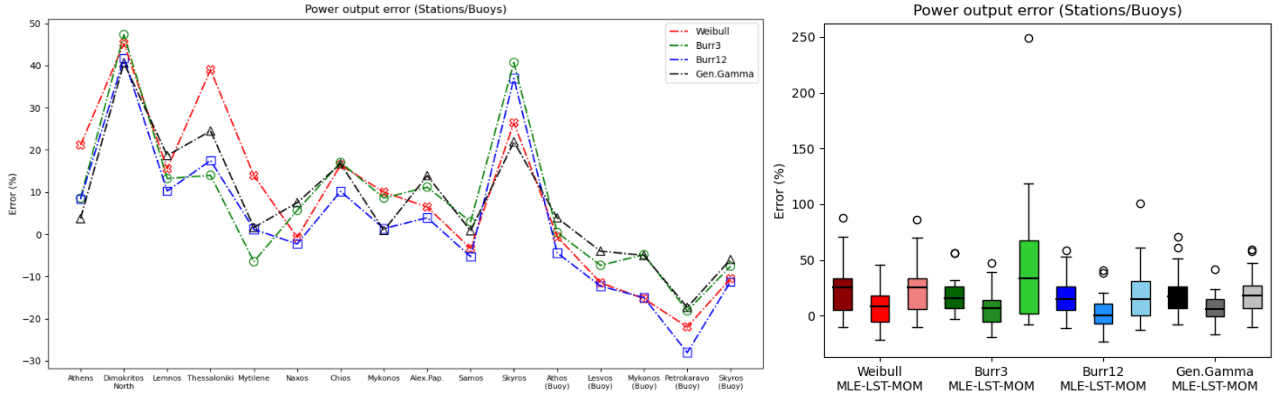

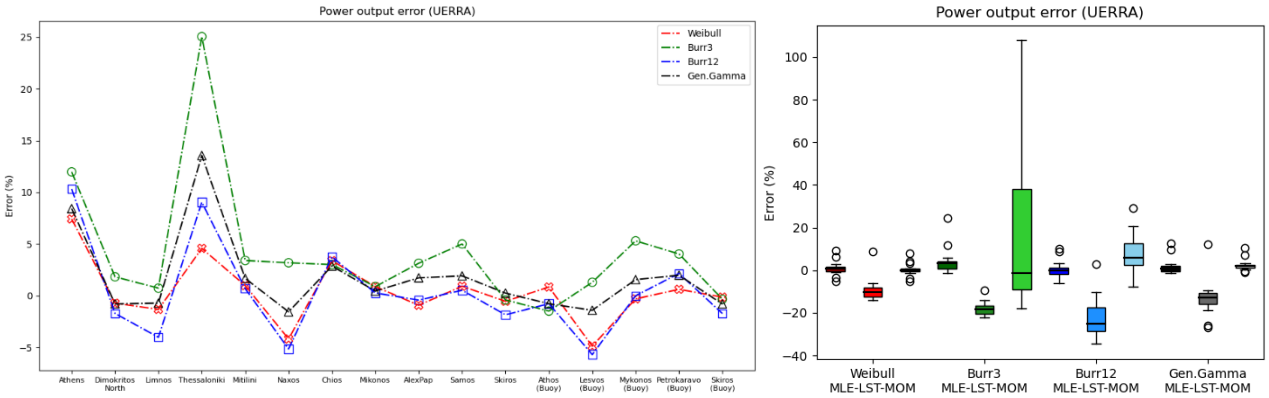


**Figure.6.3.4.1:** Relative estimation error of the mean wind power output based on the time series and wind speed distributions, a) Station-Buoys and UERRA reanalysis (left), b) distributions' parameters estimation methods (right)

In terms of the total power production based-on the reanalysis data, Figure 6.3.4.2 demonstrates the available annual power output for the entire study area along with the relative errors maps for each distribution for the reanalysis wind time series. In order to downscale the 6-hours wind time series to 1-hour timestep, linear interpolation was applied to fill the missing hourly intervals. According to Hallgren et al. (2020), with a sufficiently long time series, errors from the linear interpolation should even out, as the offshore wind speeds would be overestimated as often as underestimated. Thus, the offshore wind speed time series were adjusted to the Vestas V164 power curve for extracting the final power output, multiplied by the number of WTs per pixel.

The total annual wind power output is estimated to be more than 500 GW/y per pixel, exceeding 920 GW/y mostly in the Central-East part of the Aegean Sea (Figure 6.3.4.2f). For coastal areas, as was expected due to the low mean wind speed values and the increased variability, the potential power output is extremely low, less than 20 GW/y per pixel and the relative error for all the distributions is increased. Accordingly, the capacity factors (Figure 6.3.4.2f) reached values between 0.4 and - 0.52 for the windiest areas and less than 0.1 for the coastal areas. Finally, considering the performance of the probabilistic models, GG and B3 produced the lowest errors (Figure 6.3.4.2b,d) in the windiest areas as well as W2 and B12 had similar increased negative errors (Figure 6.3.4.2a,c).

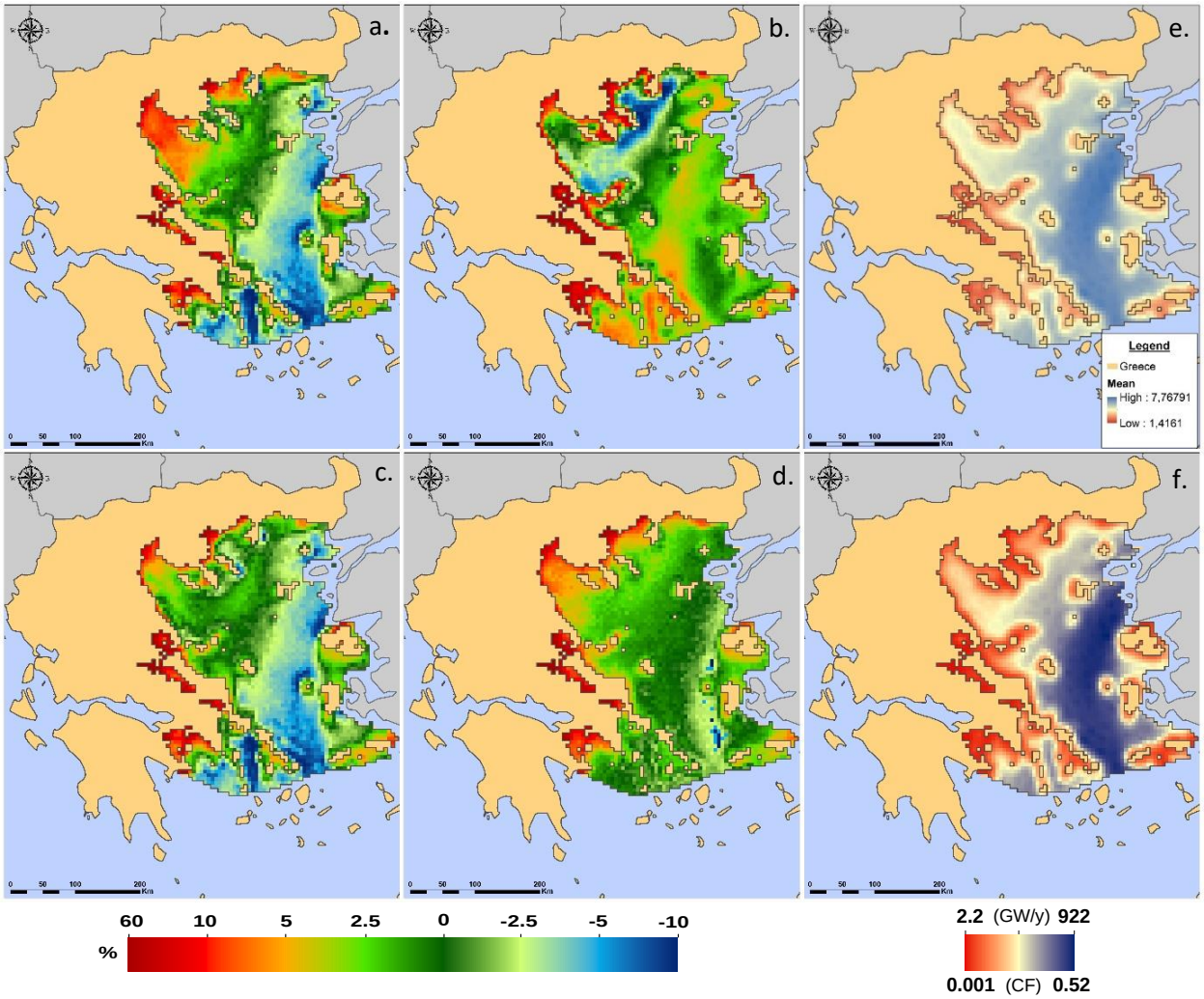


**Figure.6.3.4.2:** Relative estimation error (%) of the total wind power output for the entire UERRA reanalysis dataset (left), W2 (a), B3 (b), B12 (c), GG (d), Mean wind speed output and (e) Total annual power and capacity factors (f)

The total wind power output was predicted to be more than 500 GW/y per pixel (25 WTs) exceeding 930 GW/y mostly in the Central-East part of the Aegean Sea (Figure.6.3.4.2a). For coastal areas, as it was expected due to the low mean wind speed values and the increased variability, the potential power output is extremely low, less than 20 GW/y per pixel and the relative error for all the distribution is increased. Accordingly, the capacity factors (Figure.6.3.4.2f) reached values between 0.4 and - 0.52 for the windiest areas and less than 0.1 for the coastal areas. Finally, considering the performance of the probabilistic models, GG and B3

succeeded the lowest errors (Figure.6.3.4.2b,d) in comparison with the windiest areas in comparison with the W2 and B12 that led to similar error values (Figure.6.3.4.2a,c). As a conclusion, wind power output assessment indicates that the offshore wind resources are promising for expanding national electricity generation focused on the marine energy and offshore wind farms. Although, the bathymetry of the Eastern Aegean Sea is a tremendous drawback for such tasks and only with possible future technological improvements (e.g., floating structure for depths exceeding 200 meters), the windiest areas of the Aegean Sea will be "unlocked" for offshore wind farms development.

Analyzing the differences of the power output between the observational data and the UERRA ensembles, the differences ranged between -41% and 44%. Specifically, in Lemnos, Naxos, Mykonos and Alexandros Papadiamantis stations the lowest differences occurred, with values ranging between -4% and 14%. In addition, for the Lesvos, Mykonos and Skyros buoys the power output differences estimated at -7%, -11% and 2% respectively. Finally, maximum errors were observed for the Chios, Samos and Skyros stations as well as for Athos and Petrokaravo buoys, with values exceeding 38% and 44%.

### 6.3.5 Offshore wind resource assessment results

In the first stage of the analysis, four probabilistic models, including multiparameter distributions (B3, B12 and GG) and the two parameter W2, were analyzed based on their fitting performance. The GG, B12 and B3 distributions led to a challenging fitting performance in both the observational and reanalysis data, exhibiting a higher fitting flexibility than the W2distribution. The GG and B12 distribution models, provided the best fitting performance for all of the examined cases, especially when focusing on the high-speed tail of the distribution (similar results are noticed in Kiss & Jánosi 2008 and Carta et al. 2009). For both B3 and B12 distributions care must be taken considering the parameters' estimation using either the MLE, LSE or MOM methods. In terms of the GoF results, the three-parameter models outperformed W2 distribution, as expected, although, very small differences between the probabilistic models occurred. Furthermore, based on the extreme events' preliminary assessment, the GG, B3 and B12 distributions tended to perform better mainly for the in-situ data and because of the heavy-

tail behavior of the examined wind speed regimes. In contrast, for the estimated power output errors, and similarly to Soukissian (2013), where multi-parameter distribution models are compared to W2, the results were similar and satisfying for all the probabilistic models, highlighting that for the B12 and GG distributions the minimum percentage errors occurred. Concerning wind power output errors for the entire study area (using UERRA data), the examination of all probabilistic models showed rather low relative differences in the windiest areas of the North and Central Aegean Sea. Interestingly, the estimated offshore wind resource indicated areas of increased power output potential in the Eastern – South part of the Aegean Sea, where the total power output may be promising for future OWE deployment.

In the quest to clarify if UERRA (MESCAN-SURFEX) is suitable for offshore wind applications among previous and recent reanalysis products, a comparison is applied with similar studies across the Mediterranean. Undoubtedly, all reanalysis data have strengths and weaknesses, however, regional reanalysis products can play a pivotal role in offshore wind resource characterization and modelling because the increasing spatial resolution. Particularly, Table 6.3.5.1 illustrates correlation, bias and RMSE values from previous studies for the Aegean Sea, using ERA-Interim (Soukissian et al. 2008), ETA-NWP (Soukissian et al. 2017), WRF-Var (Giannaros et al. 2017) and RCM4 (Katopodis et al. 2019) modelled datasets, and for different time periods between 1995-2011. The resulting UERRA wind time series were adjusted to the current time frame of the studies conducted, and the results indicate similar statistical values or slightly improved scores for both the buoy and the coastal stations data. UERRA tends to preserve lower correlation metrics compared to ERA-Interim and ETA-NWP, although, decreased biases and RMSE values were found in two out of four buoys. In addition, the statistical analysis for the coastal stations highlighted better bias and correlation scores compared to the RCM4 dataset and lower biases and RMSE compared to the WRF-Var dataset.

**Table 6.3.5.1:** Statistical inter-comparison of different reanalysis products and observational data (stations and buoys) over the Greek coastal and offshore areas

| Years: 2000-2011 | | **ERA-Interim** | **ETA-NWP** | **UERRA** | Years: 2003 | | **WRF-Var** | **UERRA** |
|---|---|---|---|---|---|---|---|---|
| **Athos** | R2 | 0.83 | 0.832 | 0.75 | **Elliniko** | R2 | - | - |
| | Bias | 0.32 | 0.45 | -0.871 | | Bias | -0.32 | **-0,063** |
| | RMSE | 2.14 | 2.041 | 2.89 | | RMSE | 2.16 | **1,774** |

| | | | | | | | | |
|---|---|---|---|---|---|---|---|---|
| **Lesvos** | R2 | 0.71 | 0.809 | 0.66 | **Alex. Pap.** | R2 | - | - |
| | Bias | 0.21 | 1.329 | **0.161** | | Bias | -0.15 | -1,105 |
| | RMSE | 2.8 | 2.563 | 3.171 | | RMSE | 2.39 | **2,287** |
| **Mykonos** | R2 | 0.82 | 0.874 | 0.75 | **Lemnos** | R2 | - | - |
| | Bias | 1.18 | 1.251 | **1.067** | | Bias | 0.05 | 0,106 |
| | RMSE | 2.37 | 2.351 | **2.27** | | RMSE | 2.01 | 2,122 |
| **Skyros** | R2 | 0.76 | - | **0.82** | **Skyros** | R2 | - | - |
| | Bias | 0.03 | - | -0.103 | | Bias | 1.65 | **-0,361** |
| | RMSE | 2.45 | - | **2.06** | | RMSE | 3.03 | **2,254** |
| Years: 1995-2004 | | | **RCM4** | **UERRA** | Years: 1995-2004 | | **RCM4** | **UERRA** |
| **Elliniko** | R2 | - | 0.84 | 0.65 | **Thessaloniki** | R2 | 0.56 | **0,62** |
| | Bias | - | 0.28 | **-0.04** | | Bias | -0.96 | **0,29** |
| | RMSE | - | 0.33 | 1.764 | | RMSE | 0.99 | 2,423 |
| **Alex. Pap.** | R2 | - | - | - | **Naxos** | R2 | 0.49 | **0,77** |
| | Bias | - | - | - | | Bias | -2.9 | **1,731** |
| | RMSE | - | - | - | | RMSE | 3.01 | 3,614 |
| **Lemnos** | R2 | - | 0.67 | **0.83** | **Samos** | R2 | 0.77 | 0,65 |
| | Bias | - | -0.79 | **0.695** | | Bias | -1.52 | **1,35** |
| | RMSE | - | 0.91 | 2.488 | | RMSE | 1.59 | 2,998 |
| **Skyros** | R2 | - | 0.77 | **0.81** | **Mytilene** | R2 | 0.37 | **0,696** |
| | Bias | - | 0.25 | **-0.22** | | Bias | -0.06 | -0,55 |
| | RMSE | - | 0.72 | 1.981 | | RMSE | 0.58 | 2,133 |

Overall, downscaled UERRA (MESCAN-SURFEX) data enhance recent reanalysis products, however, increased bias issues and RMSE scores are observed, mostly due to moderate models' capability to reproduce extreme wind speeds caused by the different spatial resolutions and the observational grid density during the downscaling procedures. Especially in coastal areas with complex topographic characteristics (i.e., Naxos, Samos, Lesvos) and in most of the offshore areas (i.e., Athos, Lesvos and Mykonos buoys), these effects are reflected, however, in some, but not all locations, a value of statistical significance over the global reanalysis products is added.

ERA5 is nowadays the most important reference for wind energy studies as already discussed in the literature review section. A comparison between UERRA (MESCAN SURFEX) and ERA5 products could be beneficial. However, in spite of the fact that recent studies appraised ERA5's capability to reproduce wind speed regimes (Dörenkämper et al. 2020), numerous similarities between the two datasets were observed. Besides, in Hallgren et al. (2020), UERRA (HARMONIE)

is proposed instead of ERA5 for analyzing mesoscale phenomena like the low-level jets, while in Pelosi et al. (2020) similar statistical performances occurred for the land products of UERRA (MESCAN-SURFEX) and ERA5. In Knoop et al. (2020), the estimated power output errors between the ERA5 data and 291 European tall masts were calculated between -40.2% and 32.7%, while similar scores proportional to the UERRA results were also estimated (-44% and 38% with 5 out of 16 stations and buoys exceeding errors below 10%). All of the aforementioned studies denote the reduced RMSE and even lower bias errors for the ERA5 products, but it is noteworthy that models with coarser resolution and smoother solutions can get better scores compared to higher-resolution models, when using standard verification metrics (Olauson 2018). However, the higher-resolution datasets could have a more realistic representation of local features, especially when downscaling procedures embody a dense grid of observational data for correction purposes. Nevertheless, if an increased spatial resolution is needed for regional assessment purposes, UERRA may still be an option. In this "tight" race among reanalysis products, with the new version of the reanalysis from ECMWF, ERA6 (by 2023) and CERRA (Copernicus European Regional Re-Analysis) (by 2021), new challenges in the reanalysis data assimilation methods arise.

### 6.4.1 Stochastic wind simulation results

In Table 6.4.1.1 and Figures 6.4.1.1-2 the results of the synthetic time series generation scheme are demonstrated in accordance to the marginal seasonal characteristics, the marginal probabilistic and the second order dependence structures. Simulated observational and reanalysis wind speed data consist of 100 hourly time series of 25-years length. In order to emulate the observed and the reanalysis wind time series, any values of the synthetic time series that are below the recorded positive minimum value of the station or the reanalysis data, are set to zero.

**Table 6.4.1.1:** Estimated mean, variance, skewness and kurtosis between reanalysis and simulated data based on Weibull, Burr XII and Gen. Gamma distribution.

| **Marginal (Lesvos)** | **Mean** | **Variance** | **Skewness** | **Kurtosis** |
|---|---|---|---|---|
| Observed (Buoy) | 6.61 | 16.45 | 1.04 | 1.39 |
| UERRA (Pixels) | 5.37 | 7.29 | 0.48 | 0.06 |
| **Weibull** | **Mean** | **Variance** | **Skewness** | **Kurtosis** |

| | | | | |
|---|---|---|---|---|
| Simulated (Buoy) (20 years) | 6.93 | 17.08 | 1.24 | 1.18 |
| Simulated (UERRA) (20 years) | 6.14 | 7.31 | 0.51 | 0.42 |
| **Burr12** | **Mean** | **Variance** | **Skewness** | **Kurtosis** |
| Simulated (Buoy) (20 years) | 6.84 | 17.32 | 0.96 | 1.84 |
| Simulated (UERRA) (20 years) | 5.65 | 7.29 | 0.73 | 0.71 |
| **Gen. Gamma** | **Mean** | **Variance** | **Skewness** | **Kurtosis** |
| Simulated (Buoy) (20 years) | 6.47 | 16.91 | 1.16 | 1.76 |
| Simulated (UERRA) (20 years) | 5.21 | 7.04 | 0.49 | -0.28 |

Considering the periodical characteristics (seasonal and diurnal), there is a good agreement between the observed and simulated variance, skewness and kurtosis, although, slight differences occurred for the simulated mean values based on the different probabilistic models, due to the effect of the induced uncertainty of the long-term persistence. In particular, the B12 and W2 distributions seem to overestimate the observed marginal values, although GG underestimates the mean and kurtosis (on the reanalysis data) while preserving the overall double-periodical behaviour (Figure 6.4.1.1 and Table 6.4.1.1). Concerning the second order dependence structure, the stochastic generation scheme reproduces extremely well the observed long-term behavior of the wind speed times series (Figure 6.4..11). In addition, Figure 6.4.1.1a-b, illustrates the applicability of the climacogram function (red line) compared to the Markov process (grey line) (for $H$=0.5) and Figure 6.4.1.1c-d highlights the inapplicability of the autocorrelation function (AcF) to preserving the long-term behaviour for an increased number of lags using only two parameters (i.e., Hurst and slope).

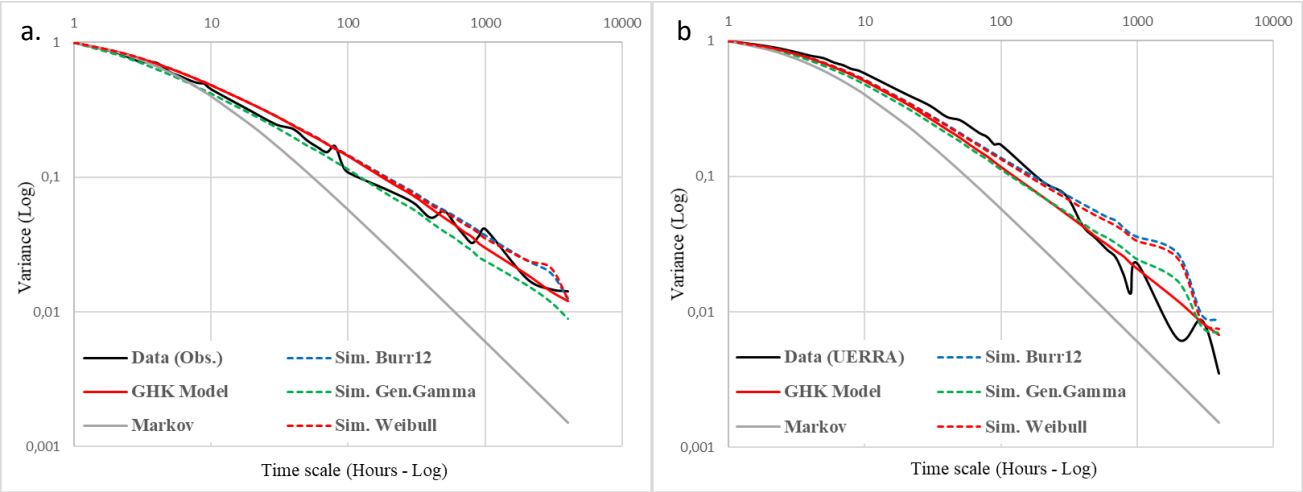

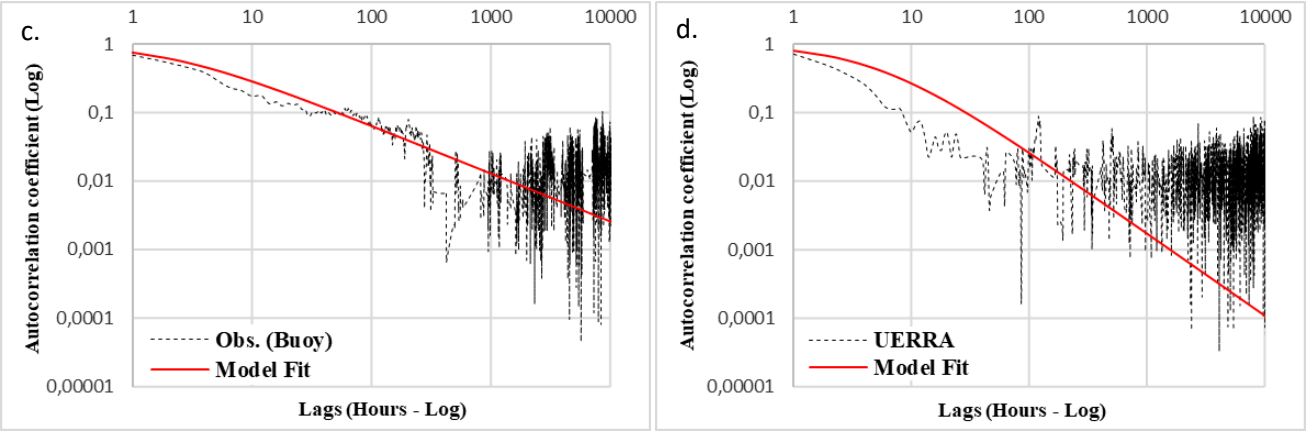


**Figure 6.4.1.1:** Empirical, modeled and simulated climacocrams for the: a) observational and b) reanalysis data. Autocorrelation coefficient plots for the: c) observational and d) reanalysis data

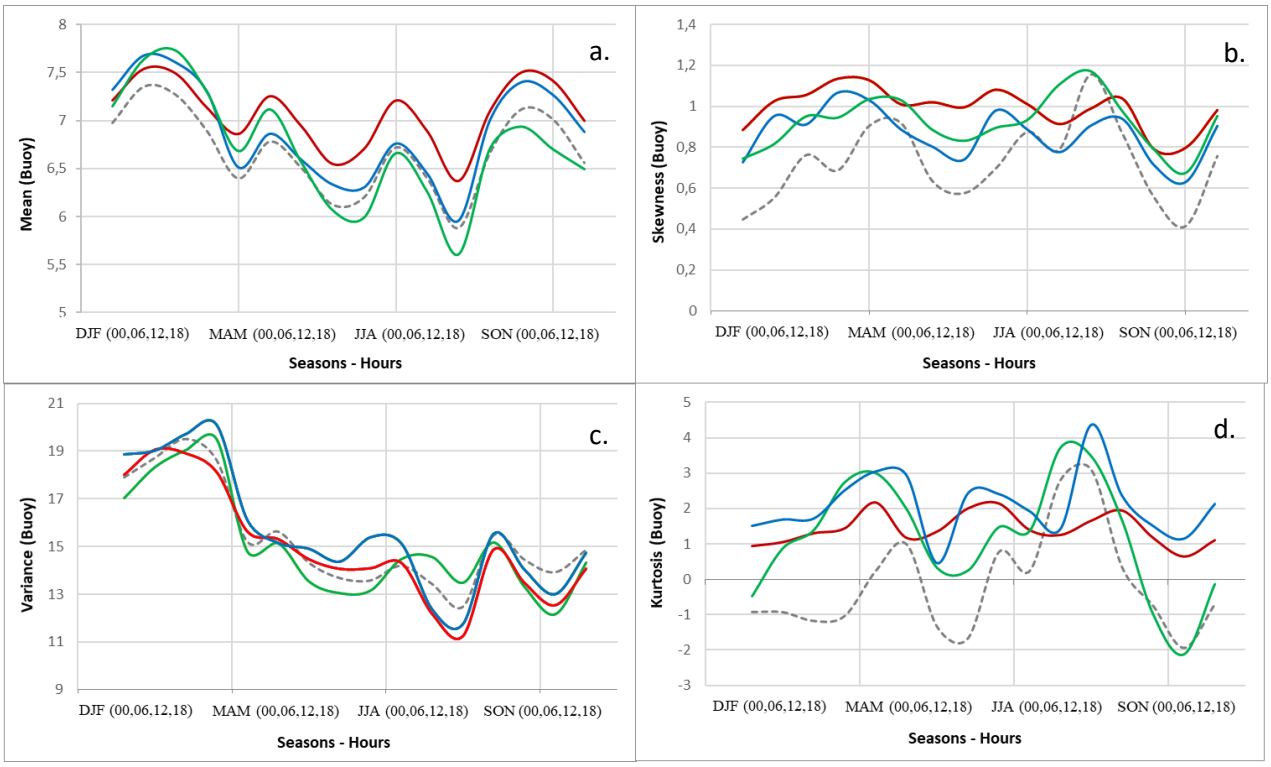

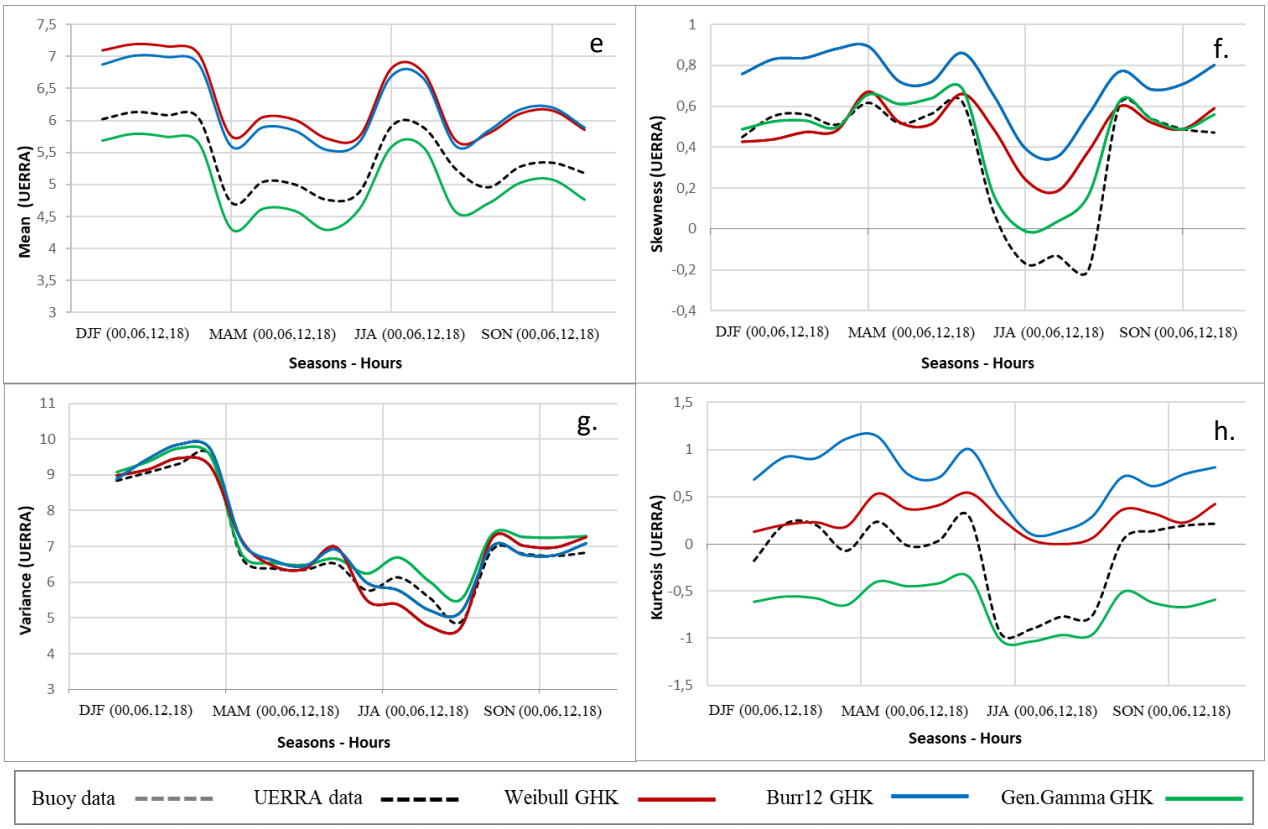


**Figure 6.4.1.2:** Seasonal-Hourly mean, variance, skewness and kurtosis plots between observational and simulated data (a-d) and reanalysis and simulated data (e-h) for Weibull, BurrXII and Gen.Gamma distributions

For illustration purposes, in Figure 6.4.1.3, a 365-day window of the observed versus the simulated wind time series is demonstrated. Note that here, the explicit preservation up to the fourth moment is adequate since preservation of additional moments slightly improved the simulated distributions. For the selected buoy examined (Lesvos), the best simulation results are obtained using the GG and the B12 distributions considering the extremes preservation, nevertheless, W2 satisfactory captures the observed and reanalysis wind time series. Furthermore, the simulated data seem to adequately preserve the intermittent characteristics (diurnal and seasonal), and it is notable that even the dry and strong etesian winds (meltemia) in the summer period, and specifically during August, are captured. The observed and the simulated wind speed time series for the selected probabilistic models are presented in Figure 6.4.1.3a-c and the CDF fitting intervals are graphically illustrated in Figure 6.4.1.3d-f respectively.

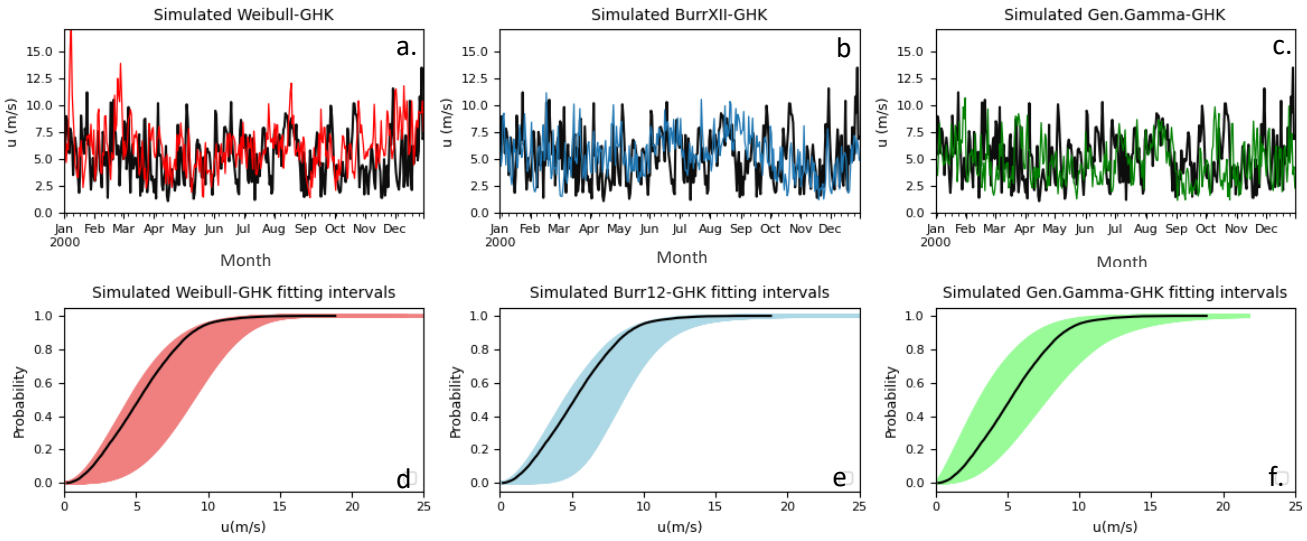


**Figure 6.4.1.3:** a-c) Indicative simulated time series using Weibull, Burr XII and Gen.Gamma distribution and d-e) Simulated CDF fitting intervals for Weibull, Burr XII and Gen.Gamma distribution

The generated wind speed time series, using the SMA-GHK scheme, compared to the observed and reanalysis data are discussed. Different scenarios were tested based on the key comparison criteria of the selected probability distribution functions, of the double periodical statistical characteristics, and of the second order dependence structure (via the climacogram). For the selected site in Lesvos, all of the distributions showed increased performance in accordance to the mean and variance of the simulated samples, however, GG preserved better the skewness and kurtosis values. Overall, the strength of the presented stochastic scheme can be highlighted particularly in non-Markovian and non-Gaussian processes, such as wind speed, in which a long-term persistence behaviour and a heavy-tail distribution are apparent and must be explicitly preserved for a large range of scales. Most research has focused on Markov autocorrelation structures in continuous-time (Zárate-Miñano et al. 2014;Loukatou et al. 2018) or in discrete-time (AR [Castellanos & Ramesar 2006;Carapelluci & Giordano 2013]; or higher-order AR; [Suomalainen et al. 2012]), while here the Hurst-Kolmogorov model is applied for the second-order dependence structure of the wind speed, ranging from small hourly-lags/scales to large hyper-annual lags/scales (of the order of decades) beyond the spectrum observed by the data. For the marginal structure, results highlight how applying a heavy-tail probability function permits for a more cohesive representation of the extreme behaviour of wind speed beyond the

Weibull distribution in addition to Castellanos & Ramesar (2006), Suomalainen et al. (2012) and Carapelluci and Giordano (2013). The double periodicity of wind speed is simulated by a mixed exponential-cosine model to preserve the double asymmetric fluctuation of the diurnal and seasonal periodicities, while for single sinus and cosine expressions [see Ephrath et al. (1996) and Carapelluci & Giordano (2013), and for non-parametric models [see Suomalainen et al. (2012) and Loukatou et al. (2018). Finally, the climacogram stochastic metric is selected for the estimation of the dependence structure from data, instead of the more common estimators of autocorrelation or power-spectrum, mainly because of the lower estimation bias.

The preservation of additional lags/scales beyond the timeseries length in both the marginal and dependence structures, is advantageous for management purposes, and can be justified by global-scale hourly wind speed analyses applying the ensemble Monte-Carlo technique as well as by the entropy extremization principle, which results in a long-term persistent rather than a Markov-type behaviour (Koutsoyiannis et al. 2018). Although the proposed methodology is able to preserve the different characteristics of the measured wind speed data for any distribution applicable in wind speed modelling, some drawbacks are noticed. The limitation of the proposed stochastic model is that the applied explicit-implicit scheme cannot capture beyond the second-order dependence structure as well as the auto-correlations between the diurnal and seasonal periodicities of wind speed, whereas it can explicitly simulate the marginal (i.e., probability density function) and second-order dependence (i.e., autocorrelation) structures of wind speed for scales ranging from hours to decades, as well as the double periodicity of wind speed in an implicit manner.

### 6.4.2 Spatial wind stochastic simulation results and discussion

Examining the spatial extension of the SMA-GHK simulation scheme to the entire study area, results indicate that model is adequately capturing the marginal probability distribution, the long-term persistence and the diurnal and seasonal periodicities. In Table 6.4.2.1 and Figure 6.4.2.1 the results of the synthetic time series are demonstrated in accordance to the marginal seasonal characteristics, the marginal probabilistic and the second order dependence structure. Simulated reanalysis wind speed data consist of 100 hourly time series of 25-years length and 1-

hour interval. In order to emulate the observed reanalysis wind time series, any values of the synthetic time series that are below the recorded positive minimum value of the station or the reanalysis data (which is around 0.1 m/s), are set to zero. It is noticed that for the distribution function the special case of the Burr XII distribution (PBF) is applied (see Table 6.4.2.1) which approximates the Weibull distribution for small hourly velocities and the Pareto distribution for larger ones. Hence, the dependence structure, marginal distribution and standardization scheme of offshore wind are based on the preliminary analysis performed in the previous sections where PBF showed an increased performance and simplicity during the standardization process.

**Table 6.4.2.1:** Estimated mean, variance, skewness and kurtosis between reanalysis and simulated data based on PBF distribution.

| **Marginal (Komotini)** | **Mean** | **Variance** | **Skewness** | **Kurtosis** |
|---|---|---|---|---|
| Observed (UERRA) | 3.679 | 5.942 | 1.281 | 5.751 |
| Simulated (UERRA) | 3.665 | 6.362 | 1.839 | 9.152 |
| **Marginal (Larissa)** | **Mean** | **Variance** | **Skewness** | **Kurtosis** |
| Observed (UERRA) | 3.713 | 7.971 | 1.714 | 8.511 |
| Simulated (UERRA) | 3.704 | 7.848 | 1.819 | 8.972 |
| **Marginal (Lemnos)** | **Mean** | **Variance** | **Skewness** | **Kurtosis** |
| Observed (UERRA) | 6.539 | 14.101 | 0.885 | 4.028 |
| Simulated (UERRA) | 6.506 | 13.916 | 0.961 | 4.322 |
| **Marginal (Cyclades)** | **Mean** | **Variance** | **Skewness** | **Kurtosis** |
| Observed (UERRA) | 7.271 | 12.211 | 0.606 | 3.361 |
| Simulated (UERRA) | 7.304 | 12.039 | 0.598 | 3.365 |

The parameters related to the dependence structure via the climacogram are estimated for the entire study area as: $k$ = 0.18 – 78 (Figure.6.4.2.1a), $q$ = 1 hour and the Hurst parameter ($H$) ranges in the interval = 0.55 - 0.78 (Figure.6.4.2.1b), whereas for the marginal distribution the shape ($c,a$) and scale ($b$) parameters are estimated in the range 1.2 - 2.5 and 1.6 - 20 for the shape parameters and 2 - 37 for the scale parameter respectively. Considering the periodical characteristics (seasonal and diurnal), there is a satisfying agreement between the observed and the simulated raw moments considering the mean, variance, skewness and kurtosis. In particular, the PBF distribution seems to slightly overestimate the observed marginal values in most cases. An indicative example is illustrated in Table 6.4.2.1 for the broader Komotini, Larissa, Lemnos and Cyclades area. Overall, the SMA-GHK model tends to overestimate and slightly underestimate mean and variance in the coastal areas and most of the offshore areas. Besides, skewness and

kurtosis seem to preserve relatively small variations; however, their periodic cycles are adequately captured. Concerning the second order dependence structure, simulated through the climacogram, the stochastic generation scheme is supremely reproducing the observed long-term behavior of the wind speed times series, as presented in Figure.6.4.2.1.

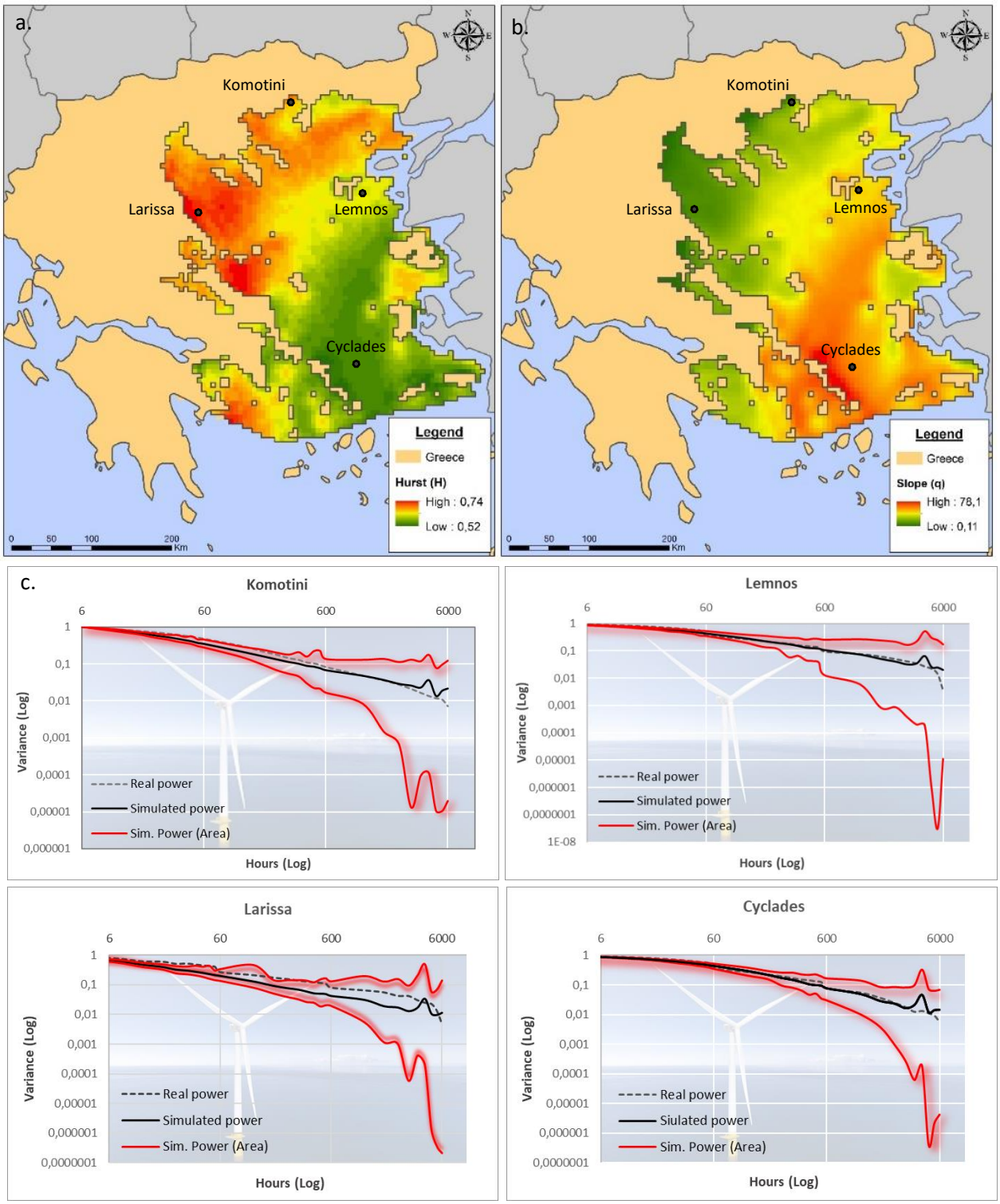

**Figure.6.4.2.1:** a) Estimated Hurst parameter (H) and b) Estimated slope (q) of the climacogram function $\gamma$ for the entire study area. c) Indicative wind power climacograms between UERRA and SMA-GHK simulated data based on the PBF distribution (Background image source: GE Renewable Energy)

Moreover, is highlighted that the variance at scale 1 of the standardized climacogram should approximate unity but it is slightly larger due to the diurnal and seasonal double periodicity effects. These effects also cause a small increase of the climacograms around diurnal and seasonal scales. Simulated wind power uncertainty for the 100 simulations is indicatively illustrated in Figure.6.4.2.1. Notable is the decreased wind power variability for the wider offshore area of Cyclades as also for some coastal parts (i.e., Larissa) although, in the latter case, weak wind power potential values occurred.

Annual energy production for both hindcasted and reanalysis wind speed data is demonstrated in Figure.6.4.2.2a-f for the different types of the selected wind turbines, i.e., 5, 8 and 10 MW respectively along with the optimal areas (light and dark green colored areas). The most promising areas occurred in the Central and Eastern part of the study area, consisting of the islands of the North Aegean Sea and Cyclades. The mean values of the hindcasted and simulated AEP is these areas ranges between 0.6 - 25 GWh/year for the 5MW wind generators, 0.4 – 38 GWh/year for the 8MW and between 0.6 – 50 GWh/year for the 10MW wind turbines respectively. Finally, Figure 6.4.2.2 is also presenting the differences of the simulated AEP compared to an indicative year (2018) of hindcasted offshore wind reanalysis data. Results indicate decreased discrepancies among the synthetic wind time series and the historical modelled data; however, the overall offshore wind patterns seem to be adequately captured from the SMA-GHK simulation scheme.

The estimated Wind Power Variability (WPV) ranges between 0.5 - 8.3 (Figure.6.4.2.3a) and the Coefficient of Variation (CV) varies from 0.5 to 2.7 with the highest wind power variability and variation located in the North-East Aegean Sea (broader Thracian Sea, Lemnos and Sporades). On the contrary, the less productive areas, in terms of the AEP, occurred in the North-West Aegean Sea (Thermaikos gulf) and the broader western part of the coastal Greek territory.

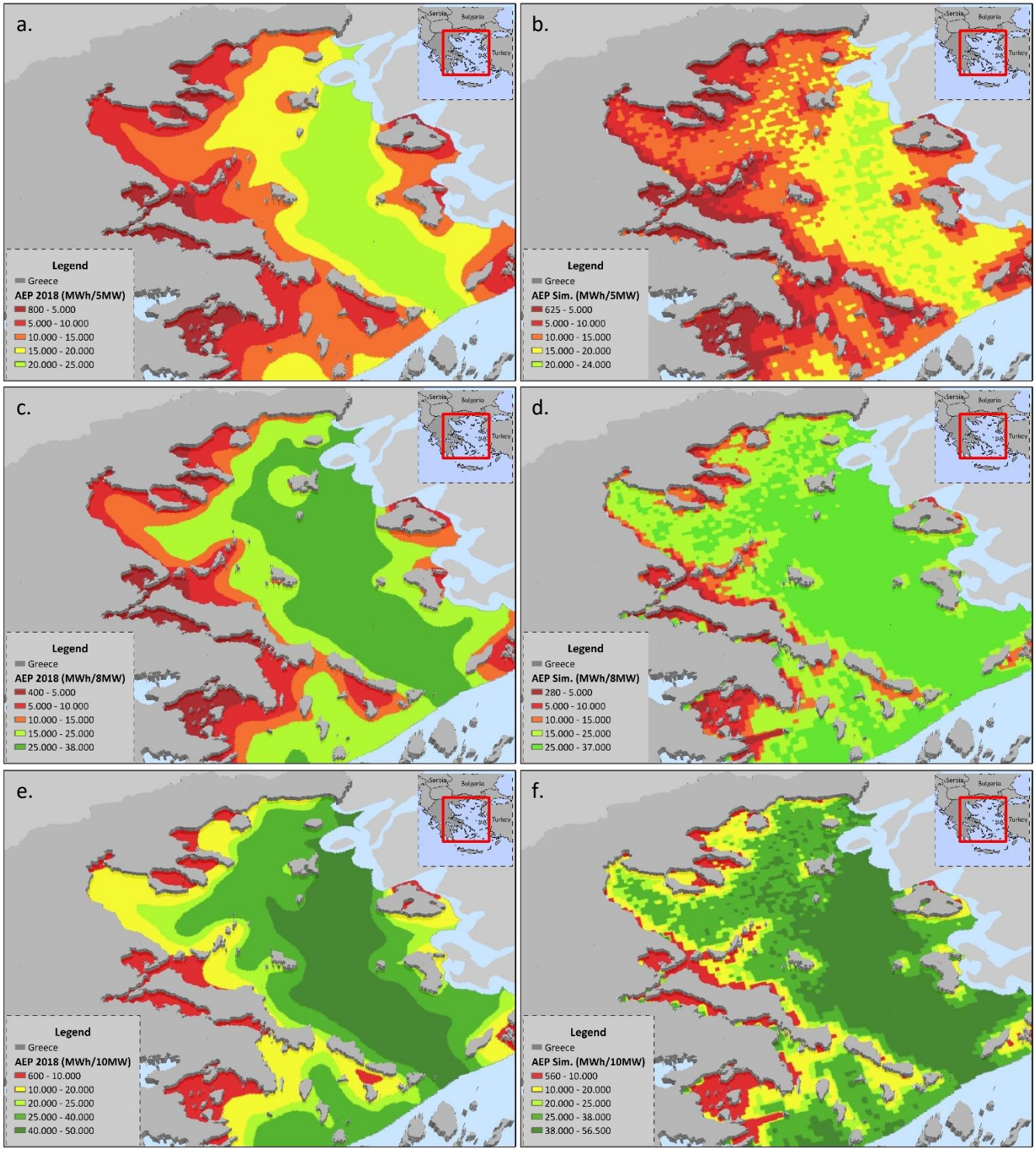


**Figure.6.4.2.2:** a,c,e) Estimated AEP from the hindcasted UERRA reanalysis wind time-series (for 2018) and b,d,f) Estimated AEP from the simulated wind speed time-series for the 5,8 and 10MW wind generators

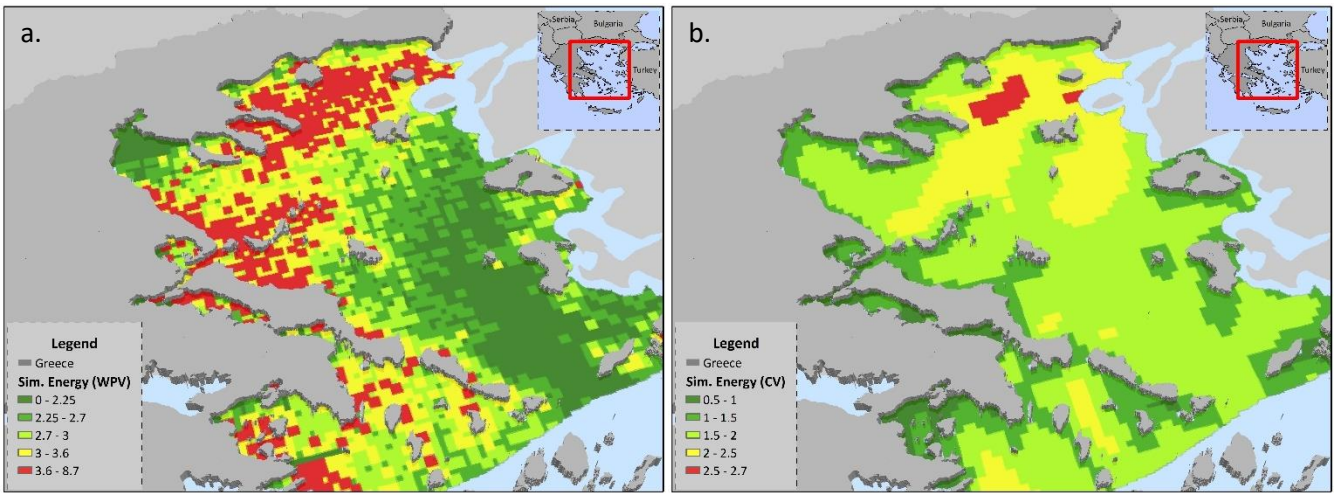


**Figure.6.4.2.3:** a) Estimated Wind Power Variability of the Simulated Annual Energy Production (via the Climacogram) and b) Coefficient of Variation (CV) of the Simulated Annual Energy Production

## 6.5 Levelized Cost of Energy and Net Present Value results

According to the above-mentioned cost and wind-related results, the spatial distribution of the total CAPEX, O&M, AEP and thus, the final LCOE and NPV estimates are presented during this section. Total CAPEX results are summarized in Figure. 6.5.1, where the costs for the bottom-fixed and the floating concepts are estimated between 18 – 35 million euros, 29 – 57 million euros and 37 - 71 million euros for the reference 5, 8 and 10MW (Figure. 6.5.1a-c) wind turbines respectively. These results are in line with existing generic sources and previous studies reviewed in Section 2, where values ranging from 2 - 5.5 million euros/MW were reported. Nevertheless, increased CAPEX costs occurred by the proposed model, mainly due to the increased WTs capacity beyond 8 MW as also, because of the increased capital investment costs for the selected floating concepts (WindFloat and Spar-Buoy).

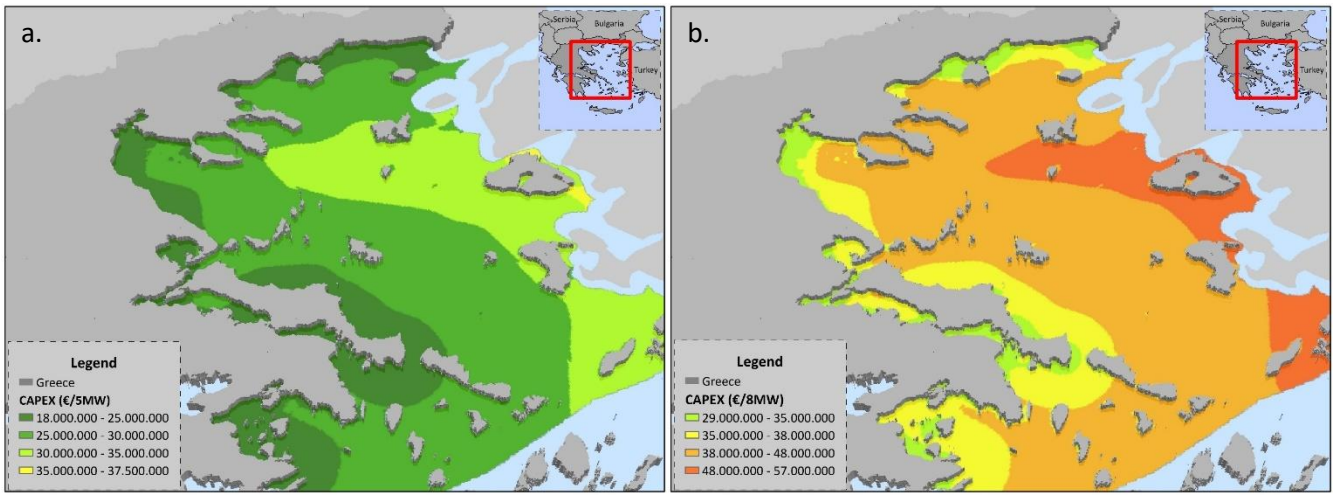

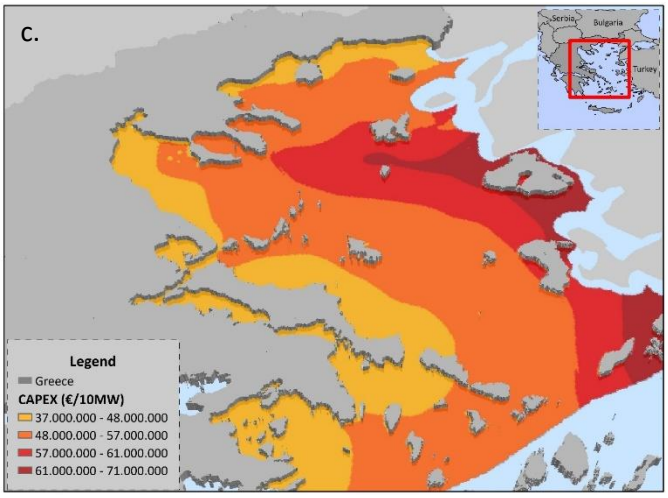


**Figure.6.5.1:** Estimated CAPEX in euros (€) for the a) 5MW b) 8MW and, c) 10MW wind turbines

Moreover, Figure 6.5.2 shows the CAPEX costs differences towards the cell size increase from 1000 meters to 2000 and 5000 meters. Results indicate a ±10% difference when the cell size increases from 1000 to 2000 meters, ±15% for an increase from 2000 to 5000 meters and finally, a ±25% difference from 1000 to 5000 meters. As expected, the higher percentage increase is mostly occurring in transitional water depth areas from 30 to 40 meters and 70 to 80 meters where the selected foundation technology differs and thus, the CAPEX cost is "adjusted" to the mean cost values between monopile and jacket structures and the jacket and floating structures. Also, when resampling from 1000 m. to 5000 m., the costs percentage differences increase, however, the pixels amount with increased differences is proportionally smaller than resampling from 1000 m. to 2000 m. In most of the far offshore areas, (beyond 20 kilometers) CAPEX differences range between -5% and +5%, hence, when only floating concepts are to be considered, the cell size increase has a minimum impact to the final cost estimates. On the contrary, when bottom-fixed concepts are under consideration, the minimum possible cell size (i.e., 1000 m.) is the optimal solution to further reduce cost uncertainties.

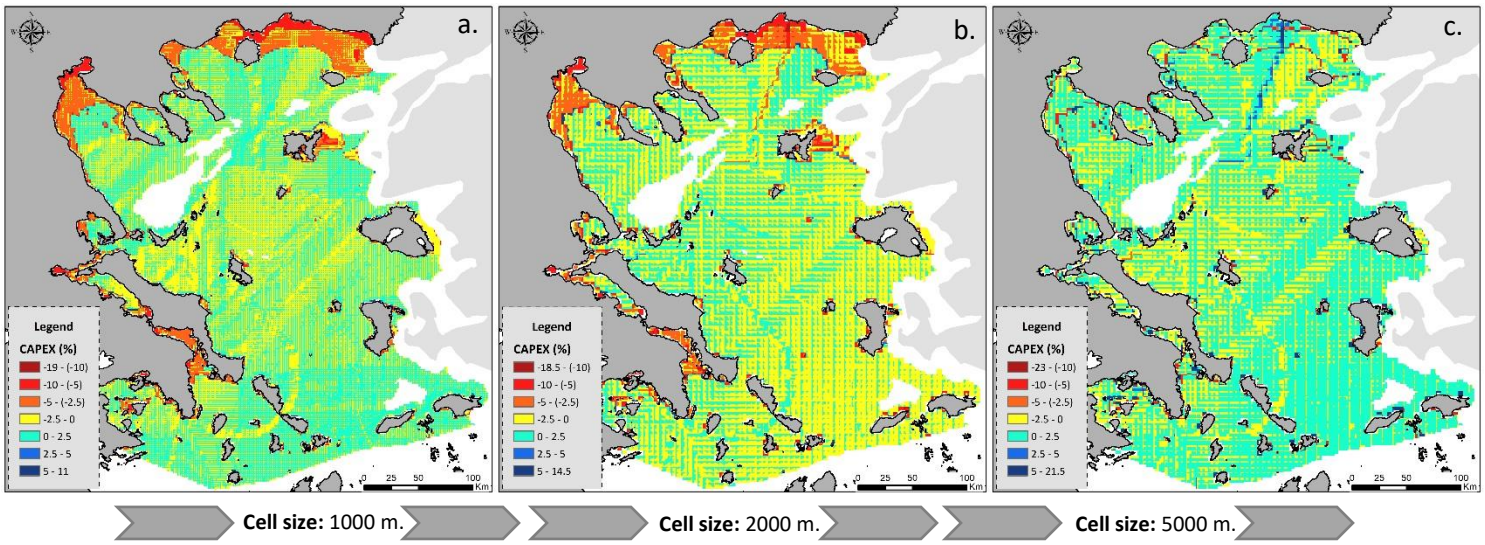


**Figure.6.5.2:** a) Estimated CAPEX percentage differences (%) between a) 1000 m. and 2000 m. cell size, b) 2000 m. and 5000 m. cell size and c) 1000 m. and 5000 m. cell size

The LCoE and NPV results, illustrated in Figure. 6.5.3, are based on the discounted values of CAPEX, O&M and Decommissioning cost (D&D) before being distributed to the energy generation during the project's lifetime. Additionally, the spatial distribution of these costs and the variability of the high- and low-cases are demonstrated. It is highlighted that those assumptions have been made considering that the final investment decision is to be taken in 2020 and the operating phase to start five years later, in 2025 until 2050. The results in Figure. 6.5.3 indicate that the costs of offshore wind energy are highly correlated to water depths, the wind resources and the total distance from the onshore network junction points and the nearest ports. In this sense, the lower water depths and higher annual energy production, the lower levelized production costs and the higher net present values occurred.

For example, regions located in the 0-70 m water depths are the least cost areas for developing offshore wind farms, with an average LCoE ranging from 95 to 120 €/MWh and NPVs up to 20 million euros for a single wind turbine (light green areas). These areas are mostly located to the Eastern part of Lemnos, Skyros and Cyclades islands as also to the Western part of Lesvos island. Results highlight that the total amount of space in short distances from the shore is limited

to the aforementioned sites, however, when a maximum water depth of 30 - 40 m. is to be considered, these areas are further reduced, mostly to the Eastern part of Lemnos Island. In contrast, available energy which costs between 80 and 100 €/MWh, is mainly located beyond 100 meters water depth to the Central and Central-East Aegean Sea (dark green areas).

In spite of the fact that these areas are located at remote distances from the shore, from potential ports and onshore transmission infrastructures, the LCoE and NPVs are promising because of the optimal wind resources and the reduced wind power availability. On the contrary, the highest LCoE and the lowest NPVs are mostly occurred on the Eastern and North-Eastern parts of the study area. In particular, these areas are located to the broader marine areas of Attica region, in the Northern and Eastern part of Evoia, in the wider Chalkidiki peninsula and the offshore areas around Sporades and Samothraki islands. These low potential offshore areas are illustrated in orange and red colors in Figure 6.5.3a,c,e and in grey and black colors in Figure 6.5.3b,d,f for the LCoE and the NPV results respectively.

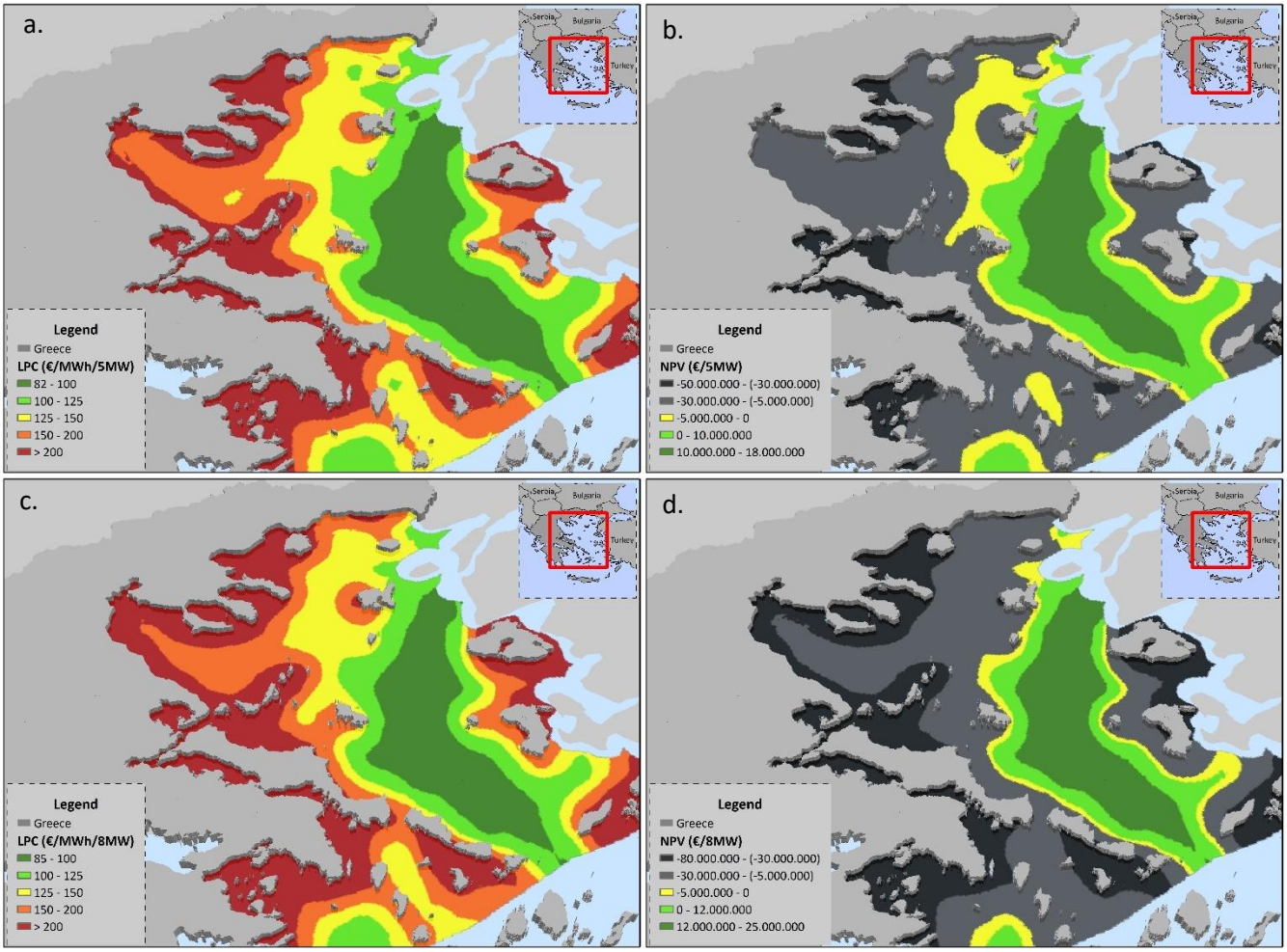

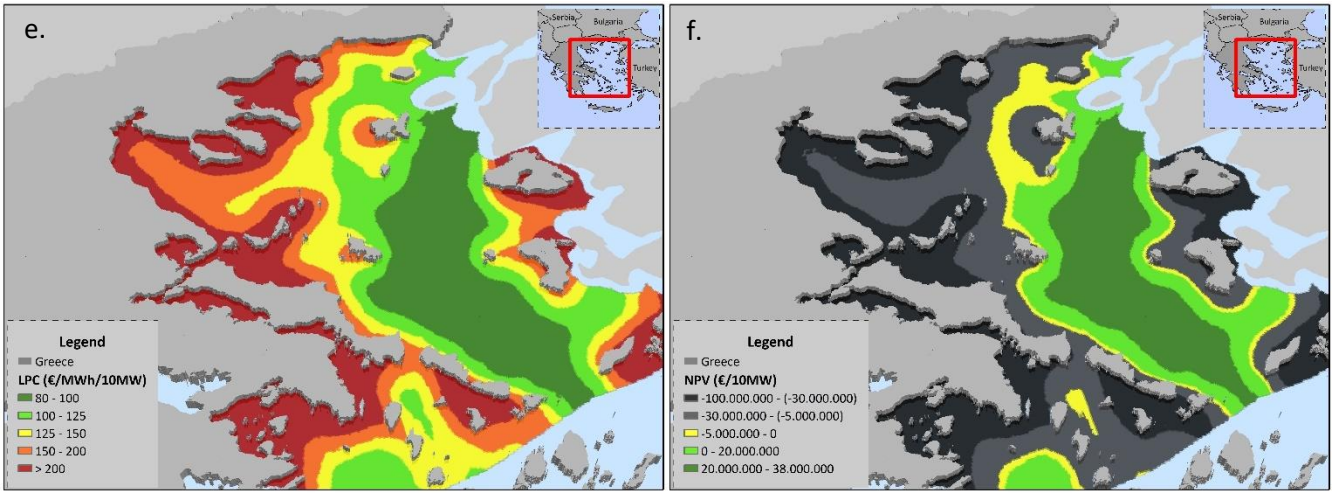


**Figure.6.5.3:** Estimated LCoE and NPV for the a-b) 5MW, c-d) 8MW, e-f) 10 MW wind generators for a lifetime of 25 years with 4% interest rate, 2% of power losses and 135 €/MWh for the electricity celling price

Moreover, Figure 6.5.4 summarizes the average CAPEX, LCoE and NPVs for the three depth bands and the associated foundation types considered: 0-30 m. (monopile), 30-70 m. (jacket), and >70 m. (floating). Moreover, the relation of cost differences with the distance from the shoreline, the nearest ports and the nearest onshore transmission junctions is also demonstrated. Some further insights of the results, illustrated in Figure. 6.5.4, highlight that the costs of offshore wind power generation increase for different installation scenarios (for the floating concepts) and different foundation cost assumptions in terms of the steel price. Surprisingly, the mean LCOE is higher and the mean NPVs are lower in shallow waters than increased water depths beyond 200 meters, reflecting the decreased energy yields in regions close to the shore. Overall, different patterns emerge from the analysis (on a WT basis) where the:

- CAPEX values for both monopile and jacket concepts preserve small differentiations, however, for the floating concepts, CAPEX decreases beyond 500 meters of water depth (approx. 0.6 million Euros) because of the cost decrease in the mooring and anchoring mechanisms;
- Sites below 70 meters water depth exceed LCoE values greater than 130 €/MWh and NPVs below 4.5 million eurosfor the entire study area;

- Sites beyond 150 meters water depth preserve the minimum LCoE values (below 100 €/MWh) and maximum NPVs (greater than 5 million Euros);
- An increase by approximately 9-10% in CAPEX slightly increases LCoE, however, has a greater impact on the NPVs by 2-3 million euros per WT (light red, grey and blue lines in Figure 6.5.4);
- Sites with greater distances from the shore preserve higher CAPEX values (1 - 1.5 million Euros), lower LCOE values (from 80 to 280 €/MWh) and the NPVs seem to significantly increase in either short and greater distances from the shore (i.e., below 8 km and beyond 45 km);
- CAPEX decreases for increased distances from the shore, mainly because of the lower installation and manufacturing costs for the floating concepts. However, the lowest LCoE values occurred in areas with distances between 70 km and 75 km from the nearest ports;
- Considering the distance from the onshore network junctions, the most promising areas observed for distances between 160 km and 180 km from the nearest junction point.

a.

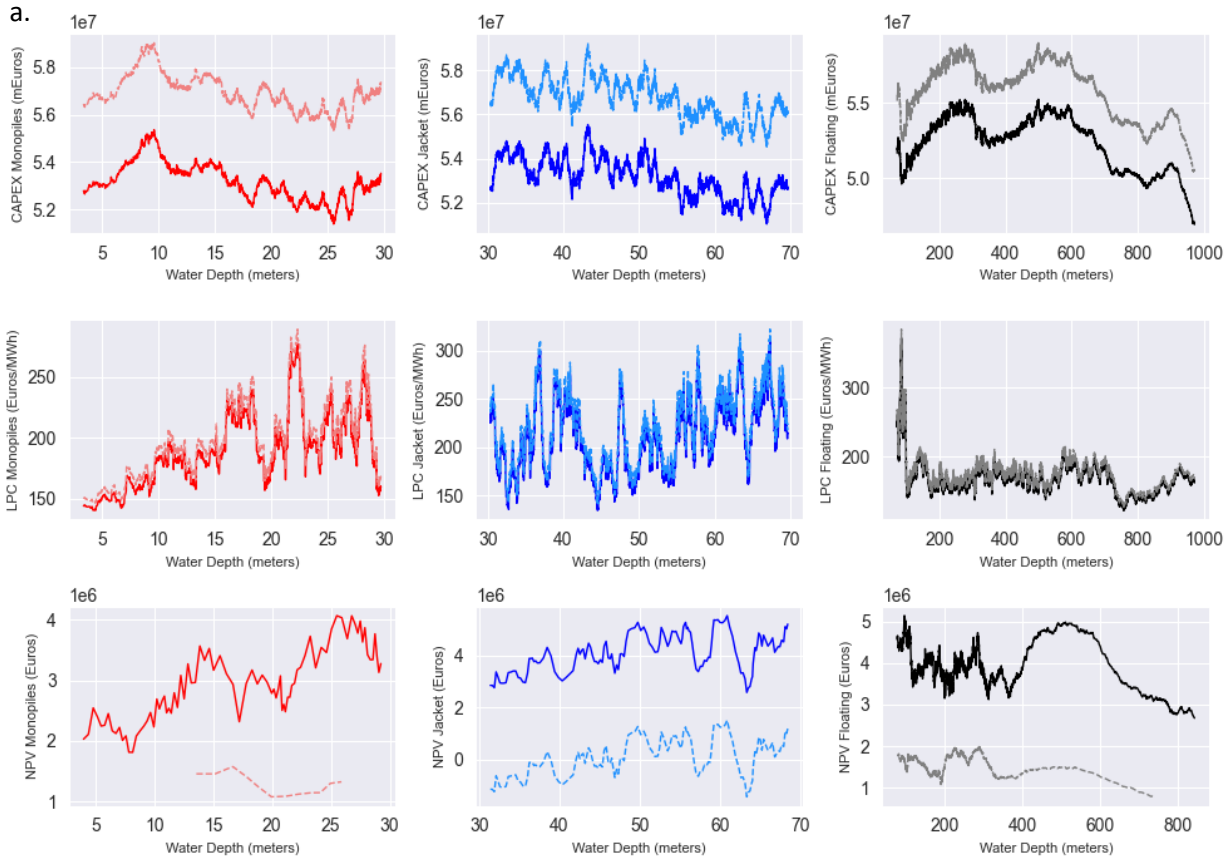

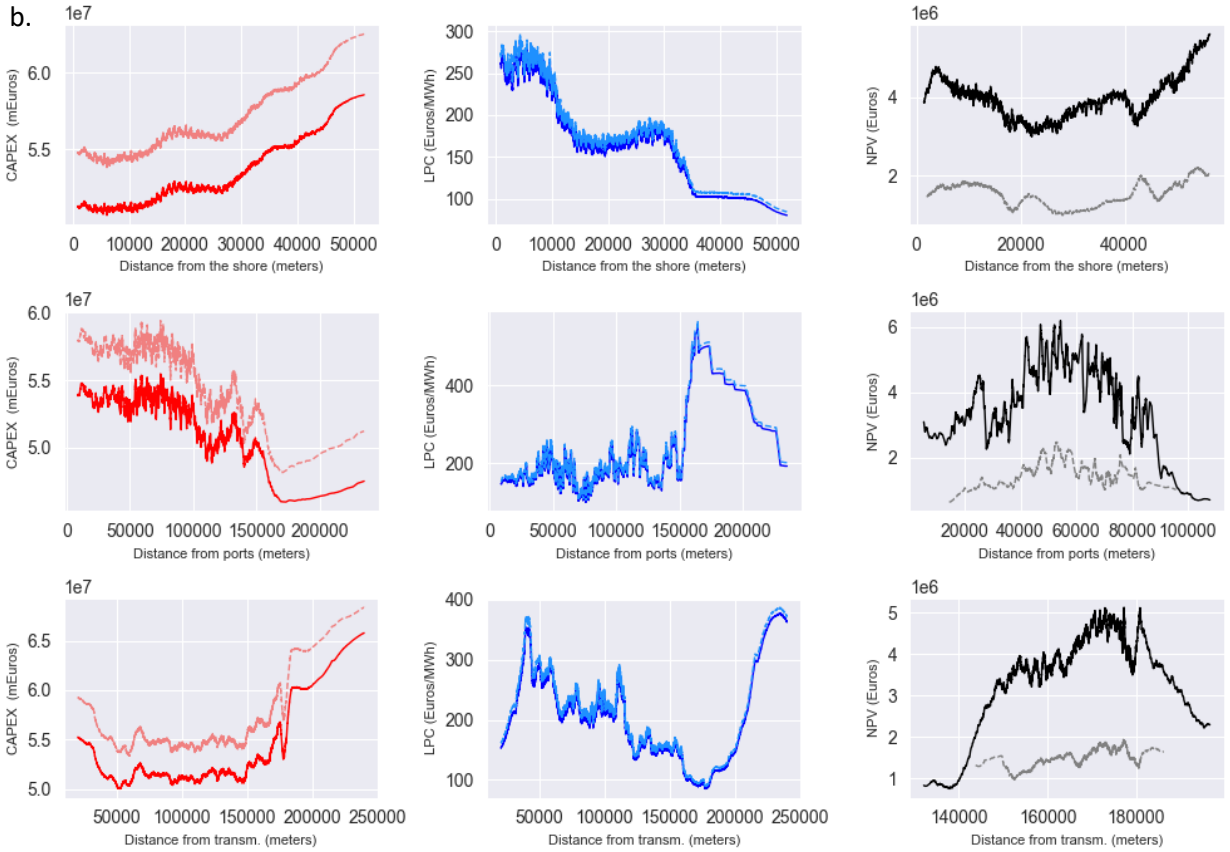


**Figure.6.5.4:** Indicative CAPEX, LCOE and NPV variations proportional to a) the water depth increase for the monopile (left), jacket (center) and floating (right) support structures, b) the distance from the shore (first row), the ports (second row) and the onshore network junctions (third row)

## 6.6 Spatial optimization model and OWF site-prospecting results

In this section, an extensive computational study is presented and discusses along with the optimal solutions representation, considering different site-prospecting scenarios and cost-related parameters configurations. Broadly speaking, the aim is to answer the questions: i) how efficient is the model on extracting global optimum solutions, ii) which is the model's capability for guaranteeing compactness, iii) which model for imposing contiguity is the fastest and more efficient in practice and finally, iv) is the model able to solve large-scale instances, considering the computational efficiency and the model's complexity, encountered in practice. All experiments were performed on an Intel-Core i5 desktop machine with a CPU of 2.3 gigahertz (GHz) and 8

gigabyte RAM with 8 processors. The MIP solver is Gurobi Optimizer 9.1.0 and the default settings were used with the following exceptions: 7 threads maximum, 8 GB RAM maximum, concurrent method for the LP relaxation, almost zero MIP gap tolerance (0.001%) and the computational time was limited to 800 seconds.

For the optimal solutions, the results returned a value of 0 or 1 for each region (cell/decision variable). A value of 1 indicates that the region selected is optimal and a value 0 is otherwise. Therefore, the model will search and sum the attributes of the optimal regions and display in tabular form. The algorithm search for optimal solution(s) begins with constraint parameters set to the total MWs of installed capacity required, the type of the WTs in each spatial unit (cell) and the capability to search for optimal solutions among NoData cells as well as in the edges of the input raster data (arrays). Finally, the Lazy Constraints parameter was invoked when solving the cut (via the Lazy constraint) models in order to guarantee contiguity for the optimal solutions. The objective function of the model presents the highest suitability score in terms of either the maximum Net Present Value (NPV) or the minimum Levelized Production Cost (LCoE) along with the maximum compactness of the available regions.

Considering the model's complexity, the inputs datasets (arrays) imposed to the model, contain 196240 cells (446 rows x 440 columns) with a cell size of 1000 meters. These spatial characteristics lead to a model with 206862 rows, 827424 columns and 2059484 nonzero variables with 1026105 quadratic objective terms. The aforementioned model parameters are reduced to 8556 rows, 34200 columns and 83674 nonzero variables with 41100 quadratic objective terms when the cell size increases to 5000 m. for a reference input raster of 8184 total cells (i.e. 93 rows and 88 columns).

### 6.6.1 Sub – criteria initialization and model set-up

The basic steps of the spatial optimization scheme set-up incorporate: i) to import all input data needed for the constraints' formulation (wind power classes, maximum distance from the shore, depths to be excluded etc.) as long as the cost-related calculations configurations for estimating the LCoE or/and NPV (energy selling price, interest rate etc.), ii) to set the OWF(s) characteristics (MWs and number of OWFs) and finally, iii) adjust the spatial optimization input

parameters (i.e. criteria weights). Figure 6.6.1.1 illustrates these steps and the overall outline of the GUI widget. It is noticed that all cost-estimations are performed "on the fly" during the running of the algorithm in order to be able to adjust and easily modify the initial parameters

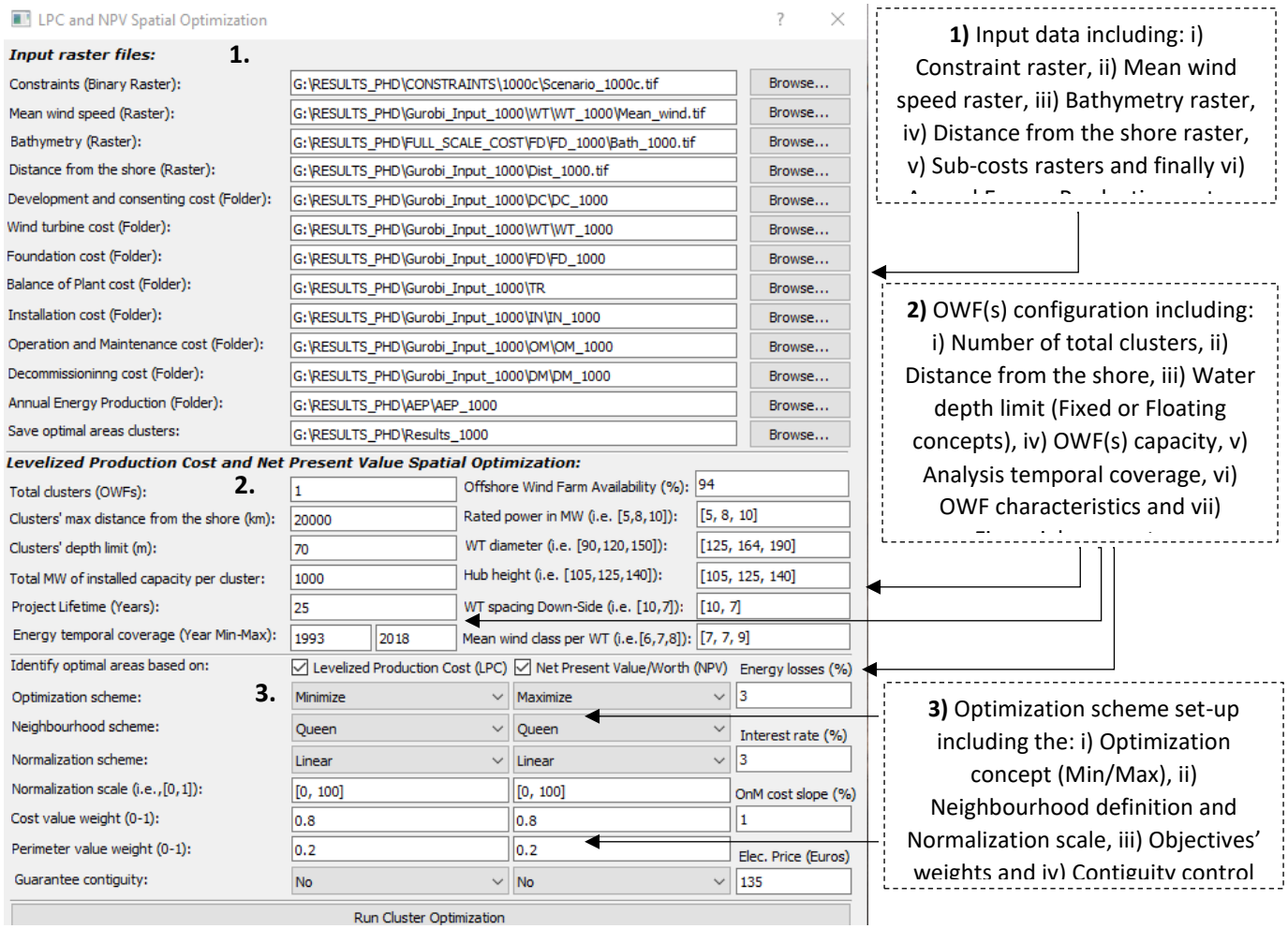


needed for each scenario.

**Figure.6.6.1.1:** Spatial optimization model set-up and initialization

In order to link Steps 1 and 2 illustrated in Figure 6.6.1.1, the associated maps are presented in Figure 6.6.1.2 that are used for the formulation of both the objective functions and the constraints of the spatial optimization routines. Thus, all data that are imported in Step 1 including: i) AEP rasters, WT cost, Foundation cost, Balance of Plant cost, Installation cost, O&M cost and Decommissioning cost rasters are used to estimate the spatial distribution of either the NPV or the LCOE for the entire study area. These estimates can be adjusted on per annual basis

(considering one year of wind data and the estimated AEP) or for the entire lifetime of a potential OWF (considering 20 or 25 years of lifetime data). The input AEP raster surfaces imported to the model include the hindcasted wind data as extracted from the UERRA reanalysis time series or the simulated data, based-on the SMA-GHK stochastic simulation scheme for one or more years of simulated wind time-series. In addition, Step 2 incorporates the total clusters (OWFs) to be extracted, the size of each OWF as also, all cost and financial expenditures parameters needed for the evaluation of the LCoE and the NPV. Moreover, the technical characteristics of the OWF in terms of the WTs capacity, rotor diameter, WTs' spacing and the wind speed classes for each WT type are used for the constraints' formulation.

In particular, WTs characteristics (MW, rotor diameter and WTs spacing) are used to calculate the optimal number of WTs per pixel. For example, using the scenario of the 1000 m. cell size, using Eq. 4.3.2.1-2 (Section 4), the total numbers of WTs per pixel is estimated as 1.25 (for the 5MW), 0.91 (for the 8MW) and 0.8 (for the 10 MW). On the contrary, by introducing the 5000 m. cell size raster surfaces, a total number of 33.7, 23.8 and 20 WTs is estimated for the 5MW, 8MW and 10MW respectively. Consequently, the constraint of the total MW required for each simulation is estimated (i.e., the total number of pixels required in order to reach a 1000 MW offshore wind farm). Furthermore, the wind class raster surface is used to define the type of WTs that can potentially be placed in each cell (pixel). Thus, for a mean wind speed below 6.5 m/s a reference 5 MW wind turbine may be placed, for mean wind speeds between 6.5 m/s and 8.5 m/s an 8 MW wind turbine is selected and for a reference mean wind speed beyond 8.5 m/s, the 10 MW wind generator is selected. It is noticed that theses wind speed limits are indicative and do not reflect an actual offshore wind class assessment campaigns required for the optimal selection of the appropriate WT model in each offshore area.

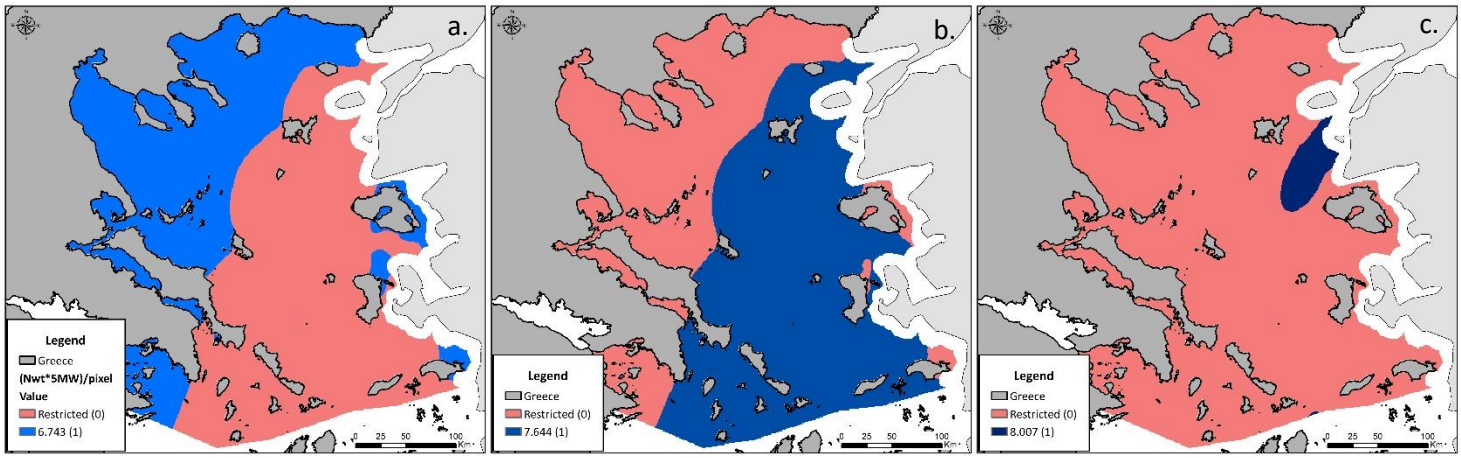

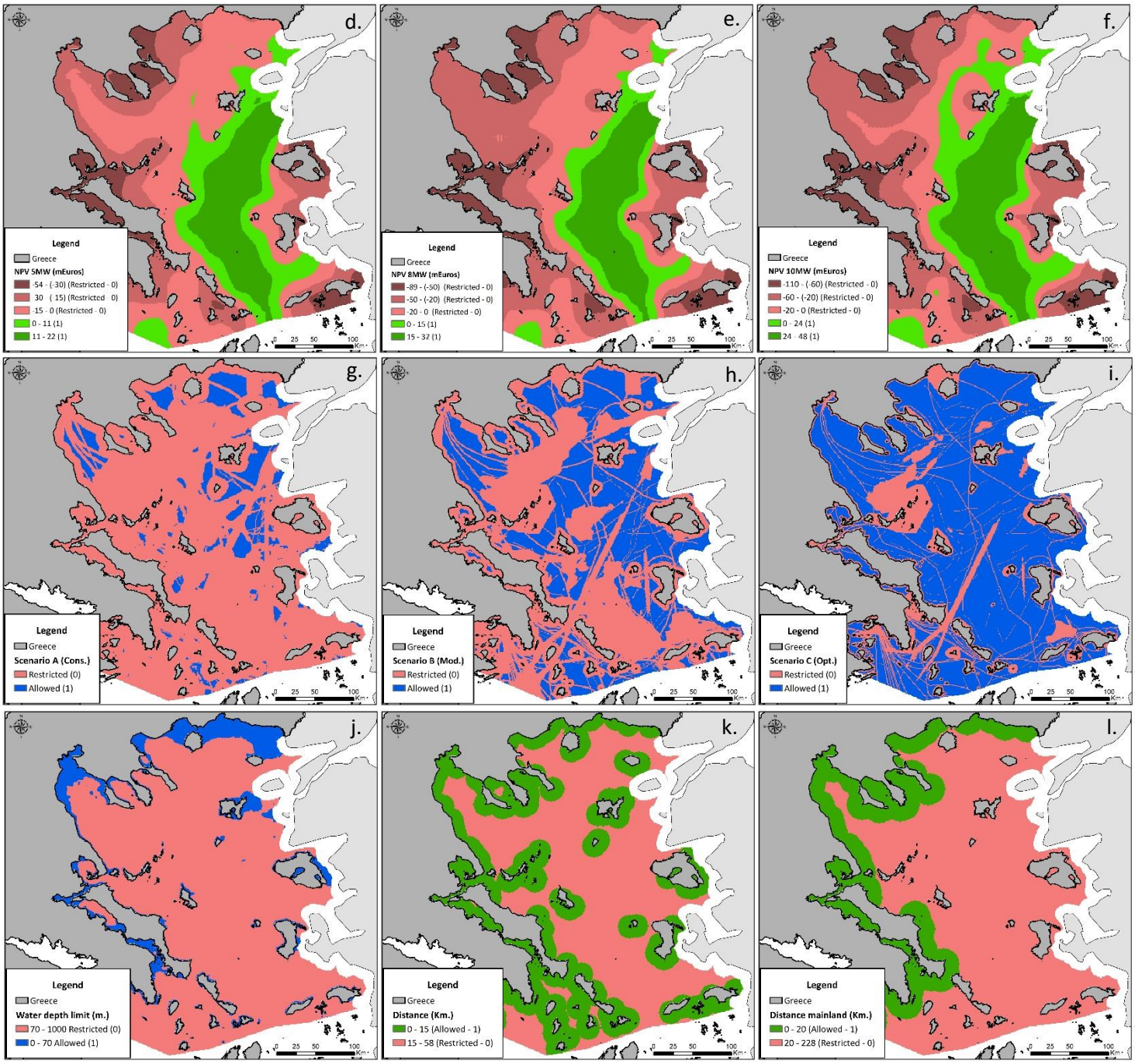


**Figure.6.6.1.2:** Optimization input raster data (arrays) including: a-c) Installed capacity per pixel according to the wind class category, d-e) Net Present Values per WT type (only positive values), g-i) Pre-defined exclusion scenario and finally, j-i) Water depth and distance from the shore restrictions

Finally, in Step 3 of the spatial optimization scheme set-up, the following parameters have to be considered by the user including: i) the optimization concept (for either the LCoE or NPV model), for example, to allocate optimal areas with the minimum LCoE values and the maximum NPVs, ii) Neighbourhood concept definition, considering the compactness estimation (Queen or Rook pattern) and the normalization scale for each objective, iii) each objective's weights, including the LCoE or/and NPV as the first objective and compactness as the second objective and finally, iv) the Contiguity control in terms of the Lazy constraint activation in order to guarantee that non-contiguous areas will be excluded during the optimization process.

### 6.6.2 Final Offshore Wind Farms location results

At this point, the empirical application of the model, presented in Section 5.7, is demonstrated along with site-prospecting results and the model's sensitivity. Thus, having set-up the initial parameters discussed in the previous Sections, the spatial optimization algorithm is ready to search for optimal areas based-on the predefined user's inputs and preferences in terms of the optimal clusters' characteristics and the optimization scheme to be applied. Combining the GIS-based cost and energy related surfaces with the final exclusion areas rasters, the optimal areas for potential OWE deployment along with the marginal production costs are estimated and mapped. Based on either the LCoE or the NPV spatial distribution with the compactness index, the optimization procedure was tested for its efficiency to identify and deliver optimal areas. Optimality was assessed in terms of the global optimum solutions, the compactness preservation as long as in terms of the optimal LCoE and NPV values identified by the solver. Different scenarios were tested, based on the number and the size of clusters for OWFs siting. Hence, the OWFs' total size, in terms of the MW of installed capacity, was set to 200, 500 and 1000 MW respectively, for a number of total clusters required set as 1,2 and 4 different clusters.

In order to validate the model's capability to allocate continuous and compact patterns upon the given weighting factors, different weights were selected for each objective. To this end, Table.6.6.2.1 and Figure.6.6.2.1 illustrate the results obtained for 25 different scenarios, using the 1000 m. rasters (i.e., the minimum cell size) for different configurations, considering the selected exclusion scenario, the OWFs' technical characteristics, the financial parameters' characteristics

and the spatial optimization technical aspects. Particularly, Table.6.6.2.2 shows the processing times (CPU time), the number of iterations, the applied weighting scheme, the number of branch and bound nodes required to find a contiguous and compact area and finally, the contiguity control success without considering the lazy constraint.

For the compactness control, results indicated that for weight values < 0.1, the shape of the optimal areas tends to be irregular. In contrast, for weight values > 0.3, the optimal areas look alike rectangles. While the compactness weight values range between 0.1 - 0.3, the optimal areas tend to reduce their irregular shape. In addition to the shape control, when the compactness weight decreases (i.e., < 0.1), the running time increases exponentially. Searching for larger areas (in terms of the MW of installed capacity) it is highlighted that as the compactness weight decreases, the final optimal areas might be fragmented, as contiguity and compactness are expressed through the objective function and not as constraint factor.

Some indicative OWFs site-prospecting configurations from the model solutions are shown Figure.6.6.2.1, where the most promising areas were located in the Northern-East and Central part of the Aegean Sea with LCoE values below 90 €/MWh and NPV in the range between 3 - $4x10^9$ euros (see Figure.6.6.2.1a-c). These estimates correspond to approximately a 1000 MW offshore wind park using floating concepts, located to the Western offshore area of Lesvos Island. In the conservative and moderate suitability scenario (red colored areas), results, considering the NPV optimization (green areas), indicate fragmented optimal solutions in terms of the contiguity control. The reason is that the negative NPVs are discarded from the optimization process and as a result, the solution space is significantly reduced. Thus, when the compactness weight is set to 0.2, a greater importance is given to the NPV objective and due to the increased variability of the NPV, the algorithm “prefers” to break the cluster and return higher NPV areas that keep the cluster compact and reduce optimality of the cost objective. In these cases, an increased compactness weight must be set or the contiguity control lazy constraint must be enabled, however, the computational effort for the algorithm to search for optimal solutions is significantly increasing.

On the contrary, when large marine areas are to be identified nearshore (see Figure.6.6.2.1d), most optimal areas are returned only for the LCoE optimization scenario with a

value of 131-159 €/MWh, located to the Eastern part of South Evoia. For the NPV optimization scenario, no optimal areas were identified due to the negative NPV values occurred at most of the marine areas below the 30 km from the shoreline. When the size of the potential OWFs decreases to approximately 200MW and the distance from the shoreline constraint is enabled (i.e., distance below 30 km from the shore), optimal areas are mostly observed to the Eastern part of Lemnos Island (Figure.6.6.2.1e-f) with LCoE values in the range between 77 - 86 €/MWh and NPV values from 670 million eurosto 810 million Euros.

Furthermore, Figure.6.6.2.1g illustrates the optimal areas for OWE deployment when the distance limit is reduced below 20 km, for a maximum depth of 40 meters with no constraints considered for the marine human activities, protected areas etc. Results highlight that these dispersed areas occurred in the broader area of the Northern Aegean Sea near Alexandroupoli, in the Western part of Thassos island and finally to Chalkidiki peninsula. LCOE values range between 147-300 €/MWh as long as the NPVs are estimated below 300 million Euros. Finally, for a 500 MW offshore wind park Figure.6.6.2.1h demonstrates the optimal areas, considering a distance from the shore restriction (below 30 km) while all optimal clusters are concentrated to the Eastern part of the Lemnos island. The final optimal LCoE and NPVs were estimated in the range between 93-104 €/MWh and 300-600 million euros respectively. Overall, the Central, North-East and Eastern marine areas in the Aegean Sea preserved most of the time the higher optimality rankings in terms of the highest NPVs and the lowest LCoE.

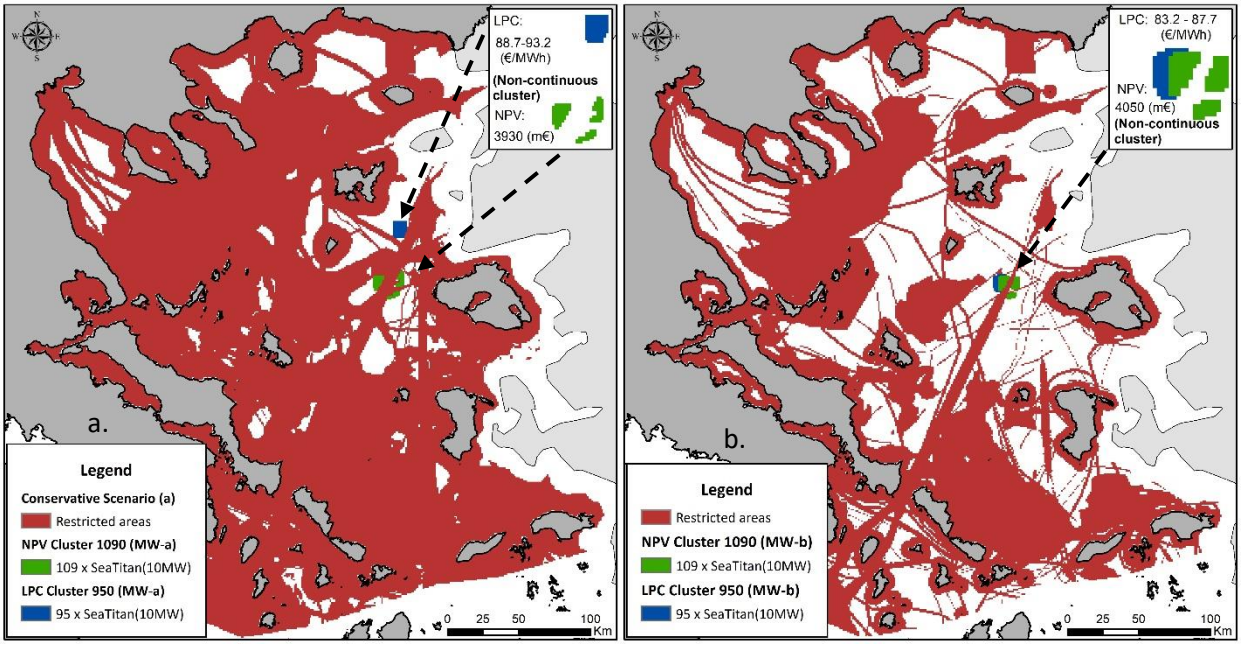

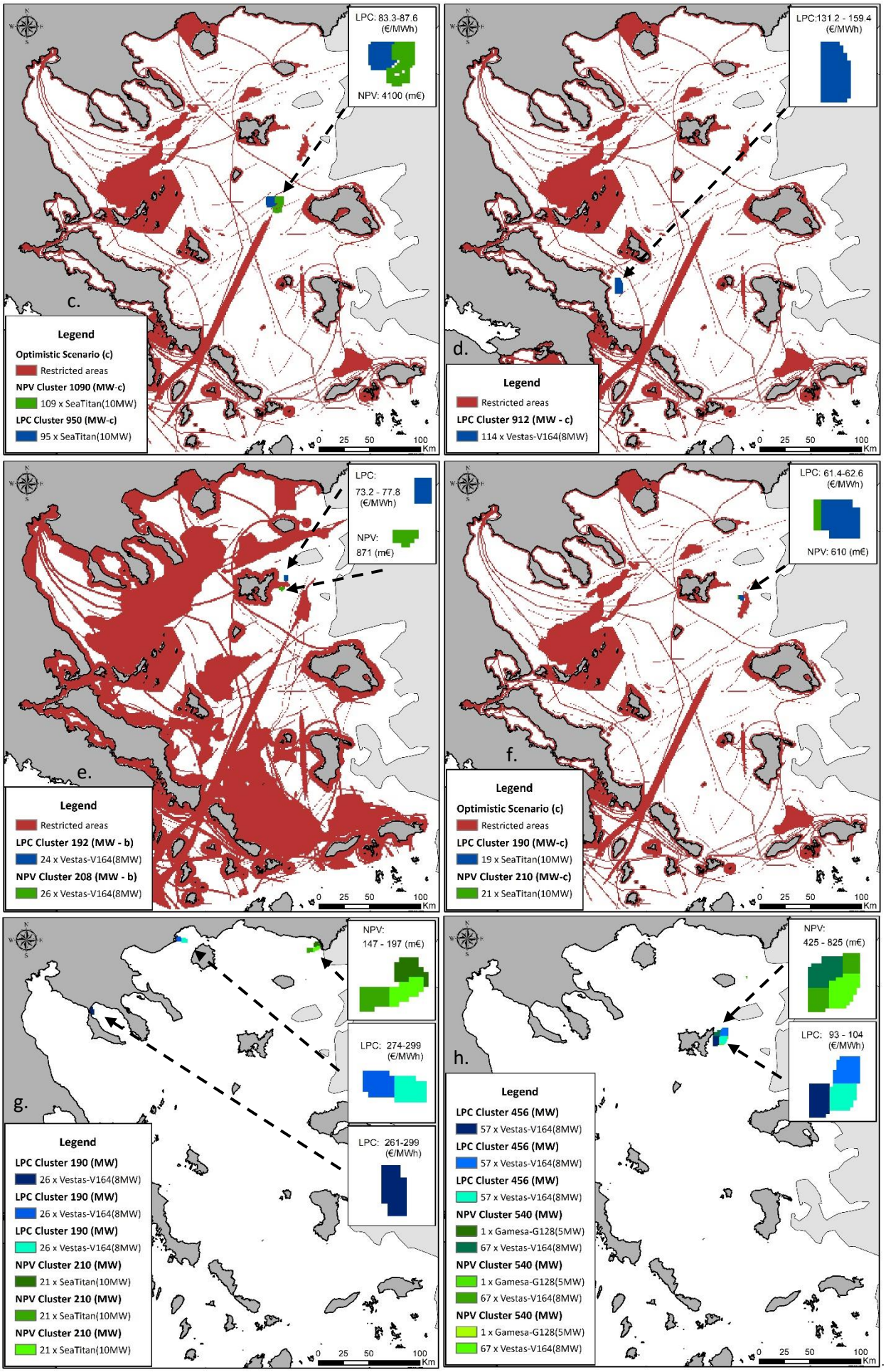
c.
LPC: 83.3-87.6 (€/MWh)
NPV: 4100 (m€)
Legend
Optimistic Scenario (c)
Restricted areas
NPV Cluster 1090 (MW-c)
109 x SeaTitan(10MW)
LPC Cluster 950 (MW-c)
95 x SeaTitan(10MW)
0 25 50 100 Km
d.
LPC:131.2 - 159.4 (€/MWh)
Legend
Restricted areas
LPC Cluster 912 (MW - c)
114 x Vestas-V164(8MW)
0 25 50 100 Km
e.
LPC: 73.2 - 77.8 (€/MWh)
NPV: 871 (m€)
Legend
Restricted areas
LPC Cluster 192 (MW - b)
24 x Vestas-V164(8MW)
NPV Cluster 208 (MW - b)
26 x Vestas-V164(8MW)
0 25 50 100 Km
f.
LPC: 61.4-62.6 (€/MWh)
NPV: 610 (m€)
Legend
Optimistic Scenario (c)
Restricted areas
LPC Cluster 190 (MW-c)
19 x SeaTitan(10MW)
NPV Cluster 210 (MW-c)
21 x SeaTitan(10MW)
0 25 50 100 Km
g.
NPV: 147 - 197 (m€)
LPC: 274-299 (€/MWh)
LPC: 261-299 (€/MWh)
Legend
LPC Cluster 190 (MW)
26 x Vestas-V164(8MW)
LPC Cluster 190 (MW)
26 x Vestas-V164(8MW)
LPC Cluster 190 (MW)
26 x Vestas-V164(8MW)
NPV Cluster 210 (MW)
21 x SeaTitan(10MW)
NPV Cluster 210 (MW)
21 x SeaTitan(10MW)
NPV Cluster 210 (MW)
21 x SeaTitan(10MW)
0 25 50 100 Km
h.
NPV: 425 - 825 (m€)
LPC: 93 - 104 (€/MWh)
Legend
LPC Cluster 456 (MW)
57 x Vestas-V164(8MW)
LPC Cluster 456 (MW)
57 x Vestas-V164(8MW)
LPC Cluster 456 (MW)
57 x Vestas-V164(8MW)
NPV Cluster 540 (MW)
1 x Gamesa-G128(5MW)
67 x Vestas-V164(8MW)
NPV Cluster 540 (MW)
1 x Gamesa-G128(5MW)
67 x Vestas-V164(8MW)
NPV Cluster 540 (MW)
1 x Gamesa-G128(5MW)
67 x Vestas-V164(8MW)
0 25 50 100 Km

**Figure 6.6.2.1:** Optimization results (optimal clusters) for: a-c) Far from the shore OWFs 1000 MW, d) Nearshore (to the mainland) OWFs 1000 MW, e) Nearshore (all coastal areas) OWFs 200 MW, f) Far from the shore OWFs 200 MW, g) Nearshore (to the mainland) OWFs 200 MW, h) Nearshore (all coastal areas) OWFs 500 MW

Overall, the results in Figure.6.6.2.1 indicate that most of the optimal areas are located far from the shore, in terms of the minimum LCoE and maximum NPV. This is mostly caused because of the restrictions occurred in the nearshore marine areas but most importantly, because of the higher wind speeds far from the shore and specifically to the Eastern and Central part of the Aegean Sea (North Aegean islands, Western Dodecanese and Cyclades). This imposes that those nearshore areas are more sensitive to planning issues, which is caused by the higher area competition and the higher share of protected areas near the coasts irrespectively to the exclusion scenario used. So far, the coastal areas may be less expensive to produce smaller amounts of electricity than far shore areas, where resources seem unlimited, but this comes in line with the increased cost sensitivity for the floating foundation concepts.

The cost sensitivity analysis has been performed and eight parameters were altered systematically to test model's sensitivity. The results are highlighted in Table 6.6.2.1 for different economic and technical aspects such as the:

1. interest rate (±2%),
2. lifetime of the wind farm (±5 years),
3. availability (±3%),
4. electricity selling price (±30%),
5. CAPEX (±15%),
6. O&M and Maintenance expenditures annual slope (±10%),
7. average power output (±15%) and power losses (±1%)
8. weather factors during the installation process and installation strategies for the floating concepts (±5%).

The parameters such as the initial investment cost (CAPEX), availability, and annual energy production exhibited similar variations of LCoE of about 15 - 20 €/MWh and for the NPV between 1000-1500 million euros (25% and 70% difference), considering a 2% difference for the interest

rate or 15% for the CAPEX and the annual energy production respectively. It is also noticed that the LCoE is more sensitive to the interest rate. The variation of 1% (increase or decrease) of power losses ensuing a change of 12% for both LCoE and the NPV respectively. When the lifetime of a potential OWF is restricted to 20 years (from 25), the LCoE increases by approximately 25-30 €/MWh and the NPV decreases from 650 to 1150 million euros respectively. Thus, shorter life span is more sensitive compared to the extended lifespan scenario. Lifetime sensitivity scenarios to the AEP have a greater effect on the LCoE and the NPV for the optimal areas as long as a 30% difference occurred for both values. Although 15 or 20 years is shorter than the design life of an OWF, it might be considered to show the cost risk of early failure of items or a decision to upgrade before 20 years as Cavazzi and Dutton (2016) and Nagababu et al. (2017) highlight in previous research studies. On the contrary, lengthening the lifetime to 30 years gave a proportionately smaller advantage of 4 - 8 €/MWh, indicating a lower benefit to be gained from "sweating the assets".

**Table 6.6.2.1:** Optimization results in terms of the final optimal areas for 200, 500 and 1000MW future OWFs. With red color is highlighted the sensitivity analysis and with blue the optimal scenarios

| Scenario | Optimal Area | Bath limit | WT combinations | LPC Values | NPV Values | IRR | CAPEX | O&M Cost | O&M Slope | Discount Rate | Avail. | PowerLosses | Lifetime | E. Price |
|---|---|---|---|---|---|---|---|---|---|---|---|---|---|---|
| | (Name) | (m) | (Count/MW) | Euros/MWh | mEuros | (%) | mEuros | mEuros/Year | (%) | (%) | (%) | (%) | (Years) | Euros/MWh |
| **1. Conservative (Fixed/Floating)** | S.Lemnos/W.Lesvos | Fixed/Floated (1000m) | 95-105 (10 MW) | 88-93 | 3161-3924 | 6.27-6.3 | 6540-6670 | 84.1-90.1 | 1 | 2 | 95 | 2 | 25 | 135 |
| **2. Moderate (Fixed/Floating)** | W.Lesvos | Fixed/Floated (1000m) | 95-105 (10 MW) | **83.3/87.6** | **3706-4033** | **6.42-6.76** | **6431-6627** | **84-89.3** | 1 | 2 | 95 | 2 | 25 | 135 |
| **3. Optimistic (Fixed/Floating)** | W.Lesvos | Fixed/Floated (1000m) | 95-105 (10 MW) | **83.2-87.4** | **3924-4142** | **6.5-6.79** | **5776-6090** | **85.5-89.9** | 1 | 2 | 95 | 2 | 25 | 135 |
| 4. Conservative (Fixed/Floating) | S.Lemnos/W.Lesvos | Fixed/Floated (1000m) | 95-105 (10 MW) | 109-115 | 1068-1744 | 3.95-4.21 | 6529-6649 | 85.8-93 | 1 | **4** | 94 | **3** | 25 | 135 |
| 5. Moderate (Fixed/Floating) | W.Lesvos | Fixed/Floated (1000m) | 95-105 (10 MW) | 102-108 | 1558-1863 | 4.05-4.28 | 6278-6540 | 85.3-92.6 | 1 | **4** | 94 | **3** | 25 | 135 |
| 6. Optimistic (Fixed/Floating) | W.Lesvos | Fixed/Floated (1000m) | 95-105 (10 MW) | 103-108.3 | 1613-1831 | 4.05-4.33 | 6322-6572 | 86.7-91.9 | 1 | **4** | 94 | **3** | 25 | 135 |
| 7. Conservative (Fixed/Floating) | S.Lemnos/W.Lesvos | Fixed/Floated (1000m) | 95-105 (10 MW) | **124.6-130** | **490-1199** | **3.19-3.63** | **6507-6681** | **83.3-91.2** | 1 | 4 | 94 | 2 | **20** | 135 |
| 8. Moderate (Fixed/Floating) | W.Lesvos | Fixed/Floated (1000m) | 95-105 (10 MW) | 116.6-123 | 959-1220 | 3.35-3.69 | 6495-6594 | 85.4-91 | 1 | 4 | 94 | 2 | **20** | 135 |
| 8. Optimistic (Fixed/Floating) | W.Lesvos | Fixed/Floated (1000m) | 95-105 (10 MW) | **166.5-122.8** | **926-1308** | **3.49-3.78** | **6278-6649** | **87.3-89.7** | 1 | 4 | 94 | 2 | **20** | 135 |
| 9. Conservative (Fixed/Floating) | W.Lesvos | Fixed/Floated (1000m) | 95-105 (10 MW) | **79.9-84** | **5.9-545** | **2.32-2.41** | **6518-6692** | **84.2-92.6** | 1 | 2 | **96** | 2 | 25 | **95** |
| 10. Moderate (Fixed/Floating) | W.Lesvos | Fixed/Floated (1000m) | 95-105 (10 MW) | **79.9-84** | **123-584** | **2.38-2.65** | **6576-6601** | **85.6-92.3** | 1 | 2 | **96** | 2 | 25 | **95** |
| 11. Optimistic (Fixed/Floating) | W.Lesvos | Fixed/Floated (1000m) | 95-105 (10 MW) | **79.9-83.2** | **631-662** | **2.38-2.72** | **6485-6583** | **87.4-91.1** | 1 | 2 | **96** | 2 | 25 | **95** |
| **12. Conservative (Nearshore)** | E.Lemnos | **Fixed/Floated (200m)** | 12 (8 MW) + 39 (10 MW) or 9 (8 MW) + 45 (10 MW) | 112-129 | 67 - 399 | 5.04-5.21 | 3456-4219 | 51 - 59 | 1 | 3 | 95 | 3 | 25 | 135 |
| **13. Moderate(Nearshore)** | E.Lemnos | **Fixed/Floated (200m)** | 12 (8 MW) + 39 (10 MW) or 9 (8 MW) + 45 (10 MW) | 105-122 | 76 - 423 | 5.12-5.3 | 3163-4073 | 49 - 55 | 1 | 3 | 95 | 3 | 25 | 135 |
| **14. Optimistic(Nearshore)** | E.Lemnos | **Fixed/Floated (200m)** | 1 (5 MW) + 65 (8 MW) or 48 (10 MW) | **104.9-114** | **83-499** | **5.24-5.38** | **2750 -2914** | **45-49** | 1 | 3 | 95 | 3 | 25 | 135 |
| **15. Conservative (Mainland)** | Lemnos | **Fixed (70m)** | 24-26 (8 MW) | **83-87** | **772-824** | **3.57-3.62** | **1081-1107** | **18.03-19** | **0.5** | 2 | 96 | 2 | 25 | **115** |
| **18. Moderate (Mainland)** | Lemnos | **Fixed (70m)** | 19-20 (10 MW) | **82-86** | **595-638** | **3.64-3.75** | **1232-1258** | **19.8-20.15** | 1 | 2 | 95 | 2 | 25 | 135 |
| **17. Optimistic(Mainland)** | Lemnos | **Fixed (70m)** | 48 or 53 (10 MW) | **87-94** | **1445 - 1552** | **3.98-4.05** | **2805-3063** | **51-52.1** | 1 | 2 | 95 | 2 | 25 | 135 |
| **18. Optimistic (Mainland)** | S.Evoia | **Fixed (70m)** | 119 (8 MW) | **131-159** | **No Solution** | **No Solution** | **4043-4142** | **74.2-76.9** | 1 | 2 | 95 | 3 | 25 | 95 |
| **19. Optimistic (Mainland)** | S.Evoia | **Fixed (70m)** | 60 (8 MW) | **120-149** | **No Solution** | **No Solution** | **4009-4065** | **84.8-86** | **2** | 2 | 95 | 3 | 25 | 95 |
| **20. No Constraints (Nearshore)** | Lemnos | **Fixed (70m)** | 5 MW/8 MW | **93-100** | **686-700** | **3.69-3.76** | **2296-2380** | **40.6-40.8** | 1 | 2 | **95** | 2 | 25 | **135** |
| **21. No Constraints (Nearshore)** | Alexandr./Thasos | **Fixed (70m)** | 24 (10 MW) | **71-73** | **594-627** | **4.42-4.73** | **1232-1265** | **20.1-20.3** | **0.5** | 2 | **96** | 2 | 25 | **95** |
| **22. No Constraints (Mainland)** | Alexandroupoli | **Fixed (70m)** | 8 MW/10 MW | **259-279** | **211-221** | **3.18-3.22** | **891-943** | **20.8-21.5** | **2** | **4** | 95 | 2 | 25 | 135 |
| **23. No Constraints (Floating)** | E.Skyros | Fixed/Floated (1000m) | 95-105 (10 MW) | **77-80** | **981-1318** | **3.99-4.06** | **5688-5886** | **93.4-99.7** | 1 | 2 | 95 | 2 | 25 | **100** |
| **24. No Constraints (Mainland)** | No solution | Fixed (70m) | No solution | **No solution** | **No solution** | **No solution** | **No solution** | **No solution** | 1 | **3** | **94** | 2 | 25 | 95 |
| 25. No Constraints (Fixed/Floating) **Lazy** | W.Lesvos | Fixed/Floated (1000m) | 95-105 (10 MW) | **91.9-93.3** | **2699-3011** | **3.99-4.2** | **5399-6267** | **78-81.3** | 2 | 3 | 94 | 3 | 25 | 100 |
| **26. No Constraints (Fixed/Floating) -15% O&M** | W.Lesvos | Fixed/Floated (1000m) | 95-105 (10 MW) | **93.1-94.4** | **2478-2856** | **6.79-6.99** | **4915 - 5297** | **70.2 - 72.9** | 2 | 3 | 96 | 3 | 25 | 135 |
| **27. No Constraints (Fixed/Floating) -15% CAP** | W.Lesvos | Fixed/Floated (1000m) | 95-105 (10 MW) | **90.3-90.8** | **2565 - 2940** | **7.99-8.25** | **5605 - 6398** | **78-81** | 2 | 3 | 96 | 3 | 25 | 135 |
| **28. No Constraints (Fixed/Floating) +15% AEP** | W.Lesvos | Fixed/Floated (1000m) | 95-105 (10 MW) | **86.4 - 87.7** | **2894 - 3056** | **8.18-8.34** | **5605 - 6398** | **78 - 81** | 2 | 3 | 96 | 3 | 25 | 135 |
| **29. No Constraints (Fixed/Floating) ±10% CAP/AEP** | W.Lesvos | Fixed/Floated (1000m) | 95-105 (10 MW) | **94.3 - 105.1** | **2399 - 2689** | **8.88-9.24** | **5169 - 5554** | **78- 81** | 2 | 3 | 96 | 3 | 25 | 135 |

Besides of NPV and LCoE, another valuable economic metric to validate a project's viability is the Internal Rate of Return (IRR). Overall, the IRR is the discount rate that sets the NPV equal to zero and it is generally accepted that the project is feasible when the IRR is greater than a benchmark rate of return (i.e., 10 - 15%). In summary, reviewing the results in Table 6.6.2.1, the economic benefits of the offshore wind projects for most of the scenarios are not promising, at least with the current assumptions made. As a result, the IRR in all cases is below 10%, where in most of the scenarios the IRR ranges between 3% and 7%. When no constraints are considered, and by reducing CAPEX or O&M or alternatively, increasing AEP, the IRR exceeds 8%. Thus, if the IRR is maximized, the financial assumptions required to determine the duration of the project, *N*, have no effect on the ideal project. Adding additional uncertainties to the investment case, such as varying electricity selling price (see Scenarios 3, 11, 15, 21), risk of CAPEX overruns, O&M variations, etc. may have a great impact on the distribution of project IRR.

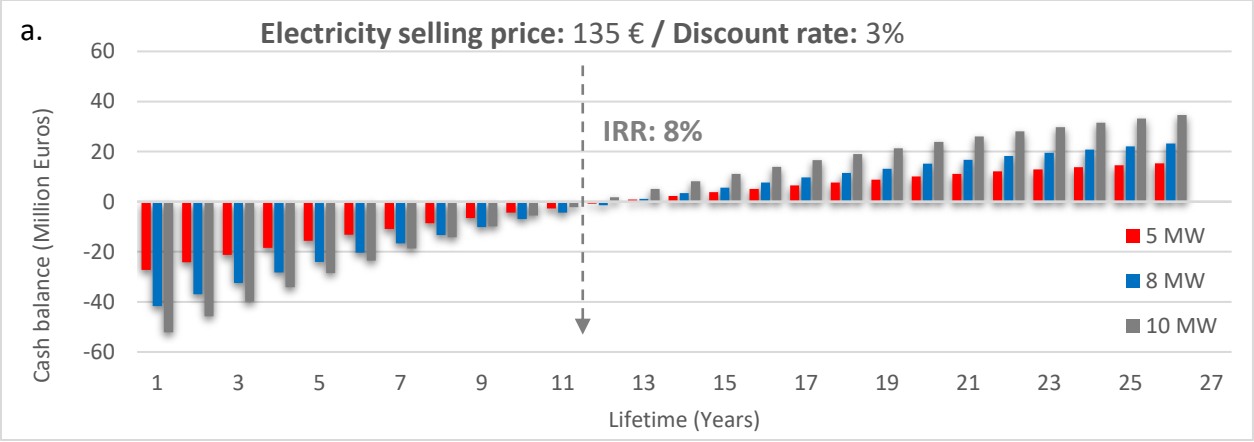


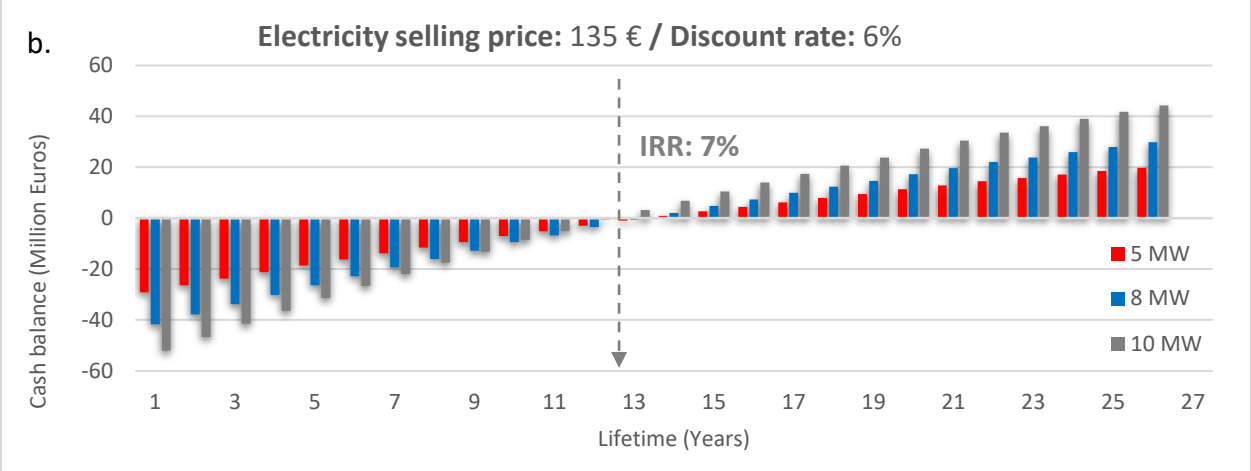

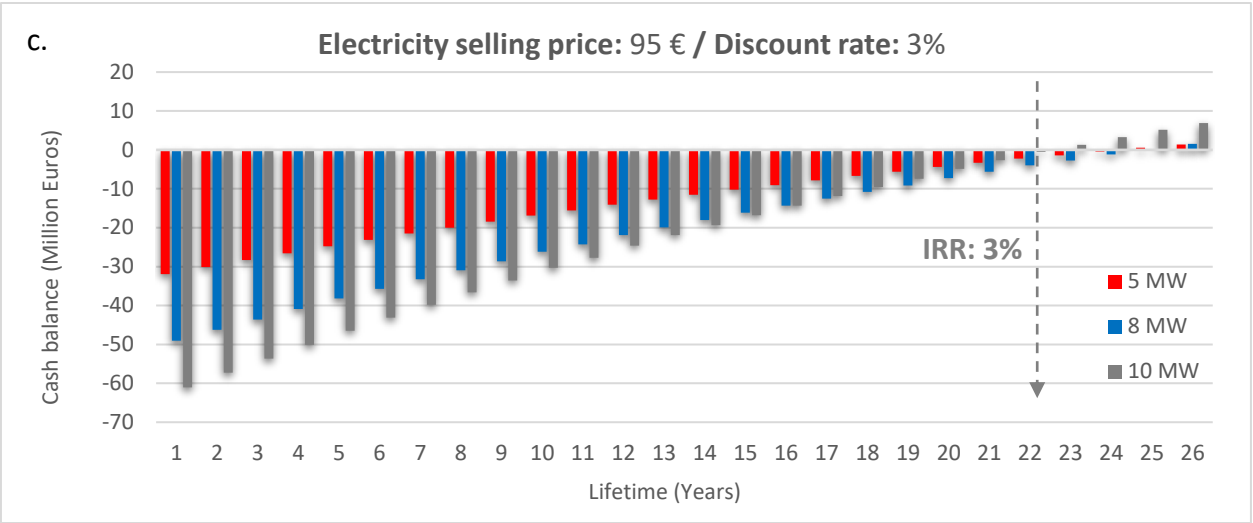


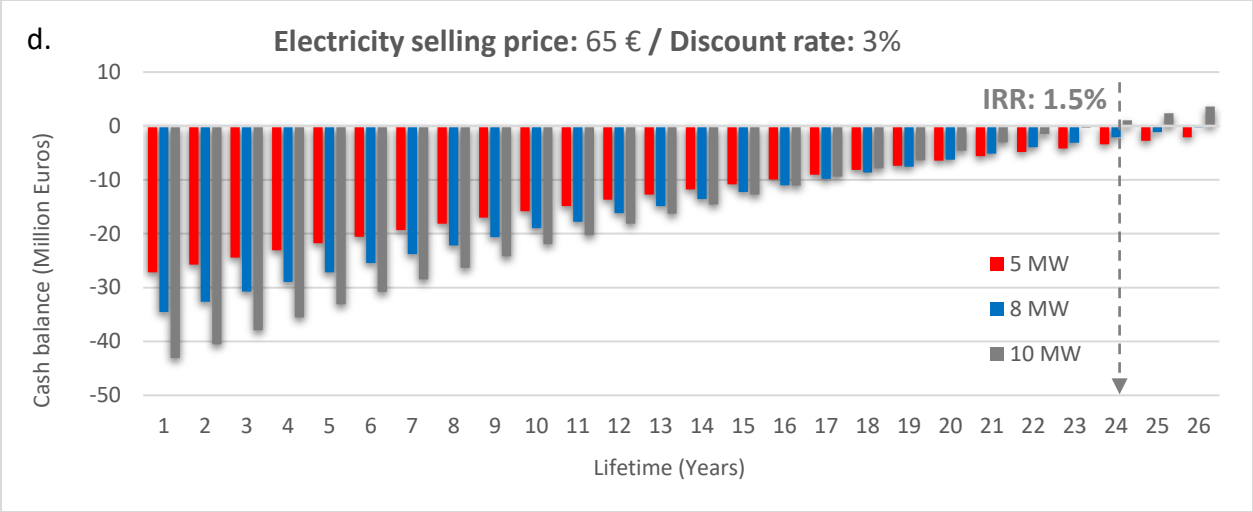


**Figure 6.6.2.2:** Cash balance results of indicative optimal solutions for and Electricity selling price of a) 65€/MWh, b) 95€/MWh, c) 135€/MWh and Discount Factor of 3% (a,c,d) and 6% (b)

Linked to IRR, Figure 6.6.2.2 illustrates the overall cashflows of some indicative optimal scenarios for the offshore wind floating concepts. Results indicate the enormous effect of the electricity selling price, the discount rate, the CAPEX and AEP variations to the resulted IRR and consequently, to the viability and the payback period of an offshore wind project. Thus, for IRR values above 6 - 7%, a payback period of approximately 11 – 12 years occurred for an electricity selling price of 135€/MWh. Potential reduction of CAPEX or in contrast an increase of the long-term AEP may lead to increased IRR values or reductions to the electricity selling prices below 115 €/MWh. On the contrary, when the electricity selling price reduces to 65 €/MWh and 95 €/MWh,

the resulted IRR is barely exceeding 1 - 3% with a payback period of 22 and 25 years (for an OWF lifetime of 25 years). It is also noticed that for the scenario of an electricity selling price of 65 €/MWh, a 10% decrease of CAPEX along with a 10% increase of AEP were considered although, the results were not promising (IRR 1.5% and a payback period of 25 years, Figure 6.6.2.2d). Moreover, a discount rate reduction by 3% (see Figures 6.6.2.2a - b), leads to an increase to the resulted IRR by 1% with a reduction to the payback period of 1-2 years. Finally, for the nearshore areas where fixed-bottom concepts are considered, an IRR of 5-6% occurred with a payback period of 14 - 18 years for an electricity selling price between 100 – 135 €/MWh.

Conclusively, the results are sensitive to the cost assumptions made in the model and presented in detail in Section 5. Cost information is scarce in the offshore wind energy industry and it is also difficult to predict future technological advancements, however, with the proposed model's adjustments numerous scenarios may be tested for either the cost- or the energy-related parameters. For example, there are potential cost reductions to be gained by standardizing foundation types and research efforts on floating turbines could significantly decrease the cost of positioning turbines in deeper waters. Moreover, the fast development of HVDC cables could lead to capital cost reductions and reduction in energy losses over long-distance transmission as also, the increasing turbine size and power rating will further impact the installation cost and the produced energy by an OWF. Based on these statements, new opportunities may arise for the Central and North Aegean area, where many promising areas occurred, however, more detailed techno-economic assessments will reveal the actual (and less uncertain) economic trade-offs for future offshore wind projects.

### 6.6.3 A simplified version of the spatial optimization scheme

Alternatively to the spatial optimization scheme illustrated in Sections 6.6.1 - 6.6.3, a simplified version may be established towards the optimum number of cells required rather than the installed capacity of a potential OWF. Consequently, the user predefines the total number of cells *N* comprising of a potential OWF, without any prior information about technical and economic aspects. Thus, all input data, for instance, cost surfaces, annual energy production or LCoE/NPV, rasters are not formulated inside the optimization process rather than inserted as

fixed input data sources. For the current simplified version, the annual energy production (*AEP*), the wind power variability (*WPV*), the bathymetric profile (*BP*) and the compactness of an optimal cluster (*CI*) are formulating the objectives of the spatial optimization scheme (Eq.6.6.3.1 - 2) subject to the constraints presented via the Eq.6.6.3.3 – 6.6.3.7. The objective function of the model should be modified adding the weight factor of each objective and can be expressed as:

$$Minimize = \sum_{(i,j \in C)} x_{ij}(w_{aep}A_{ij} + w_{wpv}E_{ij} + w_{bp}B_{ij} + w_v V_{ij})] \quad (6.6.3.1)$$

$$V_{ij} = 4 - (x_{i,j-1} + x_{i,j+1} + x_{i-1,j} + x_{i+1,j}) \quad (6.6.3.2)$$

where *C* is the set of all raster cells$_{i,j}$ with total I rows and J columns, $w_v$ is the weight for compactness, $w_{aep}$ and $w_{wpv}$ are the weights for the annual energy production and wind power variability respectively and $w_{bf}$ is the weight for the bathymetric profile raster. For each cell *ij*, $A_{i,j}$ represents the value of AEP, $E_{ij}$ the value of wind power variability, $B_{i,j}$ the bathymetry and $V_{ij}$ represents the total cell edges contribute to the cluster perimeter; $x_{ij}$ is a binary variable (0 or 1) to represent whether the cell *ij* belongs to final cluster or not.

The five constraints for the proposed model ensure that: i) the total number of selected optimal cells, equal to the desired size *N* (Eq.6.6.3.3), ii) none of the optimal cells exist at a pseudo-row or a pseudo-column of the raster (Eq.6.6.3.4 - Eq.6.6.3.7) and iii) the contiguity (referred as Lazy constraint callback via Gurobi optimizer) of the optimal solutions (Eq.6.6.3.8).

$$\sum_{(i,j \in P)} x_{i,j} = N \quad (Eq.6.6.3.3)$$

$$\sum_{j=0}^{J+1} x_{0,j} = 0 \quad (Eq.6.6.3.4)$$

$$\sum_{j=0}^{J+1} x_{I+1,j} = 0 \quad (Eq.6.6.3.5)$$

$$\sum_{i=0}^{I+1} x_{i,0} = 0 \quad (Eq.6.6.3.6)$$

$$\sum_{i=1}^{I+1} x_{i,J+1} = 0 \quad (Eq.6.6.3.7)$$

where *P* is the set of all raster cells$_{i,j}$ including 2 pseudo-rows and 2 pseudo-columns at the start and the end of the raster extent with total I+2 rows and J+2 columns. Finally, the contiguity Lazy constraint (via the BFS algorithm) is expressed as:

$$\sum_{(i,j \in S)} x_{i,j} = N - 1 \qquad \text{(Eq.6.6.3.8)}$$

where $S \dot{\subseteq} C$ is an alternative solution but with non-continuous raster cells. At first, all running tests are analyzed for a specific scenario of 8 and 32 cells and one cluster, for different compactness weights in order to assess the resulted areas shape, optimality scores and running times. Based on the *AEP* and the *WPV* spatial distribution among with the *BP* index, the optimization procedure was set up for three different scenarios for identifying optimal areas for both fixed and floating structures.

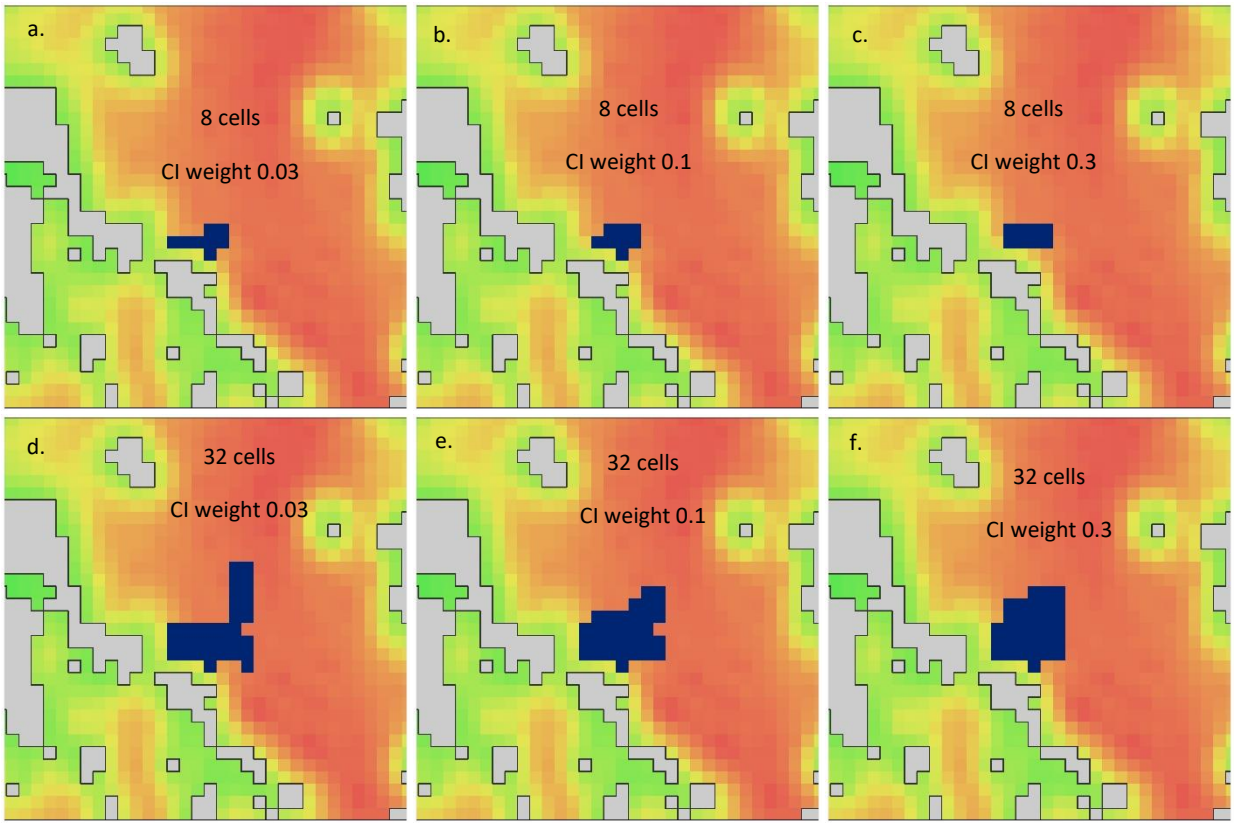


**Figure.6.6.3.1:** Optimal results for an 8 (a-c) and 32 (d-e) cells cluster area with variable compactness weight

Different alternatives are taken into consideration based on the number and the size of clusters for OWF siting. The results are demonstrated in Figures 6.6.3.1 - 2 for number of total cells *N* as 8 and 32 cells for 2, 3 and 5 different clusters. In order to validate the model's capability to allocate continuous and compact patterns upon the inherent weighting factors for the

objectives including compactness, different weights were selected for the objectives. As a result, a weight of 0.4 is selected for *AEP* and 0.2 for *WPV*, bathymetry and compactness respectively. For the first two scenarios, areas with bathymetry below 70 meters and between 70 - 200 meters were selected for bottom-fixed and floating structures. For the last scenario no restrictions were considered.

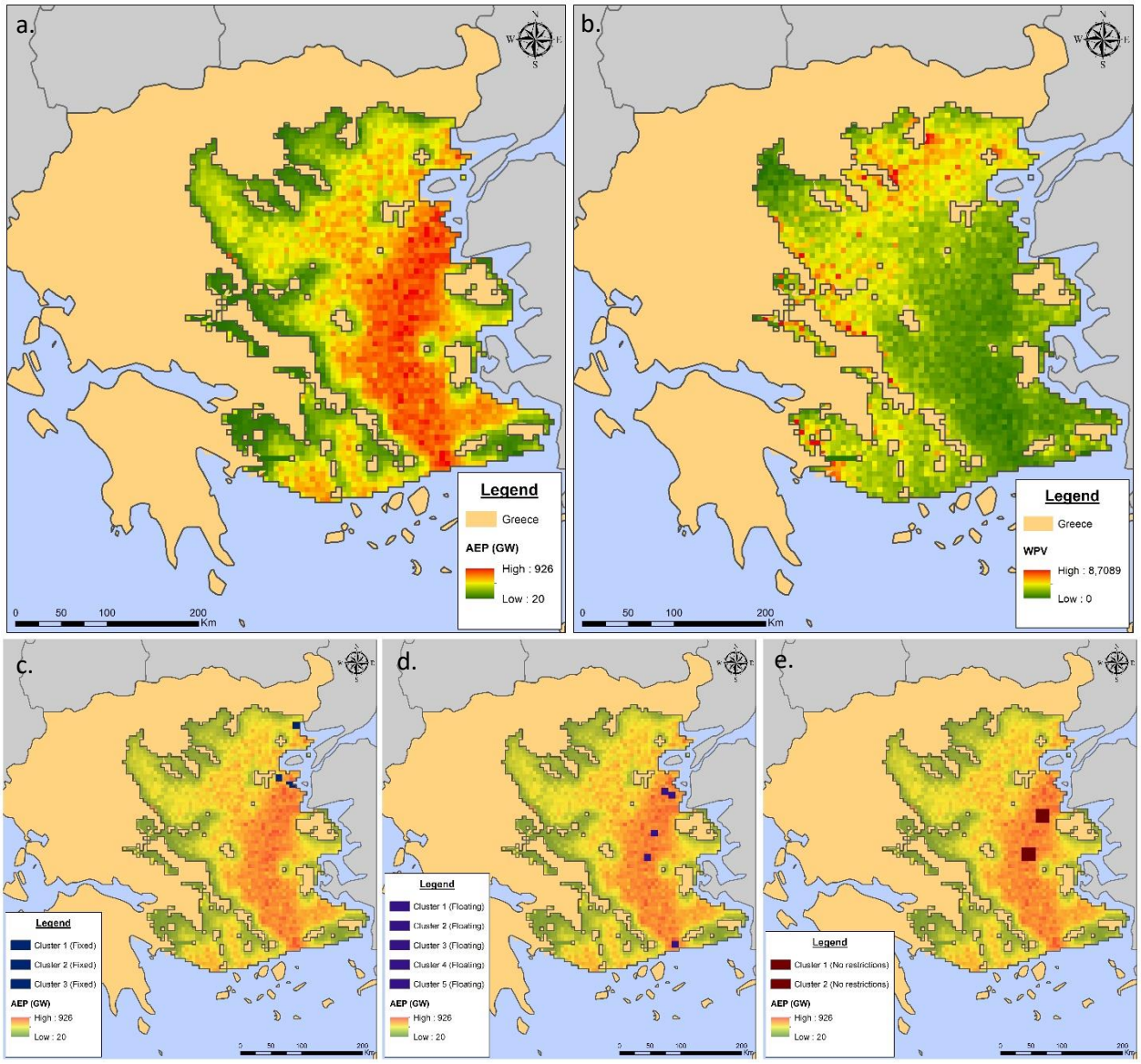


**Figure 6.6.3.2:** Optimal results for an 8 (a-c) and 32 (d-e) cells cluster area with variable compactness weight

Considering the compactness control, results in Figure 6.6.3.1 indicate that for weight values below 0.1, the shape of the optimal areas tends to be irregular. In contrast, for weight values above 0.3, the optimal areas look alike rectangles. While for compactness weight values ranging between 0.1 - 0.3 the optimal areas tend to reduce their irregular shape. In addition to the shape control, when the compactness weight decreases (i.e. < 0.1), the running time increases exponentially. Annual energy production and wind power variability results are demonstrated in Figure 6.6.3.2 along with the optimal areas for different number of cells, clusters and bathymetry values considered. The most promising areas occurred in the Central and Eastern part of the study area consisting of the North Aegean and Cyclades islands. The estimated *AEP* is these areas ranges between approximately 750 - 930 GW annually with the estimated *WPV* approximating values below 1. On the contrary, the less windy areas in terms of the *AEP* are mainly in the North-West Aegean Sea (Thermaikos gulf) and the entire Western part of the coastal Greek territory.

### 6.6.4 Sensitivity of the proposed MIP models (complex and simplified version)

The sensitivity tests were performed to study the model properties through changes in the input variables and raster surfaces (in terms of the cell size) in order to analyse their effect on the model outputs as also on the computational performance of the proposed algorithm. In location-allocation problems, it is extremely important to study the effect of altering various planning requirements and for a spatial optimization integer programming problem, the major types of parameters tuning concerning the sensitivity of the solutions that may be asked consist of:

- The effect of the **cells' quantity** in terms of the size of the study area (i.e., the cells count for the cost surface(s) introduced to the spatial optimization scheme) and the **optimal solutions spatial extent** (either in MW of installed capacity or the exact number of cells returned).
- The effect of the **cell size increase** in the computational performance of the optimization process;
- The effects of the **criteria weighting** towards solutions' optimality and algorithms computational efficiency when considering a non-linear objective function;

- The effect of **changes in the right-hand** side value on certain constraints and the inclusion or not of the Lazy constraints;
- The effect of **changes in the coefficients** of the objective function and the **gap value** or the **time limitation**;
- The effect when the **constraints are reduced** from the original problem (i.e., when asking for the algorithm to return optimal areas in terms of the MWs of installed capacity or in terms of the pixels required in the form of the total pixels count)

To assess the aforementioned parameters, during each of the runs, the following values are recorded:

- **Time LP:** the time it takes to solve the LP relaxation of the problem at node 0 (the root node of the branch-and-bound tree);
- **Objective LP:** the objective function value obtained after solving the LP relaxation of the problem at node 0 (the root node of the branch-and-bound tree);
- **Time IP:** the time (in seconds) it takes to solve the problem to optimality.
- **Objective IP:** the objective function value of the best integer feasible solution obtained during the run;
- **Upper Bound IP:** for cases in which the problem is not solved to optimality in the pre-defined time limit, the best upper bound is obtained during the run.
- **Nodes explored IP:** The total number of branch and cut nodes explored in the most recent optimization.
- **Niter IP:** The total number of simplex iterations performed during the optimization process.
- **Gap limit IP:** The MIP solver will terminate (with an optimal result) when the gap between the lower and upper objective bound is below 0001%.
- **Contiguity control:** Whether the Lazy Constraint for controlling fragmentation issues is enabled and if the final optimal clusters are continuous or not (True/False).

Analyzing the sensitivity factors of a complex spatial optimization scheme, the determination of an optimal solution in the previous sections showed sensitivity through changes

made to the right-hand side value of suitability (screening scenarios), proximity and water depth, wind class limits and the MW of installed capacity required. The effect of these changes does alter some of the selected optimal regions and therefore, the model is sensitive to the changes made on the aforementioned constraint values. In Tables Tables 6.6.4.1 (complex version) and Table 6.6.5.2 (simplified version) all computational results are demonstrated for different optimization settings in terms of the aforementioned parameters. Blue colored rows indicate successful optimization runs and red colored rows highlight the scenarios that did not succeed to guarantee the clusters' contiguity for either the LCoE or NPV cost optimization.

**Table 6.6.4.1:** Optimization results in terms of the solutions' quality and the computational performance for each scenario illustrated in Table 6.6.3.1

| Scenario | LPC/NPV | LPC/NPV | LPC/NPV | LPC/NPV | LPC/NPV | LPC/NPV | LPC/NPV | LPC/NPV | LPC/NPV |
|---|---|---|---|---|---|---|---|---|---|
| | **Values weight** | **Compactness weight** | **Nodes explored** | **Gap** | **Run Time** | **Obj. Value** | **Iterations** | **Optimal capacity** | **Contiguity** |
| | (0-1) | (0-1) | (Count) | (%) | (Seconds) | (Norm.cost) | (Count) | (MW) | (Boolean) |
| 1. Conservative (Fixed/Floating) | 0.8/0.8 | 0.2/0.2 | (98)/(1) | 0/0 | 92/**31** | 399/**12497** | 20799/**13283** | 954/1056 | TRUE/**FALSE** |
| 2. Moderate (Fixed/Floating) | 0.7/0.7 | 0.3/0.3 | (1)/(1) | 0/0 | 54/**52** | 357/**12778** | 438301/**12782** | 954/1056 | TRUE/**FALSE** |
| 3. Optimistic (Fixed/Floating) | 0.7/0.7 | 0.3/0.3 | (1976)/(1) | 0/0 | 401/56 | **336.2/13110** | 702783/16763 | 954/1056 | **TRUE/TRUE** |
| 4. Conservative (Fixed/Floating) | 0.8/0.8 | 0.2/0.2 | (87)/(1) | 0/0 | 50/**40.6** | 465/**11573** | 11120/**8138** | 954/1056 | TRUE/**FALSE** |
| 5. Moderate (Fixed/Floating) | 0.7/0.7 | 0.3/0.3 | (1)/(1) | 0/0 | 29.7/**35.7** | 414/**11720** | 74338/**23364** | 954/1056 | TRUE/**FALSE** |
| 6. Optimistic (Fixed/Floating) | 0.7/0.7 | 0.3/0.3 | (212)/(1) | 0/0 | 27.9/14 | **394/12660** | 580033/7918 | 954/1056 | **TRUE/TRUE** |
| 7. Conservative (Fixed/Floating) | 0.8/0.8 | 0.2/0.2 | (81)/(1) | 0/0 | 61/**25** | 519/**10329** | 18031/**9545** | 954/1056 | TRUE/**FALSE** |
| 8. Moderate (Fixed/Floating) | 0.7/0.7 | 0.3/0.3 | (1)/(1) | 0/0 | 30/**39** | 457/**10433** | 427218/**6883** | 954/1056 | TRUE/**FALSE** |
| 9. Optimistic (Fixed/Floating) | 0.7/0.7 | 0.3/0.3 | (1)/(1) | 0/0 | 362/36 | 438.1/10678 | 585264/5118 | 954/1056 | TRUE/TRUE |
| 10. Conservative (Fixed/Floating) | 0.8/0.8 | 0.2/0.2 | (265)/(1) | 0/0 | 75/**22** | 374/10064 | 22806/4987 | 954/1056 | TRUE/**FALSE** |
| 11. Moderate (Fixed/Floating) | 0.8/0.8 | 0.2/0.2 | (1)/(1) | 0/0 | 119/**19** | 345/10713 | 244058/15792 | 954/1056 | TRUE/**FALSE** |
| 12. Conservative (Nearshore) | 0.8/0.8 | 0.2/0.2 | (3179)/(1) | 0/0 | 556/34 | **312/12113** | 844058/5792 | 954/1056 | **TRUE/TRUE** |
| 13. Moderate(Nearshore) | 0.7/0.7 | 0.3/0.3 | (1)/(1) | 0/0 | 211/**75** | 572/**3989** | 49121/**14567** | 482-528 | TRUE/**FALSE** |
| 14. Optimistic(Nearshore) | 0.8/0.8 | 0.2/0.2 | (1)/(1) | 0/0 | 99/**41** | 557/**4083** | 9593/**4974** | 482-528 | TRUE/**FALSE** |
| 15. Conservative (Mainland) | 0.8/0.8 | 0.2/0.2 | (1341)/(1) | 0/0 | 227/42 | 460/4599 | 625242/6450 | 482-528 | TRUE/TRUE |
| 18. Moderate (Mainland) | 0.7/0.7 | 0.3/0.3 | (1)/(1) | 0/0 | 35/33 | **306/2009** | 4948/236 | 192-204 | **TRUE/TRUE** |
| 17. Optimistic (Mainland) | 0.5/0.5 | 0.5/0.5 | (789)/(64) | 0/0 | 321/84 | **315/2041** | 14789/678 | 192-204 | **TRUE/TRUE** |
| 18. Optimistic (Mainland) | 0.7/0.7 | 0.3/0.3 | (5420)/(1) | 0/0 | 170/57 | 344/5935 | 220777/93497 | 482-528 | TRUE/TRUE |
| 19. Optimistic (Mainland) | 0.6/0.6 | 0.4/0.4 | 1/- | 0/0 | 36/- | 1615/- | 6997/- | 1056/- | TRUE |
| 20. Optimistic (Mainland) | 0.6/0.6 | 0.4/0.4 | 1/- | 0/0 | 36/- | 830.57/- | 1709/- | 528/- | TRUE |
| 21. No Constraints (Nearshore) | 0.6/0.6 | 0.4/0.4 | (1445)/(1) | 0/0 | 59/32 | 558/4763 | 62787/5594 | 482-528 | TRUE/TRUE |
| 22. No Constraints (Nearshore) | 0.5/0.5 | 0.5/0.5 | (519)/(125) | 0/0 | 159/58 | **146/2175** | 92314/8798 | 192-204 | **TRUE/TRUE** |
| 23. No Constraints (Mainland) | 0.6/0.6 | 0.4/0.4 | (1445)/(67) | 0/0 | 89/61 | 299/1939 | 59814/154 | 192-204 | TRUE/TRUE |
| 24. No Constraints (Floating) | 0.7/0.7 | 0.3/0.3 | (793)/(1) | 0.21/0 | 800/800 | 418/12979 | 269549/16676 | 954/1056 | TRUE/TRUE |
| 25. No Constraints (Fixed/Floating) | **0.99/0.99** | **0.01/0.01** | (1456433)/(17456) | 0/0 | 6500/796 | **172/13011** | 824501/223456 | 954/1056 | **TRUE/TRUE** |
| 26. No Constraints (Fixed/Floating) | **0.99/0.99** | **0.01/0.01** | (1)/(1) | 0/0 | **48.72/39.29** | 166.8/13061 | 1199/6690 | 954/1056 | **FALSE/FALSE** |
| 27. No Constraints (Fixed/Floating) | **0.9/0.9** | **0.1/0.1** | (3015)/(1) | 0.33/0 | **800/56** | **252/12982** | 362371/36589 | 954/1056 | **TRUE/TRUE** |
| 28. No Constraints (Fixed/Floating) | **0.7/0.7** | **0.3/0.3** | (745)/(1) | 22.8/0 | **800/79** | **462/12863** | 517749/23290 | 954/1056 | **TRUE/TRUE** |
| 29. No Constraints (Fixed/Floating) | **0.5/0.5** | **0.5/0.5** | (55)/(83) | 38.3/0.36 | **800/800** | 706/12755 | 452997/155891 | 954/1056 | TRUE/TRUE |

Hence, considering the suitability Scenarios (A, B and C) results indicate increased computational effort and running time when the suitable areas increase, for example, in Scenarios B and C. On the contrary, when the suitability space decreases, for example in areas

with positive NPVs or for LCoE with a cut-off value below 200 €/MWh, a low compactness weight (i.e. 0.1 – 0.3) does not guarantee the contiguity of the optimal solutions (see Scenario 1,2,4, 5, 7, 8, 13 and 25-26 in Table 6.6.4.1). Considering the size of the optimal areas to be returned, results indicate a lower computational effort for OWFs of size 1000 MW (Scenarios 1 - 11) compared to the 500 MW and 200 MW (Scenarios 12 - 24). However, these differences cannot be easily quantified, due to the different configurations in terms of the economic indicators (i.e., interest rate, O&M slope, electricity celling price etc.) which have a great impact on the total remaining areas for either the LCoE or the NPV optimization scenario.

In addition, Table 6.6.4.1 presents that the differences in the compactness weight, ranging from 0.01 to 0.5, have a noteworthy impact on the model's computational effort. Differences in the compactness weight led to increased variations at the total objective values (see Scenarios 25 - 29), with values ranging between 166.8 and 706 for the LCoE and 12755 – 13061 for the NPV respectively (these values refer to the weighted objective scores and not the actual LCoE and NPV values). Thus, increased compactness weights reduce the optimality of the areas returned by the model for both LCoE and the NPV objective. On the contrary, the spatial distribution of the optimal areas for different compactness weights does not preserve increased differentiations as long as all optimal solutions are converged, and no dispersion patterns occurred. It is noticed that for a compactness weight below 0.05, all optimal clusters are fragmented (Scenario 26). Finally, for the correlation occurred between the compactness weight and the computational effort needed to obtain optimal solutions, Scenarios 25 – 29 highlight that as the compactness weight increases, the running time of the optimization process reaches the time limit that has been set to 800 seconds.

The subsequent sensitivity analysis was also focused on the reduction in the number of constraints where the number of optimal regions required was not considered in the problem. Consequently, for the simplified version of the spatial optimization schemes, all computational results are illustrated in Table 6.6.4.2. For the simplified version, similar results were observed for small differentiations of the compactness weight for values between 0.01 and 0.7. Similarly to the complex spatial optimization scheme, for compactness weights below 0.01 (for the 8 cells) and 0.05 (for the 32 cells), optimal clusters are fragmented. As a result, each objective was fixed to

0.3, 0.2 and 0.1, and the corresponding compactness weights were set as 0.01, 0.1, 0.4, and 0.7. In these cases, when the Lazy constraint of the contiguity control was enabled, no fragmentation issues occurred (see Scenarios 1, 11 and 17). However, in the aforementioned scenarios, when the Lazy constraints are enabled, the computational effort significantly increases, especially for smaller clusters, where the solution space is vast and each iteration must be validated for the contiguity check.

**Table 6.6.4.2:** Optimization results in terms of the solutions' quality and the computational performance for each scenario illustrated in Table 6.6.3.1

| Scenario | *Cells* | *AEP* | *WPV* | *BP* | *CI* | *Lazy Constraints* | *Nodes explored* | *Gap* | *Run Time* | *Obj. Value* | *Iterations* | *Contiguity* |
|---|---|---|---|---|---|---|---|---|---|---|---|---|
| | (N) | (0-1) | (0-1) | (0-1) | (0-1) | (Count) | (Count) | (%) | (sec.) | (Norm.cost) | (Count) | (Boolean) |
| **1 (Lazy)** | 8 | 0.3 | 0.3 | 0.3 | 0.1 | 149/0 | 1 | 0 | 0.83 | **6.07** | 700 | **TRUE** |
| **2** | 8 | 0.3 | 0.3 | 0.3 | 0.1 | 0 | 1 | 0 | 0.68 | **6.01** | 474 | **TRUE** |
| 3 (Lazy) | 8 | 0.2 | 0.2 | 0.2 | 0.4 | 2889/0 | 995 | 0 | 15 | 8.05 | 106102 | TRUE |
| 4 | 8 | 0.2 | 0.2 | 0.2 | 0.4 | 0 | 1895 | 0 | 21.2 | 8.05 | 130195 | TRUE |
| **5 (Lazy)** | 8 | 0.1 | 0.1 | 0.1 | **0.7** | 41960/0 | 90237 | 0 | 5678 | **10.02** | 17234568 | TRUE |
| **6** | 8 | 0.1 | 0.1 | 0.1 | **0.7** | 0 | 60088 | 0 | 1.218 | **10.02** | 8292664 | TRUE |
| 7 (Lazy) | 8 | 0.5 | 0.3 | 0.15 | 0.05 | 92/0 | 1 | 0 | 0.52 | 6.34 | 203 | TRUE |
| 8 | 8 | 0.5 | 0.3 | 0.15 | 0.05 | 0 | 1 | 0 | 0.46 | 6.34 | 169 | TRUE |
| **9 (Lazy)** | 8 | 0.5 | 0.3 | 0.19 | **0.01** | - | - | - | Time limit | - | - | - |
| **10** | 8 | 0.5 | 0.3 | 0.19 | **0.01** | 0 | 1 | 0 | 0.0007 | 5.61 | 38 | **FALSE** |
| **11 (Lazy)** | 32 | 0.3 | 0.3 | 0.3 | **0.1** | 226936/1057 | 108785 | 0 | 346 | **23.73** | 245565 | **TRUE** |
| **12** | 32 | 0.3 | 0.3 | 0.3 | 0.1 | 0 | 1 | 0 | 0.45 | **23.49** | 257 | **FALSE** |
| **13 (Lazy)** | 32 | 0.2 | 0.2 | 0.2 | **0.4** | 1214/0 | 267 | 0 | 8.75 | **23.25** | 20534 | **TRUE** |
| 14 | 32 | 0.2 | 0.2 | 0.2 | 0.4 | 0 | 664 | 0 | 7.73 | 23.85 | 41189 | TRUE |
| 15 (Lazy) | 32 | 0.1 | 0.1 | 0.1 | 0.7 | 31837/0 | 11971 | 0 | 356 | 23.92 | 1738924 | TRUE |
| 16 | 32 | 0.1 | 0.1 | 0.1 | 0.7 | 0 | 12923 | 0 | 224 | 23.92 | 1389533 | TRUE |
| 17 (Lazy) | 32 | 0.5 | 0.3 | 0.15 | 0.05 | 471234/3871 | 476507 | 0 | 4287 | 25.98 | 2876765 | TRUE |
| **18** | 32 | 0.5 | 0.3 | 0.15 | 0.05 | 0 | 1 | 0 | 0.43 | **25.94** | 272 | **FALSE** |

Considering multi-objectivity, when different weights are assigned to the remaining objectives (i.e. annual energy production, bathymetry or wind power variability), the spatial distribution of the optimal solutions also preserves decreased heterogeneity for the 32 cells and almost no differentiations for the 8 cells. Table 6.6.4.2 shows the feasible weight combinations for the four objectives to generate different optimal patterns for future OWFs. Scenarios 1-6 and 11-16 can be eventually viewed as the optimization schemes that try to equally optimize the *AEP*, *WPD* and *BP,* excluding compactness that always is considered more important. For lower compactness weights (i.e., 0.05 and 0.1) the objective value decreases (considering a

minimization problem) as long as for weights beyond 0.1, increased differences occurred to the solutions' objective values.

Evaluating the spatial optimization schemes (complex and simplified versions), the assurance of spatial contiguity embedded as a constraint factor is what makes the model more difficult to solve using exact methods. However, the increased computational resources and a wider availability of parallelized computing, solvers' improvements, and methods for reducing complexity allow increasingly larger and more complex spatial problems to be solved optimally. Results highlighted that when a time limit is set, the compactness control through the objective function appears as the best option to obtain optimal solutions with the minimum computational effort. On the contrary, when the shape of the optimal clusters is neglected and the optimality of a potential cluster is solely expressed in terms of the cost objective(s), contiguity control, via the Lazy constraint, has to be considered, however, the computational effort and time increase significantly (beyond one hour for the reference area used in these examples). Although during the computational experiments, a short number of problems were stopped after the code executed for 15 minutes, in real applications, most of the solutions are meant to last for a long time, especially when large scale simulations with a minimal spatial resolution have to be considered.

## References


1. **Aksoy H., Toprak Z.F., Aytek A., Ünal N.E., (2004):** Stochastic generation of hourly mean wind speed data, Renewable Energy:29;2111-2131
2. **Almeida P.J.A.L., Vieira M.V., Kajin M., Forero-Medina G., and Cerqueira R., (2010):** Indices of movement behavior: conceptual background, effects of scale and location errors, *Zoologia*: 27(5):674-680
3. **Cavazzi, S. and Dutton, A. G.(2016)**: An Offshore Wind Energy Geographic Information System (OWE-GIS) for assessment of the UK's offshore wind energy potential, Part 1, *Renew. Energy*: 87:212–228
4. **Benhamou S., (2004):** How to reliably estimate the tortuosity of an animal's path: straightness, sinuosity, or fractal dimension?,*Journal of Theoretical Biology*:229;209-220
5. **Bosch J., Staffell I., and Hawkes A.D., (2019):** Global levelised cost of electricity from offshore wind, *Energy*:189

6. **Burnecki K., Misiorek A., Weron R., (2005):** in Statistical Tools for Finance and Insurance (ch.13: Loss Distributions), ed. P. Čižek, W. Härdle, & R. Weron (Berlin: Springer):289
7. **Carapelluci R., Giordano L., (2013):** A methodology for the synthetic generation of hourly wind speed time series based on some known aggregate input data, Applied Energy:101;541-550
8. **Carta J.A., Ramírez P., Velázquez S., (2009):** A review of wind speed probability distributions used in wind energy analysis: Case studies in the Canary Islands, Renewable and Sustainable Energy Reviews;13:933-955
9. **Castellanos F., Ramesar V.I., (2006):** Characterization and Estimation of Wind Energy Resources Using Autoregressive Modelling and Probability Density Functions, Wind Engineering:30(1)
10. **Dicorato M., Forte G., Pisani M., and Ttrovato M., (2011):** Guideliness for assessment of investment cost for offshore wind generation, *Renewable Energy*:36;2043-2051
11. **Dimitriadis P., Koutsoyiannis D., (2018):** Stochastic synthesis approximating any process dependence and distribution, Stochastic Environmental Research and Risk Assessment:32;1493-1515
12. **Dörenkämper M., Olsen B.T., Witha B., Hahmann H., Davis N.N., Barcons J., et al., (2020):** The Making of the New European Wind Atlas, Part 2: Production and Evaluation, Geoscientific Model Development:13;5079-5102
13. **Ephrath J.E., Goudriaan J., Marani A., (1996):** Modelling diurnal patterns of air temperature, radiation wind speed and relative humidity by equations from daily characteristics, Agricultural Systems:51(4);377-393
14. **Fingerish L., Hand M., and Laxson A., (2006):** Wind Turbine Design Cost and Scaling Model. Technical Report NREL/TP-500-40566, National Renewable Energy Laboratory, CO, December 2006.
15. **Giannaros T.M., Melas D., Ziomas I., (2017):** Performance evaluation of the Weather Research and Forecasting (WRF) model for assessing wind resource in Greece, Renewable Energy;102:190-198
16. **Hallgren C., Arnqvist J., Ivanelli S., Körnich H., Vakkari V., Sahlée E., (2020):** Looking for an Offshore Low-Level Jet Champion among Recent Reanalyses: A Tight Race over the Baltic Sea, Energies:13(14);3670
17. **Ioannou A., Angus A., and Brennan F., (2018a):** A lifecycle techno-economic model of offshore wind energy for different entry and exit instances, *Applied Energ*y:221;406-404
18. **Katopodis T., Vlachogiannis D., Politi N., Gounaris N., Karozis S., Sfetsos A., (2019):** Wind resource characteristics and wind energy potential in Greece, Renewable Sustainable Energy:11
19. **Kiss P., Jánosi I.M., (2008):** Comprehensive empirical analysis of ERA-40 surface wind speed distribution over Europe, Energy Conversion and Management;49:2142-2151
20. **Knoop S., Ramakrishnan P., Wijnant I., (2020):** Dutch Offshore Wind Atlas Validation against Meteomast Wind Measurements, Energies:13(24);6558
21. **Koutsoyiannis D., Dimitriadis P., Lombardo F., Stevens S., (2018):** From Fractals to Stochastics: Seeking Theoritical Consistency in Analysis of Geophysical Data, In: Tsonis A. (eds) Advances in Nonlinear Geosciences. Springer, Cham
22. **Koutsoyiannis D., (2020):** Simple stochastic simulation of time irreversible and reversible processes, Hydrological Sciences Journal:65(4);536–551.
23. **Loukatou A., Howell S., Johnson P., Duck P., (2018):** Stochastic wind speed modelling for estimation of expected wind power output, Applied Energy:228;1328-1340

24. **Myhr A., Bjerkseter C., Ågotnes A. and Nygaard T. A., (2014):** Levelised cost of energy for offshore floating wind turbines in a life cycle perspective, *Renewable Energy*:66;714-728.
25. **Nerantzaki S., Papalexiou S.M. (2019):** Tails of Extremes: Advancing a Graphical Method and Harnessing Big Data to Assess Precipitation Extremes, Advances in Water Resources
26. **Olauson J., (2018):** ERA5: The new champion of wind power modelling, Renewable Energy:126;322-331
27. **Pelosi A., Terribile F., D'Urso G., Chirico G.B., (2020):** Comparison of ERA-5 Land and UERRA MESCAN-SURFEX Reanalysis Data with Spatially Interpolated Weather Observations for the Regional Assessment of Reference Evapotranspiration, Water:12(6);1669
28. **Perkin S., Garrett D., and Jensson P., (2015):** Optimal wind turbine selection methodology: A case-study for Búrfell, Iceland, Renewable Energy:75;165-172
29. **Scholz T.S., Lopes V.V., Estanqueiro A., (2014):** A cyclic time-dependent Markov process to model daily patterns in wind turbine power production, Enegy:67;557-568
30. **Shaffiee M., Brennan F., and Espinoza I. A., (2016):** A parametric whole life cost model for offshore wind farms, *Int. J. Life Cycle Assess.*:21;961-975
31. **Soukissian T., Prospathopoulos A., Hatzinaki M., Kabouridou M., (2008):** Assessment of the wind and wave climate of the Hellenic seas using 10-Year hindcast results. Open Ocean Eng. J.;1:1–12
32. **Soukissian T., (2013):** Use of multi-parameter distributions for offshore wind speed modelling: The Johnson $S_B$ distribution, Applied Energy;111:982-1000
33. **Soukissian T., Papadopoulos A., Skrimizeas P., Karathanasi F., Axaopoulos P., Avgoustoglou E., et al., (2017):** Assessment of offshore wind power potential in the Aegean and Ionian Seas on high-resolution hindcast model results, AIMS Energy:5(2);268-289
34. **Suomalainen K., Silva C.A., Ferrão P., Connors S., (2012):** Synthetic wind speed scenarios including diurnal effects: Implifications for wind power dimensioning, Energy:37;41-50
35. **Wang Y., (2016):** Prediction of short-term distributions of load extremes of offshore wind turbines. *China Ocean Eng*;30:851–866
36. **Zárate-Miñano R., Anghel M., Milano F., (2013):** Continuous wind speed models based on stochastic differential equations, Applied Energy:104;42-49
37. **Zhou C., Ieritano C., Hopkins W.S., (2019):** Augmenting Basin-Hopping with Techniques from Unsupervised Machine Learning: Applications in Spectroscopy and Ion Mobility, Front. Chem.;7(7):519

# 7. Conclusions and future research

This thesis has presented for the first time an integrated geospatially-explicit methodology for future offshore wind farm site-prospecting. The overarching objective was to develop a framework formulated as a Spatial Decision Support System (SDSS) (**SpOWNED-Opt**) that handles the complex spatial relationships between multiple objectives for offshore wind farms site-selection in a tractable way. The proposed SDSS can simulate major spatial, technical and economic aspects of an offshore wind farm and can be used in preliminary studies for the development and consenting stage. The analytical steps demonstrated in Section 5 and all processes depicted on Figure 5.1 offer enough flexibility to include different spatial, technical and economic configurations. Furthermore, **SpOWNED-Opt** can support the decision-makers allowing them to analyze from various viewpoints different energy planning scenarios as also to localize where is better to address the energy measures. Thus, **SpOWNED-Opt** provides a useable and useful means to model, estimate and assess the local, regional and national trade-offs for future offshore wind energy deployment.

Considering some technical aspects, invisible links to different optimization models and access to the results of complex cost functions are provided in order to quantify and assess controversial techno-economic, environmental and social objectives. Thus, the sub-modular design adopted (discretization of the site-prospecting stages) serves as an interactive development process, necessary to the successful design of an integrated SDSS, based on a system that can be easily modified to meet the current and projected needs of offshore wind energy market.

Overall, the proposed effort is currently under way on extending the choice of tools offered towards the presentation of errors and uncertainty estimates. In addition, further visualization tools and mapping representation options may be incorporated inside the GUI. Nevertheless, the **SpOWNED-Opt** structure consists of a valuable tool to foster extended discussions with researchers, experts and stakeholders to design similar tools facilitating the planning and decision processes for different classes of location-allocation problems and particularly, in the offshore wind energy sector.

In the following chapters, the conclusions for the research questions posed in the Introduction Section (Section 1.3) will be discussed along with further recommendations for

future research. Thus, the main key findings and the general conclusions focus on answering the following questions (***RQ.1 – RQ.6***):

- ***RQ.1:*** *In recent literature research if there are any existing integrated spatial modelling schemes to support OWE deployment beyond simple multi-criteria assessments?*
- ***RQ.2:*** *How to create a holistic and user-friendly Spatial Decision Support System (SDSS), based-on interconnected GIS tools and algorithms for less uncertain site-prospecting campaigns?*
- ***RQ.3:*** *How GIS structures and models can be a powerful tool to monitor, handle and assess complex spatial relationships towards OWF site-prospecting, as a multi-objective problem, using spatial modelling techniques that can be easily customized for any specific region worldwide?*
- ***RQ.4:*** *What kind of spatial optimization models and stochastic simulation schemes must be established in order to gain vital cost and energy related information leading to less uncertain results, even in the pre-planning and consenting stages?*
- ***RQ.5:*** *Which are the technical and economic characteristics of future OWFs and in an environmental and socio-economic scale of development, if energy-related investments can be sustainable and profitable for Greece?*

## 7.1 Overall SDSS considerations

Answering ***RQ.1*** and ***RQ.2***, the concept of the SDSS focused on developing a system that is capable of addressing the commonly faced spatial decision problems. These problems were categorized as: i) site selection and screening analysis, ii) site assessment in terms of a life-cycle techno-economic analysis, iii) offshore wind resource assessment and stochastic simulation of the long-term wind speeds and energy output, iv) multi-criteria spatial optimization site-prospecting and finally, v) spatial knowledge discovery in terms of the inherent uncertainties' quantification and the sensitivity analysis.

In order to demonstrate relative spatial cost differences, the SDSS provides general cost results on the basis of a bottom-up cost model that can be altered by the user. Although the testing of the model to date has been somewhat limited due to computational limitations on a desktop PC of average performance, it seems that a "comprehensive" site-prospecting methodology of the type described in this thesis is feasible. However, as with the output of any complex model, a useful sensitivity analysis is highly dependent on the modelling assumptions and the associated quality of the initial data. There may be proprietary more sophisticated methodologies of this type already in existence specifically-tailored to particular tasks or modules, however, they are not publicly available or lack of spatial or spatio-temporal perspectives at a regional or national level of development. In this sense, the development of an open-source methodology for offshore wind energy deployment at greater scales might prove useful to potential investors, regulators, and other parties at the pre-development and consenting stages. While many computational details of the described conceptual framework, continued development of **SpOWNED-Opt** as an "open source" model would ideally include publicly available standalone sub-modules.

Building on the survey of spatial modelling and spatial optimization problem-solving and described in Section 3, it reveals the main implementation routes available for their development. The conclusions that are drawn from the results described in the previous Sections indicate that:

- The integration of GIS structures with spatial analysis techniques and spatial models is a key issue in the implementation of an integrated and holistic SDSS;
- Plug-in technologies are some important means of introducing extensibility into the SDSS. This is particularly relevant for models, where plugins allow different spatial models to be made available within the system, to be extended and customized based on the trends occurred in terms of the economies of scales, the level of development and planning as long as in terms of the future projections of OWFs characteristics and configurations;
- One of the major challenges was the development of efficient computational procedures for tackling multi-scale spatio-temporal multicriteria problems considering the Least Cost Path optimization modules and the MINLP site-prospecting framework. However,

complex spatial problems are characterized by high computational demands and this is highlighted, mostly for the graph-based problems where the computational time increases non-linearly proportional to the graph size;

- A comprehensive approach to dealing with parameter uncertainties involves an in-depth uncertainty and sensitivity analysis. These issues were tackled in terms of the spatial resolution, the life-cycle techno-economic configurations and the annual energy production stochastic simulation. Results underlined the great impact of the initial wind speed data quality, the spatial resolution of the input data and the probabilistic model to be selected to efficiently simulate annual or long-term energy production;
- The effectiveness of communicating model output uncertainty, both numerically and visually is of paramount importance in order to give visualized semantic schemes to the users and the stakeholders overall, for the entire decision-making and planning processes.

Considering future research, the most immediate extension to this work would be to refine and further develop the **SpOWNED-Opt** system. As a research prototype, the proposed SDSS could be refined further through the introduction of more robust models considering the structural design of the offshore wind turbines and foundations, analytical models for the balance of plant cost estimation and more sophisticated tools to calculate installation and decommissioning costs using stochastic simulation approaches considering the uncertainty quantification due to the met-ocean conditions. In addition, richer display tools may be re-designed in order to improve the visual inspection of the results by the user and to provide data handling support for reducing computational performance. Most of these refinements could be made incrementally, owing to the object-oriented design of the system.

### 7.2 Constraints mapping and screening analysis

Regarding ***RQ.5***, employing methods for screening all unsuitable locations or reducing conflicts between different users sharing the same space has traditionally been one of the original areas for which GIS have been developed. In this research, the framework for assessing space availability has been enriched by embracing both qualitative perspectives as well as quantitative

data. The spatial factors examined refer to the site obstructions that restrict the available area for OWE deployment. Results from the screening assessment highlight that:

- Examining the water depth of the study area, it was observed that it increases sharply by limiting the areas with shallow waters and remarkable wind power potential. However, suitable areas of water depths below 70 meters occurred in the broader area of Eastern Lemnos island, in Alexandroupoli, in the Western part of Thassos island and in the Eastern offshore areas of Central Evoia;
- The installation of offshore wind farms in deeper waters was inevitable in accordance to the remaining suitable areas for all of the screening scenarios (conservative, moderate and optimistic). As a result, the installation of an offshore wind farm, in most cases, occurred in water depths beyond 100 m, which is associated with some advantageous and disadvantageous technical and economic issues described in the previous Section;
- Although the average water depth where most European offshore wind farms are installed is approximately between 15 - 30 m at a mean distance of 10 - 20 km from the shore, this cannot be the only case for the Aegean Sea because such depths were found in most cases at a maximum of 10 km from the shore and still very close to potential conflicting onshore and marine uses;
- The results were also highlighted that for the screening scenarios, more detailed input data have to be incorporated in terms of the exact fishing activities distribution as also for potential future marine activities planning (i.e. future cables and pipelines corridors). It is clear, however, that the realization of offshore wind energy projects in Greece requires at an administration level the existence of a concise legal framework related to the marine spatial planning regulations;
- Finally, an integrated screening analysis is vital to further reduce the computational effort needed for the remaining spatial optimization algorithms. As already highlighted in the results Section, a substantial decrease of the suitable areas for potential OWFs is the key to reduce the execution times of both the LCP algorithms (where entire offshore areas may be

eliminated) and the MINLP optimization scheme where the remaining pixels and possible optimal solutions lead to extracting optimal areas in the range of few hours.

Unquestionably, the alternative current and future projections of the marine activities in the Central and North Aegean Sea, as well as the possible challenges and opportunities, can enforce the decision-making process. The anticipated opportunities and threats can foster the informed strategic deployment of potential offshore wind farms, taking advantage of the cost-effective suitable locations while also balancing the interests and impacts on the marine environment. In this sense, as already highlighted in Section 2, previous omissions on planning and licensing procedures may be avoided. Moreover, stakeholders often wish to investigate the choices available if the criteria are different or if a new criterion is introduced. Furthermore, these processes must be repeated whenever the legal framework is modified or potential changes occur in terms of the materials prices evolution or the strategies to be followed during an OWF development. To overcome these obstacles, the developed approach was designed to be robust and to provide its users with the capability to insert, modify or remove the existing criteria and data without possessing any programming knowledge. As result it can be used in many different scales and study areas worldwide. This ensures the system's long-term adaptability and usability; however numerous future adaptations and improvements are needed. Further adjustments and improvements of the suitability assessment campaigns may incorporate:

- More dynamic marine spatial planning tools for assessing the spatio-temporal cumulative human activities' distribution and impact to the marine environment;
- More accurate inputs in order to further reduce uncertainties during the planning and licensing procedures;
- The integration of more transparent support schemes in order to enhance participatory processes, combining in parallel, general public's needs and preferences with the views of stakeholders.

### 7.3 Cost assessment algorithms and spatially-explicit models

In order to address ***RQ.4,*** and ***RQ.5***, the cost-related analytical expressions developed in this work are expected to assist investors, researchers, and other stakeholders to derive initial estimates for future offshore wind farm projects and trends. The development of a realistic and accurate method for life cycle cost analysis for large-scale offshore wind farms is a very complex and highly uncertain task. Nevertheless, the proposed model is based on a combined multivariate regression approach where the cost data of completed and ongoing projects provided the baseline for estimating the costs of future projects.

A cost breakdown structure was presented to identify various cost components involved in five phases of offshore wind projects, namely development and consenting (D&C), production and acquisition (P&A), installation and commissioning (I&C), operation and maintenance (O&M) and decommissioning and disposal (D&D). Multiple spatially-explicit cost models were built for each unit cost, and several mathematical tools were used to evaluate all costs incurred during the lifecycle of potential offshore wind farms in the Central and North Aegean Sea. Results indicated that the capital cost of offshore wind turbines and support structures as well as the costs associated with electrical infrastructures configurations (export cables and offshore substations) account for the largest portion of overall cost, followed by the O&M and the installation and decommissioning costs. Moreover, the installed capacity of an offshore wind farm, the wind turbines' size, the interest rate, the overall losses and the electricity celling price were identified as parameters with significant influence on LCoE and NPV.

Focusing on the non-spatial technical and economic characteristics, since the total lifetime of an offshore wind farm is relatively long (beyond 20 or even 25 years in the near future), a small change in interest rate leads to a large variation in the project's total cost. The sensitivity analysis highlighted which variables have the biggest impact on the modelled LCoE, NPV, IRR and the payback period. Altering the annual energy production, CAPEX and interest rate all had a significant impact on the final estimates, and therefore improvements on the input data should be a priority. O&M reductions had the least influence on both of the LCoE and NPV, mostly because of the ports spatial distribution assumptions made for the O&M cost estimates. Even

though, additional cost reduction studies may show that significant opportunities are available to reduce O&M, considering all maintenance facilities and infrastructures placed near to the potential OWFs on remote islets and small island of the Central Aegean Sea that are not characterized as marine protected or NATURA areas.

Considering the distance-based algorithms, the complex spatial relationships and interactions including multiple objectives for OWF transmission, installation and O&M cost evaluation and assessment were presented in a tractable way. For OWE assessment practices, the proposed framework can be selected as the starting point for advanced negotiation processes among different agents and stakeholders (local authorities, engineers' groups, system operators and industries). Furthermore, the methodology can be easily utilized in other regions by applying the three steps that were demonstrated in Section 5 based on the GIS structures and the angle-weighted LCP algorithms. Although the proposed methodology has been developed to evaluate and delineate transmission lines or potential least cost shipping routes, it can be easily extended to other path routing problems with smoothing adaptations such as road construction, pipeline routing etc.

Overall, the added value and the contribution of the proposed LCP algorithms lies on: a) the implementation of the dual graph representation for angles control and straightness penalization, b) the straightness assessment based on the customized sinuosity index to validate results upon paths' optimality and c) the smoothing techniques and obstacles avoidance performance for more accurate cost calculations and paths' delineation, considering homogenous and non-homogenous cost surfaces. On the basis of the test results, the algorithm is robust and practical. In most of the current commercial GIS software products, multi-objective problems for constrained and penalized optimum least-cost paths along with the curvature optimization is not always considered. Thus, the proposed algorithm can be applied in these software products as a standalone toolbox to improve preliminary studies for line routing and distance-based cost evaluation. Further development and improvement could incorporate:

- The integration of additional physical parameters, such as geological conditions, faults and stochastic parameters (e.g., meteorological conditions) that are always crucial for this type of spatio-temporal problems;
- Other pathfinding strategies and algorithms may be applied, like A* or hierarchical approaches as long as, dynamic programming implementations in order to further validate the algorithm's computational performance.
- The inclusion of the sinuosity index in the optimization process for further controlling the paths' straightness or even the distortion and elongation errors of the optimal paths, as applied in previous research studies, is under consideration.

As a concluding remark, and emphasizing on the distance-based costs modelling, the mapping of optimal line corridors is a useful tool to assess the costs of alternative routing paths and outline alternative strategies and scenarios for a future investment. The methods developed in this thesis may not always be ideally suited to the geographical extent but may represent an integrated multi-disciplinary attempt to bring some of the knowledge existing in other fields to the domain of geography, spatial optimization and GIS, extending spatial modelling to a wider variety of purposes.

### 7.4 Offshore wind resource assessment and wind process stochastic simulation

This part of the research (related to ***RQ.1*** and ***RQ.4***) constituted of an integrated step by step framework for the statistical and probabilistic assessment towards the stochastic generation of wind time series. Thus, long-length wind speed time series from coastal stations and offshore buoys among with the UERRA (MESCAN-SURFEX) ensembles were extracted and analyzed based on the optimal distribution selection, the marginal statistical characteristics, the second order dependence structure and the statistical similarities between the observational and reanalysis data.

In terms of the probabilistic assessment, the Burr (Type III), Burr (Type XII or PBF), and the Generalized Gamma distribution offer significantly better fits than Weibull, however, the tight differences are highlighted. Using numerous long-term observational and reanalysis wind time

series spread over a wide geographic region, the superior fit of the Generalized Gamma to the data is remarkable irrespectively of the parameters' estimation method used. However, for wind samples with heavy shaped tails in terms of the extremes, the Burr XII (PBF) exhibited a better fitting performance, mainly for the in situ data.

Considering the reanalysis performance, results revealed a fair performance of the UERRA ensembles. The examined statistical tests were found to lie within acceptable ranges in 4 stations and 2 buoys, however, the poor performance of the results, concerning bias and root mean square errors is highlighted. In contrast, monthly and seasonal statistical characteristics as well as the long-term persistence examination indicated a satisfying agreement, although the center of gravities (mean values) indicates a clear displacement between the measured and modelled wind speeds. Considering these results, further bias correction and calibration methods should be applied to the reanalysis data in order to reduce uncertainty of the estimates. An option could be to standardize or homogenize reanalysis wind speed time series since skewness and kurtosis coefficient conserved a good agreement. Thus, UERRA (MESCAN-SURFEX) data can significantly contribute to wind speed modelling and wind power generation assessment campaigns at a regional level only if the increased horizontal resolution is a pre-requisite.

Analyzing the stochastic wind simulation outputs, results suggest that if extended periods of either reanalysis or observational data are available, the proposed simulation scheme could provide very good short-period or even multidecadal historical wind time series by preserving the intermittent characteristics. The simplicity of the proposed model and the inclusion of a reduced number of parameters to capture the diurnal and seasonal periodic cycles is underlined. The results for the seasonal characteristics and the second order dependence structure were exceptional, indicating the robustness of the presented simulation scheme in Monte-Carlo experiments for sensitivity analyses, derivation of confidence intervals, uncertainty quantification etc.

Overall, the aforementioned outcomes can be further examined and validated to other wind speed regimes concerning the accuracy of the reanalysis data, the suggested probabilistic models as well as the stochastic wind explicit-implicit generation scheme. Suggestions for future research may encompass:

- The inclusion and testing of additional multi-parameter probabilistic models;
- Further customizations for a joint wind speed and wind power time series characterization and simulation;
- Expansion of the proposed framework to a two-dimensional (spatial-temporal) stochastic simulation framework, and finally,
- An extension of the proposed model for short-term prediction and forecasting campaigns including hourly and sub-hourly temporal resolutions.

### 7.5 Multiple objectives spatial optimization algorithm

For the final spatial optimization scheme, and reviewing ***RQ.1, RQ.2*** and ***RQ.3***, there are some assumptions, requirements, and limitations related to the proposed approach. The model was built on the assumption that cost objectives are higher in weight than those assigned to the compactness criterion for the sites to be exploited. However, the model applied is capable of dealing with the conflicting criteria that govern the legislative criteria and MSP regulations for OWFs site-prospecting in a rigorous manner as it can easily handle NoData values cells, fragmented areas and returns optimal compact sites for OWFs development.

One of the main advantages of this approach is that it produces solutions that precisely reflect the default preferences of the user in terms of the results' optimality. Furthermore, it relies on a rigorous and systematic mathematical approach that avoids falling in sub-optimal solutions, leading to optimal contiguous and compact sites in a promising amount of time considering the size of the study area (extent) and the spatial resolution (cell size). In this manner, stakeholders and decision makers may use the proposed spatial optimization scheme as a basis for investment decision-making including several critical variables in the costing of offshore wind projects. In addition, the tool allows testing policy or investment priorities with different future scenarios.

On the contrary, some limitations already highlighted in the previous section are mainly focusing on the model's constraints set-up. The model is sensitive to the OWFs' capacity in terms of the megawatts required for each offshore site, thus, the lower and upper bounds of the required megawatts to be installed must be taken under consideration during the modelling set-up in order

to be able to find optimal areas. For example, when a 500 MW offshore wind farm is set by the user, the algorithm "searches" for optimal combinations, in terms of the LCoE or the NPVs, by forcing the sum of the wind turbines installed per wind turbine type and count in each cell to sum up 500 MW. It is noticed that the sum of the MWs installed per cell is not always an integer number and the sum of the pixels acquired is not guaranteed that always leads to precisely 500 MW. Thus, a lower and upper bound is used in the optimization scheme (i.e., search for optimal solutions in the range between 480 MW and 520 MW). Thus, the wind turbines' capacity that is pre-defined (e.g., 3,5,10 MWs) and the combinations occurred based on the wind class characteristics may lead to solutions outside the pre-defined bounds.

Moreover, when the compactness weight reduces to zero, to guarantee contiguity, the BFS Lazy Constraint is enabled and as a result, the pool of optimal solutions increases drastically among with the computational effort for the algorithm to find optimal solutions. With the current algorithm's configurations, most of the times, contiguity is guaranteed via the objective function for compactness weights greater than 0.05. However, when the solution space increases (i.e., no constraints are considered in terms of the areas excluded or negative NPVs are discarded), the compactness weight must be greater than 0.05 for guaranteeing continuous solutions. Regarding the "simplified" version of the spatial optimization scheme (see Section 6.6.5), when the optimal areas to be extracted are set in terms of the cells acquired and not by the MWs of installed capacity, the complexity of the optimization problem is reduced and the computational effort decreases. Particularly, the number of the constraints equations is reduced (no capacity constraints), however, when the number of the total objectives increases (3 objectives or more) caution must be taken when considering each objective's weight.

Overall, the inherent complexity of spatial and geographical problems poses great challenges to solving demanding spatial optimization problems. Research upon spatial optimization problems will likely remain an important and active area as long as there is an increasing exigency to develop techniques for solving this type of problems efficiently and effectively in terms of the solutions quality and the computational performance. This is driven by growing needs to better reflect real-world problems, to further reduce uncertainties but also the recognition that even small economic efficiencies, especially in the field of RES planning, can

result in million euros in savings for private and public companies, municipalities, and governments. However, huge investment planning efforts and increased technical prerequisites lead to spatial problems that are more difficult to be solved because of larger planning applications and greater spatial detail. It is clear, then, that spatial problem-solving will continue to challenge spatial optimization applications, as new models are defined, existing models are enhanced, and more challenging spatial optimization schemes are encountered. In addition, the proposed method may consist of the basis to produce benchmark solutions and to compare such solutions with efficient heuristic methods for location-allocation problems. Such a comparison may help to decide whether a heuristic is a justifiable choice.

Considering the multi-objectivity of such problems, the model presents to designers all inherent trade-offs upon different objectives, such as AEP and capital and operational expenditures. With this extra “degree of freedom”, designers may have a clearer understanding of the possibilities and the associated trade-offs and they can be better equipped to identify optimal offshore areas for RES deployment that meet their desires. Hence, further research can identify techniques to:

- Reduce the complexity and the number of constraints to guarantee spatial compactness and contiguity in spatial MILP and/or MINLP models. In general, examination of the spatial distribution of the input data could be used as a guide to reduce the problem size;
- Additionally, heuristics can be applied and compared to the exact methods proposed in this thesis in order to minimize the number of variables and constraints required to represent a MINLP model;
- Finally, considering compactness and the shape of the spatial clusters, additional constraints may be integrated in order to control the shape of the optimal areas returned, for example, single line continuous areas, rectangular or ever more complex shapes (i.e., hexagonal, cyclic etc.).

### 7.6 SDSS Graphical User Interface effectiveness and robustness

**SpOWNED-Opt**, through its graphical user interface, provided a framework that allows researchers to develop robust and sustainable tools and to accelerate software development timeframes in the field of spatial modelling and overall, Geosciences. To this extent, and answering ***RQ.1*** and ***RQ.2***, the requirements of scientific application development such as sophisticated models' integration, visualization tools, testing and validating results and easily applying sensitivity analysis campaigns, are all provided and tested in this Thesis. Nevertheless, researchers and developers can easily climax new capabilities or expose existing libraries through Python via inbuilt libraries, or "callout" to other software packages with simplified customizations. Considering that **SpOWNED-Opt** is built upon Qt and makes use of Qt Designer and PyQt5, outsourcing modelling schemes can be easily connected and integrated to the **SpOWNED-Opt** workflows. This is particularly useful in collaborative development between different disciplines or teams and as already stated, the enclosure of more sophisticated and robust modules may be an option.

With regards to the issue of data management, the approach followed in the current SDSS allows the processing of large amounts of data, supports complex processes such analysis and visualization at different scales and also provides analysis adapted to the requirements of the examined problem. Its functions are based on the advantages provided by managing complex relationships, parameters and restrictions via a powerful and simultaneously friendly GUI for either experienced or non-experienced users. The designed approach also facilitates data connection from different sources, produces results compatible to other systems and GIS platforms and identifies the data needed to solve the site-prospecting problems. Keeping this in mind, limitations of this work can be identified in the context that is specifically tailored to OWFs site-prospecting campaigns. Nevertheless, the major limitations of this approach are noticed in terms of the data acquisition and storage to a structured database. For these reasons, several **SpOWNED-Opt** use cases for enhancing, supporting and commercializing spatial optimization modelling are reported. These include:

- Simple workflows for the full automation of operations typically performed by a user interacting with one or more pieces of software, such as pre- or post-processing operations;
- Customized visualization of large complex data stored, for example in NetCDF files or during the wind process stochastic simulation and energy output estimation;
- Simple distributable software products, which can be provided to users, collaborators or "customers". These would usually have a customized graphical user interface and components for input, computation and then visualization;
- Multi-disciplinary research and development, which involves multiple different teams with different skill bases, software development capabilities and background modelling and analysis technologies.

Using an advanced software platform technology like **SpOWNED-Opt**, allows scientists to easily exploit opportunities in both spatial- and energy-related domains. The system has demonstrated an attractive compromise to fostering the inclusion of spatio - temporal considerations within decision-making processes.

## 7.7 Concluding remarks

Offshore wind energy is one of the most important and most promising renewable energy sources in Greece. However, offshore wind farms have also controversial effects on human activities and the environment, thus, triggers public concerns. These concerns are not adequately represented in current state-of-the-art siting procedures of offshore wind farms in a holistic manner. Therefore, the aim of this thesis was to further extend and improve current site-prospecting decision-making tools and in summary, a systematic modelling scheme in the form of a SDSS, is now in place for OWFs site-prospecting campaigns.

Focusing on the spatio-temporal decision-making part of this research, high-performance computing and big data analysis will potentially allow not only to improve the models and validate them, but also to create models of this level of detail for entire regions and countries. The better the models are, the more accurate strategic pathways in integrated spatial- and energy- planning can be supported by the investors, planners, researchers and the general public as Camargo and

Stoeglehner (2018) pinpointed a few years ago. The literature review in Sections 2 and 3 demonstrated the need to develop such models, specifically for the offshore wind sector that are able to better represent the uncertainties of the unit energy costs by identifying efficiencies and technical improvements, whilst still considering and optimizing socio-economic and environmental concerns. Moreover, and according to Mytilinou and Kolios (2017), the impact of Net Present Value and Levelized Production Cost on the economic objectives has not been fully considered and will be further investigated in the future, especially when considering spatially-explicit suitability campaigns and viability measures for future offshore wind farms. Thus, the revealed outcomes may have an important impact in the future of RES deployment in countries with substantial offshore wind resources and will help decision-makers for their next cost-efficient investments.

Focusing on the "spatial aspects" of the proposed SDSS, spatial optimization problems can be characterized by the type of information represented by the solution. Some problems seek optimal locations for lines (e.g., transmission corridors), and some for areas or zones (in this case, optimal allocation of continuous and compact marine areas). As Malczewski and Jankowski (2020) have underlined, the use of integrated spatial optimization schemes in terms of the solutions' optimality, quality and uncertainty as also, in terms of the models' sensitivity is still an exception rather than the rule. The effectiveness of communicating model outputs uncertainty, both numerically and visually, is of paramount importance especially in spatial decision-making problems, where model results fail to disclose full information.

In this context, the models used in this thesis aimed to visualize information uncertainty and systematically evaluate the effectiveness of the proposed solutions by communicating the results of spatially-explicit uncertainty. Overall, computational systems such as GIS impose a systematic framework of data models and replicable processing, allowing data and results to be shared and discussed rigorously and objectively. Improved methods and techniques as the one proposed in this thesis can certainly help, as can ever-greater processing power. Yet, the experience of the last 20 years suggests that there are rather few purely technical solutions to substantial real-world problems.

## References


1. **Camargo L.R. and Stoeglehner G., (2018):** Spatiotemporal modelling for integrated spatial and energy planning, Energy, Sustainability and Society:8(32)
2. **Goodchild M.F. and Longley P.A., (2019):** Geographic Information Science, At M.M. Fischer and P. Nijkamp (eds.) – Handbook of Regional Science, Springer-Verlag GmbH Germany
3. **Malczewski J. and Jankowski P., (2020):** Emerging trends and research frontiers in spatial multicriteria analysis, International Journal of Geographic Information Science:34(7);1267-1282
4. **Mytilinou V. and Kolios A.J., (2017):** A multi-objective optimization approach applied to offshore wind farm location selection, J. Ocean Eng. Mar. Energy:3;265-284
5. **Resch B., Sagl G., Tornros T., Bachmaier A., Eggers J.B. et al. (2014):** GIS-Based Planning and Modelling for Renewable Energy: Challenges and Future Research Avenues, ISPRS Int. J. Geo-Inf.:3;662-692